UNIWERSYTET MARII CURIE-SKŁODOWSKIEJ
W LUBLINIE
Szkoła Doktorska Nauk Ścisłych i Przyrodniczych

Dziedzina: **Nauki ścisłe i przyrodnicze**
Dyscyplina: **Nauki chemiczne**

Jędrzej Kozak
nr albumu: 261777

Analiza bezpośrednia i w przepływie wybranych substancji biologicznie czynnych z wykorzystaniem czujników sitodrukowanych

(Direct and flow analysis of selected biologically active substances using screen-printed sensors)

Rozprawa doktorska przygotowywana pod kierunkiem naukowym
prof. dr hab. Katarzyny Tyszczuk-Rotko

w Instytucie Nauk Chemicznych

LUBLIN, 2023

Pragnę złożyć serdeczne podziękowania Pani Promotor

prof. dr hab. Katarzynie Tyszczuk-Rotko

za nieocenioną pomoc, cenne wskazówki, cierpliwość i wyrozumiałość

w trakcie przygotowywania niniejszej rozprawy doktorskiej.

Spis treści

Lista publikacji będących podstawą rozprawy doktorskiej

Publikacja 1

K. Tyszczuk-Rotko, **J. Kozak**, M. Sztanke, K. Sztanke, I. Sadok, *A screen-printed sensor coupled with flow system for quantitative determination of a novel promising anticancer agent candidate*, Sensors, 20 (18) (2020) 5217-5227.

(IF_{2020} = 3,576 MEiN = 100 pkt.)

Publikacja 2

J. Kozak, K. Tyszczuk-Rotko, M. Wójciak, I. Sowa, *Electrochemically activated screen-printed carbon sensor modified with anionic surfactant (aSPCE/SDS) for simultaneous determination of paracetamol, diclofenac and tramadol*, Materials, 14 (13) (2021) 3581-3596.

(IF_{2021} = 3,748 MEiN = 140 pkt.)

Publikacja 3

J. Kozak, K. Tyszczuk-Rotko, M. Wójciak, I. Sowa, M. Rotko, *First screen-printed sensor (electrochemically activated screen-printed boron-doped diamond electrode) for quantitative determination of rifampicin by adsorptive stripping voltammetry*, Materials, 14 (15) (2021) 4231-4242.

(IF_{2021} = 3,748 MEiN = 140 pkt.)

Publikacja 4

K. Tyszczuk-Rotko, **J. Kozak**, B. Czech, *Screen-printed voltammetric sensors—tools for environmental water monitoring of painkillers,* Sensors, 22 (7) (2022) 2437-2454.

(IF_{2022} = 3,9 MEiN = 100 pkt.)

Publikacja 5

J. Kozak, K. Tyszczuk-Rotko, M. Wójciak, I. Sowa, M. Rotko, *Electrochemically pretreated sensor based on screen-printed carbon modified with Pb nanoparticles for determination of testosterone,* Materials, 15 (14) (2022) 4948-4964.

(IF_{2022} = 3,4 MEiN = 140 pkt.)

Publikacja 6

J. Kozak, K. Tyszczuk-Rotko, I. Sadok, K. Sztanke, M. Sztanke, *Application of a screen-printed sensor modified with carbon nanofibers for the voltammetric analysis of an anticancer disubstituted fused triazinone,* International Journal of Molecular Sciences, 23 (5) (2022) 2429-2442.

(IF_{2022} = 5,6 MEiN = 140 pkt.)

Publikacja 7

J. Kozak, K. Tyszczuk-Rotko, R. Metelka, *Quantification of anti-cancer antibiotic bleomycin using an electrochemically pretreated and decorated with lead nanoparticles screen-printed sensor,* International Journal of Molecular Sciences, 24 (1) (2022) 472-484.

(IF_{2022} = 5,6 MEiN = 140 pkt.)

Publikacja 8

J. Kozak, K. Tyszczuk-Rotko, K. Sztanke, M. Sztanke, *Sensitive and selective voltammetric sensor based on anionic surfactant-modified screen-printed carbon for the quantitative analysis of an anticancer active fused azaisocytosine-containing congener,* International Journal of Molecular Sciences, 24 (1) (2023) 564-574.

(IF_{2022} = 5,6 MEiN = 140 pkt.)

Publikacja 9

J. Kozak, K. Tyszczuk-Rotko, *Screen-printed gold sensor for ultrasensitive voltammetric analysis of the antipsychotic drug thioridazine,* Measurement, 217 (2023) 113107.

(IF_{2022} = 5,6 MEiN = 200 pkt.)

Publikacja 10

J. Kozak, K. Tyszczuk-Rotko, D. Gorylewski, *A nanoporous screen-printed carbon sensor for environmental and clinical monitoring of the antibiotic ciprofloxacin***,** Measurement (zaakceptowana do druku 26.09.2023 r., dołączono mail potwierdzający akceptację).

(IF_{2022} = 5,6 MEiN = 200 pkt.)

Łączny IF: <u>46,372</u>

Łączna liczba punktów MEiN: <u>1440</u>

Współpraca naukowa

Część badań do cyklu publikacji będących podstawą niniejszej rozprawy doktorskiej zrealizowano przy współpracy z:

1. **Prof. dr hab. Magdaleną Wójciak i prof. dr hab. Ireneuszem Sową** - Zakład Chemii Analitycznej, Uniwersytet Medyczny w Lublinie;
2. **Dr hab. Małgorzatą Sztanke, prof. UM i Prof. dr hab. Krzysztofem Sztanke –** Katedra Nauk Podstawowych, Uniwersytet Medyczny w Lublinie;
3. **Dr Radovanem Metelką** - Uniwersytet w Pardubicach, Katedra Chemii Analitycznej, Wydział Technologii Chemicznej, Pardubice, Czechy;
4. **Dr Iloną Sadok –** Katolicki Uniwersytet Lubelski Jana Pawła II, Wydział Medyczny, Instytut Nauk Biologicznych, Katedra Chemii;
5. **Dr Michałem Kuryło** - Centralne Laboratorium Miejskiego Przedsiębiorstwa Wodociągów i Kanalizacji w Lublinie.

Wstęp

W dzisiejszych czasach kilka tysięcy związków pełni rolę substancji czynnych preparatów farmaceutycznych. Ze względu na stale rosnącą produkcję i spożycie preparatów farmaceutycznych coraz większa liczba substancji leczniczych przenika do środowiska, zwłaszcza do ekosystemów wodnych. Farmaceutyki przedostają się do środowiska naturalnego zarówno podczas ich wytwarzania, stosowania, jak i utylizacji. Do źródeł zanieczyszczeń środowiska naturalnego substancjami czynnymi preparatów farmaceutycznych i ich metabolitami można zaliczyć: ścieki komunalne, których całkowite oczyszczenie tradycyjnymi metodami jest niemożliwe, niewłaściwa utylizacja przeterminowanych i niewykorzystanych leków, ścieki z przemysłu farmaceutycznego, a także odpady z gospodarstw, gdzie stosowane są różnego rodzaju leki weterynaryjne. Najczęściej wykrywanymi w próbkach środowiskowych grupami farmaceutyków są: leki przeciwbólowe i przeciwzapalne, antybiotyki, środki hormonalne oraz leki psychotropowe. Obecność tych substancji w środowisku wywiera szkodliwy wpływ na zdrowie zwierząt, jak również ludzi. Przykładowo, żeńskie hormony powodują feminizację ryb, a zanieczyszczenie antybiotykami skutkuje pojawieniem się coraz większej liczby wieloopornych szczepów bakterii, co przekłada się na znaczny spadek skuteczności sprawdzonych metod leczenia.

Mając na uwadze mnogość zagrożeń wynikających z obecności farmaceutyków w środowisku, niezwykle istotne jest monitorowanie ich ilości zarówno w próbkach środowiskowych, jak i płynach ustrojowych. W tym celu stosowana jest cała gama metod analitycznych, najczęściej metod chromatograficznych, które pomimo wielu zalet posiadają też wady, tj. kosztowna aparatura, często czasochłonny etap przygotowania próbki do analizy, a także duże zużycie odczynników. Metody elektroanalityczne, w tym woltamperometria, umożliwiają wykrywanie i ilościowe oznaczenie wielu związków organicznych. Woltamperometria charakteryzuje się wysoką czułością, niewielkim zużyciem odczynników i małą objętością próbek, niskim kosztem aparatury i analizy, a także możliwością miniaturyzacji i wykorzystania czujników w analizatorach przenośnych. Wśród stale rosnącej liczby opracowywanych czujników elektrochemicznych dużym zainteresowaniem cieszą się czujniki sitodrukowane. Urządzenia te wpisują się w popularny trend miniaturyzacji aparatury pomiarowej, znajdują bowiem zastosowanie w analizie polowej dzięki kompatybilności z analizatorami przenośnymi. Czujniki te składają się zazwyczaj z układu trzech

elektrod nadrukowanych z użyciem tuszów przewodzących na wspólnym podłożu ceramicznym lub plastikowym. Woltamperometria jak każda metoda analityczna, nie jest wolna od interferencji, które mogą wpływać na wynik analizy. Ich źródłem mogą być np. składniki złożonych matryc analizowanych próbek.

Niniejsza praca poświęcona jest opracowaniu nowych, woltamperometrycznych procedur oznaczania wybranych związków biologicznie czynnych z użyciem czujników sitodrukowanych oraz doborze odpowiedniego sposobu minimalizacji interferencji występujących podczas analizy próbek biologicznych i środowiskowych. W trakcie prowadzonych badań skupiono się na następujących grupach związków: związkach o działaniu przeciwzapalnym i przeciwbólowym, związkach o właściwościach przeciwnowotworowych, przeciwpsychotycznych, antybiotykach i hormonach. Dzięki elektrochemicznej aktywacji i/lub modyfikacji powierzchni stosowanych czujników, odpowiednio dobranym sposobom minimalizacji interferencji (zastosowanie: układu przepływowego, wstępnego odbiałczania próbek, modyfikacji powierzchni surfaktantem, dodatku do roztworu czynnika kompleksującego, krótkich czasów nagromadzania czy dużego rozcieńczenia próbek) oraz optymalizacji procedur woltamperometrycznych możliwe było selektywne oznaczania wybranych związków na bardzo niskich poziomach stężeń rzędu 10^{-9} – 10^{-13} mol L^{-1}.

Cel badań

Celem badań prowadzonych w ramach realizacji niniejszej rozprawy doktorskiej było opracowanie woltamperometrycznych procedur oznaczania wybranych związków biologicznie czynnych w próbkach środowiskowych i płynach ustrojowych z wykorzystaniem czujników sitodrukowanych, które będą charakteryzować się lepszymi parametrami analitycznymi w porównaniu do tych opisanych w literaturze.

Cele szczegółowe pracy to:

- zaprezentowanie nowych możliwości zastosowania czujników sitodrukowanych do analizy śladowej wybranych związków biologicznie czynnych;
- poprawa parametrów czujników sitodrukowanych poprzez elektrochemiczną aktywację elektrody pracującej i/lub modyfikację jej powierzchni surfaktantem, nanocząsteczkami ołowiu lub warstwą nanomateriałów węglowych;
- charakterystyka powierzchni elektrod sitodrukowanych z wykorzystaniem nowoczesnych technik instrumentalnych oraz określanie charakteru procesów elektrodowych;
- optymalizacja procedur przygotowania czujników i oznaczania wybranych związków biologicznie czynnych;
- opracowaniu procedur minimalizacji interferencji pochodzących od składników próbek środowiskowych i biologicznych;
- zastosowanie opracowanych procedur elektrochemicznych do oznaczania wybranych związków biologicznie czynnych w próbkach środowiskowych i biologicznych.

1. Aktualny stan wiedzy

1.1. Czujniki sitodrukowane

Wykorzystanie metod elektroanalitycznych w analizie związków biologicznie czynnych znacznie wzrosło w ciągu ostatniej dekady. Wynika to m.in. z faktu iż zarówno reakcje biologiczne zachodzące w ludzkim organizmie jak i reakcje elektrochemiczne na granicy faz elektroda-roztwór przebiegają z udziałem przenoszenia elektronów. Wiele ważnych procesów fizjologicznych, enzymatycznych i biochemicznych działa w oparciu o mechanizm elektrochemicznego utleniania/redukcji. Jedną z najczęściej stosowanych metod elektroanalitycznych jest woltamperometria, która została wprowadzona w latach 20-tych XX wieku przez czechosłowackiego chemika Jaroslava Heyrovsky'ego. Woltamperometria polega na badaniu zależności wartości mierzonego natężenia prądu w funkcji przyłożonego potencjału. Metoda ta pozwala na uzyskanie informacji jakościowych i ilościowych dotyczących badanych elektroaktywnych jonów i cząsteczek. Przy użyciu woltamperometrii możliwe jest oznaczanie śladowych stężeń dużej liczby związków organicznych, jak również prostych jonów uzyskując w większości przypadków granice wykrywalności rzędu $10^{-9} – 10^{-10}$ mol L^{-1}. Niewątpliwymi zaletami woltamperometrii są również: prostota i względnie krótki czas analizy, dokładność i precyzja oznaczeń, możliwość analizy bardzo małych objętości próbek oraz względnie niski koszt aparatury [1-5].

Wśród całej gamy elektrod wykorzystywanych w woltamperometrii na szczególną uwagę zasługują elektrody sitodrukowane (ang. *screen-printed electrodes*, SPEs). SPEs pojawiły się w latach 90-tych XX w. i od tego czasu są coraz częściej stosowane ze względu na niską cenę, odtwarzalność elektrody do elektrody, niezawodność oraz możliwość masowej produkcji. Ponadto, niewątpliwymi zaletami SPEs jest możliwość wykorzystania tego rodzaju elektrod wraz z przenośnymi analizatorami do badań próbek w miejscu ich pobrania w terenie, dzięki czemu nie zachodzi konieczność ich transportu do laboratorium i przechowywania. Możliwa jest praca z niewielkimi objętościami próbek i odczynników, a co za tym idzie, produkcja minimalnej ilości ścieków. Technika sitodruku to proces, w którym tusz jest nadrukowywany na stałą powierzchnię poprzez przeciskanie go przez siatkę zawierającą szablon obrazu jaki chcemy uzyskać. Typowy czujnik sitodrukowany składa się z układu trzech elektrod, pracującej, odniesienia i pomocniczej

umieszczonych zwykle na podłożu ceramicznym lub z tworzywa sztucznego jak polichlorek winylu czy poliwęglan, a także na podłożach elastycznych, papierze lub poliestrach (Rys. 1). Czynnikami mającymi wpływ na zaprojektowanie skutecznego czujnika sitodrukowanego są m.in. skład tuszu, temperatura jego utwardzania, metoda wstępnej obróbki i chropowatość powierzchni. Właściwości i użyteczność tuszu przewodzącego zależą od właściwości reologicznych, dyspersji, powierzchni właściwej i gęstości cząstek. Głównymi składnikami tuszów przewodzących są rozpuszczalniki, nanoczastęczki i związki przewodzące oraz organiczne spoiwo. Najczęściej stosowane tusze do produkcji SPEs zawierają materiały przewodzące, takie jak grafit, grafen, fullereny, a także inne nanomateriały węglowe jak nanorurki czy nanowłókna. Szeroko stosowane są również tusze przewodzące mające w swoim składzie metale, zwykle srebro, złoto, platyna itp. Srebrny tusz jest używany do drukowania ścieżek przewodzących i elektrod pseudoodniesienia, podczas gdy tusze węglowe i złote są używane do drukowania elektrod pracujących. Różnice w składzie tuszów węglowych mają istotny wpływ na efektywność transportu elektronów i wydajność analityczną SPEs.

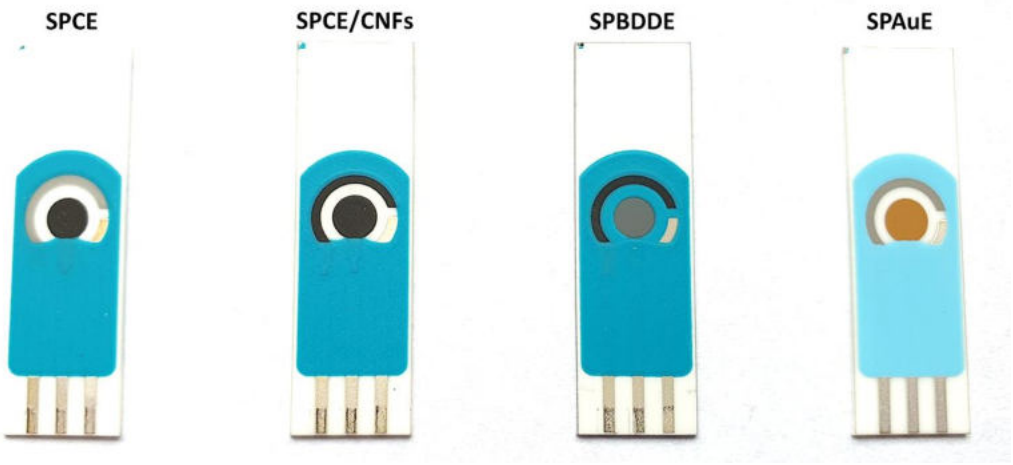

Rys. 1. Dostępne w handlu czujniki sitodrukowane wykorzystywane w trakcie badań (SPCE – sitodrukowana elektroda węglowa, SPCE/CNFs – sitodrukowana elektroda węglowa modyfikowana warstwą nanowłókien węglowych, SPBDDE – sitodrukowana elektroda diamentowa domieszkowana borem, SPAuE – sitodrukowana elektroda złota) [opracowanie własne].

W celu dostosowania SPEs do różnorakich zastosowań analitycznych oprócz doboru odpowiedniego materiału do produkcji elektrody pracującej ich właściwości

można też zmieniać za pomocą różnych modyfikatorów (Rys. 2) [6-8]. Obecnie w analityce najczęściej stosuje się SPEs modyfikowane nanomateriałami węglowymi np. nanorurkami [9] i nanowłóknami [10], nanocząsteczkami metali i tlenków metali [11], polimerami [12, 13], a także cieczami jonowymi [14, 15]. Rosnącym zainteresowaniem cieszą się także w ostatnich latach bioczujniki oparte na SPEs, do których zwykle zaliczane są SPEs modyfikowane enzymami [16, 17], przeciwciałami [18] lub kwasami nukleinowymi [19]. Modyfikacji SPEs można dokonać podobnie jak w przypadku konwencjonalnych elektrod poprzez nakroplenie roztworu modyfikatora lub elektroosadzania z roztworu, może się to również odbywać na etapie drukowania tuszu na powierzchnie nośnika. Do najczęstszych celów modyfikacji powierzchni elektrody pracującej należy zaliczyć zwiększenie powierzchni aktywnej, poprawę kinetyki transferu elektronów lub selektywności czujnika.

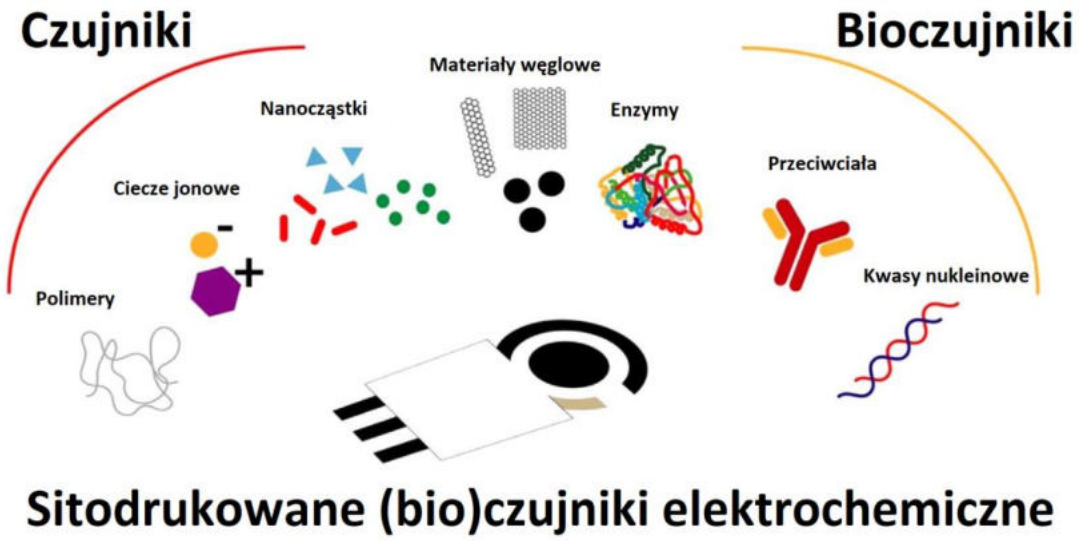

Rys. 2. Rodzaje modyfikatorów SPEs [8].

Interesujące własności SPEs w połączeniu z mnogością materiałów, jakie można wykorzystać do ich produkcji, a także modyfikatorów powierzchni, jakie można zastosować, pozwalają na oznaczanie zarówno jonów metali [20], jak i szerokiej gamy związków organicznych [21] na niskich poziomach stężeń. Dodatkowo, pojawienie się i rozwój bioczujników umożliwia również oznaczanie biomarkerów (w tym nowotworowych), a także patogenów np. wirusa SARS-CoV-2 [6], a uniwersalność SPEs sprawia iż są one świetnym narzędziem analitycznym w obszarach badań środowiska, farmaceutyków oraz żywności.

1.2. Przyczyny występowania interferencji w woltamperometrycznej analizie związków organicznych oraz sposoby ich minimalizacji/eliminacji

Woltamperometria posiada wiele zalet tj. względnie niski koszt wykorzystywanych urządzeń, prostota wykonania pomiarów, wysoka czułość i precyzja oznaczeń. Jednak jak każda metoda analityczna woltamperometria również nie jest wolna od interferencji. Do głównych przyczyn występowania interferencji podczas woltamperometrycznych oznaczeń związków organicznych należy zaliczyć:

- blokowanie powierzchni elektrody przez produkty i półprodukty reakcji elektrodowych oraz związki organiczne i jony metali obecne w próbce,
- nakładanie się pików analitu i interferenta.

Blokowanie powierzchni elektrody pracującej przez adsorbujące się produkty lub półprodukty zachodzących reakcji elektrodowych, jak również przez składniki złożonych matryc analizowanych próbek, stanowi istotny czynnik ograniczający praktyczne wykorzystanie technik elektrochemicznych. Może znacznie utrudnić, a nawet uniemożliwić wykonanie analizy. Eliminację lub minimalizację problemu blokowania powierzchni elektrody można zrealizować na wiele sposobów, przy czym dobierając odpowiedni sposób należy mieć na uwadze typ czujnika i materiału elektrodowego, mechanizm blokowania, rodzaj stosowanej metody elektroanalitycznej oraz matrycy próbki [22].

Jednym ze sposobów pozwalających ograniczyć zanieczyszczenie powierzchni elektrody jest prowadzenie pomiarów w układzie przepływowym. Układ ten pozwala na skrócenie czasu kontaktu próbki z powierzchnią elektrody, a także usuwanie z niej produktów i półproduktów reakcji elektrochemicznych przez co ogranicza ich osadzanie na elektrodzie pracującej [22, 23]. SPEs znajdują zastosowanie w połączeniu z różnego rodzaju układami przepływowymi (Rys. 3). Można tu wymienić analizę przepływowo-wstrzykową (ang. *Flow-Injection Analysis, FIA)*, gdzie układ składa się z celki pomiarowej, pompy perystaltycznej, rurek i zaworu wstrzykowego. Uproszczoną wersją FIA jest bezprzewodowa analiza przepływowo-wstrzykowa (ang. *Batch Injection Analysis, BIA*), w której wykorzystuje się jedynie celkę elektrochemiczną i elektroniczną mikropipetę dozującą próbkę bezpośrednio na powierzchnię elektrody zanurzonej w roztworze elektrolitu. Układ do BIA może być zatem wykorzystywany w analizie poza laboratorium, pozwala także uniknąć problemów występujących w FIA

jak np. obecności pęcherzyków powietrza. SPEs mogą być również stosowane w detektorach elektrochemicznych do wysokosprawnej chromatografii cieczowej (ang. *High-Performance Liquid Chromatography, HPLC*) [23, 24].

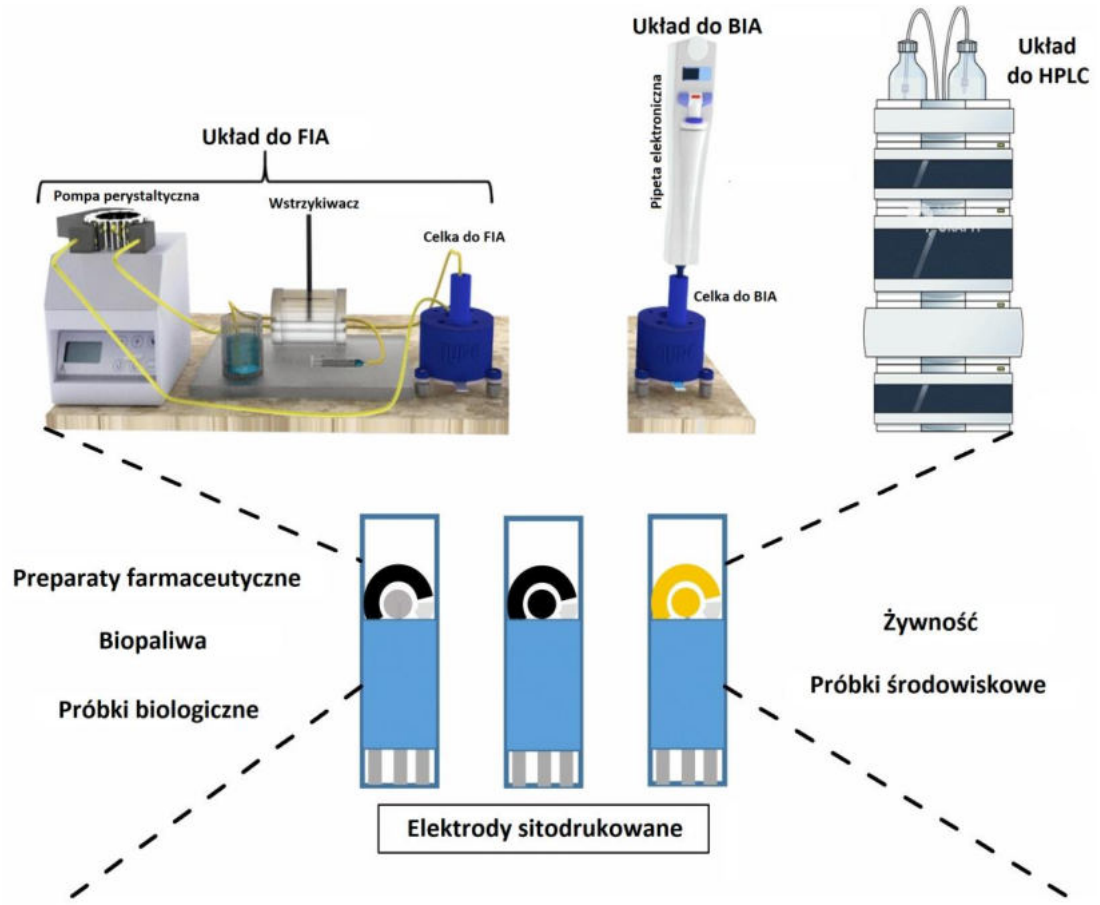

Rys. 3. Układy przepływowe współpracujące z czujnikami sitodrukowanymi [23].

Zanieczyszczenie powierzchni elektrody pracującej składnikami matrycy można ograniczyć również wskutek jej odpowiedniej modyfikacji. Zastosowanie znajdują tutaj surfaktanty i polimery. Surfaktanty adsorbują się na powierzchni elektrody pracującej przez co zapobiegają jej zanieczyszczaniu przez organiczne makrocząsteczki i jony metali obecne w analizowanych próbkach. Dodatkową zaletą modyfikacji elektrody surfaktantem może być wzrost intensywności sygnału analitycznego oznaczanej substancji jeśli w warunkach prowadzenia pomiaru istnieje ona w roztworze jako jon o znaku przeciwnym do znaku jonu surfaktantu. Dochodzi wówczas do elektrostatycznego przyciągania pomiędzy surfaktantem i analitem [25]. Zabezpieczenie powierzchni elektrody przed adsorpcją potencjalnych interferentów można uzyskać w podobny sposób wykorzystując modyfikację filmem polimeru np. Nafionu (sulfonowanego kopolimeru tetrafluoroetenu) czy polisiloksanów [26, 27]. Znanym

działaniem prewencyjnym ograniczającym blokowanie elektrod jest prowadzenie nagromadzania analitu przy użyciu krótkich impulsów potencjałowych. Potencjał impulsu katodowego jest dobierany tak, żeby zachodziła adsorpcja analitu, a potencjał impulsu anodowego tak, by zdesorbować substancję powierzchniowo czynną przy dalszym nagromadzaniu analitu. Nagromadzanie impulsowe pozwala na minimalizację interferencji pochodzących od surfaktantów obecnych w próbkach wód [28].

Próbki o bogatej matrycy takie jak krew czy surowica zawierają znaczne ilości rozpuszczonych białek, które adsorbując się na powierzchni elektrody mogą uniemożliwić wykonanie analizy. W takim przypadku próbkę można poddać wstępnemu przygotowaniu strącając białka np. przy pomocy mocnego kwasu, wówczas po odwirowaniu otrzymujemy próbkę wolną od białek. Sposób ten może być jednak zastosowany tylko w przypadku gdy analit występuje w postaci wolnej, a nie związanej z białkami [29]. Kolejnym sposobem minimalizacji zanieczyszczenia elektrody składnikami matrycy próbki jest zapewnienie odnawialności jej powierzchni po każdym pomiarze. W tym celu można wprowadzić etap elektrochemicznego oczyszczania do procedury pomiarowej lub zastosować elektrody modyfikowane osadzanymi *in-situ* nanocząstkami lub błonką metali np. bizmutu czy antymonu, które są usuwane po każdym pomiarze wraz z ewentualnymi zanieczyszczeniami. Można również korzystać z elektrod wykonanych z materiałów cechujących się dużą odpornością na osadzanie zanieczyszczeń, czego świetnym przykładem jest elektroda diamentowa domieszkowana borem (ang. *boron-doped diamond electrode, BDDE*). Jej podatność na zanieczyszczanie można dodatkowo zmniejszyć uwodorniając jej powierzchnię. Innymi sposobami jakie można odnaleźć w literaturze jest podgrzewanie elektrody podczas wykonywania analizy oraz stosowanie elektrod jednorazowego użytku [22].

Interferencje wynikające z nakładania się pików również można eliminować modyfikując powierzchnie elektrody pracującej polimerem. Wspomniany wcześniej Nafion oprócz zabezpieczenia elektrody przed adsorpcją zanieczyszczeń posiada właściwości kationowymienne dzięki czemu eliminuje interferencje pochodzące od anionów [30]. Grupą polimerów pozwalających uzyskać niezwykle wysoką selektywność i specyficzność oznaczeń są polimery z odciskiem molekularnym (ang. *Molecularly Imprinted Polymers, MIPs*). MIPs to syntetyczne polimery selektywne względem konkretnego analitu lub grupy związków strukturalnie zbliżonych. Ogólna zasada odcisku molekularnego opiera się na procesie syntezy, w którym funkcjonalne

i sieciujące monomery są kopolimeryzowane w obecności docelowego analitu, który pełni rolę szablonu/matrycy molekularnej. Szablon wdrukowany niejako w usieciowaną matrycę tworzy w niej puste i specyficzne miejsca wiążące komplementarne do cząsteczki analitu. Zaletami MIPs są m.in. niski koszt przygotowania, wysoka stabilność i specyficzność, dzięki której mogą z powodzeniem w wielu przypadkach zastępować drogie, biologiczne analogi np. przeciwciała [31, 32]. W sytuacji gdy na sygnał analitu nakłada się sygnał pochodzący od obecnych w próbce jonów metali skutecznym sposobem minimalizacji tego typu interferencji jest wprowadzenie do roztworu odpowiedniego reagenta np. EDTA, DTPA, którego zadaniem jest skompleksowanie przeszkadzających jonów metali [33].

2. Badania własne

Przeprowadzone w ramach niniejszej rozprawy doktorskiej badania miały na celu opracowanie woltamperometrycznych procedur oznaczania wybranych związków biologicznie czynnych (tj. związków o działaniu przeciwzapalnym i przeciwbólowym, związków o właściwościach przeciwnowotworowych, przeciwpsychotycznych, antybiotyków i hormonów) z wykorzystaniem czujników sitodrukowanych, które będą charakteryzować się lepszymi parametrami analitycznymi w porównaniu do tych opisanymi w literaturze. Użyteczność zoptymalizowanych procedur została potwierdzona poprzez zastosowanie ich w analizie próbek o różnej matrycy. W ramach badań:

- zoptymalizowano skład elektrolitu podstawowego, potencjał i czasu nagromadzania analitów oraz parametry techniki rejestracji sygnału analitycznego (**Rozdz. 2.2**);
- scharakteryzowano powierzchnie czujników sitodrukowanych z wykorzystaniem nowoczesnych technik instrumentalnych (**Rozdz. 2.3**);
- określono charakter zachodzących procesów elektrodowych (**Rozdz. 2.4**);
- wyznaczono parametry analityczne oraz zbadano selektywność procedur (**Rozdz. 2.5**);
- zastosowano opracowane procedury w analizie próbek biologicznych, środowiskowych i preparatów farmaceutycznych (**Rozdz. 2.6**).

2.1. Charakterystyka oznaczanych związków biologicznie czynnych

Wraz z rozwojem medycyny w ostatnich dziesięcioleciach gwałtownie wzrosła produkcja i spożycie preparatów farmaceutycznych, które pozwoliły wyeliminować wiele chorób i poprawiły jakość ludzkiego życia. Obecnie około 3000 różnych związków chemicznych pełni rolę substancji czynnych farmaceutyków, a roczna wielkość produkcji przekracza setki ton. Wzrost spożycia leków skutkuje wzrostem zanieczyszczenia środowiska, zwłaszcza wodnego substancjami czynnymi tych leków i ich metabolitami. Farmaceutyki, które docierają do zbiorników wodnych, zarówno powierzchniowych, jak i podziemnych, pochodzą z wielu różnych źródeł (Rys. 4). Pierwszym z nich są ścieki komunalne,

które zawierają duże ilości farmaceutyków pochodzących z ludzkich odchodów, a także nieodpowiednia utylizacja przeterminowanych lub niewykorzystanych leków. Innym ważnym źródłem środków farmaceutycznych są odpady rolne i zwierzęce, zwłaszcza te ostatnie, ponieważ w dużych gospodarstwach prowadzących intensywną hodowlę zwierzęta są one często karmione paszami zawierającymi leki, a odchody są często wykorzystywane w rolnictwie jako dodatki do gleby, skąd po wymyciu przedostają się do wód gruntowych. Kolejnym ważnym źródłem są ścieki z przemysłu farmaceutycznego, w których występują wysokie stężenia substancji czynnych.

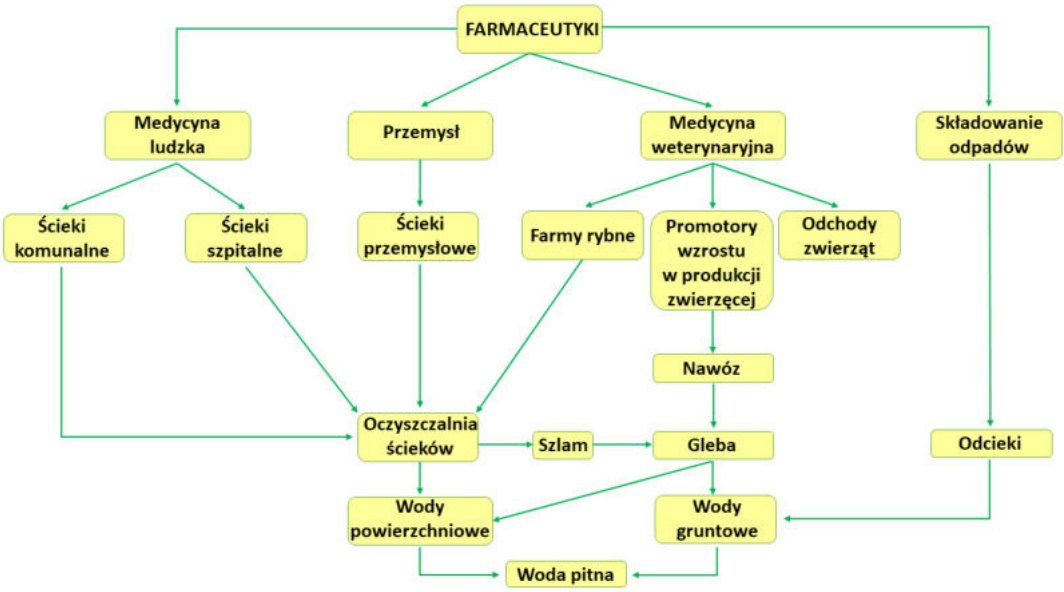

Rys. 4. Źródła zanieczyszczeń środowiska substancjami czynnymi preparatów farmaceutycznych oraz ich obieg [opracowanie własne].

Pomimo występowania coraz większej liczby farmaceutyków w ekosystemach wodnych stosunkowo niewiele jest informacji na temat ich toksyczności w stężeniach środowiskowych. Do najczęściej wykrywanych w próbkach środowiskowych grup farmaceutyków możemy zaliczyć: niesteroidowe leki przeciwzapalne (NLPZ), innego rodzaju środki przeciwbólowe, antybiotyki, środki hormonalne, β-blokery, leki psychotropowe, przeciwnowotworowe, antyretrowirusowe oraz leki regulujące gospodarkę lipidową [34-36].

W trakcie prowadzonych badań skupiono się na następujących grupach związków: związkach o działaniu przeciwzapalnym i przeciwbólowym, związkach o właściwościach przeciwnowotworowych, przeciwpsychotycznych, antybiotykach

i hormonach.

Leki przeciwnowotworowe zgodnie z ich właściwościami terapeutycznymi, farmakologicznymi i chemicznymi można podzielić na dwie grupy: leki przeciwnowotworowe (L01) i terapia hormonalna (L02). Leki przeciwnowotworowe dzieli się na pięć grup: L01A - środki alkilujące, L01B - antymetabolity, L01C - alkaloidy roślinne i inne substancje naturalne, L01D - antybiotyki cytotoksyczne i substancje pokrewne oraz L01X - inne środki przeciwnowotworowe. Tymczasem w terapii hormonalnej wykorzystuje się hormony - L02A oraz antyhormony i środki pokrewne - L02B. Leki stosowane w leczeniu nowotworów odznaczają się wysoką toksycznością oddziałując negatywnie na ludzkie komórki i układ hormonalny [37]. Leki te na ogół nie są dobrze metabolizowane i zwykle są wydalane przez pacjentów w postaci niezmienionej wraz z kałem i moczem. Ponieważ leczenie raka odbywa się w szpitalach, ale także u pacjentów ambulatoryjnych leczonych w domu, wykazano, że ścieki pochodzące ze szpitali i ścieki domowe stanowią istotne źródło leków przeciwnowotworowych w ekosystemach wodnych. Ponadto wykazano, że ścieki z fabryk farmaceutycznych, w których leki te są produkowane, również zawierają ich podwyższone stężenia. Wiele leków przeciwnowotworowych to oporne, trwałe lub „pseudotrwałe" zanieczyszczenia organiczne obecne w ściekach i często nie są usuwane przez wtórne i trzeciorzędowe oczyszczanie w oczyszczalniach ścieków, przez co mogą stanowić zagrożenie dla ekosystemów wodnych [38]. Ze względu na toksyczność leków przeciwnowotworowych i ich przedostawanie do środowiska konieczne jest monitorowanie stężeń tych leków zarówno w próbkach środowiskowych, jak i płynach ustrojowych pacjentów poddawanych leczeniu.

W ramach współpracy z naukowcami z Uniwersytetu Medycznego w Lublinie opracowano procedury oznaczania trzech nowo otrzymanych związków o właściwościach przeciwnowotworowych [**RD1**, **RD6** i **RD8**]. Badane związki zostały krótko scharakteryzowane poniżej.

8-(4-metoksyfenylo)-4-okso-4,6,7,8-tetrahydroimidazo[2,1-c][1,2,4]triazyno -3-karboksylan etylu, EIMTC (Rys. 5A) to związek chemiczny o strukturze zbliżonej do zasad azotowych wchodzących w skład nukleotydów kwasów nukleinowych. Cechuje się on niewielką toksycznością *in vitro* i *in vivo*, szerokim spektrum działania p-nowotworowego oraz dobrą biodostępnością. EIMTC wykazuje skuteczne działanie przeciwko komórkom szpiczaka mnogiego, raka

piersi i szyjki macicy [39-41].

8-(4-chlorofenylo)-3-fenylo-7,8-dihydroimidazo[2,1-c][1,2,4]triazyno-4-(6H)-on, 4-Cl-PIMT (Rys. 5B) jest najbardziej obiecującym kandydatem na lek przeciwnowotworowy spośród skondensowanych, dipodstawionych triazynonów. 4-Cl-PIMT wykazuje działanie antyproliferacyjne na komórki szpiczaka krwi obwodowej, co wskazuje na możliwą użyteczność związku w leczeniu tego rodzaju nowotworów hematologicznych. Ponadto, związek ten okazał się mieć silne właściwości antymigracyjne w komórkach raka szyjki macicy, co sugeruje jego wysoki potencjał w zapobieganiu przerzutom [42].

Kolejną substancją o podobnej budowie jest 3-(4-nitrofenylo)-8-(2,3-dimetylofenylo)-7,8-dihydroimidazo[2,1-c][1,2,4]triazyn-4(6H)-on, NDIT (Rys. 5C). NDIT wywołuje zahamowanie wzrostu nowotworów wywodzących się z komórek nabłonkowych tj. nowotworu piersi, szyjki macicy, płuc i jajników, przy czym najsilniejszy efekt cytostatyczny uzyskano w przypadku raka piersi i szyjki macicy. W świetle aktualnej wiedzy mechanizm jego działania przeciwnowotworowego może być związany z selektywną aktywacją (poprzez redukcję z udziałem szeregu flawoprotein) tego proleku zawierającego pierścień aromatyczny z grupą nitrową w tkance nowotworowej do substancji przeciwnowotworowej (tj. cytotoksyczny rodnik nitroanionu i cytotoksyczna cząsteczka hydroksyloaminy) Ponadto stwierdzono, że NDIT wykazuje niewielką toksyczność w stosunku do prawidłowych komórek nabłonkowych linii komórkowej Vero [43-45].

Opracowano również procedurę oznaczania wykorzystywanego powszechnie w terapii onkologicznej cytostatycznego antybiotyku, bleomycyny [**RD7**]. Bleomycyna, BLM (Rys. 5D) jest mieszaniną naturalnych, strukturalnie podobnych antybiotyków glikopeptydowych wytwarzanych przez bakterię *Streptomyces verticillus*. Klinicznie stosowana bleomycyna zawiera głównie bleomycynę A2 i B2 oraz niewielkie ilości innych podfrakcji. W połączeniu z innymi chemioterapeutykami BLM znajduje zastosowanie w leczeniu wielu typów nowotworów. Jest lekiem pierwszego rzutu w leczeniu chłoniaka Hodgkina, ale znajduje również zastosowanie w leczeniu chłoniaków nieziarniczych oraz nowotworów głowy, szyi i skóry. W terapii skojarzonej z cisplatyną i etopozydem wykazuje wysoką skuteczność w leczeniu raka jądra. BLM znajduje również zastosowanie w leczeniu złośliwego wysięku opłucnowego oraz w skleroterapii

u pacjentów z malformacjami naczyniowymi. Szerokie zastosowanie BLM wynika z faktu, że powoduje ona mielosupresję i immunosupresję na stosunkowo niskim poziomie [46-52].

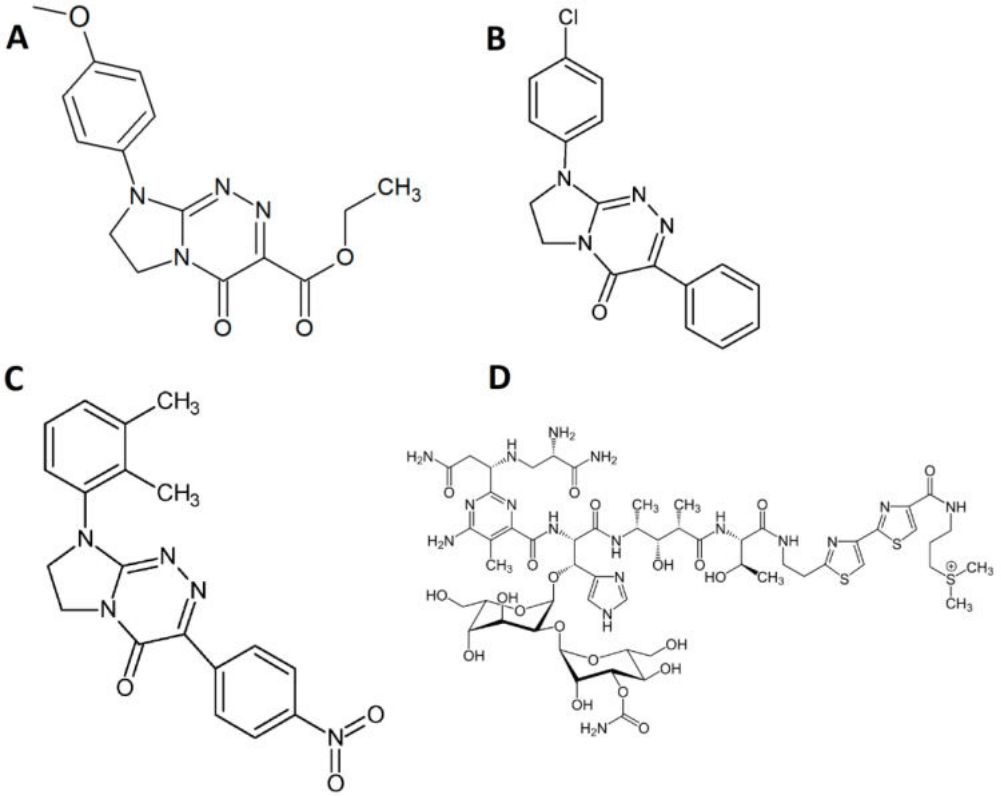

Rys. 5. Wzory strukturalne: A) EIMTC, B) 4-Cl-PIMT, C) NDIT, D) BLM [opracowanie własne].

Inną grupą związków, która była podstawą badań do niniejszej rozprawy były substancje biologicznie czynne o właściwościach przeciwzapalnych i przeciwbólowych. Substancje te należą do najczęściej stosowanych farmaceutyków na świecie i są powszechnie podawane w objawowym leczeniu różnych chorób. Leki z tej grupy mają największy udział w całkowitej zawartości farmaceutyków w ściekach szpitalnych [53]. Leki przeciwbólowe to zróżnicowana grupa leków stosowanych w celu złagodzenia bólu. Złagodzenie bólu można osiągnąć poprzez działanie leków przeciwbólowych na obwodowy i ośrodkowy układ nerwowy. Istnieją trzy główne grupy leków przeciwbólowych: narkotyczne (opioidy), nienarkotyczne (np. paracetamol) i niesteroidowe leki przeciwzapalne (NLPZ, np. naproksen, diklofenak) [54]. W ramach prowadzonych badań opracowano procedurę jednoczesnego oznaczania paracetamolu, diklofenaku

i tramadolu [**RD2**].

Acetaminofen (N-acetylo-p-aminofenol, Rys. 6A) jest znany jako paracetamol (PA) lub tylenol i jest szeroko stosowany na świecie w celu łagodzenia umiarkowanego bólu i obniżenia gorączki. Działanie przeciwbólowe i przeciwgorączkowe PA jest podobne do aspiryny (kwasu acetylosalicylowego), ale zwykle preferuje się PA, zwłaszcza u pacjentów wrażliwych na kwas acetylosalicylowy. Pojedyncze dawki PA wykazują działanie przeciwbólowe w ostrych zespołach bólowych, bez jakichkolwiek skutków ubocznych, jednak przedawkowanie PA może skutkować kumulacją toksycznych metabolitów, co może powodować ciężkie, a czasem śmiertelne uszkodzenia wątroby i nerek [55].

Diklofenak (DF, Rys. 6B) jest niesteroidowym lekiem przeciwzapalnym (NLPZ), stosowanym w celu złagodzenia bólu spowodowanego urazem lub chorobą przewlekłą. Jest szeroko stosowany na całym świecie w celach leczniczych i weterynaryjnych. DF obecny w środowisku ulega degradacji w bardzo niewielkim stopniu. Może powodować spadek populacji ryb i ptaków, powodując niewydolność nerek [54, 56]. Zgodnie z dyrektywą Parlamentu Europejskiego i Rady Unii Europejskiej (2013/39/UE) DF jest substancją podlegającą monitoringowi w środowisku wodnym na terenie całej Unii Europejskiej.

Tramadol, (1R,2R)-2-[(dimetyloamino)metylo]-1-(3-metoksyfenylo) cykloheksanol (TR, Rys. 6C) jest syntetycznym opioidowym lekiem przeciwbólowym stosowanym w leczeniu ostrego i przewlekłego bólu. Związek ten działa na receptor μ-opioidowy oraz na układ serotoninergiczny i noradrenergiczny. Typowe dawkowanie doustne tramadolu mieści się w zakresie od 50 do 100 mg co 4 do 6 godzin. Maksymalna dawka leku wynosi 400 mg na dobę. Przedawkowanie tramadolu może powodować nudności, depresję oddechową, wymioty, śpiączkę, zawroty głowy i tachykardię [57].

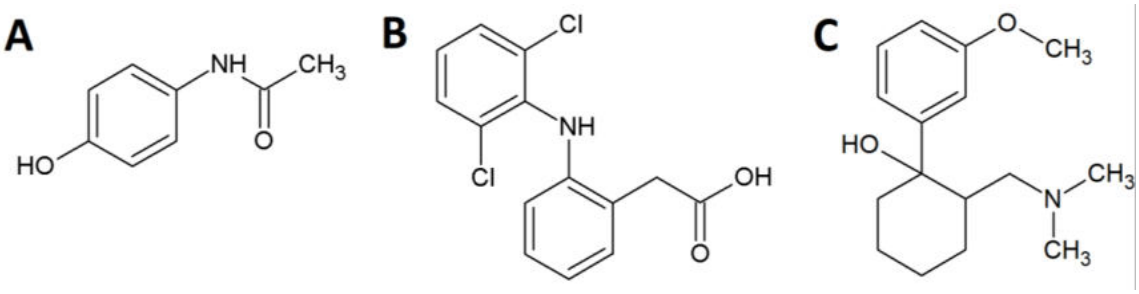

Rys. 6. Wzory strukturalne: A) PA, B) DF i C) TR [opracowanie własne].

Kolejną grupą związków, które były przedmiotem prowadzonych badań były antybiotyki. Spożywanie obecnie ogromnej ilości antybiotyków w walce z chorobami, ale także w celu wspomagania wzrostu zwierząt, m.in. w akwakulturach, mleczarniach czy fermach drobiu, przyczynia się do obecności tych biologicznie aktywnych związków w środowisku. Znaczna ilość antybiotyków jest wydalana w postaci niezmienionej lub w postaci aktywnych metabolitów. Z tego powodu ścieki szpitalne, weterynaryjne, a nawet komunalne często zawierają wysokie stężenia antybiotyków. Ponadto procesy ich usuwania ze ścieków są mało efektywne [58-60]. Ze względu na ciągłe wprowadzanie antybiotyków do środowiska, organizmy wodne i glebowe są na nie przewlekle narażone. Ponadto, ponieważ są aktywne w bardzo niskich stężeniach, działają toksycznie na organizmy, a w połączeniu z innymi lekami i/lub związkami ksenobiotycznymi występuje efekt synergistyczny. Antybiotyki stanowią poważne zagrożenie dla glonów i roślin wodnych. Stwierdzono, że wiele z nich jest inhibitorami fotosyntezy, ponieważ mogą blokować łańcuch przenoszenia elektronów fotosystemu II w chloroplastach i zwiększać stres oksydacyjny. Mikroorganizmy, w tym bakterie i grzyby, rozwijają oporność na substancje przeciwbakteryjne w wyniku ekspozycji na niskie stężenia przez kilka generacji, co prowadzi do wytworzenia szczepów opornych na większość popularnie stosowanych antybiotyków [34]. W trakcie prowadzonych prac badawczych opracowano procedurę oznaczania ryfampicyny [**RD3**] .

Ryfampicyna ((3-[[(4-metylo-1-piperazynylo)-imino]-metylo]) ryfamycyna) (RIF, Rys. 7) jest półsyntetycznym antybiotykiem makrocyklicznym, będącym pochodną ryfamycyny, otrzymywaną w procesie fermentacji przeprowadzanym przez szczep *Streptomyces mediterranei*. Ryfampicyna jest antybiotykiem pierwszego rzutu wraz z izoniazydem, pirazynamidem, etambutolem i streptomycyną w leczeniu gruźlicy płuc i pozapłucnej. RIF jest również stosowana w leczeniu trądu i niektórych rodzajów zapalenia kości i szpiku oraz zapalenia wsierdzia. Działanie tego antybiotyku polega na hamowaniu DNA-zależnej polimerazy RNA w komórkach bakteryjnych, co skutkuje zatrzymaniem ich wzrostu [61-63].

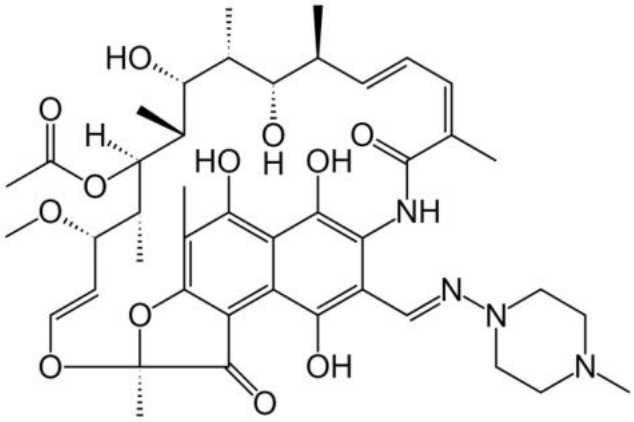

Rys. 7. Wzór strukturalny RIF [opracowanie własne].

W ramach badań poświęcono uwagę również grupie związków biologicznie czynnych jakimi są hormony. Substancje te regulują wiele rodzajów funkcji komórkowych i fizjologicznych w organizmie człowieka, takich jak reprodukcja, wzrost i różnicowanie komórek, tkanek i narządów. Hormony sterydowe obecne w środowisku wodnym stanowią zagrożenie dla bytujących w nim organizmów już w stężeniach rzędu ng L^{-1}. Dotyczy to zarówno syntetycznych jak i naturalnie wytwarzanych hormonów sterydowych tj. estron, 17β-estradiol, progesteron i testosteron [64]. Ten ostatni stał się przedmiotem prowadzonych badań, a opracowana procedura oznaczania testosteronu została opisana w publikacji [**RD5**].

Testosteron (17β-hydroksyandrost-4-en-3-on) (TST, Rys. 8) jest głównym endogennym sterydem androgenno-anabolicznym u ludzi. W organizmie człowieka wytwarzany jest głównie w jądrach mężczyzn i w niewielkich ilościach w jajnikach kobiet i nadnerczach u obu płci. U mężczyzn TST odgrywa kluczową rolę w rozwoju narządów układu rozrodczego, takich jak jądra i prostata, a także w promowaniu drugorzędowych cech płciowych, takich jak zwiększona masa mięśniowa, masa kostna i wzrost włosów na ciele. Ponadto TST jest niezbędny dla zdrowia i dobrego samopoczucia, zapobiega także osteoporozie. Nadużywanie testosteronu jest powszechne wśród sportowców, którzy chcą zwiększyć siłę i zdolności regeneracyjne, co czyni go najczęściej zgłaszaną, nadużywaną substancją sterydową. Światowa Agencja Antydopingowa zakazała jego stosowania w celu zapewnienia uczciwej rywalizacji sportowej i ochrony sportowców przed możliwymi niepożądanymi skutkami ubocznymi, takimi jak zawał serca, nadciśnienie, choroby wątroby czy zaburzenia psychiczne [65, 66].

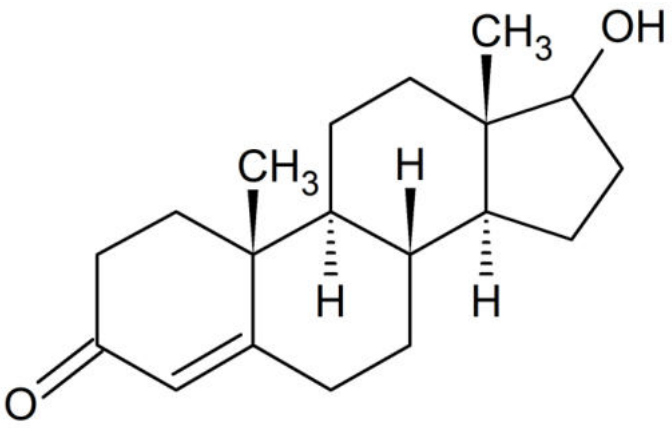

Rys. 8. Wzór strukturalny TST [opracowanie własne].

Ostatnią grupą związków, która była przedmiotem niniejszych badań były substancje przeciwpsychotyczne. Związki te stanowią podstawowy sposób leczenia zaburzeń psychotycznych, w tym schizofrenii. Leki z tej grupy są powszechnie stosowane w leczeniu objawów psychotycznych, takich jak paranoja, omamy, pobudzenie i delirium. Są również stosowane w leczeniu depresji psychotycznej, choroby afektywnej dwubiegunowej i lęku. Lekiem przeciwpsyhotycznym, któremu poświęcono uwagę i którego procedurę oznaczania opracowano jest tiorydazyna [**RD9**].

Tiorydazyna (10-[2-(1-metylo-2-piperydylo)etylo]-2-(metylotio)-10H fenotiazyna) (TDZ, Rys. 9) jest stosowana w leczeniu schizofrenii, w przypadku braku odpowiedzi na inne leki przeciwpsychotyczne. Mechanizm działania tego leku polega na regulowaniu poziomu substancji takich jak serotonina, dopamina i glutaminian w ludzkim mózgu, których nieodpowiednie ilości wywołują objawy schizofrenii. Oprócz schizofrenii TDZ jest stosowana do kontrolowania manii i pobudzenia, może być wykorzystywana w leczeniu lęków i problemów behawioralnych u dzieci. TDZ jest również lekiem używanym w walce z infekcjami wywołanymi przez oporny na metycylinę szczep *Staphylococcus aureus* i wielooporny szczep *Mycobacterium tuberculosis* [67-69].

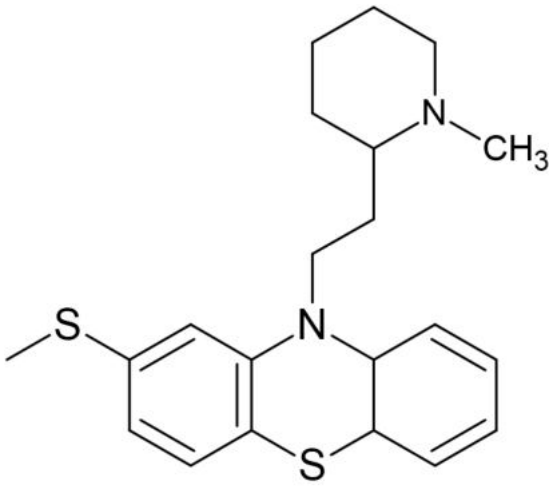

Rys. 9. Wzór strukturalny TDZ [opracowanie własne].

2.2. Woltamperometryczne procedury oznaczania wybranych związków biologicznie czynnych

Pomiary elektrochemiczne prowadzono z wykorzystaniem analizatora elektrochemicznego μAutolab (Holandia) sterowanego przez oprogramowanie GPES (techniki woltamperometrycznych) lub oprogramowanie FRA podczas rejestracji widm elektrochemicznej spektroskopii impedancyjnej (EIS) i krzywych pojemności różniczkowej. W toku prowadzonych badań we wszystkich pracach [**RD1 – RD9**] z wyjątkiem artykułu [**RD4**] (artykuł przeglądowy), dokonano optymalizacji składu roztworu elektrolitu podstawowego, czasu mieszania (t) lub czasu ($t_{acc.}$) i potencjału nagromadzania ($E_{acc.}$). Ponadto, w każdej procedurze optymalizacji poddawano parametry techniki rejestracji sygnału analitycznego woltamperometrii impulsowo-różnicowej (DPV) lub woltamperometrii fali prostokątnej (SWV). W przypadku DPV optymalizowano następujące parametry: amplitudę (ΔE_A), szybkość skanowania (ν) i czas modulacji (t_m), natomiast stosując SWV optymalizowano częstotliwość (f), krok potencjału (ΔE) i amplitudę (E_{SW}). Zoptymalizowane, wymienione powyżej parametry podsumowano w tabeli 1, a opracowane woltamperometryczne procedury zaprezentowano schematycznie w tabeli 2.

Tabela 1. Zestawienie składu roztworu i parametrów opracowanych procedur.

Analit	Elektroda	Technika	Skład roztworu	Zakres rejestracji woltamperogramów i zoptymalizowane parametry	Praca
EIMTC	SPCE/CNFs	SWV	0,075 mol L^{-1} H_2SO_4	od -0,2 do -0,9 V; t = 45 s; f = 50 Hz; E_{SW} = 50 mV; ΔE = 7 mV;	[**RD1**]
PA, DF, TR	aSPCE/SDS	DPAdSV	0,075 mol L^{-1} bufor octanowy (pH = 4,0 ± 0,1) + 15 mg L^{-1} SDS + 1 × 10^{-5} mol L^{-1} DTPA	od 0 do 2 V; $E_{acc.}$ = -0,4 V; $t_{acc.}$ = 120 s; ΔE_A = 150 mV; ν = 250 mV s^{-1}; t_m = 10 ms	[**RD2**]
RIF	aSPBDDE	DPAdSV	0,1 mol L^{-1} PBS (pH = 3,0 ± 0,1)	od -0,25 do 1 V; $E_{acc.}$ = -0,45 V; $t_{acc.}$ = 120 s; ΔE_A = 150 mV; ν = 100 mV s^{-1}; t_m = 5 ms	[**RD3**]
TST	pSPCE/PbNPs	DPAdSV	0,075 mol L^{-1} bufor octanowy (pH = 4,5 ± 0,1) + 7,5 × 10^{-5} mol L^{-1} Pb(II)	od -1,1 do -1,7 V; $E_{acc.}$ = -1,1 V; $t_{acc.}$ = 120 s; ΔE_A = 150 mV; ν = 175 mV s^{-1}; t_m = 5 ms	[**RD5**]
4-Cl-PIMT	SPCE/CNFs	SWAdSV	0,025 mol L^{-1} HNO_3	od -0,2 do -1 V; $E_{acc.}$ = 0,1 V; $t_{acc.}$ = 120 s; f = 75 Hz; E_{SW} = 150 mV; ΔE = 7 mV	[**RD6**]
BLM	pSPCE/PbNPs	SWAdSV	0,05 mol L^{-1} bufor octanowy (pH = 4,6 ± 0,1) + 5 × 10^{-5} mol L^{-1} Pb(II) + 1 × 10^{-5} mol L^{-1} DTPA	od -1 do -1,7 V; $E_{acc.}$ = -1 V; $t_{acc.}$ = 120 s; f = 50 Hz; E_{SW} = 50 mV; ΔE = 10 mV	[**RD7**]
NDIT	SPCE/SDS	DPAdSV	0,01 mol L^{-1} HNO_3 + 10 mg L^{-1} SDS	od -0,2 do -1,1 V; t = 45 s; ΔE_A = 175 mV; ν = 150 mV s^{-1};	[**RD8**]

				t_m = 5 ms	
TDZ	SPAuE	DPAdSV	0,1 mol L^{-1} PBS (pH = 2,6 ± 0,1)	od 0 do 1,2 V; $E_{acc.}$ = -0,2 V; $t_{acc.}$ = 60 s; ΔE_A = 100 mV; ν = 75 mV s^{-1}; t_m = 10 ms	[**RD9**]

SPCE/CNFs – sitodrukowana elektroda węglowa modyfikowana nanowłóknami węglowymi; aSPCE/SDS – elektrochemicznie aktywowana sitodrukowana elektroda węglowa modyfikowana dodecylosiarczanem sodu; aSPBDDE – elektrochemicznie aktywowana sitodrukowana elektroda diamentowa domieszkowana borem; pSPCE/PbNPs – elektrochemicznie wstępnie przygotowana sitodrukowana elektroda węglowa modyfikowana nanocząstkami ołowiu; SPCE/SDS – sitodrukowana elektroda węglowa modyfikowana dodecylosiarczanem sodu; SPAuE – sitodrukowana elektroda złota; PBS – buforowana fosforanem sól fizjologiczna; SWV – woltamperometria fali prostokątnej; SWAdSV – adsorpcyjna woltamperometria stripingowa fali prostokątnej; DPAdSV – impulsowo-różnicowa adsorpcyjna woltamperometria stripingowa

Tabela 2. Schematy procedur oznaczania: A) EIMTC [**RD1**], B) PA, DF i TR [**RD2**], C) RIF [**RD3**], D) TST [**RD5**], E) 4-Cl-PIMT [**RD6**], F) BLM [**RD7**], G) NDIT [**RD8**], H) TDZ [**RD9**].

Schemat procedury	Praca
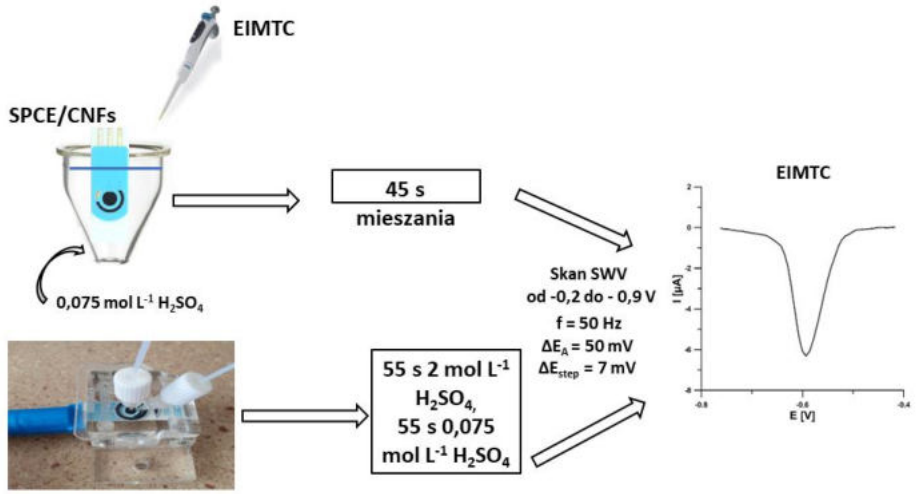	[**RD1**]
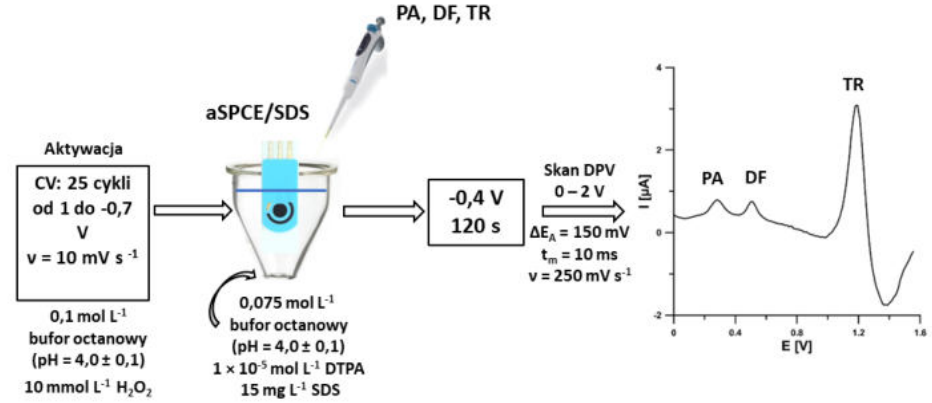	[**RD2**]
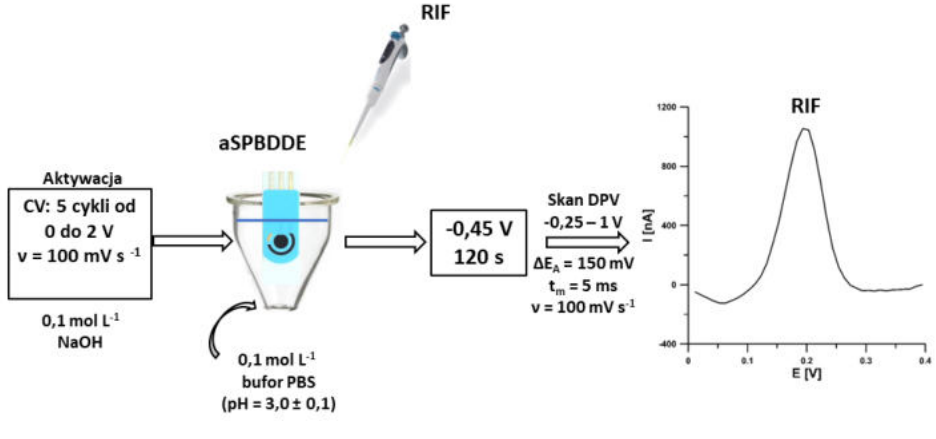	[**RD3**]

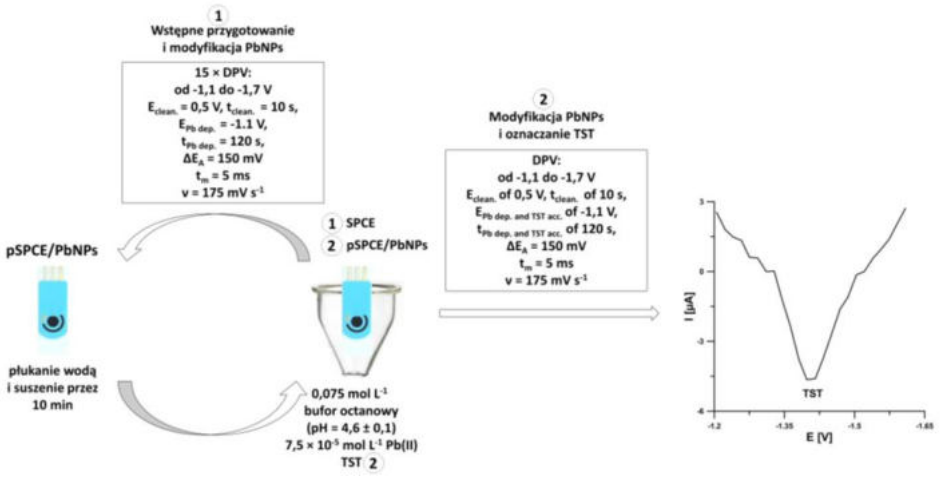
1
Wstępne przygotowanie
i modyfikacja PbNPs
15 × DPV:
od -1,1 do -1,7 V
$E_{clean.}$ = 0,5 V, $t_{clean.}$ = 10 s,
$E_{Pb\ dep.}$ = -1.1 V,
$t_{Pb\ dep.}$ = 120 s,
ΔE_A = 150 mV
t_m = 5 ms
v = 175 mV s^{-1}
pSPCE/PbNPs
płukanie wodą
i suszenie przez
10 min
1 SPCE
2 pSPCE/PbNPs
0,075 mol L^{-1}
bufor octanowy
(pH = 4,6 ± 0,1)
7,5 × 10^{-5} mol L^{-1} Pb(II)
TST 2
2
Modyfikacja PbNPs
i oznaczanie TST
DPV:
od -1,1 do -1,7 V
$E_{clean.}$ of 0,5 V, $t_{clean.}$ of 10 s,
$E_{Pb\ dep.\ and\ TST\ acc.}$ of -1,1 V,
$t_{Pb\ dep.\ and\ TST\ acc.}$ of 120 s,
ΔE_A = 150 mV
t_m = 5 ms
v = 175 mV s^{-1}
I [µA]
TST
E [V]

[**RD5**]

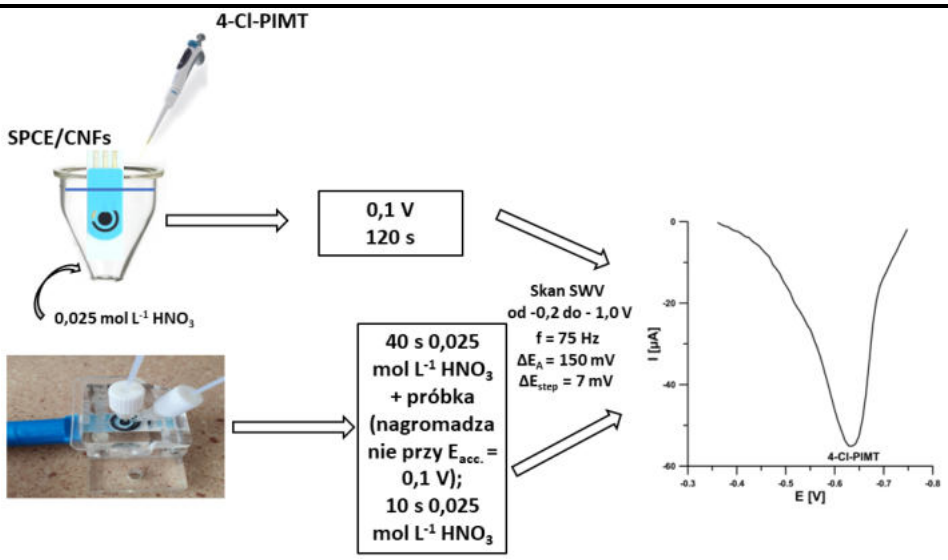
4-Cl-PIMT
SPCE/CNFs
0,025 mol L^{-1} HNO_3
0,1 V
120 s
40 s 0,025
mol L^{-1} HNO_3
+ próbka
(nagromadza
nie przy $E_{acc.}$ =
0,1 V);
10 s 0,025
mol L^{-1} HNO_3
Skan SWV
od -0,2 do - 1,0 V
f = 75 Hz
ΔE_A = 150 mV
ΔE_{step} = 7 mV
I [µA]
4-Cl-PIMT
E [V]

[**RD6**]

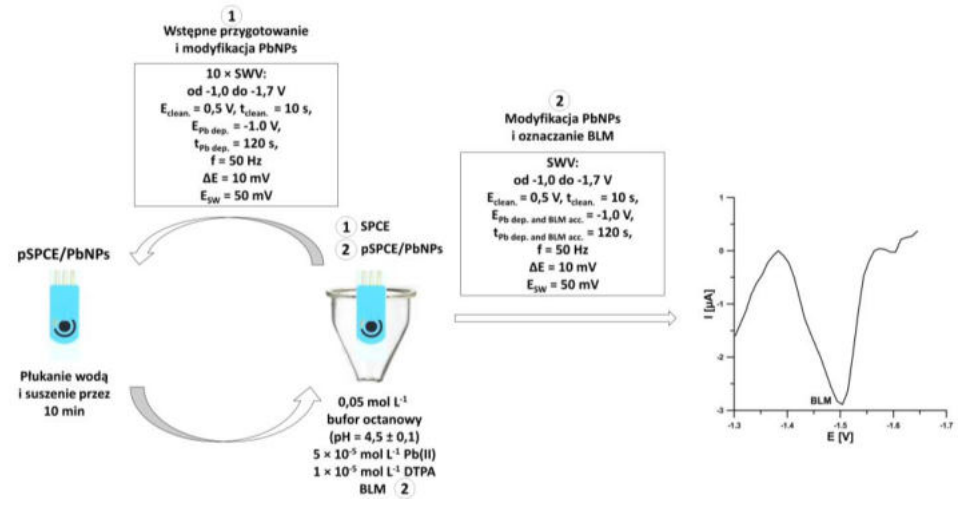
1
Wstępne przygotowanie
i modyfikacja PbNPs
10 × SWV:
od -1,0 do -1,7 V
$E_{clean.}$ = 0,5 V, $t_{clean.}$ = 10 s,
$E_{Pb\ dep.}$ = -1.0 V,
$t_{Pb\ dep.}$ = 120 s,
f = 50 Hz
ΔE = 10 mV
E_{SW} = 50 mV
pSPCE/PbNPs
Płukanie wodą
i suszenie przez
10 min
1 SPCE
2 pSPCE/PbNPs
0,05 mol L^{-1}
bufor octanowy
(pH = 4,5 ± 0,1)
5 × 10^{-5} mol L^{-1} Pb(II)
1 × 10^{-5} mol L^{-1} DTPA
BLM 2
2
Modyfikacja PbNPs
i oznaczanie BLM
SWV:
od -1,0 do -1,7 V
$E_{clean.}$ = 0,5 V, $t_{clean.}$ = 10 s,
$E_{Pb\ dep.\ and\ BLM\ acc.}$ = -1,0 V,
$t_{Pb\ dep.\ and\ BLM\ acc.}$ = 120 s,
f = 50 Hz
ΔE = 10 mV
E_{SW} = 50 mV
I [µA]
BLM
E [V]

[**RD7**]

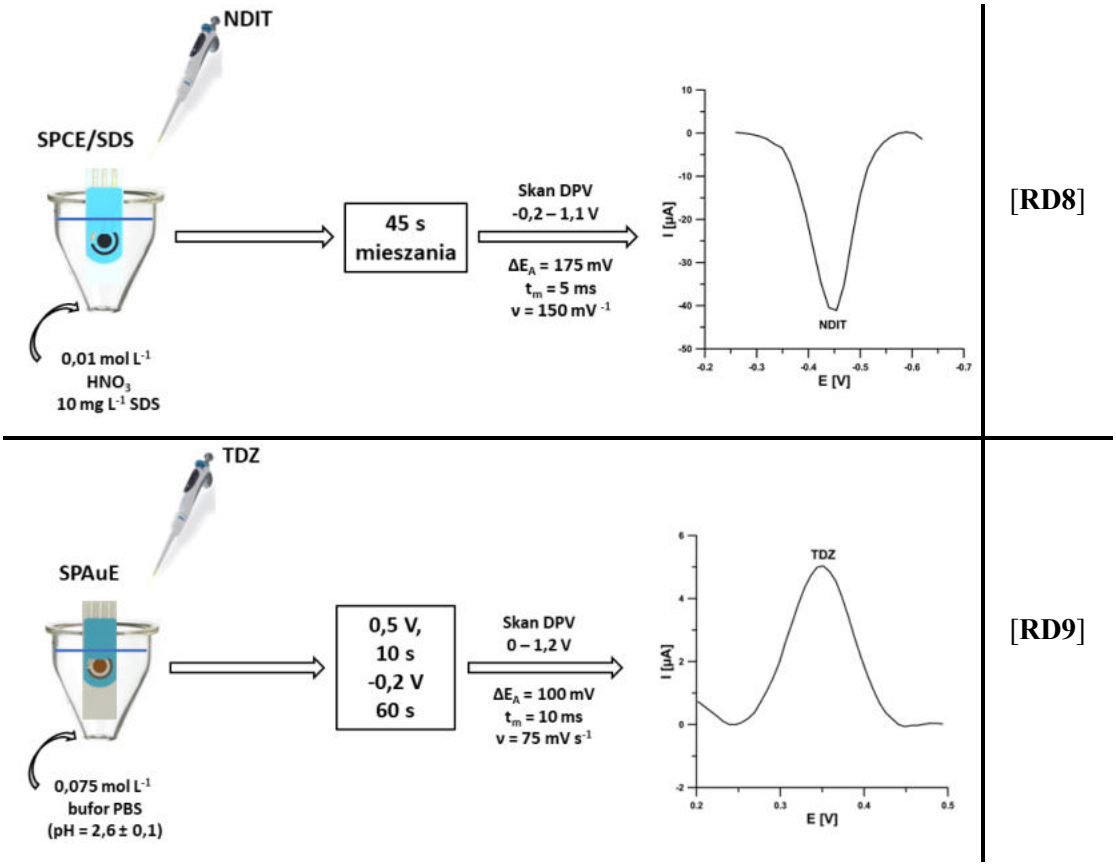

W publikacji przeglądowej [**RD4**] zebrane zostały informacje dotyczące wykorzystania czujników sitodrukowanych w woltamperometrycznej analizie substancji czynnych leków przeciwbólowych (paracetamolu, diklofenaku, tramadolu, ibuprofenu, ketoprofenu, naproksenu i kwasu acetylosalicylowego) w próbkach wód. W pracy zaprezentowano porównanie parametrów analitycznych procedur oznaczania wyżej wymienionych związków. Opisane zostały również różnego rodzaju modyfikacje SPEs i ich wpływ na parametry oraz użyteczność stosowanych czujników.

2.3. Charakterystyka stosowanych czujników sitodrukowanych

W celu wyjaśnienia wpływu modyfikacji i/lub aktywacji elektrod na zmianę ich morfologii oraz parametrów elektrochemicznych, a tym samym na sygnały analityczne badanych związków, wykorzystano szereg technik instrumentalnych. Technikami wykorzystanymi w celu zobrazowania morfologii powierzchni stosowanych elektrod były skaningowa (SEM) i transmisyjna (TEM) mikroskopia elektronowa oraz profilometria optyczna. Metody spektroskopii dyspersji energii promieniowania rentgenowskiego (EDS) i rentgenowskiej spektroskopii

fotoelektronów (XPS) posłużyły do analizy składu pierwiastkowego materiału elektrodowego. Informacji na temat parametrów elektrochemicznych elektrod dostarczyły badania z wykorzystaniem woltamperometrii cyklicznej (CV) i elektrochemicznej spektroskopii impedancyjnej (EIS) wykonane w 0,1 mol L^{-1} roztworze KCl zawierającym 5×10^{-3} mol L^{-1} $K_3[Fe(CN)_6]$. Dzięki EIS możliwe było zmierzenie oporu przenoszenia ładunku (R_{ct}) dla każdej ze stosowanych elektrod. W celu obliczenia powierzchni aktywnych (A_S) elektrod pracujących rejestrowano woltamperogramy cykliczne w szerokim zakresie szybkości rejestracji sygnału (ν). Obliczeń A_S dokonano w oparciu o zależności natężenia prądu piku utleniania Fe(II) (I_p) od pierwiastka kwadratowego z ν ($\nu^{1/2}$) i równania Randlesa-Ševčíka [70]. Dodatkowo na podstawie uzyskanych woltamperogramów cyklicznych obliczono wartości względnego rozdzielenia pików (χ^0) utleniania i redukcji dla układu redoks Fe^{2+}/Fe^{3+}. Wartości te informują o efektywności przenoszenia elektronów pomiędzy elektrodą pracującą a cząsteczkami analitu obecnymi w roztworze, im wartość bliższa teoretycznej (jedności), tym efektywniej zachodzi przenoszenie elektronów.

Rejestracja krzywych pojemności różniczkowej warstwy podwójnej na granicy faz elektroda-elektrolit podstawowy w obecności wysokich stężeń surfaktantu i/lub analitów pozwoliła zbadać adsorpcję tychże związków na powierzchni stosowanych elektrod pracujących.

2.3.1. Czujniki z elektrodą pracującą modyfikowaną nanomateriałem węglowym

W publikacjach [**RD1**] i [**RD6**] oznaczenia związków o właściwościach przeciwnowotworowych prowadzono przy użyciu sitodrukowanej elektrody węglowej modyfikowanej nanowłóknami węglowymi (SPCE/CNFs). Modyfikacja SPCE nanowłóknami węglowymi skutkowała 2-krotnym wzrostem sygnałów analitycznych EIMTC (Rys. 10A) i 10-krotnym w przypadku 4-Cl-PIMT (Rys. 10B), w porównaniu z sygnałami uzyskanymi na elektrodzie niemodyfikowanej, co jest wynikiem wzrostu powierzchni aktywnej elektrody pracującej (0,061 vs. 0,081 cm^2) [28]. Powierzchnie SPCE i SPCE/CNFs zobrazowano przy pomocy SEM (Rys, 10C i 10D). Uzyskane obrazy pozwoliły zaobserwować różnice w morfologii powierzchni SPCE niemodyfikowanej i SPCE pokrytej warstwą nanowłókien węglowych. Badania EIS pokazały, że obecność CNFs na powierzchni SPCE przyczynia się do znacznego spadku oporu przenoszenia ładunku (R_{ct}) (197,3 vs.

63,5 Ω cm^2) (Rys. 10E). Podjęto również próby wykorzystania elektrod modyfikowanych innymi materiałami węglowymi (wielościennymi nanorurkami węglowymi – MWCNTs oraz grafenem), jednak modyfikacje te nie przyniosły oczekiwanych rezultatów.

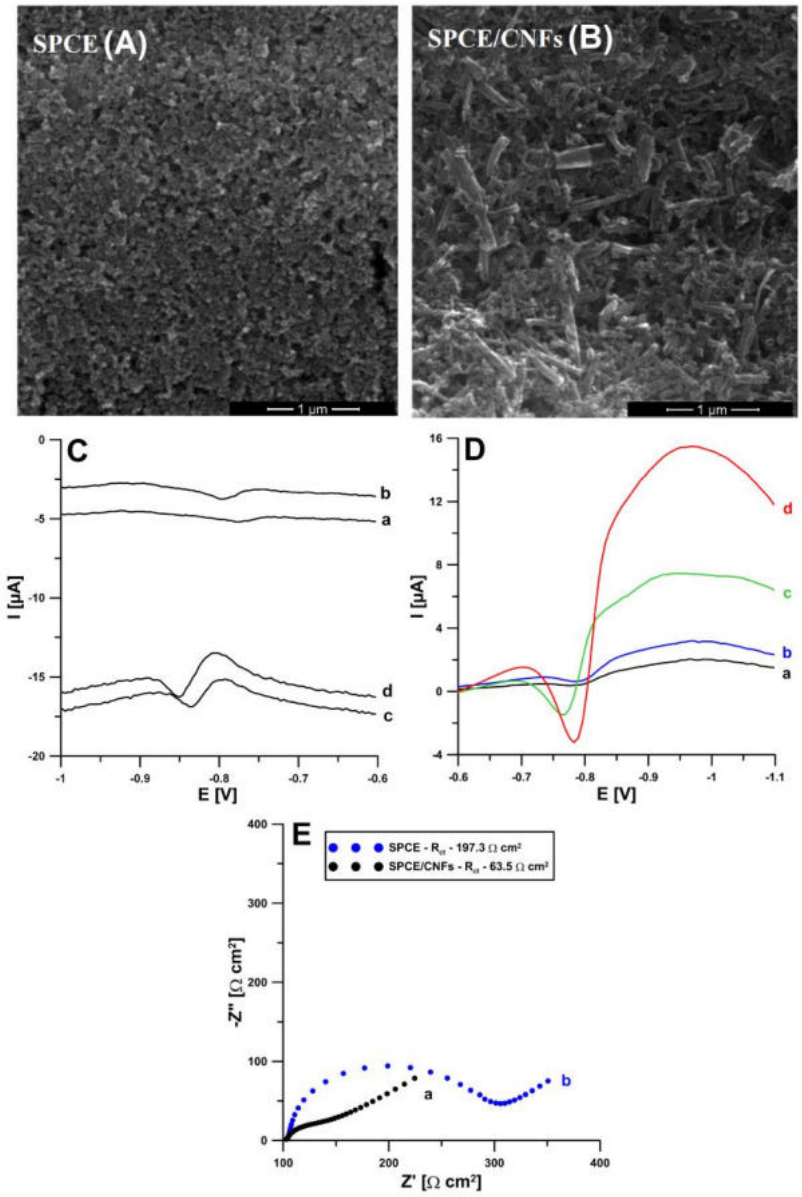

Rys. 10. Obrazy SEM powierzchni: A) SPCE i B) SPCE/CNFs [**RD1**]. C) Woltamperogramy zarejestrowane podczas oznaczania 5×10^{-7} mol L^{-1} (a i c) oraz 1×10^{-6} mol L^{-1} (b i d) EIMTC na SPCE (a i b) i SPCE/CNFs (c i d) [**RD1**]. D) Woltamperogramy zarejestrowane podczas oznaczania 5×10^{-8} mol L^{-1} (a i c) oraz 1×10^{-7} mol L^{-1} (b i d) 4-Cl-PIMT na SPCE (a i b) i SPCE/CNFs (c i d). E) Widma EIS SPCE/CNFs (a) i SPCE (b) [**RD6**].

2.3.2. Czujniki o aktywowanej powierzchni elektrody pracującej

Tusze wykorzystywane do produkcji elektrod sitodrukowanych oprócz głównego składnika przewodzącego zawierają również różnego rodzaju organiczne rozpuszczalniki i pasty wiążące (np. żywica poliestrowa czy etyloceluloza), których obecność może prowadzić do spowolnienia kinetyki reakcji elektrochemicznych. Wstępne przygotowanie (aktywacja) elektrod ma na celu poprawę ich właściwości elektrochemicznych poprzez usunięcie organicznych składników tuszu lub zanieczyszczeń. Istnieje wiele sposobów wstępnego przygotowania SPEs, w tym aktywacja elektrochemiczna, która polega zwykle na przyłożeniu do elektrody stałego potencjału przez krótki czas lub zmianie potencjału w zakresie ekstremalnych potencjałów anodowych i/lub katodowych z wykorzystaniem woltamperometrii cyklicznej (CV) [71-74]. Wykorzystanie elektrochemicznej aktywacji/wstępnego przygotowania elektrod pracujących stanowiło istotny element badań opisanych w publikacjach [**RD2**, **RD3**, **RD5** i **RD7**].

W pracy [**RD3**] do oznaczania ryfampicyny (RIF) wykorzystano elektrochemicznie aktywowaną sitodrukowaną elektrodę diamentową domieszkowaną borem (aSPBDDE). Aktywację SPBDDE wykonano w roztworze 0,1 mol L^{-1} NaOH rejestrując 5-krotnie woltamperogramy cykliczne w przedziale potencjału 0 – 2 V. Wskutek aktywacji uzyskano 8-krotne wzmocnienie sygnału analitycznego RIF (Rys. 11A). Zarejestrowane widma impedancyjne wykazały, że efektem aktywacji jest znaczny spadek oporu przenoszenia ładunku (R_{ct}) (SPBDDE – 105,4 i aSPBDDE – 286,5 Ω cm^2) (Rys. 11B). Podjęto próby zastosowania aktywacji wykonanej w roztworze 0,1 mol L^{-1} buforu octanowego o pH = 4 zawierającym 10 mmol L^{-1} H_2O_2. Aktywacja ta nie pozwoliła jednak na uzyskanie tak dużego wzmocnienia sygnału jak aktywacja w roztworze NaOH (Rys. 11A).

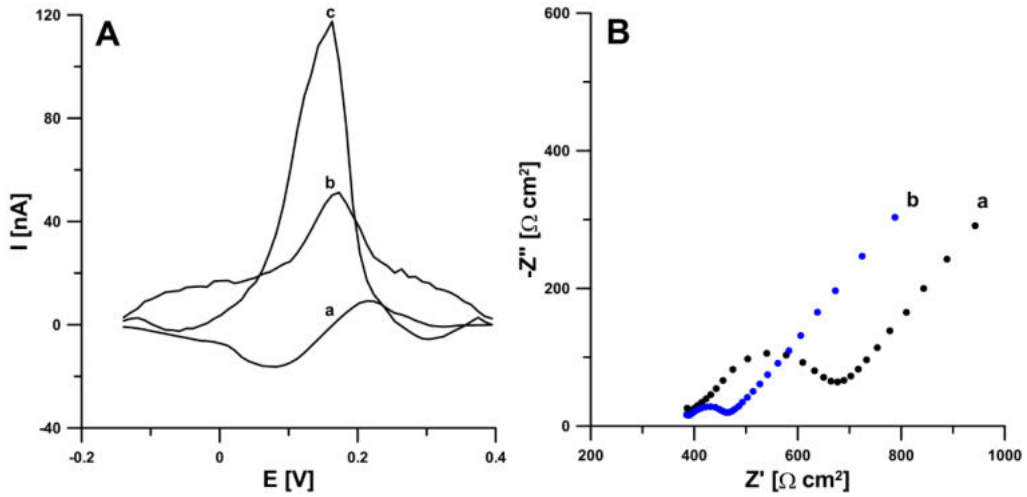

Rys. 11. A) Woltamperogramy zarejestrowane podczas oznaczania 2×10^{-10} mol L^{-1} RIF na SPBDDE nieaktywowanej (a) i SPBDDE aktywowanej w roztworze: buforu octanowego o pH = 4 z dodatkiem 10 mmol L^{-1} H_2O_2 (b) i NaOH (c). B) Widma EIS uzyskane dla SPBDDE (a) i aSPBDDE (aktywowanej w roztworze NaOH) (b) [**RD3**].

Z użyciem CV zbadano jak aktywacja wpływa na A_S elektrody pracującej. W tym celu zarejestrowano woltamperogramy cykliczne w zakresie ν od 50 do 400 mV s^{-1} (Rys. 12A i 12B). Na ich podstawie wykreślono zależność natężenia prądu piku utleniania Fe(II) (I_p) od pierwiastka kwadratowego z szybkości skanowania ($\nu^{1/2}$) (Rys. 12C). Badania pokazały, że elektrochemiczna aktywacja SPBDDE wpływa nieznacznie na wielkość A_S (0,0146 vs. 0,0157 cm^2).

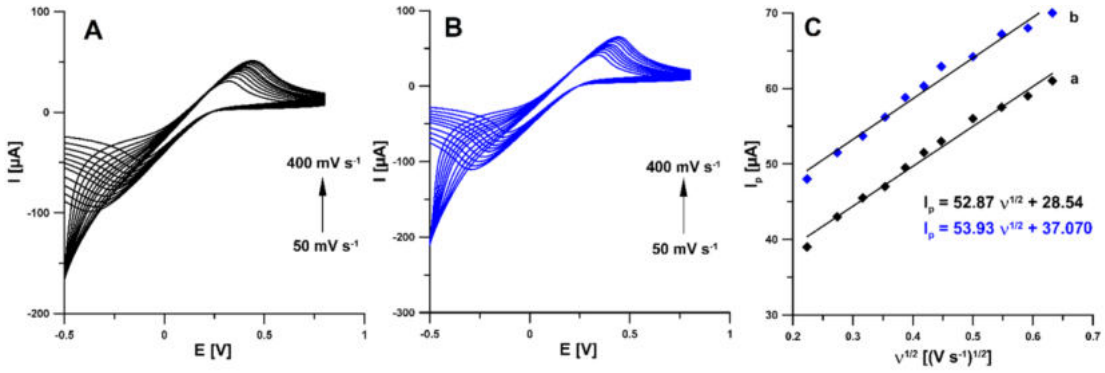

Rys. 12. Woltamperogramy cykliczne zarejestrowane na SPBDDE (A) i aSPBDDE (B). C) Zależność $I_p = f(\nu^{1/2})$ wykreślona dla SPBDDE (a) i aSPBDDE (b) [**RD3**].

Morfologię otrzymanego czujnika scharakteryzowano przy użyciu SEM, a także profilometrii optycznej i porównano z nieaktywowaną SPBDDE. Otrzymane obrazy SEM (Rys. 13A) pozwoliły zauważyć zmiany w powierzchni elektrody pracującej tj. zwiększenie liczby porów, co jest prawdopodobnie związane z częściowym usunięciem organicznego spoiwa wiążącego drobiny materiału tworzącego elektrodę. Ocena zmian strukturalnych powierzchni elektrod przy pomocy profilometrii optycznej wykazała natomiast wzrost chropowatości powierzchni (R_a: 0,451 vs. 0,517 μm) i całkowitej wysokości profilu (R_t: 7,833 vs. 10,627 μm) wskutek aktywacji SPBDDE (Rys. 13B).

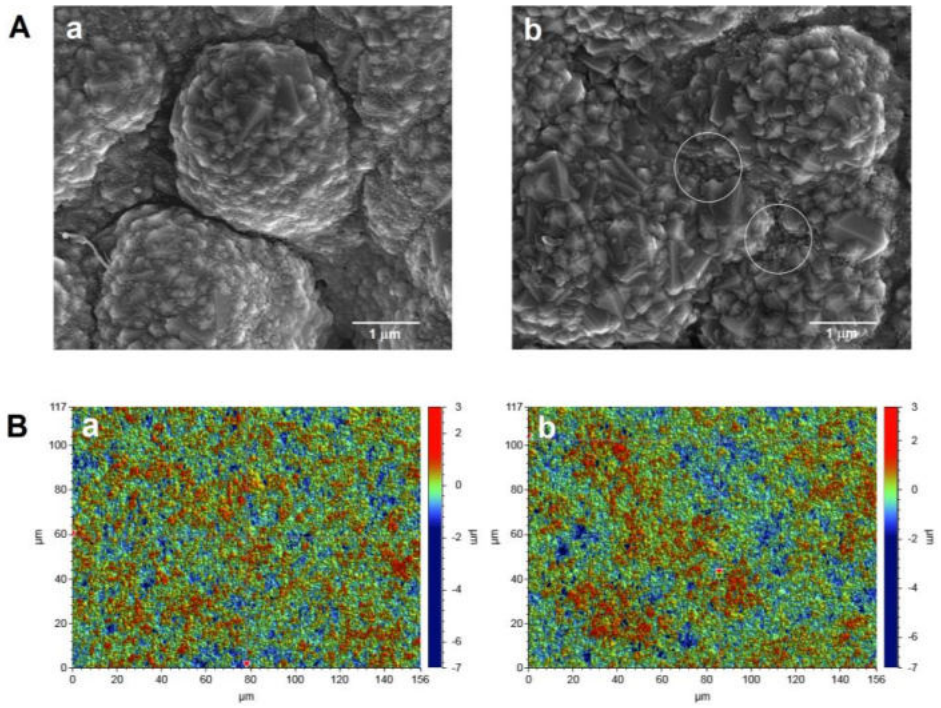

Rys. 13. A) Obrazy SEM i B) profile optyczne SPBDDE (a) i aSPBDDE (b) [**RD3**].

2.3.3. Czujniki z elektrodą pracującą modyfikowaną surfaktantem

W publikacji [**RD2**], w procedurze jednoczesnego oznaczania paracetamolu (PA), diklofenaku (DF) i tramadolu (TR) wykorzystano elektrochemicznie aktywowaną sitodrukowaną elektrodę węglową modyfikowaną dodatkowo surfaktantem anionowym – dodecylosiarczanem sodu (aSPCE/SDS). Czujnik zanurzony był w 0,1 mol L^{-1} buforze octanowym o pH = 4 zawierającym 10 mmol L^{-1} H_2O_2. Aktywacja polegała na wykonaniu 25 skanów CV w zakresie potencjałów od 1 do -0,7 V (ν = 10 mV s^{-1}). Aktywacja SPCE pozwoliła uzyskać

wyższy sygnał analityczny TR (2,7 vs. 1,8 μA), przy czym jej wpływ na sygnały PA i DF był znikomy (Rys. 14A). Obrazy SEM powierzchni pokazały wzrost ilości porów w materiale elektrody wskutek aktywacji (Rys. 14B i 14C).

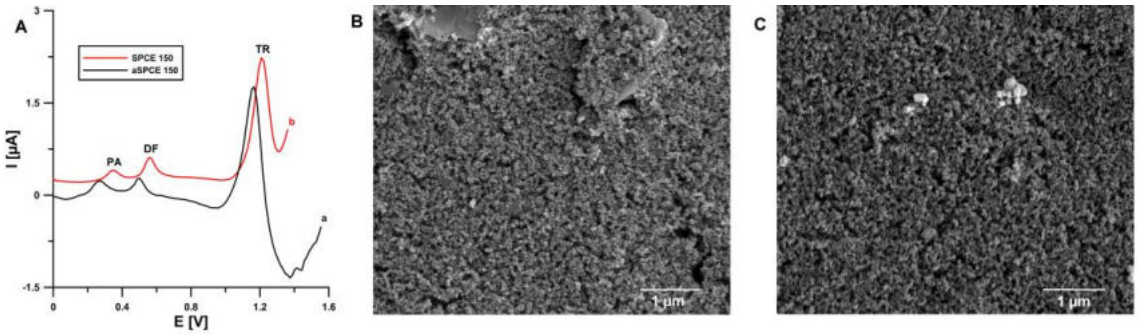

Rys. 14. A) Woltamperogramy zarejestrowane dla 2×10^{-6} mol L^{-1} PA, 1×10^{-7} mol L^{-1} DF i 2×10^{-5} mol L^{-1} TR na aSPCE (a) i SPCE (b). Obrazy SEM powierzchni SPCE (B) i aSPCE (c) [**RD2**].

Elektrochemicznie aktywowana SPCE była dodatkowo modyfikowana SDS. Surfaktant o odpowiednim stężeniu był wprowadzany do roztworu elektrolitu podstawowego. Rejestrując krzywe pojemności różniczkowej warstwy podwójnej na granicy faz elektroda pracująca-elektrolit podstawowy wykazano adsorpcję SDS na powierzchni aSPCE (Rys. 15A). Zaadsorbowany na powierzchni elektrody surfaktant nadaje jej ładunek ujemny, przez co dochodzi do elektrostatycznego przyciągania pomiędzy jonami surfaktantu i analitu występującego w roztworze w postaci kationowej. Dzięki tego rodzaju oddziaływaniom możliwe było uzyskanie znacznego wzmocnienia sygnału analitycznego TR (Rys. 15B). Badania EIS wykazały, że tego rodzaju elektrochemiczna aktywacja również przyczynia się do spadku R_{ct} (388,7 vs. 950,6 Ω cm^2) (Rys. 15C). Zarejestrowane zostały również woltamperogramy cykliczne w zakresie ν od 5 do 500 mV s^{-1}. Na podstawie uzyskanych zależności $Ip = f(v^{1/2})$ (Rys. 15D) i równania Randlesa-Ševčíka obliczono A_S dla SPCE, aSPCE i aSPCE/SDS, które wyniosły odpowiednio 0,056, 0,054 i 0,059 cm^2, co pokazuje, że ani aktywacja, ani modyfikacja SDS-em nie wpływa na wielkość A_S elektrod.

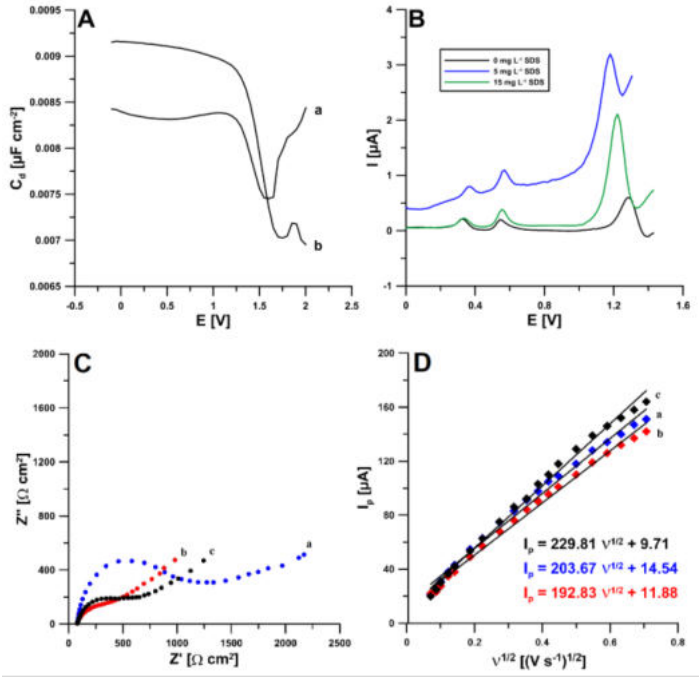

Rys. 15. A) Krzywe pojemności różniczkowej warstwy podwójnej na granic faz aSPCE/bufor octanowy o pH = 4 w obecności: 0 (a) i 15 (b) mg L^{-1} SDS. B) Woltamperogramy zarejestrowane dla 2×10^{-6} mol L^{-1} PA, 1×10^{-7} mol L^{-1} DF i 5×10^{-6} mol L^{-1} TR w obecności 0, 5 i 15 mg L^{-1} SDS. C) Wykresy Nyquista otrzymane dla SPCE (a), aSPCE (b) i aSPCE/SDS (c). D) Zależność Ip = f($\nu^{1/2}$) wykreślona dla: SPCE (a), aSPCE (b) i aSPCE/SDS [**RD2**].

W procedurze oznaczania związku przeciwnowotworowego NDIT [**RD8**] zastosowano SDS jako modyfikator SPCE. Adsorpcję surfaktantu na powierzchni elektrody potwierdzono rejestrując krzywe pojemności różniczkowej (Rys. 16A). Efektem modyfikacji SPCE był blisko 4-krotny przyrost wielkości sygnałów analitycznych NDIT (Rys. 16B). Stężenie SDS poddano optymalizacji by uzyskać jak najwyższe natężenia prądu pików NDIT przy jednoczesnym zachowaniu powtarzalności sygnałów (Rys. 16C). Za optymalne stężenie tego surfaktantu uznano 10 mg L^{-1}. Badania CV wykonane w zakresie ν od 5 do 300 mV s^{-1} pozwoliły zauważyć, że modyfikacja SDS-em powierzchni SPCE skutkuje spadkiem wartości χ^0 z 4,12 dla elektrody niemodyfikowanej do 2,86, co potwierdza, że warstwa zaadsorbowanego SDS przyczynia się do poprawy efektywności przenoszenia elektronów (Rys. 16D). Modyfikacja elektrody SDS-em nie wpłynęła na wielkość A_S (Rys. 16E).

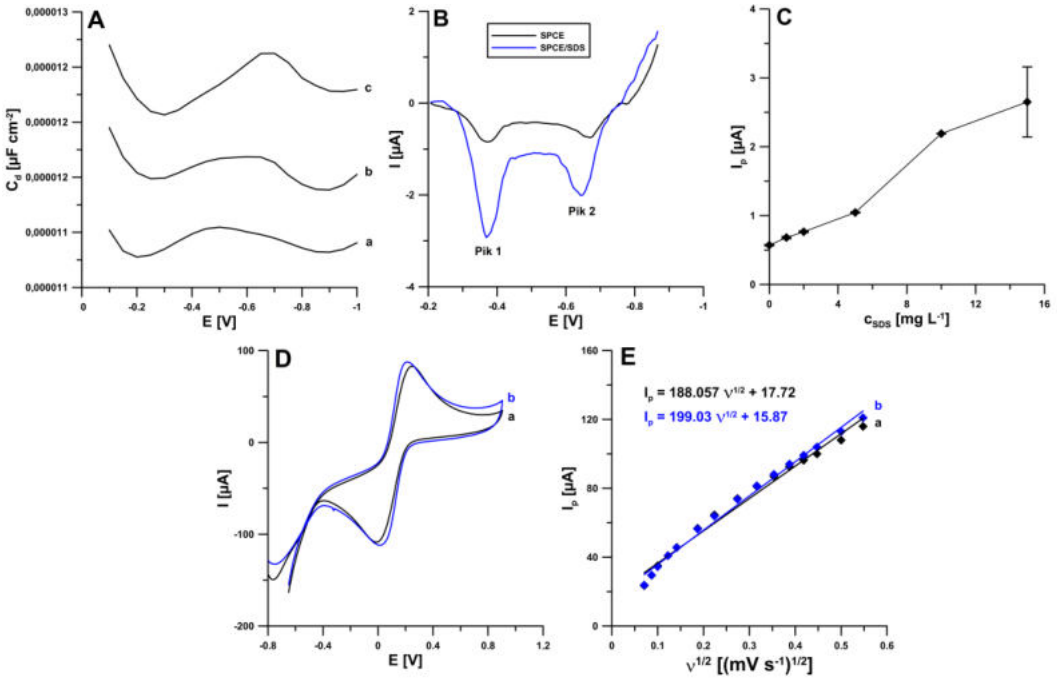

Rys. 16. A) Krzywe pojemności różniczkowej warstwy podwójnej na granic faz SPCE/elektrolit podstawowy w obecności: 0 (a) i 10 (b) i 20 (c) mg L^{-1} SDS. B) Woltamperogramy zarejestrowane dla 5 × 10^{-8} mol L^{-1} NDIT na SPCE (a) i SPCE/SDS (b) (10 mg L^{-1} SDS). C) Wpływ stężenia SDS na sygnał 5 × 10^{-8} mol L^{-1} NDIT. D) Krzywe CV zarejestrowane na SPCE (a) i SPCE/SDS (b) (ν = 150 mV s^{-1}). E) Zależność $I_p = f(\nu^{1/2})$ wykreślona dla: SPCE (a) i SPCE/SDS (b) [**RD8**].

2.3.4. Czujniki z elektrodą pracującą modyfikowaną metalem

W pracach [**RD5**] i [**RD7**] zostały przedstawione procedury oznaczania odpowiednio testosteronu (TST) i bleomycyny (BLM), na poddanej wstępnemu przygotowaniu sitodrukowanej elektrodzie węglowej modyfikowanej osadzanymi *in-situ* nanocząstkami ołowiu (pSPCE/PbNPs). Wstępne przygotowanie elektrod polegało na wykonaniu 15 skanów DPV [**RD5**] lub 10 skanów SWV [**RD7**] w zoptymalizowanych warunkach i w roztworach, w których wykonywano docelowe oznaczenia analitów. Elektrody następnie opłukiwano wodą, suszono i umieszczano ponownie w tych samych roztworach by wykonać oznaczenie analitu. Badania z wykorzystaniem metod CV i EIS wykazały, że wstępne przygotowanie w obu przypadkach nie wpływa na wartości A_S i R_{ct}, powoduje jednak znaczącą poprawę kształtu sygnałów analitycznych, a także ich powtarzalność. Modyfikacja nanocząstkami ołowiu natomiast jest niezbędna do

zaobserwowania sygnałów analitycznych TST i BLM (Rys. 17A i 17B). Informacji na temat prawdopodobnego wyjaśnienia poprawy kształtu i powtarzalności sygnałów dostarczyły badania elektrod z użyciem rentgenowskiej spektroskopii fotoelektronów (XPS). Uzyskane tą metodą widma, a w szczególności poddany dekonwolucji sygnał Pb4f pokazuje, że w przypadku SPCE/PbNPs mamy do czynienia z przewagą tlenków ołowiu nad ołowiem w postaci metalicznej (Rys. 17C), natomiast jeśli chodzi o pSPCE/PbNPs sytuacja jest odwrotna (Rys. 17D). Przewaga metalicznego ołowiu może skutkować lepszą odtwarzalnością osadzania składającej się z nanocząstek błonki ołowiu, co z kolei przekłada się na lepszą powtarzalność i kształt sygnałów analitycznych TST i BLM.

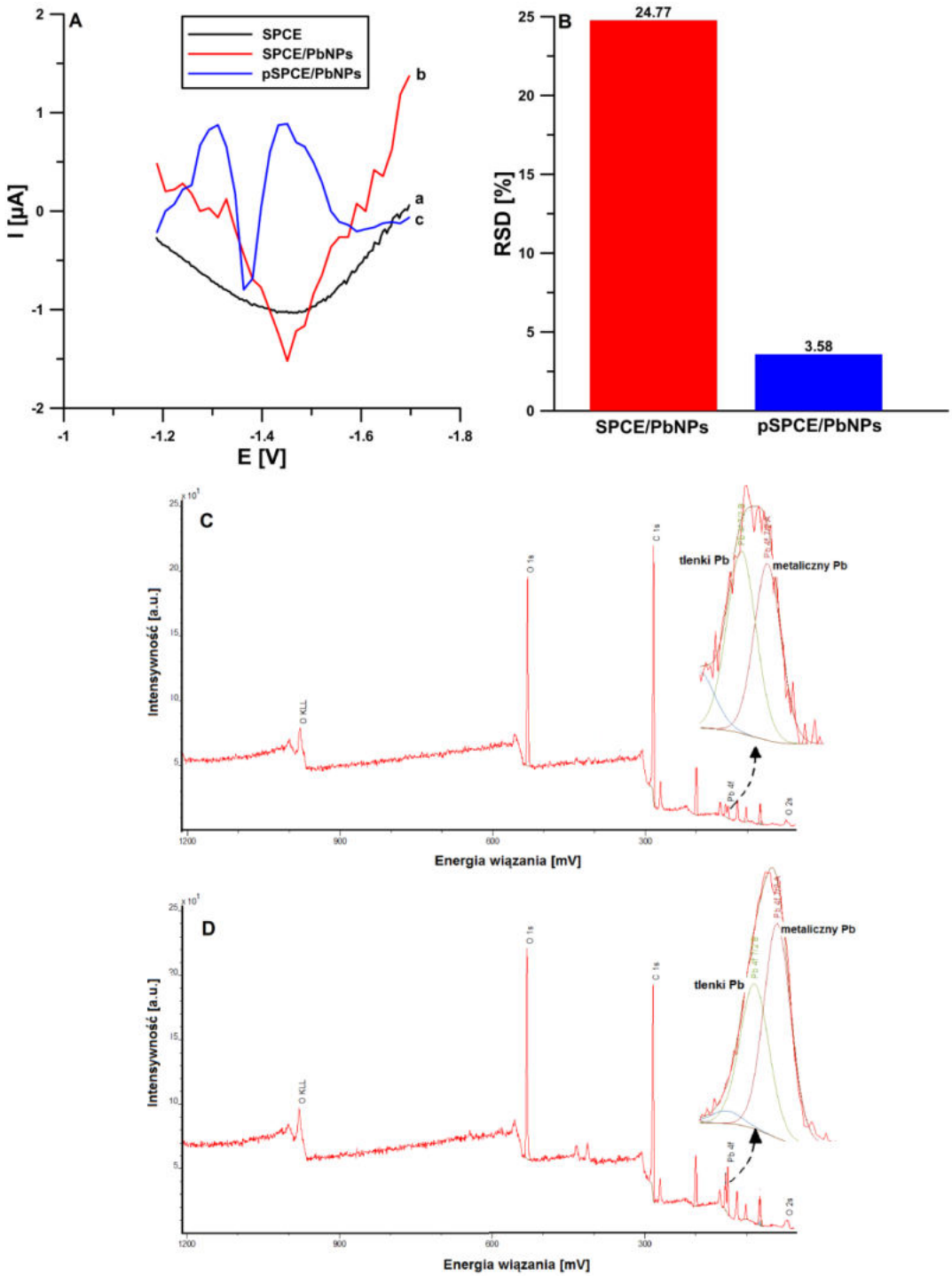

Rys. 17. A) Woltamperogramy uzyskane dla 2×10^{-9} mol L^{-1} TST na SPCE (a), SPCE/PbNPs (b) i pSPCE/PbNPs (c). B) Wykres słupkowy przedstawiający względne odchylenie standardowe (RSD) pomiarów wykonanych dla 2×10^{-9} mol L^{-1} TST (n = 10) [**RD5**]. Widma XPS: SPCE/PbNPs (C) i pSPCE/PbNPs (D) [**RD7**].

Obecność ołowiu w postaci nanocząstek została potwierdzona za pomocą SEM i transmisyjnej mikroskopii elektronowej (TEM) w połączeniu ze spektroskopią dyspersji energii promieniowania rentgenowskiego (EDS) (Rys. 18).

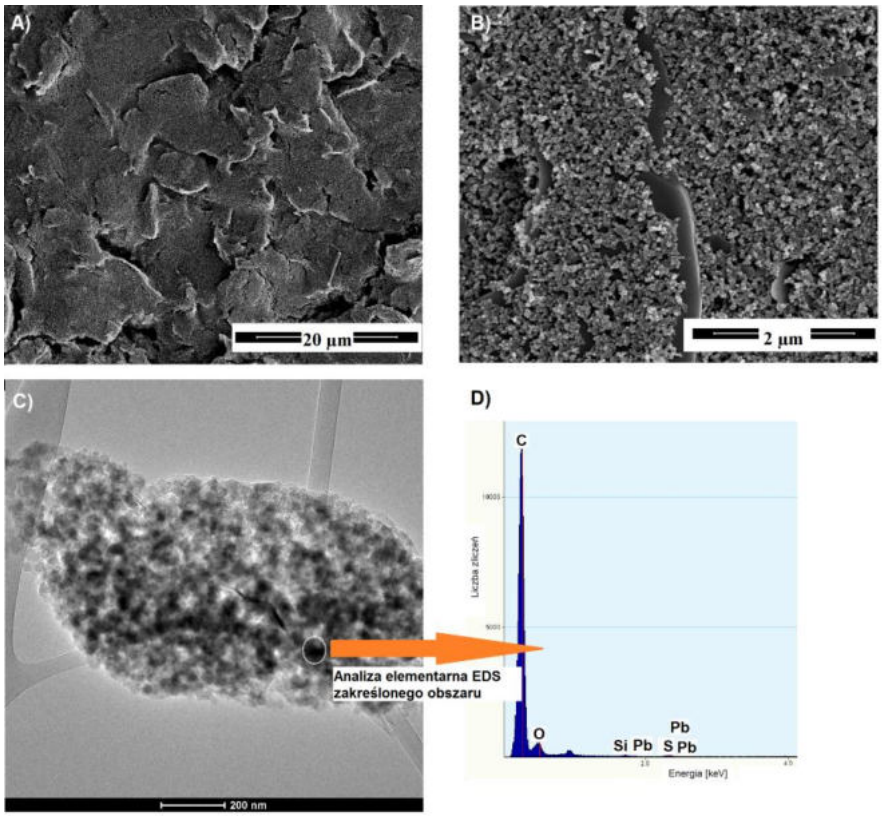

Rys. 18. Obrazy SEM (A i B) i TEM (C) powierzchni pSPCE/PbNPs. D) Widmo EDS zaznaczonego fragmentu pSPCE/PbNPs [**RD5**].

Stosując EIS i CV (Rys. 19) wykazano, że modyfikacja nanocząstkami ołowiu powoduje spadek R_{ct} (121,3 vs. 146,7 Ω cm^2), a przede wszystkim znaczące zwiększenie A_S elektrody pracującej (0,072 cm^2 dla SPCE i 0,22 cm^2 dla pSPCE/PbNPs), co znajduje odzwierciedlenie we wzroście sygnałów analitycznych zarówno TST, jak i BLM.

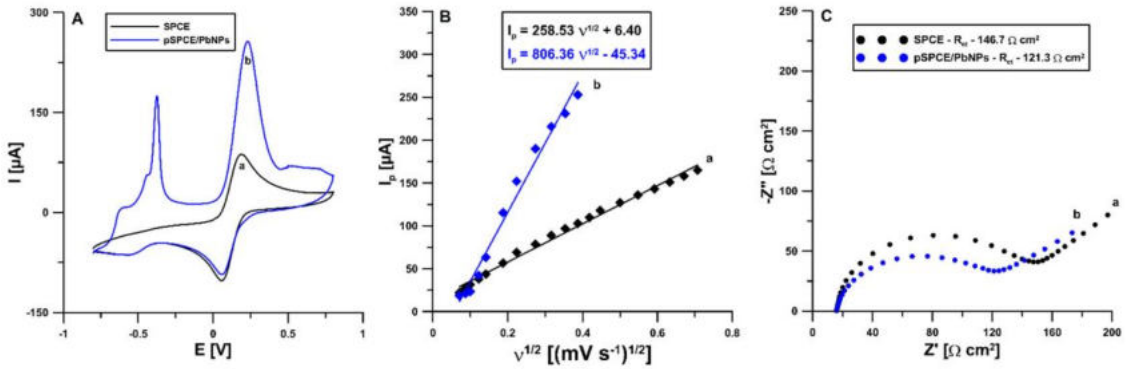

Rys. 19. A) Krzywe CV zarejestrowane na SPCE (a) i pSPCE/PbNPs (b) dla ν = 100 mV s^{-1}. B) Zależność $I_p = f(\nu^{1/2})$ wykreślona dla: SPCE (a) i pSPCE/PbNPs (b) (ν od 5 do 150 mV s^{-1}). C) Widma EIS SPCE (a) i pSPCE/PbNPs (b) [**RD5**].

W publikacji [**RD9**] opisana została woltamperometryczna procedura oznaczania tiorydazyny (TDZ) na handlowo dostępnej sitodrukowanej elektrodzie złotej (SPAuE). Odpowiedź SPAuE na obecność analitu porównano z odpowiedzią SPCE i SPCE modyfikowanej elektrochemicznie błonką złota (SPCE/AuF). Błonka złota osadzana była na powierzchni SPCE metodą *ex-situ* z roztworu 0,2 mol L^{-1} H_2SO_4 zawierającego 2 × 10^{-4} mol L^{-1} $HAuCl_4$, przykładając potencjał -0,2 V przez 90 s. Na wszystkich trzech elektrodach zarejestrowano woltamperogramy dla czterech wzrastających stężeń TDZ (1 × 10^{-9}, 2 × 10^{-9}, 5 × 10^{-9} i 1 × 10^{-8} mol L^{-1}). Uzyskane krzywe pozwoliły zauważyć, że modyfikacja SPCE błonką złota skutkuje znaczącym wzmocnieniem sygnału (Rys. 20B) względem niemodyfikowanej SPCE (Rys. 20A). Najwyższe I_p TDZ otrzymano jednak stosując SPAuE (Rys. 20C). Na podstawie wykonanych pomiarów wykreślono zależności I_p od stężenia TDZ, dzięki czemu możliwe było obliczenie czułości każdej z elektrod. Najwyższą czułością wynoszącą 0,15 µmol nA^{-1} charakteryzuje się SPAuE (Rys. 20F), a SPCE/AuF nieznacznie niższą (0,11 µmol nA^{-1}) (Rys. 20E). Wśród porównywanych elektrod najniższą czułość wykazała SPCE (0,012 µmol nA^{-1}) (Rys. 20D), około 10-krotnie niższą niż SPCE/AuF i SPAuE. Ogromny wzrost czułości elektrod złotej i modyfikowanej złotem wynika najprawdopodobniej z silnego powinowactwa siarki do złota. Atomy siarki, zwłaszcza w grupach tiolowych, adsorbują się na powierzchni złota, tworząc silne wiązania kowalencyjne [75-77]. TDZ posiadająca dwa atomy siarki w cząsteczce, w tym jeden w grupie

tiometylowej, najprawdopodobniej ulega silnej adsorpcji na powierzchni elektrod złotych.

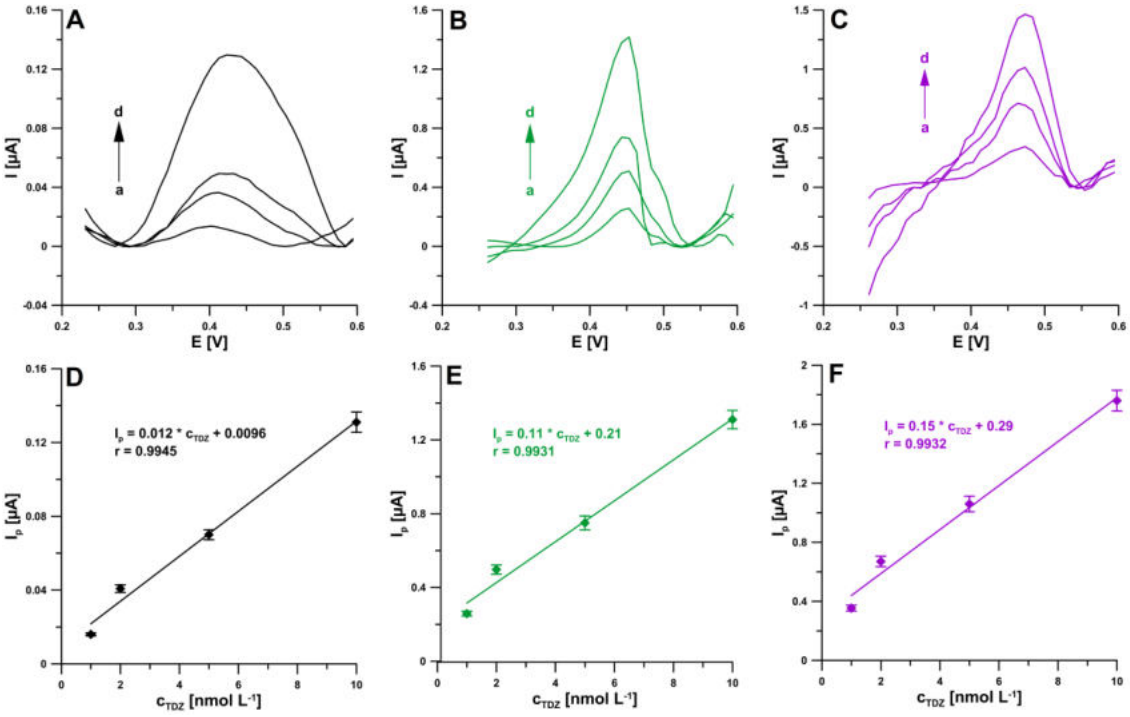

Rys. 20. Woltamperogramy uzyskane podczas oznaczania 1×10^{-9} (a), 2×10^{-9} (b), 5×10^{-9} (c) i 1×10^{-8} (d) mol L^{-1} TDZ na SPCE (A), SPCE/AuF (B) i SPAuE (C). Zależności liniowe pomiędzy I_p i stężeniem TDZ (1×10^{-9} – 1×10^{-8} mol L^{-1}) uzyskane na SPCE (D), SPCE/AuF (E) i SPAuE (F) [**RD9**].

Wszystkie trzy elektrody scharakteryzowano wykorzystując metody EIS i CV. Rysunek 21A przedstawia krzywe CV zarejestrowane na SPCE, SPCE/AuF i SPAuE przy ν = 100 mV s^{-1}. Zarówno na SPCE/AuF, jak i SPAuE uzyskano wzmocnienie sygnału utleniania Fe(II) do Fe(III) (107 µA dla SPCE/AuF i 112 µA dla SPAuE) względem SPCE (81,1 µA). Dla każdej z elektrod obliczono χ^0 i wartość najbliższą wartości teoretycznej (χ^0 = 1) uzyskano dla SPAuE, co świadczy o najefektywniejszym przenoszeniu elektronów spośród badanych elektrod. Dodatkowo, w oparciu o wykonane pomiary CV (5-300 mV s^{-1}) oraz zależność $I_p = f(\nu^{1/2})$ (Rys. 21B) i równania Randlesa-Sevcika obliczono A_S elektrod. Badania EIS wykazały, że modyfikacja SPCE błonką złota powoduje znaczne obniżenie R_{ct}. Najniższą wartość R_{ct} w porównaniu z pozostałymi elektrodami uzyskano dla SPAuE (Rys. 21C). W tabeli 3 zestawiono wszystkie wymienione parametry, których analiza pozwala jednoznacznie

stwierdzić, że ze względu na efektywność przenoszenia elektronów, wysoką czułość oraz dużą powierzchnię aktywną, SPAuE posiada najlepsze właściwości spośród testowanych czujników.

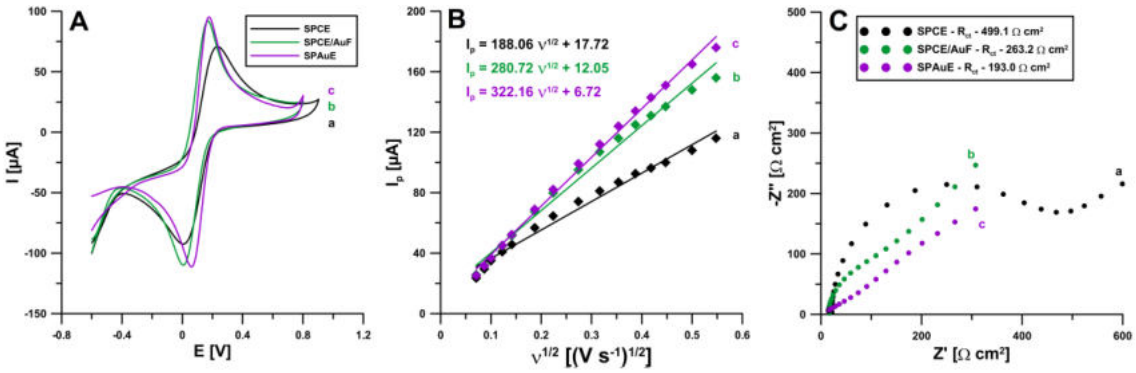

Rys. 21. A) Krzywe CV zarejestrowane na SPCE (a), SPCE/AuF (b) i SPAuE (c) dla ν = 100 mV s^{-1}. B) Zależność $I_p = f(\nu^{1/2})$ wykreślona dla: SPCE (a), SPCE/AuF (b) i SPAuE (c) (ν od 5 do 300 mV s^{-1}). C) Widma EIS SPCE (a), SPCE/AuF (b) i SPAuE (c) [**RD9**].

Tabela 3. Charakterystyka elektrochemiczna SPCE, SPCE/AuF i SPAuE wykonana z wykorzystaniem metod CV i EIS [**RD9**].

Elektroda	**As [cm^2]**	**R_{ct} [Ω cm^2]**	**χ^0 (ν = 100 mV s^{-1})**	**Czułość [µM nA^{-1}]**
SPCE	0,052	499,1	3,45	0,012
SPCE/AuF	0,078	263,2	2,68	0,11
SPAuE	0,089	193,0	1,90	0,15

Morfologię powierzchni i skład pierwiastkowy wszystkich trzech elektrod zbadano za pomocą SEM-EDS (Rys. 22). Wykazano, że w przypadku SPCE/AuF błonka złota składa się z nanocząstek o średnicy ekwiwalentnej w zakresie od 44,59 do 88,86 nm. SPAuE natomiast składa się z cząstek i aglomeratów złota o wielkości od 143,93 do 2100,23 nm.

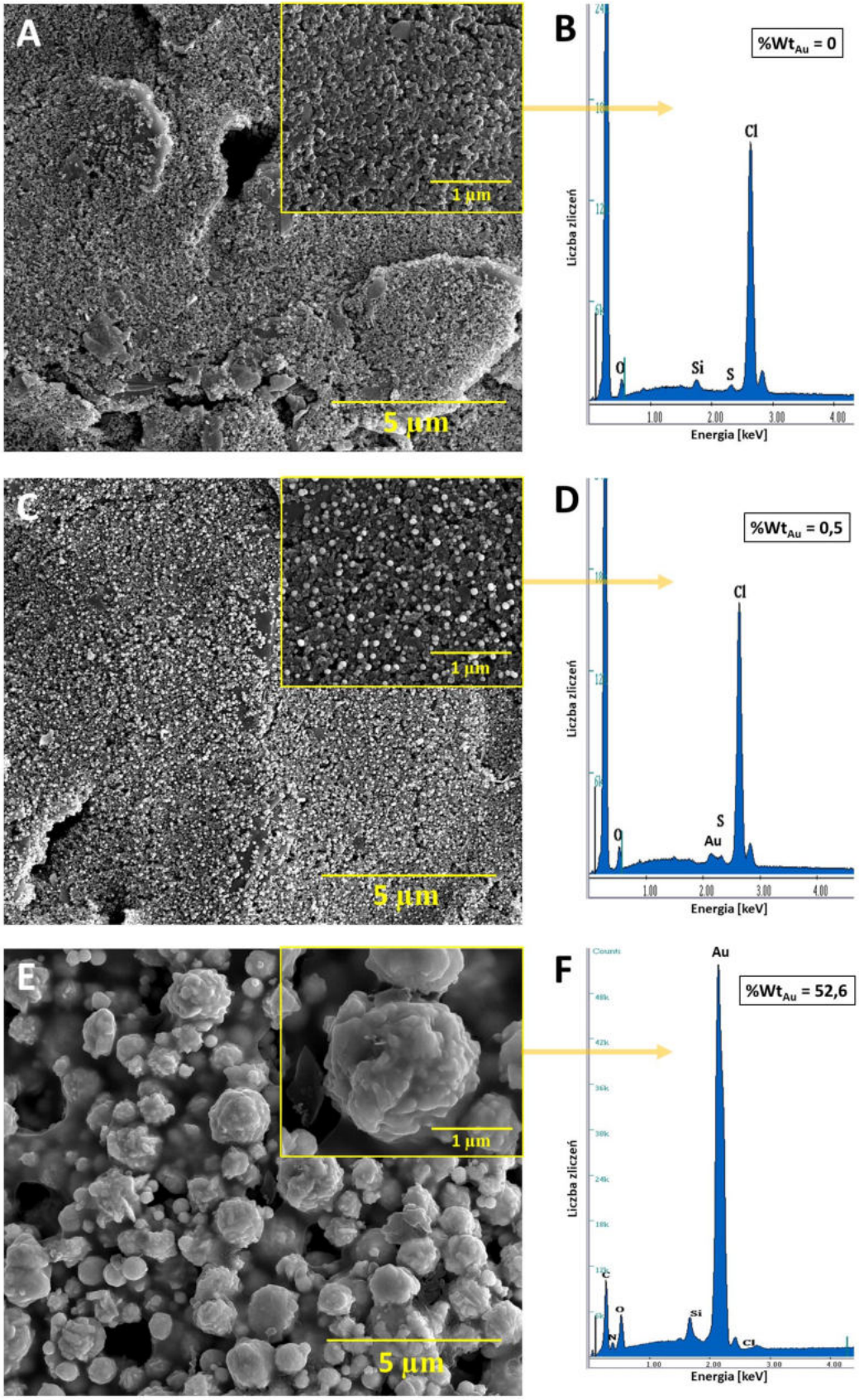

Rys. 22. Obrazy SEM SPCE (A), SPCE/AuF (C) i SPAuE (E). Widma EDS SPCE (B), SPCE/AuF (D) i SPAuE (F).

2.4. Badanie charakteru procesów elektrodowych

Charakter procesów utleniania lub redukcji badanych substancji zbadano z użyciem metody CV. Na podstawie uzyskanych woltamperogramów cyklicznych wykreślono zależności natężenia prądu piku analitu (I_p) w funkcji pierwiastka kwadratowego z szybkości skanowania ($\nu^{1/2}$), której liniowy przebieg wskazuje na transport substancji od/do powierzchni elektrody na drodze dyfuzji. W przypadku gdy zależność ta jest nieliniowa mamy do czynienia z adsorpcją analitu na powierzchni elektrody. Potwierdzenie dyfuzyjnego bądź adsorpcyjnego charakteru procesu elektrodowego stanowi również zależność pomiędzy logarytmem natężenia prądu piku ($\log I_p$) a logarytmem z szybkości skanowania ($\log\nu$). Wartość współczynnika nachylenia prostej regresji bliska 0,5 potwierdza dyfuzję, a wartość bliska 1 wskazuje na adsorpcję badanej substancji. W przypadku gdy współczynnik przyjmuje wartości pośrednie np. 0,7, nie jest możliwe jednoznaczne określenie, czy proces jest kontrolowany w pełni adsorpcyjnie, czy dyfuzyjnie. Charakter procesu można wówczas określić mianem mieszanego [78].

W tabeli 4 podsumowano szczegółowe parametry zależności uzyskanych na podstawie badań CV wykonanych dla badanych substancji, a wybrane woltamperogramy cykliczne i wykreślone zależności przedstawione zostały na rysunkach 23 i 24.

Tabela 4. Zestawienie wyników badań CV procesów elektrodowych [**RD1**, **RD3, RD5-RD9]**, .

Analit	**Zakres ν [mV s^{-1}]**	**$I_p = f(\nu^{1/2})$**	**log Ip = f(log ν)**	**Charakter procesu elektrodowego**	**Praca**
EIMTC	20 – 500	$I_p = 3{,}61 * \nu^{1/2} + 1{,}91$ r = 0,9868	$\log I_p = 0{,}49 * \log\nu + 0{,}61$ r = 0,9918	Dyfuzja	[**RD1**]
RIF	15 – 500	$I_p = 0{,}082 * \nu^{1/2} – 0{,}29$ r = 0,9959	$\log I_p = 0{,}77 * \log\nu – 1{,}86$ r = 0,9994	Proces mieszany	[**RD3**]
TST	5 – 250	Nieliniowa	-	Adsorpcja	[**RD5**]
4-Cl-PIMT	20 – 450	Nieliniowa	$\log I_p = 1{,}011 * \log\nu – 0{,}16$ r = 0,9586	Adsorpcja	[**RD6**]

BLM	5 – 200	$I_p = 0,3 * \nu^{1/2} – 0,57$ r = 0,9979	log I_p = 0,81 * log ν – 1,24	Proces mieszany	[**RD7**]
NDIT	5 – 300	Pik 1: $I_p = 3,24 * \nu^{1/2} – 5,35$ r = 0,9944 Pik 2: $I_p = 4,91 * \nu^{1/2} – 5,8$ r = 0,9984	Pik 1: log I_p = 0,68 * log ν + 0,042 r = 0,9940 Pik 2: log I_p = 0,65 * log ν + 0,33 r = 0,9955	Proces mieszany	[**RD8**]
TDZ	5 – 400	Nieliniowa	log I_p = 1,01 * log ν – 2,22 r = 0,9954	Adsorpcja	[**RD9**]

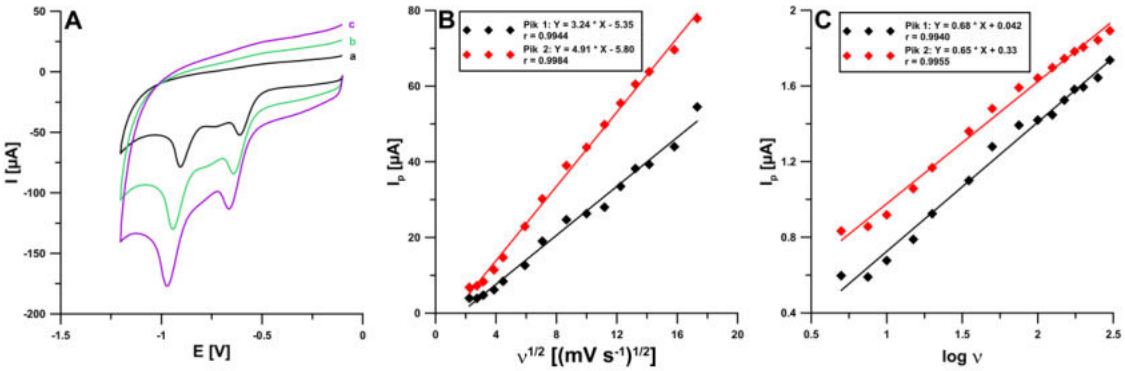

Rys. 23. A) Woltamperogramy cykliczne zarejestrowane dla 1 × 10^{-5} mol L^{-1} NDIT przy ν 50 (a), 100 (b) i 150 mV s^{-1} (c). B) Zależności $I_p = f(\nu^{1/2})$. C) Zależności log I_p = f(log ν) [**RD8**].

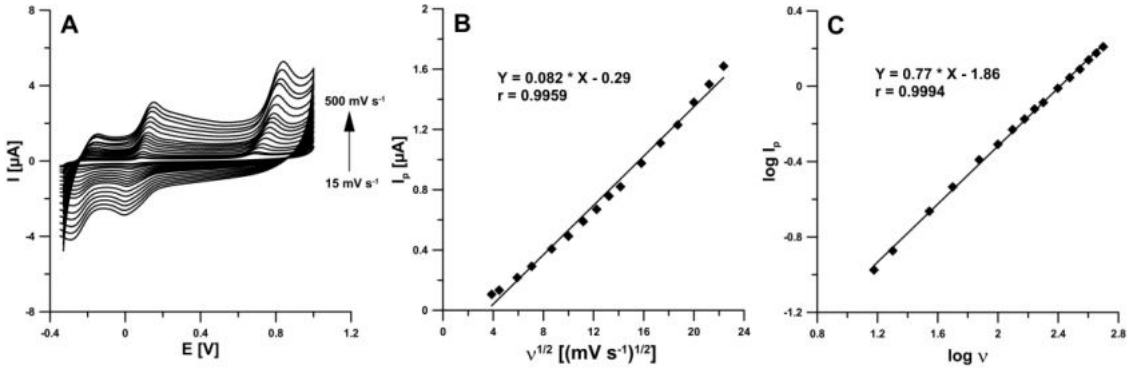

Rys. 24. A) Woltamperogramy cykliczne zarejestrowane dla 5×10^{-6} mol L^{-1} RIF przy ν od 15 do 500 mV s^{-1} (c). B) Zależność $I_p = f(\nu^{1/2})$. C) Zależność log I_p = f(log ν) [**RD3**].

W publikacji **RD2** charakter procesu elektrodowego określono w oparciu o krzywe pojemności różniczkowej warstwy podwójnej na granicy faz elektroda pracująca/elektrolit podstawowy (Rys. 25). Zarówno w obecności PA, jak i DF na zarejestrowanych krzywych zaobserwowano pojawienie się pików desorpcji tych związków, co potwierdza, że ulegają one adsorpcji na powierzchni elektrody. W przypadku TR brak pików desorpcji na krzywych świadczy iż kationy TR docierają do powierzchni elektrody na drodze dyfuzji, a następnie przyciągane są przez ujemnie naładowane „głowy" SDS.

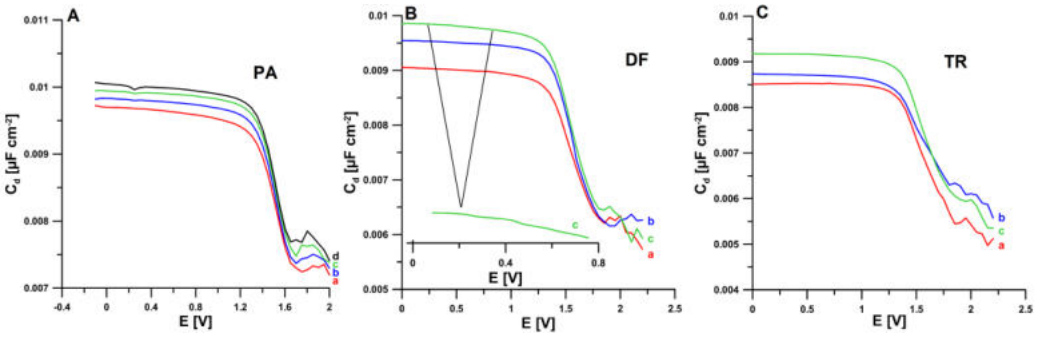

Rys. 25. Krzywe pojemności różniczkowej warstwy podwójnej na granicy faz aSPCE/bufor octanowy o pH = 4,0 w obecności 15 mg L^{-1} SDS i: A) 2×10^{-7} (a), 2×10^{-6} (b), 2×10^{-5} (c) i 2×10^{-4} mol L^{-1} PA (d). B) 2×10^{-7} (a), 2×10^{-6} (b) i 2×10^{-5} mol L^{-1} DF (c). C) 2×10^{-7} (a), 2×10^{-6} (b) i 2×10^{-5} mol L^{-1} TR (c) [**RD2**].

W pracy **[RD7]** na podstawie wyników badań CV charakter procesu elektrodowy określono jako mieszany, co wskazuje na udział adsorpcji w procesie

elektroredukcji BLM na powierzchni pSPCE/PbNPs. Adsorpcję analitu potwierdzono również rejestrując krzywe pojemności różniczkowej, na których w obecności BLM widoczne były trzy piki desorpcji (Rys. 26).

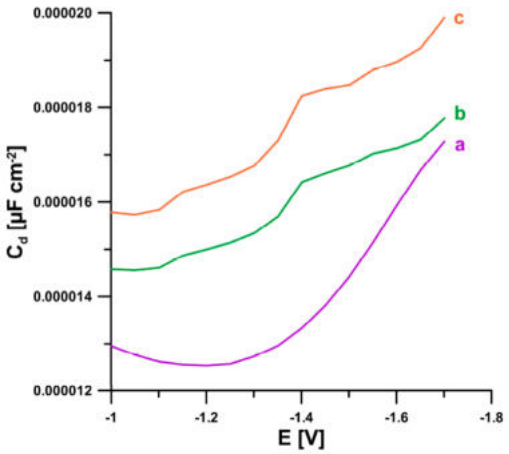

Rys. 26. Krzywe pojemności różniczkowej warstwy podwójnej na granicy faz pSPCE/PbNPs/bufor octanowy (pH = 4,5) w obecności: 0 (a), 2×10^{-6} (b) i 5×10^{-6} mol L^{-1} BLM (c) [**RD7**].

Badania CV dostarczają informacji na temat mechanizmu reakcji elektrodowej. Pozwalają na określenie czy reakcja utleniania bądź redukcji analitu zachodzi jedno- czy wielostopniowo, jaka liczba elektronów i protonów bierze w niej udział oraz czy jest ona odwracalna.

W trakcie badań starano się poznać mechanizm ulteniania bądź redukcji oznaczanych związków. W przypadku części analitów informacje o dobrze poznanych mechanizmach reakcji zaczerpnięto z literatury [**RD3**, **RD5**, **RD8**]. Dodatkowo w pracach **RD1** i **RD6** obliczono liczbę protonów i elektronów biorących udział w reakcjach elektrodowych na podstawie zależności potencjału piku analitu (E_p) w funkcji pH. W pracy [**RD9**] natomiast do wyznaczenia liczby elektronów biorących udział w reakcji utleniania TDZ do formy rodnikokationu posłużono się zależnością E_p w funkcji logv. Ustalono, że reakcja ta zachodzi z udziałem dwóch elektronów (Rys. 27).

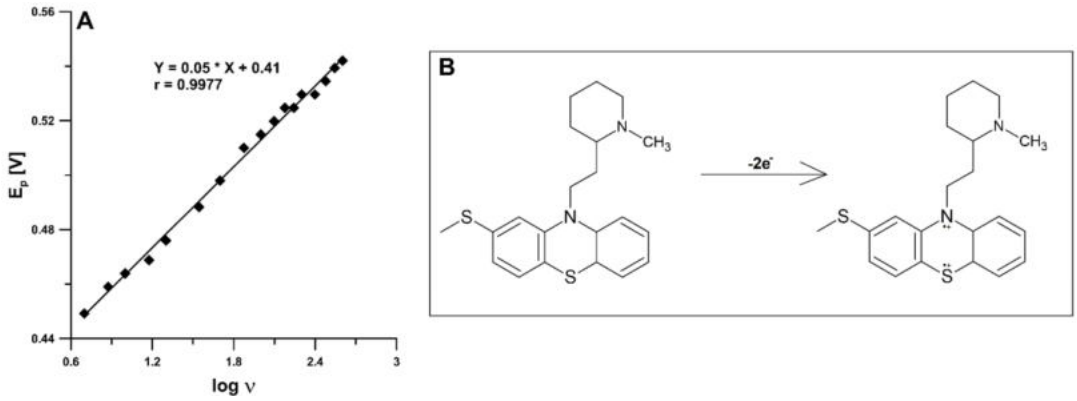

Rys. 27. A) Zależność E_p TDZ vs. logv. B) Mechanizm reakcji utleniania TDZ [**RD9**].

2.5. Parametry analityczne opracowanych procedur i selektywność

W zoptymalizowanych warunkach wykonano pomiary do krzywych kalibracyjnych oznaczanych substancji. Przykładowe woltamperogramy uzyskane dla wzrastających stężeń analitów zostały przedstawione na Rysunku 28. Granice wykrywalności (LOD) i oznaczalności (LOQ) obliczono na podstawie następujących wzorów: LOD = 3 SD_a/b i LOQ = 10 SD_a/b, gdzie „SD_a" to odchylenie standardowe z wyrazu wolnego równania krzywej kalibracyjnej (n = 3), a „b" oznacza średnią wartość współczynnika kierunkowego krzywej kalibracyjnej. W trakcie prowadzonych badań wyznaczono także powtarzalność sygnałów analitycznych badanych substancji, jak również odtwarzalność elektrody do elektrody. Powtarzalność określano obliczając względne odchylenie standardowe (RSD) z dziesięciu pomiarów wykonanych dla określonego stężenia analitu na jednej elektrodzie, natomiast odtwarzalność elektrody do elektrody na podstawie RSD obliczonego dla dziewięciu lub sześciu pomiarów wykonanych na trzech (lub dwóch [**RD2**]) niezależnie przygotowanych elektrodach dla tego samego stężenia analitu.

Dodatkowo, zbadano wpływ potencjalnych interferentów tj. prostych jonów nieorganicznych oraz szeregu związków organicznych, na sygnały analityczne analitów. W przypadku procedur zastosowanych do analizy próbek środowiskowych zbadano wpływ 2 mg L^{-1} surfaktantu niejonowego, Tritonu X-100 na sygnały analitów. Było to podyktowane faktem, iż w środowisku wodnym obecne są związki organiczne o działaniu powierzchniowo czynnym odpowiadającym 0,2 – 2 mg L^{-1} Tritonu X-100 [79]. W procedurze jednoczesnego

oznaczania PA, DF i TR [**RD2**] zbadano również wpływ surfaktantu kationowego (bromku cetylotrimetyloamoniowego, CTAB). Wszystkie wymienione parametry analityczne opracowanych procedur podsumowano w tabeli 5. W jednej z kolumn przestawione zostały nadmiary badanych interferentów względem określonych stężeń analitów, które nie powodują zmian sygnałów większych niż ±10 %. W procedurach, w których zaobserwowano znaczny wpływ obecności jonów metali na sygnały analityczne badanych substancji [**RD2**, **RD7**], do roztworu elektrolitu podstawowego dodawano roztwór soli sodowej kwasu pentetynowego (DTPA) celem skompleksowana przeszkadzających jonów.

Tabela 5. Parametry analityczne procedur oznaczania EIMTC, PA, DF, TR, RIF, TST, 4-Cl-PIMT, BLM, NDIT i TDZ z wykorzystaniem czujników sitodrukowanych [**RD1-RD3, RD5-RD9**].

Analit	**Elektroda**	**Metoda**	**Zakres liniowy krzywej kalibracyjnej [mol L^{-1}]**	**LOD [mol L^{-1}]**	**LOQ [mol L^{-1}]**	**Powtarzalność RSD [%] (n = 10)**	**Odtwarzalność RSD [%] (n = 9)**	**Selektywność**	**Praca**
EIMTC	SPCE/CNFs	SWV	$2 \times 10^{-9} – 2 \times 10^{-8}$ $2 \times 10^{-8} – 2 \times 10^{-7}$	5×10^{-10}	$1{,}7 \times 10^{-9}$	2,9	3,4	Ca(II)-**50x**, (Mg(II), Cl(-I), UA, GLU, ADN, DOP)-**5x**, EPI-**2,5x**, (E2, AA)-**0,5x**	[**RD1**]
PA	aSPCE/SDS	DPAdSV	$5 \times 10^{-8} – 2 \times 10^{-5}$	$1{,}49 \times 10^{-8}$	$4{,}96 \times 10^{-8}$	2,7	2,5 (n = 6)	Pb(II)-**1000x**, Mo(VI)-**200x**, (GLU, Mg(II))-**100x**, Ca(II)-**40x**, Cl(-I)-**20x**, (Cd(II), Fe(III), Ni(II), AA)-**10x**, Cu(II)-**2x**, **2 mg L^{-1}** Triton X-100, **2 mg L^{-1}** CTAB	[**RD2**]
DF			$1 \times 10^{-9} – 2 \times 10^{-7}$	$2{,}1 \times 10^{-10}$	$6{,}9 \times 10^{-10}$	1,2	3,1 (n = 6)	(Cl(-I), GLU)-**2500x**, Pb(II)-**1000x**, (Mg(II), Mo(VI))-**500x**, (Fe(III), Ca(II), AA)-**100x**, (Cu(II), Ni(II))-**25x**, Cd(II)-**10x**, , **2 mg L^{-1}** Triton X-100, **2 mg L^{-1}** CTAB	
TR		DPV	$1 \times 10^{-8} – 2 \times 10^{-7}$ $2 \times 10^{-7} – 2 \times 10^{-6}$	$1{,}71 \times 10^{-9}$	$5{,}69 \times 10^{-9}$	1,8	3,5 (n = 6)	GLU-**2500x**, Pb(II)-**1000x**, Ca(II)-**500x**, Mg(II)-**250x**, Fe(III)-**100x**, Mo(VI)-**50x**, (Cd(II), Ni(II), Cl(-I))-**25x**, Cu(II)-**10x**, AA-**5x**, , **2 mg L^{-1}** Triton X-100, **2 mg L^{-1}** CTAB	
RIF	aSPBDDE	DPAdSV	$2 \times 10^{-12} – 2 \times 10^{-11}$ $2 \times 10^{-11} – 2 \times 10^{-10}$	$2{,}2 \times 10^{-13}$	$7{,}3 \times 10^{-13}$	2,5	5,2	(Mg(II), Ca(II))-**1000x**, EPI-**400x**, AMX-**200x**, (Fe(III),	[**RD3**]

			$2 \times 10^{-10} – 2 \times 10^{-9}$ $2 \times 10^{-9} – 2 \times 10^{-8}$					Cd(II), Cu(II), Pb(II), Ni(II), V(V), DOP, AA, UA, ASA, GLU)-**100x**, **2 mg L^{-1}** Triton X-100	
TST	pSPCE/PbNPs	DPAdSV	$1 \times 10^{-11} – 1 \times 10^{-10}$ $1 \times 10^{-10} – 2 \times 10^{-9}$ $2 \times 10^{-9} – 2 \times 10^{-8}$	$2{,}2 \times 10^{-12}$	$7{,}3 \times 10^{-12}$	3,6	-	Ni(II)-**10000x**, Mg(II)-**5000x**, GLU-**2000x**, (Ca(II), Cu(II), AA, ADN)-**1000x**, DOP-**500x**, (UA, EPI)-**200x**, (Fe(III), V(V))-**100x**	[**RD5**]
4-Cl-PIMT	SPCE/CNFs	SWAdSV	$5 \times 10^{-10} – 1 \times 10^{-8}$ $1 \times 10^{-8} – 1 \times 10^{-7}$	$9{,}9 \times 10^{-11}$	$3{,}3 \times 10^{-10}$	2,2	5,1	GLU-**2000x**, (EPI, AA, UA, Cl(-I))-**1000x**, (Ca(II), ADN)-**200x**, (Mg(II), DOP)-**100x**, Fe(III)-**40x**	[**RD6**]
BLM	pSPCE/PbNPs	SWAdSV	$1 \times 10^{-10} – 2 \times 10^{-9}$ $2 \times 10^{-9} – 2 \times 10^{-8}$	$2{,}8 \times 10^{-11}$	$9{,}3 \times 10^{-11}$	3,3	7,5	EPI-**2500x**, (Mg(II), Ca(II), GLU, DOP, UA, AA)-**1000x**, V(V)-**500x**, Ni(II)-**200x**, (Fe(III), Cd(II), Cu(II), ADN, TST)-**100x**, **2 mg L^{-1}** Triton X-100	[**RD7**]
NDIT	SPCE/SDS	DPAdSV	$1 \times 10^{-9} – 2 \times 10^{-6}$	$2{,}9 \times 10^{-10}$	$9{,}6 \times 10^{-10}$	3,5	-	(Fe(III), Ca(II), Mg(II), Cl(-I), GLU, EPI, AA, UA)-**1000x**, DOP-**100x**	[**RD8**]
TDZ	SPAuE	DPAdSV	$1 \times 10^{-11} – 2 \times 10^{-10}$ $2 \times 10^{-10} – 2 \times 10^{-9}$ $2 \times 10^{-9} – 2 \times 10^{-8}$	$2{,}9 \times 10^{-12}$	$9{,}8 \times 10^{-12}$	3,5	6,25	(Fe(III), Ni(II), Mg(II), Ca(II), Cu(II), Cd(II), Pb(II), GLU)-**1000x**, (UA, ADN)-**100x**, EPI-**20x**, DOP-**10x**, **2 mg L^{-1}** Triton X-100	[**RD9**]

GLU – glukoza, ADN – adenina, EPI – epinefryna (adrenalina), DOP – dopamina, UA – kwas moczowy, AA – kwas askorbinowy, E2 – estradiol, ASA – kwas acetylosalicylowy, AMX – amoksycylina, TST – testosteron

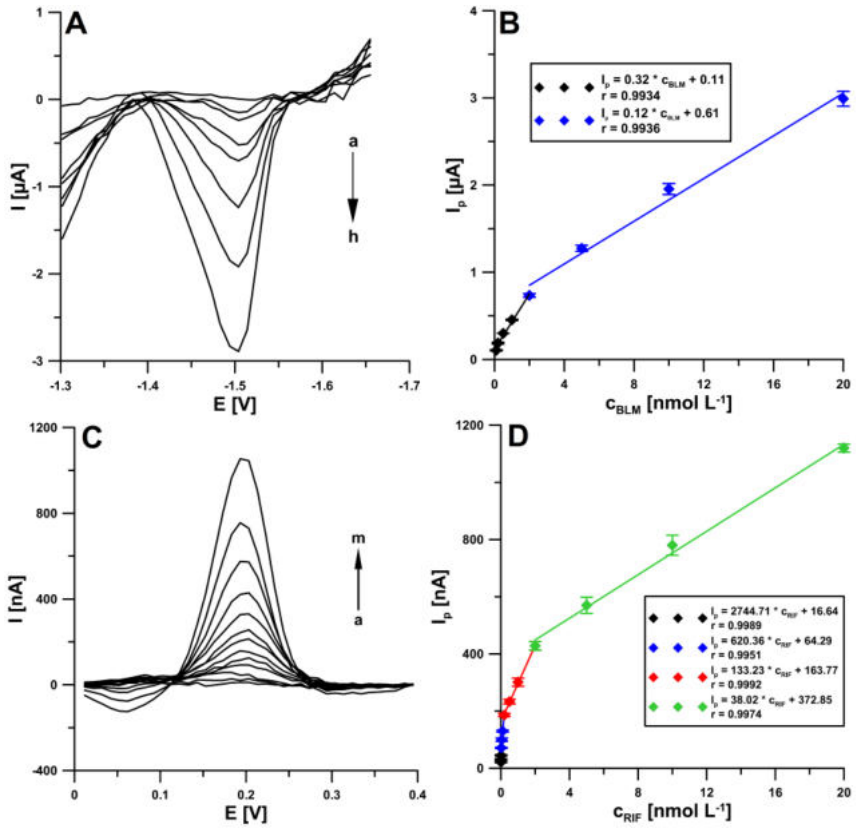

Rys. 28. Woltamperogramy otrzymane podczas oznaczania wzrastających stężeń: A) BLM (a → h, $1 \times 10^{-10} – 2 \times 10^{-8}$ mol L^{-1}) [**RD7**] i C) RIF (a → m, $2 \times 10^{-12} – 2 \times 10^{-8}$ mol L^{-1}) [**RD3**]. Zakresy liniowe krzywych kalibracyjnych: B) BLM i D) RIF.

2.6. Zastosowanie opracowanych procedur i sposoby minimalizacji interferencji

Użyteczność zoptymalizowanych woltamperometrycznych procedur oznaczania wybranych związków biologicznie czynnych zweryfikowano wykonując analizy próbek płynów ustrojowych, próbek środowiskowych (wody rzeczne, ścieki komunalne i szpitalne), a także preparatów farmaceutycznych. Procedurę jednoczesnego oznaczania PA, DF i TR [**RD2**] wykorzystano m.in. do oznaczenia zawartości tych związków w preparatach farmaceutycznych, a uzyskane wyniki wykazują zgodność z zawartością deklarowaną przez producenta. Wyniki wykonanych oznaczeń podsumowano w tabeli 6, a przykładowe woltamperogramy otrzymane podczas analiz przedstawiono na rysunku 29.

Tabela. 6. Zastosowanie opracowanych woltamperometrycznych procedur.

Analit	Próbka	Wartość deklarowana przez producenta	Dodano [mol L^{-1}]	Oznaczono woltamperometrycznie ± SD (n=3) [mol L^{-1}]	Oznaczono metodą porównawczą ± SD (n=3) [mol L^{-1}]	Odzysk* [%]	Błąd względny** [%]	Praca
EIMTC	Surowica ludzka	-	5×10^{-8}	$4{,}86 \times 10^{-8} \pm 0{,}17 \times 10^{-8}$ [a]	$5{,}21 \times 10^{-8} \pm 0{,}05 \times 10^{-8}$ [b]	97,2	7,2	[**RD1**]
		-	1×10^{-7}	$0{,}99 \times 10^{-7} \pm 0{,}03 \times 10^{-7}$ [a]	$0{,}96 \times 10^{-7} \pm 0{,}03 \times 10^{-7}$ [b]	99	3	
PA	Woda z rzeki Bystrzycy	-	2×10^{-7}	$1{,}91 \times 10^{-7} \pm 0{,}09 \times 10^{-7}$ [c]	-	97	-	[**RD2**]
DF		-	2×10^{-8}	$2{,}01 \times 10^{-8} \pm 0{,}02 \times 10^{-8}$ [c]	-	100,5	-	
TR		-	2×10^{-8}	$2{,}04 \times 10^{-8} \pm 0{,}06 \times 10^{-8}$ [d]	-	102	-	
PA	Surowica ludzka	-	2×10^{-7}	$2{,}04 \times 10^{-7} \pm 0{,}01 \times 10^{-7}$ [c]	-	102	-	
DF		-	2×10^{-8}	$1{,}97 \times 10^{-8} \pm 0{,}1 \times 10^{-8}$ [c]	-	98,5	-	
TR		-	2×10^{-8}	$2 \times 10^{-8} \pm 0{,}04 \times 10^{-8}$ [d]	-	100	-	
PA	Lek 1	325 mg	-	321,3 ± 3,8 mg [f]	-	-	$1{,}1^{***}$	
TR		37,5 mg	-	38,3 ± 2,1 mg [f]	-	-	$2{,}1^{***}$	
DF	Lek 2	25 mg	-	25 ± 0,64 mg [f]	-	-	$0{,}0^{***}$	
RIF	Woda z rzeki Bystrzycy	-	1×10^{-10}	$9{,}73 \times 10^{-11} \pm 0{,}24 \times 10^{-11}$ [c]	< LOD [e]	97,3	-	[**RD3**]
		-	5×10^{-9}	$4{,}57 \times 10^{-9} \pm 0{,}11 \times 10^{-9}$ [c]	$4{,}71 \times 10^{-9} \pm 0{,}25 \times 10^{-9}$ [e]	91,4	3	
	Mocz bydlęcy	-	1×10^{-10}	$9{,}2 \times 10^{-11} \pm 0{,}07 \times 10^{-11}$ [c]	< LOD [e]	92	-	

		-	5×10^{-9}	$4{,}93 \times 10^{-9} \pm 0{,}04 \times 10^{-9}$ [c]	$4{,}76 \times 10^{-9} \pm 1{,}8 \times 10^{-9}$ [e]	98,6	3,6	
TST	Oczyszczone ścieki komunalne	-	3×10^{-11}	$2{,}96 \times 10^{-11} \pm 0{,}12 \times 10^{-11}$ [c]	-	98,7	-	[**RD5**]
		-	2×10^{-10}	$2{,}09 \times 10^{-10} \pm 0{,}17 \times 10^{-10}$ [c]	-	104,5	-	
	Mocz ludzki (materiał odniesienia)	-	3×10^{-11}	$2{,}97 \times 10^{-11} \pm 0{,}12 \times 10^{-11}$ [c]	-	99	-	
		-	2×10^{-10}	$2{,}01 \times 10^{-10} \pm 0{,}26 \times 10^{-10}$ [c]	-	100,5	-	
4-Cl-PIMT	Surowica ludzka	-	2×10^{-9}	$2{,}1 \times 10^{-9} \pm 0{,}07 \times 10^{-9}$ [g]	$2{,}32 \times 10^{-9} \pm 0{,}34 \times 10^{-9}$ [h]	105	9,48	[**RD6**]
		-	2×10^{-8}	$2{,}01 \times 10^{-8} \pm 0{,}06 \times 10^{-8}$ [g]	$1{,}97 \times 10^{-9} \pm 0{,}03 \times 10^{-9}$ [h]	100,7	2,18	
BLM	Oczyszczone ścieki komunalne	-	5×10^{-10}	$4{,}8 \times 10^{-10} \pm 0{,}12 \times 10^{-10}$ [g]	-	96	-	[**RD7**]
		-	2×10^{-9}	$1{,}93 \times 10^{-9} \pm 0{,}04 \times 10^{-9}$ [g]	-	96,5	-	
	Mocz ludzki (materiał odniesienia)	-	2×10^{-9}	$2{,}07 \times 10^{-9} \pm 0{,}04 \times 10^{-9}$ [g]	-	103,5	-	
		-	4×10^{-9}	$3{,}96 \times 10^{-9} \pm 0{,}02 \times 10^{-9}$ [g]	-	99	-	
NDIT	Surowica ludzka	-	2×10^{-8}	$2{,}01 \times 10^{-8} \pm 0{,}09 \times 10^{-8}$ [c]	-	100,5	-	[**RD8**]
		-	5×10^{-8}	$5{,}04 \times 10^{-8} \pm 0{,}14 \times 10^{-8}$ [c]	-	100,8	-	
TDZ	Oczyszczone ścieki komunalne	-	5×10^{-11}	$5 \times 10^{-11} \pm 0{,}21 \times 10^{-11}$ [c]	-	100	-	[**RD9**]
		-	2×10^{-10}	$1{,}97 \times 10^{-10} \pm 0{,}02 \times 10^{-10}$ [c]	-	98,5	-	
	Surowica ludzka	-	5×10^{-11}	$5{,}03 \times 10^{-11} \pm 0{,}24 \times 10^{-11}$ [c]	-	100,6	-	
		-	2×10^{-10}	$2{,}05 \times 10^{-10} \pm 0{,}1 \times 10^{-10}$ [c]	-	102,5	-	

a – SWV; b – UHPLC-ESI-MS/MS (ultrawysokosprawna chromatografia cieczowa sprzężona z tandemową spektrometrią mas, z jonizacją przez elektrorozpylanie); c – DPAdSV; d – DPV; e – HPLC/PDA (wysokosprawna chromatografia cieczowa z detektorem diodowym); f – wartość w przeliczeniu na jedną tabletkę preparatu; g – SWAdSV; h – UHPLC-ESI-MS (ultrawysokosprawna chromatografia cieczowa sprzężona ze spektrometrią mas, z jonizacją przez elektrorozpylanie); *Odzysk [%] =

(Oznaczono woltamperometrycznie × 100) / Dodano; **Błąd względny [%] = ((|Oznaczono metodą porównawczą – Oznaczono woltamperometrycznie|) / Oznaczono woltamperometrycznie) × 100; *** Błąd względny [%] = (|Oznaczono woltamperometrycznie – Wartość deklarowana przez producenta| / Wartość deklarowana przez producenta) × 100

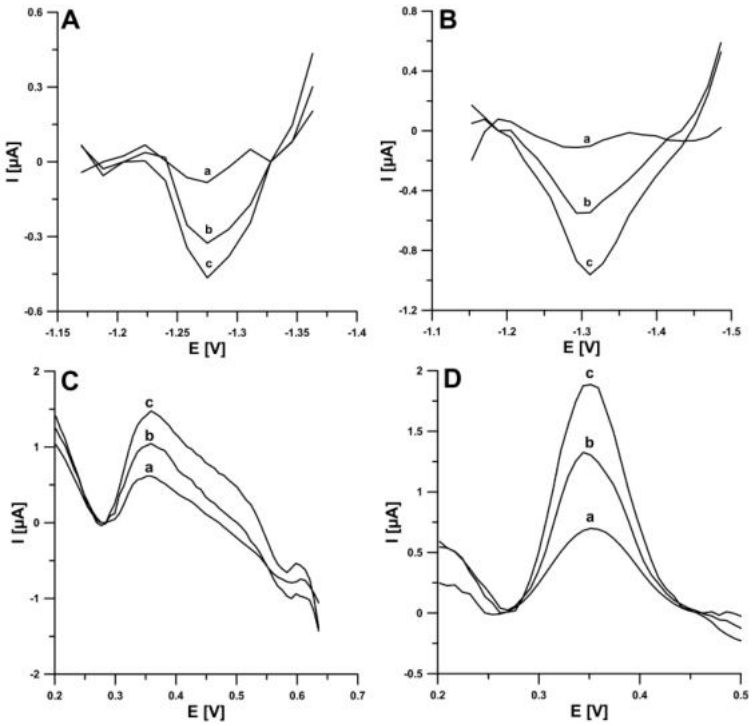

Rys. 29. Woltamperogramy otrzymane podczas oznaczania: A) TST w próbce materiału odniesienia-moczu ludzkim: a) próbka + 3×10^{-11}, b) jak (a) + 3×10^{-11}, c) jak (a) + 6×10^{-11} mol L^{-1} TST; B) TST w próbce oczyszczonych ścieków komunalnych: a) próbka 3×10^{-11}, b) jak (a) + 3×10^{-11}, c) jak (a) + 6×10^{-11} mol L^{-1} TST [**RD5**]; C) TDZ w próbce surowicy ludzkiej: a) próbka + 5×10^{-11}, b) jak (a) + 5×10^{-11}, c) jak (a) + 1×10^{-10} mol L^{-1} TDZ; D) TDZ w próbce surowicy ludzkiej: a) próbka + 2×10^{-10}, b) jak (a) + 2×10^{-10}, c) jak (a) + 4×10^{-10} mol L^{-1} TDZ [**RD9**].

Warto podkreślić, że w zdecydowanej większości analizowane próbki nie były w żaden sposób przygotowywane przed pomiarami (próbki moczu i ścieków). Próbki wód rzecznych i preparatów farmaceutycznych poddano jedynie filtracji z użyciem filtrów strzykawkowych. W przypadku próbek surowicy ludzkiej, do próbek dodawano roztwór kwasu trichlorooctowego (TCA) celem strącenia rozpuszczonych w nich białek, które mogłyby blokować powierzchnię stosowanej elektrody. Po strąceniu białka próbki poddawane były wirowaniu, a określoną objętość uzyskanego w ten sposób supernatantu dodawano do naczynka pomiarowego i analizowano.

Jednym ze sposobów minimalizacji interferencji pochodzących od matrycy próbek było zastosowanie układu przepływowego. Analizę próbek surowicy ludzkiej prowadzono z użyciem klasycznej analizy przepływowo-wstrzykowej (FIA) [**RD1**],

a po każdym pomiarze układ wraz z elektrodą przepłukiwano roztworem H_2SO_4 o wyższym stężeniu niż elektrolit podstawowy (2,0 vs. 0,075 mol L^{-1}) celem dokładnego oczyszczenia. Analizę przepływową próbek surowicy przedstawiono także w publikacji [**RD6**]. W procedurze oznaczania 4-Cl-PIMT po etapie nagromadzania analitu na powierzchni elektrody pracującej do celki przepływowej doprowadzono roztwór elektrolitu podstawowego (0,025 mol L^{-1} HNO_3). Miało to na celu usunięcie roztworu próbki z przestrzeni przyelektrodowej aby zmniejszyć prawdopodobieństwo redukcji interferentów w etapie rejestracji sygnału analitycznego. Zbadano w jakim stopniu rosnąca objętość surowicy dodawanej do roztworu pomiarowego wpływa na sygnał analitu (Rys. 30). Stwierdzono, że zastosowanie układu przepływowego minimalizuje tłumienie sygnału 4-Cl-PIMT przez składniki matrycy próbki.

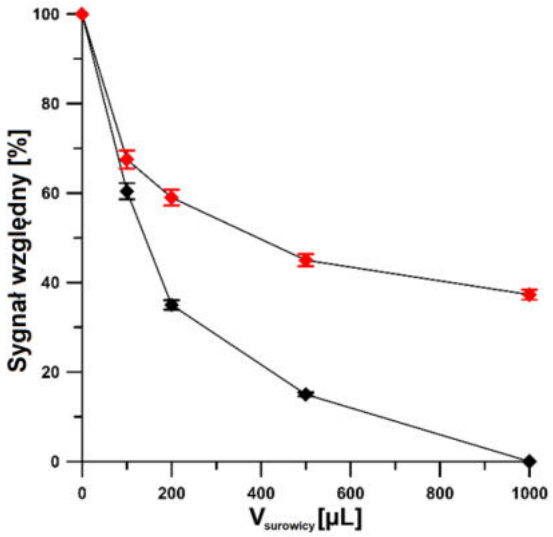

Rys. 30. Wpływ surowicy ludzkiej na prąd piku 5×10^{-9} mol L^{-1} 4-Cl-PIMT w układzie klasycznym (czarny) i przepływowym (czerwony) [**RD6**].

Dodatkowo w procedurze tej skrócono czas nagromadzania analitu ze 120 do 30 s, co również zmniejsza adsorpcję potencjalnych interferentów na powierzchni elektrody pracującej. Minimalizację interferencji przez skrócenie czasu analizy zastosowano także podczas oznaczania RIF [**RD3**].

W procedurze jednoczesnego oznaczania PA, DF i TR [**RD2**], a także w procedurze oznaczania NDIT [**RD8**] jako modyfikator elektrody pracującej zastosowano SDS. Dzięki zaadsorbowanemu na powierzchni elektrody surfaktantowi możliwe było uzyskanie wzmocnienia sygnałów pochodzących od analitów. Dodatkową zaletą modyfikacji surfaktantem jest zabezpieczenie elektrody przed zanieczyszczeniem

przez obecne w próbce związki organiczne. Badania pokazały, że zaadsorbowany SDS pozwala zminimalizować wpływ CTAB i Tritonu X-100 na sygnały analityczne PA, DF i TR (Rys. 31) [**RD2**].

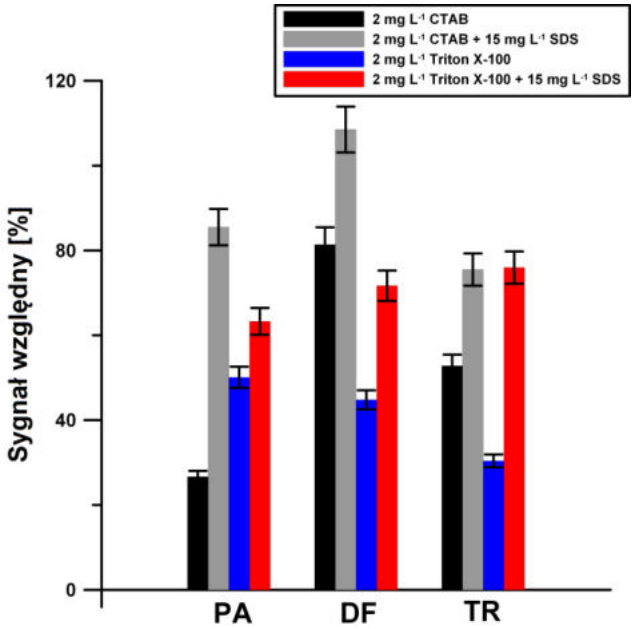

Rys. 31. Wpływ 2 mg L^{-1} Triton X-100 i CTAB na sygnały PA, DF i TR bez i w obecności SDS [**RD2**].

Kolejnym sposobem minimalizacji wpływu obecnych w próbkach związków organicznych jest jej rozcieńczenie. We wszystkich pracach, w przypadku analizy próbek płynów ustrojowych i próbek środowiskowych anality oznaczano w próbkach rozcieńczonych od 10 do 10000 razy. Duże krotności rozcieńczeń były możliwe w przypadku oznaczania związków, które w określonych próbkach osiągają wysokie stężenia.

2.7. Porównanie opracowanych procedur z danymi literaturowymi

Ze względu na opracowywanie ciągle to nowych czujników stosowanych w woltamperometrii możliwe jest rozszerzenie możliwości aplikacyjnych tej metody analitycznej. W literaturze jest szereg prac opisujących zastosowanie czujników elektrochemicznych w oznaczeniach PA, DF, TR, RIF, TST, BLM i TDZ. W tabeli 7 przedstawiono porównanie opracowanych procedur oznaczania tych związków, wybranymi procedurami opisanymi w literaturze [9, 28, 66, 68, 80-111], które charakteryzują się najkorzystniejszymi parametrami analitycznymi. W przypadku

procedur oznaczania PA, DF, TR, RIF, TST i BLM uzyskano jedne z najniższych granic wykrywalności spośród woltamperometrycznych procedur opisanych w literaturze. Te charakteryzujące się lepszymi parametrami analitycznymi wykorzystywały czujniki, których opracowanie było wysoce czaso- i pracochłonne i wymagało często kilkudniowej syntezy modyfikatorów. Ponadto, zaprezentowana w pracy [**RD2**] procedura jest jedyną pozwalającą na jednoczesne oznaczenie PA, DF i TR, natomiast procedury oznaczania RIF [**RD3**] i BLM [**RD7**] były w momencie opublikowania prac pierwszymi przykładami zastosowania czujników sitodrukowanych w analizie tych związków. Procedura pozwalająca na oznaczanie TDZ przy użyciu SPAuE [**RD9**] cechuje się wyjątkowo wysoką czułością, dzięki której możliwe było uzyskanie około tysiąc razy niższej granicy wykrywalności niż w przypadku innych opisanych dotychczas procedur. Związki przeciwnowotworowe: EIMTC, 4-Cl-PIMT i NDIT są substancjami nowo zsyntezowanymi, w związku z czym brak jest w literaturze danych na temat ich woltamperometrycznych oznaczeń, a przedstawione w pracach [**RD1**], [**RD4**] i [**RD6**] procedury są pierwszymi sposobami analizy tychże związków. Niezwykle istotny jest również fakt, iż we wszystkich opracowanych procedurach bazowano na dostępnych handlowo czujnikach sitodrukowanych, które były ewentualnie poddawane prostym, szybkim i wysoce skutecznym modyfikacjom i pozwalają na bezpośrednią analizę większości próbek.

Tabela 7. Porównanie opracowanych procedur oznaczania PA, DF, TR, RIF, TST, BLM i TDZ z opisanymi w literaturze procedurami charakteryzującymi się najkorzystniejszymi parametrami analitycznymi.

Elektroda	Metoda	Zakres liniowy [mol L^{-1}]	LOD [mol L^{-1}]	Zastosowanie	Lit.
Paracetamol (PA)					
Co MPs/Pt	SWV	$5 \times 10^{-7} – 1 \times 10^{-4}$	$4{,}2 \times 10^{-7}$	Preparaty farmaceutyczne	[80]
ZMCPE	DPV	$1 \times 10^{-5} – 6 \times 10^{-5}$	$6{,}8 \times 10^{-7}$	-	[81]
$NiFe_2O_4$/Gr/ CPE	SWV	$1 \times 10^{-8} – 9 \times 10^{-6}$	$3{,}6 \times 10^{-9}$	Preparaty farmaceutyczne, surowica, mocz	[82]
SPCE/MW CNTs-	DPAdSV	$5 \times 10^{-9} – 5 \times 10^{-6}$	$1{,}4 \times 10^{-9}$	Woda rzeczna, ścieki	[28]

COOH				komunalne	
Sm_2O_3@ZrO_2/CNTs/ GCE	SWV	$3,7 \times 10^{-9} – 2,2 \times 10^{-6}$	$3,4 \times 10^{-10}$	Preparaty farmaceutyczne, krew	[83]
COOH-CNTs/ZnO/ NH_2-CNTs/GCE	SWASV	$2,5 \times 10^{-11} – 1,8 \times 10^{-8}$	$4,7 \times 10^{-14}$	Preparaty farmaceutyczne, surowica, ślina, mocz	[84]
aSPCE/SDS	DPAdSV	$5 \times 10^{-8} – 2 \times 10^{-5}$	$1,49 \times 10^{-8}$	Woda z rzeki, surowica, preparaty farmaceutyczne	[**RD2**]
Diklofenak (DF)					
La_2O_3@SF-L Cu_2S/GCE	DPV	$1 \times 10^{-8} – 9 \times 10^{-4}$	$1,7\times 10^{-9}$	Preparaty farmaceutyczne, surowica, mocz	[85]
Ru-TiO_2/CPE	SWV	$1 \times 10^{-7} – 2 \times 10^{-6}$	$1,48 \times 10^{-9}$	Preparaty farmceutyczne, mocz	[86]
Aptamer-polydopamine@Fe_3O_4-GCE	DPV	-	$1,1 \times 10^{-10}$	Surowica	[87]
SPCE/MW CNTs-COOH	DPAdSV	$1 \times 10^{-10} – 2 \times 10^{-8}$	3×10^{-11}	Woda rzeczna, ścieki komunalne	[28]
SPCE/MW CNTs-COOH	DPAdSV	$1 \times 10^{-10} – 1 \times 10^{-8}$	$2,8 \times 10^{-11}$	Woda rzeczna	[9]
COOH-CNTs/ZnO/ NH_2-CNTs/GCE	SWASV	$7,5 \times 10^{-11} – 2,1 \times 10^{-8}$	$7,8 \times 10^{-14}$	Preparaty farmaceutyczne, surowica, ślina, mocz	[84]
aSPCE/SDS	DPAdSV	$1 \times 10^{-9} – 2 \times 10^{-7}$	$2,1 \times 10^{-10}$	Woda z rzeki, surowica, preparaty farmaceutyczne	[**RD2**]
Tramadol (TR)					
MIP-MWCNT/ CPE	SWV	$1 \times 10^{-8} – 2 \times 10^{-5}$	4×10^{-9}	Preparaty farmaceutyczne, mocz	[88]

f-MWCNTs/ AuNPs/PGE	DPV	$1{,}2 \times 10^{-8} – 1 \times 10^{-7}$ $1 \times 10^{-7} – 3 \times 10^{-6}$	5×10^{-9}	Mocz	[89]
GO-MWCNTs/ CPE	DPV	$2 \times 10^{-9} – 1{,}1 \times 10^{-3}$	$1{,}5 \times 10^{-10}$	Preparaty farmaceutyczne, surowica	[90]
Polypyrrole @Sol-Gel MIP/f-MWCNT/ GCE	SWV	$2 \times 10^{-10} – 2 \times 10^{-9}$	3×10^{-11}	Preparaty farmaceutyczne, mocz	[91]
CNFs/SPE	SWV	$5 \times 10^{-11} – 1 \times 10^{-7}$	$1{,}6 \times 10^{-11}$	Mocz	[92]
Au disc micro-electrode	AFFTCV	$5{,}7 \times 10^{-12} – 3{,}4 \times 10^{-9}$	$1{,}2 \times 10^{-12}$	Mocz, surowica	[93]
aSPCE/SDS	DPV	$1 \times 10^{-8} – 2 \times 10^{-7}$ $2 \times 10^{-7} – 2 \times 10^{-6}$	$1{,}71 \times 10^{-9}$	Woda z rzeki, surowica, preparaty farmaceutyczne	[**RD2**]
Ryfampicyna (RIF)					
$Ni(OH)_2$@rGO/SPCE	DPV	$1 \times 10^{-9} – 2 \times 10^{-7}$ $2 \times 10^{-7} – 5 \times 10^{-5}$	3×10^{-9}	Preparaty farmaceutyczne, surowica	[94]
3D pRGO/GCE	DPV	$1 \times 10^{-9} – 1 \times 10^{-7}$	$2{,}7 \times 10^{-10}$	Mleko	[95]
PbF/GCE	SWAdSV	$2{,}5 \times 10^{-10} – 1 \times 10^{-8}$	9×10^{-11}	Preparaty farmaceutyczne	[96]
MWCNTs-CeO_2 /GCE	DPAdSV	$1 \times 10^{-13} – 1 \times 10^{-6}$	$3{,}4 \times 10^{-14}$	Surowica	[97]
DNA/CPE	DPAdSV	-	8×10^{-15}	Surowica	[98]
$CoFe_2O_4$@CdSe/GCE	SWAdSV	$1 \times 10^{-16} – 1 \times 10^{-7}$	$4{,}55 \times 10^{-17}$	Preparaty farmaceutyczne, surowica	[99]
aSPBDDE	DPAdSV	$2 \times 10^{-12} – 2 \times 10^{-11}$ $2 \times 10^{-11} – 2 \times 10^{-10}$ $2 \times 10^{-10} – 2 \times 10^{-9}$ $2 \times 10^{-9} – 2 \times 10^{-8}$	$2{,}2 \times 10^{-13}$	Mocz, woda z rzeki	[**RD3**]
Testosteron (TST)					
GCE/CTAB	SWAdSV	$1 \times 10^{-8} – 7 \times 10^{-8}$	$1{,}2 \times 10^{-9}$	Preparaty farmaceutyczne,	[66]

				mocz	
GCE/BiF + CTAB	SWAdSV	$1 \times 10^{-9} – 4{,}5 \times 10^{-8}$	3×10^{-10}	Preparaty farmaceutyczne, mocz	[100]
MD/CNTs	DPV	$1 \times 10^{-10} – 1 \times 10^{-6}$	$1{,}4 \times 10^{-11}$	Ślina	[101]
AuE/DMIP	SWV	$1 \times 10^{-14} – 1 \times 10^{-13}$	1×10^{-14}	Mocz	[102]
SPE/MIP	CV	$3{,}5 \times 10^{-18} – 3{,}5 \times 10^{-15}$	$3{,}5 \times 10^{-17}$	Mocz	[103]
pSPCE/ PbNPs	DPAdSV	$1 \times 10^{-11} – 2 \times 10^{-10}$ $2 \times 10^{-10} – 2 \times 10^{-9}$ $2 \times 10^{-9} – 2 \times 10^{-8}$	$2{,}2 \times 10^{-12}$	Mocz, ścieki komunalne	[**RD5**]
Bleomycyna (BLM)					
HMDE	AdSV	$1 \times 10^{-9} – 1 \times 10^{-7}$	5×10^{-10}	Surowica	[104]
AuE/DNA (E-DNA sensor)	SWV	$1 \times 10^{-10} – 1 \times 10^{-6}$	1×10^{-10}	Surowica	[105]
ITO/MB-DNA	DPV	$1 \times 10^{-10} – 1 \times 10^{-7}$	$3{,}3 \times 10^{-11}$	Surowica	[106]
AuE/DNA	DPV	$1 \times 10^{-12} – 1 \times 10^{-7}$	$7{,}4 \times 10^{-13}$	Surowica	[107]
pSPCE/ PbNPs	SWAdSV	$1 \times 10^{-10} – 2 \times 10^{-9}$ $2 \times 10^{-9} – 2 \times 10^{-8}$	$2{,}8 \times 10^{-11}$	Mocz, ścieki komunalne	[**RD7**]
Tiorydazyna (TDZ)					
Bi/PSi/ CNTPE	DPV	$1 \times 10^{-7} – 2{,}6 \times 10^{-4}$	3×10^{-8}	Osocze	[68]
SPCE/ FeV NPs	DPV	$2 \times 10^{-8} – 1 \times 10^{-4}$	8×10^{-9}	Surowica	[108]
β-CD/CPE	DPV	$1 \times 10^{-8} – 1 \times 10^{-7}$	7×10^{-9}	Preparaty farmaceutyczne	[109]
NGO-500/SPCE	DPV	$4 \times 10^{-8} – 1{,}5 \times 10^{-4}$	4×10^{-9}	Mocz, surowica	[110]
Ru-Bi_2S_3/GCE	DPV	$5 \times 10^{-9} – 1{,}4 \times 10^{-3}$	1×10^{-9}	Surowica	[111]
SPAuE	DPAdSV	$1 \times 10^{-11} – 2 \times 10^{-10}$ $2 \times 10^{-10} – 2 \times 10^{-9}$ $2 \times 10^{-9} – 2 \times 10^{-8}$	$2{,}9 \times 10^{-12}$	Surowica, ścieki komunalne	[**RD9**]

Co MPs/Pt – elektroda platynowa modyfikowana mikrocząstkami kobaltu; ZMCPE – pastowa elektroda węglowa modyfikowana nanocząstkami ZrO_2; $NiFe_2O_4$/Gr/CPE – pastowa elektroda węglowa modyfikowana nanokompozytem grafenu i $NiFe_2O_4$; Sm_2O_3@ZrO_2/CNTs/GCE – elektroda z węgla

szklistego modyfikowana kompozytem Sm_2O_3 i ZrO_2; La_2O_3@SF-L Cu_2S/GCE – elektroda z węgla szklistego modyfikowana kompozytem La_2O_3 i Cu_2S; Ru-TiO_2/CPE – pastowa elektroda węglowa modyfikowana nanocząstkami TiO_2 domieszkowanymi rutenem; SPCE/MWCNTs-COOH – sitoddrukowana elektroda węglowa modyfikowana wielościennymi nanorurkami węglowymi, funkcjonalizowanymi grupami karboksylowymi; COOH-CNTs/ZnO/NH_2-CNTs/GCE – elektroda z węgla szklistego modyfikowana nanorurkami węglowymi funkcjonalizowanymi grupami aminowymi i karboksylowymi oraz warstwą tlenku cynku pomiędzy nimi; SWASV – anodowa woltamperometria stripingowa fali prostokątnej; MIP-MWCNT/CPE – pastowa elektroda węglowa modyfikowana polimerem z odciskiem molekularnym i wielościennymi nanorurkami węglowymi; f-MWCNTs/AuNPs/PGE – ołówkowa elektroda grafitowa modyfikowana funkcjonalizowanymi, wielościennymi nanorurkami węglowymi i nanoczątkami złota; GO-MWCNTs/CPE – pastowa elektroda węglowa modyfikowana tlenkiem grafenu i wielościennymi nanorurkami węglowymi; Polypyrrole@Sol-Gel MIP/f-MWCNT/GCE – elektroda z węgla szklistego modyfikowana polimerem z odciskiem molekularnym i funkcjonalizowanymi, wielościennymi nanorurkami węglowymi; CNFs/SPE – elektroda sitodrukowana modyfikowana nanowłóknami węglowymi; AFFTCV – adsorpcyjna woltamperometria cykliczna z transformacją Fouriera; $CoFe_2O_4$@CdSe/GCE – elektroda z węgla szklistego modyfikowana nanoczątkami $CoFe_2O_4$@CdSe o strukturze rdzeń-powłoka; DNA/CPE – pastowa elektroda węglowa modyfikowana DNA; MWCNTs-CeO_2/GCE – elektroda z węgla szklistego modyfikowana wielościennymi nanorurkami węglowymi i nanopręty tlenku ceru; PbF/GCE – elektroda z węgla szklistego modyfikowana błonką ołowiu; 3D pRGO/GCE – elektroda z węgla szklistego modyfikowana trójwymiarowym, porowatym zredykowanym tlenkiem grafenu; Ni$(OH)_2$@rGO/SPCE – sitodrukowana elektroda węglowa modyfikowana nanofilmem wodorotlenku niklu i zredukowanym tlenkiem grafenu; GCE/CTAB – GCE modyfikowana CTAB; GCE/BiF + CTAB – GCE modyfikowana błonką bizmutu i CTAB; MD/CNTs – elektroda pastowa oparta na nanorurkach węglowych modyfikowana maltodekstryną; AuE/DMIP – elektroda złota modyfikowana dwuwarstwowym polimerem z odciskiem molekularnym; SPE/MIP – elektroda sitodrukowana modyfikowana polimerem z odciskiem molekularnym; AuE/DNA – elektroda złota modyfikowana DNA; HMDE – wisząca kroplowa elektroda rtęciowa; ITO/MB-DNA – elektroda z tlenku indowo-cynowego modyfikowana błękitem metylenowym i DNA; Ru-Bi_2S_3/GCE – GCE modyfikowana siarczkiem bizmutu domieszkowanym rubidem; NGO-500/SPCE – SPCE modyfikowana sferycznymi mikrostrukturami NiO i Gd_2O_3; β-CD/CPE – CPE modyfikowana β-cyklodekstryną; SPCE/FeV NPs – SPCE modyfikowana nanocząstkami wanadanu żelaza; Bi/PSi/CNTPE – pastowa elektroda oparta na nanorurkach węglowych modyfikowana bizmutem i porowatym krzemem

3. Dalsze perspektywy zastosowania czujników sitodrukowanych

W trakcie trwania studiów doktoranckich opracowano również procedurę oznaczania antybiotyku ciprofloksacyny (CFX) na nanoporowatej sitodrukowanej elektrodzie węglowej (NPSPCE) [**RD10**]. Schemat zoptymalizowanej procedury został przedstawiony na rysunku 32. Otrzymane wyniki zostały opisane w pracy wysłanej do czasopisma Measurement (IF = 5,6, 200 pkt MEiN). Z uwagi na fakt, iż praca została zaakceptowana w dzień przed złożeniem rozprawy doktorskiej (dołączono mail potwierdzający akceptację) i nie miała jeszcze nadanego numeru DOI, opis przeprowadzonych badań i ich rezultat przedstawiono w rozdziale dotyczącym dalszych perspektyw zastosowania czujników sitodrukowanych.

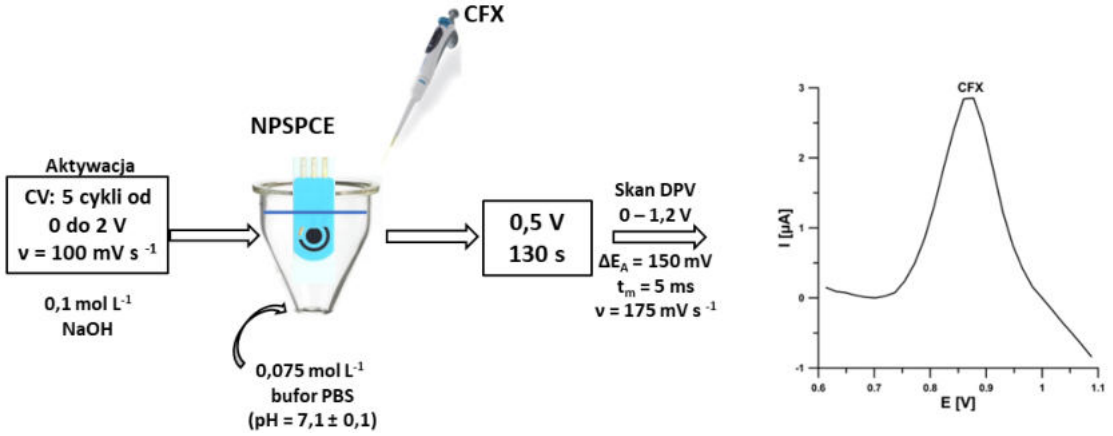

Rys. 32. Schemat procedury oznaczania CFX [opracowanie własne].

Ciprofloksacyna (CFX, Rys. 33) jest antybiotykiem fluorochinolonowym drugiej generacji, skutecznym zarówno wobec bakterii Gram-ujemnych, jak i Gram-dodatnich. CFX jest stosowana w leczeniu szerokiego zakresu infekcji układu moczowego, oddechowego i pokarmowego. Ponadto jest lekiem z wyboru w leczeniu infekcji kości i stawów, infekcji skóry oraz chorób przenoszonych drogą płciową. CFX jest substancją, która po podaniu doustnym jest wydalana w około 50% przez drogi moczowe i jednym z najczęściej wykrywanych w środowisku antybiotyków [112-113].

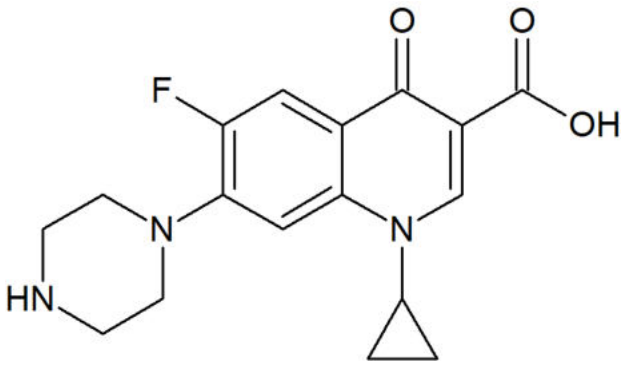

Rys. 33. Wzór strukturalny CFX [opracowanie własne].

W zaproponowanej procedurze [**RD10**] sitodrukowana elektroda węglowa (SPCE) była aktywowana w ten sam sposób, co sitodrukowana elektroda diamentowa domieszkowana borem (SPBDDE) w pracy [**RD3**], czyli metodą CV z użyciem zasady sodowej. Podobnie jak w tamtym przypadku aktywacja przyczyniła się do znacznego (ok. 10-krotnego, Rys. 34A) wzrostu natężenia prądu piku (I_p) analitu. Badania EIS wykazały spadek wartości R_{ct} względem elektrody nieaktywowanej (784,9 vs. 406 **Ω** cm^2) (Rys. 34B). Dodatkowo wartości względnego rozdzielenia pików (χ^0) utleniania redukcji układu redoks Fe^{2+}/Fe^{3+} (Rys. 34C) potwierdziły poprawę efektywności przenoszenia elektronów dzięki zastosowaniu aktywacji. Wartość χ^0 dla elektrody aktywowanej wynosi 2,39 i jest bliższa wartości teoretycznej ($\chi^0 = 1$) niż χ^0 uzyskane dla SPCE (4,47). Badania CV wykonane dla ν w zakresie 7,5 – 200 mV s^{-1} posłużyły do wykreślenia zależności $I_p = f(\nu^{1/2})$ (Rys. 34D), na podstawie których obliczono A_S obu elektrod. W przypadku SPCE aktywacja spowodowała istotne zwiększenie A_S (0,042 vs. 0,074 cm^2). Obrazowanie powierzchni elektrod przy użyciu SEM uwidoczniło przyczynę tak dużej zmiany. Na obrazach SEM (Rys. 35A i 35B) można zauważyć, że wskutek aktywacji doszło do zmian morfologii powierzchni SPCE z wytworzeniem wysoce porowatej struktury. Średnica ekwiwalentna porów została wyznaczona przy pomocy oprogramowania „NIS-Elements" i zawierała się w zakresie 17,68 – 167,46 nm, przy średniej wartości 58,7 ± 31,29 nm (n = 100), co pokazuje, że elektrochemiczna aktywacja anodowa SPCE z użyciem zasady sodowej prowadzi do wytworzenia sitodrukowanej elektrody węglowej o strukturze nanoporowatej (NPSPCE). Bazując na wynikach niniejszych badań i badań przedstawionych w pracy [**RD3**] można wyciągnąć wniosek, że ten sam rodzaj aktywacji może w różny sposób wpłynąć na parametry elektrody wyjściowej, w zależności od materiału, z którego jest ona wyprodukowana.

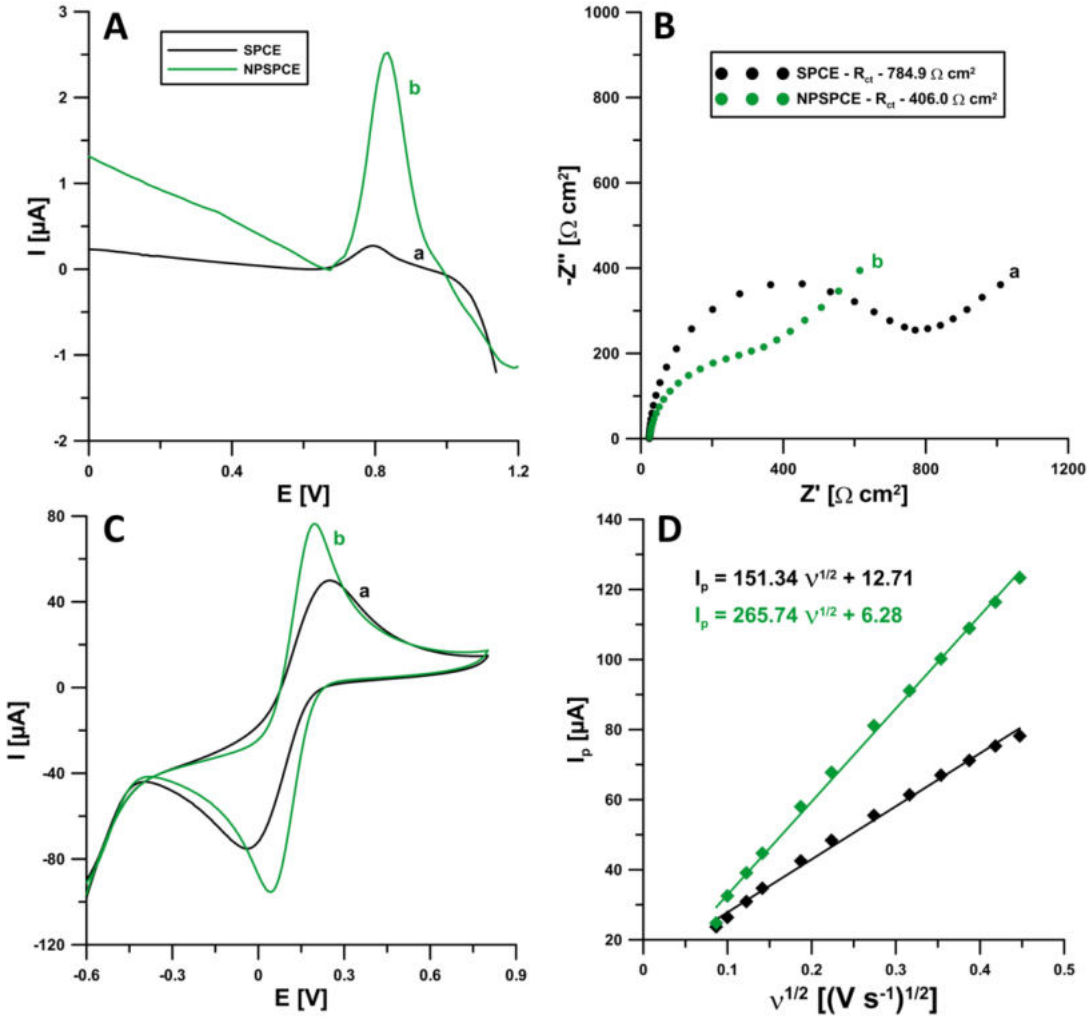

Rys. 34. Woltamperogramy uzyskane dla 5 × 10^{-8} mol L^{-1} CFX na SPCE (a) i NPSPCE (b). B) Widma EIS uzyskane dla SPBDDE (a) i aSPBDDE (b). C) Krzywe CV zarejestrowane na SPCE (a) i NPSPCE (b) (ν = 100 mV s^{-1}). D) Zależność Ip = f($\nu^{1/2}$) wykreślona dla SPCE (a) i NPSPCE (b) [**RD10**].

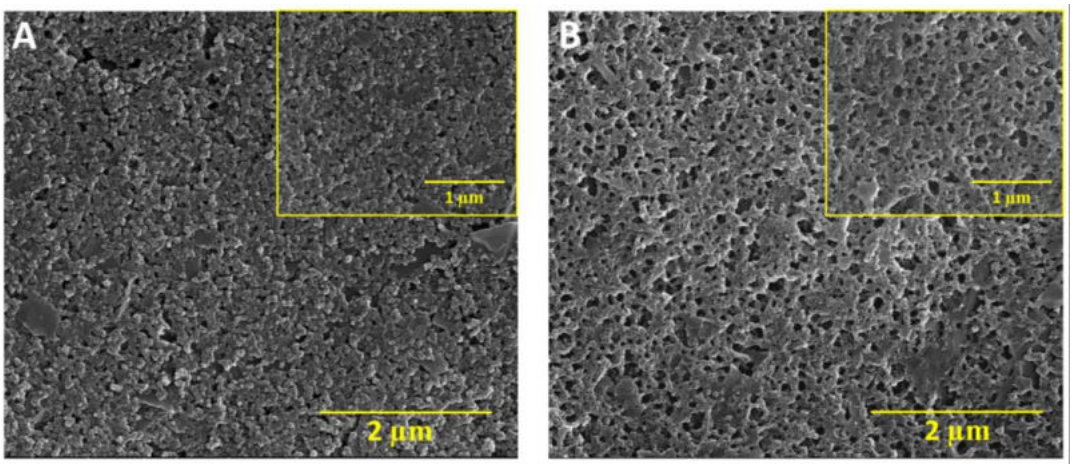

Rys. 35. Obrazy SEM powierzchni SPCE (A) i NPSPCE (B) [**RD10**].

Charakter procesu elektrodowego określono przy użyciu metody CV. Na podstawie uzyskanych woltamperogramów cyklicznych (Rys. 36A) wykreślono zależności $I_p = f(\nu^{1/2})$ oraz $\log I_p = f(\log \nu)$. Nieliniowy przebieg pierwszej z nich (Rys. 36B) i wartość współczynnika kierunkowego prostej regresji (0,93) w drugiej (Rys. 36C) jednoznacznie wskazują na adsorpcyjny charakter elektroutleniania CFX na NPSPCE.

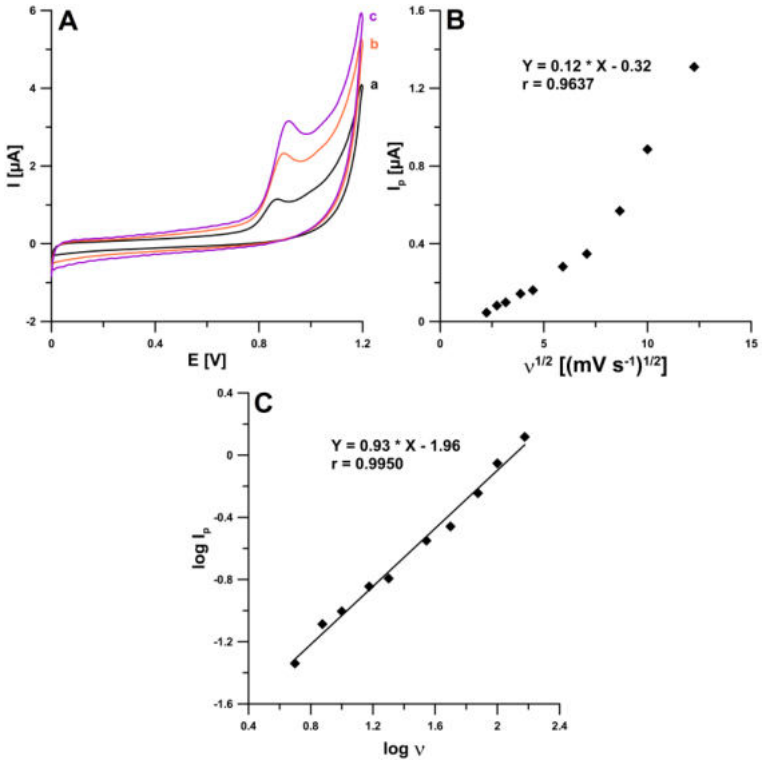

Rys. 36. A) Woltamperogramy cykliczne zarejestrowane dla 1×10^{-6} mol L^{-1} CFX przy ν 50 (a), 100 (b) i 150 mV s^{-1} (c). B) Zależność $I_p = f(\nu^{1/2})$. C) Zależność $\log I_p = f(\log \nu)$ [**RD10**].

W zoptymalizowanych warunkach krzywa kalibracyjna jest liniowa w zakresie stężeń CFX od 5×10^{-10} do 3×10^{-8} mol L^{-1} (Rys. 37A i B). Obliczone granice wykrywalności i oznaczalności wynoszą odpowiednio $6{,}3 \times 10^{-11}$ i $2{,}1 \times 10^{-10}$ mol L^{-1}. Uzyskana LOD jest najniższą spośród woltamperometrycznych oznaczeń CFX na czujnikach sitodrukowanych. Porównanie wyników otrzymanych z użyciem NPSPCE z procedurami o najkorzystniejszych parametrach analitycznych umieszczono w tabeli 8. Zbadano również wpływ potencjalnych interferentów, zarówno nieorganicznych jonów (Fe^{3+}, Cu^{2+}, Ca^{2+}, Pb^{2+}, Cd^{2+}, Mg^{2+} i Ni^{2+}) jak i związków organicznych (glukozy, adrenaliny, dopaminy, kwasu moczowego i kwasu askorbinowego) na sygnał

analityczny 1×10^{-6} mol L^{-1} CFX. Zaobserwowano, że 1000-krotny nadmiar badanych interferentów nie powoduje zmiany intensywności sygnału CFX większej niż 10% wartości początkowej, podobnie jak dodatek 2 mg L^{-1} Tritonu X-100.

Tabela 8. Porównanie parametrów analitycznych procedur oznaczania CFX.

Elektroda	Metoda	Zakres liniowy [mol L^{-1}]	LOD [mol L^{-1}]	Zastosowanie	Lit.
rGO/PPR/ GCE	DPV	$2 \times 10^{-9} – 4 \times 10^{-4}$	2×10^{-9}	Surowica	[114]
MMWCNTs @MIP /CPE	DPV	$5 \times 10^{-9} – 8{,}5 \times 10^{-7}$	$1{,}7 \times 10^{-9}$	Preparaty farmaceutyczne, mocz, surowica	[115]
ChCl/CPE	SWV	$5 \times 10^{-9} – 2 \times 10^{-4}$	$3{,}6 \times 10^{-10}$	Krople do oczu, jaja, woda z rzeki	[116]
MIP/PGE	SWV	$1 \times 10^{-9} – 1 \times 10^{-3}$	$7{,}6 \times 10^{-11}$	Preparaty farmaceutyczne	[117]
Ag-β-CD/GCE	DPV	$1 \times 10^{-10} – 5 \times 10^{-8}$	$2{,}8 \times 10^{-11}$	Surowica, wody powierzchniowe	[118]
NPSPCE	DPAdSV	$5 \times 10^{-10} – 3 \times 10^{-8}$	$6{,}3 \times 10^{-11}$	Mocz, ścieki komunalne, ścieki szpitalne	[**RD10**]

rGO/PPR/GCE – GCE modyfikowana czerwienią polifenolową i zredukowanym tlenkiem grafenu; MMWCNTs@MIP/CPE – CPE modyfikowana MIP i magnetycznymi wielościennymi nanorurkami węglowymi; ChCl/CPE – CPE modyfikowana chlorkiem choliny; MIP/PGE – ołówkowa elektroda grafitowa modyfikowana MIP; Ag-β-CD/GCE – GCE nanocząstkami srebra modyfikowanymi β-cyklodekstryną

Użyteczność proponowanej procedury sprawdzono wykonując oznaczenia CFX w próbkach moczu ludzkiego, ścieków komunalnych i ścieków szpitalnych. Woltamperogramy otrzymane podczas analiz zaprezentowano na rysunkach 37C-E. Dzięki niskiej granicy wykrywalności możliwe było zminimalizowanie interferencji poprzez duże rozcieńczenie próbki. Ze względu na fakt, iż CFX osiąga w moczu stężenie rzędu 10^{-4}-10^{-6} mol L^{-1}, próbki rozcieńczono 10000-krotnie. W przypadku ścieków komunalnych i szpitalnych rozcieńczenia były odpowiednio 10- i 20-krotne. Wszystkie próbki analizowano metodą dodatku wzorca. Uzyskane wartości odzysków w przedziale 97,1-103,5% dowodzą niewielkiego wpływu matrycy próbek na sygnał analitycznych (Tabela 9). Ponadto, należy zauważyć, że możliwe było oznaczenie rzeczywistego stężenia CFX w próbkach ścieków szpitalnych.

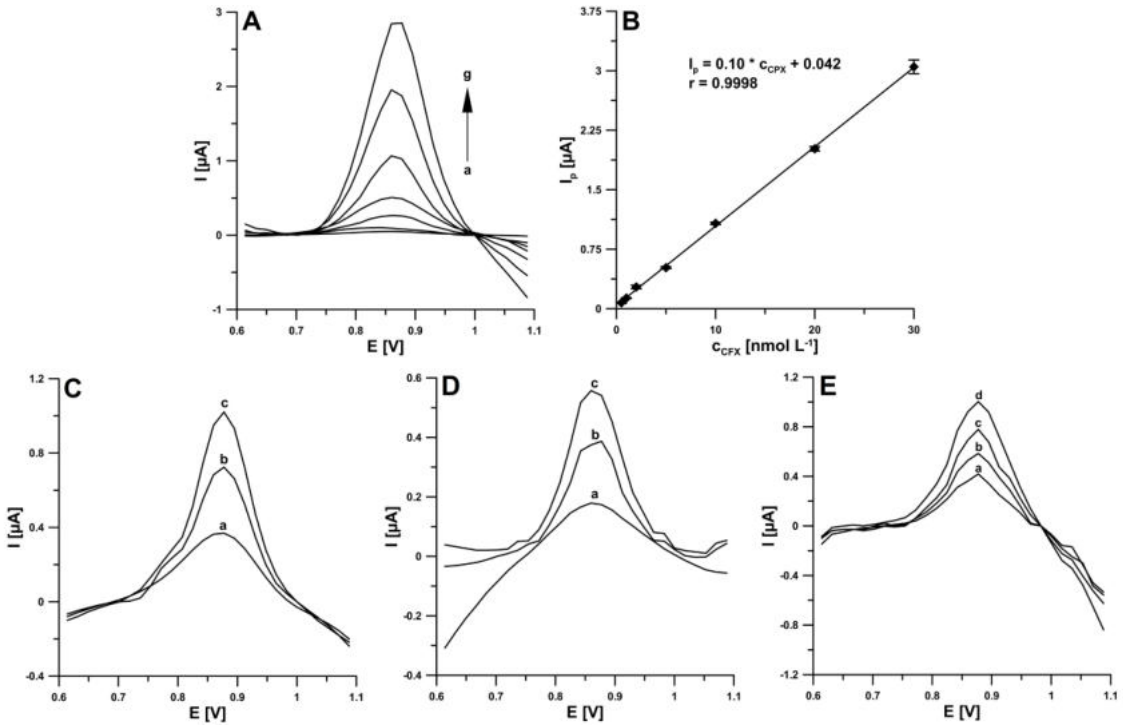

Rys. 37. A) Woltamperogramy otrzymane podczas oznaczania wzrastających stężeń CFX (a → g, 5×10^{-10} – 3×10^{-8} mol L^{-1}). B) Zakres liniowy krzywej kalibracyjnej CFX. Woltamperogramy otrzymane podczas oznaczania: C) CFX w próbce materiału odniesienia-moczu ludzkim: a) próbka + 2×10^{-9}, b) jak (a) + 2×10^{-9}, c) jak (a) + 4×10^{-9} mol L^{-1} CFX; D) CFX w próbce oczyszczonych ścieków komunalnych: a) próbka + 2×10^{-9}, b) jak (a) + 2×10^{-9}, c) jak (a) + 4×10^{-9} mol L^{-1} CFX; E) CFX w próbce ścieków szpitalnych: a) próbka, b) jak (a) + 5×10^{-9}, c) jak (a) + 1×10^{-8}, d) jak (a) + $1{,}5 \times 10^{-8}$ mol L^{-1} CFX [**RD10**].

Tabela 9. Wyniki oznaczania CFX.

Próbka	**Dodano [mol L^{-1}]**	**Oznaczono ± SD (n=3) [mol L^{-1}]**	**Odzysk* [%]**
Mocz ludzki (materiał odniesienia)	2×10^{-9}	$2{,}07 \times 10^{-9} \pm 0{,}08 \times 10^{-9}$	103,5
	5×10^{-9}	$4{,}92 \times 10^{-9} \pm 0{,}11 \times 10^{-9}$	98,4
Oczyszczone ścieki komunalne	2×10^{-9}	$1{,}96 \times 10^{-9} \pm 0{,}07 \times 10^{-9}$	98
	5×10^{-9}	$5{,}14 \times 10^{-9} \pm 0{,}11 \times 10^{-9}$	102,2
Ścieki szpitalne	0	$1{,}04 \times 10^{-8} \pm 0{,}05 \times 10^{-8}$	-
	5×10^{-9}	$1{,}5 \times 10^{-8} \pm 0{,}004 \times 10^{-8}$	97,1

4. Podsumowanie i wnioski

W ramach niniejszej rozprawy doktorskiej:

- Opracowano woltamperometryczne procedury oznaczania związków o działaniu przeciwnowotworowym (8-(4-metoksyfenylo)-4-okso-4,6,7,8-tetrahydroimidazo[2,1-c][1,2,4]triazyno-3-karboksylanu etylu - EIMTC [**RD1**] i 8-(4-chlorofenylo)-3-fenylo-7,8-dihydroimidazo[2,1-c][1,2,4]triazyno-4-(6H)-onu - 4-Cl-PIMT [**RD6**] na sitodrukowanej elektrodzie węglowej modyfikowanej warstwą nanowłókien węglowych (SPCE/CNFs), 3-(4-nitrofenylo)-8-(2,3-dimetylofenylo)-7,8-dihydroimidazo[2,1-c][1,2,4]triazyn-4(6H)-onu (NDIT) na sitodrukowanej elektrodzie węglowej modyfikowanej dodecylosiarczanem sodu (SPCE/SDS) [**RD8**], bleomycyny (BLM) na wstępnie przygotowanej elektrochemicznie sitodrukowanej elektrodzie węglowej modyfikowanej nanocząstkami ołowiu (pSPCE/PbNPs) [**RD7**]) i przeciwbólowym (paracetamolu (PA), diklofenaku (DF) i tramadolu (TR) na elektrochemicznie aktywowanej sitodrukowanej elektrodzie węglowej modyfikowanej SDS (aSPCE/SDS) [**RD2**]) oraz procedurę oznaczania antybiotyku ryfampicyny (RIF) na elektrochemicznie aktywowanej sitodrukowanej elektrodzie diamentowej domieszkowanej borem (aSPBDDE) [**RD3**], procedurę oznaczania testosteronu (TST) na pSPCE/PbNPs [**RD5**] oraz procedurę oznaczania związku przeciwpsychotycznego, tiorydazyny (TDZ) na sitodrukowanej elektrodzie złotej (SPAuE) [**RD9**].

- W publikacji przeglądowej [**RD4**] dokonano podsumowania danych literaturowych dotyczących woltamperometrycznych procedur oznaczania związków o właściwościach przeciwbólowych (paracetamolu, diklofenaku, tramadolu, ibuprofenu, ketoprofenu, naproksenu i kwasu acetylosalicylowego) w próbkach wód przy użyciu czujników sitodrukowanych.

- Wzmocnienie sygnałów analitycznych oznaczanych związków, poprawę ich kształtu i powtarzalności, jednocześnie minimalizując interferencje wynikające z obecności składników analizowanych próbek uzyskano dzięki elektrochemicznej aktywacji lub/i modyfikacji powierzchni elektrod sitodrukowanych warstwą nanowłókien węglowych, surfaktantem lub nanocząstkami ołowiu.

- Zmiany w strukturze i właściwościach elektrochemicznych czujników zbadano z wykorzystaniem szerokiej gamy technik instrumentalnych, takich jak skaningowa (SEM) i transmisyjna (TEM) mikroskopia elektronowa, profilometria optyczna, spektroskopia dyspersji energii promieniowania rentgenowskiego (EDS) oraz rentgenowska spektroskopia fotoelektronów (XPS), woltamperometria cykliczna (CV) i elektrochemiczna spektroskopia impedancyjna (EIS). Uzyskane wyniki wykazały, że elektrochemiczna aktywacja lub/i modyfikacja powierzchni przyczynia się do zmiany jej mikroskopowej struktury, zmniejszenie oporu przenoszenia ładunku (R_{ct}), zwiększenie powierzchni aktywnej (A_S) i poprawy efektywności przenoszenia elektronów, a tym samym do poprawy parametrów analitycznych opracowanych procedur.

- Określono charakter zachodzących procesów elektrodowych dla badanych związków. Stwierdzono, że w przypadku procedur oznaczania PA, DF, TST, 4-Cl-PIMT i TDZ proces elektrodowy ma charakter adsorpcyjny. Natomiast w opracowanej procedurze oznaczania RIF, BLM i NDIT mamy do czynienia z charakterem mieszanym, zaś w przypadku oznaczania EIMTC i TR z procesem dyfuzyjnym.

- Przeprowadzono ocenę selektywności opracowanych procedur. Wyznaczono nadmiary możliwych interferentów, które nie wpływają na zmianę sygnału analitycznego oznaczanych związków o więcej niż ±10%. W przypadku procedur oznaczania EIMTC [**RD1]** i 4-Cl-PIMT [**RD6**] wykorzystano układ przepływowy do analizy próbek surowicy. Umożliwiło to skuteczne usuwanie zanieczyszczeń i pozostałości produktów reakcji elektrodowej analitu po każdym pomiarze. W celu minimalizacji interferencji stosowano również wstępne odbiałczanie próbek, krótkie czasy nagromadzania analitów, modyfikacje powierzchni surfaktantem, dodatek do roztworu czynnika kompleksującego (soli sodowej kwasu pentetynowego, DTPA), czy duże rozcieńczenie próbek (możliwe dzięki bardzo niskim wartościom granic wykrywalności i oznaczalności).

- Wykonano pomiary do krzywych kalibracyjnych oznaczanych związków, wyznaczono zakresy liniowe oraz obliczono granice wykrywalności i oznaczalności. Stwierdzono, że zoptymalizowane procedury charakteryzują się

szerokimi zakresami liniowymi krzywych kalibracyjnych, a także pozwoliły uzyskać jedne z najniższych lub najniższe granice wykrywalności spośród woltamperometrycznych procedur opisanych w literaturze. W przypadku oznaczeń RIF ($2{,}2 \times 10^{-13}$ mol L^{-1}) [**RD3**] i BLM ($2{,}8 \times 10^{-11}$ mol L^{-1}) [**RD7**] obliczone granice wykrywalności są najniższymi jakie uzyskano na czujnikach sitodrukowanych, natomiast granica wykrywalności obliczona dla TDZ ($2{,}9 \times 10^{-12}$ mol L^{-1}) [**RD9**] jest najniższą spośród wszystkich opisanych woltamperometrycznych oznaczeń tego związku. Warto podkreślić, że procedury oznaczania RIF i BLM stanowią pierwsze zastosowania czujników sitodrukowanych w analizie tych związków. Ponadto, procedury oznaczania trzech związków o właściwościach przeciwnowotworowych – EIMTC [**RD1**], 4-Cl-PIMT [**RD6**] i NDIT [**RD8**] są pierwszymi metodami analizy ilościowej tych substancji.

- Potwierdzono praktyczną użyteczność opracowanych procedur do analizy wybranych związków w próbkach biologicznych (mocz, surowica) i środowiskowych (wody rzeczne, ścieki komunalne i ścieki szpitalne). W przypadku procedury oznaczania PA, DF i TR przeprowadzono również analizę preparatów farmaceutycznych. Należy podkreślić, że większość analizowanych próbek nie była poddawana przygotowaniu przed przystąpieniem do pomiarów. Próbki wód rzecznych i preparatów farmaceutycznych poddano jedynie filtracji, a próbki surowicy poddano odbiałczaniu. Wysokie wartości odzysków, zbliżone do 100% dowodzą minimalnego wpływu matrycy próbek na uzyskane sygnały analityczne. Zgodność wyników uzyskanych za pomocą opracowanych procedur z wynikami uzyskanymi przy użyciu metod porównawczych, takich jak wysokosprawna chromatografia cieczowa z detektorem diodowym (HPLC/PDA), ultrawysokosprawna chromatografia cieczowa sprzężona ze spektrometrią mas (UHPLC-ESI-MS) lub tandemowa spektrometria mas (UHPLC-ESI-MS/MS), potwierdza możliwość efektywnego wykorzystania opracowanych procedur do analizy próbek rzeczywistych.

- Wykonano dodatkowe badania pokazujące potencjał wykorzystania nanoporowatej sitodrukowanej elektrody węglowej (NPSPCE) w woltamperometrycznych oznaczeniach antybiotyku ciprofloksacyny (CFX) [**RD10**]. Elektrochemiczna aktywacja spowodowała wytworzenie porowatej

struktury elektrody pracującej. Przyczyniła się ona również do zwiększenia A_S, spadku R_{ct}, poprawy efektywności przenoszenia elektronów i wzmocnienia sygnału CFX. Obliczona granica wykrywalności ma najniższą wartością osiągniętą na czujnikach sitodrukowanych. Zoptymalizowaną procedurę zastosowano do oznaczania CFX w próbkach wody rzecznej, ścieków komunalnych i szpitalnych. Warto zaznaczyć, że jest to pierwszy przypadek oznaczenia rzeczywistego stężenia CFX w próbce ścieków szpitalnych**.**

5. Literatura

[1] K. Srivastava, S. S. Upadhyay, C. R. Rawool, N. S. Punde, A. S. Rajpurohit, Current Analytical Chemistry 15 (2019) 249.

[2] C. Batchelor-McAuley, E. Kätelhön, E.O. Barnes, R.G. Compton, E. Laborda, A. Molina, ChemistryOpen. 4 (2015) 224.

[3] J.R. Ortenero, N.P. Dugos, A.N. Soriano, E.M. T. Borres, A.M.T. Juan Sing, M.D. A. Pararuan, E.L. R. Tined, Applied Science and Engineering Progress 16 (2022) 5700.

[4] A. Martin Santos, A. Wong, A. Araújo Almeida, O. Fatibello-Filho, Talanta. 174 (2017) 610.

[5] E.P. Achterberg, M. Gledhill, K. Zhu, Molecular Sciences and Chemical Engineering, 2018.

[6] A. García-Miranda Ferrari, S.J. Rowley-Neale, C.E. Banks, Talanta Open 3 (2021) 100032.

[7] G. Paimard, E. Ghasali, M. Baeza, Chemosensors 11 (2023) 113.

[8] S. Singh, J. Wang, S. Cinti, ECS Sensor Plus 1 (2022) 023401.

[9] A. Sasal, K. Tyszczuk-Rotko, M. Wójciak, I. Sowa, Materials 13 (2020) 781.

[10] C.T. Fakude, O.A. Arotiba, F. Arduini, N. Mabuba, Electroanalysis 32 (2020) 2650.

[11] D. Antuña-Jiménez, M.B. González-García, D. Hernández-Santos, P. Fanjul-Bolado, Biosensors 10 (2020) 9.

[12] I. Seguro, P. Rebelo, J.G. Pacheco, C. Delerue-Matos, Sensors 22 (2022) 2819.

[13] M.M. El-Beshlawy, F.M. Abdel-Haleem, A.H. Kamel, A. Barhoum, Chemosensors 11 (2022) 3.

[14] W. Niamsi, N. Larpant, P.K. Kalambate, V. Primpray, C. Karuwan, N. Rodthongkum, W. Laiwattanapaisal, Biosensors 12 (2022) 852.

[15] T.A. Ali, Z.F. Akl, Journal of Radioanalytical Nuclar Chemistry 328 (2021) 267.

[16] V.A. Arlyapov, S.S. Kamanin, O.A. Kamanina, A.N. Reshetilov, Nanotechnologies in Russia 12 (2017) 658.

[17] D. Manoj, I. Auddy, S. Nimbkar, S. Chittibabu, S. Shanmugasundaram, International Journal of Food Science 2020 (2020) 1696201.

[18] X. Wang, Z. Zhang, G. Wu, C. Xu, J. Wu, X. Zhang, J. Liu, Analytical Methods. 14 (2022) 7.

[19] Q. Ye, Z. Zhang, J. Liu, X. Wang, Analytical Methods 14 (2022) 2961.
[20] J. Barton, M.B.G. García, D.H. Santos, P. Fanjul-Bolado, A. Ribotti, M. McCaul, D. Diamond, P. Magni, Microchimica Acta 183 (2016) 503.
[21] H.M. Mohamed, TrAC Trends in Analytical Chemistry. 82 (2016) 1.
[22] J. Barek, Chemosensors 9 (2021) 12.
[23] A.L. Squissato, R.A.A. Munoz, C.E. Banks, E.M. Richter, ChemElectroChem 7 (2020) 2211.
[24] N.F. Barros Azeredo, M.S. Ferreira Santos, J.R. Sempionatto, J. Wang, L. Angnes, Analytical Chemistry 94 (2022) 250.
[25] M.R. Housaindokht, F. Janati-Fard, N. Ashraf, Journal of Surfactants and Detergents 24 (2021) 873.
[26] R. Couto, M. Quinaz, Sensors 16 (2016) 1015.
[27] K. Tyszczuk-Rotko, I. Sadok, M. Barczak, Microporous and Mesoporous Materials 230 (2016) 109.
[28] A. Sasal, K. Tyszczuk-Rotko, M. Wójciak, I. Sowa, M. Kuryło, Materials. 13 (2020) 3091.
[29] M.M. Salim, S. Ashraf, H.M. Hashem, F. Belal, Scientific Reports 12 (2022) 14289.
[30] R. García-González, M.T. Fernández-Abedul, A. Costa-García, Talanta. 107 (2013) 376.
[31] M. Khasanah, M. Mudasir, A. Kuncaka, E. Sugiharto, G. Supriyanto, S. Wafiroh, Indonesian Journal of Chemistry 10 (2010) 295.
[32] S. Dehdashtian, B. Hashemi, Chemical Papers 74 (2020) 157.
[33] Y. Yang, Y. Peng, F. Zhao, B. Zeng, Sensors 3 (2003) 524.
[34] M. Ortúzar, M. Esterhuizen, D.R. Olicón-Hernández, J. González-López, E. Aranda, Frontiers in Microbiology 13 (2022) 869332.
[35] A. Szymonik, J. Lach, Inżynieria i Ochrona Środowiska, 15(3) (2012) 249.
[36] R.H. Perry, Physical Chemistry Chemical Physics 23 (2021) 1221.
[37] C. Nassour, S.J. Barton, S. Nabhani-Gebara, Y. Saab, J. Barker, Environmental Science and Pollution Research 27 (2020) 1339.
[38] D. Li, H. Chen, H. Liu, D. Schlenk, J. Mu, S. Lacorte, G.-G. Ying, L. Xie, Environment International 153 (2021) 106543.
[39] K. Sztanke, J. Rzymowska, M. Niemczyk, I. Dybała, A.E. Kozioł, European Journal of Medicinal Chemistry 41 (2006) 539.

[40] K. Sztanke, New Ethyl 7,8-Dihydro-6H-Imidazo[2,1-c][1,2,4]Triazine-4-oxo-3-Carboxylates and Method for Obtaining Them. Polish Patent 196751, 31 January 2008.

[41] M. Sztanke, J. Rzymowska, K. Sztanke, Molecular and Cellular Biochemistry 418 (2016) 179.

[42] K. Sztanke, K. Pasternak, M. Sztanke, M. Kandefer-Szerszeń, A.E. Kozioł, I. Dybała, Bioorganic & Medicinal Chemistry Letters 19 (2009) 5095.

[43] M. Sztanke, J. Rzymowska, M. Janicka, K. Sztanke, Arabian Journal of Chemistry 12 (2019) 4044.

[44] M. Sztanke, K. Sztanke, Derivatives of 3-(4-nitrophenyl)-7,8-dihydroimidazo[2,1-c][1,2,4]triazin-4(6H)-one Substituted by phenyl, alkylphenyl, dialkylphenyl and alkoxyphenyl, Method for Obtaining Them and Medical Application. Polish Patent PL 225419, 28 April 2017.

[45] L. Chiavassa, F. Camilo, M. La Scalea, Journal of the Brazilina Chemical Society 32 (2021) 889.

[46] G.K. Shiu, T.J. Goehl, W.H. Pitlick, Journal of Pharmaceutical Sciences. 68 (1979) 232.

[47] T. Miura, Journal of Biochemistry 157 (2015) 217.

[48] J. Galba, L. Veizerová, J. Piešťanský, M. Mego, L. Novotný, S. Dokupilová, K. Maráková, E. Havránek, P. Mikuš, Journal of Liquid Chromatography & Related Technologies. 38 (2015) 294.

[49] O. Falay, E. Öztürk, Y. Bölükbaşı, T. Gümüş, S. Örnek, M. Özbalak, M. Çetiner, O. Demirkol, B. Ferhanoğlu, Leukemia & Lymphoma. 58 (2017) 1114.

[50] V. Murray, J. Chen, L. Chung, International Journal of Molecular Sciences 19 (2018) 1372.

[51] Y. Li, C. Huang, J. Zheng, H. Qi, Talanta 103 (2013) 8.

[52] [1] J.M. Mack, E.C. Peterson, S.E. Crary, J.H. Moran, K. Neville, C.D. Pierce, G.T. Richter, Pediatric Blood & Cancer 69 (2022).

[53] S. Aydin, M.E. Aydin, A. Ulvi, Environmental Science and Pollution Research 26 (2019) 36887.

[54] E. Felis, K. Miksch, Water Science and Technology 60 (2009) 2253.

[55] F. Cao, Q. Dong, C. Li, J. Chen, X. Ma, Y. Huang, D. Song, C. Ji, Y. Lei, Sensors and Actuators B: Chemical 256 (2018) 143–150.

[56] K. Kimuam, N. Rodthongkum, N. Ngamrojanavanich, O. Chailapakul, N. Ruecha, Microchemical Journal 155 (2020) 104744.

[57] Z. Bagherinasab, H. Beitollahi, M. Yousefi, M. Bagherzadeh, M. Hekmati, Microchemical Journal 156 (2020) 104803.

[58] B. Nas, T. Dolu, S. Koyuncu, Water, Air & Soil Pollution 232 (2021) 127.

[59] X. Ma, Z. Wang, Processes 10 (2022) 124.

[60] A.F. Martins, T.G. Vasconcelos, D.M. Henriques, C.D.S. Frank, A. König, K. Kümmerer, Clean Soil Air Water 36 (2008) 264.

[61] M. Tilinca, G. Hancu, E. Mircia, D. Iriminescu, A. Rusu, R. A. Vlad, E. Barabas, Farmacia 65 (2017) 219.

[62] S. Kumar, P.J. Bouic, B. Rosenkranz, Acta Chromatographica 31 (2019) 92.

[63] A. Srivastava, D. Waterhouse, A. Ardrey, S.A. Ward, Journal of Pharmaceutical and Biomedical Analysis 70 (2012) 523.

[64] R. Lyubimenko, O.I. Gutierrez Cardenas, A. Turshatov, B.S. Richards, A.I. Schäfer, Applied Catalysis B: Environmental 291 (2021) 120097.

[65] R.N. Goyal, V.K. Gupta, S. Chatterjee, Analytica Chimica Acta 657 (2010) 147.

[66] A. Levent, A. Altun, Y. Yardım, Z. Şentürk, Electrochimica Acta 128 (2014) 54.

[67] L. Karadurmus, D. Kır, S. Kurbanoglu, S.A. Ozkan, Current Pharmaceutical Analysis 15 (2019) 413.

[68] A. Ensafi, P. Hedayati, M.M. Abarghoui, B. Rezaei, Electroanalysis 29 (2017) 2461.

[69] C. Koventhan, V. Vinothkumar, S.-M. Chen, P. Veerakumar, K.-C. Lin, Journal of Electroanalytical Chemistry 898 (2021) 115600.

[70] K. Sipa, M. Brycht, A. Leniart, P. Urbaniak, A. Nosal-Wiercińska, B. Pałecz, S. Skrzypek, Talanta 176 (2018) 625.

[71] M.I. González-Sánchez, B. Gómez-Monedero, J. Agrisuelas, J. Iniesta, E. Valero, Journal of Electroanalytical Chemistry 839 (2019) 75.

[72] M.I. González-Sánchez, B. Gómez-Monedero, J. Agrisuelas, J. Iniesta, E. Valero, Electrochemistry Communications 91 (2018) 36.

[73] H. Wei, J.-J. Sun, Y. Xie, C.-G. Lin, Y.-M. Wang, W.-H. Yin, G.-N. Chen, Analytica Chimica Acta 588 (2007) 297.

[74] X. Yuan, L. Ma, J. Zhang, Y. Zheng, Applied Surface Science 544 (2021) 148760.

[75] E. Pensa, E. Cortés, G. Corthey, P. Carro, C. Vericat, M.H. Fonticelli, G. Benítez, A.A. Rubert, R.C. Salvarezza, Accounts of Chemical Research 45 (2012) 1183.

[76] L.J. Opuchlik, J. Pawłowska, S. Sęk, R. Bilewicz, Journal of Electroanalytical Chemistry 825 (2018) 22.

[77] N.P. Shetti, S.J. Malode, S.T. Nandibewoor, Analytical Methods 7 (2015) 8673.

[78] D. K. Gosser, VCH: Ney York, NY, USA, 1993.

[79] M. Grabarczyk, A. Koper, Electroanalysis 23 (2011) 1442.

[80] M. Doulache, B. Saidat, M. Trari, Russian Journal of Electrochemistry 53 (2017) 461.

[81] S.B. Matt, S. Raghavendra, M. Shivanna, M. Sidlinganahalli, D.M. Siddalingappa, Journal of Inorganic and Organometallic Polymers and Materials 31 (2021) 511.

[82] A. Afkhami, H. Khoshsafar, H. Bagheri, T. Madrakian, Analytica Chimica Acta 831 (2014) 50.

[83] T. Teker, M. Aslanoglu, Microchemical Journal 158 (2020) 105234.

[84] T. Kokab, A. Shah, M.A. Khan, M. Arshad, J. Nisar, M.N. Ashiq, M.A. Zia, ACS Applied Nano Materials 4 (2021) 4699.

[85] B. Baniahmad, H. Hassani Nadiki, S. Jahani, N. Nezamabadi-Pour, A. Toolabi, M.M. Foroughi, Frontiers in Chemistry 10 (2022) 889590.

[86] L. Killedar, D. Ilager, N.P. Shetti, T.M. Aminabhavi, K. Raghava Reddy, Journal of Molecular Liquids. 340 (2021) 116891.

[87] T. Rohani, S.Z. Mohammadi, N. Gholamhosein Zadeh, M.B. Askari, Microchemical Journal 166 (2021) 106274.

[88] A. Afkhami, H. Ghaedi, T. Madrakian, M. Ahmadi, H. Mahmood-Kashani, Biosensors and Bioelectronics 44 (2013) 34.

[89] S. Kolahi-Ahari, B. Deiminiat, G.H. Rounaghi, Journal of Electroanalytical Chemistry 862 (2020) 113996.

[90] M.A. Mohamed, S.A. Atty, N.N. Salama, C.E. Banks, Electroanalysis 29 (2017) 1038.

[91] B. Deiminiat, G.H. Rounaghi, M.H. Arbab-Zavar, Sensors and Actuators B: Chemical 238 (2017) 651.

[92] Z. Jahromi, E. Mirzaei, A. Savardashtaki, M. Afzali, Z. Afzali, Microchemical Journal 157 (2020) 104942.

[93] P. Norouzi, R. Dinarvand, M. Reza Ganjali, A. Sadat Emami Meibodi, Analytical Letters 40 (2007) 2252.

[94] E. Sharafi, S. Sadeghi, New Journal of Chemistry 47 (2023) 500.

[95] K. Zhang, Y. Wang, H. Wang, F. Li, Y. Zhang, N. Zhang, Analytical Methods 14 (2022) 2304.

[96] K. Tyszczuk, M. Korolczuk, Electroanalysis 21 (2009) 101.

[97] N. Zhang, M. Brites Helu, K. Zhang, X. Fang, H. Yin, J. Chen, S. Ma, A. Fang, C. Wang, Nanomaterials 10 (2020) 391.

[98] S.Th. Girousi, I.Ch. Gherghi, M.K. Karava, Journal of Pharmaceutical and Biomedical Analysis 36 (2004) 851.

[99] K. Asadpour-Zeynali, F. Mollarasouli, Biosensors and Bioelectronics 92 (2017) 509.

[100] A. Levent, A. Altun, S. Taş, Y. Yardım, Z. Şentürk, Electroanalysis 27 (2015) 1219.

[101] L.A. Gugoasa, R.-I. Stefan-van Staden, B. Calenic, J. Legler, Journal of Molecular Recognition 28 (2015) 10.

[102] H. Fourou, M. Braiek, A. Bonhomme, F. Lagarde, A. Zazoua, N. Jaffrezic-Renault, Analytical Letters 51 (2018) 312.

[103] M.-H. Lee, J.L. Thomas, W.-C. Liu, Z.-X. Zhang, B.-D. Liu, C.-H. Yang, H.-Y. Lin, Microchimica Acta 186 (2019) 695.

[104] X. Tan, J. Hu, Q. Li, Analyst 122 (1997) 991.

[105] B.-C. Yin, D. Wu, B.-C. Ye, Analytical Chemistry 82 (2010) 8272.

[106] J. Chang, P. Gai, H. Li, F. Li, Talanta. 190 (2018) 492.

[107] S. Lu, M. Yang, X. Li, X. Liu, Y. Yin, Y. Cao, Amplified detection of bleomycin based on an electrochemically driven recycling strategy, Analytical Methods 6 (2014) 5573.

[108] G. Kesavan, M. Pichumani, S.-M. Chen, C.-J. Wu, Journal of Alloys and Compounds 885 (2021) 160880.

[109] A. Ferancova, E. Korgova, Journal of Electroanalytical Chemistry 492 (2000) 74.

[110] V. Vinothkumar, G. Kesavan, S.-M. Chen, Journal of Electroanalytical Chemistry 895 (2021) 115535.

[111] R. Sakthivel, S. Kubendhiran, S.-M. Chen, Journal of the Taiwan Institute of Chemical Engineers 111 (2020) 270.

[112] L. Fotouhi, Z. Atoofi, M.M. Heravi, Talanta 103 (2013) 194.

[113] A. Pollap, K. Baran, N. Kuszewska, J. Kochana, Journal of Electroanalytical Chemistry 878 (2020) 114574.

[114] R. Chauhan, A.A.S. Gill, Z. Nate, R. Karpoormath, Journal of Electroanalytical Chemistry. 871 (2020) 114254.

[115] H. Bagheri, H. Khoshsafar, S. Amidi, Y. Hosseinzadeh Ardakani, Analytical Methods 8 (2016) 3383.

[116] W.D. Adane, B.S. Chandravanshi, M. Tessema, Sensing and Bio-Sensing Research 39 (2023) 100547.

[117] C. Yan, J. Li, T. Meng, X. Liu, R. Zhang, Y. Chen, G. Wang, International Journal of Electrochemical Science (2016) 6466.

[118] A.A.S. Gill, S. Singh, Z. Nate, C. Pawar, R. Chauhan, N.B. Thapliyal, R. Karpoormath, R. Patel, Journal of Pharmaceutical and Biomedical Analysis 203 (2021) 114219.

6. Streszczenie w języku polskim

Niniejsza rozprawa doktorska obejmuje cykl 10 prac [**RD1-RD10**] (w tym 9 opublikowanych i 1 zaakceptowanej do druku) w czasopismach z listy filadelfijskiej o łącznym współczynniku wpływu IF równym 46,372 i 1440 punktach MEiN. Nadrzędnym celem badań było opracowanie woltamperometrycznych procedur oznaczania wybranych związków biologicznie czynnych, należących do grup substancji przeciwnowotworowych, przeciwbólowych, antybiotyków, hormonów i substancji psychotropowych, w próbkach środowiskowych i płynach ustrojowych z wykorzystaniem czujników sitodrukowanych. Cele szczegółowe dotyczyły między innymi poprawy parametrów czujników sitodrukowanych poprzez elektrochemiczną aktywację elektrody pracującej lub/i modyfikację jej powierzchni, charakterystyki otrzymanych czujników z wykorzystaniem szerokiej gamy technik, minimalizacji interferencji pochodzących od składników próbek i zastosowania opracowanych procedur w analizie próbek rzeczywistych.

Związki biologicznie czynne będące przedmiotem badań do niniejszej rozprawy doktorskiej występują w płynach ustrojowych na poziomie stężeń rzędu 10^{-5}-10^{-8} mol L^{-1}. Ponadto, większość z nich stanowi śladowe zanieczyszczenia środowiska wodnego (stężenia rzędu 10^{-9}-10^{-12} mol L^{-1}) i jest zagrożeniem dla organizmów wodnych, jak również organizmu człowieka. W oznaczeniach woltamperometrycznych stosuje się całą gamę elektrod pracujących, a dobór elektrody determinuje możliwość prowadzenia oznaczeń na niskich poziomach stężeń. W trakcie prowadzonych badań skupiono się na grupie czujników sitodrukowanych z uwagi na ich zalety, tzn. niski koszt produkcji, odpowiedni poziom odtwarzalności elektrod, dostępność oraz możliwość zastosowania w analizatorach przenośnych. W literaturze można odnaleźć prace dotyczące zastosowania tych czujników w analizie wybranych do niniejszej rozprawy grup związków. Niemniej jednak w większości przypadków uzyskane parametry analityczne nie pozwalają na oznaczanie rzeczywistych stężeń tych związków w płynach ustrojowych i próbkach środowiskowych. W związku z powyższym istotne wydaje się opracowanie woltamperometrycznych procedur oznaczania charakteryzujących się niższymi granicami wykrywalności i oznaczalności oraz lepszą selektywnością w porównaniu z metodami opisanymi w literaturze.

Opracowano woltamperometryczne procedury oznaczania związków o działaniu przeciwnowotworowym (8-(4-metoksyfenylo)-4-okso-4,6,7,8-

tetrahydroimidazo[2,1-c][1,2,4]triazyno-3-karboksylanu etylu - EIMTC [**RD1**] i 8-(4-chlorofenylo)-3-fenylo-7,8-dihydroimidazo[2,1-c][1,2,4]triazyno-4-(6H)-onu - 4-Cl-PIMT [**RD6**] na sitodrukowanej elektrodzie węglowej modyfikowanej warstwą nanowłókien węglowych (SPCE/CNFs), 3-(4-nitrofenylo)-8-(2,3-dimetylofenylo)-7,8-dihydroimidazo[2,1-c][1,2,4]triazyn-4(6H)-onu (NDIT) na sitodrukowanej elektrodzie węglowej modyfikowanej dodecylosiarczanem sodu (SPCE/SDS) [**RD8**], bleomycyny (BLM) na wstępnie przygotowanej elektrochemicznie sitodrukowanej elektrodzie węglowej modyfikowanej nanocząstkami ołowiu (pSPCE/PbNPs) [**RD7**]) i przeciwbólowym (paracetamolu (PA), diklofenaku (DF) i tramadolu (TR) na elektrochemicznie aktywowanej sitodrukowanej elektrodzie węglowej modyfikowanej SDS (aSPCE/SDS) [**RD2**]) oraz procedurę oznaczania antybiotyku ryfampicyny (RIF) na elektrochemicznie aktywowanej sitodrukowanej elektrodzie diamentowej domieszkowanej borem (aSPBDDE) [**RD3**], procedurę oznaczania testosteronu (TST) na pSPCE/PbNPs [**RD5**] oraz procedurę oznaczania związku przeciwpsychotycznego, tiorydazyny (TDZ) na sitodrukowanej elektrodzie złotej (SPAuE) [**RD9**]. Cykl prac wchodzących w skład niniejszej rozprawy doktorskiej zawiera również prace przeglądową [**RD4**], w której podsumowano woltamperometryczne procedury oznaczania związków o działaniu przeciwbólowym (paracetamolu, diklofenaku, tramadolu, ibuprofenu, ketoprofenu, naproksenu i kwasu acetylosalicylowego) z użyciem czujników sitodrukowanych. Opisane w literaturze procedury pogrupowano biorąc pod uwagę rodzaj stosowanych czujników sitodrukowanych (czujniki modyfikowane nanomateriałami węglowymi, modyfikowane polimerami oraz czujniki elektrochemicznie aktywowane).

W trakcie prowadzonych badań zoptymalizowano procedury przygotowania czujników i oznaczania wybranych związków. Zbadano jak na wartość natężenia prądu pików oznaczanych związków i ich powtarzalność wpływa szereg czynników takich jak: rodzaj i pH elektrolitu podstawowego, czas i potencjał nagromadzania analitu (w przypadku adsorpcyjnego i mieszanego procesu elektrodowego), a także parametry techniki rejestracji sygnału – woltamperometrii impulsowo-różnicowej (DPV) (amplitudę, szybkość rejestracji sygnału i czas modulacji) lub woltamperometrii fali prostokątnej (SWV) (amplitudę, krok potencjału i częstotliwość).

Elektrochemiczną aktywację lub/i modyfikację powierzchni elektrod sitodrukowanych surfaktantem lub nanocząstkami ołowiu zastosowano w celu wzmocnienia sygnałów analitycznych oznaczanych związków, poprawy powtarzalności

sygnałów i ich kształtu oraz minimalizacji interferencji od składników próbek. Zmiany w strukturze, składzie powierzchni i właściwościach elektrochemicznych czujnika potwierdzono na podstawie badań wykonanych z wykorzystaniem szerokiej gamy technik instrumentalnych, takich jak skaningowa (SEM) i transmisyjna (TEM) mikroskopia elektronowa, profilometria optyczna, spektroskopia dyspersji energii promieniowania rentgenowskiego (EDS) i rentgenowska spektroskopia fotoelektronów (XPS), woltamperometria cykliczna (CV) i elektrochemiczna spektroskopia impedancyjna (EIS). Poza wykazaniem zmian w morfologii powierzchni stwierdzono, że elektrochemiczna aktywacja lub/i modyfikacja powierzchni przyczynia się do zmniejszenia oporu przenoszenia ładunku (R_{ct}), zwiększenia powierzchni aktywnej (A_S) i poprawy efektywności przenoszenia elektronów.

Przy użyciu woltamperometrii cyklicznej określono także charakter procesów elektrodowych zachodzących na powierzchni stosowanych elektrod. Wykazano, że transport EIMTC do powierzchni SPCE/CNFs zachodzi na drodze dyfuzji, a związek ten redukuje się w sposób nieodwracalny dając jeden pik. Jeden pik zaobserwowano również w przypadku nieodwracalnej redukcji 4-Cl-PIMT na SPCE/CNFs i testosteronu na pSPCE/PbNPs, a także nieodwracalnego utleniania tiorydazyny na SPAuE. W tych czterech przypadkach stwierdzono adsorpcyjny charakter procesów elektrodowych. Podczas oznaczania bleomycyny na pSPCE/PbNPs rejestrowano trzy piki redukcji przy jednoczesnym braku piku utleniania, natomiast nieodwracalna redukcja NDIT na SPCE/SDS zachodziła dwustopniowo. W obu przypadkach charakter procesu elektrodowego określono jako mieszany. Charakter mieszany procesu elektrodowego stwierdzono również w przypadku utleniania ryfampicyny na aSPBDDE. Związek ten daje trzy piki anodowe i dwa katodowe. W przypadku procedury jednoczesnego oznaczania paracetamolu, diklofenaku i tramadolu charakter procesu elektrodowego określono rejestrując krzywe pojemności różniczkowej warstwy podwójnej na granicy faz elektroda/elektrolit podstawowy. Widoczne na krzywych piki desorpcji paracetamolu i diklofenaku potwierdzają adsorpcję tych związków na aSPCE/SDS, natomiast nie zaobserwowano piku desorpcji tramadolu, co świadczy o dyfuzyjnym charakterze procesu. W oparciu o badania własne lub dane literaturowe starano się przedstawić prawdopodobny mechanizm reakcji elektrodowych, jakim ulegają oznaczane związki.

Jednym z etapów prowadzonych badań było sprawdzenie selektywności opracowanych procedur. W tym celu badano wpływ wzrastających stężeń możliwych

interferentów (jonów metali i związków organicznych) na sygnał analityczny oznaczanych substancji. W przypadku procedury oznaczania EIMTC [**RD1**] i 4-Cl-PIMT [**RD6**] zastosowano układ przepływowy do analizy próbek surowicy. Pozwoliło to na wymycie zanieczyszczeń i pozostałości produktów reakcji elektrodowej analitu po każdym pomiarze. W celu minimalizacji interferencji stosowano również wstępne odbiałczanie próbek, krótkie czasy nagromadzania analitów, modyfikacje powierzchni surfaktantem, dodatek do roztworu czynnika kompleksującego (soli sodowej kwasu pentetynowego, DTPA), czy duże rozcieńczenie próbek (możliwe dzięki bardzo niskim wartościom granic wykrywalności i oznaczalności).

W trakcie prowadzonych badań wykonano pomiary do krzywych kalibracyjnych oznaczanych związków, obliczono granice wykrywalności i oznaczalności. Stwierdzono, że zoptymalizowane procedury charakteryzują się szerokimi zakresami liniowymi krzywych kalibracyjnych, a także jednymi z najniższych lub najniższymi granicami wykrywalności spośród woltamperometrycznych procedur opisanych w literaturze. Granice wykrywalności obliczone dla oznaczeń RIF ($2{,}2 \times 10^{-13}$ mol L^{-1}) [**RD3**] i BLM ($2{,}8 \times 10^{-11}$ mol L^{-1}) [**RD7**] są najniższymi jakie uzyskano na czujnikach sitodrukowanych. Natomiast granica wykrywalności obliczona dla TDZ ($2{,}9 \times 10^{-12}$ mol L^{-1}) [**RD9**] jest najniższą spośród wszystkich opisanych woltamperometrycznych oznaczeń tego związku. Należy podkreślić, że zaproponowane procedury oznaczania RIF i BLM są pierwszymi wykorzystującymi czujniki sitodrukowane. Ponadto, procedury oznaczania trzech związków o właściwościach przeciwnowotworowych – EIMTC [**RD1**], 4-Cl-PIMT [**RD6**] i NDIT [**RD8**], są pierwszymi sposobami analizy ilościowej tych substancji.

Celem potwierdzenia praktycznej użyteczności opracowanych procedur do analizy wybranych związków wykonano analizy próbek biologicznych (mocz, surowica) i środowiskowych (wody rzeczne, ścieki komunalne i ścieki szpitalne). W przypadku procedury oznaczania PA, DF i TR analizowano również preparaty farmaceutyczne. Warto nadmienić, że większość analizowanych próbek nie była w żaden sposób przygotowywana przed pomiarami. Próbki wód rzecznych i preparatów farmaceutycznych poddano jedynie filtracji, a próbki surowicy poddano odbiałczaniu. Wartość odzysków bliskie 100% świadczą o niewielkim wpływie matrycy próbek na sygnał analityczny. Zgodność wyników uzyskanych z tymi otrzymanymi z wykorzystaniem metod porównawczych (wysokosprawną chromatografią cieczową z detektorem diodowym (HPLC/PDA), ultrawysokosprawną chromatografią cieczową

sprzężoną ze spektrometrią mas (UHPLC-ESI-MS) lub tandemową spektrometrią mas (UHPLC-ESI-MS/MS)) świadczą o możliwości zastosowania opracowanych procedur w analizie próbek rzeczywistych.

Dodatkowe badania (praca zaakceptowana 26.09.2023r. w czasopiśmie Measurement) pokazały perspektywę wykorzystania nanoporowatej sitodrukowanej elektrody węglowej (NPSPCE) w woltamperometrycznych oznaczeniach antybiotyku ciprofloksacyny (CFX) [**RD10**]. Porowatą strukturę elektrody pracującej uzyskano dzięki elektrochemicznej aktywacji. Przyczynia się ona do spadku R_{ct}, zwiększenia A_S, poprawę efektywności przenoszenia elektronów i wzmocnienia sygnału CFX. Obliczona granica wykrywalności jest najniższą jaką uzyskano na czujnikach sitodrukowanych. Zoptymalizowaną procedurę zastosowano do oznaczania CFX w próbkach wody rzecznej, ścieków komunalnych i szpitalnych. Warto dodać, że po raz pierwszy przy użyciu czujników sitodrukowanych oznaczono rzeczywiste stężenie CFX w próbce ścieków szpitalnych.

7. Streszczenie w języku angielskim

This doctoral dissertation comprises series of 10 papers **[RD1-RD10]** (9 published and 1 accepted for publication) in journals indexed in the Philadelphia list, with a combined Impact Factor (IF) of 46.372 and 1440 points from the Polish Ministry of Education and Science. The primary goal of the research was to develop voltammetric procedures for the determination of selected biologically active compounds, belonging to groups of anticancer, analgesic, antibiotic, hormonal, and psychotropic substances, in environmental samples and body fluids using screen-printed sensors. Specific objectives included improving the parameters of screen-printed sensors through electrochemical activation of the working electrode and/or modification of its surface, characterizing the obtained sensors using various techniques, minimizing interferences from sample components, and applying the developed procedures to real sample analysis.

The biologically active compounds studied in this doctoral dissertation are present in body fluids at concentrations on the order of 10^{-5} to 10^{-8} mol L^{-1}. Moreover, most of them are trace contaminants in the aquatic environment (concentrations on the order of 10^{-9} to 10^{-12} mol L^{-1}), posing a threat to aquatic organisms as well as humans. A wide range of working electrodes is used in voltammetric determinations and the choice of electrode determines the possibility of conducting determinations at low concentration levels. The research focused on screen-printed sensors due to their advantages, such as low production cost, adequate electrode reproducibility, availability, and suitability for use in portable analyzers. Although the literature contains studies on the application of these sensors in the analysis of compounds related to this dissertation, in most cases the obtained analytical parameters do not allow for the determination of real concentrations of these compounds in body fluids and environmental samples. Therefore, it is crucial to develop voltammetric procedures with lower detection and quantification limits and better selectivity compared to methods described in the literature.

Voltammetric procedures were developed for the determination of compounds with anticancer activity (8-(4-methoxyphenyl)-4-oxo-4,6,7,8-tetrahydroimidazo[2,1-c][1,2,4]triazin-3-ethyl carboxylate - EIMTC **[RD1]** and 8-(4-chlorophenyl)-3-phenyl-7,8-dihydroimidazo[2,1-c][1,2,4]triazin-4(6H)-one - 4-Cl-PIMT **[RD6]** on a screen-printed carbon electrode modified with carbon nanofibers (SPCE/CNFs), 3-(4-

nitrophenyl)-8-(2,3-dimethylphenyl)-7,8-dihydroimidazo[2,1-c][1,2,4]triazin-4(6H)-one (NDIT) on a screen-printed carbon electrode modified with sodium dodecyl sulfate (SPCE/SDS) **[RD8]**, bleomycin (BLM) on an electrochemically pretreated screen-printed carbon electrode modified with lead nanoparticles (pSPCE/PbNPs) **[RD7]**, and analgesic compounds (paracetamol (PA), diclofenac (DF) and tramadol (TR)) on an electrochemically activated screen-printed carbon electrode modified with SDS (aSPCE/SDS) **[RD2]**, as well as a procedure for the determination of the antibiotic rifampicin (RIF) on an electrochemically activated boron-doped diamond screen-printed electrode (aSPBDDE) **[RD3]**. This also includes procedures for the determination of testosterone (TST) on pSPCE/PbNPs [RD5] and the antipsychotic compound thioridazine (TDZ) on a screen-printed gold electrode (SPAuE) **[RD9]**.

The research also included a review paper **[RD4]** summarizing voltammetric procedures for the determination of analgesic compounds (paracetamol, diclofenac, tramadol, ibuprofen, ketoprofen, naproxen, and acetylsalicylic acid) using screen-printed sensors. The described procedures were categorized based on the type of screen-printed sensors used (sensors modified with carbon nanomaterials, modified with polymers and electrochemically activated sensors).

During the research, the procedures for sensor preparation and compound determination were optimized. The influence of various factors, such as the type and pH of the supporting electrolyte, accumulation time and potential (for adsorptive and mixed electrode processes), and signal registration parameters (differential pulse voltammetry (DPV – amplitude, scan rate and modulation time) or square-wave voltammetry (SWV) – amplitude, step potential and frequency), was investigated with respect to the current intensity of the analyte peaks and their repeatability.

Electrochemical activation and/or modification of the screen-printed electrode surface with surfactants or lead nanoparticles were employed to enhance the analytical signals of the determined compounds, improve the repeatability and shape of the signals, and minimize interference from sample components. Changes in the structure, surface composition, and electrochemical properties of the sensors were confirmed using a wide range of instrumental techniques, including scanning (SEM) and transmission (TEM) electron microscopy, optical profilometry, energy-dispersive X-ray spectroscopy (EDS) and X-ray photoelectron spectroscopy (XPS), cyclic voltammetry (CV), and electrochemical impedance spectroscopy (EIS). In addition to changes in surface morphology, it was observed that electrochemical activation and/or

modification of the surface contributed to a decrease in charge transfer resistance (R_{ct}), an increase in active surface area (A_S), and improved electron transfer efficiency.

The electrochemical processes occurring on the surface of the employed electrodes were determined using cyclic voltammetry. It was found that the transport of EIMTC to the SPCE/CNFs surface occurs through diffusion, and this compound is irreversibly reduced to give a single peak. Irreversible reduction was also observed for 4-Cl-PIMT on SPCE/CNFs, testosterone on pSPCE/PbNPs, and irreversible oxidation of thioridazine on SPAuE. In these four cases, the electrochemical process was characterized as adsorptive. During the determination of bleomycin on pSPCE/PbNPs, three reduction peaks were observed in the absence of an oxidation peak, while the irreversible reduction of NDIT on SPCE/SDS occurred in two steps. In both cases, the electrochemical process was classified as mixed. A mixed electrochemical process was also observed during the oxidation of rifampicin on aSPBDDE, which exhibited three anodic peaks and two cathodic peaks. In the simultaneous determination of paracetamol, diclofenac, and tramadol, the nature of the electrochemical process was determined by recording differential capacity curves at the electrode/supporting electrolyte interface. The desorption peaks of paracetamol and diclofenac confirmed the adsorption of these compounds on aSPCE/SDS, while no desorption peak was observed for tramadol, indicating a diffusive process. Based on the conducted research and available literature data, an attempt was made to propose the likely mechanism of the electrochemical reactions undergone by the determined compounds.

One of the stages of the research was to test the selectivity of the developed procedures. To achieve this, the influence of increasing concentrations of potential interferents (metal ions and organic compounds) on the analytical signal of the determined substances was examined. For the determination procedures of EIMTC **[RD1]** and 4-Cl-PIMT **[RD6]**, a flow system was applied to analyze serum samples, allowing for the removal of impurities and remnants of the reaction products of the analyte after each measurement. To minimize interferences, pre-deproteination of the samples, short accumulation times, surface modifications with surfactants, the addition of complexing agents (sodium pentethenate, DTPA) to the solution, and dilution of the samples were employed due to the very low detection and quantification limits.

During the research, calibration curves for the determined compounds were constructed, and detection and quantification limits were calculated. The optimized procedures were found to have broad linear ranges in the calibration curves and some of

the lowest detection limits among voltammetric procedures described in the literature. The detection limits calculated for RIF (2.2×10^{-13} mol L^{-1}) **[RD3]** and BLM (2.8×10^{-11} mol L^{-1}) **[RD7]** are the lowest achieved on screen-printed sensors. Furthermore, the detection limit calculated for TDZ (2.9×10^{-12} mol L^{-1}) **[RD9]** is the lowest among all described voltammetric determinations of this compound. It is worth noting that the proposed determination procedures for RIF and BLM are the first to utilize screen-printed sensors. Additionally, the procedures for the determination of three compounds with anticancer properties – EIMTC **[RD1]**, 4-Cl-PIMT **[RD6]**, and NDIT **[RD8]** – represent the first quantitative methods for the analysis of these substances.

To confirm the practical usefulness of the developed procedures for the analysis of selected compounds, analyses of biological (urine, serum) and environmental (river water, municipal sewage, and hospital sewage) samples were performed. In the case of the determination procedure for PA, DF, and TR, pharmaceutical formulations were also analyzed. It is worth mentioning that most of the analyzed samples were not subjected to any preparation before measurements. River water and pharmaceutical formulations were only filtered, and serum samples were only deproteinated. The recoveries close to 100% indicate minimal interference from the sample matrix on the analytical signal. The agreement between the results obtained with the developed procedures and those obtained using comparative methods (high-performance liquid chromatography with a diode array detector (HPLC/PDA), ultra-high-performance liquid chromatography coupled with mass spectrometry (UHPLC-ESI-MS), or tandem mass spectrometry (UHPLC-ESI-MS/MS)) demonstrates the potential for the application of the developed procedures in the analysis of real samples.

Additional research (The paper was accepted on September 26, 2023, in the Measurement journal.) revealed the prospect of using nanoporous screen-printed carbon electrodes (NPSPCE) in voltammetric determinations of the antibiotic ciprofloxacin (CFX) [**RD10**]. The porous structure of the working electrode was achieved through electrochemical activation, contributing to a decrease in R_{ct}, an increase in A_S, improved electron transfer efficiency, and enhanced CFX signal. The calculated detection limit is the lowest achieved on screen-printed sensors. The optimized procedure was applied to determine CFX in samples of river water, municipal sewage, and hospital sewage. It is worth adding that, for the first time, real CFX concentrations were determined using screen-printed sensors in hospital sewage samples.

8. Osiągnięcia naukowe

W tabeli 10 podsumowano osiągniecia naukowe uzyskane w trakcie studiów doktoranckich.

Tabela 10. Podsumowanie osiągnięć naukowych.

Prace naukowe			
Liczba artykułów naukowych:		**IF**	**Punkty MEiN**
a) wchodzących w skład rozprawy doktorskiej	10	46,372	1440
b) niewchodzących w skład rozprawy doktorskiej.	4	14,886	440
Łącznie	**14**	**61,258**	**1880**
Rozdziały w monografiach	9 (łączna liczba punktów MEiN – 180)		
Prezentacje wyników			
Liczba prezentacji:			
a) międzynarodowych			
- poster	5		
b) krajowych			
- komunikat	6		
- poster	17*		
Łącznie	**28**		

* Wyróżnienie posteru pt. „Zastosowanie modyfikowanego czujnika sitodrukowanego w analizie EIMTC – związku o właściwościach przeciwnowotworowych”, VII Ogólnopolska konferencja naukowa Innowacje w Praktyce – 20.10.2020 r., Lublin;

Spis publikacji niewchodzących w skład rozprawy doktorskiej:

1. I. Sadok, K. Tyszczuk-Rotko, R. Mroczka, **J. Kozak**, M. Staniszewska**,** *Improved voltammetric determination of kynurenine at the Nafion covered glassy carbon electrode – application in samples delivered from human cancer cells*, International Journal of Tryptophan Research, 14 (2021) 1-14.

   ($IF_{2021-2022}$ = 4,4 MEiN = 100 pkt.)

2. K. Tyszczuk-Rotko, **J. Kozak**, A. Węzińska, *Electrochemically activated screen-printed carbon electrode for determination of ibuprofen*, Applied Sciences 11 (21) (2021) 9908–9915.

   (IF_{2021} = 2,838 MEiN = 100 pkt.)

3. K. Tyszczuk-Rotko, R. Olchowski, **J. Kozak**, O. Sekerzh-Zenkovich, R. Dobrowolski, *Modified mesoporous carbon material (Pb-N-CMK-3) obtained by a hard-templating route, dicyandiamide impregnation and electrochemical lead particles deposition as an electrode material for the U(VI) ultratrace determination*, Materials 14 (21) (2021) 6490–6504.

   (IF_{2021} = 3,748 MEiN = 140 pkt.)

4. K. Tyszczuk-Rotko, D. Gorylewski, **J. Kozak**, *Supporting electrolyte manipulation for simple improvement of the sensitivity of trace vanadium(V) determination at a lead-coated glassy carbon electrode*, Sensors 22 (21) (2022) 8209-8220.

   (IF_{2022} = 3,9 MEiN = 100 pkt.)

Rozdziały w monografiach:

1. K. Tyszczuk-Rotko, A. Sasal, **J. Kozak**, M. Rotko, *Czujniki sitodrukowane – przygotowanie, charakterystyka i zastosowanie*, Nauka i przemysł – metody spektroskopowe w praktyce, nowe wyzwania i możliwości, UMCS, Lublin 2020, str. 189-198, ISBN 978-83-227-9369-5.

2. **J. Kozak**, K. Tyszczuk-Rotko, A. Sasal, *Nowy węglowy czujnik sitodrukowany w analizie śladowej talu(I)*, Nauka i przemysł – lubelskie spotkania studenckie, UMCS, Lublin 2020, str. 112-114, ISBN 978-83-227-9370-1.

3. A. Sasal, K. Tyszczuk-Rotko, **J. Kozak**, *Woltamperometryczna metoda oznaczania diklofenaku na elektrodzie sitodrukowanej modyfikowanej nanorurkami węglowymi*, Nauka i przemysł – lubelskie spotkania studenckie, UMCS, Lublin 2020, str. 234-236, ISBN 978-83-227-9370-1.

4. **J. Kozak**, K. Tyszczuk-Rotko, *Czujniki sitodrukowane w jednoczesnej analizie paracetamolu, diklofenaku i tramadolu*, Nauka i przemysł – lubelskie spotkania studenckie, UMCS, Lublin 2021, str. 115-118, ISBN 9788322795033.

5. K. Tyszczuk-Rotko, A. Sasal, **J. Kozak**, *Zastosowanie czujników sitodrukowanych w analizie śladowej pozostałości farmaceutyków w próbkach wód*, Nauka i przemysł – metody spektroskopowe w praktyce, nowe wyzwania i możliwości, UMCS, Lublin 2021, str. 65-68, ISBN 978-83-227-9504-0.

6. **J. Kozak**, K. Tyszczuk-Rotko, D. Gorylewski, *Wykorzystanie technik woltamperometrycznych w analizie śladowej testosteronu,* Nauka i przemysł – lubelskie spotkania studenckie, UMCS, Lublin 2022, str. 115-118, ISBN 978-83-227-9603-0.

7. D. Gorylewski, K. Tyszczuk-Rotko, **J. Kozak**, *Związki przeciwwirusowe – właściwości, zastosowanie i analiza z wykorzystaniem technik woltamperometrycznych*, Nauka i przemysł – lubelskie spotkania studenckie, UMCS, Lublin 2022, str. 115-118, ISBN 978-83-227-9603-0.

8. D. Gorylewski, K. Tyszczuk-Rotko, **J. Kozak**, *Elektrochemiczne procedury oznaczania związku arsenoorganicznego – roksarsonu*, Nauka i przemysł – lubelskie spotkania studenckie, UMCS, Lublin 2023, str. 164-166, ISBN 9788322797013.

9. **J. Kozak**, K. Tyszczuk-Rotko, D. Gorylewski, *Wykorzystanie technik woltamperometrycznych w analizie antybiotyków*, Nauka i przemysł – lubelskie spotkania studenckie, UMCS, Lublin 2023, str. 144-147, ISBN 9788322797013.

Wykaz posterów i prezentacji wygłoszonych na konferencjach i sympozjach naukowych o zasięgu krajowym i międzynarodowym:

1. **J. Kozak**, K. Tyszczuk-Rotko, A. Sasal, *Woltamperometryczna procedura oznaczania Tl(I) z użyciem modyfikowanego czujnika sitodrukowanego*, VII Ogólnopolska konferencja naukowa INNOWACJE W PRAKTYCE – 20.10.2020 r., Lublin (poster);
2. **J. Kozak**, K. Tyszczuk-Rotko, A. Sasal, *Zastosowanie modyfikowanego czujnika sitodrukowanego w analizie EIMTC – związku przeciwnowotworowego,* VII Ogólnopolska konferencja naukowa INNOWACJE W PRAKTYCE – 20.10.2020 r., Lublin (poster);
3. **J. Kozak**, K. Tyszczuk-Rotko, A. Sasal, *Zastosowanie modyfikowanych czujników sitodrukowanych w analizie śladowej talu(I),* XVII Konferencja z cyklu "Elektroanaliza w teorii i praktyce" – 19-20.11.2020 r., on-line (poster);
4. **J. Kozak**, K. Tyszczuk-Rotko, A. Sasal, *Woltamperometryczna procedura oznaczania EIMTC – nowego związku o właściwościach przeciwnowotworowych,* XVII Konferencja z cyklu "Elektroanaliza w teorii i praktyce" – 19-20.11.2020 r., on-line (poster);
5. **J. Kozak**, K. Tyszczuk-Rotko, *Woltamperometryczna procedura jednoczesnego oznaczania paracetamolu, diklofenaku i tramadolu z wykorzystaniem czujników sitodrukowanych,* II edycja Konferencji dla Młodych Naukowców nt. Biologia, Chemia i Środowisko - SPOJRZENIE MŁODYCH NAUKOWCÓW, 24-25.04.2021 r., Kraków, on-line (prezentacja ustna);
6. **J. Kozak**, K. Tyszczuk-Rotko, *Modyfikowany czujnik sitodrukowany do ilościowego oznaczania nowego związku o właściwościach przeciwnowotworowych,* II edycja Konferencji dla Młodych Naukowców nt. Biologia, Chemia i Środowisko - SPOJRZENIE MŁODYCH NAUKOWCÓW, 24-25.04.2021 r., Kraków, on-line (poster);
7. **J. Kozak**, K. Tyszczuk-Rotko, *Czujniki sitodrukowane w jednoczesnej analizie paracetamolu, diklofenaku i tramadolu*, IX Ogólnopolskie Sympozjum „Nauka i przemysł – lubelskie spotkania studenckie", 28.06.2021 r., Lublin, on-line (poster);

8. **J. Kozak**, K. Tyszczuk-Rotko, M. Sztanke, K. Sztanke, I. Sadok, *Determination of promising anticancer agent candidate using screen-printed carbon sensor modified with carbon nanofibers*, 3rd International Workshop on Functional Nanostructured Materials, 6-8.10.2021 r., Kraków, on-line (poster);

9. **J. Kozak**, K. Tyszczuk-Rotko, M. Wójciak, I. Sowa, M. Rotko, *Application of electrochemically activated screen-printed boron-doped diamond electrode for quantification of rifampicin*, 3rd International Workshop on Functional Nanostructured Materials, 6-8.10.2021 r., Kraków, on-line (poster);

10. **J. Kozak**, K. Tyszczuk-Rotko, *Woltamperometryczna procedura oznaczania ryfampicyny z wykorzystaniem elektrochemicznie aktywowanego czujnika sitodrukowanego,* XI Polska Konferencja Chemii Analitycznej, 19-23.06.2022 r., Łódź (prezentacja ustna);

11. **J. Kozak**, K. Tyszczuk-Rotko, D. Gorylewski, *Pierwsza metoda analityczna oznaczania nowego związku o właściwościach przeciwnowotworowych,* XI Polska Konferencja Chemii Analitycznej, 19-23.06.2022 r., Łódź (poster);

12. **J. Kozak**, K. Tyszczuk-Rotko, D. Gorylewski, *Wykorzystanie technik woltamperometrycznych w analizie śladowej testosteronu*, X Ogólnopolskie Sympozjum „Nauka i przemysł – lubelskie spotkania studenckie", 27.06.2022 r., Lublin (prezentacja ustna);

13. D. Gorylewski, K. Tyszczuk-Rotko, **J. Kozak**, *Związki przeciwwirusowe – właściwości, zastosowanie i analiza z wykorzystaniem technik woltamperometrycznych*, X Ogólnopolskie Sympozjum „Nauka i przemysł – lubelskie spotkania studenckie", 27.06.2022 r., Lublin (poster);

14. **J. Kozak**, K. Tyszczuk-Rotko, D. Gorylewski, *Modified screen-printed sensor for determination of anticancer drug candidate*, I Międzynarodowa Konferencja Doktorantów pt. „ŚRODOWISKO-ROŚLINA-ZWIERZĘ-PRODUKT", 26.04.2022 r., Lublin (poster);

15. K. Tyszczuk-Rotko, **J. Kozak**, D. Gorylewski, M. Rotko, *The determination of Cr(VI) using catalytic adsorptive stripping voltammetric technique*, 15th Pannonian International Symposium on Catalysis, 4-8.09.2022 r., Jastrzębia Góra (poster);

16. K. Tyszczuk-Rotko, B. Czech, D. Gorylewski, **J. Kozak**, M. Rotko, *Voltammetric procedurę for U(VI) determination with the use of TiO_2/Al_2O_3 photocatalyst*, 15th Pannonian International Symposium on Catalysis, 4-8.09.2022 r., Jastrzębia Góra (poster);

17. **J. Kozak**, K. Tyszczuk-Rotko, D. Gorylewski, *Zastosowanie elektrochemicznie aktywowanego czujnika sitodrukowanego w analizie śladowej ryfampicyny*, 64. Zjazd Polskiego Towarzystwa Chemicznego, 11-16.09.2022 r., Lublin (prezentacja ustna);

18. D. Gorylewski, K. Tyszczuk-Rotko, **J. Kozak**, *Wanad – właściwości, zastosowanie i analiza woltamperometryczna*, 64. Zjazd Polskiego Towarzystwa Chemicznego, 11-16.09.2022 r., Lublin (prezentacja ustna);

19. D. Gorylewski, K. Tyszczuk-Rotko, **J. Kozak**, *Nowa, bardzo czuła woltamperometryczna procedura oznaczania wanadu(V) z wykorzystaniem elektrody z węgla szklistego modyfikowanej błonką ołowiu*, IX Ogólnopolska Konferencja Naukowa Innowacje w Praktyce, 20-21.10.2022 r., Lublin (poster);

20. D. Gorylewski, K. Tyszczuk-Rotko, **J. Kozak**, *Czujnik sitodrukowany modyfikowany nanowłóknami węglowymi w analizie nowego związku przeciwnowotworowego*, IX Ogólnopolska Konferencja Naukowa Innowacje w Praktyce, 20-21.10.2022 r., Lublin (poster);

21. D. Gorylewski, K. Tyszczuk-Rotko, **J. Kozak**, *Zastosowanie woltamperometrii stripingowej do analizy śladowej V(V) – wykorzystanie elektrody GCE/PbFE*, III Ogólnopolska Studencka Konferencja Naukowa „Bliżej Chemii", 7-8.01.2023 r., on-line (poster);

22. D. Gorylewski, K. Tyszczuk-Rotko, **J. Kozak**, *Wykorzystanie prostego w przygotowaniu czujnika GCE/CTAB do woltamperometrycznego oznaczania śladowych ilości roksarsonu*, Fizykochemia Granic Faz – Metody Instrumentalne, 16-20.04.2023 r., Lublin (prezentacja ustna);

23. K. Tyszczuk-Rotko, **J. Kozak**, D. Gorylewski, *Woltamperometryczna procedura oznaczania tiorydazyny z wykorzystaniem czujnika sitodrukowanego*, Krakowska Konferencja Węglowa Krak-C, 25-26.05.2023 r., Kraków (poster);

24. K. Tyszczuk-Rotko, D. Gorylewski, **J. Kozak**, *Czuła i selektywna woltamperometryczna procedura oznaczania roksarsonu w próbkach środowiskowych*, Krakowska Konferencja Węglowa Krak-C, 25-26.05.2023 r., Kraków (poster);

25. **J. Kozak**, K. Tyszczuk-Rotko, D. Gorylewski, Wykorzystanie technik woltamperometrycznych w analizie antybiotyków, XI Ogólnopolskie Sympozjum „Nauka i przemysł – lubelskie spotkania studenckie", 26.06.2023 r., Lublin (poster);

26. D. Gorylewski, K. Tyszczuk-Rotko, **J. Kozak**, Elektrochemiczne procedury oznaczania związku arsenoorganicznego – roksarsonu, XI Ogólnopolskie Sympozjum „Nauka i przemysł – lubelskie spotkania studenckie", 26.06.2023 r., Lublin (poster);

27. **J. Kozak**, K. Tyszczuk-Rotko, D. Gorylewski, Aleksy Keller, *Zastosowanie sitodrukowanej elektrody złotej w woltamperometrycznych oznaczeniach tiorydazyny*, 65. Zjazd Polskiego Towarzystwa Chemicznego, 18-22.09.2023 r., Toruń (poster);

28. **J. Kozak**, K. Tyszczuk-Rotko, D. Gorylewski, Aleksy Keller, *Elektrochemicznie aktywowane czujniki sitodrukowane w analizie śladowej antybiotyków*, 65. Zjazd Polskiego Towarzystwa Chemicznego, 18-22.09.2023 r., Toruń (poster);

9. Inne osiągnięcia

1. Zagraniczny staż naukowy w Uniwersytecie w Pardubicach (Czechy) w ramach projektu „PROM – Międzynarodowa wymiana stypendialna doktorantów i kadry akademickiej” (19-23.09.2022 r.), opiekun stażu: dr Radovan Metelka;
2. Stypendium za osiągnięcia naukowe z Własnego Funduszu Stypendialnego UMCS w Lublinie, uzyskane w roku akademickim 2022/2023;
3. Nagroda za zajęcie I miejsca w konkursie „Ad astra” dla wybitnych młodych naukowców UMCS w Lublinie za osiągnięcia naukowe z lat 2021-2022 w kategorii Nauki Ścisłe i Przyrodnicze.

ANEKS – TEKSTY PUBLIKACJI BĘDĄCYCH PRZEDMIOTEM ROZPRAWY DOKTORSKIEJ I OŚWIADCZENIA WSPÓŁAUTORÓW

RD1

K. Tyszczuk-Rotko, **J. Kozak**, M. Sztanke, K. Sztanke, I. Sadok, *A screen-printed sensor coupled with flow system for quantitative determination of a novel promising anticancer agent candidate*, Sensors, 20 (18) (2020) 5217-5227.

sensors

MDPI

Article

A Screen-Printed Sensor Coupled with Flow System for Quantitative Determination of a Novel Promising Anticancer Agent Candidate

Katarzyna Tyszczuk-Rotko [1,*], Jędrzej Kozak [1], Małgorzata Sztanke [2], Krzysztof Sztanke [3] and Ilona Sadok [4]

1 Faculty of Chemistry, Institute of Chemical Sciences, Maria Curie-Skłodowska University in Lublin, 20-031 Lublin, Poland; jedrekkozak@onet.pl
2 Chair and Department of Medical Chemistry, Medical University of Lublin, 20-093 Lublin, Poland; malgorzata.sztanke@umlub.pl
3 Laboratory of Bioorganic Synthesis and Analysis, Chair and Department of Medical Chemistry, Medical University of Lublin, 20-093 Lublin, Poland; krzysztofsztanke@umlub.pl
4 Laboratory of Separation and Spectroscopic Method Application, Centre for Interdisciplinary Research, Faculty of Science and Health, The John Paul II Catholic University of Lublin, 20-708 Lublin, Poland; ilona.sadok@kul.pl
* Correspondence: ktyszczuk@poczta.umcs.lublin.pl

Received: 23 August 2020; Accepted: 11 September 2020; Published: 13 September 2020

Abstract: A carbon nanofibers modified screen-printed carbon sensor (SPCE/CNFs) was applied for the determination of a novel promising anticancer agent candidate (ethyl 8-(4-methoxyphenyl)-4-oxo-4,6,7,8-tetrahydroimidazo[2,1-*c*][1,2,4]triazine-3-carboxylate, EIMTC) using square-wave voltammetry (SWV). It is the first method for the quantitative determination of EIMTC. The modified screen-printed sensor exhibited excellent electrochemical activity in reducing EIMTC. The peak current of EIMTC was found to be linear in two concentration ranges of 2.0×10^{-9} – 2.0×10^{-8} mol L^{-1} and 2.0×10^{-8} – 2.0×10^{-7} mol L^{-1}, with a detection limit of 5.0×10^{-10} mol L^{-1}. The connection of flow-cell for the SPCE/CNFs with SWV detection allowed for the successful determination of EIMTC in human serum samples. Ultra-high-performance liquid chromatography coupled to electrospray ionization triple quadrupole mass spectrometry (UHPLC-ESI-MS/MS) acted as a comparative method in the serum samples analysis.

Keywords: anticancer agent candidate; voltammetric analysis; screen-printed sensor; flow system; liquid chromatography

1. Introduction

Ethyl 8-(4-methoxyphenyl)-4-oxo-4,6,7,8-tetrahydroimidazo[2,1-*c*][1,2,4]triazine-3-carboxylate (PubChem CID: 11507951), namely EIMTC (Figure 1), is an interesting electroactive small molecule for our current electrochemical research needs. EIMTC has been shown to possess a fully defined molecular structure, and a low toxicity in vitro and in vivo [1–3]. The same compound has been reported as the most promising innovative nucleobase-like structure (belonging to a class of fused azaisocytosine-containing congeners) with a broad spectrum of anticancer activity (i.e., in multiple myeloma cells and tumor cells of the cervix and breast) as well as good bioavailability and permeability properties [3]. Its methods of synthesis, a complete structural, physico-chemical and pharmacological characterization, have been published earlier together with all the derivatives belonging to the same class of molecules [1–3]. EIMTC has been proposed as a novel anticancer drug candidate with potential applicability in the treatment of multiple myelomas due to its remarkable antiproliferative activity in

human multiple myeloma cells (i.e., resistant as well as susceptible to thalidomide) combined with a less toxic effect on normal cells. In addition, this potential anticancer drug candidate has been shown to induce growth arrest in cancer cells and evoke higher necrosis rates in tumor than in non-tumoral cells of the same epithelial origin [3].

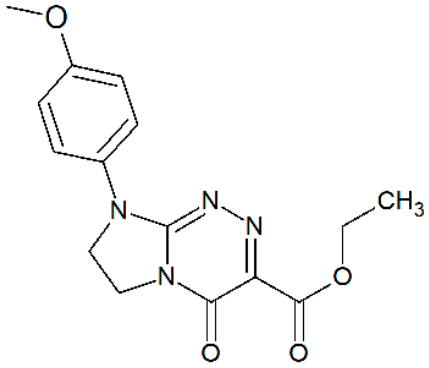

Figure 1. The structure of the investigated EIMTC.

Despite the above-mentioned utilities, no analytical method of EIMTC determination has been developed as of yet. Therefore, the present paper is aimed at developing and optimizing the first electrochemical procedure that allows the quantitative determination of this novel anticancer agent candidate. In the studies, unmodified and modified with carbon nanofibers screen-printed carbon sensors (SPCE and SPCE/CNFs, respectively) were applied for the voltammetric determination of EIMTC.

It is worth mentioning that electrochemical methods, including among others voltammetry, offer a high sensitivity with relatively low-cost instrumentation and analysis [4]. In turn, due to the mass production nature, availability and low cost of screen-printed electrodes, they are now a good approach to the preparation of voltammetric sensors [5–9]. Moreover, the application of nanomaterials together with screen-printing fabrication is a very actual subject of research of particular importance especially for environmental monitoring and medical diagnostics, but also in other fields of analytical applications [10]. One of the attractive carbon nanomaterials for the sensor fabrication are carbon nanofibers (CNFs). The beginning of their electrochemical applications can be dated to early 2000s [11]. Until now, CNFs have found numerous applications, which are connected with their attractive properties, especially their large number of edge-plane sites and their high surface active group-to-volume ratio [12,13]. Furthermore, CNFs can be easily functionalized to suit a particular detection mechanism [13].

2. Materials and Methods

2.1. Instrumentations

All voltammetric measurements were carried out using an electrochemical potentiostat (μAutolab, Eco Chemie, Utrecht, The Netherlands) connected to a personal computer operated by GPES 4.9 software. The 4 mm diameter sensors (SPCE – ref. 110 and SPCE/CNFs – ref. 110CNF) were provided by DropSens, Llanera, Spain. The sensors were immersed in a classic quartz cell (volume 10 mL) or a commercially available methacrylate wall-jet flow-cell (ref. FLWCL, DropSens, Llanera, Spain). The experiments on flow system were carried out using a peristaltic pump type MS-CA (Ismatec, Wertheim, Germany) and sample injection with a 500 μL sample loop (Valco Instruments Co. Inc., Houston, USA).

The images of sensors surface were recorded using a high-resolution scanning electron microscope Quanta 3D FEG (FEI, Hillsboro, USA).

The UHPLC-ESI-MS/MS system was used consisting of a model 1290 infinity ultra-high performance liquid chromatograph (Agilent Technologies, USA) connected to a 6460 triple quadrupole mass spectrometer (Agilent Technologies, USA) equipped with an electrospray ion source (Agilent Jet

Stream) operating in the positive ion mode. The instrument was controlled using Agilent MassHunter Acquisition software v.B.08. The data were analyzed by Agilent MassHunter Quantitative Analysis software v.B.07. The chromatography was performed on a Zorbax Eclipse Plus-C18 Rapid resolution HT column (2.1 mm × 50 mm × 1.8 µm) protected by a Zorbax Eclipse Plus-C18 Narrow Bore Guard Column (2.1 mm × 12.5 mm × 5 µm), both purchased from Agilent Technologies.

2.2. Chemicals

The EIMTC was synthesized from 2-hydrazinylidene-1-(4-methoxyphenyl)imidazolidine and diethyl 2-hydroxyiminomalonate according to the synthetic approach published earlier [1,2]. The chemical structure of the analyzed compound was determined by consistent spectroscopic data (including IR, ^{1}H NMR, EI-MS), whereas its high level of purity was confirmed by a sharp melting point (150–151 °C) and found elemental analyses being within ±0.4% of the theoretical values for each element analyzed.

The solutions of sulfuric acid, acetic acid, and acetate buffers of different pH were prepared from Sigma-Aldrich reagents. The Merck (Darmstadt, Germany) standard solutions of Ca^{2+}, Mg^{2+}, Fe^{3+}, Cl^- as well as Sigma-Aldrich (Saint Louis, USA) reagents (adenine, dopamine, epinephrine, glucose, uric acid, ascorbic acid and estradiol) were used in interference studies. For voltammetric measurements, 1.0×10^{-3} mol L^{-1} solution of EIMTC was prepared in *N*,*N*-dimethylformamide (Sigma-Aldrich, Saint Louis, USA). For UHPLC-ESI-MS/MS analysis, methanol (hypergrade, Merck, Darmstadt, Germany) and formic acid (LC-MS, Sigma-Aldrich, Saint Louis, USA) were used.

2.3. Sample Preparation

The 100 µL of human serum sample 100-times diluted in ultrapure water (Sigma-Aldrich, Saint Louis, USA) spiked with an appropriate concentration of EIMTC was transferred to a centrifugal tube, mixed with 25 µL of 7.5% (*w*/*v*) trichloroacetic acid solution (TCA, Sigma-Aldrich, Saint Louis, USA) for protein precipitation, vortexed well, and centrifuged at 14,000× *g* for 15 min at 4 °C (5415R Centrifuge, Eppendorf, Germany). The collected supernatant was centrifuged once again (14,000× *g*, 15 min, 4 °C), and the clear aliquot was analyzed in triplicate by the SWV and UHPLC-ESI-MS/MS methods.

2.4. SWV Analysis

In the case of measurements performed in a classic electrochemical cell, the standard solution of EIMTC was added to the supporting electrolyte of 0.075 mol L^{-1} H_2SO_4, mixed for 45 s (open circuit potential), and SWV curves were registered. In flow system, in the first step of analysis 2 mol L^{-1} H_2SO_4 for 55 s was directed through the cell in order to clean the electrode surface. Then, 500 µL of 0.075 mol L^{-1} solution of H_2SO_4 containing an appropriate concentration of EIMTC or the sample added to 0.075 mol L^{-1} solution of H_2SO_4 was injected. After 55 s (open circuit potential) from the moment of sample injection, SWV measurements were carried out. The flow rates of each solution were about 3 mL min^{-1}. For SWV, the optimum parameters are as follows: initial potential of −0.2 V, final potential of −0.9 V, frequency (*f*) of 50 Hz, square-wave amplitude (ΔE_A) of 50 mV, and step potential (ΔE_{step}) of 7 mV. The signal of EIMTC was measured after subtracting the background.

2.5. UHPLC-ESI-MS/MS Analysis

The ionization parameters were as follows: nebulizer: 35 psi; gas temperature: 300 °C; gas flow: 10 L min^{-1}; sheath gas temperature: 325 °C; sheath gas flow: 10 L min^{-1}; and capillary voltage: 4000 V. The mobile phase consisted of two solutions: A (0.1% (*v*/*v*) formic acid in water) and B (methanol). The gradient program was as follows: 0–5 min—5% to 70% B; 5–7 min—5% B (column re-equilibration). The column temperature and mobile phase rate were 40°C and 0.3 mL min^{-1}, respectively. The injection volume was 5 µL. The analyte's ions were monitored in Multiple Reaction Monitoring (MRM) mode. MRM transitions: *m*/*z* 317 > 289 (quantifier, fragmentor: 140 V; collision energy: 20 eV) and *m*/*z* 317 > 245 (qualifier, fragmentor: 140 V; collision energy: 22 eV).

3. Results and Discussion

3.1. Voltammetric Behaviour of EIMTC

The electrochemical behavior of EIMTC at the unmodified SPCE and carbon nanofibers modified SPCE is shown in Figure 2. Before SWV curve registration, the solution was mixed for 45 s (open circuit potential). It can be seen that the reduction peaks of EIMTC at the SPCE were weak, while the EIMTC responses were considerably improved at the SPCE/CNFs. The reason for better performance of SPCE/CNFs was explained in our earlier works [14,15]. In those papers, the active surface areas of the SPCE and SPCE/CNFs were calculated using cyclic voltammetric studies in 0.1 mol L^{-1} solution of KCl and 5.0×10^{-3} mol L^{-1} $K_3[Fe(CN)_6]$ and the Randles–Sevcik equation. It was found that modification of the electrode increases its active surface (Figure 3).

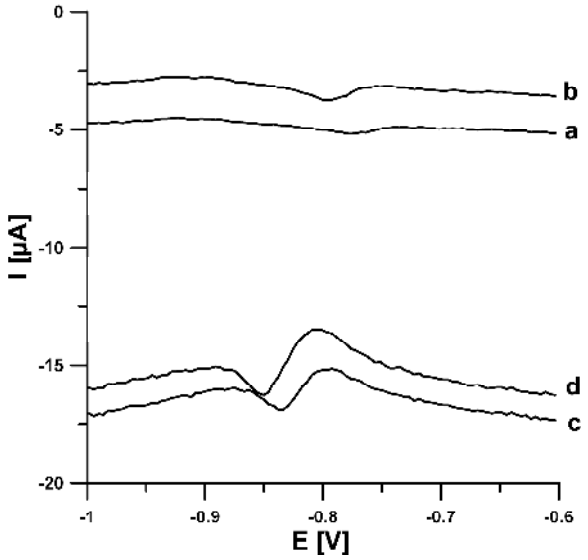

Figure 2. Square-wave voltammograms of 5.0×10^{-7} mol L^{-1} (a and c) and 1.0×10^{-6} mol L^{-1} (b and d) EIMTC in 0.1 mol L^{-1} acetate buffer solution of pH 4.5 at the screen-printed carbon sensor (SPCE) (a and b) and carbon nanofibers modified screen-printed carbon sensors (SPCE/CNFs) (c and d). The SWV parameters: open circuit potential, t of 45 s, initial E of −0.6 V, final E of −1.0 V, f of 50 Hz, ΔE_A of 25 mV, and ΔE_{step} of 4 mV.

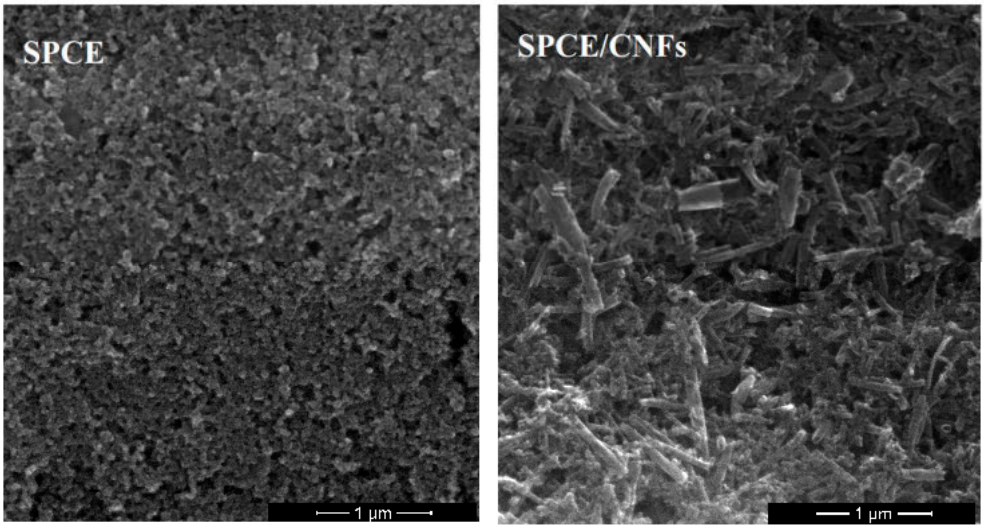

Figure 3. SEM images of SPCE and SPCE/CNFs.

In the next part of the experiments, cyclic voltammograms (CVs) were recorded in the range of −0.2–(−0.75)V to get information about the behavior of EIMTC at the SPCE/CNFs. Figure 4A represents CV curves recorded for 1.0×10^{-5} mol L^{-1} EIMTC in 0.1 mol L^{-1} acetate buffer of pH 4.5 with scan rates (ν) of 50, 100, and 150 mV s^{-1}. As it can be seen, well-defined irreversible reduction peaks of EIMTC were obtained. To ascertain the effect of scan rate on the reduction peak current of EIMTC, the scan rate studies were carried out in the range of 20–500 mV s^{-1}. The linearity of peak current (I_p) of EIMTC vs. $\nu^{1/2}$ plot (Figure 4B) indicated that the reduction of EIMTC at the SPCE/CNFs is diffusion controlled, which was further confirmed by the slope value (0.49) of logI_p vs. logν plot (Figure 4C) [16]. Furthermore, the I_p values of 2.0×10^{-7} mol L^{-1} EIMTC were almost stable during changes in the potential (0–(−0.8)V) applied to the electrode, which also confirmed that the reduction of EIMTC is diffusion-controlled at the SPCE/CNFs. While the potential does not significantly affect the EIMTC signal, mixing of the solution prior the SWV curves registration (open circuit potential) is very important. As can be seen in Figure 4D, the I_p value of 2.0×10^{-7} mol L^{-1} EIMTC reached maximum at the solution mixing time (t) of 45 s. It is connected with the facilitated diffusion of EIMTC molecules to the electrode surface during solution mixing [17].

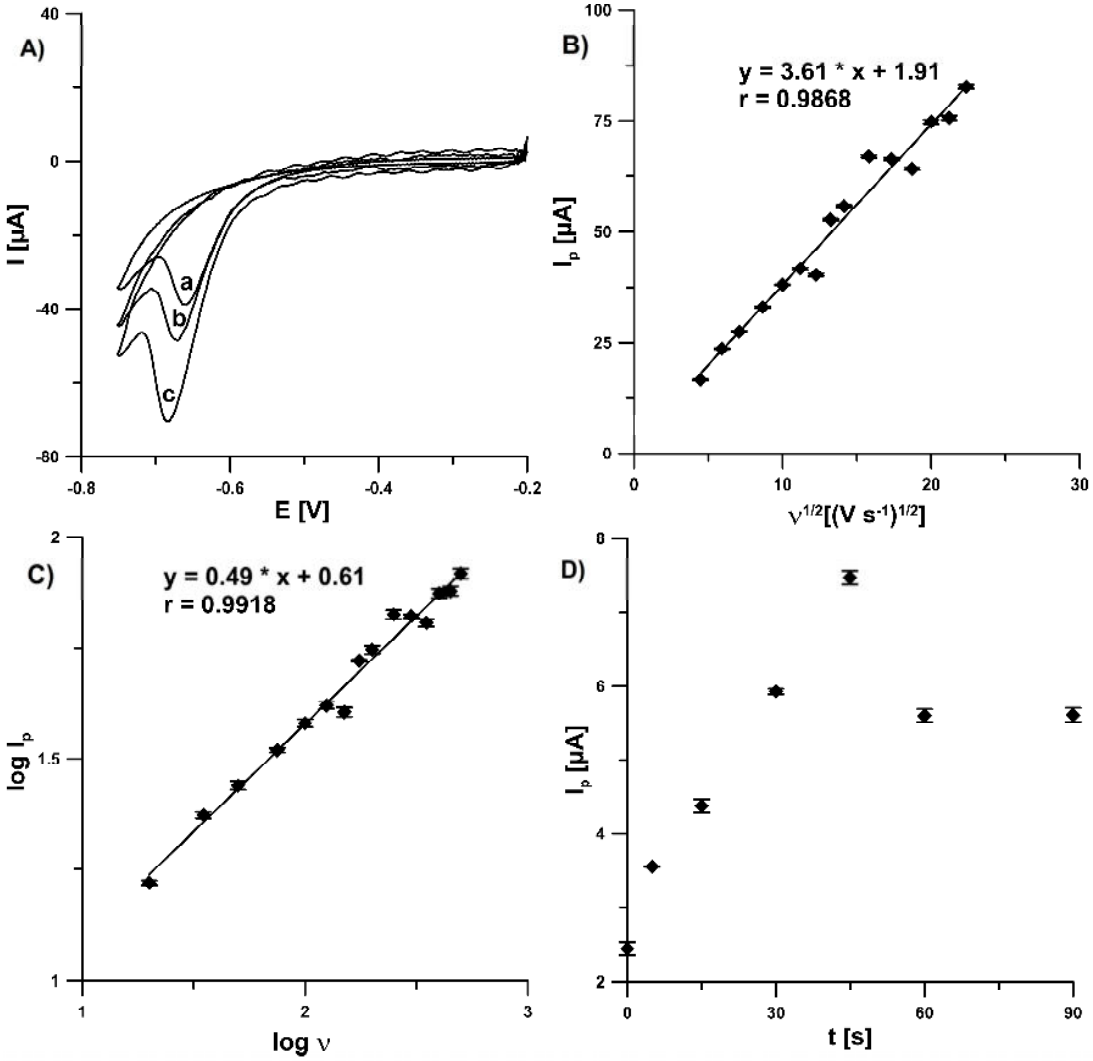

Figure 4. (**A**) Cyclic voltammograms of 1.0×10^{-5} mol L^{-1} EIMTC at ν of 50 (a), 100 (b) and 150 mV s^{-1} (c). The dependence between (**B**) *Ip* and $v^{1/2}$ and (**C**) log*Ip* and log*v*. (**D**) Effect of *t* on I_p of 2.0×10^{-7} mol L^{-1} EIMTC (open circuit potential). The average values of I_p are shown with the standard deviation of n = 3.

3.2. Effect of pH

The pH dependence of 5.0×10^{-7} mol L^{-1} EIMTC at the SPCE/CNFs was investigated using 0.1 mol L^{-1} sulfuric acid, acetic acid, and acetate buffer (pH of 3.5–6.0). From the plot of I_p of EIMTC vs. pH (Figure 5A) it is clear that peak current is affected by the pH value. The best result with respect to sensitivity accompanied with a well-defined response was obtained in the H_2SO_4 solution, so this solution was used in further studies. The linearity of peak potential (E_p) of EIMTC vs. pH plot (Figure 5B) was obtained in the pH range of 2.9–6.0 (r = 0.9950). The slope of the equation was found to be 51 mV pH^{-1}. This closeness of the slope to the expected theoretical value of 59 mV pH^{-1} suggested that the number of electrons is equal to the hydrogen ions taking part in the electrode reaction.

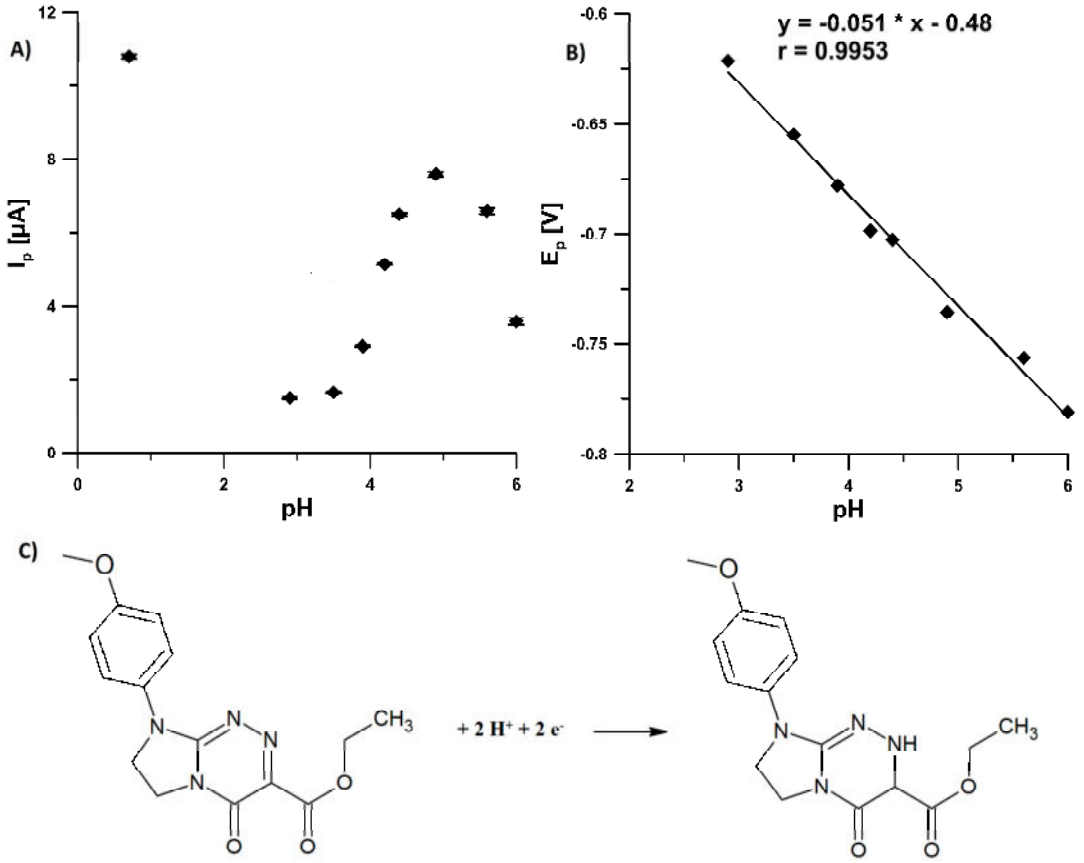

Figure 5. Effect of pH on: (**A**) I_p and (**B**) E_p of 5.0×10^{-7} mol L^{-1} EIMTC (open circuit potential, t of 45 s). The SWV parameters: initial E of −0.2 V, final E of −0.9 V, f of 50 Hz, ΔE_A of 25 mV and ΔE_{step} of 4 mV. (**C**) The mechanism proposed for the reduction of EIMTC. The average values of I_p are shown with the standard deviation of n = 3.

EIMTC is a small molecule possessing in a privileged triazinone scaffold the azomethine grouping of ketimine type (C=N) that can be reduced electrochemically. The reduction of this C=N grouping in the analyzed molecule, leads to the protonated CH–NH grouping. This is consistent with previous studies on electrochemical behavior of monocyclic as well as fused triazinones [18,19]. The one-step reduction process at the SPCE/CNFs surface occurs through an electron-gain mechanism, including the transfer of two electrons and two protons (Figure 5C).

Moreover, the effect of selected supporting electrolyte (H_2SO_4) concentration (0.025–0.2 mol L^{-1}) on the peak current of 5.0×10^{-7} mol L^{-1} EIMTC at the SPCE/CNFs was studied. The highest signals were obtained at a concentration of 0.075 mol L^{-1} and at higher concentrations of H_2SO_4 the EIMTC signals are almost stable. Therefore, 0.075 mol L^{-1} H_2SO_4 solution was selected for further experiments.

3.3. Effect of SWV Parameters

The dependence of the reduction in peak current (I_p) of 5.0×10^{-7} mol L^{-1} EIMTC on the square-wave frequency (f) was studied in the range of 10–125 Hz at the SPCE/CNFs (Figure 6A). The I_p values were found to increase linearly, with increasing f to 50 Hz, and then to decrease. That is why f to 50 Hz was chosen for further studies. Next, the effect of step potential (ΔE_{step}) on the 5.0×10^{-7} mol L^{-1} EIMTC signals was examined from 2 to 9 mV (f to 50 Hz and ΔE_A of 25 mV). The highest EIMTC signal was obtained at ΔE_{step} of 7 mV (Figure 6B). Furthermore, the influence of square-wave amplitude (ΔE_A) on the 5.0×10^{-7} mol L^{-1} EIMTC responses was examined in the rage of 25–100 mV (Figure 6C, f to 50 Hz and ΔE_{step} of 7 mV). The maximum value of EIMTC signal (5.0 µA) was achieved at ΔE_A of 100 mV. However, due to the much lower background current and a slight difference in EIMTC peak current (4.6 vs. 5.0 µA), ΔE_A of 50 mV was selected for further experiments.

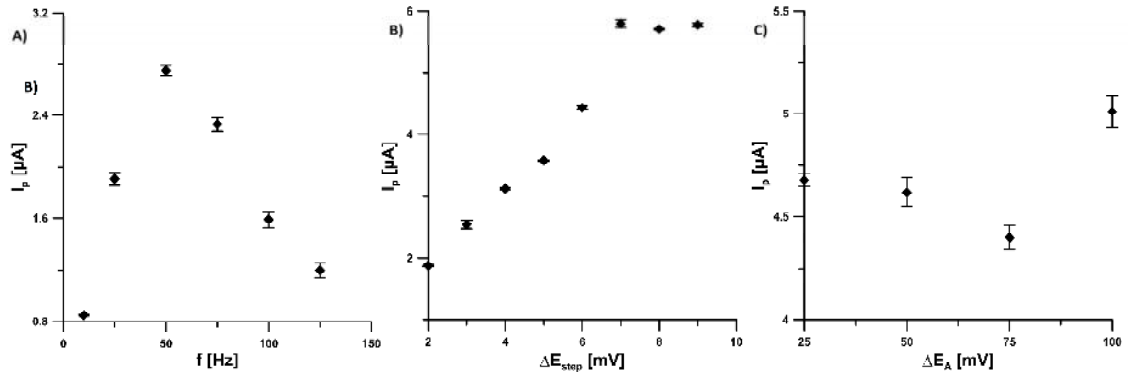

Figure 6. Effect of (**A**) f (10–125 Hz), (**B**) ΔE_{step} (2–9 mV) and (**C**) ΔE_A (25–100 mV) on 5.0×10^{-7} mol L^{-1} EIMTC responses. The average values of I_p are shown with the standard deviation of n = 3.

3.4. Interferences

The presence of common ions (Ca^{2+}, Mg^{2+}, Fe^{3+}, and Cl^-) and organic compounds (uric acid, ascorbic acid, glucose, adenine, dopamine, epinephrine, and estradiol) in human serum samples may alter electrochemical EIMTC signals and consequently affect the selectivity. The tolerance concentration ratios with respect to 5.0×10^{-7} mol L^{-1} EIMTC for interferences at 10% level were examined. The results given in Table 1 show that Fe^{3+}, estradiol, and ascorbic acid have a maximum effect on the determination of EIMTC.

Table 1. Results of interference studies for the determination of 5.0×10^{-7} mol L^{-1} EIMTC at the SPCE/CNFs.

Species	Tolerance Limits
Ca^{2+}	50
Mg^{2+}, Cl^-, uric acid, glucose, adenine, dopamine	5
epinephrine	2.5
Fe^{3+}, estradiol, ascorbic acid	0.5

The preliminary analysis of human serum samples spiked with 5.0×10^{-8} mol L^{-1} EIMTC in the classical electrochemical cell did not bring expected results. No EIMTC signals were observed. This signal attenuation was related to the serum sample matrix. Therefore, flow-injection analysis in a commercially available wall-jet flow-cell was proposed to resolve this problem. It is well known that the electrochemical detection under hydrodynamically controlled conditions reveals some benefits. Among others, the shear forces of the flowing liquid continuously regenerate the working electrode surface and remove reaction products [20]. Consequently, the selectivity under flow analytical conditions can be improved, which was confirmed by our research (see Section 3.6).

3.5. Calibration Curve in Flow System, Precision and Reproducibility

The SPCE/CNFs sensor coupled with flow system was used for the quantitative determination of a novel promising anticancer agent candidate EIMTC. The flow conditions and SWV parameters are described in Section 2.4. The responses were linear with EIMTC concentrations ranging from 2.0×10^{-9} to 2.0×10^{-8} mol L^{-1} and 2.0×10^{-8} to 2.0×10^{-7} mol L^{-1} (Figure 7A,B). The limits of detection (LOD) and quantification (LOQ) were determined 5.0×10^{-10} and 1.7×10^{-9} mol L^{-1}, respectively, according to the definitions of LOD = $3SD_a/b$ and LOQ = $10SD_a/b$ (SD_a—standard deviation of intercept (n = 3); b—slope of calibration curve) [21].

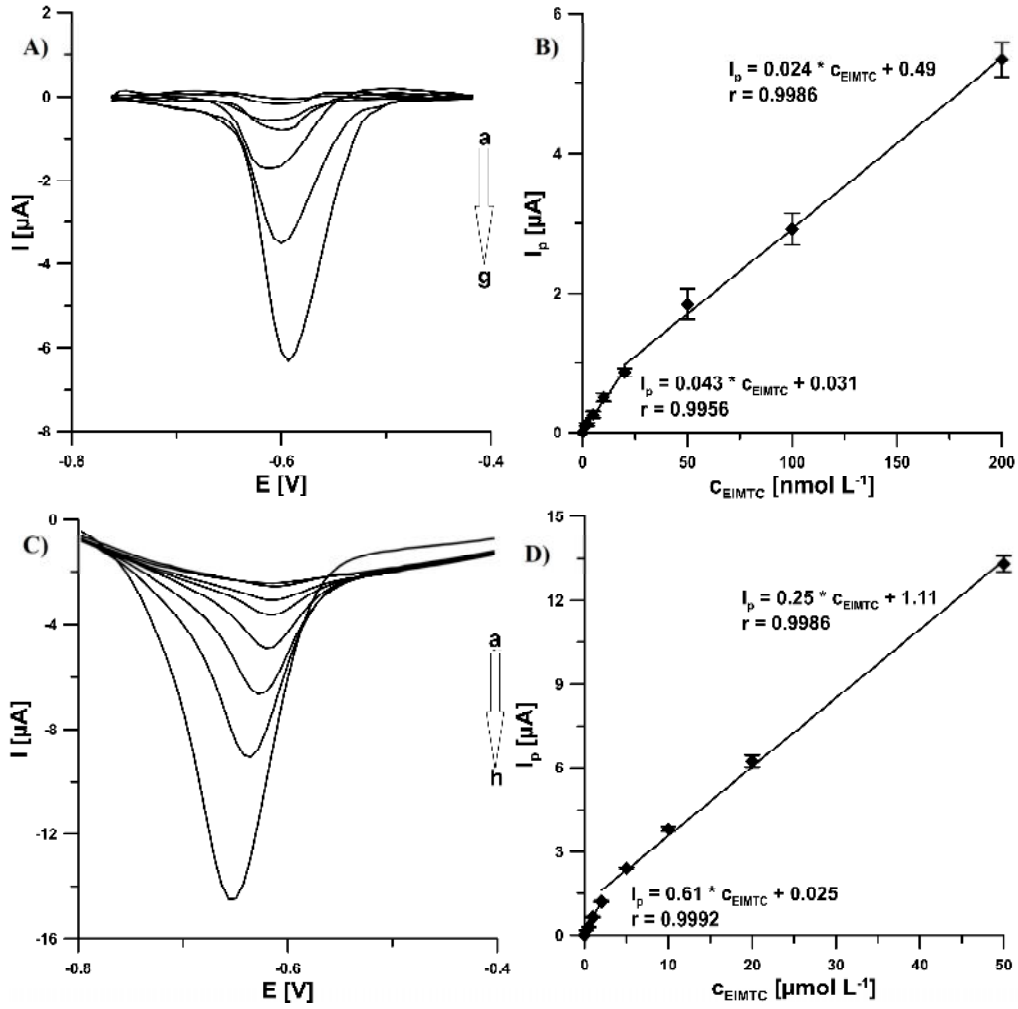

Figure 7. (**A**) SWV curves registered in flow system at the SPCE/CNFs in 0.075 mol L^{-1} H_2SO_4 solution containing increasing concentrations of EIMTC: 2.0×10^{-9} (a), 5.0×10^{-9} (b), 1.0×10^{-8} (c), 2.0×10^{-8} (d), 5.0×10^{-8} (e), 1.0×10^{-7} (f), 2.0×10^{-7} (g) mol L^{-1}. (**B**) Linear ranges of the calibration graph of EIMTC in flow system at the SPCE/CNFs. (**C**) SWV curves registered in flow system at the SPCE in 0.075 mol L^{-1} H_2SO_4 solution containing increasing concentrations of EIMTC: 2.0×10^{-7} (a), 5.0×10^{-7} (b), 1.0×10^{-6} (c), 2.0×10^{-6} (d), 5.0×10^{-6} (e), 1.0×10^{-5} (f), 2.0×10^{-5} (g), 5.0×10^{-5} (h) mol L^{-1}. (**D**) Linear ranges of the calibration graph of EIMTC in flow system at the SPCE. The average values of I_p are shown with the standard deviation of n = 9. After 55 s (open circuit potential) from the moment of sample injection (500 µL sample loop), SWV measurements were carried out. The SWV parameters: initial E of −0.2 V, final E of −0.9 V, f of 50 Hz, ΔE_A of 50 mV, and ΔE_{step} of 7 mV.

The relative standard deviation (RSD) values of 2.9% and 5.2% calculated for ten repeated measurements of 2.0×10^{-8} and 2.0×10^{-7} mol L^{-1} EIMTC at the SPCE/CNFs, respectively, confirmed

the satisfactory precision of the signals at the SPCE/CNFs. In turn, the RSD values of 3.4% and 4.7% (n = 9) calculated for the same EIMTC concentrations but using three electrodes, indicated the acceptable reproducibility of the sensor.

Moreover, in order to confirm the advantage of using the SPCE/CNFs instead of the unmodified SPCE in the EIMTC determinations, the voltammetric measurements to the calibration curve were also made at the SPCE (Figs. 7C and 7D). The calibration curve was linear in two ranges from 2.0×10^{-7} to 2.0×10^{-6} mol L^{-1} and from 2.0×10^{-6} to 5.0×10^{-5} mol L^{-1}, with detection and quantification limits of 3.4×10^{-8} and 1.1×10^{-7} mol L^{-1}, respectively. The comparison demonstrates that the SPCE/CNFs provides two orders of magnitude lower detection and quantifications limits.

3.6. Serum Samples Assay in Flow System

To establish the utility of the developed flow voltammetric procedure in biological samples, EIMTC was determined in the spiked human serum samples. The calibration graph was used for the determination of spiked serum samples. The results obtained for the SWV and UHPLC-ESI-MS/MS analysis are listed in Table 2. The recovery obtained was 97.2% and 99.0%. The relative error values of 3.0% and 7.2% show satisfactory agreement with the cooperative UHPLC-ESI-MS/MS method. It was also confirmed by the t-Student test. The calculated t values ($t_{exp.}$) are 1.98 and 0.71, which is below the critical value equal to 2.78 (level of significance of 0.05, number of degrees of freedom (f) of 4, $f = n_1 + n_2 - 2$) [22]. Moreover, the results indicate that there is no significant effect of the sample serum matrix on the voltammetric EIMTC signal, and the developed SWV procedure in a flow system is feasible for EIMTC analysis in real biological samples.

Table 2. Results obtained for EIMTC in human serum samples using SWV at the SPCE/CNFs and UHPLC-ESI-MS/MS.

	EIMTC Concentration [mol L^{-1}] ± SD (n = 3)			**Recovery [%]**	**Relative Error [%]**	$t_{exp.}$
	Added	**Found SWV**	**Found UHPLC-ESI-MS/MS**			
Human serum	5.0×10^{-8}	$4.86 \times 10^{-8} \pm 0.17 \times 10^{-8}$	$5.21 \times 10^{-8} \pm 0.05 \times 10^{-8}$	97.2	7.2	1.98
	1.0×10^{-7}	$0.99 \times 10^{-7} \pm 0.03 \times 10^{-7}$	$0.96 \times 10^{-7} \pm 0.03 \times 10^{-7}$	99.0	3.0	0.71

4. Conclusions

In the present studies, the first analytical method was proposed for sensitive and selective determination of a novel promising anticancer agent candidate (EIMTC) using the carbon nanofibers modified screen-printed carbon sensor. The modified sensor showed great improvement to the EIMTC reduction electrode process compared to the unmodified sensor (LOD: 5.0×10^{-10} mol L^{-1} vs. 3.4×10^{-8} mol L^{-1} and 1.7×10^{-9} mol L^{-1} vs. 1.1×10^{-7} mol L^{-1}, respectively). The reason for enhanced detection performance at the SPCE/CNFs is related to an increase in the number of active sites, as we showed earlier [14,15]. Furthermore, the electrochemical responses of EIMTC at the SPCE/CNFs were characterized by the CV technique and the results indicated that the reduction process of EIMTC is diffusion-controlled. The diffusion of EIMTC molecules to the electrode surface was facilitated during solution mixing before the SWV curve registration. Moreover, the flow system successfully resolved the problem with the influence of the human serum matrix on the EIMTC signal. The application of the developed voltammetric procedure for analysis of human serum samples was successfully demonstrated. The results show satisfactory agreement with the cooperative UHPLC-ESI-MS/MS method. The proposed method is characterized by a wide linear range, low detection and quantification limits, as well as satisfactory precision and reproducibility.

Author Contributions: Conceptualization, K.T.-R. and J.K.; methodology, K.T.-R. and J.K.; investigation, K.T.-R., J.K., M.S., K.S. and I.S.; writing—original draft preparation, K.T.-R. and J.K.; writing—review and editing, K.T.-R., J.K., M.S., K.S. and I.S.; supervision, K.T.-R. All authors have read and agreed to the published version of the manuscript.

Funding: This research received no external funding.

Acknowledgments: The authors gratefully acknowledge the use of the services and facilities of the Center for Interdisciplinary Research of The John Paul II Catholic University of Lublin, Lublin, Poland, supported by the European Union from European Regional Development Fund under the Operational Programme Development of Eastern Poland 2007–2013 (agreement POPW.01.03.00-06-003/09-00).

Conflicts of Interest: The authors declare no conflict of interest.

References

1. Sztanke, K.; Rzymowska, J.; Niemczyk, M.; Dybała, I.; Kozioł, A.E. Synthesis, Crystal structure and anticancer activity of novel derivatives of ethyl 1-(4-oxo-8-aryl-4,6,7,8-tetrahydroimidazo[2,1-c][1,2,4]triazin-3-yl)formate. *Eur. J. Med. Chem.* **2006**, *41*, 539–547. [CrossRef] [PubMed]
2. Sztanke, K. New Ethyl 7,8-Dihydro-6H-Imidazo[2,1-c][1,2,4]Triazine-4-oxo-3-Carboxylates and Method for Obtaining Them. Polish Patent 196751, 31 January 2008.
3. Sztanke, M.; Rzymowska, J.; Sztanke, K. In vitro effects of a new fused azaisocytosine-like congener on relative cell proliferation, necrosis and cell cycle in cancer and normal cell cultures. *Mol. Cell. Biochem.* **2016**, *418*, 179–188. [CrossRef] [PubMed]
4. Rosolina, S.M.; Chambers, J.Q.; Xue, Z.-L. Direct analysis of palladium in active pharmaceutical ingredients by anodic stripping voltammetry. *Anal. Chim. Acta* **2016**, *914*, 47–52. [CrossRef] [PubMed]
5. Li, M.; Li, Y.-T.; Li, D.-W.; Long, Y.-T. Recent developments and applications of screen-printed electrodes in environmental assays—A review. *Anal. Chim. Acta* **2012**, *734*, 31–44. [CrossRef] [PubMed]
6. Blasco, C.A.; Plana, N.S.; Cruz, J.M.; Cortada, M.E. Voltammetric determination of metal ions beyond mercury electrodes. A review. *Anal. Chim. Acta* **2017**, *990*, 11–53.
7. Raymundo-Pereira, P.A.; Gomes, N.O.; Carvalho, J.H.S.; Machado, S.A.S.; Oliveira, O.N., Jr.; Janegitz, B.C. Simultaneous detection of quercetin and carbendazim in wine samples using disposable electrochemical sensors. *ChemElectroChem* **2020**, *7*, 3074–3081. [CrossRef]
8. Silva, R.R.; Raymundo-Pereira, P.A.; Campos, A.M.; Wilson, D.; Otoni, C.G.; Barud, H.S.; Costa, C.A.R.; Domeneguetti, R.R.; Balogh, D.T.; Ribeiro, S.J.L.; et al. Microbial nanocellulose adherent to human skin used in electrochemical sensors to detect metal ions and biomarkers in sweat. *Talanta* **2020**, *218*, 121153. [CrossRef] [PubMed]
9. Raymundo-Pereira, P.A.; Gomes, N.O.; Machado, S.A.S.; Oliveira, O.N., Jr. Simultaneous, ultrasensitive detection of hydroquinone, paracetamol and estradiol for quality control of tap water with a simple electrochemical method. *J. Electroanal. Chem.* **2019**, *848*, 113319. [CrossRef]
10. Trojanowicz, M. Impact of nanotechnology on design of advanced screen-printed electrodes for different analytical applications. *TrAC-Trends Anal. Chem.* **2016**, *84*, 22–47. [CrossRef]
11. Marken, F.; Gerrard, M.L.; Mellor, I.M.; Mortimer, R.J.; Madden, C.E.; Fletcher, S.; Holt, K.; Foord, J.S.; Dahm, R.H.; Page, F. Voltammetry at carbon nanofiber electrodes. *Electrochem. Commun.* **2001**, *3*, 177–180. [CrossRef]
12. Huang, J.; Liu, Y.; You, T. Carbon nanofiber based electrochemical biosensors: A review. *Anal. Methods* **2010**, *2*, 202–211. [CrossRef]
13. Kour, R.; Arya, S.; Young, S.-J.; Gupta, V.; Bandhoria, P.; Khosla, A. Review—Recent advances in carbon nanomaterials as electrochemical biosensors. *J. Electrochem. Soc.* **2020**, *167*, 037555. [CrossRef]
14. Sasal, A.; Tyszczuk-Rotko, K.; Wójciak, M.; Sowa, I. First electrochemical sensor (screen-printed carbon electrode modified with carboxyl functionalized multiwalled carbon nanotubes) for ultratrace determination of diclofenac. *Materials* **2020**, *13*, 781. [CrossRef] [PubMed]
15. Sasal, A.; Tyszczuk-Rotko, K.; Wójciak, M.; Sowa, I.; Kuryło, M. Simultaneous analysis of paracetamol and diclofenac using MWCNTs-COOH modified screen-printed carbon electrode and pulsed potential accumulation. *Materials* **2020**, *13*, 3091. [CrossRef] [PubMed]
16. Gosser, D.K. *Cyclic Voltammetry: Simulation and Analysis of Reaction Mechanism*; VCH: New York, NY, USA, 1993.

17. Sasal, A.; Tyszczuk-Rotko, K.; Chojecki, M.; Korona, T.; Rotko, M. Direct determination of paracetamol in environmental samples using screen-printed carbon/carbon nanofibers sensor—Experimental and theoretical studies. *Electroanalysis* **2020**, *32*, 1618–1628. [CrossRef]
18. Ludvik, J.; Zuman, P. Electrochemical proof of the single bond character of the N–N bonds in some 1,2,4-triazines. *Indian J. Chem.* **2003**, *42A*, 847–848.
19. Stępniowska, A.; Sztanke, M.; Tuzimski, T.; Korolczuk, M.; Sztanke, K. A simple stripping voltammetric method for the determination of a new anticancer prodrug in serum. *Biosens. Bioelectron.* **2017**, *94*, 584–588. [CrossRef] [PubMed]
20. Tóth, K.; Štulic, K.; Kutner, W.; Fehér, Z.; Lindner, E. Electrchemical detction in liquid flow analitical techniques: Characterization and classification (IUPAC Technical Report). *Pure Appl. Chem.* **2004**, *76*, 1119–1138.
21. Mocak, J.; Bond, A.M.; Mitchell, S.; Scollary, G. A statistical overview of standard (IUPAC and ACS) and new procedures for determining the limits of detection and quantification: Application to voltammetric and stripping techniques. *Pure Appl. Chem.* **1997**, *69*, 297–328. [CrossRef]
22. Konieczki, P.; Namiesnik, J. *Quality Assurance and Quality Control in the Analytical Chemical Laboratory: A Practical Approach*; CRC Press: Boca Raton, FL, USA, 2009.

RD 2

J. Kozak, K. Tyszczuk-Rotko, M. Wójciak, I. Sowa, *Electrochemically activated screen-printed carbon sensor modified with anionic surfactant (aSPCE/SDS) for simultaneous determination of paracetamol, diclofenac and tramadol*, Materials, 14 (13) (2021) 3581-3596.

materials

MDPI

Article

Electrochemically Activated Screen-Printed Carbon Sensor Modified with Anionic Surfactant (aSPCE/SDS) for Simultaneous Determination of Paracetamol, Diclofenac and Tramadol

Jędrzej Kozak [1], Katarzyna Tyszczuk-Rotko [1,*], Magdalena Wójciak [2,*] and Ireneusz Sowa [2]

[1] Faculty of Chemistry, Institute of Chemical Sciences, Maria Curie-Skłodowska University in Lublin, 20-031 Lublin, Poland; jedrekkozak@onet.pl
[2] Department of Analytical Chemistry, Medical University of Lublin, 20-093 Lublin, Poland; i.sowa@umlub.pl
* Correspondence: ktyszczuk@poczta.umcs.lublin.pl (K.T.-R.); magdalena.wojciak@umlub.pl (M.W.)

Abstract: In this work, an electrochemically activated screen-printed carbon electrode modified with sodium dodecyl sulfate (aSPCE/SDS) was proposed for the simultaneous determination of paracetamol (PA), diclofenac (DF), and tramadol (TR). Changes of surface morphology and electrochemical behaviour of the electrode after the electrochemical activation with H_2O_2 and SDS surface modification were studied by scanning electron microscopy (SEM), cyclic voltammetry (CV), and electrochemical impedance spectroscopy (EIS). The influence of various parameters on the responses of the aSPCE/SDS such as pH and concentration of the buffer, SDS concentration, and techniques parameters were investigated. Using optimised conditions ($E_{acc.}$ of −0.4 V, $t_{acc.}$ of 120 s, ΔE_A of 150 mV, ν of 250 mV s^{-1}, and t_m of 10 ms), the aSPCE/SDS showed a good linear response in the concentration ranges of 5.0×10^{-8}–2.0×10^{-5} for PA, 1.0×10^{-9}–2.0×10^{-7} for DF, and 1.0×10^{-8}–2.0×10^{-7} and 2.0×10^{-7}–2.0×10^{-6} mol L^{-1} for TR. The limits of detection obtained during the simultaneous determination of PA, DF, and TR are 1.49×10^{-8} mol L^{-1}, 2.10×10^{-10} mol L^{-1}, and 1.71×10^{-9} mol L^{-1}, respectively. The selectivity of the aSPCE/SDS was evaluated by examination of the impact of some inorganic and organic substances that are commonly present in environmental and biological samples on the responses of PA, DF, and TR. Finally, the differential pulse adsorptive stripping voltammetric (DPAdSV) procedure using the aSPCE/SDS was successfully applied for the determination of PA, DF, and TR in river water and serum samples as well as pharmaceuticals.

Keywords: electrochemically activated screen-printed carbon electrode modified with sodium dodecyl sulfate; simultaneous determination of paracetamol; diclofenac and tramadol; differential pulse adsorptive stripping voltammetry; river water; human serum and pharmaceutical formulation samples

Citation: Kozak, J.; Tyszczuk-Rotko, K.; Wójciak, M.; Sowa, I. Electrochemically Activated Screen-Printed Carbon Sensor Modified with Anionic Surfactant (aSPCE/SDS) for Simultaneous Determination of Paracetamol, Diclofenac and Tramadol. *Materials* **2021**, *14*, 3581. https://doi.org/10.3390/ma14133581

Academic Editor: Suzy Surblé

Received: 28 May 2021
Accepted: 23 June 2021
Published: 26 June 2021

1. Introduction

Paracetamol (PA), also called acetaminophen, is a widely used pain reliever and antipyretic drug. However, it has no anti-inflammatory effect. Paracetamol is the main ingredient in many cold and flu medications. It is usually used to relieve headaches, toothaches, backaches, muscle aches, and other minor aches. An overdose of paracetamol may result in the accumulation of toxic metabolites that can cause acute and sometimes fatal nephro- and hepatotoxicity [1–3].

Diclofenac (DF) is a well-known, non-steroidal anti-inflammatory drug (NSAID) for the treatment of post-traumatic pain and pain in chronic diseases. It exhibits activities characteristic of this group of drugs, i.e., anti-inflammatory, antipyretic, analgesic, and inhibiting platelet aggregation. Despite its undoubted advantages, it can be very dangerous for living organisms. It causes an increase in blood pressure and thus strokes and worsens the functioning of the liver [2,4].

Tramadol (TR) is an opioid drug, a synthetic analog of codeine. It is a centrally acting pain reliever and is used to treat mild to severe pain. Tramadol can be used alone or in combination with NSAIDs to deal with cases associated with severe acute or chronic pain, lower back pain, and postoperative pain management. Overdosing on tramadol can cause slow or ceased breaths because this substance can accumulate in the body, causing critical levels of poisoning [5,6].

The presented pharmaceuticals may be present in the environment and have a negative impact, e.g., diclofenac affects the quality of water and is harmful to fish.

Due to the possible side effects for humans as well as the negative impact on the environment, it is extremely important to develop sensitive and accurate methods for the determination of the presented drugs in samples of biological fluids and environmental samples. There are many analytical methods such as high-performance liquid chromatography (HPLC) [7–9], liquid chromatography-tandem mass spectrometry (LC-MS/MS) [10–12], gas chromatography-mass spectrometry (GC-MS) [13–15], and spectrophotometry [16–18], which are used to determine paracetamol, diclofenac, and tramadol. However, these methods are generally costly, requiring a time-consuming sample preparation step. Compared to other analytical techniques, electrochemical methods, including voltammetry, are simple, relatively cheap, and more sensitive. In this type of procedures, apart from classic electrodes, we can use screen-printed sensors with many advantages, i.e., low cost, simplicity of construction and operation, diversification of the selection of electrode materials, portability, and ease in modification of the electrodes for various uses [19]. In the literature, we can find procedures for the determination of paracetamol alone or in the presence of various compounds [2,3,19–29], diclofenac [2,30–32], and tramadol [33] using screen-printed electrodes but there is no article showing the simultaneous determination of these three compounds.

In this work, for the first time, an electrochemically activated screen-printed carbon sensor (aSPCE) modified with an anionic surfactant (sodium dodecyl sulfate, SDS) was prepared and applied for the simultaneous determination of paracetamol, diclofenac, and tramadol. The activation can functionalize the electrode surface, increase the active surface or remove surface contamination [34,35]. Due to the adsorption of surfactants on the electrode surface, its properties change, which influences the reaction speed. Furthermore, surfactants effectively stabilize the voltammetric response by protecting the electrode surface from contamination. It has been shown that surfactants can increase the accumulation of some electroactive molecules on the electrode surface, which results in an improvement in the analytical signal and an increase in the sensitivity of the developed method [36–46].

2. Materials and Methods

2.1. Apparatus

Voltammetric measurements were performed using a μAutolab analyzer (Eco Chemie, Utrecht, The Netherlands) controlled by GPES 4.9 software. All experiments were carried out in a 10 mL quartz electrochemical cell using commercially available screen-printed sensors (Ref. C150, DropSens, Llanera, Spain,), which were activated electrochemically prior to measurements. These sensors consisted of a screen-printed carbon working electrode (SPCE), a platinum screen-printed auxiliary electrode, and a silver screen-printed pseudo-reference electrode. The μAutolab analyzer (Eco Chemie, Utrecht, The Netherlands), controlled in this case by FRA 4.9 software, was also used to record the differential capacity curves and Nyquist plots by the electrochemical impedance spectroscopy (EIS) method.

Microscopic images of the SPCE surface were obtained with a high-resolution scanning electron microscope Quanta 3D FEG (FEI, Hillsboro, FL, USA). The experiments were carried out under required conditions (acceleration voltage of 5.0 kV, horizontal field width of 5.97 μm, working distance of 9.0 mm).

HPLC analyses were performed on a VWR Hitachi Elite LaChrom HPLC (Tokyo, Japan) with PDA detector using an XB-C18 reversed phase core-shell column (Kinetex, Phenomenex, Aschaffenburg, Germany) (25 cm × 4.6 mm i.d., 5 μm).

2.2. Reagents and Solutions

All solutions were prepared with Sigma-Aldrich or Merck reagents purchased from Merck KGaA company (Darmstadt, Germany). Appropriate amounts of paracetamol sulfate potassium salt (PA), diclofenac sodium salt (DF), and tramadol hydrochloride (TR) (Sigma-Aldrich, St. Louis, MO, USA) were dissolved in deionized water to obtain 0.01 mol L^{-1} solutions of PA and TR and 0.001 mol L^{-1} solution of DF. These solutions were diluted with deionized water as needed. A SDS (sodium dodecyl sulfate) solution was obtained by dissolving a weighed amount of Sigma-Aldrich reagent in deionized water. When selecting the base electrolyte and examining the effect of pH on the signals of the analytes, 0.1 mol L^{-1} solutions of sulfuric acid, acetic acid, and acetate buffers with pH values of 3.5 ± 0.1, 4.0 ± 0.1, 4.5 ± 0.1, 5.0 ± 0.1, 5.5 ± 0.1, and 6.0 ± 0.1 were used. DTPA (diethylenetriaminepentaacetic acid) solution was prepared in deionized water using Sigma-Aldrich reagent. The influence of interferents such as Ca(II), Mg(II), Fe(III), Ni(II), Cd(II), Pb(II), Cu(II), V(V), Mo(VI), and Cl^- was checked using Merck standard solutions. The effect of organic substances was checked using Sigma-Aldrich reagents: glucose, ascorbic acid, Triton X-100, and cetyltrimethylammonium bromide (CTAB). The solutions were prepared using ultrapurified water (>18 MW cm, Milli-Q system, Millipore, UK). HPLC-grade acetonitrile and trifluoroacetic acid (TFA) were from Merck.

2.3. Preparation of aSPCE/SDS

The screen-printed carbon electrode surface was electrochemically activated before the measurements [34]. Activation consisted of 25 repetitive voltammetric cycles between 1.0 and −0.7 V at a scan rate of 10 mV s^{-1} in 0.1 mol L^{-1} acetate buffer of pH = 4.0 ± 0.1 containing 10 mmol L^{-1} H_2O_2. After activation, the sensor was rinsed with deionized water and allowed to air dry. Then, the electrode surface was modified with SDS during analysis of PA, DF, and TR by immersing the SPCE in a supporting electrolyte solution (acetate buffer of pH = 4.0 ± 0.1) containing 15 mg L^{-1} SDS.

2.4. Voltammetric Analysis

Voltammetric measurements of PA, DF, and TR in optimized conditions were carried out in a solution composed of 0.075 mol L^{-1} acetate buffer (pH of 4.0 ± 0.1), 1.0×10^{-5} mol L^{-1} DTPA and 15 mg L^{-1} SDS. The procedure consists of an accumulation step at a potential ($E_{acc.}$) of −0.4 V for a time ($t_{acc.}$) of 120 s. Differential pulse adsorptive stripping voltammetric (DPAdSV) curves were recorded from 0 to 2 V with an amplitude (ΔE_A) of 150 mV, a scan rate (ν) of 250 mV s^{-1}, and a modulation time (t_m) of 10 ms. The background curve was subtracted from each voltammogram. The average values of peak current (I_p) are shown with the standard deviation of n = 3.

2.5. HPLC/PDA Analysis

For high-performance liquid chromatography photodiode array detection (HPLC/PDA), a mixture of acetonitrile and water with 0.025% of trifluoroacetic acid was used as mobile phase. The acetonitrile concentration in the eluent increased constantly from 12 to 80% during 0–30 min. The flow rate was 1.0 mL min^{-1} and temperature was set at 25°C. The injection volume was 20 µL. All samples were analyzed in triplicate, at a wavelength of 248 nm, 273 nm, and 277 nm for paracetamol, tramadol, and diclofenac, respectively.

2.6. Real Sample Analysis

Bystrzyca river water (Lublin, Poland), pharmaceuticals (first tablets containing PA (325 mg) and TR (37.5 mg) (Polfarmex S.A., Kutno, Poland) and second tablets containing DF (25 mg) (GSK, Brentford, UK)), and normal human serum from Merck (Darmstadt, Germany) were tested. River water samples were spiked with appropriate concentrations of the analytes and filtered through a 0.45 µm Millipore filter. Pharmaceuticals were prepared as follows. Three tablets of each drug were weighed and the average tablet weights were determined. Then, the three tablets of each drug were powdered in a mortar

and the samples with corresponding average weight of one tablet were dissolved in 100 mL of deionized water. The samples were subsequently placed in an ultrasonic bath for 10 min and filtered through a 0.45 µm Millipore filter. Frozen human serum was thawed at room temperature. Then, 100 µL of the human serum sample 100 times diluted in deionized water spiked with appropriate concentrations of the analytes was transferred to a centrifugal tube, mixed with 50 µL of 7.5% (*w*/*v*) trichloroacetic acid solution (Sigma-Aldrich) for protein precipitation, centrifuged at 4000× *g* for 10 min, and filtered through a 0.45 µm Millipore filter. The collected supernatant was analyzed in triplicates by the optimized voltammetric procedure and HPLC/PDA methods.

3. Results and Discussion

3.1. Microscopic and Electrochemical Characteristic of Sensors

The preliminary studies (Figure 1A) showed that the application of electrochemical treatment of the SPCE surface with H_2O_2 [34] shifts the peak potentials of PA, DF, and TR towards less positive potential values (0.35 vs. 0.26 V for PA, 0.56 vs. 0.50 V for DF, and 1.19 vs. 1.17 V for TR) and contributes to a significant enhancement of the analytical signal of TR (1.6 vs. 2.6 µA for 2.0 × 10^{-5} mol L^{-1}), with a statistically insignificant change in the peak current of PA and DF. The surface morphology of the bare SPCE and the electrochemically activated screen-printed carbon electrode (aSPCE) was examined by SEM. It was found that electrochemical activation leads to visible changes on the surface of the working electrode as the number and size of the pores increase (Figure 1B,C). This is because the organic ink constituents or contaminants introduced into the printing stage can be removed by electrochemical treatment in H_2O_2 [34].

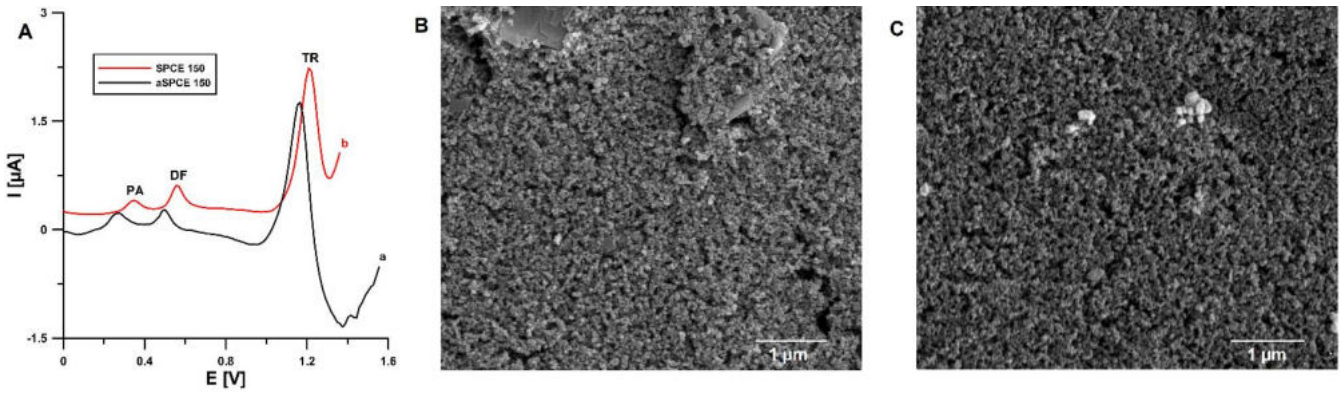

Figure 1. (**A**) Voltammograms of 2 × 10^{-6} mol L^{-1} PA, 1 × 10^{-7} mol L^{-1} DF, and 2 × 10^{-5} mol L^{-1} TR in 0.1 mol L^{-1} CH_3COOH/CH_3COONa buffer of pH 4.0 ± 0.1 recorded at the bare SPCE (a) and electrochemically activated SPCE (b). The DPAdSV parameters: $E_{acc.}$ of −0.25 V, $t_{acc.}$ of 30 s, ΔE_A of 50 mV, t_m of 50 ms, and ν of 140 mV s^{-1}. SEM images with 25,000× magnification of bare SPCE (**B**) and aSPCE (**C**).

Further modification of the activated electrode surface with sodium dodecyl sulfate during the analysis of PA, DF, and TR in a supporting electrolyte solution containing SDS allows for a significant increase in the TR peak (0.74 vs. 1.7 µA for 5.0 × 10^{-6} mol L^{-1} of TR and 15 mg L^{-1} SDS), with a statistically insignificant change in the peak current of PA and DF (Figure 2A). Figure 2B shows the changes in the intensity of the TR peak current with the changing concentration of SDS. The oxidation peak current increased with the concentration of SDS, increasing from 0 to 15.0 mg L^{-1}, and the response decreased when the amount of SDS further increased. The increase of the TR peak current can be explained by the electrostatic attraction between TR cations (the acidic environment) and polar groups ('heads') of the SDS molecules [1]. While the excess of SDS immobilizes the electrode surface, the film becomes detached and decreases the adsorption amount of tramadol. The surface morphology of the activated electrode surface modified with sodium dodecyl sulfate (aSPCE/SDS) imaged using SEM does not differ from the un-

modified electrode (aSPCE) (results not shown). This is because the used concentration of SDS is below the critical micelle concentration and the surfactant in agglomerates is not visible [40]. Moreover, the influence of other surfactants (Triton X-100 and CTAB) on the analytical signals of PA, DF, and TR at the aSPCE was studied (see Section 3.5). However, the PA, DF, and TR signals decreased in the presence of CTAB and Triton-X in the supporting electrolyte.

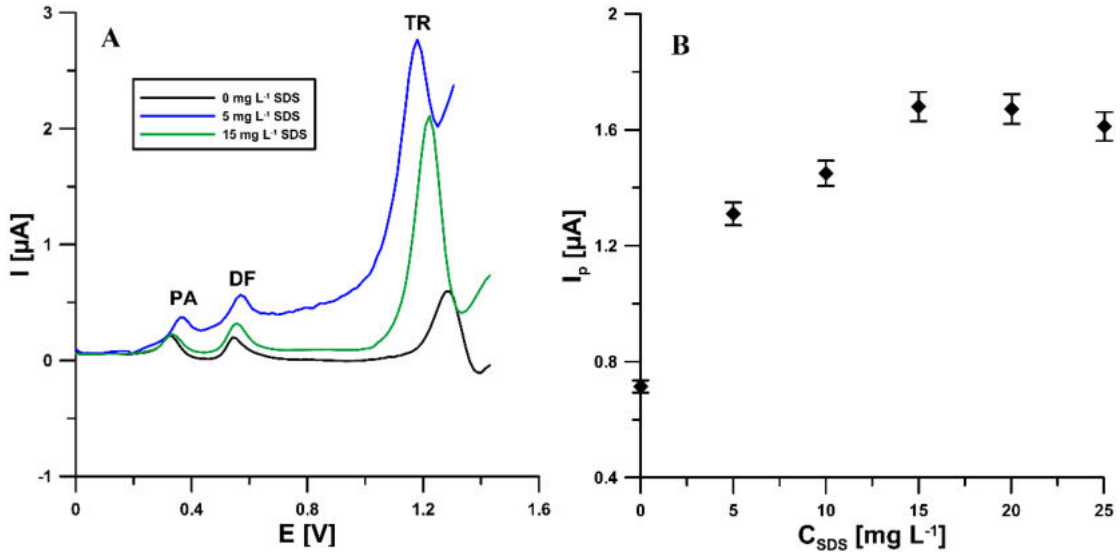

Figure 2. (**A**) Voltammograms of 2×10^{-6} mol L^{-1} PA, 1×10^{-7} mol L^{-1} DF, and 5.0×10^{-6} mol L^{-1} TR in 0.1 mol L^{-1} CH_3COOH/CH_3COONa buffer of pH 4.0 ± 0.1 containing 0, 5, and 15 mg L^{-1} SDS. (**B**) Influence the SDS concentration on voltammetric response of 5.0×10^{-6} mol L^{-1} TR. The DPAdSV parameters as in Figure 1A.

In order to characterize the influence of the modifications on the electrochemical properties of the sensor, measurements using electrochemical impedance spectroscopy (EIS) and cyclic voltammetry (CV) were performed. The impedance spectra (Nyquist plots) were recorded at a potential of 0.25 V in the frequency range from 10 kHz to 0.1 Hz, from a solution of 0.1 mol L^{-1} CH_3COOH/CH_3COONa buffer of pH = 4.0 ± 0.1 containing 1×10^{-3} mol L^{-1} PA, DF, or TR. As can be seen in Figure 3A obtained for the supporting electrolyte containing PA (selected example), electrochemical activation of the electrode causes a significant reduction in the value of the charge transfer resistance (R_{ct}) (red curve) compared to the unactivated electrode (blue curve) (388.7 vs. 950.6 Ω cm^2). It has also been shown that the modification of the aSPCE surface with SDS causes a slight increase in R_{ct} (black curve) compared to the activated electrode (388.7 vs. 487.6 Ω cm^2). In addition, the active surface areas (A_s) of the SPCE, aSPCE, and aSPCE/SDS were calculated using the Randles–Sevcik equation [47]. Figure 3B shows the relationship between anodic peak currents (I_p) and the square root of the scan rates ($v^{1/2}$). For the bare SPCE, aSPCE, and aSPCE/SDS, the A_s is equal to 0.056, 0.054, and 0.059 cm^2, respectively. The A_s is almost the same for all studied electrodes.

To sum up, the SPCE morphology surface changed greatly after electrochemical treatment with H_2O_2. This contributes to lowering the charge transfer resistance of the electrode. The SDS modification slightly increases the charge transfer resistance of the activated electrode but does not block the electrode surface, whereas the active surface areas for the bare SPCE, aSPCE, and aSPCE/SDS are almost the same.

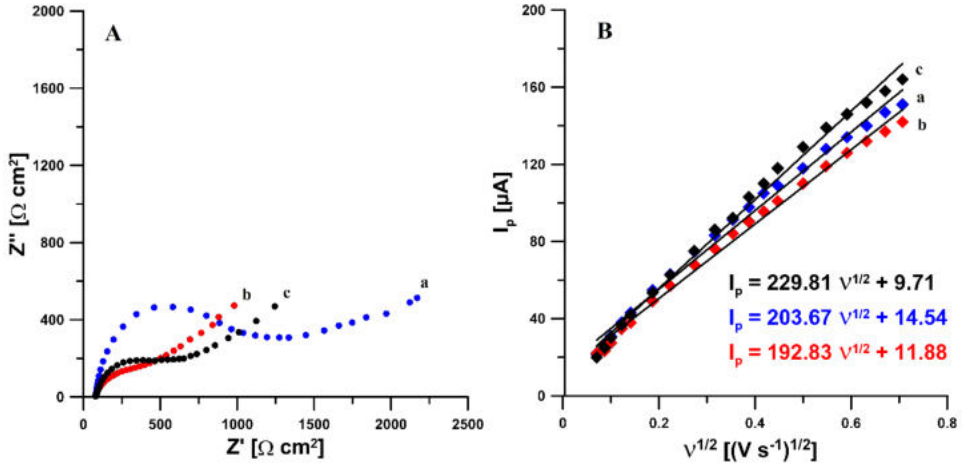

Figure 3. (**A**) Nyquist plots of SPCE (a), aSPCE (b), and aSPCE/SDS recorded at a potential of 0.25 V, in the frequency range from 10 kHz to 0.1 Hz, from a solution of 0.1 mol L^{-1} CH_3COOH/CH_3COONa buffer of pH = 4.0 ± 0.1 containing 1 × 10^{-3} mol L^{-1} PA. (**B**) Dependence between anodic peak currents and the square root of scan rates obtained in 0.1 mol L^{-1} KCl containing 5.0 mmol L^{-1} $K_3[Fe(CN)_6]$ at the SPCE (a), aSPCE (b), and aSPCE/SDS (c), ν range: 5.0–500 mV s^{-1}.

3.2. Influence of pH

The effect of the type and pH of the supporting electrolyte on the signals of 2 × 10^{-6} mol L^{-1} PA, 1 × 10^{-7} mol L^{-1} DF, and 2 × 10^{-5} mol L^{-1} TR was investigated for 0.1 mol L^{-1} of H_2SO_4, CH_3COOH solutions, and CH_3COOH/CH_3COONa buffers with pH of 3.5 ± 0.1, 4.0 ± 0.1, 4.5 ± 0.1, 5.0 ± 0.1, 5.5 ± 0.1, and 6.0 ± 0.1. The corresponding data are presented in Figure 4A. As can be seen for the simultaneous determination of PA and TR, a sulfuric acid solution should be used as the supporting electrolyte. However, in the case of the simultaneous determination of PA, DF, and TR, the acetate buffer at pH of 4.0 ± 0.1 is the best choice considering the peak currents. In addition, the influence of the concentration of the selected supporting electrolyte on the voltammetric response of the analytes was also checked (Figure 4B) and it was shown that the highest peak current values were obtained for 0.075 mol L^{-1} CH_3COOH/CH_3COONa buffer of pH of 4.0 ± 0.1, hence it was used for further research.

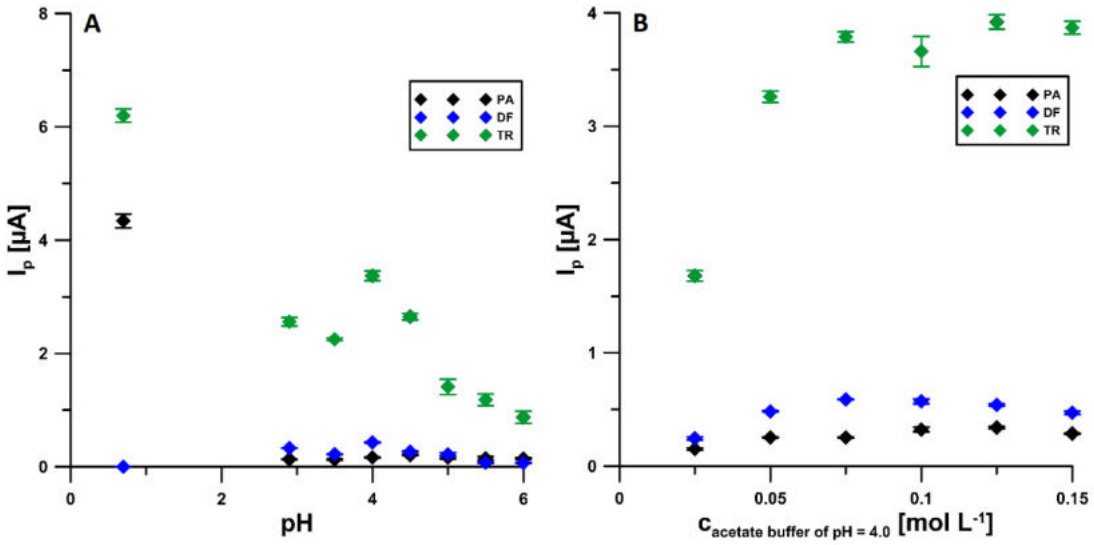

Figure 4. Effect of pH (**A**) and the concentration of the CH_3COOH/CH_3COONa buffer solution with a pH of 4.0 ± 0.1 (**B**) on the signals of 2 × 10^{-6} mol L^{-1} PA, 1 × 10^{-7} mol L^{-1} DF, and 2 × 10^{-5} mol L^{-1} TR. The DPAdSV parameters as in Figure 1A.

3.3. Adsorption Studies

The information on the electrochemical response of PA, DF, and TR on the aSPCE/SDS was obtained from the analysis of differential capacity curves. For each analyte, measurements were made at a frequency of 200 Hz in the potential range of −0.1 to 2 V. Based on the obtained results, it can be concluded that the SDS used as a modifier adsorbs onto the aSPCE surface, which is evidenced by the difference in the curves of the double layer interface aSPCE/acetate buffer of pH = 4.0 in the absence and presence of 15 mg L^{-1} SDS (Figure 5A). No adsorption peaks of any of the analytes occurred in the potential range used. However, in the presence of PA, a desorption peak can be seen at a potential of 0.25 V, the height of which increases with the increasing concentration of PA in the solution (Figure 5B). This proves the strong adsorption of PA. In the case of adding DF, for a concentration of 2×10^{-6} mol L^{-1} and higher, two very small desorption peaks (0.3 and 0.45 V) can be noticed, which may indicate slight adsorption of this analyte on the aSPCE/SDS surface (Figure 5C). Figure 5D shows the differential capacity curves recorded for increasing TR concentrations. No peak was observed here, which makes it possible to conclude that TR existing in the cationic form reaches the electrode by diffusion and becomes electrostatically attracted by the surface adsorbed SDS anions.

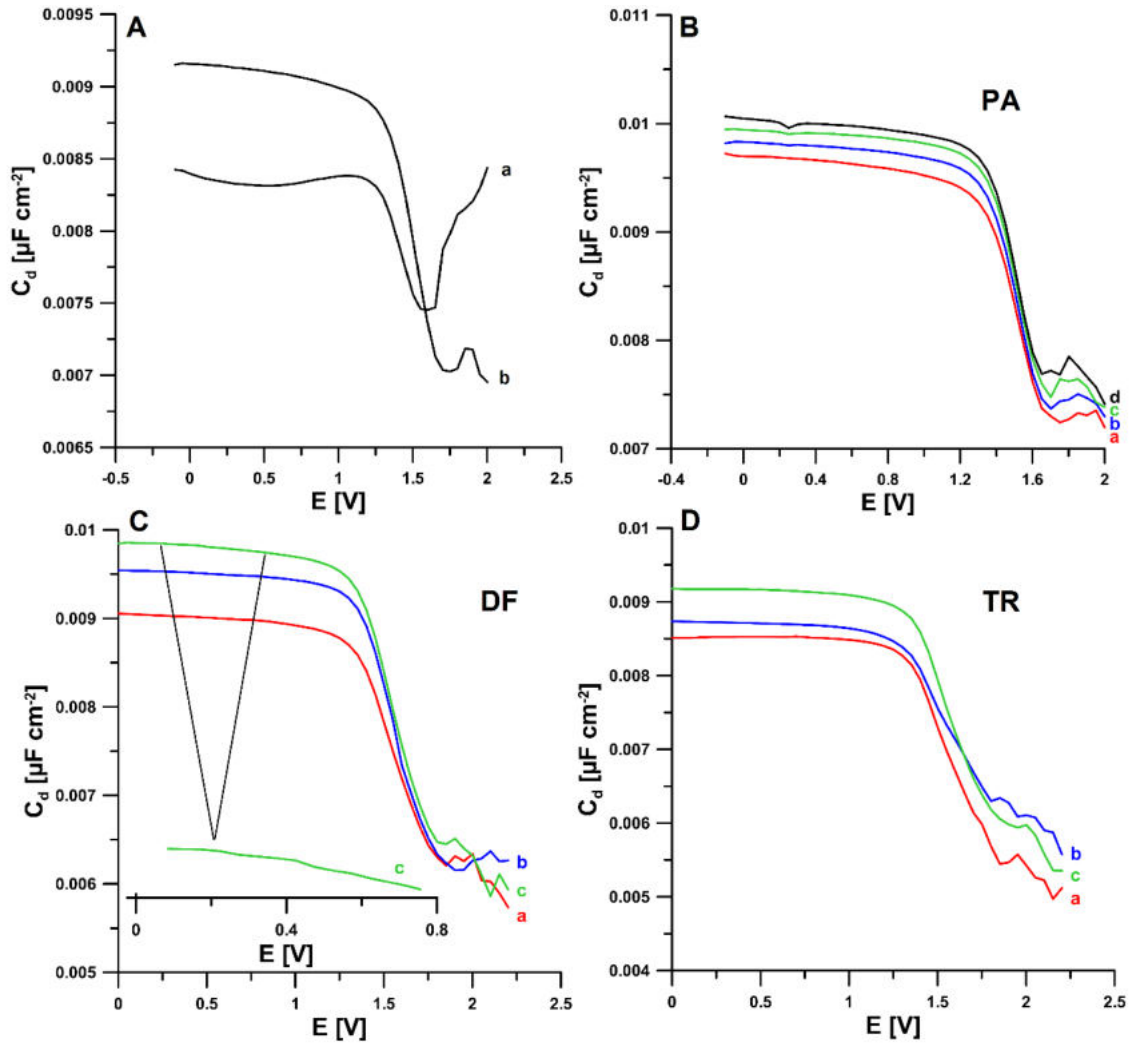

Figure 5. The differential capacity-potential curves of the double layer interface aSPCE/acetate buffer of pH = 4.0 ± 0.1 in the presence of: (**A**) 0 (a) and 15 (b) mg L^{-1} SDS, (**B**) 15 mg L^{-1} SDS and (a) 2×10^{-7}, (b) 2×10^{-6}, (c) 2×10^{-5}, (d) 2×10^{-4} mol L^{-1} PA, (**C**) 15 mg L^{-1} SDS and (a) 2×10^{-7}, (b) 2×10^{-6}, (c) 2×10^{-5} mol L^{-1} DF, (**D**) 15 mg L^{-1} SDS and (a) 2×10^{-7}, (b) 2×10^{-6}, (c) 2×10^{-5} mol L^{-1} TR.

3.4. Optimization of Procedure Parameters

In order to find the most optimal conditions for the analysis of PA, DF, and TR at the aSPCE/SDS, the effect of parameters such as the accumulation potential ($E_{acc.}$) and time ($t_{acc.}$), amplitude (ΔE_A), scan rate (ν), and modulation time (t_m) on the peak currents was investigated. The effect of E_{acc} was tested in the range from 0 to −0.5 V with the $t_{acc.}$ of 30 s. The highest signals were obtained at a potential of −0.4 V (Figure 6A). Then, for the selected value of the potential, the effect of $t_{acc.}$ in the range of 15–300 s was investigated. The $t_{acc.}$ of 120 s was chosen (Figure 6B), but the accumulation stage can be extended to obtain lower detection limits.

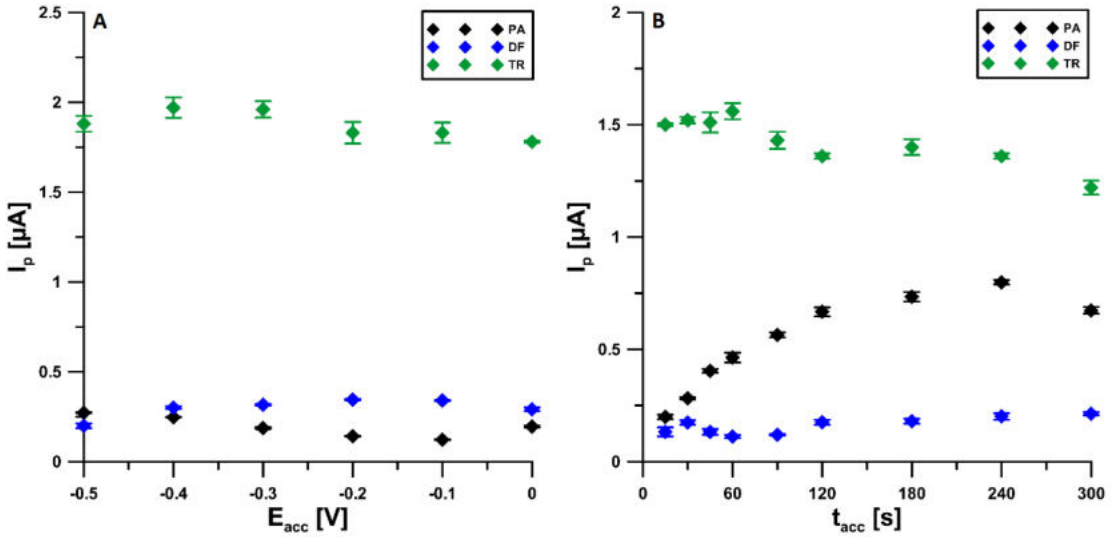

Figure 6. Influence of $E_{acc.}$ (**A**) and $t_{acc.}$ (**B**) on voltammetric response of 2×10^{-6} mol L^{-1} PA, 1×10^{-7} mol L^{-1} DF, and 1×10^{-5} mol L^{-1}TR. The DPAdSV parameters: ΔE_A of 50 mV, t_m of 50 ms, and ν of 140 mV s^{-1}.

The ΔE_A varied from 25 to 175 mV. For further experiments, the value of 150 mV was selected (Figure 7A). Then, the effect of ν in the range of 50–300 mV s^{-1} was checked. It was found that the highest PA and DF signals were recorded for ν equal to 250 mV s^{-1} and this value was considered as the most optimal. For ν equal to 300 mV s^{-1}, the TR peak was higher, but the PA and DF signals decreased (Figure 7B). The last analyzed parameter was t_m checked in the range of 2 to 40 ms. The highest signals of all three tested compounds were recorded for the t_m of 10 ms (Figure 7C).

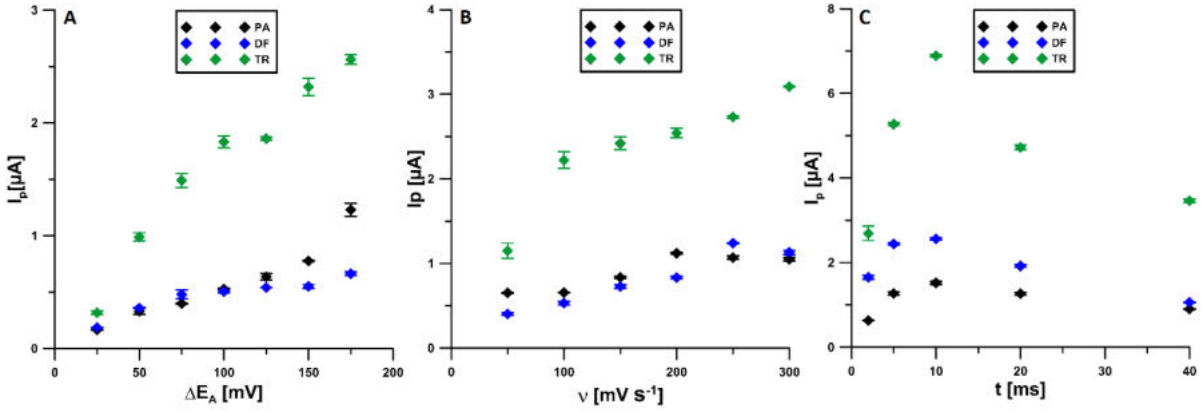

Figure 7. Influence of ΔE_A (**A**), ν (**B**), and t_m (**C**) on voltammetric response of 2×10^{-6} mol L^{-1}PA, 1×10^{-7} mol L^{-1} DF, and 1×10^{-5} mol L^{-1} TR. The DPAdV parameters: $E_{acc.}$ of −0.4 V and $t_{acc.}$ of 120 s.

3.5. Selectivity

In the optimized conditions, the influence of potential interferents on the determination of PA, DF, and TRA was investigated. The tolerance limit was defined as the concentration, which gave an error of $\leq 10\%$ in the determination of 5×10^{-6} mol L^{-1} PA, 2×10^{-7} mol L^{-1} DF, and 2×10^{-6} mol L^{-1} TR. It needs to be highlighted that the addition of 1.0×10^{-5} mol L^{-1} DTPA to the supporting electrolyte solution was applied. This was to minimize the interference from metal ions due to their complexation with DTPA. It was noticed that an excess of glucose (up to 100-fold), ascorbic acid (up to 10-fold), Fe(III) (up to 10-fold), Ca(II) (up to 40-fold), Cu(II) (up to 2-fold), Mg(II) (up to 100-fold), Cd(II) (up to 10-fold), Pb(II) (up to 1000-fold), Ni(II) ions (up to 10-fold), Mo(VI) (up to 200-fold), and Cl(-I) (up to 20-fold) had negligible effects on the assay of PA. It was observed that an excess of glucose (up to 2500-fold), ascorbic acid (up to 100-fold), Fe(III) (up to 100-fold), Ca(II) (up to 100-fold), Cu(II) (up to 25-fold), Mg(II) (up to 500-fold), Cd(II) (up to 10-fold), Pb(II) (up to 1000-fold), Ni(II) (up to 25-fold), Mo(VI) (up to 500-fold), and Cl(-I) (up to 2500-fold ex) had negligible effects on the assay of DF. Moreover, an excess of glucose (up to 2500-fold), ascorbic acid (up to 5-fold), Fe(III) (up to 100-fold), Ca(II) (up to 500-fold), Cu(II) (up to 10-fold), Mg(II) (up to 250-fold), Cd(II) (up to 25-fold), Pb(II) (up to 1000-fold), Ni(II) (up to 25-fold), Mo(VI) (up to 50-fold), and Cl(-I) (up to 25-fold) had negligible effects on the assay of TR.

Due to the fact that natural waters contain surfactants with a surface active effect comparable to the effect of 0.2 to 2 mg L^{-1} of Triton X-100 [48], the influence of 2 mg L^{-1} of Triton X-100 on the voltammetric response of 5×10^{-6} mol L^{-1} PA, 2×10^{-7} mol L^{-1} DF, and 2×10^{-6} mol L^{-1} TR was investigated. Moreover, the influence of cationic surfactant (CTAB) was studied. As can be seen in Figure 8, the adsorption of SDS on the aSPCE surface contributes to minimizing the effect of the surfactants (Triton X-100 and CTAB) on the analytical signal of all analyzed substances. In the presence of 2 ppm of Triton X -100, 2 ppm of CTAB, and 15 mg L^{-1} SDS in the supporting electrolyte, the signals do not fall below 60% of their original values and are well formed and easy to measure.

3.6. Analytical Characteristic

Under the optimized conditions, the ability of the aSPCE/SDS for individual and simultaneous determination of PA, DF, and TR was studied. The results are summarized in Table 1. Figure 9 shows the voltammograms and linear ranges of the calibration plots obtained during simultaneous determination of PA, DF, and PA. The limits of detection (LOD) and quantification (LOQ) obtained during simultaneous determination of PA, DF, and TR are 14.87, 0.21, and 1.71 nmol L^{-1}, and 49.56, 0.69, and 5.69 nmol L^{-1}, respectively, according to the definitions of LOD = $3SD_a/b$ and LOQ = $10SD_a/b$ (SD_a—standard deviation of intercept (n = 3); b—slope of calibration curve) [49]. Table 2 shows the comparison techniques used for the determination of PA, DF, and TR. It should be clearly emphasized that the proposed voltammetric procedure using the aSPCE/SDS mostly allows a significantly lower LOD to be obtained than those obtained for other techniques [7–12,14,16–18,47]. In the case of the article [9], the calculated LOD of TR is lower (5.33×10^{-10} vs. 1.71×10^{-9} mol L^{-1}), but the first concertation of TR from the calibration graph is higher than the one obtained at the aSPCE/SDS (1.67×10^{-8} vs. 1.0×10^{-8} mol L^{-1}). On the other hand, in the article [15], the LOD is equal to the first concertation of TR, which is incorrect. Moreover, both techniques [9,15] require more expensive equipment, the procedures are more laborious, and more reagents are used. Furthermore, it should be emphasized that this is the first electrochemical sensor for simultaneous determination of PA, DF, and TR.

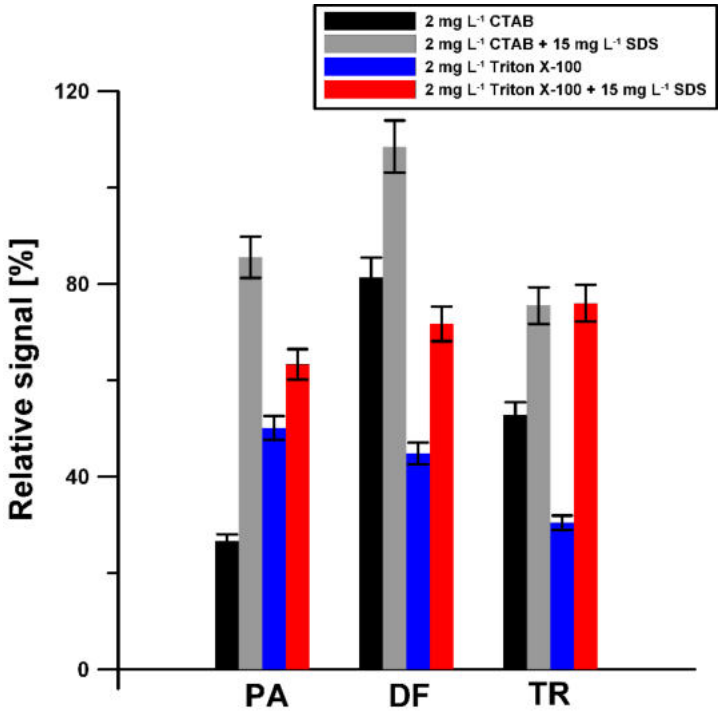

Figure 8. Influence of 2 ppm Triton X-100 and CTAB on voltammetric response of 5×10^{-6} mol L^{-1} PA, 2×10^{-7} mol L^{-1} DF, and 2×10^{-6} mol L^{-1} TR in the absence and presence of 15 mg L^{-1} SDS.

Table 1. Analytical parameters obtained for individual and simultaneous determination of PA, DF, and TR at the aSPCE/SDS.

Parameter	PA	DF	TR	PA, DF, and TR
Linear range (nmol L^{-1})	50–100000	1–200	10–200 200–2000	50–20,000 (PA) 1–200 (DF) 10–200 (TR) 200–2000 (TR)
Calibration graph equation I_p (μA) c_{PA} (μmol L^{-1}) c_{DF} (nmol L^{-1}) c_{TR} (μmol L^{-1})	$I_p = 0.30c_{PA} + 0.77$	$I_p = 14.27c_{DF} + 0.063$	$I_p = 5.95c_{TR} + 0.33$ $I_p = 1.63c_{TR} + 1.31$	$I_p = 0.44c_{PA} + 0.10$ $I_p = 11.62c_{DF} + 0.024$ $I_p = 5.51c_{TR} + 0.34$ $I_p = 1.61\ c_{TR} + 1.23$
Correlation coefficient (r)	0.9947	0.9967	0.9940 0.9947	0.9983 (PA) 0.9996 (DF) 0.9945 (TR) 0.9952 (TR)
LOD (nmol L^{-1})	12.93	0.12	2.47	14.87 (PA) 0.21(DF) 1.71 (TR)
LOQ (nmol L^{-1})	43.09	0.39	8.24	49.56 (PA) 0.69 (DF) 5.69 (TR)

Additionally, the precision was verified for the determination of 5×10^{-6} mol L^{-1} PA, 2×10^{-7} mol L^{-1} DF, and 2×10^{-7} mol L^{-1} TR with ten replicates. The results were 2.7, 1.2, and 1.8%, respectively, indicating the satisfactory repeatability of the signals at the aSPCE/SDS. The reproducibility was assessed based on voltammograms registered in the solution containing 1×10^{-6} mol L^{-1} PA, 1×10^{-8} mol L^{-1} DF, and 2×10^{-7} mol L^{-1} TR at three freshly prepared electrodes. The RSD was calculated as 2.5, 3.1, and 3.5% (n = 6), respectively, confirming the acceptable reproducibility of the aSPCE/SDS.

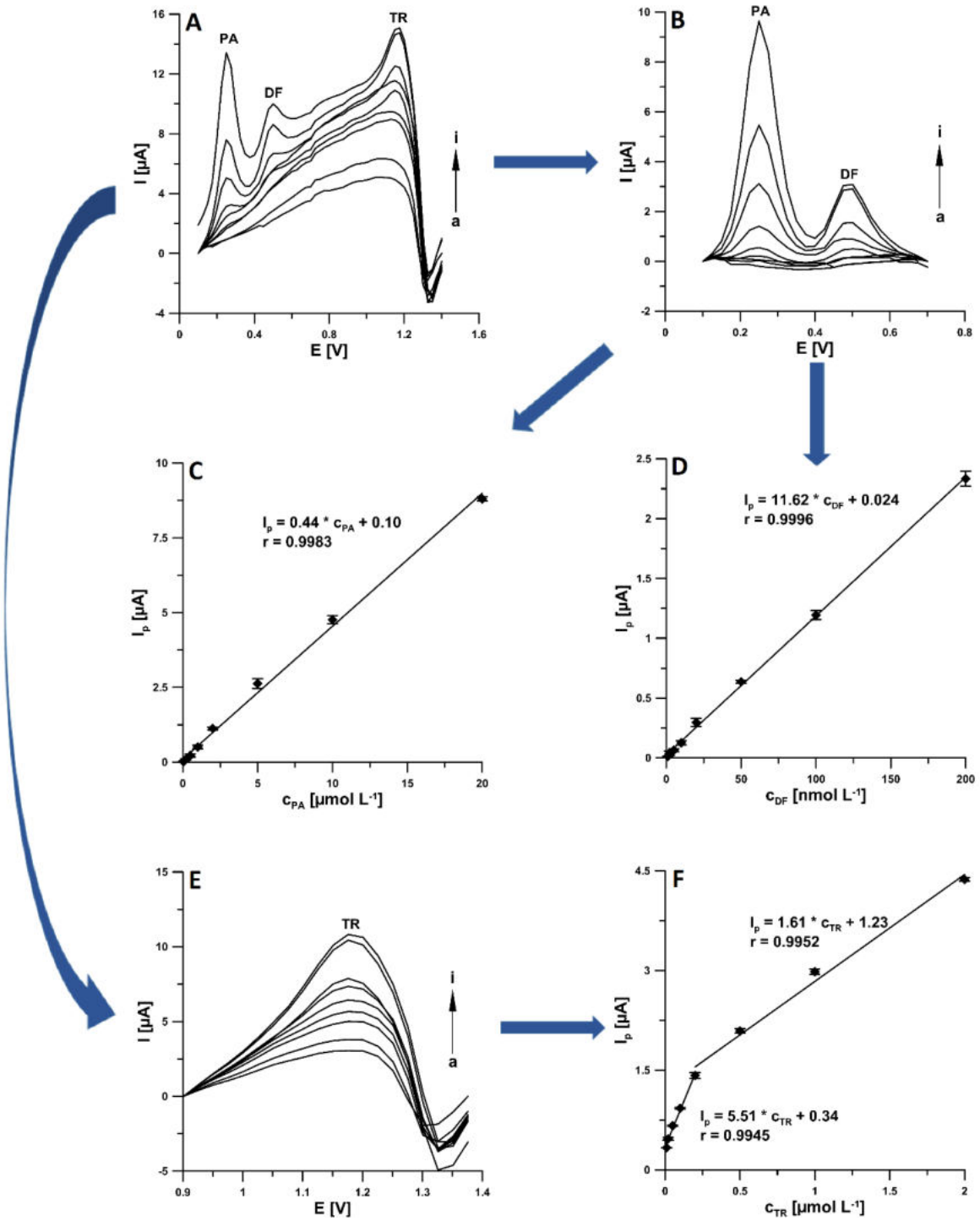

Figure 9. (**A**) Voltammograms obtained at the aSPCE/SDS in 0.075 mol L^{-1} CH_3COOH/CH_3COONa buffer solution of pH 4.0 ± 0.1 containing increasing concentrations of PA (a–i, 0.05, 0.1, 0.2, 0.5, 1, 2, 5, 10, 20 µmol L^{-1}), DF (a–i, 0.001, 0.002, 0.005, 0.01, 0.02, 0.05, 0.1, 0.2, 0.2 µmol L^{-1}), TR (a–i, 0.01, 0.02, 0.05, 0.1, 0.2, 0.5, 1, 2, 2 µmol L^{-1}). (**B**) Segment of voltammograms (A) in the potential range of 0.1–0.7 V. Linear range of the calibration curve of PA (**C**) and DF (**D**,**E**) Segment of voltammograms (A) in the potential range of 0.9–1.4 V. (**F**) Linear ranges of the calibration curve of TR. The DPAdSV parameters: $E_{acc.}$ of −0.4 V, $t_{acc.}$ of 120 s, ΔE_A of 50 mV, t_m of 10 ms, and ν of 250 mV s^{-1}.

Table 2. Comparison of techniques for analysis of PA, DF, and TR.

Method	Analyte	Linear Range (mol L^{-1})	LOD (mol L^{-1})	Application	Ref.
HPLC	PA	5.74×10^{-4}–9.93×10^{-4}	1.50×10^{-5}	Pharmaceutical formulations	[7]
HPLC	DF	3.14×10^{-9}–2.30×10^{-6} 1.26×10^{-8}–1.97×10^{-6}	3.77×10^{-10} 1.57×10^{-9}	Hospital wastewater, human serum	[8]
HPLC	TR	1.67×10^{-8}–1.0×10^{-6}	5.33×10^{-10}	Urine, plasma	[9]
LC-MS/MS	PA	8.28×10^{-7}–3.31×10^{-4}	2.21×10^{-8}	Human plasma	[10]
LC-MS/MS	DF	1.57×10^{-8}–3.14×10^{-5}	6.29×10^{-9}	Cow plasma	[11]
LC-MS/MS	TR	6.67×10^{-8}–8.33×10^{-7}	8.66×10^{-9}	Pharmaceutical formulations	[12]
GC-MS	PA	4.97×10^{-4}–3.31×10^{-3}	1.32×10^{-4}	Pharmaceutical formulations	[47]
GC-MS	DF	7.86×10^{-10}–1.57×10^{-7}	3.93×10^{-10}	Human plasma	[14]
GC-MS	TR	1.50×10^{-9}–1.0×10^{-6} 1.83×10^{-8}–8.33×10^{-7} 8.33×10^{-9}–1.0×10^{-6}	1.50×10^{-9} 8.33×10^{-9} 2.67×10^{-9}	Plasma, urine, saliva	[15]
Spectrophotometry	PA	0–9.94×10^{-4}	-	Pharmaceutical formulations	[16]
Spectrophotometry	DF	1.57×10^{-5}–2.52×10^{-4}	-	Pharmaceutical formulations	[17]
Spectrophotometry	TR	5.67×10^{-6}–1.43×10^{-5}	-	Pharmaceutical formulations	[18]
DPAdSV	PA	5.0×10^{-8}–2.0×10^{-5}	1.49×10^{-8}	River water, human serum, pharmaceutical formulations	This work
	DF	1.0×10^{-9}–2.0×10^{-7}	2.10×10^{-10}		
	TR	1.0×10^{-8}–2.0×10^{-7} 2.0×10^{-7}–2.0×10^{-6}	1.71×10^{-9}		

3.7. Sample Analysis

In order to confirm the usefulness of the developed voltammetric procedure at the aS-PCE/SDS, the simultaneous determination of PA, DF, and TR was carried out in Bystrzyca river water samples and human serum samples, the results of which are presented in Table 3. The recovery values obtained by DPV were between 97.0 and 102.0%, which corresponds to a satisfactory degree of accuracy of the method. The HPLC/PDA was used as a comparative method for the determination of PA, DF, and TR in river water and human serum samples. However, the concentrations of PA, DF, and TR were below the detection limits of the chromatographic method. The calculated LOD by HPLC/PDA for PA, DF, and TR was 2.4×10^{-7}, 5.2×10^{-7}, and 2.7×10^{-7} mol L^{-1}, respectively. Moreover, the contents of the analytes, PA and TR in the pharmaceutical tablets 1 and DF in the pharmaceutical tablets 2, were determined. The results are summarized in Table 4. The obtained values are consistent with the values declared by the manufacturer. The calculated relative errors (0–2.1%) indicated that there were no important matrix interferences for the pharmaceuticals analyzed by the proposed DPAdSV procedure at the SPCE/SDS.

Table 3. The results of simultaneous PA, DF, and TR determination in river water and human serum samples.

Sample	PA Concentration (nmol L^{-1}) ± SD (n = 3)			Recovery * (%)
	Added	Found DPAdSV	Found HPLC/PDA	
Bystrzyca river	0	<LOD	<LOD	-
	200	191 ± 9.0	<LOD	97.0
Human serum	0	<LOD	<LOD	-
	200	204 ± 1.2	<LOD	102.0

Table 3. *Cont.*

Sample	DF concentration (nmol L^{-1}) ± SD (n = 3)			Recovery * (%)
	Added	Found DPAdSV	Found HPLC/PDA	
Bystrzyca river	0	<LOD	<LOD	-
	20	20.1 ± 0.2	<LOD	100.5
Human serum	0	<LOD	<LOD	-
	20	19.7 ± 1.0	<LOD	98.5
Sample	**TR concentration (nmol L^{-1}0 ± SD (n = 3)**			**Recovery * (%)**
	Added	**Found DPAdSV**	**Found HPLC/PDA**	
Bystrzyca river	0	<LOD	<LOD	-
	20	20.4 ± 0.6	<LOD	102.0
Human serum	0	<LOD	<LOD	-
	20	20.0 ± 0.4	<LOD	100.0

* Recovery (%) = (Found DPAdSV × 100)/Added.

Table 4. The results obtained during the determination of PA, DF, and TR in pharmaceutical formulations at the aSPCE/SDS.

Tablets	Compound	Label Value (mg)	Determined DPAdSV (mg) ± SD (n = 3)	Relative Error * (%)
1	PA	325.0	321.3 ± 3.8	1.1
	TR	37.5	38.3 ± 2.1	2.1
2	DF	25.0	25.0 ± 0.64	0.0

* Relative error (%) = (|DPAdSV value − label value|/label value) × 100.

4. Conclusions

In summary, in this study, an electrochemically activated screen-printed carbon electrode modified with sodium dodecyl sulfate (aSPCE/SDS) was introduced for the first time for the simultaneous analysis of paracetamol (PA), diclofenac (DF), and tramadol (TR). The electrochemical activation of the SPCE surface using CV in acetate buffer of pH = 4.0 ± 0.1 containing H_2O_2 significantly changes the electrode surface morphology and reduces the charge transfer resistance. The modification with SDS allows for the enhancement of the TR signal, while not negatively affecting the PA and DF signals, and greatly minimizes the influence of surfactants (Triton X-100 and CTAB) on the analytical signal of all analyzed substances. The DPAdSV procedure with the aSPCE/SDS allows for selective determination of low PA, DF, and TR concentrations. The LODs and LOQs obtained during simultaneous determination of PA, DF, and TR are 14.87 and 49.56 nmol L^{-1}, 0.21 and 0.69 nmol L^{-1}, and 1.71 and 5.69 nmol L^{-1}, respectively. The developed sensor was successfully used to determine PA, DF, and TR in river water and human serum samples as well as in pharmaceutical preparations. The concentrations of PA, DF, and TR determined by DPAdSV method in river water and human serum samples were below the detection limits of the chromatographic method (HPLC/PDA). The obtained results show that the procedure can be used as a quick, simple, and cheap alternative to other methods. Moreover, it should be highlighted that the further advantage of the aSPCE/SDS sensor is it portability, which is very promising for quick field analysis.

Author Contributions: Conceptualization, J.K. and K.T.-R.; methodology, J.K. and K.T.-R.; investigation, J.K., K.T.-R., M.W. and I.S.; writing—original draft preparation, J.K. and K.T.-R.; writing—review and editing, J.K., K.T.-R., M.W. and I.S.; supervision, K.T.-R. All authors have read and agreed to the published version of the manuscript.

Funding: This research received no external funding.

Institutional Review Board Statement: Not applicable.

Informed Consent Statement: Not applicable.

Data Availability Statement: Not applicable.

Conflicts of Interest: The authors declare no conflict of interest.

References

1. Yunusoğlu, O.; Allahverdiyeva, S.; Yardım, Y.; Şentürk, Z. A simple approach to simultaneous electroanalytical quantification of acetaminophen and tramadol using a boron-doped diamond electrode in the existence of sodium dodecyl sulfate. *Electroanalysis* **2020**, *32*, 429–436. [CrossRef]
2. Sasal, A.; Tyszczuk-Rotko, K.; Wójciak, M.; Sowa, I.; Kuryło, M. Simultaneous analysis of paracetamol and diclofenac using MWCNTs-COOH modified screen-printed carbon electrode and pulsed potential accumulation. *Materials* **2020**, *13*, 3091. [CrossRef] [PubMed]
3. Cao, F.; Dong, Q.; Li, C.; Chen, J.; Ma, X.; Huang, Y.; Song, D.; Ji, C.; Lei, Y. Electrochemical sensor for detecting pain reliever/fever reducer drug acetaminophen based on electrospun CeBiOx nanofibers modified screen-printed electrode. *Sens. Actuators B* **2018**, *256*, 143–150. [CrossRef]
4. Kimuama, K.; Rodthongkumb, N.; Ngamrojanavanichc, N.; Chailapakuld, O.; Ruecha, N. Single step preparation of platinum nanoflowers/reduced graphene oxide electrode as a novel platform for diclofenac sensor. *Microchem. J.* **2020**, *155*, 104744. [CrossRef]
5. Hassannezhad, M.; Hosseini, M.; Ganjali, M.R.; Arvand, M. A graphitic carbon nitride (g-C3N4/Fe3O4) nanocomposite: An efficient electrode material for the electrochemical determination of tramadol in human biological fluids. *Anal. Methods* **2019**, *11*, 2064–2071. [CrossRef]
6. Rokhsefid, N.; Shishehbore, M.R. Synthesis and characterization of an Au nanoparticles/graphene nanosheet nanocomposite and its application for the simultaneous determination of tramadol and acetaminophen. *Anal. Methods* **2019**, *11*, 5150–5159. [CrossRef]
7. Ali, A.; Athar, M.M.; Ahmed, M.; Nadeem, K.; Murtaza, G.; Farooq, U.; Salman, M. Stability-indicating HPLC-PDA assay for simultaneous determination of paracetamol, thiamine and pyridoxal phosphate in tablet formulations. *Acta Pharm.* **2019**, *69*, 249–259. [CrossRef]
8. Soheili-Azad, P.; Yaftian, M.R.; Dorraji, M.S.S. Zn/Al-layered double hydroxide–graphene oxide nanocomposite use in the solid-phase extraction–preconcentration and HPLC determination of diclofenac. *Chem. Pap.* **2020**, *74*, 4419–4432. [CrossRef]
9. Hamid, Y.; Fat'Hi, M.R. A simple vortex-assisted graphene oxide nanosheets dispersive micro-solid phase extraction combined with high-performance liquid chromatography for UV-Vis detection of tramadol in biological samples. *Sep. Sci. Technol.* **2018**, *53*, 1689–1697. [CrossRef]
10. Kam, R.K.; Chan, M.H.; Wong, H.T.; Ghose, A.; Dondorp, A.M.; Plewes, K.; Tarning, J. Quantitation of paracetamol by liquid chromatography–mass spectrometry in human plasma in support of clinical trial. *Future Sci. OA* **2018**, *4*, FSO331. [CrossRef]
11. Yang, Y.J.; Liu, X.W.; Kong, X.J.; Qin, Z.; Li, S.H.; Jiao, Z.H.; Li, J.Y. An LC–MS/MS method for the quantification of diclofenac sodium in dairy cow plasma and its application in pharmacokinetics studies. *Biomed. Chromatogr.* **2019**, *33*, e4520. [CrossRef]
12. Abdel-Megied, A.M.; Bahr El-din, K.M. Development of a novel LC-MS/MS method for detection and quantification of tramadol hydrochloride in presence of some mislabeled drugs: Application to counterfeit study. *Biomed Chromatogr.* **2019**, *33*, e4486. [CrossRef] [PubMed]
13. Saito, T.; Morita, S.; Inoue, S.; Yamamoto, I.; Inokuchi, S. GC-MS assay for acetaminophen in human hair segments. *Forensic Toxicol.* **2008**, *26*, 27–30. [CrossRef]
14. Shah, I.; Barker, J.; Naughton, D.P.; Barton, S.J.; Ashraf, S.S. Determination of diclofenac concentrations in human plasma using a sensitive gas chromatography mass spectrometry method. *Chem. Cent. J.* **2016**, *10*, 52. [CrossRef]
15. Adlnasab, L.; Shahdousti, P.; Ahmar, H. Layered double hydroxide intercalated with tyrosine for ultrasonic-assisted microextraction of tramadol and methadone from biological samples followed by GC/MS analysis. *Microchim. Acta* **2020**, *187*, 265. [CrossRef]
16. Behera, S.; Ghanty, S.; Ahmad, F.; Santra, S.; Banerjee, S. UV-Visible spectrophotometric method development and validation of assay of paracetamol tablet formulation. *J. Anal. Bioanal. Tech.* **2012**, *3*, 1000151. [CrossRef]
17. Darweesh, S.A.; Khalaf, H.S.; Al-Khalisy, R.S.; Yaseen, H.M.; Mahmood, R.M. Advancement and validation of new derivatives spectrophotometric method for individual and simultaneous estimation of diclofenac sodium and nicotinamide. *Orient. J. Chem.* **2018**, *34*, 1625–1632. [CrossRef]
18. Glavanović, S.; Glavanović, M.; Tomišić, V. Simultaneous quantitative determination of paracetamol and tramadol in tablet formulation using UV spectrophotometry and chemometric methods. *Spectrochim. Acta A Mol. Biomol. Spectrosc.* **2016**, *157*, 258–264. [CrossRef]
19. Bagherinasab, Z.; Beitollahi, H.; Yousefi, M.; Bagherzadeh, M.; Hekmati, M. Rapid sol gel synthesis of BaFe12O19 nanoparticles: An excellent catalytic application in the electrochemical detection of tramadol in the presence of acetaminophen. *Microchem. J.* **2020**, *156*, 104803. [CrossRef]
20. Demir, N.; Atacan, K.; Ozmen, M.; Bas, S.Z. Design of a new electrochemical sensing system based on MoS2–TiO2/reduced graphene oxide nanocomposite for the detection of paracetamol. *New J. Chem.* **2020**, *44*, 11759–11767. [CrossRef]
21. Sasal, A.; Tyszczuk-Rotko, K.; Chojecki, M.; Korona, T.; Nosal-Wiercińska, A. Direct determination of paracetamol in environmental samples using screen-printed carbon/carbon nanofibers sensor—Experimental and theoretical studies. *Electroanalysis* **2020**, *32*, 1618–1628. [CrossRef]

22. Ibáñez-Redín, G.; Wilson, D.; Gonçalves, D.; Oliveira, O.N., Jr. Low-cost screen-printed electrodes based on electrochemically reduced graphene oxide-carbon black nanocomposites for dopamine, epinephrine and paracetamol detection. *J. Colloid Interface Sci.* **2018**, *515*, 101–108. [CrossRef] [PubMed]
23. Raymundo-Pereira, P.A.; Gomes, N.O.; Machado, S.A.S.; Oliveira, O.N., Jr. Simultaneous, ultrasensitive detection of hydroquinone, paracetamol and estradiol for quality control of tap water with a simple electrochemical method. *J. Electroanal. Chem.* **2019**, *848*, 113319. [CrossRef]
24. Serrano, N.; Castilla, Ò.; Ariño, C.; Diaz-Cruz, M.S.; Díaz-Cruz, J.M. Commercial screen-printed electrodes based on carbon nanomaterials for a fast and cost-effective voltammetric determination of paracetamol, ibuprofen and caffeine in water samples. *Sensors* **2019**, *19*, 4039. [CrossRef] [PubMed]
25. Mahmoud, B.G.; Khairy, M.; Rashwan, F.A.; Banks, C.E. Simultaneous voltammetric determination of acetaminophen and isoniazid (hepatotoxicity-related drugs) utilizing bismuth oxide nanorod modified screen-printed electrochemical sensing platforms. *Anal. Chem.* **2017**, *89*, 2170–2178. [CrossRef]
26. Zhanga, Y.; Jiangc, X.; Zhanga, J.; Zhangc, H.; Lia, Y. Simultaneous voltammetric determination of acetaminophen and isoniazid using MXene modified screen-printed electrode. *Biosens. Bioelectron.* **2019**, *130*, 315–321. [CrossRef] [PubMed]
27. Ortiz-Aguayo, D.; Bonet-San-Emeterio, M.; del Valle, M. Simultaneous voltammetric determination of acetaminophen, ascorbic acid and uric acid by use of integrated array of screen-printed electrodes and chemometric tools. *Sensors* **2019**, *19*, 3286. [CrossRef]
28. Deroco, P.B.; Fatibello-Filho, O.; Arduini, F.; Moscone, D. Effect of different carbon blacks on the simultaneous electroanalysis of drugs as water contaminants based on screen-printed sensors. *Electroanalysis* **2019**, *31*, 2145–2154. [CrossRef]
29. Karikalan, N.; Karthik, R.; Chen, S.-M.; Velmurugan, M.; Karuppiah, C. Electrochemical properties of the acetaminophen on the screen printed carbon electrode towards the high performance practical sensor applications. *J. Colloid Interface Sci.* **2016**, *483*, 109–117. [CrossRef]
30. de Carvalhoa, R.C.; Bettsa, A.J.; Cassidya, J.F. Diclofenac determination using CeO2 nanoparticle modified screen-printed electrodes—A study of background correction. *Microchem. J.* **2020**, *158*, 105258. [CrossRef]
31. Sasal, A.; Tyszczuk-Rotko, K.; Wójciak, M.; Sowa, I. First electrochemical sensor (screen-printed carbon electrode modified with carboxyl functionalized multiwalled carbon nanotubes) for ultratrace determination of diclofenac. *Materials* **2020**, *13*, 781. [CrossRef]
32. Zhang, C.; Cao, Z.; Zhang, G.; Yan, Y.; Yang, X.; Chang, J.; Song, Y.; Jia, Y.; Pan, P.; Mi, W.; et al. An electrochemical sensor based on plasma-treated zinc oxide nanoflowers for the simultaneous detection of dopamine and diclofenac sodium. *Microchem. J.* **2020**, *158*, 105237. [CrossRef]
33. Jahromi, Z.; Mirzael, E.; Savardashtaki, A.; Afzali, M.; Afzali, Z. A rapid and selective electrochemical sensor based on electrospun carbon nanofibers for tramadol detection. *Microchem. J.* **2020**, *157*, 104942. [CrossRef]
34. González-Sánchez, M.I.; Gómez-Monedero, B.; Agrisuelas, J.; Iniesta, J.; Valero, E. Highly activated screen-printed carbon electrodes by electrochemical treatment with hydrogen peroxide. *Electrochem. Commun.* **2018**, *91*, 36–40. [CrossRef]
35. González-Sánchez, M.I.; Gómez-Monedero, B.; Agrisuelas, J.; Iniesta, J.; Valero, E. Electrochemical performance of activated screen printed carbon electrodes for hydrogen peroxide and phenol derivatives sensing. *J. Electroanal. Chem.* **2019**, *839*, 75–82. [CrossRef]
36. Tigari, G.; Manjunatha, J.G. A surfactant enhanced novel pencil graphite and carbon nanotube composite paste material as an effective electrochemical sensor for determination of riboflavin. *J. Sci. Adv. Mater. Dev.* **2020**, *5*, 56–64. [CrossRef]
37. Atta, N.F.; Darwish, S.A.; Khalil, S.E.; Galal, A. Effect of surfactants on the voltammetric response and determination of an antihypertensive drug. *Talanta* **2007**, *72*, 1438–1445. [CrossRef] [PubMed]
38. da Silva, E.M.; de Oliveira, G.C.; de Sequeira, A.B.; Terezo, A.J.; Castilho, M. Development of a composite electrode based on graphite and polycaprolactone for the determination of antihypertensive drugs. *Microchem. J.* **2020**, *158*, 105228. [CrossRef]
39. Yardim, Y. Sensitive detection of capsaicin by adsorptive stripping voltammetry at a boron-doped diamond electrode in the presence of sodium dodecylsulfate. *Electroanalysis* **2011**, *23*, 2491–2497. [CrossRef]
40. Kumar, N.; Goyal, R.N. A simple and highly selective determination of telmisartan at sodium dodecyl sulfate modified pyrolytic graphite surface. *Electroanalysis* **2018**, *30*, 892–900. [CrossRef]
41. Raril, C.; Manjunatha, J.G.; Tigari, G. Low-cost voltammetric sensor based on an anionic surfactant modified carbon nanocomposite material for the rapid determination of curcumin in natural food supplement. *Instrum. Sci. Tech.* **2020**, *48*, 561–582. [CrossRef]
42. Pınar, P.T. Electrooxidation and low-tech determination of pantoprazole on a disposable pencil graphite electrode by the use of cationic surfactant. *Acta Chim. Slov.* **2020**, *67*, 212–220. [CrossRef] [PubMed]
43. Nurdin, I.; Fitri, H.R.; Widiatmoko, P.; Devianto, H.; Prakoso, T. The effect of cationic CTAB on the performance of graphene electrode for supercapacitor. *IOP Conf. Ser. Mater. Sci. Eng.* **2020**, *823*, 012038. [CrossRef]
44. Angelis, P.N.; de Cassia Mendonca, J.; de Rocha, L.R.; Capelari, T.B.; Prete, M.C.; Segatelli, M.G.; Borsato, D.; Tarley, C.R.T. Feasibility of a nano-carbon black paste electrode for simultaneous voltammetric determination of antioxidants in food samples and biodiesel in the presence of surfactant. *Electroanalysis* **2020**, *32*, 1198–1207. [CrossRef]
45. Ziyadinova, G.; Ziganshina, E.; Budnikov, H. Voltammetric sensing and quantification of eugenol using nonionic surfactant self-organized media. *Anal. Methods* **2013**, *5*, 4750–4756. [CrossRef]

46. Kamenicka, B.; Bartaskova, A.; Svancara, I.; Weidlich, T. Applicability of voltammetric determination of diclofenac at carbon paste electrodes to the analysis of aqueous solutions purified by adsorption and/or ionic liquid-based ion exchange. *Monatsh. Chem.* **2019**, *150*, 429–437. [CrossRef]
47. Gosser, D.K. *Cyclic Voltammetry: Simulation and Analysis of Reaction Mechanism*; VCH: New York, NY, USA, 1993.
48. Grabarczyk, M.; Koper, A. How to determine uranium faster and cheaper by adsorptive stripping voltammetry in water samples containing surface active compounds. *Electroanalysis* **2011**, *23*, 1442–1446. [CrossRef]
49. Mocak, J.; Bond, A.M.; Mitchell, S.; Scollary, G. A statistical overview of standard (IUPAC and ACS) and new procedures for determining the limits of detection and quantification: Application to voltammetric and stripping techniques. *Pure Appl. Chem.* **1997**, *69*, 297–328. [CrossRef]

RD3

J. Kozak, K. Tyszczuk-Rotko, M. Wójciak, I. Sowa, M. Rotko, *First screen-printed sensor (electrochemically activated screen-printed boron-doped diamond electrode) for quantitative determination of rifampicin by adsorptive stripping voltammetry*, Materials, 14 (15) (2021) 4231-4242.

materials

MDPI

Article

First Screen-Printed Sensor (Electrochemically Activated Screen-Printed Boron-Doped Diamond Electrode) for Quantitative Determination of Rifampicin by Adsorptive Stripping Voltammetry

Jędrzej Kozak [1], Katarzyna Tyszczuk-Rotko [1,*], Magdalena Wójciak [2], Ireneusz Sowa [2] and Marek Rotko [1]

[1] Faculty of Chemistry, Institute of Chemical Sciences, Maria Curie-Skłodowska University in Lublin, 20-031 Lublin, Poland; jedrekkozak@onet.pl (J.K.); marekrotko@poczta.umcs.lublin.pl (M.R.)
[2] Department of Analytical Chemistry, Medical University of Lublin, 20-093 Lublin, Poland; magdalena.wojciak@umlub.pl (M.W.); i.sowa@umlub.pl (I.S.)
* Correspondence: ktyszczuk@poczta.umcs.lublin.pl

Abstract: In this paper, a screen-printed boron-doped electrode (aSPBDDE) was subjected to electrochemical activation by cyclic voltammetry (CV) in 0.1 M NaOH and the response to rifampicin (RIF) oxidation was used as a testing probe. Changes in surface morphology and electrochemical behaviour of RIF before and after the electrochemical activation of SPBDDE were studied by scanning electron microscopy (SEM), CV and electrochemical impedance spectroscopy (EIS). The increase in number and size of pores in the modifier layer and reduction of charge transfer residence were likely responsible for electrochemical improvement of the analytical signal from RIF at the SPBDDE. Quantitative analysis of RIF by using differential pulse adsorptive stripping voltammetry in 0.1 mol L^{-1} solution of PBS of pH 3.0 ± 0.1 at the aSPBDDE was carried out. Using optimized conditions (E_{acc} of −0.45 V, t_{acc} of 120 s, ΔE_A of 150 mV, ν of 100 mV s^{-1} and t_m of 5 ms), the RIF peak current increased linearly with the concentration in the four ranges: 0.002–0.02, 0.02–0.2, 0.2–2.0, and 2.0–20.0 nM. The limits of detection and quantification were calculated at 0.22 and 0.73 pM. The aSPBDDE showed satisfactory repeatability, reproducibility, and selectivity towards potential interferences. The applicability of the aSPBDDE for control analysis of RIF was demonstrated using river water samples and certified reference material of bovine urine.

Keywords: electrochemically activated screen-printed boron-doped diamond sensor; first screen-printed sensor for rifampicin determination; differential pulse adsorptive stripping voltammetry; river water and urine samples

Citation: Kozak, J.; Tyszczuk-Rotko, K.; Wójciak, M.; Sowa, I.; Rotko, M. First Screen-Printed Sensor (Electrochemically Activated Screen-Printed Boron-Doped Diamond Electrode) for Quantitative Determination of Rifampicin by Adsorptive Stripping Voltammetry. *Materials* **2021**, *14*, 4231. https://doi.org/10.3390/ma14154231

Academic Editor: Alvaro Caballero

Received: 23 June 2021
Accepted: 26 July 2021
Published: 29 July 2021

1. Introduction

Rifampicin (RIF) ((3-[[(4-methyl-1-piperazinyl)-imino]-methyl])-rifamycin) is a semi-synthetic macrocyclic antibiotic, which is a derivative of rifamycin antibiotics produced by fermentation of the strain *Streptomyces mediterranei*. Rifampicin is an odorless red powder that is very slightly soluble in water, acetone, alcohol, and ether. It is soluble in methanol and ethyl acetate, and easily soluble in chloroform [1,2]. Rifampicin is a first-line antibiotic along with isoniazid, pyrazinamide, ethambutol, and streptomycin in the treatment of pulmonary and extrapulmonary tuberculosis and has a unique role in killing semi-dormant tubercle bacilli (*Mycobacterium tuberculosis*) [3]. In a standard treatment procedure for tuberculosis, all four drugs are administered in various combinations over the first 2 months, and isoniazid and rifampicin are continued for the next 4 months [4]. RIF is also used for the treatment of leprosy, and some types of osteomyelitis and endocarditis. The action of this antibiotic is based on the inhibition of DNA-dependent RNA polymerase in bacterial cells, resulting in suspending their growth [5].

Inappropriate dosage during the long-term treatment period often leads to drug resistance and even death despite the disease being curable. Therefore, possible drug dosing irregularities are monitored. The simplest approach to detecting dosing abnormalities is to assess the patients' urine levels of rifampicin. Therefore, many methods are used to determine rifampicin, including supercritical fluid chromatography (SFC) [2], high-performance liquid chromatography (HPLC) [3], fluorescence quenching [4], liquid chromatography-tandem mass spectrometry (LC-MS/MS) [5–7], ultra performance liquid chromatography (UPLC) [8], and spectrophotometry [1,9]. Electrochemical methods such as amperometry [10] and voltammetry [11–13] are also used here.

One of the popular electrodes working in voltammetry is a boron-doped diamond electrode (BDDE), which is an alternative to classical carbon electrodes. A diamond, a wide gap insulator, can be converted into a metal conductor with strong boron doping [14]. Most BDDEs are produced by the chemical vapor deposition technique and the properties of the electrode can be manipulated depending on the doping agent (B and C), surface termination, impurity level (sp3/sp2 ratio), morphological factors, and crystallographic orientation [15]. The BDDE provides superior chemical stability, low background current, a very wide potential window of water stability, low double-layer capacitance, chemical inertness, and long life-time [16,17]. One of the most valuable properties of BDDEs is the electrogeneration of hydroxyl radicals under polarization at high anodic potentials resulting in a low electrochemical activity for the oxygen evolution reaction and a high chemical reactivity for organics oxidation [18]. Furthermore, BDDEs are stable at extreme temperatures and pressures and resistant to fouling, so are ideal for the application of portable sensors for in situ measurements over extended periods of time, even in harsh environments [19].

The aim of the work presented here was to develop a simple, fast and highly sensitive voltammetric procedure for the determination of RIF in urine and water samples using an electrochemically activated screen-printed boron-doped diamond electrode (aSPBDDE). It should be noted that for the first time rifampicin was determined using a screen-printed sensor.

2. Materials and Methods

2.1. Apparatus

Voltammetric experiments were undertaken using a μAutolab analyzer (Eco Chemie, Utrecht, The Netherlands) controlled by GPES 4.9 software. The measurements were performed in a classic electrochemical cell with a commercially available screen-printed sensor (Metrohm-DropSens, Oviedo, Spain). The same analyzer controlled by FRA 4.9 software was also used to record Nyquist plots in the electrochemical impedance spectroscopy (EIS) method. The three-electrode sensor consisted of a boron-doped diamond (BDD) working electrode, a carbon auxiliary electrode, and a silver pseudo-reference electrode. In order to characterize the aSPBDDE, the optical profiles and the microscopic images of the sensors were recorded using a Contour GT-K1 optical profilometer (Veeco, New York, NY, USA) and a high-resolution scanning electron microscope Quanta 3D FEG (FEI, Hillsboro, OR, USA). The optical profiles were obtained using vertical scanning interferometry (VSI) mode with magnification of 40×. The SEM experiments were carried out under conditions (acceleration voltage of 5.0 kV, horizontal field width of 5.97 μm, working distance of 9.8 mm, magnification of 25,000×). Chromatographic measurements were performed on a VWR Hitachi Elite LaChrom HPLC system equipped with a spectrophotometric detector (PDA), an XB-C18 reversed phase core-shell column (Kinetex, Phenomenex, Aschaffenburg, Germany) (25 cm × 4.6 mm i.d., 5 μm), and EZChrom Elite software (version 3.2 SP2, Merck, Germany).

2.2. Reagents and Solutions

Rifampicin (Sigma-Aldrich, Darmstadt, Germany) was dissolved in ethanol to prepare 1.0 mM stock solution. This solution was diluted in 0.1 M phosphate buffer saline (PBS)

with a pH value of 7.5 ± 0.1. The dilutions were prepared each day. The effect of the pH of the supporting electrolyte on the RIF signal was investigated using 0.1 mol L^{-1} PBS solutions with a pH value of: 3.0 ± 0.1, 4.5 ± 0.1, 6.0 ± 0.1, 7.5 ± 0.1, 8.5 ± 0.1, 9.5 ± 0.1, and 11.0 ± 0.1. The effect of inorganic interferences was examined using standard solutions (Merck) of: Mg(II), Ca(II), Cu(II), Cd(II), Pb(II), Ni(II), Fe(III), and V(V). The influence of organic substances was checked for reagents purchased from Sigma-Aldrich: glucose, ascorbic acid, dopamine, epinephrine, uric acid, acetylsalicylic acid, amoxicillin, and from Fluka—Triton X-100. Acetonitrile and trifluoroacetic acids (TFA) were HPLC-grade (Merck, Darmstadt, Germany). All solutions were prepared using ultrapurified water (>18 MW cm, Milli-Q system, Millipore, UK).

2.3. Preparation of Activated Screen-Printed Boron-Doped Diamond Electrode (aSPBDDE)

Before each series of measurements (after each solution change in the electrochemical cell), the SPBDDE was electrochemically activated. The activation consisted of five voltammetric cycles between 0 and 2 V at a scan rate of 100 mV s^{-1} in a solution of NaOH at a concentration of 0.1 M. After activation, the sensor was rinsed with deionized water and used for RIF determination.

2.4. Rifampicin (RIF) Differential Pulse Adsorptive Stripping Voltammetric (DPAdSV) Analysis

Voltammetric analysis of RIF under optimized conditions were carried out in 0.1 M solution of PBS (pH of 3.0 ± 0.1). An accumulation potential (E_{acc}) of −0.45 V was applied during stirring for 120 s (accumulation time—t_{acc}). The differential pulse adsorptive stripping voltammetric (DPAdSV) curves were recorded in the potential range from −0.25 to 1 V with an amplitude (ΔE_A) of 150 mV, a scan rate (ν) of 100 mV s^{-1}, and a modulation time (t_m) of 5 ms. The background curve was subtracted from each voltammogram. The average values of Ip are shown with the standard deviation of n = 3.

2.5. RIF High-Performance Liquid Chromatography (HPLC)/PDA Analysis

HPLC conditions were based on the literature [20]. Separation was achieved using a mixture of acetonitrile and water with 0.025% of trifluoroacetic acid (50:50, *v*/*v*) as the mobile phase. The flow rate was 1.0 mL min^{-1} and temperature was set at 25 °C. The injection volume was 20 µL. All samples were analysed in triplicate at a wavelength of 330 nm. Quantification was performed using the calibration curve constructed based on peak areas of standard solutions of RIF.

3. Results and Discussion

3.1. Characteristics of aSPBDDE Sensors

According to the literature data, activation can functionalize the electrode surface, increase the active surface, or remove surface contamination [21,22]. Therefore, in the first stage of the research, electrochemical activation (five voltammetric cycles between 0 and 2 V at a scan rate of 100 mV s^{-1}) in two different solutions (0.1 M NaOH and 0.1 M acetate buffer of pH 4.0 containing 10 mmol L^{-1} H_2O_2) was applied. The studies showed that electrochemical activation of the electrode contributes to a significant increase in the RIF peak current. The signals obtained showed that the activation with NaOH was much more effective (Figure 1A). In order to test the influence of activation on the electrochemical properties of the electrodes, measurements were performed using cyclic voltammetry (CV) and electrochemical impedance spectroscopy (EIS). Impedance spectra (Nyquist plots) were recorded in the frequency range from 1 MHz to 0.1 Hz at a potential of 0.2 V, from a solution of 0.1 M KCl containing 5.0 mM $K_3[Fe(CN)_6]$. As can be seen in Figure 1B, electrochemical activation of the electrode (blue curve) significantly reduces the charge transfer resistance (R_{ct}) compared to the unactivated electrode (black curve) (105.4 vs. 286.5 Ω cm^2). The electrochemical activation of the SPBDDE changes the surface morphology, reduces the R_{ct} but does not change the active surface areas (A_s) of the SPBDDE and aSPBDDE, which were 0.0146 ± 0.000510 and 0.0157 ± 0.000470 cm^2, respectively. The active surface areas

were calculated using CV measurements in 0.1 M solution of KCl containing 5.0 mM $K_3[Fe(CN)_6]$ based on the Randles–Sevcik equation [23] and the dependence between anodic peak currents and the square root of the scan rates (Figure 2).

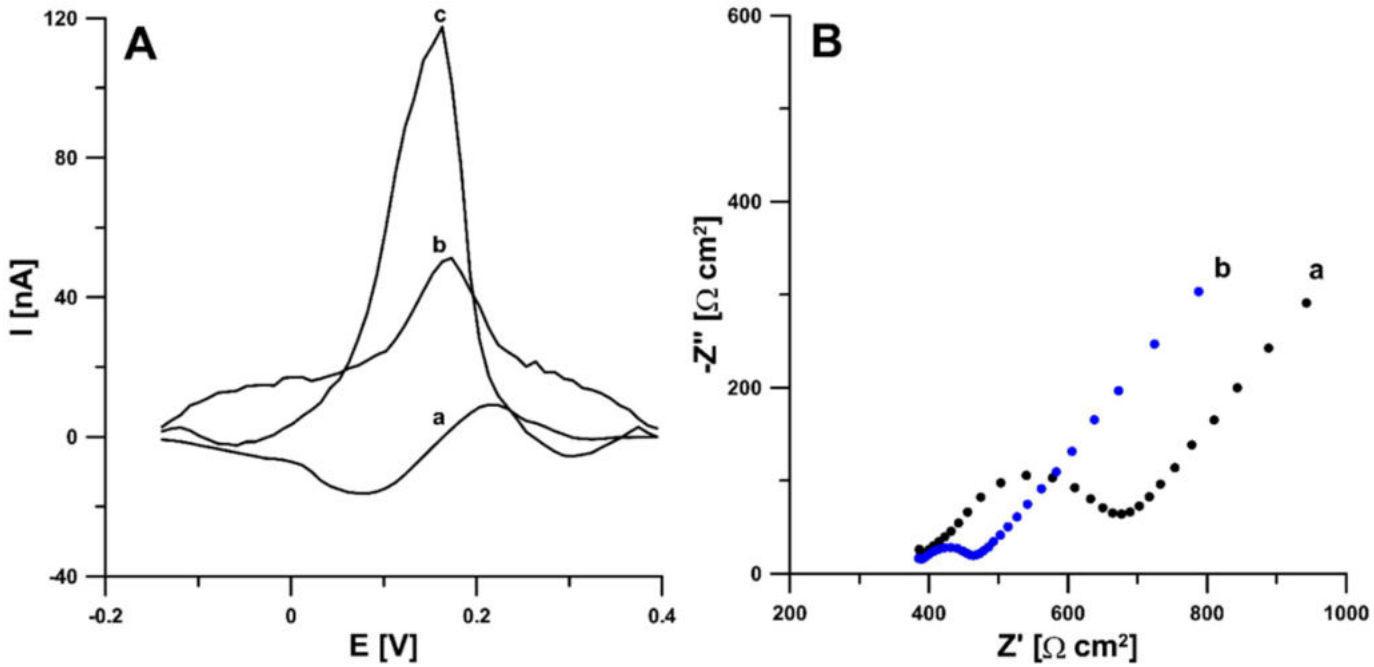

Figure 1. (**A**) Voltammograms of 0.2 nM rifampicin (RIF) in 0.1 M phosphate buffer saline (PBS) of pH 7.5 obtained at the bare screen-printed boron-doped diamond electrode (SPBDDE) (a), electrochemically activated in 0.1 M acetate buffer of pH 4.0 containing 10 mM H_2O_2 SPBDDE (b) and electrochemically activated in 0.1 M NaOH SPBDDE (c). The differential pulse adsorptive stripping voltammetric (DPAdSV) parameters: Eacc of −0.25 V, tacc of 60 s, ΔE_A of 50 mV, ν of 100 mV s^{-1} and t_m of 10 ms. (**B**) Nyquist plots of SPBDDE (a) and aSPBDDE (b).

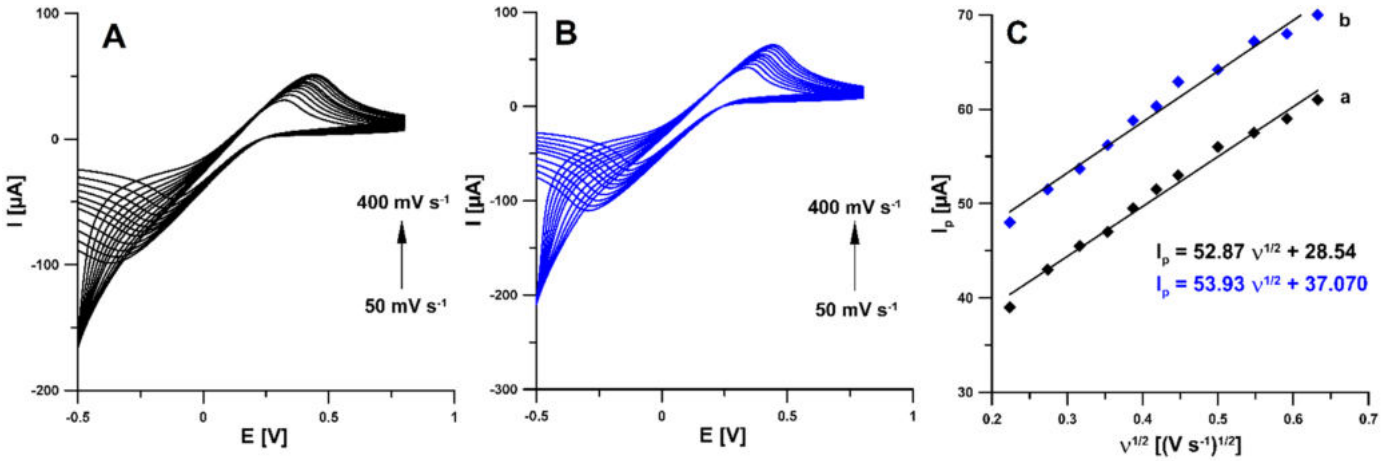

Figure 2. Cyclic voltammograms recorded in a solution of 0.1 M KCl containing 5.0 mM $K_3[Fe(CN)_6]$ at the bare SPBDDE (**A**) and electrochemically activated in 0.1 M NaOH SPBDDE (**B**). (**C**) Dependence between anodic peak currents and the square root of the scan rates for the bare SPBDDE (a) and aSPBDDE (b), ν range of 50–400 mV s^{-1}.

The surface morphology of the bare SPBDDE and the electrochemically activated electrode (aSPBDDE) was examined using scanning electron microscopy (SEM) and optical profilometry. It was found that electrochemical activation causes visible changes in the surface of the working electrode, increasing the number and size of pores in the modifier layer located near the support surface (Figure 3A). This is related to the removal of organic

binders existing on the electrode surface [21]. Changes in the structure of the electrode surface after activation were also found using optical profilometry. The examination of the electrodes using an optical profilometer showed an increase in surface roughness and total height of the profile (R_a: 0.451 and 0.517 µm, and R_t: 7.833 and 10.627 µm for the SPBDDE and the aSPBDDE, respectively) (Figure 3B).

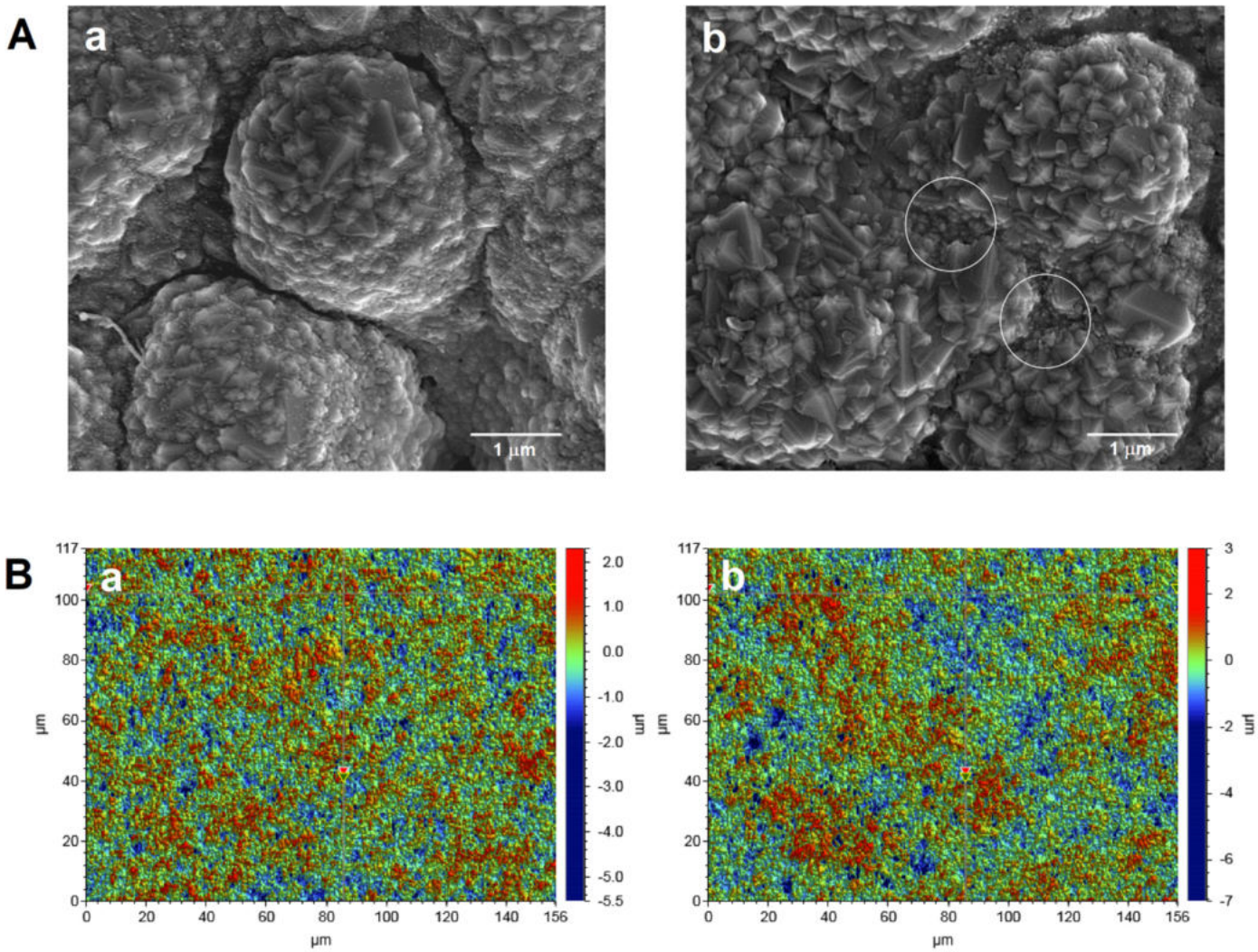

Figure 3. (**A**) Scanning electron microscope (SEM) images and (**B**) optical profiles of SPBDDE (a) and aSPBDDE (b).

3.2. Influence of pH and Concentration of Supporting Electrolyte

In order to select the optimal pH of the base electrolyte, the electrochemical behavior of 0.1 and 0.2 nM RIF in 0.1 M PBS was examined over a pH range of 3.0 to 11.0 (Figure 4A). It was observed that, with increasing pH, the peak potential shifts to less positive potential values. The maximum RIF peak current was observed at pH of 3.0 ± 0.1 and this value was considered suitable for further studies. Moreover, the influence of PBS concentration ranging from 0.025 to 0.175 M was checked (Figure 4B). The highest analytical signal of RIF was obtained for 0.1 and 0.125 M PBS and, therefore, finally the concentration of 0.1 M PBS pH 3.0 ± 0.1 was considered optimal.

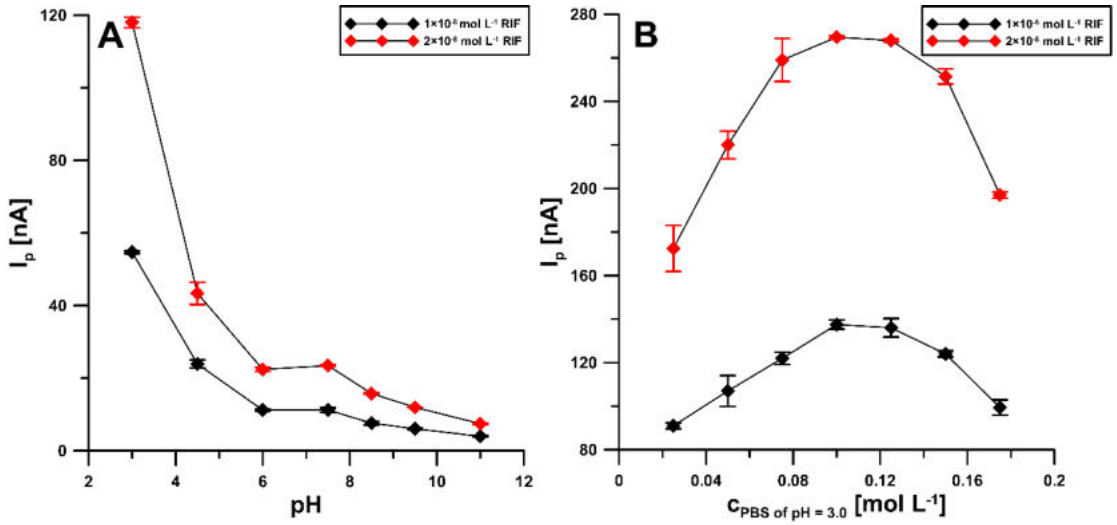

Figure 4. Influence of pH value (**A**) and concentration of the PBS solution of pH 3.0 ± 0.1 (**B**) on RIF peak current. The DPAdSV parameters: Eacc of −0.25 V, tacc of 60 s, ΔE_A of 50 mV, ν of 100 mV s^{-1} and t_m of 10 ms.

3.3. Cyclic Voltammetry (CV) Behaviour of RIF

The electrochemical behaviour of RIF was examined at the aSPBDDE in the 0.1 M solution of PBS (pH of 3.0) containing 5.0 µM RIF using cyclic voltammetry and the recorded voltammograms are depicted in Figure 5A. As can be seen, RIF was oxidized quasi-reversibly. The partially reversible oxidation of RIF also occurs in voltammetric procedures using a glassy carbon electrode modified with a gold nanoparticles/polymelamine nanocomposite [24] and a carbon paste electrode [25]. In the potential range used, three anode peaks at potentials about −0.17, 0.10 and 0.75 V and two cathode peaks at potentials about 0.02 and −0.25 V were visible (ν = 100 mV s^{-1}). Two protons and two electrons are involved in the oxidation of RIF to RIF-quinone [24]. Taking into account the peak current and signal repeatability, the second oxidation RIF peak at potential about 0.10 V was selected for studies. On the basis of the obtained values of the RIF oxidation peak currents for the different scan rates from 15 to 500 mV s^{-1}, the relationship between the peak current (Ip) and the square root of scan rate ($\nu^{1/2}$) indicated that the oxidation processes of RIF are controlled by diffusion at the aSPBDDE (Figure 5B). Moreover, the relationship between the log of the peak current (log Ip) and the log of the scan rate (log ν) was plotted (Figure 5C). The slope of 0.77 observed in the plot of log Ip vs. log ν indicated that this process was not purely diffusion- or adsorption-controlled.

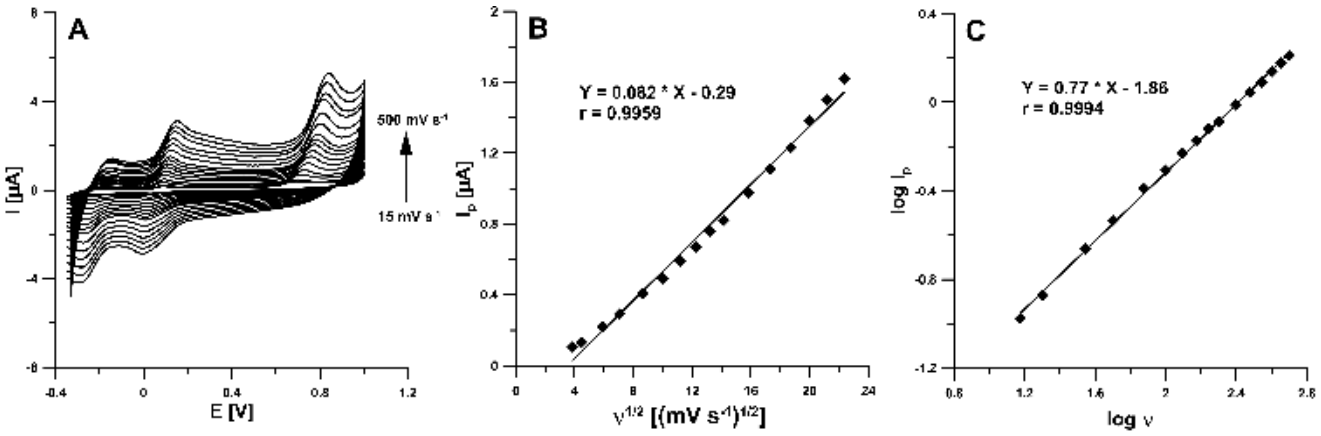

Figure 5. (**A**) Cyclic voltammograms recorded in 0.1 M solution of PBS (pH 3.0 ± 0.1) containing 5.0 µM RIF at different scan rates, (**B**) the dependence between Ip and $\nu^{1/2}$, (**C**) dependence between log Ip and log ν for ν from 15 to 500 mV s^{-1}.

3.4. Optimization of DPAdSV Parameters

In order to obtain the best analytical signal of RIF, the effect of various parameters, including accumulation potential (Eacc) and time (tacc), amplitude (ΔE_A), scan rate (ν), and modulation time (t_m), on the RIF peak current was investigated. The influence of Eacc on the RIF peak current was examined in the range from 0 to −0.7 V with the tacc of 60 s. The peak current increased strongly, reaching a maximum at a potential of −0.45 V. As the potential was shifted towards more negative values, the peak current remained almost constant, hence a potential of −0.45 V was chosen as the optimal RIF accumulation potential (Figure 6A). For a potential of −0.45 V, the effect of accumulation time in the range of 15–300 s was investigated. As can be seen in Figure 6B, taking into account the highest peak currents of RIF, the t_{acc} of 300 s can be considered as an optimum. However, in order to reduce analysis time, the t_{acc} of 120 s was selected for further experiments.

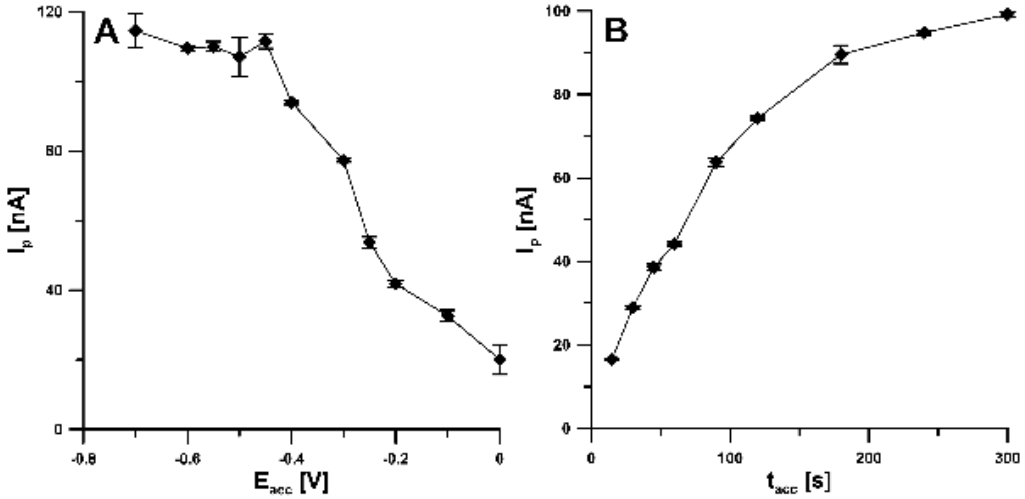

Figure 6. Influence of Eacc (**A**) and tacc (**B**) on the analytical signal of 1.0 and 0.5 nM RIF, respectively.

For ν of 100 mV s^{-1} and t_m of 10 ms, the amplitude was varied from 25 to 200 mV. The highest RIF signal was obtained at an amplitude value of 150 mV (Figure 7A). Then, the effect of the scan rate, ranging from 25 to 200 mV s^{-1} (ΔE_A of 150 mV, t_m of 10 ms), was tested. The RIF peak current reached its maximum value at a scan rate of 100 mV s^{-1}, while a further increase in the scan rate resulted in a significant decrease in peak current. A scan rate of 100 was found to be optimal (Figure 7B). In addition, the modulation time was varied from 2 to 40 ms (ΔE_A of 150 mV, ν of 100 mV s^{-1}). For t_m of 5 ms, the highest RIF signal was obtained (Figure 7C).

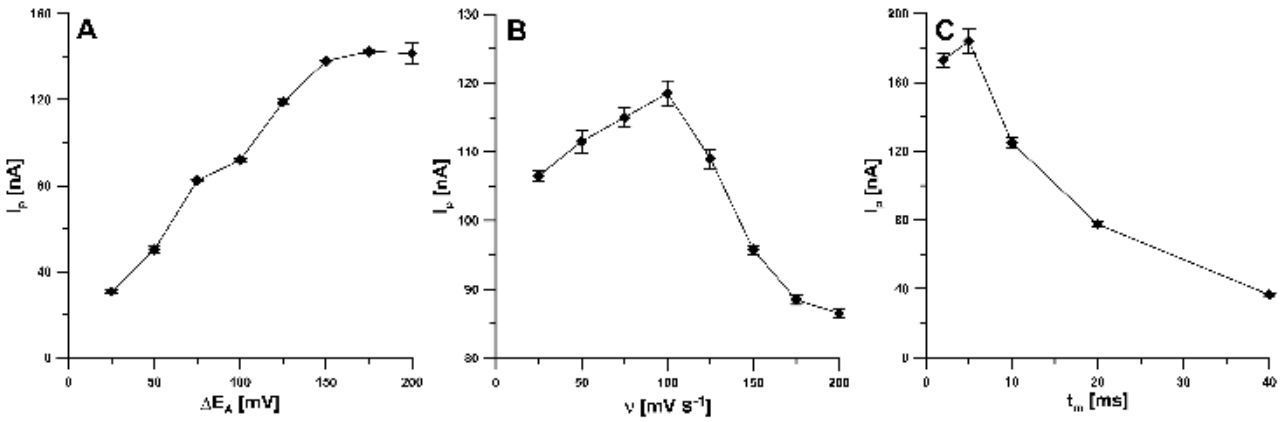

Figure 7. Effect of ΔE_A (**A**), ν (**B**) and t_m (**C**) on analytical response of 0.5 nM RIF. The DPAdSV parameters: E_{acc} of −0.45 V and t_{acc} of 120 s.

3.5. Interference Studies

In order to test the selectivity of the proposed sensor, the influence of interferents potentially occurring in natural waters and biological fluids on the RIF voltammetric response was tested (Figure 8). The tolerance limit was defined as the concentration that gave an error of ≤10% in the determination of 0.5 nM RIF. The results obtained showed that Mg(II) (up to 1000-fold excess), Ca(II) (up to 1000-fold excess), epinephrine (EPI, up to 400-fold excess), amoxicillin (AMX, up to 200-fold excess), Fe(III) (up to 100-fold excess), Cd(II) (up to 100-fold excess), Cu(II) (up to 100-fold excess), Pb(II) (up to 100-fold excess), Ni(II) (up to 100-fold excess), V(V) (up to 100-fold excess), dopamine (DOP, up to 100-fold excess), ascorbic acid (AA, up to 100-fold excess), uric acid (UA, up to 100-fold excess), acetylsalicylic acid (ASA, up to 100-fold excess), and glucose (GLU, up to 100-fold excess) had negligible effects on the assay of RIF. Natural waters contain surfactants with a surface active effect comparable to Triton X-100 in a concentration of 0.2 to 2 ppm [26]. For this reason, the DPAdSV response of 0.5 nM RIF in the presence of 2 ppm Triton X-100 was checked and it was found that the peak current did not change by more than ±10%. Interference studies showed that the developed procedure is characterized by satisfactory selectivity and can be used for the determination of RIF in natural water samples and biological fluids without a complicated sample preparation step.

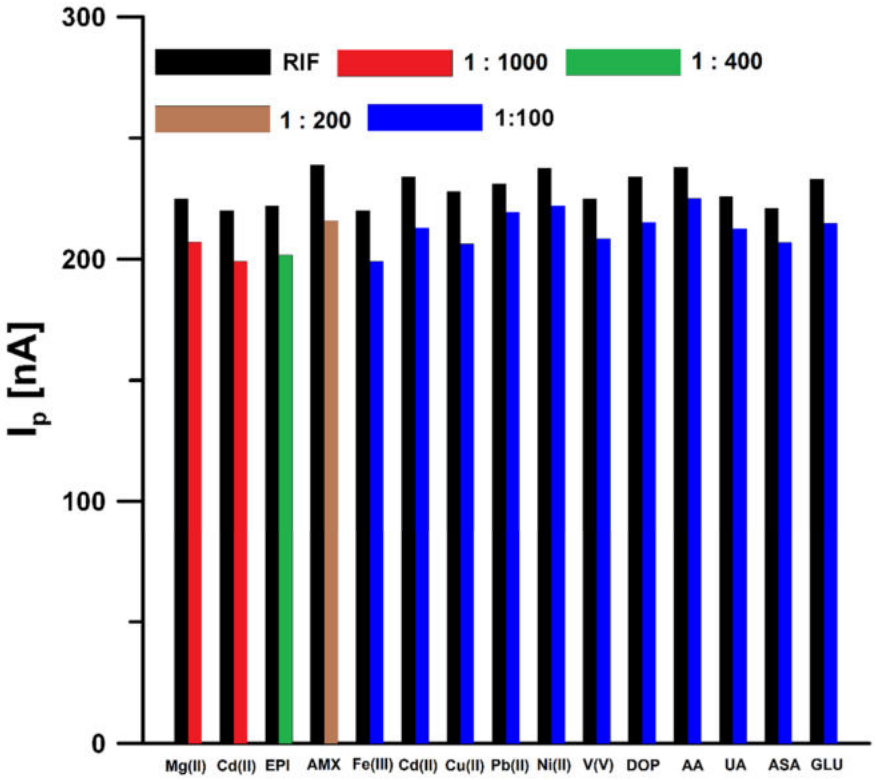

Figure 8. Histogram bars of the RIF peak current in the presence of interferents.

3.6. Analytical Characteristic

Under optimized conditions, RIF was determined in the concentration range of 2 pmol L^{-1}–20 nmol L^{-1} using differential pulse adsorptive stripping voltammetry (DPAdSV). It was found that the RIF peak current increased linearly with the concentration in the four ranges: 0.002–0.02 nM (I_p [nA] = 2744.71 ± 71.52 × c_{RIF} [nM] + 16.64 ± 0.20), 0.02–0.2 nM (I_p [nA] = 620.36 ± 21.52 × c_{RIF} [nM] + 64.29 ± 2.79), 0.2–2.0 nM (I_p [nA] = 133.23 ± 8.54 × c_{RIF} [nM] + 163.77 ± 6.52), and 2.0–20.0 nM (I_p [nA] = 38.020 ± 1.14 × c_{RIF} [nM] + 372.85 ± 19.54). Figure 9 shows the voltammograms and linear ranges of the rifampicin calibration plots at the aSPBDDE. The limits of detection (LOD) and quantification (LOQ) were calculated at 0.22 and 0.73 pM, respectively, according to the

definitions of LOD = 3SDa/b and LOQ = 10SDa/b (SDa—standard deviation of intercept (n = 3); b—slope of calibration curve) [27].

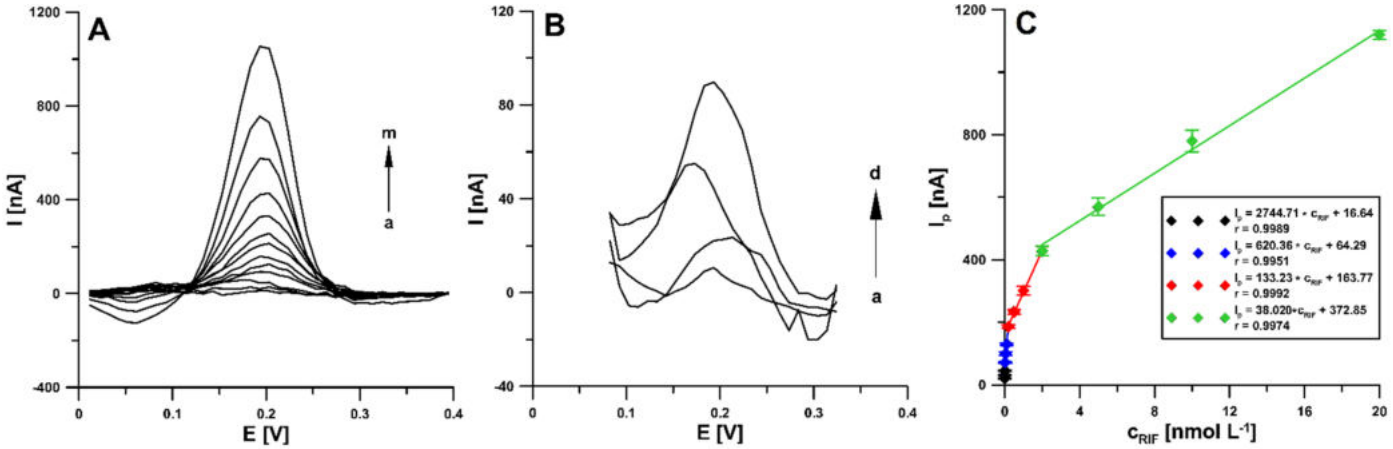

Figure 9. (**A**) DPAdSV curves recorded at the aSPBDDE in the PBS solution of pH 3.0 ± 0.1 containing increasing concentrations of RIF: (a) 0.002, (b) 0.005, (c) 0.01, (d) 0.02, (e) 0.05, (f) 0.1, (g) 0.2, (h) 0.5, (i) 1.0, (j) 2.0, (k) 5.0, (l) 10.0, (m) 20.0 nM. (**B**) DPAdSV curves for the RIF concentration: (a) 0.002, (b) 0.005, (c) 0.01, (d) 0.02 nM. (**C**) Calibration plot of RIF. The DPAdSV parameters: Eacc of −0.45 V, tacc of 120 s, ΔE_A of 150 mV, ν of 100 mV s^{-1} and t_m of 5 ms.

Table 1 presents a comparison of the different methods of RIF determination. It should be clearly stated that the developed voltammetric procedure for the determination of rifampicin enables the achievement of a much lower limit of detection than other methods [1,3–5,8,10]. When it comes to voltammetry, there are only three procedures in the literature in which the detection limit was lower than in this paper [28–30]. However, these procedures require time-consuming preparation of working electrodes, which consists of complex, multi-step modifier synthesis processes. Moreover, it is particularly noteworthy that in this work a screen-printed sensor was used for the first time to quantify RIF.

Table 1. Comparison of different methods for RIF determination.

Method	Linear Range (μM)	LOD (μM)	Application	Ref.
Spectrophotometry	6.08–60.80	4.25	Pharmaceutical formulations	[1]
Fluorescence quenching	0.61–1000.0	0.085	Human urine	[4]
HPLC	0–2.0	5.86	Herbal extracts, liver microsomes	[3]
LC-MS/MS	0.030–7.78	0.30	Human plasma	[5]
UPLC	0.0790–31.60	-	Human plasma	[8]
Amperometry	-	1.69	Pharmaceutical formulations, urine	[10]
DPAdSV	0.0000020–0.020	0.00000022	Bovine urine, river water	This work

Moreover, repeatability was checked for the determination of 0.1 nM RIF and a relative standard deviation (RSD) of 2.5% (n = 10) was obtained. This RSD value proves the good repeatability of the RIF analytical signal at the aSPBDDE. The reproducibility was assessed on the basis of measurements made during the determination of 0.05 nM RIF at three sensors. The RSD value was 5.2%, which confirmed the acceptable reproducibility of the sSPBDDE.

3.7. Real Sample Analysis

In order to check the usefulness of the developed RIF determination DPAdSV procedure using the aSPBDDE, the analysis of the Bystrzyca river (Lublin, Poland) and bovine urine (certified reference material, ERM-BB386, Sigma-Aldrich) samples was performed. The measurements were done by voltammetric and chromatographic method (HPLC/PDA). The results are shown in Table 2. After collecting samples from the river,

they were filtered using 0.45 μm Millipore filter and stored in the refrigerator. River water samples spiked with 0.001 and 0.05 μM RIF and bovine urine samples spiked with 1.0 and 50.0 μM were analysed by the standard addition method. It should be added that to reduce interference from the sample matrix, the accumulation step was shortened to 30 s. According to our knowledge, there is no information in the literature on the concentration of RIF in environmental water samples but the concentration in urine is given. The average concentration of RIF in the urine of patients treated with this antibiotic is in the range of 55.0–67.0 μM [4]. The very low detection and quantification limits of the DPAdSV procedure (0.22 pM) obtained and a high concentration of RIF in urine samples allow for multiple dilution of the sample in the electrolyte solution, which contributes to minimizing the interference from the sample matrix. A 10-fold dilution of river water samples and 10,000-fold dilution of bovine urine samples were used for voltammetric measurements. The recovery values attained by the proposed voltammetric procedure were between 91.4% and 98.6% and indicate satisfactory accuracy of the method. Moreover, as can be seen in Table 2, no significant difference was observed between the concentrations of RIF determined by the DPAdSV at the aSPBDDE and the HPLC/PDA (the relative error values are 3.0% for Bystrzyca river samples and 3.6% for bovine urine samples). It should be added that the comparison of the results could only be done for higher RIF concentrations (river water sample spiked with 0.05 μM and bovine urine sample spiked with 50.0×10^{-5} μM), whereas for lower ones (0.001 and 1.0 μM), HPLC/PDA determinations were outside the LOD method. The DPAdSV curves obtained during the determination of RIF in Bystrzyca river water and bovine urine samples are shown in Figure 10.

Table 2. The results of RIF determination in river water and bovine urine samples.

Sample	RIF Concentration (μM) ± SD (n = 3)				Recovery * (%)	Relative Error ** (%)
	Added	Found DPAdSV	RIF Concentration Found in Electrochemical Cell	Found HPLC/PDA		
Bystrzyca river	0.001	0.000973 ± 0.0000240	0.0000973 ± 0.00000240	<LOD	97.3	-
	0.05	0.0457 ± 0.00110	0.00457 ± 0.000110	0.0471 ± 0.00250	91.4	3.0
Bovine urine	1.0	0.920 ± 0.0070	0.0000920 ± 0.00000070	<LOD	92.0	-
	50.0	49.30 ± 0.40	0.00493 ± 0.000040	47.60 ± 0.018	98.6	3.6

* Recovery (%) = (Found DPAdSV × 100)/Added; ** Relative error (%) = ((|Found HPLC/PDA − Found DPAdSV|)/Found HPLC/PDA) × 100.

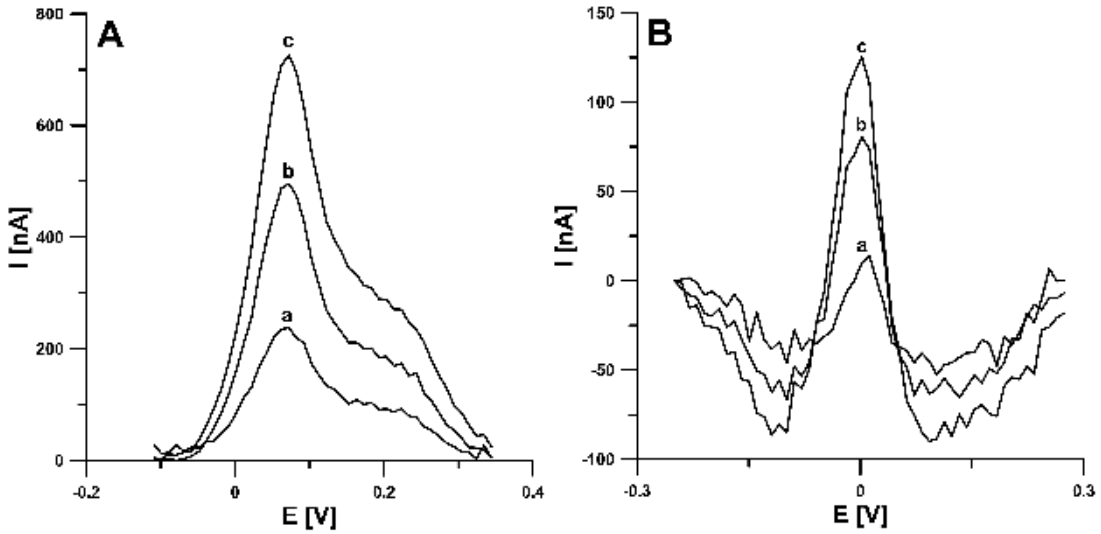

Figure 10. DPAdSV curves obtained for the determination of RIF in Bystrzyca river water sample (**A**): (a) 1 mL of sample + 0.1, (b) as (a) + 0.1, (c) as (a) + 0.2 nM RIF and bovine urine sample (**B**): 1 μL of sample + 0.1, (b) as (a) + 0.1, (c) as (a) + 0.2 nM RIF. The DPAdSV parameters: Eacc of −0.45 V, tacc of 30 s, ΔE_A of 150 mV, ν of 100 mV s^{-1} and t_m of 5 ms.

4. Conclusions

In summary, in this study a simple, fast, and cost-effective differential pulse adsorptive stripping voltammetric procedure (DPAdSV) using an electrochemically activated screen-printed boron-doped diamond electrode (aSPBDDE) for quantification of rifampicin (RIF) was developed. For the first time, a screen-printed sensor was introduced for analysis of RIF. The electrochemical activation of the electrode surface using cyclic voltammetry (CV) in 0.1 mol L^{-1} NaOH resulted in changes in its morphology and a decrease in the charge transfer resistance, which translated into a significant increase in the RIF oxidation peak current. Moreover, the electrochemical behaviour of RIF in 0.1 M PBS (pH of 3.0 $\pm$ 0.1) was characterized by CV. The results obtained show that the oxidation of RIF at the aSPBDDE was not purely diffusion- or adsorption-controlled. The DPAdSV procedure developed using the aSPBDDE showed good selectivity and sensitivity. The calculated LOD and LOQ values were 0.22 and 0.73 pM, respectively. The DPAdSV procedure at the aSPBBDE was successfully used for the determination of RIF in river water and bovine urine samples. The recovery values (91.4% and 98.6%) and the good agreement with the results obtained by the DPAdSV procedure and by the referenced HPLC/PDA method (relative errors of 3.6 and 4.0%) showed satisfactory accuracy of the method. The results obtained revealed the analytical usefulness of the presented voltammetric procedure for RIF analysis in body fluids and natural water samples.

Author Contributions: Conceptualization, J.K. and K.T.-R.; methodology, J.K. and K.T.-R.; investigation, J.K., K.T.-R., M.W., I.S. and M.R.; writing—original draft preparation, J.K. and K.T.-R.; writing—review and editing, J.K., K.T.-R., M.W., I.S. and M.R.; supervision, K.T.-R. All authors have read and agreed to the published version of the manuscript.

Funding: This research received no external funding.

Institutional Review Board Statement: Not applicable.

Informed Consent Statement: Not applicable.

Data Availability Statement: The data presented in this study are available on request from the corresponding author.

Conflicts of Interest: The authors declare no conflict of interest.

References

1. Tilinca, M.; Hancu, G.; Mircia, E.; Iriminescu, D.; Rusu, A.; Vlad, R.A.; Barabás, E. Simultaneous determination of isoniazid and rifampicin by UV spectrophotometry. *Farmacia* **2017**, *65*, 219–224.
2. Wei, L.; Wang, J.; Yan, Z.-Y. Development of a sensitive and rapid method for rifampicin impurity analysis using supercritical fluid chromatography. *J. Pharm. Biomed. Anal.* **2015**, *114*, 341–347.
3. Kumar, S.; Bouic, P.J.; Rosenkranz, B. A validated stable HPLC method for the simultaneous determination of rifampicin and 25-O-desacetyl rifampicin—evaluation of in vitro metabolism. *Acta Chromatogr.* **2019**, *31*, 92–98. [CrossRef]
4. Chatterjee, K.; Kuo, C.W.; Chen, A.; Chen, P. Detection of residual rifampicin in urine via fluorescence quenching of gold nanoclusters on paper. *J. Nanobiotechnol.* **2015**, *13*, 46. [CrossRef]
5. Srivastava, A.; Waterhouse, D.; Ardrey, A.; Ward, S.A. Quantification of rifampicin in human plasma and cerebrospinal fluid by a highly sensitive and rapid liquid chromatographic–tandem mass spectrometric method. *J. Pharm. Biomed. Anal.* **2012**, *70*, 523–528. [CrossRef] [PubMed]
6. Oswald, S.; Peters, J.; Venner, M.; Siegmund, W. LC–MS/MS method for the simultaneous determination of clarithromycin, rifampicin and their main metabolites in horse plasma, epithelial lining fluid and broncho-alveolar cells. *J. Pharm. Biomed. Anal.* **2011**, *55*, 194–201. [CrossRef]
7. Rakuša, Ž.T.; Roškar, R.; Andrejc, A.K.; Lušin, T.T.; Faganeli, N.; Grabnar, I.; Mrhar, A.; Kristl, A.; Trontelj, J. Fast and simple LC-MS/MS method for rifampicin quantification in human plasma. *Int. J. Anal. Chem.* **2019**, *2019*, 4848236.
8. van Ewijk-Beneken Kolmer, E.W.J.; Teulen, M.J.A.; van der Hombergh, E.C.A.; van Erp, N.E.; te Brake, L.H.M.; Aarnoutse, R.E. Determination of protein-unbound, active rifampicin in serum by ultrafiltration and ultra performance liquid chromatography with UV detection. A method suitable for standard and high doses of rifampicin. *J. Chromatogr. B* **2017**, *1063*, 42–49. [CrossRef]
9. Szipszky, C.; Van Aartsen, D.; Criddle, S.; Rao, P.; Zentner, I.; Justine, M.; Mduma, E.; Mpagama, S.; Al-Shaer, M.H.; Peloquin, C.; et al. Determination of rifampin concentrations by urine colorimetry and mobile phone readout for personalized dosing in tuberculosis treatment. *J. Pediatric Infect. Dis. Soc.* **2021**, *10*, 104–111. [CrossRef] [PubMed]

10. Alonso-Lomillo, M.A.; Dominguez-Renedo, O.; Arcos-Martinez, M.J. Optimization of a cyclodextrin-based sensor for rifampicin monitoring. *Electrochim. Acta* **2005**, *50*, 1807–1811. [CrossRef]
11. Tyszczuk, K.; Korolczuk, M. New protocol for determination of rifampicine by adsorptive stripping voltammetry. *Electroanalysis* **2009**, *21*, 101–106. [CrossRef]
12. Rawool, C.R.; Srivastava, A.K. A dual template imprinted polymer modified electrochemical sensor based on Cu metal organic framework/mesoporous carbon for highly sensitive and selective recognition of rifampicin and isoniazid. *Sens. Actuators B Chem.* **2019**, *288*, 493–506. [CrossRef]
13. Zou, J.; Huang, L.-L.; Jiang, X.-Y.; Jiao, F.-P.; Yu, J.-G. Electrochemical behaviors and determination of rifampicin on graphene nanoplatelets modified glassy carbon electrode in sulfuric acid solution. *Desalination Water Treat.* **2018**, *120*, 272–281. [CrossRef]
14. Watanabe, T.; Shimizu, T.K.; Tateyama, Y.; Kim, Y.; Kawai, M.; Einaga, Y. Giant electric double-layer capacitance of heavily boron-doped diamond electrode. *Diam. Relat. Mater.* **2010**, *19*, 772–777. [CrossRef]
15. Divyapriya, G.; Nidheesh, P.V. Electrochemically generated sulfate radicals by boron doped diamond and its environmental applications. *Curr. Opin. Solid State Mater. Sci.* **2021**, *25*, 100921. [CrossRef]
16. Zhi, J.; Luo, D. Fabrication and electrochemical behavior of vertically aligned boron-doped diamond nanorod forest electrodes. *Electrochem. Commun.* **2009**, *11*, 1093–1096.
17. Shi, D.; Liu, L.; Zhai, Z.; Chen, B.; Lu, Z.; Zhang, C.; Yuan, Z.; Zhou, M.; Yang, B.; Huang, N.; et al. Effect of oxygen terminated surface of boron-doped diamondmthin-film electrode on seawater salinity sensing. *J. Mater. Sci. Technol.* **2021**, *86*, 1–10. [CrossRef]
18. Kapałka, A.; Fóti, G.; Comninellis, C. Investigations of electrochemical oxygen transfer reaction on boron-doped diamond electrodes. *Electrochim. Acta* **2007**, *53*, 1954–1961. [CrossRef]
19. McLaughlin, M.H.S.; Pakpour-Tabrizi, A.C.; Jackman, R.B. A detailed EIS study of boron doped diamond electrodes with gold nanoparticles for high sensitivity mercury detection. *Sci. Rep.* **2021**, *11*, 9505. [CrossRef] [PubMed]
20. Goutal, S.; Auvity, S.; Legrand, T.; Hauquier, F.; Cisternino, S.; Chapy, H.; Saba, W.; Tournier, N. Validation of a simple HPLC-UV method for rifampicin determination in plasma: Application to the study of rifampicin arteriovenous concentration gradient. *J. Pharmaceut. Biomed.* **2016**, *123*, 173–178. [CrossRef] [PubMed]
21. González-Sánchez, M.I.; Gómez-Monedero, B.; Agrisuelas, J.; Iniesta, J.; Valero, E. Highly activated screen-printed carbon electrodes by electrochemical treatment with hydrogen peroxide. *Electrochem. Commun.* **2018**, *91*, 36–40. [CrossRef]
22. González-Sánchez, M.I.; Gómez-Monedero, B.; Agrisuelas, J.; Iniesta, J.; Valero, E. Electrochemical performance of activated screen printed carbon electrodes for hydrogen peroxide and phenol derivatives sensing. *J. Electroanal. Chem.* **2019**, *839*, 75–82. [CrossRef]
23. Gosser, D.K. *Cyclic Voltammetry: Simulation and Analysis of Reaction Mechanism*; VCH: New York, NY, USA, 1993.
24. Amidi, S.; Hosseinzadeh Ardakani, Y.; Amiri-Aref, M.; Ranjbari, E.; Sepehri, Z.; Bagheri, H. Sensitive electrochemical determination of rifampicin using gold nanoparticles/poly-melamine nanocomposite. *RSC Adv.* **2017**, *7*, 40111–40118. [CrossRef]
25. Hammam, E.; Beltagi, A.M.; Ghoneim, M.M. Voltammetric assay of rifampicin and isoniazid drugs, separately and combined in bulk, pharmaceutical formulations and human serum at a carbon paste electrode. *Microchem. J.* **2004**, *77*, 53–62. [CrossRef]
26. Grabarczyk, M.; Koper, A. How to determine uranium faster and cheaper by adsorptive stripping voltammetry in water samples containing surface active compounds. *Electroanalysis* **2011**, *23*, 1442–1446. [CrossRef]
27. Mocak, J.; Bond, A.M.; Mitchell, S.; Scollary, G. A statistical overview of standard (IUPAC and ACS) and new procedures for determining the limits of detection and quantification: Application to voltammetric and stripping techniques. *Pure Appl. Chem.* **1997**, *69*, 297–328. [CrossRef]
28. Zhang, N.; Brites Helu, M.; Zhang, K.; Fang, X.; Yin, H.; Chen, J.; Ma, S.; Fang, A.; Wang, C. Multiwalled Carbon Nanotubes-CeO2 Nanorods: A "Nanonetwork" Modified Electrode for Detecting Trace Rifampicin. *Nanomaterials* **2020**, *10*, 391. [CrossRef]
29. Asadpour-Zeynali, K.; Mollarasouli, F. Novel electrochemical biosensor based on PVP capped CoFe2O4@CdSe core-shell nanoparticles modified electrode for ultra-trace level determination of rifampicin by square wave adsorptive stripping voltammetry. *Biosens. Biolelectron.* **2017**, *92*, 509–516. [CrossRef]
30. Girousi, S.T.; Gherghi, I.C.; Karava, M.K. DNA-modified carbon paste electrode applied to the study of interaction between rifampicin (RIF) and DNA in solution and at the electrode surface. *J. Pharm. Biomed. Anal.* **2004**, *36*, 851–858. [CrossRef]

RD4

K. Tyszczuk-Rotko, **J. Kozak**, B. Czech, *Screen-printed voltammetric sensors—tools for environmental water monitoring of painkillers,* Sensors, 22 (7) (2022) 2437-2454.

sensors

MDPI

Review

Screen-Printed Voltammetric Sensors—Tools for Environmental Water Monitoring of Painkillers

Katarzyna Tyszczuk-Rotko *, Jędrzej Kozak and Bożena Czech

Faculty of Chemistry, Institute of Chemical Sciences, Maria Curie-Skłodowska University in Lublin, 20-031 Lublin, Poland; jedrekkozak@onet.pl (J.K.); bczech@hektor.umcs.lublin.pl (B.C.)
* Correspondence: katarzyna.tyszczuk-rotko@mail.umcs.pl; Tel.: +48-81-537-5585

Abstract: The dynamic production and usage of pharmaceuticals, mainly painkillers, indicates the growing problem of environmental contamination. Therefore, the monitoring of pharmaceutical concentrations in environmental samples, mostly aquatic, is necessary. This article focuses on applying screen-printed voltammetric sensors for the voltammetric determination of painkillers residues, including non-steroidal anti-inflammatory drugs, paracetamol, and tramadol in environmental water samples. The main advantages of these electrodes are simplicity, reliability, portability, small instrumental setups comprising the three electrodes, and modest cost. Moreover, the electroconductivity, catalytic activity, and surface area can be easily improved by modifying the electrode surface with carbon nanomaterials, polymer films, or electrochemical activation.

Keywords: screen-printed sensor; voltammetric analysis; painkillers; environmental water monitoring

Citation: Tyszczuk-Rotko, K.; Kozak, J.; Czech, B. Screen-Printed Voltammetric Sensors—Tools for Environmental Water Monitoring of Painkillers. *Sensors* **2022**, *22*, 2437. https://doi.org/10.3390/s22072437

Academic Editor: Craig E. Banks

Received: 14 January 2022
Accepted: 20 March 2022
Published: 22 March 2022

1. Introduction

Increased production and consumption of over-the-counter drugs such as painkillers, e.g., diclofenac, ibuprofen, naproxen, ketoprofen, or acetaminophen, are connected with their increased excretion and presence in wastewater from homes and hospitals [1–8]. There are different sources for the contamination of surface and underground waters with drug residue, including the pharmaceutical industry, farming and veterinary, healthcare centers, and households (incorrect waste management in case of expired drugs). Some residues of the pharmaceutical substances, together with sewage, enter wastewater treatment plans (WWTP), which unfortunately are not adjusted to degrade those highly specific compounds [9,10]. Interestingly, about 2000 active pharmaceutical ingredients are administered worldwide [11]. The greatest input of pharmaceuticals into the environment have, however, treated wastewater [12–15]. It was established that 30–90% of oral doses are excreted as active substances (Table 1) [16]. Conventional WWTP are not designed to remove pharmaceuticals; therefore, the removal rates vary (Table 1). The fate of pharmaceuticals in WWTP and the environment is affected by the pharmaceutical properties, including their persistence and connected half-life. Solubility, transformation products, bioaccumulation potential, and, first of all mobility, affect their toxicity [16].

Insufficient removal from wastewater influents was a main background for the application of various wastewater treatment methods: filtration [17], adsorption [18–21], Advanced Oxidation Processes [22–25], UV [26,27], ozonation [28–31], H_2O_2 [32,33], photocatalysis [34–40], Fenton and photo-Fenton process [41–43], electro-catalysis [44,45], electro-Fenton [46] etc.

Although the reported concentrations of pharmaceuticals in the environmental matrices are generally low—usually less than 1 μg L^{-1}, but their huge usage and abundance in the environment make the authorities worried about the long-term impact on animals and humans (Table 1) [47]. Although there are no requirements to detect and limit the concentration of pharmaceuticals in wastewater and water, some of them have been identified as a priority for further study, including paracetamol and diclofenac [48].

Despite the large differences in the removal rates, it is known that sorption, adsorption, sedimentation, and biotransformation in WWTP occurred [49–54]. Hydrophobic or electrostatic interactions are responsible for the sorption of drugs [55]. However, highly hydrophilic acidic drugs such as acetylsalicylic acid, ibuprofen, ketoprofen, naproxen, and diclofenac (pKa 4.2–4.9) are not sorbed and remain in the water [50]. The other negative effect can arise from the presence of metabolized (mainly its hydroxy and carboxy derivatives) drugs as they can form conjugates with similar or even increased toxicity in comparison to the parent drug [6]. It was established that the presence of drugs in the water revealed significant oxidative stress and caused histological changes in *Cyprinus Carpio* tissues [56] or disrupted microalgal growth.

The presence of those substances in surface waters has a toxic action on fish and other water organisms and can cause an increase in the incidence of some diseases, e.g., cancer (female sex hormones). The presence of antibiotics in water is connected with the observed increase in drug resistance of various microorganisms, even pathogenic ones. Constant exposure to pharmaceuticals in drinking water has endangered the most sensitive groups such as infants, the elderly, or patients with kidney, liver failure, or cancer. Due to the presence of estrogens in the water, feminization of male individuals and an increase in the incidence of breast and testicular cancer are noted [57–59]. Some of the pharmaceuticals present in water (i.e., anticancer drugs) can penetrate the blood-placenta barrier revealing teratogenic and embryotoxic effects endangering pregnant women in particular [60,61].

Induction of oxidative stress is connected with the production of reactive oxygen species (ROS) (such as hydroxyl radicals ($^{\bullet}OH$), superoxide radicals ($O_2^{\bullet -}$), and hydrogen peroxide (H_2O_2) responsible for peroxidation of membranes' polyunsaturated fatty acids and proteins [62]. In the studies considering the 98 pharmaceuticals detected in different water matrices (treated wastewater, surface water, and groundwater), it was established that 11 out of 49 pharmaceuticals were found to exert human health risk from ingesting contaminated surface water of India [63]. The growing problem of contamination of the water environment forces the use of various methods of removing pollutants and constant monitoring.

Residual pharmaceuticals in water samples are determined with laboratory methods, such as fluid/gas chromatography coupled with mass spectrometry. Unfortunately, these methods are expensive (cost of devices + cost of analysis) and frequently, among others, relate to the very low concentration of analytes in water samples (at ng L^{-1} or pg L^{-1} levels) and the costly and time-consuming initial sample preparation stage [64–68]. Compared to that, the voltammetric techniques are characterized by their low cost, simplicity of the analytic process, and the possibility to accumulate the analyte onto the surface of the working electrode before the appropriate electrode process, which eliminates the need to apply additional concentrating techniques (e.g., the extraction to solid phase) [69].

Table 1. The concentrations and removal rates of painkillers in the environmental matrices.

Drug	Excretion and Metabolites	WWTP Removal Rate (%)	Wastewater Influent (ng/L)	Wastewater Effluent (ng/L)	Surface Water (ng/L)
diclofenac	5–10% unchanged, metabolites: glucuronide, sulfate conjugates [49]	9–60 [50] 57.9 [47]	up to 302 [50] 191,000 [47]	1300–3300 [51] Up to 5450 [50] 10,000 [52] 80,000 [47]	up to 490 [50] 1200 [48] 1410 [53]

Table 1. *Cont.*

Drug	Excretion and Metabolites	WWTP Removal Rate (%)	Wastewater Influent (ng/L)	Wastewater Effluent (ng/L)	Surface Water (ng/L)
ibuprofen	1% unchanged Metabolites: (+)-2-40-(2-Hydroxy-2-methylpropyl)-phenylpropionic acid (25%) and (+)-2-40-(2-carboxypropyl)-phenylpropionic acid (37%), conjugated ibuprofen (14%) [49]	78–100 [50] 94.8 [47]	5533 [50] 344,000 [47]	711 [50] 18,000 [47]	400 [50] 126 [53]
naproxen	<1 unchanged, metabolites: 6-o-Desmethyl naproxen (o1%), conjugates (66–92%) [49]	50–98 [50]	611,000 [50]	33,900 [50] 10,000 [52]	297 [53] 390 [48] 400 [50]
ketoprofen	Metabolites: Glucuronide conjugates [49]	15–100 [50]	5700 [50] 1000–10,000 [54]	1620 [50]	120 [48] 329 [50]
paracetamol	80% as conjugates, metabolites: Sulphate conjugate (30%), paracetamol cysteinate, mercapturate (5%) [49]	91–99 [50]	292,000 [50] 1000–10,000 [54]	1480 [50] 100,000 [52]	10,000 [48] 66 [50]
acetylsalicylic acid	Metabolites: Salicylic acid (10%), salicyluric acid (75%), salicylic phenolic (10%) and acyl (5%) glucuronides, gentisic acid (o1%) [49]	0 [50]	1000–10,000 [54]	1510 [50]	<50 [50]

In the 1990s, screen printing technology for the preparation of electrochemical sensors was introduced. The screen-printed electrodes (SPEs) became objects of numerous research efforts aimed at investigating their practical application. The low manufacturing costs, appropriate repeatability levels, and electrochemical properties, all make them an attractive analytical tool [70–77].

The manufacture of screen-printed electrodes is the process of designing appropriate ink (print) composition and then pressing it through the appropriate template (screen) onto the carrier surface (most often ceramic or polymer). Both the ink composition and the area of the working electrode can be modified, e.g., with nanoparticles/metal films, polymer, or enzyme, depending on the application-specific requirements [70–77]. The entire electrode system (reference, counter, and working electrodes) is printed on the same substrate surface (Figure 1).

The key feature of the screen-printed electrodes, among other electrochemical sensors, is their miniaturization, enabling them to apply in portable/field devices. The application of the screen-printed electrodes in the carrying out measurements in situ enable minimalization or even elimination of errors, reduces the test time, and consequently, costs usually connected with sampling, transport, and storage of representative samples [78]. This justifies the thesis saying that there is a significant need to develop field devices for monitoring waters that will allow us to evaluate water quality at the sampling location in an easy and fast manner. Recent years saw the growing interest in the development of such devices. The use of portable devices is one of the development trends in environmental analytics [79].

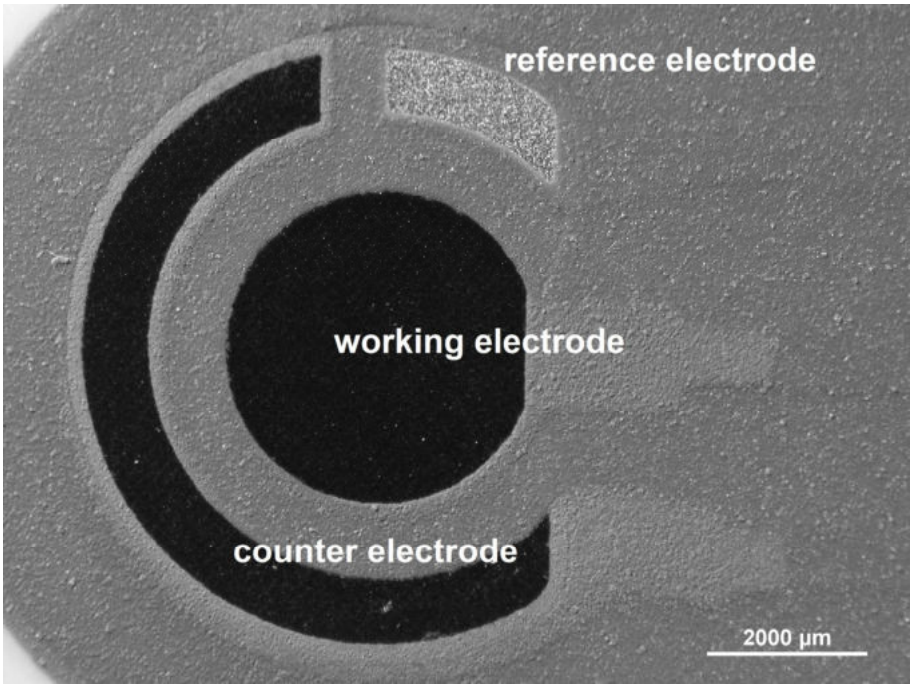

Figure 1. Optical microscopic image of screen-printed carbon electrode (SPCE, Metrohm DropSens, Oviedo, Spain).

A lot of papers describe the application of electrochemical sensors for the determination of residues of pharmaceuticals and screen-printed sensors [74,75,80]. Most electrochemical methods allow for the quantitative determination of these compounds in pharmaceutical preparations, biological samples, and beverages. However, the literature has available articles on the development of electrochemical sensors to determine pharmaceuticals, including painkillers in water samples. This article focuses on a summary of achievements in the field of screen-printed voltammetric sensors application in environmental water monitoring of painkillers.

2. Application of Screen-Printed Voltammetric Sensors for the Painkillers Determination in the Environmental Water Samples

Non-steroidal anti-inflammatory drugs (NSAIDs) are an important class of drugs because they are widely used to treat muscle pain and inflammatory rheumatic diseases, and this is an increasing trend. This fact, combined with improper disposal and ineffectiveness of wastewater treatment, leads to the ubiquitous presence of these drugs in the environment [81]. Diclofenac (DF), ibuprofen (IB), acetylsalicylic acid (AS), naproxen (NP) and ketoprofen (KP) belong to the NSAIDs (Figure 2A–E). Diclofenac exhibits activities characteristic of this group of drugs, i.e., anti-inflammatory, antipyretic, analgesic, and inhibiting platelet aggregation [82,83]. It is used to relieve symptoms of many illnesses, including non-articular rheumatism, osteoarthritis, sports injuries, and rheumatoid arthritis. In the proposed daily dose (50–150 mg), DF is completely tolerated [84]. Although no problems are caused when an appropriate amount of DF is used, its excessive or continuous use may cause symptoms such as epigastric discomfort, gastric ulcer, hematuria; meantime, the accumulated mass of toxic substances can cause kidney and liver dysfunctions [85]. Furthermore, the ubiquity of DF in the environment impairs fish health and water quality due to its poor degradation [86]. Ibuprofen ((2–4 isobutyphenyl) propionic acid is commonly prescribed to treat chronic and acute pain and many rheumatic and musculoskeletal disorders. IB is also used to reduce fever [87]. Its action is due to the inhibition of cyclooxygenases, which are involved in the synthesis of prostaglandins involved in producing pain, inflammation, and fever [88]. Acetylsalicylic acid (aspirin) is an anti-inflammatory,

antipyretic, and analgesic drug. Thanks to its effectiveness, it has a place in treating antithrombotic coronary heart disease, prevention of colon cancer, fever, headaches, and Alzheimer's disease [89,90]. Naproxen (2-(6-methoxy-2-naphthyl)propionic acid) is an antipyretic and anti-inflammatory compound applied in the treatment of nonrheumatic inflammation, migraine, and gout [91]. Association therapy with paracetamol and naproxen has also been reported to benefit patients with pain related to rheumatoid arthritis. The naproxen drug should be given with precaution to elderly patients and patients with hemophilia, gastrointestinal bleeding, and platelet coagulation dysfunction. [92]. Ketoprofen is an arylpropionic acid derivative with anti-inflammatory, antipyretic, and analgesic properties [93]. It relieves pain associated with rheumatic and nonrheumatic inflammatory disorders, vascular headaches, and dysmenorrhea [94]. It is well absorbed after oral and rectal administration, and it can be administered by injection and transdermally. KP is metabolized in the liver and mainly excreted in urine [93].

Paracetamol (N-acetyl-p-aminophenol, Figure 2F), also known as acetaminophen or Tylenol, is extensively used to relieve moderate pain and reduce fever globally [95]. It has no anti-inflammatory effect. PA is the main ingredient in many cold and flu medications [82]. The antipyretic effect of this drug is related to the inhibition of prostaglandin synthesis in the central nervous system [83]. An overdose of PA may result in the accumulation of toxic metabolites that can cause acute and sometimes fatal nephro- and hepatotoxicity [82]. As a widely used pharmaceutical, PA is present in the environment, its concentration found in environmental water samples ranges from 1 to 10 nM.

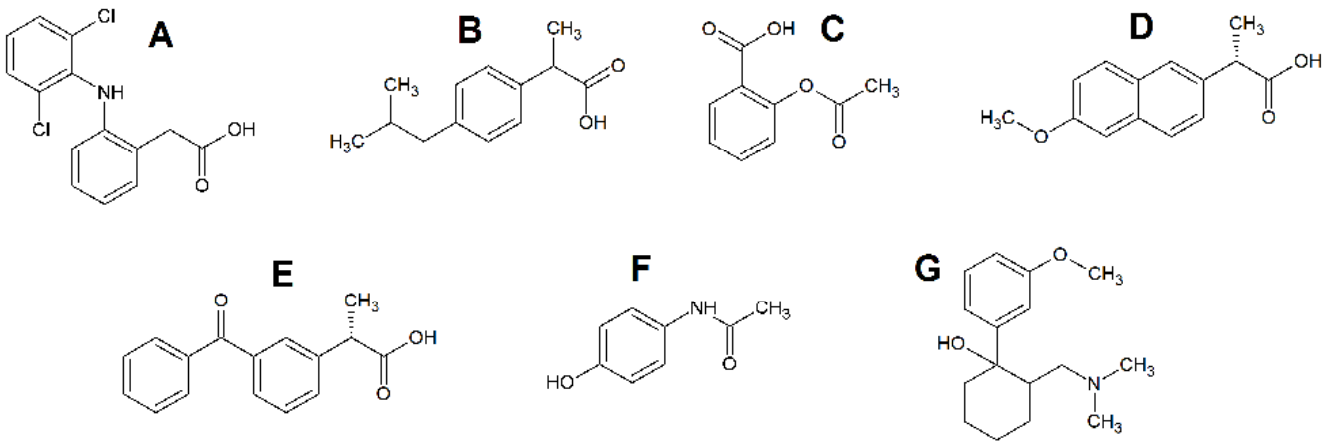

Figure 2. The structural formulas of diclofenac (**A**), ibuprofen (**B**), acetylsalicylic acid (**C**), naproxen (**D**), ketoprofen (**E**), paracetamol (**F**) and tramadol (**G**).

Tramadol, (1R,2R)-2-[(dimethylamino)methyl]-1-(3-methoxyphenyl)cyclohexanol, TR, Figure 2G, is an l-opioid recipient agonist that acts on analgesic centrally is applied initially for treating modest to severe pain [96]. TR is a commonly misused drug that can lead to addiction or even death, although it has a preferable safety profile than other opioid analgesic drugs such as morphine or hydrocodone [97]. The typical dosage requirement for oral consumption of TR ranges between 50 and 100 mg per 4 to 6 h. The maximal dose of the drug will be 400 mg every day. Overdosing of TR can cause nausea, respiratory depression, vomiting, coma, dizziness, and tachycardia.

In the literature are few articles describing the use of screen-printed sensors in the monitoring of painkillers residues (DF, PA, IB, and TR) in environmental waters samples [82,83,98–104]. These sensors have also found application in the determination of painkillers in pharmaceutical preparations and biological samples, e.g., urine and serum [84–87,96,97,105–113]. There are no studies on voltammetric procedures to determine acetylsalicylic acid and naproxen in water samples in the literature. However, there are single procedures for determining AS [89,90,114] and NP [92,115] on screen-printed

electrodes in pharmaceuticals and/or human physiological fluids. There are no attempts to use screen-printed sensors to analyze ketoprofen in any type of sample.

2.1. SPEs Modified with Carbon Nanomaterials

Carbon nanomaterials are very attractive for the mass production of SPEs and represent a significant opportunity to increase the analytical sensitivity of these devices, enabling new sensing applications [116,117]. These materials are characterized by excellent electrical conductivity, low electrical resistance, large surface area, and good physical and chemical stability [118]. In addition, the possibility of functionalization of their surface leads to an increase in analytical efficiency, including sensitivity and selectivity [119]. Carbon nanomaterials used as SPEs modifiers include mainly carbon black (CB), graphene-related materials, carbon nanofibers (CNFs), various forms of carbon nanotubes—single-, double-, and multiwalled (SWCNTs, DWCNTs, and MWCNTs), carbon nanohorns (CNHs), as well as carbon nano-onions (CNOs) [117,120–123].

In the literature, few articles describe the use of screen-printed sensors modified with carbon materials to monitor painkillers residues in environmental water samples [83,98,99,101,102]. The comparison of these assay procedures is presented in Table 2. The lowest detection limit of paracetamol for the accumulation time of 90 s (LOD, 0.54 nM) was obtained using a screen-printed carbon/carbon nanofibers sensor (SPCE/CNFs) [98]. Sasal et al. [98] described the application of a commercially available SPCE/CNFs sensor and differential pulse adsorptive stripping voltammetry (DPAdSV) for the direct determination of the low (real) concentration of PA in environmental water samples. This was done by monitoring the oxidation current of PA after adsorption of molecules onto the SPCE/CNFs surface at the potential of −0.95 V. According to the literature data, a PA oxidation mechanism at the SPCE/CNFs is associated with the formation of N-acetyl-p-quinoneimine (NAPQI) [99]. The adsorption of PA onto the electrode surface was confirmed by electrochemical impedance spectroscopy (EIS), cyclic voltammetry (CV), and theoretical studies. Moreover, the authors found that the SPCE/CNFs sensor presented better performance than the screen-printed sensors with carbon or carbon/multiwalled carbon nanotubes working electrodes. It was related to the developed active surface of the SPCE/CNFs, which mediates PA adsorption. Under optimized conditions, the DPAdSV measurements were performed in 0.1 M H_2SO_4 containing 0.01 μM EDTA to minimize the influence effect of interfering metal ions. The developed analytical procedure using SPCE/CNFs was applied to the direct determination of PA (in the range of 5–200 nM) in water samples collected from two Polish rivers and sea with the recovery values between 96.2 to 104.6%.

In [102], Sasal et al. proposed a DPAdSV voltammetric procedure at the commercially available screen-printed carbon sensor modified with carboxyl functionalized multiwalled carbon nanotubes (SPCE/MWCNTs-COOH) for the trace analysis of diclofenac (DF) (Figure 3). The authors stated that DF is irreversibly oxidized, and the oxidation process of DF is not purely diffusion-or adsorption-controlled at the SPCE/MWCNTs-COOH. Moreover, the number of electrons involved in the DF oxidation process equals 2. These results are consistent with the literature data, which proposed that DF is oxidized to 5-hydrohydiclofenac by losses of $2e^-$ and $2H^+$ [124,125]. The SPCE/MWCNTs-COOH provided a higher sensitivity and wider linear range than the SPCE (0.019 vs. 0.040 μA/nM and 0.5–200.0 vs. 1.0–200 nM, respectively). It is connected with the fact that the application of MWCNTs-COOH improved the electron transfer process and the active surface area of the electrode. The proposed DPAdSV procedure is characterized by simplicity, sensitivity, and time-saving. For the first time, the electrochemical sensor was applied to determine the real concentration of DF (0.42 ± 0.080 nmol L^{-1}) in the river water samples without the sample pre-treatment step.

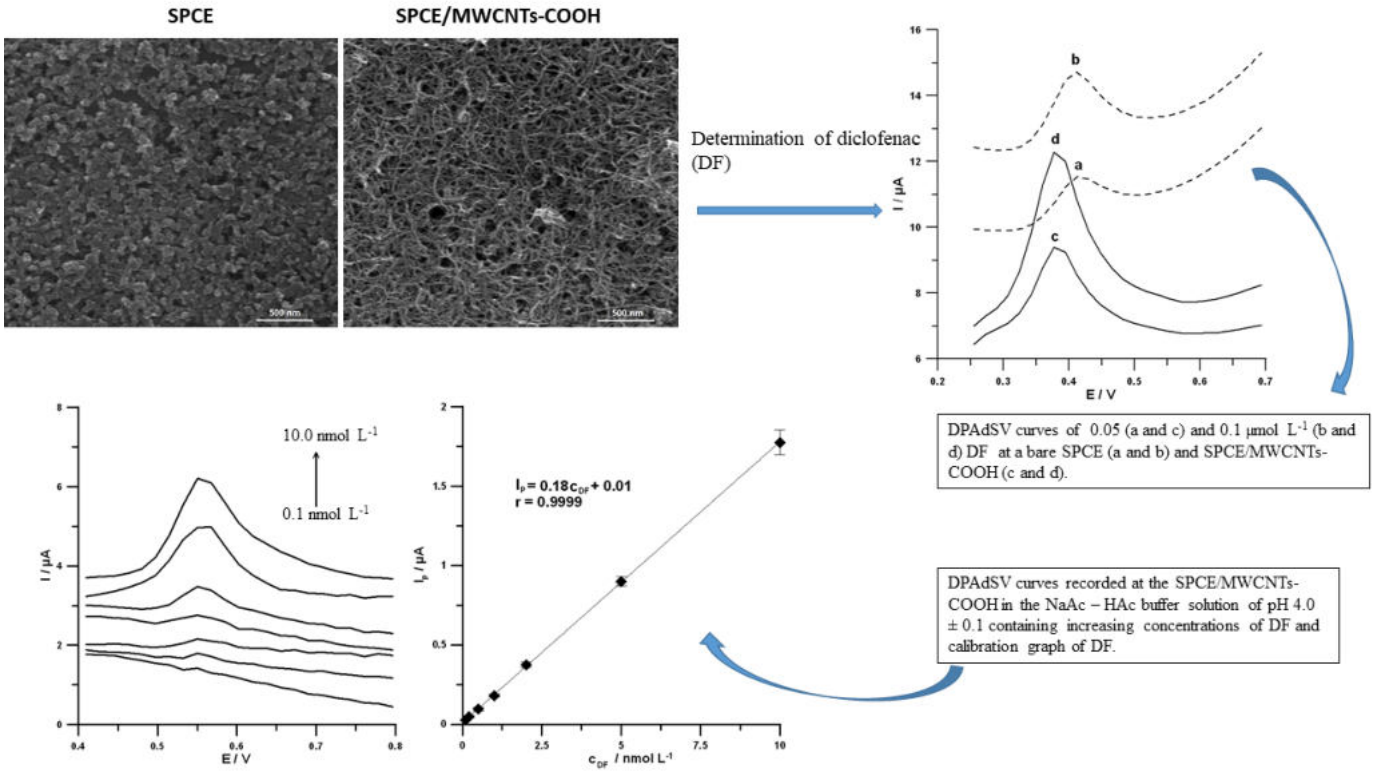

Figure 3. SEM images and DPAdSV curves recorded at the SPCE and SPCE/MWCNTs-COOH. DPAdSV curves recorded at the surface of the SPCE/MWCNTs-COOH in solution containing increasing concentrations of DF: 0.1, 0.2, 0.5, 1.0, 2.0, 5.0 and 10.0 nmol L^{-1}, and calibration graph of DF [102].

In voltammetric measurements, even a low concentration of surface-active substances can block the active surface of the electrode. Therefore, UV irradiation or microwave heating of the samples are suggested for the elimination of this type of interference. There are also other simple ways to minimize interferences from the organic matrix of samples, e.g., the application of potential pulses for accumulation. In that approach, the potential of cathode pulses was chosen in a way that made it represent the maximum adsorption of the determined element and the potential of anode pulses to desorb the interfering surfactants [126]. This method of eliminating interference from surfactants was described by Sasal et al. in [83]. The authors proposed using the DPAdSV technique, a commercially available SPCE/MWCNTs-COOH sensor, and pulsed potential accumulation for individual and simultaneous determination of paracetamol and diclofenac. The scheme of the individual steps of the optimized voltammetric procedure is presented in Figure 4. Moreover, the authors found that the application of carboxyl functionalized multiwalled carbon nanotubes and pulsed potential accumulation contributes to improving PA and DF peaks currents. The amplification of the PA and DF signals is related to a greater number of active centers at the SPCE/MWCNTs-COOH than at the SPCE. Based on the cyclic voltammetric examination, it was found that the PA and DF are irreversibly oxidized at the SPCE/MWCNTs-COOH, and these processes are not purely diffusion or adsorption controlled. The DPAdSV procedure with SPCE/MWCNTs-COOH shows the low LODs of 1.4 nM for PA and 0.03 nM for DF. The DPAdSV procedure at the SPCE/MWCNTs-COOH was successfully applied for the simultaneous analysis of PA and DF in spiked river water samples with recovery values between 96.5% and 104.8%. Moreover, the voltammetric procedure proposed by Sasal et al. allowed for the direct determination of PA (24.3 ± 0.5 nM) and DF (3.7 ± 0.7 nM) in the wastewater samples purified in a sewage treatment plant.

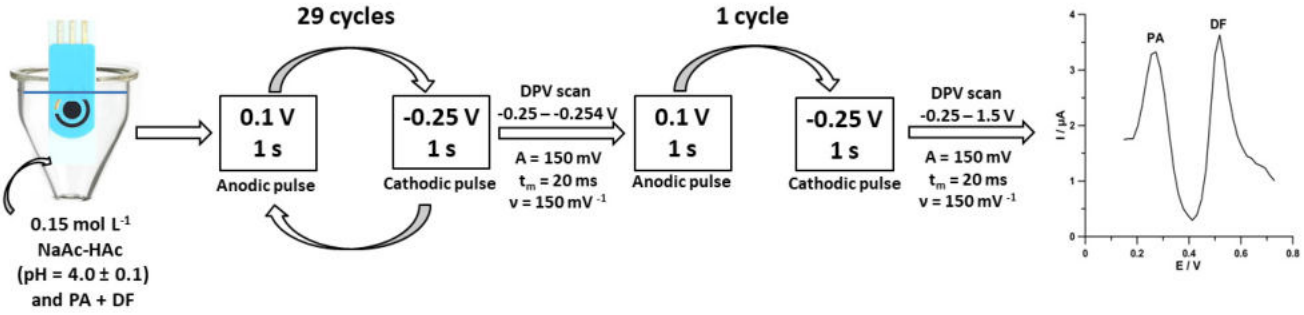

Figure 4. Scheme of voltammetric measurements of PA and DF at the SPCE/MWCNTs-COOH [83].

Serrano et al. [99] compared the analytical performances of the commercially available screen-printed carbon electrode (SPCE), multiwalled carbon nanotubes modified screen-printed carbon electrode (SPCNTE), screen-printed carbon electrode modified with carbon nanofibers (SPCNFE), and screen-printed graphene electrode (SPGPHE) for the individual and simultaneous determination of ibuprofen, paracetamol, and caffeine. The authors suggest that the SPCNFE was the most suitable carbon-based electrode for the voltammetric determination of the selected analytes in water at trace levels. Moreover, the applicability of SPCNFE for the analysis of environmental water samples was demonstrated by the simultaneous determination of PA, IB, and CF in spiked tap water samples. The good recoveries (103.1, 99.5, and 97.6% for PA, IB, and CF, respectively) and reproducibility (RSD of 8.93, 0.96, and 8.63% for PA, IB, and CF, respectively) were obtained. In hospital wastewater samples, only PA (7.74 µM) was determined. The IB and CF were not detected since the studied hospital wastewater sample did not contain IB, and the concentration of CF was below the LOD obtained for the SPCNFE.

In paper [101], Deroco et al. described the use of carbon black as a modifying nanomaterial of SPEs. The application of CB film onto the SPE surface contributed to the improvement of electrocatalytic activity for the $[Fe(CN)_6]^{3-/4-}$ redox probe, and paracetamol and levofloxacin (LVF) signals. The authors stated that PA and LVF oxidation processes were fully controlled by diffusion, and these processes involved an equal number of electrons and protons. The developed sensor was successfully used to analyze PA (6.0, 10.0, and 70.0 µM) and LVF (2.0, 9.0, and 60.0 µM) in spiked river water samples with recovery values between 98.3 and 106.0%.

Table 2. Summary of voltammetric procedures to determine painkillers residues at the screen-printed electrodes modified with carbon materials in environmental water samples.

Electrode	Analyte	Method	Linear Range [µM]	LOD [µM]	Application	Ref.
SPCE/CNFs	PA	DPAdSV	0.002–0.05 0.1–2.0	0.00054	river water, sea water	[98]
SPCE/MWCNTs-COOH	DF	DPAdSV	0.0001–0.01	0.000028	river water	[102]
SPCE/MWCNTs-COOH	PA DF	DPAdSV (PPA)	0.005–5.0 0.0001–0.02	0.0014 0.000030	wastewater, river water	[83]

Table 2. *Cont.*

Electrode	Analyte	Method	Linear Range [μM]	LOD [μM]	Application	Ref.
SPCE	PA	DPV	13.20–377.0	7.17	tap water, hospital wastewater	[99]
SPCNTE			2.64–33.70	0.66		
SPCNFE			1.98–33.70	0.66		
SPGPHE			3.31–23.20	0.66		
SPCE	IB		18.40–489.60	5.33		
SPCNTE			9.21–155.10	2.91		
SPCNFE			19.40–114.40	5.82		
SPGPHE			30.50–86.30	9.21		
SPCE	CF		24.70–480.0	7.21		
SPCNTE			20.60–480.0	6.18		
SPCNFE			61.80–330.0	2.06		
SPGPHE			15.50–44.80	4.63		
CB/SPCE	PA	SWV	0.80–30.0	2.60	river water	[101]
	LVF		0.90–70.0	0.42		

PA–paracetamol; DF–diclofenac; IB–ibuprofen; CF–caffeine; LVF–levofloxacin; DPAdSV–differential-pulse adsorptive stripping voltammetry; PPA–pulsed potential accumulation; DPV–differential-pulse voltammetry; SWV–square-wave voltammetry; SPCE–screen-printed carbon electrode; SPCE/MWCNTs-COOH–carboxyl functionalized multiwalled carbon nanotubes modified screen-printed carbon electrode; SPCNTE–screen-printed carbon electrode modified with carbon nanotubes; SPCE/CNFs (SPCNFE)–screen-printed carbon electrode modified with carbon nanofibers; SPGPHE–screen-printed graphene electrode; CB/SPCE–screen-printed carbon electrode modified with carbon black.

2.2. SPEs Electrochemically Pretreated

SPEs consist of working electrodes made of conductive inks based on platinum, gold, silver, or carbon, the latter being the most used material because it is universal and cheap. Conductive inks from screen-printed carbon electrodes (SPCEs) contain carbon with organic solvents, binding pastes (e.g., polyester resin, ethylcellulose, or epoxy-based polymeric binder), and some additives that provide functional properties. The presence of these additional non-conductive materials can lead to a slowdown in the kinetics of heterogeneous electrochemical reactions. Therefore, much attention has been paid to developing surface treatment methods to improve the electrochemical properties of the SPCEs. The main purpose of the SPCEs pre-treatment was to remove organic ink components or contaminants and increase surface roughness or functionality [127–129]. Several methods of pre-treatment of SPEs can be found in the literature, such as heat treatment [127], oxygen plasma treatment [128], chemical treatment [129], polishing [130,131], and electrochemical treatment [132–134]. Electrochemical treatments allow the in situ easy activation of SPCEs. They usually hold the electrode at a constant potential for a short time or potential cycling to extreme anodic and/or cathodic potentials [127,135]. Table 3 shows summary of voltammetric procedures for painkillers residues determination at the electrochemically pretreated screen-printed electrodes electrochemically.

In paper [82], Kozak et al. proposed an electrochemically activated (25 voltammetric cycles from 1.0 to −0.7 V at a scan rate of 10 mV s^{-1} in a solution containing 0.1 M acetate buffer of pH = 4.0 ± 0.1 and 10 mM H_2O_2) screen-printed carbon electrode modified with sodium dodecyl sulfate (aSPCE/SDS) for the simultaneous determination of paracetamol, diclofenac, and tramadol. At the moment, there is the first paper describing the voltammetric procedure of tramadol determination with the use of screen-printed electrodes in environmental water samples [82]. The electrochemical activation contributes to the removal of the organic ink constituents or contaminants introduced into the printing stage, which consequently changes the morphology of the electrode surface and reduces the charge transfer resistance. Furthermore, the modification of the electrode surface with SDS contributes to the TR signal amplification and minimizes the influence of surfactants (Triton X-100 and CTAB). The author proved the adsorption of PA and DF onto the SPCE/SDS surface by analyzing differential capacity curves and stated that TR existing in the cationic

form reaches the electrode surface by diffusion and is electrostatically attractive for the surface covered by SDS anions. The aSPCE/SDS showed a good linear response in the concentration ranges of 0.05–2.0 μM for PA, 0.001–0.2 μM for DF, and 0.01–0.2 and 0.2–2.0 μM for TR. The limits of detection obtained during the simultaneous determination of PA, DF, and TR are 0.015 μM, 0.00021 μM, and 0.0017 μM, respectively. The DPAdSV procedure with the aSPCE/SDS was successfully applied for the determination of PA, DF, and TR in river water and serum samples (the recovery values between 97.0 and 102.0%) as well as pharmaceuticals (the relative errors between determined and label values are in the ranges of 0 and 2.1%).

Table 3. Summary of voltammetric procedures for painkillers residues determination at the electrochemically pretreated screen-printed electrodes or modified with polymer film in environmental water samples.

Electrode	Analyte	Method	Linear Range [μM]	LOD [μM]	Application	Ref.
aSPCE/SDS	DF PA TR	DPAdSV	0.001–0.2 0.05–20.0 0.01–0.2 0.2–2.0	0.00021 0.015	river water	[82]
electrochemically pretreated SPCE	PA HQ E2	DPV	0.5–10.0 0.5–10.0 0.5–10.0	0.22 0.19 0.89	tap water	[100]
electrochemically pretreated SPGE	IB	SWV	0.80–30.0	6.30	river water, wastewater	[104]
MIP/SPCE	DF	DPV	0.1–10	0.07	river water, tap water	[103]

PA–paracetamol; DF–diclofenac; HQ–hydroquinone; E2–estradiol; IB–ibuprofen; DPAdSV–differential-pulse adsorptive stripping voltammetry; DPV–differential-pulse voltammetry; SWV–square-wave voltammetry; aSPCE/SDS–activated screen-printed carbon electrode modified with sodium dodecyl sulfate; electrochemically pretreated SPCE–electrochemically pretreated screen-printed carbon electrode; electrochemically pretreated SPGE–electrochemically pretreated screen-printed graphite electrode; MIP/SPCE–screen-printed carbon electrode modified with molecularly imprinted polymer.

In paper [100], Raymounds-Pereira et al. proposed electrochemically pretreated (2 voltammetric cycles from −2.5 to 2.5 V at a scan rate of 100 mV s^{-1} in 0.5 M sulfuric acid solution) screen-printed carbon electrode (SPCE) for the determination of hydroquinone (HQ), paracetamol and estradiol (E2) in tap water. The authors concluded that pre-treatment did not affect the morphology of the electrode surface and did not introduce functional groups to the surface but removed non-conducting residues from the printing ink. This consequently contributed to the improvement of the sensor's conductivity (the charge-transfer resistance decreased from 30 to 5 kΩ due to the pre-treatment) and sensitivity of the voltammetric procedure. The ability to determine PA, HQ, and E2 was verified by taking voltammetric measurements with tap water samples spiked with analytes in the concentration range of 1–7 μM). The results were compared to those obtained by high-performance liquid chromatography (HPLC). Using the Student's test the author found that the voltammetric procedures yielded the same results as the standard method HPLC.

Amin et al. [104] show the application of electrochemically pretreated screen-printed graphite electrode (SPGE) to the electrochemical oxidation and detection of ibuprofen (IB). An SPGE surface was pretreated (conditioned) by applying a fixed potential of 1.6 V for 3 min vs. Ag pseudo reference electrode. Using pretreated SPGE, detection limits were improved 12.5 times to instrumental detection limits, thereby, LOD of 6.30 μM was achieved.

2.3. SPEs Modified with Polymers

Polymers are widely used modifiers for electrodes and SPEs. The most frequently used polymers for this purpose are conductive polymers that combine conventional properties

of polymers with the electronic properties of metals and/or semiconductors. Mainly polyacetylene, polyaniline, polypyrrole, or polythiophene are used here [136,137]. In addition, it was found that the use of a conductive polymer to modify the electrode surface increases the electrical conductivity, high chemical stability, good magnetic properties, high electron affinity, optical properties, and low ionization potential [138]. Another group of polymers that can be used to modify the surface of the electrodes are ion-exchange polymers, one example of which is the well-known Nafion–perfluorinated sulfonated cation-exchanger [138]. Today, molecularly imprinted polymers (MIPs) in combination with electrochemical sensors are of great interest. MIP modified electrodes have proven the usefulness of both small and large biomolecules, such as proteins or DNA [139,140]. MIPs are typically prepared by forming a three-dimensional polymer network around a molecular template via a cross-linking step. Removal of this matrix creates binding cavities that retain the shape, size, and orientation of the target molecule, leading to a high selectivity in the recognition process [141,142]. MIPs offer some clear advantages, including very good stability with a high surface area over a wide range of experimental conditions and solvents, becoming powerful alternatives to biorecognition elements such as antibodies. Because of their high selectivity, simple synthesis methods, high stability, low cost, and good engineering capability, MIPs receive great attention as recognition elements in various fields, especially in electrochemical sensing [143,144]. The polymer layer on the surface of the electrodes can be applied in several ways. Most often it is done by dropping a polymer solution [145] or electropolymerization [137,146,147]. Other methods described in the literature are dispensing, inkjet printing, screen-printing, electrodeposition, electrospray, or pen-writing [138].

Seguro et al. [103] proposed a disposable voltammetric molecularly imprinted polymer screen-printed carbon sensor (MIP/SPCE) for the selective determination of diclofenac (Table 3). MIP preparation was achieved by cyclic voltammetry, using dopamine as a monomer in the presence of DF. The MIP/SPCE showed adequate selectivity (in comparison with other drug molecules), intra-day repeatability of 7.5%, inter-day repeatability of 11.5%, a linear range between 0.1 and 10 μM, and a limit of detection and quantification of 70 and 200 nM, respectively. Its applicability was demonstrated by the determination of DF in spiked water samples (river and tap water).

3. Conclusions

Monitoring the water environment for the presence and content of residues of pharmaceuticals, including painkillers a significant issue for contemporary analytical chemistry. This review demonstrates the applications of screen-printed sensors for the sensitive determination of environmental water pollutants (painkillers). Several examples described in this review paper show that the developed simple, sensitive, and selective voltammetric procedures with screen-printed sensors can be good tools for this purpose. The screen-printed electrodes modified with carbon nanomaterials, polymer film, or electrochemically activated showed advantageous electroconductivity, catalytic activity, and surface area. Moreover, the screen-printed sensors are potentially applicable not only in laboratory measurements but also in-field analysis. Due to their electrochemical properties, simplicity, disposability, short response time, and miniaturization, screen-printed sensors can find application in environmental water monitoring.

The screen-printed sensors area is expected to grow with new application domains. Future work will focus on improving the analytical parameters of screen-printed sensors to adjust them to the relative concentrations of the analytes in the environmental water samples, and on developing procedures and sensors for new substances AS, NP, KP) with analgesic properties. More attention should be given to expected interfering species and proven or possible strategies for mitigating their effects and improving selectivity. Moreover, sensor miniaturization, shortening the analysis time, reducing the volume of analyzed samples, and using reagents should be the aim of subsequent studies.

Author Contributions: Conceptualization, K.T.-R. and J.K.; investigation, K.T.-R., J.K. and B.C.; writing—original draft preparation, K.T.-R., J.K. and B.C.; writing—review and editing, K.T.-R., J.K. and B.C.; supervision, K.T.-R. All authors have read and agreed to the published version of the manuscript.

Funding: This research received no external funding.

Institutional Review Board Statement: Not applicable.

Informed Consent Statement: Not applicable.

Data Availability Statement: The data presented in this study are available on request from the corresponding author.

Conflicts of Interest: The authors declare no conflict of interest.

References

1. de Jesus Gaffney, V.; Mota-Filipe, H.; Pinto, R.A.; Thiemermann, C.; Loureiro, M.; Cardoso, V.V.; Benoliel, M.J.; Almeida, C.M. Chemical and biochemical characterization and in vivo safety evaluation of pharmaceuticals in drinking water. *Environ. Toxicol. Chem.* **2016**, *35*, 2674–2682. [CrossRef] [PubMed]
2. Farré, M.I.; Pérez, S.; Kantiani, L.; Barceló, D. Fate and toxicity of emerging pollutants, their metabolites and transformation products in the aquatic environment. *Trend. Anal. Chem.* **2008**, *27*, 991–1007. [CrossRef]
3. Szymonik, A.; Lach, J.; Malińska, K. Fate and removal of pharmaceuticals and illegal drugs present in drinking water and wastewater. *Ecol. Chem. Eng. S* **2017**, *24*, 65–85. [CrossRef]
4. Khan, A.H.; Khan, N.A.; Ahmed, S.; Dhingra, A.; Singh, C.P.; Khan, S.U.; Mohammadi, A.A.; Changani, F.; Yousefi, M.; Alam, S.; et al. Application of Advanced Oxidation Processes Followed by Different Treatment Technologies for Hospital Wastewater Treatment. *J. Clean Prod.* **2020**, *269*, 122411. [CrossRef]
5. Kosma, C.I.; Lambropoulou, D.A.; Albanis, T.A. Occurrence and Removal of PPCPs in Municipal and Hospital Wastewaters in Greece. *J. Hazard. Mater.* **2010**, *179*, 804–817. [CrossRef]
6. Angeles, L.F.; Mullen, R.A.; Huang, I.J.; Wilson, C.; Khunjar, W.; Sirotkin, H.I.; McElroy, A.E.; Aga, D.S. Assessing Pharmaceutical Removal and Reduction in Toxicity Provided by Advanced Wastewater Treatment Systems. *Environ. Sci. Water Res. Technol.* **2020**, *6*, 62–77. [CrossRef]
7. Brillas, E. A Critical Review on Ibuprofen Removal from Synthetic Waters, Natural Waters, and Real Wastewaters by Advanced Oxidation Processes. *Chemosphere* **2022**, *286*, 131849. [CrossRef]
8. Larsson, D.G.J.; de Pedro, C.; Paxeus, N. Effluent from Drug Manufactures Contains Extremely High Levels of Pharmaceuticals. *J. Hazard. Mater.* **2007**, *148*, 751–755. [CrossRef]
9. Boroń, M.; Pawlas, K. Pharmaceuticals in aquatic environment–literature review. *Probl. Hig. Epidemiol.* **2015**, *96*, 357.
10. de Morais, J.L.; Zamora, P.P. Use of Advanced Oxidation Processes to Improve the Biodegradability of Mature Landfill Leachates. *J. Hazard. Mater.* **2005**, *123*, 181–186. [CrossRef]
11. Burns, E.E.; Carter, L.J.; Snape, J.; Thomas-Oates, J.; Boxall, A.B.A. Application of Prioritization Approaches to Optimize Environmental Monitoring and Testing of Pharmaceuticals. *J. Toxicol. Environ. Health B* **2018**, *21*, 115–141. [CrossRef]
12. Carballa, M.; Omil, F.; Ternes, T.; Lema, J.M. Fate of Pharmaceutical and Personal Care Products (PPCPs) during Anaerobic Digestion of Sewage Sludge. *Water Res.* **2007**, *41*, 2139–2150. [CrossRef] [PubMed]
13. Evgenidou, E.N.; Konstantinou, I.K.; Lambropoulou, D.A. Occurrence and Removal of Transformation Products of PPCPs and Illicit Drugs in Wastewaters: A Review. *Sci. Total Environ.* **2015**, *505*, 905–926. [CrossRef] [PubMed]
14. Hu, X.; Xie, H.; Zhuang, L.; Zhang, J.; Hu, Z.; Liang, S.; Feng, K. A Review on the Role of Plant in Pharmaceuticals and Personal Care Products (PPCPs) Removal in Constructed Wetlands. *Sci. Total Environ.* **2021**, *780*, 146637. [CrossRef] [PubMed]
15. Fan, X.; Gao, J.; Li, W.; Huang, J.; Yu, G. Determination of 27 Pharmaceuticals and Personal Care Products (PPCPs) in Water: The Benefit of Isotope Dilution. *Front. Environ. Sci. Eng.* **2020**, *14*, 8. [CrossRef]
16. OECD. Pharmaceutical Residues in Freshwater: Hazards and Policy Responses. In *OECD Studies on Water*; OECD: Paris, France, 2019; ISBN 978-92-64-77633-3.
17. Pompei, C.M.E.; Campos, L.C.; da Silva, B.F.; Fogo, J.C.; Vieira, E.M. Occurrence of PPCPs in a Brazilian Water Reservoir and Their Removal Efficiency by Ecological Filtration. *Chemosphere* **2019**, *226*, 210–219. [CrossRef]
18. Adeola, A.O.; de Lange, J.; Forbes, P.B.C. Adsorption of Antiretroviral Drugs, Efavirenz and Nevirapine from Aqueous Solution by Graphene Wool: Kinetic, Equilibrium, Thermodynamic and Computational Studies. *Appl. Surf. Sci. Adv.* **2021**, *6*, 100157. [CrossRef]
19. Babas, H.; Kaichouh, G.; Khachani, M.; Karbane, M.E.; Chakir, A.; Guenbour, A.; Bellaouchou, A.; Warad, I.; Zarrouk, A. Equilibrium and Kinetic Studies for Removal of Antiviral Sofosbuvir from Aqueous Solution by Adsorption on Expanded Perlite: Experimental, Modelling and Optimization. *Surf. Interfaces* **2021**, *23*, 100962. [CrossRef]
20. Bhadra, B.N.; Jhung, S.H. Adsorptive Removal of Wide Range of Pharmaceuticals and Personal Care Products from Water Using Bio-MOF-1 Derived Porous Carbon. *Micropor. Mesopor. Mater.* **2018**, *270*, 102–108. [CrossRef]

21. Karunanayake, A.G.; Todd, O.A.; Crowley, M.L.; Ricchetti, L.B.; Pittman, C.U.; Anderson, R.; Mlsna, T.E. Rapid Removal of Salicylic Acid, 4-Nitroaniline, Benzoic Acid and Phthalic Acid from Wastewater Using Magnetized Fast Pyrolysis Biochar from Waste Douglas Fir. *Chem. Eng. Sci.* **2017**, *319*, 75–88. [CrossRef]
22. Jafarinejad, S. Cost-Effective Catalytic Materials for AOP Treatment Units. In *Applications of Advanced Oxidation Processes (AOPs) in Drinking Water Treatment*; Gil, A., Galeano, L.A., Vicente, M.Á., Eds.; Springer International Publishing: Cham, Switzerland, 2017; Volume 67, pp. 309–343. ISBN 978-3-319-76881-6.
23. Michael, I.; Frontistis, Z.; Fatta-Kassinos, D. Removal of Pharmaceuticals from Environmentally Relevant Matrices by Advanced Oxidation Processes (AOPs). In *Comprehensive Analytical Chemistry*; Elsevier: Amsterdam, The Netherlands, 2013; Volume 62, pp. 345–407. ISBN 978-0-444-62657-8.
24. Nie, C.; Shao, N.; Wang, B.; Yuan, D.; Sui, X.; Wu, H. Fully Solar-Driven Thermo- and Electrochemistry for Advanced Oxidation Processes (STEP-AOPs) of 2-Nitrophenol Wastewater. *Chemosphere* **2016**, *154*, 604–612. [CrossRef] [PubMed]
25. Krishnan, R.Y.; Manikandan, S.; Subbaiya, R.; Biruntha, M.; Govarthanan, M.; Karmegam, N. Removal of Emerging Micropollutants Originating from Pharmaceuticals and Personal Care Products (PPCPs) in Water and Wastewater by Advanced Oxidation Processes: A Review. *Environ. Technol. Innov.* **2021**, *23*, 101757. [CrossRef]
26. Chevremont, A.-C.; Boudenne, J.-L.; Coulomb, B.; Farnet, A.-M. Fate of Carbamazepine and Anthracene in Soils Watered with UV-LED Treated Wastewaters. *Water Res.* **2013**, *47*, 6574–6584. [CrossRef] [PubMed]
27. Pai, C.-W.; Wang, G.-S. Treatment of PPCPs and Disinfection By-Product Formation in Drinking Water through Advanced Oxidation Processes: Comparison of UV, UV/Chlorine, and UV/H_2O_2. *Chemosphere* **2022**, *287*, 132171. [CrossRef]
28. Ahmad, N.A.; Yuzir, M.A.; Yong, E.L.; Abdullah, N.; Salim, M.R. Removal of Bisphenol A (BPA) in Surface Water by Ozone Oxidation Process. *Appl. Mech. Mater.* **2015**, *735*, 210–214. [CrossRef]
29. Beltrán, F.J.; Pocostales, P.; Alvarez, P.; Oropesa, A. Diclofenac Removal from Water with Ozone and Activated Carbon. *J. Hazard. Mater.* **2009**, *163*, 768–776. [CrossRef]
30. Hamdi El Najjar, N.; Touffet, A.; Deborde, M.; Journel, R.; Karpel Vel Leitner, N. Kinetics of Paracetamol Oxidation by Ozone and Hydroxyl Radicals, Formation of Transformation Products and Toxicity. *Sep. Purif. Technol.* **2014**, *136*, 137–143. [CrossRef]
31. Lee, C.O.; Howe, K.J.; Thomson, B.M. Ozone and Biofiltration as an Alternative to Reverse Osmosis for Removing PPCPs and Micropollutants from Treated Wastewater. *Water Res.* **2012**, *46*, 1005–1014. [CrossRef]
32. Andreozzi, R.; Caprio, V.; Marotta, R.; Vogna, D. Paracetamol Oxidation from Aqueous Solutions by Means of Ozonation and H_2O_2/UV System. *Water Res.* **2003**, *37*, 993–1004. [CrossRef]
33. Sharma, J.; Mishra, I.M.; Kumar, V. Mechanistic Study of Photo-Oxidation of Bisphenol-A (BPA) with Hydrogen Peroxide (H_2O_2) and Sodium Persulfate (SPS). *J. Environ. Manag.* **2016**, *166*, 12–22. [CrossRef]
34. Abramović, B.; Kler, S.; Šojić, D.; Laušević, M.; Radović, T.; Vione, D. Photocatalytic Degradation of Metoprolol Tartrate in Suspensions of Two TiO_2-Based Photocatalysts with Different Surface Area. Identification of Intermediates and Proposal of Degradation Pathways. *J. Hazard. Mater.* **2011**, *198*, 123–132. [CrossRef] [PubMed]
35. Bahnemann, D. Photocatalytic Water Treatment: Solar Energy Applications. *J. Sol. Energy* **2004**, *77*, 445–459. [CrossRef]
36. Guo, W.; Zhao, S.; Li, G.; Li, J.; Chen, F.; Chen, R. Chlorine-Enhanced Photocatalytic Degradation of PPCPs over Bi_2MoO_6/$(BiO)_2CO_3$ Heterostructures. *J. Environ. Chem. Eng.* **2021**, *9*, 106597. [CrossRef]
37. Kumar, R.; Akbarinejad, A.; Jasemizad, T.; Fucina, R.; Travas-Sejdic, J.; Padhye, L.P. The Removal of Metformin and Other Selected PPCPs from Water by Poly(3,4-Ethylenedioxythiophene) Photocatalyst. *Sci. Total Environ.* **2021**, *751*, 142302. [CrossRef] [PubMed]
38. Yang, H.; Wang, W.; Wu, X.; Siddique, M.S.; Su, Z.; Liu, M.; Yu, W. Reducing ROS Generation and Accelerating the Photocatalytic Degradation Rate of PPCPs at Neutral PH by Doping Fe-N-C to g-C3N4. *Appl. Catal B Environ.* **2022**, *301*, 120790. [CrossRef]
39. Zhang, Q.; Chen, P.; Tan, C.; Chen, T.; Zhuo, M.; Xie, Z.; Wang, F.; Liu, H.; Cai, Z.; Liu, G.; et al. A Photocatalytic Degradation Strategy of PPCPs by a Heptazine-Based CN Organic Polymer (OCN) under Visible Light. *Environ. Sci. Nano* **2018**, *5*, 2325–2336. [CrossRef]
40. Asif, A.H.; Wang, S.; Sun, H. Hematite-Based Nanomaterials for Photocatalytic Degradation of Pharmaceuticals and Personal Care Products (PPCPs): A Short Review. *Curr. Opin. Green Sustain. Chem.* **2021**, *28*, 100447. [CrossRef]
41. Qian, H.; Yu, G.; Hou, Q.; Nie, Y.; Bai, C.; Bai, X.; Wang, H.; Ju, M. Ingenious Control of Adsorbed Oxygen Species to Construct Dual Reaction Centers ZnO@FePc Photo-Fenton Catalyst with High-Speed Electron Transmission Channel for PPCPs Degradation. *Appl. Catal B Environ.* **2021**, *291*, 120064. [CrossRef]
42. Wu, J.; Wang, B.; Cagnetta, G.; Huang, J.; Wang, Y.; Deng, S.; Yu, G. Nanoscale Zero Valent Iron-Activated Persulfate Coupled with Fenton Oxidation Process for Typical Pharmaceuticals and Personal Care Products Degradation. *Sep. Purif. Technol.* **2020**, *239*, 116534. [CrossRef]
43. Savun-Hekimoğlu, B.; Ince, N.H. Decomposition of PPCPs by Ultrasound-Assisted Advanced Fenton Reaction: A Case Study with Salicylic Acid. *Ultrason. Sonochem.* **2017**, *39*, 243–249. [CrossRef]
44. Guo, M.; Feng, Y.; Li, X.; Yan, G.; Wang, X.; Li, X.; Zhang, S.; Yu, Y. Enhanced Degradation of Pharmaceuticals and Personal Care Products (PPCPs) by Three-Dimensional Electrocatalysis Coupled Biological Aerated Filter. *J. Environ. Chem. Eng.* **2021**, *9*, 106035. [CrossRef]
45. Wang, W.; Lu, Y.; Luo, H.; Liu, G.; Zhang, R.; Jin, S. A Microbial Electro-Fenton Cell for Removing Carbamazepine in Wastewater with Electricity Output. *Water Res.* **2018**, *139*, 58–65. [CrossRef] [PubMed]

46. Yang, H.; Zhou, M.; Yang, W.; Ren, G.; Ma, L. Rolling-Made Gas Diffusion Electrode with Carbon Nanotube for Electro-Fenton Degradation of Acetylsalicylic Acid. *Chemosphere* **2018**, *206*, 439–446. [CrossRef] [PubMed]
47. Rashid, S.S.; Liu, Y.-Q. Comparison of Life Cycle Toxicity Assessment Methods for Municipal Wastewater Treatment with the Inclusion of Direct Emissions of Metals, PPCPs and EDCs. *Sci. Total Environ.* **2021**, *756*, 143849. [CrossRef]
48. Boxall, A.B.A. The Environmental Side Effects of Medication: How Are Human and Veterinary Medicines in Soils and Water Bodies Affecting Human and Environmental Health? *EMBO Rep.* **2004**, *5*, 1110–1116. [CrossRef]
49. Kasprzyk-Hordern, B.; Dinsdale, R.M.; Guwy, A.J. The Occurrence of Pharmaceuticals, Personal Care Products, Endocrine Disruptors and Illicit Drugs in Surface Water in South Wales, UK. *Water Res.* **2008**, *42*, 3498–3518. [CrossRef]
50. Ziylan, A.; Ince, N.H. The Occurrence and Fate of Anti-Inflammatory and Analgesic Pharmaceuticals in Sewage and Fresh Water: Treatability by Conventional and Non-Conventional Processes. *J. Hazard. Mater.* **2011**, *187*, 24–36. [CrossRef]
51. Stülten, D.; Zühlke, S.; Lamshöft, M.; Spiteller, M. Occurrence of Diclofenac and Selected Metabolites in Sewage Effluents. *Sci. Total Environ.* **2008**, *405*, 310–316. [CrossRef]
52. Wu, D.; Sui, Q.; Yu, X.; Zhao, W.; Li, Q.; Fatta-Kassinos, D.; Lyu, S. Identification of Indicator PPCPs in Landfill Leachates and Livestock Wastewaters Using Multi-Residue Analysis of 70 PPCPs: Analytical Method Development and Application in Yangtze River Delta, China. *Sci. Total Environ.* **2021**, *753*, 141653. [CrossRef]
53. Al-Baldawi, I.A.; Mohammed, A.A.; Mutar, Z.H.; Abdullah, S.R.S.; Jasim, S.S.; Almansoory, A.F.; Ismail, N. 'Izzati Application of Phytotechnology in Alleviating Pharmaceuticals and Personal Care Products (PPCPs) in Wastewater: Source, Impacts, Treatment, Mechanisms, Fate, and SWOT Analysis. *J. Clean. Prod.* **2021**, *319*, 128584. [CrossRef]
54. Bayati, M.; Ho, T.L.; Vu, D.C.; Wang, F.; Rogers, E.; Cuvellier, C.; Huebotter, S.; Inniss, E.C.; Udawatta, R.; Jose, S.; et al. Assessing the Efficiency of Constructed Wetlands in Removing PPCPs from Treated Wastewater and Mitigating the Ecotoxicological Impacts. *Int. J. Hyg. Environ. Health* **2021**, *231*, 113664. [CrossRef] [PubMed]
55. Liu, F.; Zhao, J.; Wang, S.; Du, P.; Xing, B. Effects of Solution Chemistry on Adsorption of Selected Pharmaceuticals and Personal Care Products (PPCPs) by Graphenes and Carbon Nanotubes. *Environ. Sci. Technol.* **2014**, *48*, 13197–13206. [CrossRef] [PubMed]
56. Stepanova, S.; Praskova, E.; Chromcova, L.; Plhalova, L.; Prokes, M.; Blahova, J.; Svobodova, Z. The Effects of Diclofenac on Early Life Stages of Common Carp (Cyprinus Carpio). *Environ. Toxicol. Pharmacol.* **2013**, *35*, 454–460. [CrossRef] [PubMed]
57. Webb, S.; Ternes, T.; Gibert, M.; Olejniczak, K. Indirect human exposure to pharmaceuticals via drinking water. *Toxicol. Lett.* **2003**, *142*, 157–167. [CrossRef]
58. Maggioni, S.; Balaguer, P.; Chiozzotto, C.; Benfenati, E. Screening of endocrine-disrupting phenols, herbicides, steroid estrogens, and estrogenicity in drinking water from the waterworks of 35 Italian cities and from PET-bottled mineral water. *Environ. Sci. Pollut. Res.* **2013**, *20*, 1649–1660. [CrossRef] [PubMed]
59. Brody, J.G.; Aschengrau, A.; McKelvey, W.; Swartz, C.H.; Kennedy, T.; Ruthann, A.R. Breast cancer risk and drinking water contaminated by wastewater: A case control study. *Environ. Health* **2006**, *5*, 28. [CrossRef] [PubMed]
60. Aschengrau, A.; Weinberg, J.M.; Janulewicz, P.A.; Romano, M.E.; Gallagher, L.G.; Winter, M.R.; Martin, B.R.; Vieira, V.M.; Webster, T.F.; White, R.F.; et al. Affinity for risky behaviors following prenatal and early childhood exposure to tetrachloroethylene (PCE)-contaminated drinking water: A retrospective cohort study. *Environ. Health* **2011**, *10*, 102. [CrossRef]
61. Zwiener, C. Occurrence and analysis of pharmaceuticals and their transformation products in drinking water treatment. *Anal. Bioanal. Chem.* **2007**, *387*, 1159–1162. [CrossRef]
62. Hena, S.; Gutierrez, L.; Croué, J.-P. Removal of Pharmaceutical and Personal Care Products (PPCPs) from Wastewater Using Microalgae: A Review. *J. Hazard. Mater.* **2021**, *403*, 124041. [CrossRef]
63. Sengar, A.; Vijayanandan, A. Human health and ecological risk assessment of 98 pharmaceuticals and personal care products (ppcps) detected in indian surface and wastewaters. *Sci. Total Environ.* **2022**, *807*, 150677. [CrossRef]
64. Kasprzyk-Hordern, B.; Dąbrowska, A.; Vieno, N.; Kronberg, L.; Nawrocki, J. Occurrence of acidic pharmaceuticals in the Warta River in Poland. *Chem. Anal.* **2007**, *52*, 289–303.
65. Caban, M.; Lis, E.; Kumirska, J.; Stepnowski, P. Determination of pharmaceutical residues in drinking water in Poland using a new SPE-GC-MS(SIM) method based on Speedisk extraction disks and DIMETRIS derivatization. *Sci. Total Environ.* **2015**, *538*, 402–411. [CrossRef] [PubMed]
66. Mirasole, C.; Di Carro, M.; Tanwar, S.; Magi, E. Liquid chromatography–tandem mass spectrometry and passive sampling: Powerful tools for the determination of emerging pollutants in water for human consumption. *J. Mass Spectrom.* **2016**, *51*, 814–820. [CrossRef] [PubMed]
67. Ma, R.; Wang, B.; Lu, S.; Zhang, Y.; Yin, L.; Huang, J.; Deng, S.; Wang, Y.; Yu, G. Characterization of pharmaceutically active compounds in Dongting Lake, China: Occurrence, chiral profiling and environmental risk. *Sci. Total Environ.* **2016**, *268*, 557–558. [CrossRef]
68. Paíga, P.; Santos, L.H.M.L.M.; Delerue-Matos, C. Development of a multi-residue method for the determination of human and veterinary pharmaceuticals and some of their metabolites in aqueous environmental matrices by SPE-UHPLC-MS/MS. *J. Pharm. Biomed.* **2017**, *135*, 75–86. [CrossRef]
69. Wang, J. *Stripping Analysis, Principles, Instrumentation and Applications*; VCH Publishers: Hoboken, NJ, USA, 1985.
70. Couto, R.A.S.; Lima, J.L.F.C.; Quinaz, M.B. Recent developments, characteristics and potential applications of screen-printed electrodes in pharmaceutical and biological analysis. *Talanta* **2016**, *146*, 801–814. [CrossRef]

71. Barton, J.; García, M.B.; Santos, D.H.; Fanjul-Bolado, P.; Ribotti, A.; McCaul, M.; Diamond, D.; Magni, P. Screen-printed electrodes for environmental monitoring of heavy metal ions: A review. *Microchim. Acta* **2016**, *183*, 503–517. [CrossRef]
72. Niu, X.; Lan, M.; Zhao, H.; Chen, C.; Li, Y.; Zhu, X. Review: Electrochemical Stripping Analysis of Trace Heavy Metals Using Screen-Printed Electrodes. *Anal. Lett.* **2013**, *46*, 2479–2502. [CrossRef]
73. Trojanowicz, M. Impact of nanotechnology on design of advanced screen-printed electrodes for different analytical applications. *Trends Anal. Chem.* **2016**, *84*, 22–47. [CrossRef]
74. Arduini, F.; Micheli, L.; Moscone, D.; Palleschi, G.; Piermarini, S.; Ricci, F.; Volpe, G. Electrochemical biosensors based on nanomodified screen-printed electrodes: Recent applications in clinical analysis. *Trends Anal. Chem.* **2016**, *79*, 114–126. [CrossRef]
75. Hughes, G.; Westmacott, K.; Honeychurch, K.C.; Crew, A.; Pemberton, R.M.; Hart, J.P. Recent advances in the fabrication and application of screen-printed electrochemical (bio) sensors based on carbon materials for biomedical, agri-food and environmental analyses. *Biosensors* **2016**, *6*, 50. [CrossRef] [PubMed]
76. Cinti, S.; Arduini, F. Graphene-based screen-printed electrochemical (bio)sensors and their applications: Efforts and criticisms. *Biosens. Bioelectron.* **2017**, *89*, 107122. [CrossRef] [PubMed]
77. Tyszczuk-Rotko, K.; Szwagierek, A. Green Electrochemical Sensor for Caffeine Determination in Environmental Water Samples: The Bismuth Film Screen-Printed Carbon Electrode. *J. ElectroChem. Soc.* **2017**, *164*, B342. [CrossRef]
78. Hayat, A.; Marty, J.L. Disposable Screen Printed Electrochemical Sensors: Tools for Environmental Monitoring. *Sensors* **2014**, *14*, 10432–10453. [CrossRef]
79. Namieśnik, J. Modern Trends in Monitoring and Analysis of Environmental Pollutants. *Pol. J. Environ. Stud.* **2001**, *10*, 127–140.
80. Feier, B.; Florea, A.; Cristea, C.; Sandulescu, R. Electrochemical detection and removal of pharmaceuticals in waste waters. *Curr. Opin. Electrochem.* **2018**, *11*, 1–11. [CrossRef]
81. Torrinha, Á.; Martins, M.; Tavares, M.; Delerue-Matos, C.; Morais, S. Carbon paper as a promising sensing material: Characterization and electroanalysis of ketoprofen in wastewater and fish. *Talanta* **2021**, *226*, 122111. [CrossRef]
82. Kozak, J.; Tyszczuk-Rotko, K.; Wójciak, M.; Sowa, I. Electrochemically Activated Screen-Printed Carbon Sensor Modified with Anionic Surfactant (aSPCE/SDS) for Simultaneous Determination of Paracetamol, Diclofenac and Tramadol. *Materials* **2021**, *14*, 3581. [CrossRef]
83. Sasal, A.; Tyszczuk-Rotko, K.; Wójciak, M.; Sowa, I.; Kuryło, M. Simultaneous analysis of paracetamol and diclofenac using MWCNTs-COOH modified screen-printed carbon electrode and pulsed potential accumulation. *Materials* **2020**, *13*, 3091. [CrossRef]
84. Jahani, P.M.; Mohammadi, S.Z.; Khodabakhshzadeh, A.; Cha, J.W.; Asl, M.S.; Jang, H.W.; Shokouhimehr, M.; Zhang, K.; Van Le, Q.; Peng, W. Simultaneous voltammetric detection of morphine and diclofenac using graphene nanoribbon modified screen-printed electrode. *Int. J. Electrochem. Sci.* **2020**, *15*, 9037–9048. [CrossRef]
85. Zhang, C.; Cao, Z.; Zhang, G.; Yan, Y.; Yang, X.; Chang, J.; Song, Y.; Jia, Y.; Pan, P.; Mi, W.; et al. An electrochemical sensor based on plasma-treated zinc oxide nanoflowers for the simultaneous detection of dopamine and diclofenac sodium. *Microchem. J.* **2020**, *158*, 105237. [CrossRef]
86. Kimuama, K.; Rodthongkumb, N.; Ngamrojanavanichc, N.; Chailapakuld, O.; Ruecha, N. Single step preparation of platinum nanoflowers/reduced graphene oxide electrode as a novel platform for diclofenac sensor. *Microchem. J.* **2020**, *155*, 104744. [CrossRef]
87. Tyszczuk-Rotko, K.; Kozak, J.; Węzińska, A. Electrochemically activated screen-printed carbon electrode for determination of ibuprofen. *Appl. Sci.* **2021**, *11*, 9908. [CrossRef]
88. Bushra, R.; Aslam, N. An overview of clinical pharmacology of ibuprofen. *Oman Med. J.* **2010**, *25*, 155–161. [CrossRef] [PubMed]
89. Diouf, A.; Moufid, M.; Bouyahya, D.; Österlund, L.; El Bari, N.; Bouchikhi, B. An electrochemical sensor based on chitosan capped with gold nanoparticles combined with a voltammetric electronic tongue for quantitative aspirin detection in human physiological fluids and tablets. *Mater. Sci. Eng.* **2020**, *110*, 110665. [CrossRef] [PubMed]
90. Kruanetr, S.; Prabhu, R.; Pollard, P.; Fernandez, C. Pharmaceutical electrochemistry: The electrochemical detection of aspirin utilising screen printed Graphene electrodes as sensors platforms. *Surf. Eng. Appl. Electrochem.* **2015**, *51*, 283–289. [CrossRef]
91. Stefano, J.S.; Montes, R.H.O.; Richter, E.M.; Munoz, R.A.A. Flow-injection analysis with multiple-pulse amperometry for simultaneous determination of paracetamol and naproxen using a homemade flow cell for screen-printed electrodes. *J. Braz. Chem. Soc.* **2014**, *25*, 484–491. [CrossRef]
92. Kondori, T.; Tajik, S.; Akbarzadeh, T.N.; Beitollahi, H.; Graiff, C.; Jang, H.W.; Shokouhimehr, M. Synthesis and characterization of bipyridine cobalt(II) complex modified graphite screen printed electrode: An electrochemical sensor for simultaneous detection of acetaminophen and naproxen. *RSC Adv.* **2021**, *11*, 3049–3057. [CrossRef]
93. Kuczyńska, J.; Nieradko-Iwanicka, B. The effect of ketoprofen lysine salt on mucosa of rat stomach after ethyl alcohol intoxication. *Biomed. Pharmacother.* **2021**, *141*, 111938. [CrossRef]
94. Molina-Garcia, L.; Santos, J.L.M.; Ruiz-Medina, A.; Llorent-Martinez, E.J. Determination of ketoprofen based on its quenching effect in the fluorescence of quantum dots. *J. Food Drug Anal.* **2013**, *21*, 426–431. [CrossRef]
95. Cao, F.; Dong, Q.; Li, C.; Chen, J.; Ma, X.; Huang, Y.; Song, D.; Ji, C.; Lei, Y. Electrochemical sensor for detecting pain reliever/fever reducer drug acetaminophen based on electrospun CeBiOx nanofibers modified screen-printed electrode. *Sens. Actuators B* **2018**, *256*, 143–150. [CrossRef]

96. Jahani, P.M.; Mohammadi, S.Z.; Khodabakhshzadeh, A.; Asl, M.S.; Jang, H.W.; Shokouhimehr, M.; Zhang, K.; Van Le, Q.; Peng, W. Simultaneous voltammetric detection of acetaminophen and tramadol using molybdenum tungsten disulfide-modified graphite screen-printed electrode. *Int. J. Electrochem. Sci.* **2020**, *15*, 9024–9036. [CrossRef]
97. Sima, V.; Cristea, C.; Bodoki, E.; Duţu, G.; Săndulescu, R. Screen-printed electrodes modified with HRP-zirconium alkoxide film for the development of a biosensor for acetaminophen detection. *Cent. Eur. J. Chem.* **2010**, *8*, 1034–1040.
98. Sasal, A.; Tyszczuk-Rotko, K.; Chojecki, M.; Korona, T.; Nosal-Wiercińska, A. Direct determination of paracetamol in environmental samples using screen-printed carbon/carbon nanofibers sensor—Experimental and theoretical studies. *Electroanalysis* **2020**, *32*, 1618–1628. [CrossRef]
99. Serrano, N.; Castilla, O.; Ariño, C.; Diaz-Cruz, M.S.; Diaz-Cruz, J.M. Commercial screen-printed electrodes based on carbon nanomaterials for a fast and cost-effective voltammetric determination of paracetamol, ibuprofen and caffeine in water samples. *Sensors* **2019**, *19*, 4039. [CrossRef]
100. Raymundo-Pereira, P.A.; Gomes, N.O.; Machado, S.A.S.; Oliveira, O.N., Jr. Simultaneous, ultrasensitive detection of hydroquinone, paracetamol and estradiol for quality control of tap water with a simple electrochemical method. *J. Electroanal. Chem.* **2019**, *848*, 113319. [CrossRef]
101. Deroco, P.B.; Fatibello-Filho, O.; Arduini, F.; Moscone, D. Effect of different carbon blacks on the simultaneous electroanalysis of drugs as water contaminants based on screen-printed sensors. *Electroanalysis* **2019**, *31*, 2145–2154. [CrossRef]
102. Sasal, A.; Tyszczuk-Rotko, K.; Wójciak, M.; Sowa, I. First electrochemical sensor (screen-printed carbon electrode modified with carboxyl functionalized multiwalled carbon nanotubes) for ultratrace determination of diclofenac. *Materials* **2020**, *13*, 781. [CrossRef] [PubMed]
103. Seguro, I.; Pacheco, J.G.; Delerue-Matos, C. Low cost, easy to prepare and disposable electrochemical molecularly imprinted sensor for diclofenac detection. *Sensors* **2021**, *21*, 1975. [CrossRef] [PubMed]
104. Amin, S.; Soomro, M.T.; Memon, N.; Solangi, A.R.; Uddin, S.; Qureshi, T.; Behzad, A.R. Disposable screen printed graphite electrode for the direct determination of ibuprofen in surface water. Environ. *Nanotechnol. Monit. Manag.* **2014**, *1–2*, 8–13.
105. Saciloto, T.R.; Cervini, P.; Cavalheiro, É.T.G. Simultaneous voltammetric determination of acetaminophen and caffeine at a graphite and polyurethane screen-printed composite electrode. *J. Braz. Chem. Soc.* **2013**, *24*, 1461–1468. [CrossRef]
106. Gilmartin, M.A.T.; Hart, J.P. Rapid detection of paracetamol using a disposable, surface-modified screen-printed carbon electrode. *Analyst* **1994**, *119*, 2431–2437. [CrossRef]
107. Ma, L.-L.; He, Y.; Qin, D.; Chang, A.; Huang, A.; Xie, X.-J.; Zhang, Y. Fabrication, characterization and performance evaluation of screen-printed carbon electrodes: Determination of acetaminophen in Tylenol. Chinese. *J. Anal. Chem.* **2021**, *49*, 21187–21196. [CrossRef]
108. Khairy, M.; Banks, C.E. A screen-printed electrochemical sensing platform surface modified with nanostructured ytterbium oxide nanoplates facilitating the electroanalytical sensing of the analgesic drugs acetaminophen and tramadol. *Microchim. Acta* **2020**, *187*, 126. [CrossRef]
109. Zhang, Y.; Jiang, X.; Zhang, J.; Zhang, H.; Li, Y. Simultaneous voltammetric determination of acetaminophen and isoniazid using MXene modified screen-printed electrode. *Biosens. Bioelectron.* **2019**, *130*, 315–321. [CrossRef]
110. Wei, Z.; Guo, S.; Cheng, L.; Li, T.; Zhang, Y.; Yang, H. Simultaneous determination of acetaminophen and tyrosine using screen-printed electrochemical sensor based on MWCNTs-doped poly(glycine)/poly(acrylic acid) conducting polymers. *Int. J. Electrochem. Sci.* **2019**, *14*, 6748–6758. [CrossRef]
111. De Carvalhoa, R.C.; Bettsa, A.J.; Cassidya, J.F. Diclofenac determination using CeO2 nanoparticle modified screen-printed electrodes—A study of background correction. *Microchem. J.* **2020**, *158*, 105258. [CrossRef]
112. Baezzat, M.R.; Tavakkoli, N.; Zamani, H. Construction of a new electrochemical sensor based on MoS_2 nanosheets modified-graphite screen printed electrode for simultaneous determination of diclofenac and morphine. *Anal. Bioanal. Chem. Res.* **2022**, *9*, 153–162.
113. Apetrei, I.M.; Bejinaru, A.A.; Boev, M.; Apetrei, C.; Buzia, O.D. Determination of ibuprofen based on screen-printed electrodes modified with carbon nanofibers. *Farmacia* **2017**, *65*, 790–795.
114. Zhao, C.; Lin, J. Electrochemically reduced graphene oxide modified screen-printed electrodes for sensitive determination of acetylsalicylic acid. *Int. J. Electrochem. Sci.* **2017**, *12*, 10177–10186. [CrossRef]
115. Baj-Rossi, C.; Jost, T.R.; Cavallini, A.; Grassi, F.; De Micheli, G.; Carrara, S. Continuous monitoring of Naproxen by a cytochrome P450-based electrochemical sensor. *Biosens. Bioelectron.* **2014**, *53*, 283–287. [CrossRef] [PubMed]
116. Yaghoubian, H.; Tajik, S.; Beitollahi, H.; Sarhadi, H.; Sheikhshoaie, I. Fe_2MoO_4 magnetic nanocomposite modified screenprinted graphite electrode as a voltammetric sensor for simultaneous determination of nalbuphine and diclofenac. *J. Mater. Sci. Mater. Electron.* **2021**, *32*, 17311–17323. [CrossRef]
117. Cumba, L.R.; Camisasca, A.; Giordani, S.; Foster, R.J. Electrochemical properties of screen-printed carbon nano-onion electrodes. *Molecules* **2020**, *25*, 3884. [CrossRef] [PubMed]
118. Kozak, J.; Tyszczuk-Rotko, K.; Sadok, I.; Sztanke, K.; Sztanke, M. Application of a screen-printed sensor modified with carbon nanofibers for the voltammetric analysis of an anticancer disubstited fused triazinone. *Int. J. Mol. Sci.* **2022**, *23*, 2429. [CrossRef] [PubMed]

119. Ibáñez-Redín, G.; Furuta, R.H.M.; Wilson, D.; Shimizu, F.M.; Shimizu, F.M.; Materon, E.M.; Arantes, L.M.R.B.; Melendez, M.E.; Carvalho, A.L.; Reis, R.M.; et al. Screen-printed interdigitated electrodes modified with nanostructured carbon nano-onion films for detecting the cancer biomarker CA19-9. *Mater. Sci. Eng. C* **2019**, *99*, 1502–1508. [CrossRef]
120. Kaewket, K.; Karuwan, C.; Sonsupap, S.; Maensiri, S.; Ngamchuea, K. Anti-fouling effects of carbon nanofiber in electrochemical sensing of phenolic compounds. *J. Electrochem. Soc.* **2021**, *168*, 067501. [CrossRef]
121. Della Pelle, F.; Angelini, C.; Sergi, M.; Del Carlo, M.; Pepe, A.; Compagnone, D. Nano carbon black-based screen-printed sensor for carbofuran, isoprocarb, carbaryl and fenobucarb detection: Application to grain samples. *Talanta* **2018**, *186*, 389–396. [CrossRef]
122. Bounegru, A.V.; Apetrei, C. Voltamperometric sensors and biosensors based on carbon nanomaterials used for detecting of caffeic acid-a review. *Int. J. Mol. Sci.* **2020**, *21*, 9275. [CrossRef]
123. Sipa, K.; Brycht, M.; Leniart, A.; Skrzypek, S. The application of carbon nanomaterials as electrode surface modifiers for the voltammetric sensing of nitroxinil—A comparative studies. *J. Electroanal. Chem.* **2019**, *848*, 113294. [CrossRef]
124. Goyal, R.N.; Chatterjee, S.; Agrawal, B. Electrochemical investigations of diclofenac at edge plane pyrolytic graphite electrode and its determination in human urine. *Sens. Actuators B Chem.* **2010**, *145*, 743–748. [CrossRef]
125. Medsen, K.G.; Skonberg, C.; Jurva, U.; Cornett, C.; Hansen, S.H.; Johansen, T.N.; Olsen, J. Bioactivation of diclofenac in vitro and In Vivo: Correlation to electrochemical studies. *Chem. Res. Toxicol.* **2008**, *21*, 1107–1119. [CrossRef] [PubMed]
126. Korolczuk, M. Application of pulsed potential accumulation for minimization of interferences from surfactants in voltammetric determination of traces of Cr(VI). *Electroanalysis* **2000**, *12*, 837–840. [CrossRef]
127. González-Sánchez, M.I.; Gómez-Monedero, B.; Agrisuelas, J.; Iniesta, J.; Valero, E. Highly activated screen-printed carbon electrodes by electrochemical treatment with hydrogen peroxide. *Electrochem. Commun.* **2018**, *91*, 36–40. [CrossRef]
128. Yuan, X.; Ma, L.; Zhang, J.; Zheng, Y. Simple pre-treatment by low-oxygen plasma activates screen-printed carbon electrode: Potential for mass production. *Appl. Surf. Sci.* **2021**, *544*, 148760. [CrossRef]
129. Wei, H.; Sun, J.-J.; Xie, Y.; Lin, C.-G.; Wang, Y.-M.; Yin, W.-H.; Chen, G.-N. Enhanced electrochemical performance at screen-printed carbon electrodes by a new pretreating procedure. *Anal. Chim. Acta* **2007**, *588*, 297–303. [CrossRef] [PubMed]
130. Lee, J.; Arrigan, D.W.M.; Silvester, D.S. Mechanical polishing as an improved surface treatment for platinum screen-printed electrodes. *Sens. Bio-Sens. Res.* **2016**, *9*, 38–44. [CrossRef]
131. Cumba, L.R.; Foster, C.W.; Brownson, D.A.C.; Smith, J.P.; Iniesta, J.; Thakur, B.; do Carmo, D.R.; Banks, C.E. Can the mechanical activation (polishing) of screen-printed electrodes enhance their electroanalytical response? *Analyst* **2016**, *141*, 2791–2799. [CrossRef]
132. Montiel, N.F.; Parrilla, M.; Beltran, V.; Nuyts, G.; Van Durme, F.; De Wael, K. The opportunity of 6-monoacetymorphine to selectively detect heroin at prenodized screen printed electrodes. *Talanta* **2021**, *226*, 122005. [CrossRef]
133. De Oliveira Silva, R.; da Silva, E.A.; Fiorucci, A.R.; Ferreira, V.S. Electrochemically activated multiwalled carbon nanotubes modified screen-printed electrode for voltammetric determination of sulfentrazone. *J. Electroanal. Chem.* **2019**, *835*, 220–226. [CrossRef]
134. Kozak, J.; Tyszczuk-Rotko, K.; Wójciak, M.; Sowa, I.; Rotko, M. First screen-printed sensor (electrochemically activated screen-printed boron-doped diamond electrode) for quantitative determination of rifampicin by adsorptive stripping voltammetry. *Materials* **2021**, *14*, 4231. [CrossRef]
135. González-Sánchez, M.I.; Gómez-Monedero, B.; Agrisuelas, J.; Iniesta, J.; Valero, E. Electrochemical performance of activated screen-printed carbon electrodes for hydrogen peroxide and phenol derivatives sensing. *J. Electroanal. Chem.* **2019**, *839*, 75–82. [CrossRef]
136. Cinto, S. Polymeric materials for printed-based electroanalytical (bio)applications. *Chemosensors* **2017**, *5*, 31. [CrossRef]
137. Raj, M.; Gupta, P.; Goyal, R.N.; Shim, Y.-B. Graphene/conducting polimer nano-composite loaded screen printed carbon sensor for simultaneous determination of dopamine and 5-hydroxytryptamine. *Sens. Actuators B Chem.* **2017**, *239*, 993–1002. [CrossRef]
138. Valasii, L.; Tsimpliaras, D.; Katseli, V.; Economou, A.; Svancara, I.; Stoces, M.; Mikysek, T.; Prodromidis, M. Disposable nafion-modified screen-printed graphite electrodes for the rapid voltammetric assay of caffeine. *Insights Anal. Electrochem.* **2015**, *1*, 2470–9867. [CrossRef]
139. Kumar, D.; Prasad, B.B. Multiwalled carbon nanotubes embedded molecularly imprinted polimer-modified screen printed carbon electrode for the quantitative analysis of C-reactive protein. *Sens. Actuators B Chem.* **2012**, *171–172*, 1141–1150. [CrossRef]
140. Stoica, B.E.; Gavrila, A.-M.; Sarbu, A.; Iovu, H.; Brisset, H.; Miron, A.; Iordache, T.-V. Uncovering the behaviour of screen-printed carbon electrodes modified with polymers molecularly imprinted with lipopolysaccharide. *Electrochem. Commun.* **2021**, *124*, 106965. [CrossRef]
141. Ekomo, V.M.; Branger, C.; Bikanga, R.; Florea, A.-M.; Istamboilie, G.; Calas-Blanchard, C.; Noguer, T.; Sarbu, A.; Brisset, H. Detection of Bisphenol A in aqueous medium by screen printed carbon electrodes incorporating electrochemical molecularly imprinted polymers. *Biosens. Bioelectron.* **2018**, *112*, 156–161. [CrossRef]
142. Ayankojo, A.G.; Reut, J.; Opik, A.; Syritski, V. Sulfamethizole-imprinted polymer on screen-printed electrodes: Towards the design of a portable environmental sensor. *Sens. Actuators B Chem.* **2020**, *320*, 128600. [CrossRef]
143. Rebelo, P.; Pacheco, J.G.; Cordeiro, M.N.D.S.; Melo, A.; Delerue-Matos, C. Azithromycin electrochemical detection using a molecularly imprinted polymer prepared on a disposable screen-printed electrode. *Anal. Methods* **2020**, *12*, 1486–1494. [CrossRef]

144. Motaharian, A.; Hosseini, M.R.M.; Naseri, K. Determination of psychotropic drug chlorpromazine using screen printed carbon electrodes modified with novel MIP-MWCNTs nano-composite prepared by suspension polymerization method. *Sens. Actuators B Chem.* **2019**, *288*, 356–362. [CrossRef]
145. Antiochia, R.; Gorton, L. A new osmium-polymer modified screen-printed graphene electrodefor fructose detection. *Sens. Actuators B Chem.* **2014**, *195*, 287–293. [CrossRef]
146. Chakkarapani, L.D.; Brandl, M. Carbon screen-printed electrode coated with poly(toluidine blue) as an electrochemical sensor for the detection of tyramine. *Eng. Proc.* **2020**, *2*, 51–56.
147. Faradilla, P.; Setiyanto, H.; Mannurung, R.V.; Saraswaty, V. Electrochemical sensor based on screen printed carbon electrode–zinc oxide nano particles/molecularly imprinted-polymer (SPCE–ZnONPs/MIP) for detection of sodium dodecyl sulfate (SDS). *RSC Adv.* **2022**, *12*, 743–752. [CrossRef]

RD5

J. Kozak, K. Tyszczuk-Rotko, M. Wójciak, I. Sowa, M. Rotko, *Electrochemically pretreated sensor based on screen-printed carbon modified with Pb nanoparticles for determination of testosterone,* Materials, 15 (14) (2022) 4948-4964.

materials

MDPI

Article

Electrochemically Pretreated Sensor Based on Screen-Printed Carbon Modified with Pb Nanoparticles for Determination of Testosterone

Jędrzej Kozak [1], Katarzyna Tyszczuk-Rotko [1,*], Magdalena Wójciak [2], Ireneusz Sowa [2] and Marek Rotko [1]

[1] Institute of Chemical Sciences, Faculty of Chemistry, Maria Curie-Skłodowska University in Lublin, 20-031 Lublin, Poland; jedrekkozak@onet.pl (J.K.); marek.rotko@poczta.umcs.lublin.pl (M.R.)
[2] Department of Analytical Chemistry, Medical University of Lublin, 20-093 Lublin, Poland; magdalena.wojciak@umlub.pl (M.W.); i.sowa@umlub.pl (I.S.)
* Correspondence: katarzyna.tyszczuk-rotko@mail.umcs.pl

Abstract: Testosterone (TST), despite its good properties, may be harmful to the human organism and the environment. Therefore, monitoring biological fluids and environmental samples is important. An electrochemically pretreated screen-printed carbon sensor modified with Pb nanoparticles (pSPCE/PbNPs) was successfully prepared and used for the determination of TST. The surface morphology and electrochemical properties of unmodified and modified sensors were characterized by cyclic voltammetry (CV), electrochemical impedance spectroscopy (EIS), scanning and transmission electron microscopy (SEM and TEM), and energy-dispersive X-ray spectroscopy (EDS). Selective determinations of TST at the pSPCE/PbNPs were carried out by differential pulse adsorptive stripping voltammetry (DPAdSV, $E_{Pb\ dep.and\ TST\ acc.}$ of −1.1 V, $t_{Pb\ dep.and\ TST\ acc.}$ of 120 s, ΔE_A of 50 mV, ν of 175 mV s^{-1}, and t_m of 5 ms) in a solution containing 0.075 mol L^{-1} acetate buffer of pH = 4.6 ± 0.1, and 7.5 × 10^{-5} mol L^{-1} $Pb(NO_3)_2$. The analytical signal obtained at the potential around −1.42 V (vs. silver pseudo-reference electrode) is related to the reduction process of TST adsorbed onto the electrode surface. The use of pSPCE/PbNPs allows obtaining a very low limit of TST detection (2.2 × 10^{-12} mol L^{-1}) and wide linear ranges of the calibration graph (1.0 × 10^{-11}–1.0 × 10^{-10}, 1.0 × 10^{-10}–2.0 × 10^{-9}, and 2.0 × 10^{-9}–2.0 × 10^{-8} mol L^{-1}). The pSPCE/PbNPs were successfully applied for the determination of TST in reference material of human urine and wastewater purified in a sewage treatment plant without preliminary preparation.

Keywords: testosterone; electrochemical preparation; screen-printed carbon sensor; lead nanoparticles; differential-pulse adsorptive stripping voltammetry; human urine; wastewater

Citation: Kozak, J.; Tyszczuk-Rotko, K.; Wójciak, M.; Sowa, I.; Rotko, M. Electrochemically Pretreated Sensor Based on Screen-Printed Carbon Modified with Pb Nanoparticles for Determination of Testosterone. *Materials* **2022**, *15*, 4948. https://doi.org/10.3390/ma15144948

Academic Editors: Michael Moustakas and Catherine Dendrinou-Samara

Received: 29 June 2022
Accepted: 14 July 2022
Published: 15 July 2022

1. Introduction

Hormones regulate many types of cellular and physiological functions in the human body, such as reproduction, growth, and differentiation [1]. Testosterone (TST), chemically known as 17β-hydroxyandrost-4-en-3-one, is the principal endogenous androgenic–anabolic steroid in humans. In the human body, it is produced primarily in the testes of males and in the ovaries of females, while small amounts are produced by adrenal glands in both sexes [2,3]. In men, TST plays a key role in the development of male reproductive tissues such as the testis and prostate, as well as in promoting secondary sexual characteristics such as increased muscle, bone mass, and the growth of body hair. Moreover, TST is essential for health and well-being as well as the prevention of osteoporosis. Testosterone abuse is widespread among sportsmen willing to increase aggressiveness, strength, and recovery, making it the most frequently reported substance in steroid misuse. The World Anti-Doping Agency prohibited its use to ensure fair play and protect athletes from possible adverse side effects such as heart attack, high blood pressure, liver disease, or mental effects [2,4]. TST can be an ingredient in pharmaceuticals. In the urine of an average man, TST is present at a

level of 10^{-8} mol L^{-1}, but in the case of hormone therapy using TST, these concentrations can be several times higher [5]. Currently, we are dealing with increasing pollution of the environment with various types of pharmaceuticals, including hormones. TST is one of the organic micropollutants present in the environment and in natural waters and can cause adverse biological effects on humans and wildlife below the physiological levels (sub-ng L^{-1}) [6,7]. Due to the fact that TST concentrations detected in the environment are in the order of 10^{-12}–10^{-11} mol L^{-1} (groundwater [8] and municipal wastewater [9]), it is necessary to develop highly sensitive methods of measuring this hormone.

Among the popular analytical methods used for the detection of TST, chromatographic methods can be indicated, e.g., high-performance liquid chromatography coupled with tandem mass spectrometry (HPLC-MS/MS) [10], isotope dilution ultra-performance liquid chromatography–tandem mass spectrometry (ID-UPLC-MS/MS) [11], liquid chromatography coupled with mass spectrometry (LC-MS) [12,13], and gas chromatography coupled with mass spectrometry (GC-MS) [14,15]. Other methods that allow us to determine TST are capillary electrophoresis (CE) [16,17] and the molecularly imprinted plasmon resonance method [18]. While chromatographic methods are extremely effective, most have many disadvantages, such as cost and long and complicated sample pretreatment, usually involving different types of derivatization, extraction, and purification prior to analysis.

On the other hand, electrochemical methods provide fast, low-cost on-site analysis with high specificity and high sensitivity [4,6]. However, there are only a few studies available on the voltammetric determination of testosterone. Most of them show the use of conventional working electrodes such as glassy carbon electrodes modified in various ways—modified with a lead film (PbFE) [19], a cationic surfactant (GCE/CTAB) [4], or a cationic surfactant and a bismuth film (GCE/CTAB/BiF) [3]. It can also include maltodextrin-modified paste electrodes based on various carbon materials (graphite, graphene, carbon nanotubes, and fullerene C_{60}) [1], the hanging mercury drop electrode (HMDE) [20], the edge plane pyrolytic graphite electrode modified with single-walled carbon nanotubes (SWNTs-EPPGE) [2], and a gold electrode modified with a double-layered molecularly imprinted polymer (AuE/DMIP) [21]. The lowest detection limit at the conventional working electrode, equal to 1.0×10^{-14} mol L^{-1}, was obtained on the AuE/DMIP. However, the preparation of this electrode requires many reagents and a multi-step procedure consisting of cleaning the gold surface and electrodepositing the first conductive polymer layer, and then another one forming the DMIP. The final step is to remove the testosterone template and dry the electrode.

Unlike individual working electrodes in electrochemical analysis, all electrodes of screen-printed sensors (SPEs), i.e., reference, working, and counter electrodes, are printed and integrated on the same substrate. SPEs represent a modern analytical chemistry trend in miniaturization [22,23]. Screen-printed electrodes have advantages such as simplicity of construction and operation, diversification of the selection of electrode materials, low cost, design flexibility, reliability for detecting different substances, portability, and simplicity of modification of the electrodes for various uses [24]. An SPE is a good electrode due to its mass production, low cost, and low background current [25]. Conductive inks from screen-printed carbon electrodes (SPCEs) contain carbon with organic solvents, bonding pastes (e.g., polyester resin, ethyl cellulose, or epoxy-based polymer binder), and some additives that provide functional properties. The presence of these additional non-conductive materials can lead to a slowdown in the kinetics of heterogeneous electrochemical reactions [26]. The main purpose of the SPCE pretreatment is to remove the organic components of the ink or contaminants and to increase the surface roughness or functionality [27]. The following methods of pretreatment of SPEs can be found in the literature—heat treatment [27], oxygen plasma treatment [28], chemical treatment [29], polishing [30,31], and electrochemical treatment [32–34].

Nanomaterials are chemical substances or materials that are manufactured and used at a very small scale [35]. Among the nanomaterials, carbon nanomaterials are often used today as electrode modifiers. We can distinguish here graphene, carbon black (CB), carbon

nanofibers (CNFs), carbon nanotubes (CNTs), and carbon nanohorns (CNHs). Carbon nanomaterials have proven to be efficient electrode materials as they exhibit remarkable electronic, mechanical, and chemical properties; high surface areas; low electrical resistance; excellent electrical conductivity; and low cost. Additionally, the ability to functionalize their surfaces with antibodies, nucleic acids, or catalysts can lead to enhanced analytical performance, including sensitivity and selectivity [36–38]. Another group of commonly used nanomaterials is nanoparticles (NPs), mainly metal nanoparticles. Due to their small size, nanoparticles can increase the surface area of the electrode used. In addition, metallic nanoparticles can increase the mass transport speed and provide fast electron transfer between the electroactive species and the electrode surface, which increases the sensitivity of the electrodes used [39,40].

Only one study describes the determination of testosterone using screen-printed sensors [41]. The TST determination procedure presented in the article [41] used SPEs modified with molecularly imprinted polymer (MIP). A very low LOD was obtained on this electrode, equal to 3.5×10^{-17} mol L^{-1}. However, the preparation of the SPE/MIP is laborious and time-consuming and requires steps such as electropolymerizing the MIP on the surface of the working electrode in the presence of a high concentration of TST as a template and then removing this template. Therefore, a very simple procedure for the preparation of the modified screen-printed sensor was proposed while maintaining the high sensitivity and selectivity of the sensor. In this work, the combination of the valuable properties of screen-printed carbon electrode (SPCE) and lead nanoparticles (PbNPs), as well as the electrochemical pretreatment step in the fabrication of a novel voltammetric sensor of TST, was proposed for the first time. The use of a lead film glassy carbon electrode for TST determination was described in the literature [19]. However, as far as we know, the application of an electrochemically pretreated screen-printed carbon sensor modified with Pb nanoparticles (pSPCE/PbNPs) has never been reported. Moreover, it is the first time a voltammetric sensor has been used in TST determinations not only in body fluids (urine) but also in environmental samples (wastewater). It is worth adding that the samples do not require preliminary preparation. To specify the advantages of PbNPs and the use of the electrochemical pretreatment step, the pSPCE/PbNPs were characterized by cyclic voltammetry (CV), electrochemical impedance spectroscopy (EIS), scanning and transmission electron microscopy (SEM and TEM), and energy-dispersive X-ray spectroscopy (EDS).

2. Materials and Methods

2.1. Apparatus

Transmission electron microscopy (TEM) analysis was performed by means of a high-resolution transmission electron microscope Tecnai G2 T20 X-TWIN (FEI) equipped with an energy dispersive X-ray spectrometer (EDS). The samples were prepared for analysis by scratching the film from the surface of the electrode and placing it on a TEM copper grid. Moreover, microscopic images of the pSPCE/PbNPs surface were attained with a high-resolution scanning electron microscope Quanta 3D FEG (FEI, USA) (acceleration voltage of 5.0 kV, working distance of 9.3 mm, magnification of 25,000×).

All voltammetric studies were made using a μAutolab electrochemical analyzer (Eco Chemie, Utrecht, The Netherlands) controlled by GPES 4.9 software. The standard quartz electrochemical cell with a volume of 10 mL composed of a commercially available screen-printed carbon sensor (SPCE, DropSens, Spain, Ref. C150) was applied for experiments. The SPCE sensor consisted of a screen-printed carbon working electrode, a platinum screen-printed auxiliary electrode, and a silver screen-printed pseudo-reference electrode. The μAutolab analyzer controlled by FRA 4.9 software was used for electrochemical impedance spectroscopy (EIS) measurements.

HPLC analyses were performed on a VWR Hitachi Elite LaChrom HPLC with a PDA detector using an Ascentis Express C18 column (15 cm × 2.1 mm i.d., 2.7 μm).

2.2. Reagents and Solutions

Appropriate amounts of Merck reagent (Darmstadt, Germany), testosterone propionate, were dissolved in ethanol to obtain a 10^{-3} mol L^{-1} solution of TST. This solution was diluted with ethanol to obtain a 10^{-4} mol L^{-1} solution of TST or with 0.1 mol L^{-1} acetate buffer of pH = 4.6 ± 0.1 to obtain 10^{-5} or 10^{-6} mol L^{-1} solutions of TST. The supporting electrolyte, acetate buffer of pH = 4.6 ± 0.1, was prepared with reagents (CH_3COONa and CH_3COOH) purchased from Merck. The 10^{-3} mol L^{-1} stock solutions of Fe(III), Ca(II), Cu(II), Mg(II), Cd(II), Ni(II), V(V), glucose (GL), dopamine (DA), ascorbic acid (AA), uric acid (UA), epinephrine (EP), and adenine (AD) were prepared from Merck reagents in deionized water before starting the set of experiments and stored at 4 °C in the dark until used. HPLC-grade acetonitrile was purchased from Merck. The solutions were prepared using ultra-purified water supplied by a Milli-Q system.

2.3. Fabrication of pSPCE/PbNPs and Voltammetric Determination of TST

The scheme of sensor fabrication and voltammetric measurements of TST at the pSPCE/PbNPs is presented in Figure 1. The commercially available SPCE was simultaneously electrochemically pretreated and electrochemically decorated by lead nanoparticles (PbNPs) in 0.075 mol L^{-1} acetate buffer of pH = 4.6 ± 0.1 containing 7.5×10^{-5} mol L^{-1} $Pb(NO_3)_2$. After placing a fresh electrode in the solution, 15 consecutive differential-pulse voltammograms were recorded (an electrochemical cleaning step at a potential of 0.5 V ($E_{clean.}$) for 10 s ($t_{clean.}$), modification of the surface with PbNPs at a potential of −1.1 V ($E_{Pb\ dep.}$) for 120 s ($t_{Pb\ dep.}$), a scan rate (ν) of 175 mV s^{-1}, an amplitude (ΔE_A) of 50 mV, a modulation time (t_m) of 5 ms, and a differential-pulse scan from −1.1 to −1.7 V). Then, after rinsing the electrode with water, it was allowed to dry for 10 min at room temperature. The sensor was electrochemically pretreated only once before a series of measurements of TST.

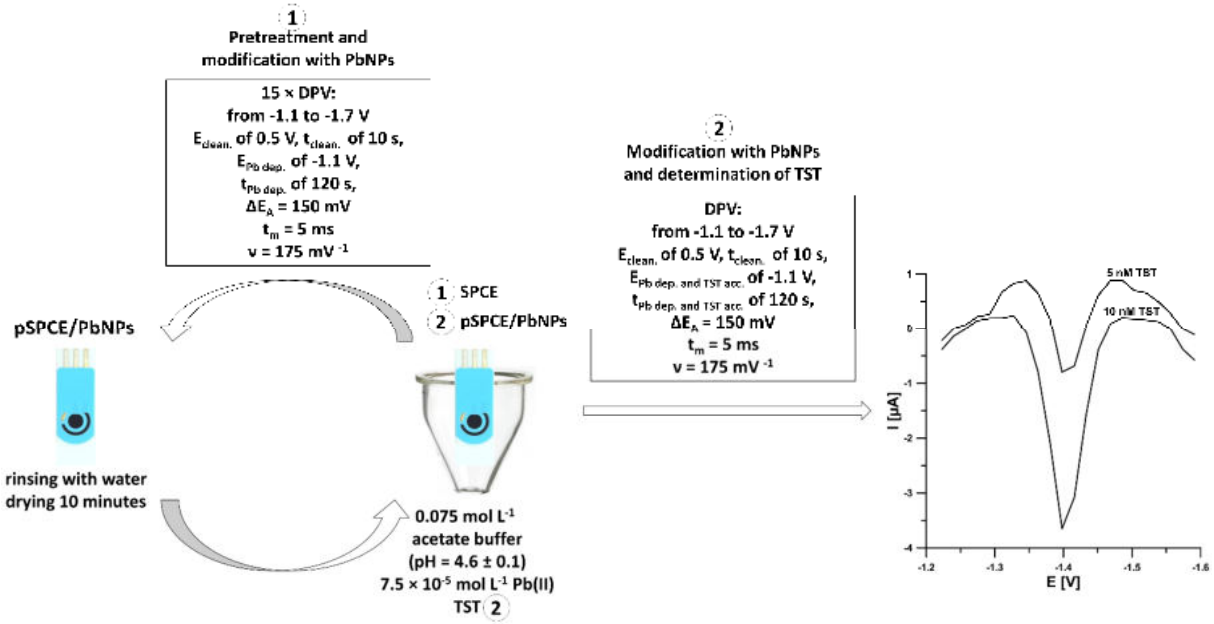

Figure 1. Scheme of sensor fabrication and voltammetric measurements of TST at the pSPCE/PbNPs.

The pSPCE/PbNPs fabricated were used for TST determination in the same solution (0.075 mol L^{-1} acetate buffer of pH = 4.6 ± 0.1 containing 7.5×10^{-5} mol L^{-1} $Pb(NO_3)_2$) in which it had been prepared. Only a specified amount of TST standard solution (concentration of TST in the range of 1.0×10^{-11}–2.0×10^{-8} mol L^{-1}) or sample was introduced into the supporting electrolyte. The procedure consists of an electrochemical cleaning step at a potential of 0.5 V ($E_{clean.}$) for 10 s ($t_{clean.}$), simultaneous modification of the surface with PbNPs, and accumulation of TST at a potential ($E_{Pb\ dep.\ and\ TST\ acc.}$) of −1.1 V for a time

($t_{Pb\ dep.\ and\ TST\ acc.}$) of 120 s. Differential-pulse scans were registered from −1.1 to −1.7 V with ν of 250 mV s^{-1}, ΔE_A of 150 mV, and t_m of 5 ms.

2.4. HPLC/PDA Analysis

Chromatographic conditions were established based on the literature [42] with slight modification. A mixture of acetonitrile and water (65:35 *v*/*v*) at a flow rate of 0.25 mL min^{-1} was used as the mobile phase. The temperature was set at 30 °C. The injection volume was 10 µL, and the analytical wavelength was 240 nm.

2.5. Sample Analysis

The reference material of human urine (Medidrug Basis-line U) and wastewater purified in a sewage treatment plant (Lublin, Poland) were analyzed using the DPAdSV and HPLC/PDA methods. The desired concentrations of TST were added to the samples, and they were directly analyzed without any separation steps.

3. Results and Discussion

3.1. Characteristics of Sensors

In the first phase of the research, the differential-pulse adsorptive stripping voltammetry (DPAdSV) technique was used to characterize TST behavior at the pSPCE/PbNPs sensor. The studies were performed in 0.1 mol L^{-1} acetate buffer of pH equal to 4.6 ± 0.1 containing 7.5 × 10^{-5} mol L^{-1} $Pb(NO_3)_2$ and 2.0 × 10^{-9} mol L^{-1} TST. For comparison, the DPAdSV curves were recorded under the same conditions at the unmodified SPCE and the SPCE/PbNPs that was not electrochemically pretreated. The studies (Figure 2A) showed that the use of modification with lead nanoparticles was necessary to obtain a reduction in the TST signal. Moreover, the application of electrochemical pretreatment of the SPCE (15 consecutive DPV measurements: 0.5 V for 10 s, −1.1 V for 120 s, scan from −1.1 to −1.7 V in the solution used further for TST determinations, rinsing with water and drying for 10 min) practically does not change the TST peak current (1.80 vs. 1.74 µA), but significantly improves its shape and shifts the peak potential of TST towards less negative potential values (−1.45 vs. −1.36 V). Furthermore, the electrochemical pretreatment significantly improves the repeatability of the analytical signal (Figure 2B, 2.0 × 10^{-9} mol L^{-1} TST RSD of 24.77 vs. 3.58%, *n* = 10). In summary, the electrochemical pretreatment step was crucial for a nicely shaped and repeatable signal, which has already been described in the literature [33]. It is worth adding that in contrast to the works described so far [43], in the electrochemical pretreatment step, the same solution and parameters as for the TST determination were used, which simplifies the electrode preparation step and reduces the consumption of reagents.

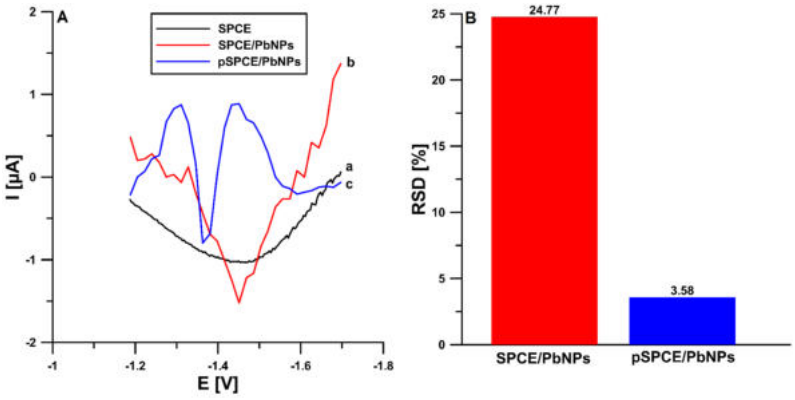

Figure 2. (**A**) DPAdSV curves of 2 × 10^{-9} mol L^{-1} TST recorded at the unmodified SPCE (**a**), modified with PbNPs (**b**), and the electrochemically pretreated SPCE/PbNPs (**c**). (**B**) Histogram bars of the repeatability of the TST signal (relative standard deviation (RSD), 2 × 10^{-9} mol L^{-1} TST, *n* = 10) at the SPCE/PbNPs and pSPCE/PbNPs.

The interfacial electron transport ability of the unmodified SPCE and the electrochemically pretreated SPCE/PbNPs was studied using EIS and CV techniques in 0.1 mol L^{-1} KCl containing 5.0 mmol L^{-1} $K_3(Fe(CN)_6)$. The CV curve displayed a pair of well-defined redox peaks of $(Fe(CN)_6)^{3-/4-}$ at the unmodified SPCE (Figure 3A, curve a). In the case of the pSPCE/PbNPs (Figure 3A, curve b), the peak-to-peak separation (ΔE) increases from 123.6 to 169.0 mV, which is ascribed to the inhibition of the electrochemical reaction process by the PbNPs modification and electrochemical pretreatment. Moreover, the rate of the electron transfer at the SPCE and the pSPCE/PbNPs was calculated as the relative peak separations (χ^0) by dividing ΔE by 59 mV. The χ^0 values for the SPCE and pSPCE/PbNPs were greater than the theoretical value ($\chi^0 = 1$) and were equal to 2.09 and 2.86, respectively. Furthermore, the pSPCE/PbNPs show a higher anodic current intensity than the SPCE. The new peak at a potential around −0.5 V is related to the oxidation of lead from the pSPCE/PbNPs surface. The obtained results indicate that the PbNPs modification and electrochemical pretreatment inhibit the electron transfer kinetics. In addition, the Randles–Sevcik equation, CV curves recorded at scan rates of 5–150 mV s^{-1}, and the dependence between the anodic peak current (I_p) and the square root of the scan rate ($v^{1/2}$) (Figure 3B) were used to calculate of the electrochemically active electrode area (A_s) of the SPCE and pSPCE/PbNPs [44]. The A_s values of the SPCE and pSPCE/PbNPs were calculated to be 0.072 and 0.22 cm^2, respectively. It is evident that the PbNPs modification and electrochemical pretreatment significantly increase the A_s. Moreover, the impedance spectra (Nyquist plots) were recorded at the SPCE and pSPCE/PbNPs in the frequency range from 50 kHz to 1 Hz (Figure 3C). According to the experimental results, the charge transfer resistance (R_{ct}) values obtained for the SPCE and pSPCE/PbNPs are 146.7 and 121.3 Ω, respectively. The pSPCE/PbNPs are characterized by lower R_{ct} and good conductivity.

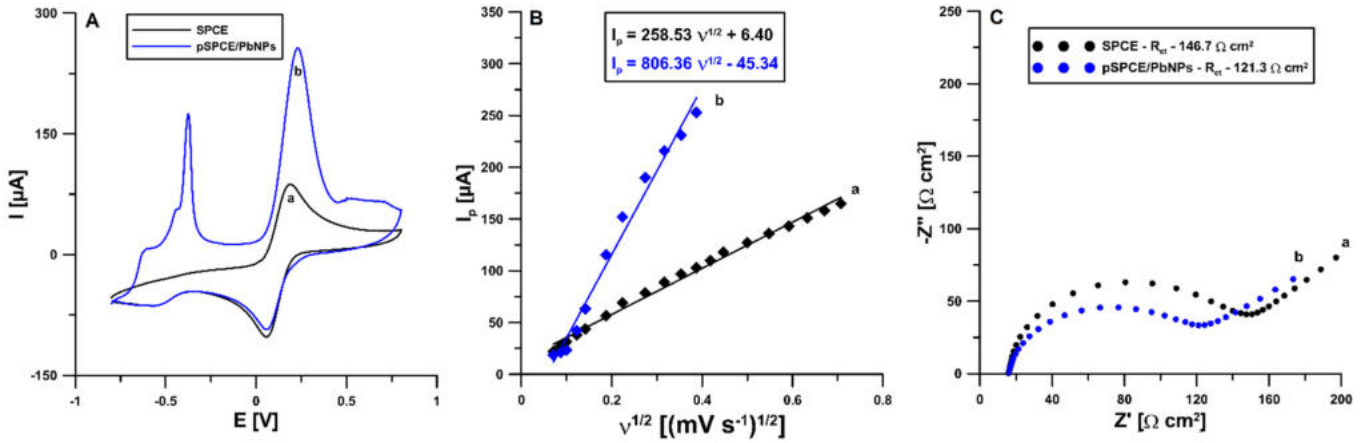

Figure 3. (**A**) Cyclic voltammograms recorded at the SPCE (**a**) and pSPCE/PbNPs (**b**) using the scan rate of 100 mV s^{-1}; (**B**) the relationship between the anodic peak current (I_p) and the square root of the scan rate ($\upsilon^{1/2}$) obtained at the SPCE (**a**) and pSPCE/PbNPs using the scan rate from 5 to 150 mV s^{-1}; (**C**) Nyquist plots of the SPCE (**a**) and pSPCE/PbNPs (**b**) registered at a potential of 0.2 V, in the frequency range from 50 kHz to 1 Hz. All results were performed in 0.1 mol L^{-1} KCl and 5.0 mmol L^{-1} $K_3(Fe(CN)_6)$.

In order to specify the advantages of PbNPs and the use of the electrochemical pretreatment step, the pSPCE/PbNPs were also characterized by scanning and transmission electron microscopy (SEM and TEM) and energy-dispersive X-ray spectroscopy (EDS). The SEM image of the pSPCE/PbNPs shows cracks formed during the drying of the SPCE surface (Figure 4A). Moreover, the characteristic structure of the carbon layer obtained by the screen-printing technique is visible in the higher resolution SEM image (Figure 4B). However, the presence of electrochemically deposited lead nanoparticles (PbNPs) was only detected using a high-resolution transmission microscope equipped with an energy

dispersive X-ray spectrometer (EDS) (Figure 4C,D). The EDS analysis confirms that the black dots contain very small amounts of lead (mass % = 0.11), which confirms that the electrochemically deposited lead is rewarded in the form of nanoparticles.

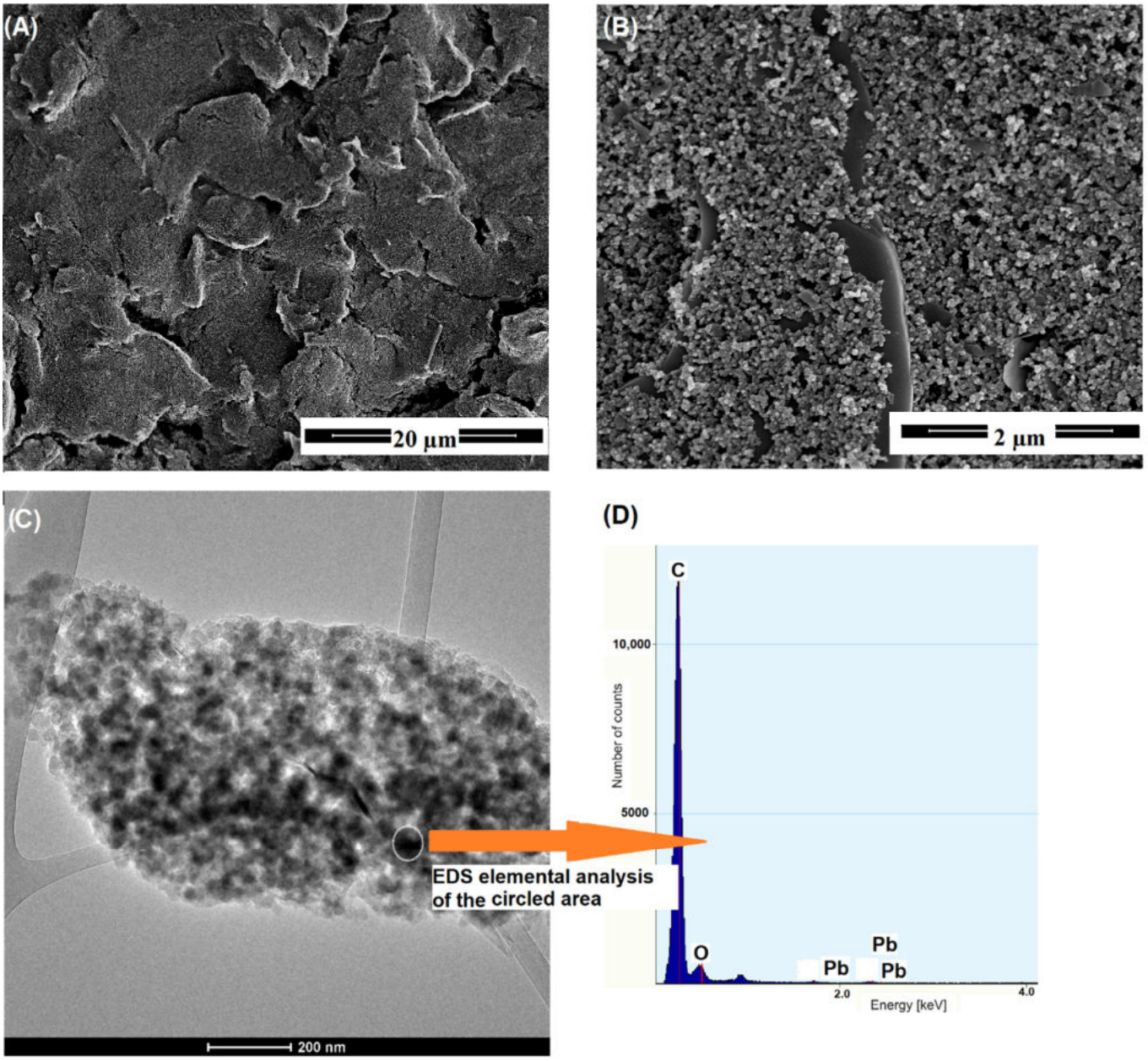

Figure 4. The SEM (**A**,**B**) and TEM (**C**) images of the pSPCE/PbNPs surface. (**D**) The EDS spectrum of the highlighted fragment of the pSPCE/PbNPs. The concentration of $Pb(NO_3)_2$ was 7.5×10^{-5} mol L^{-1}.

3.2. Mechanism and Optimization Procedure

In order to identify the involved TST reduction mechanism at the pSPCE/PbNPs, the effect of scan rate was investigated. The cyclic voltammograms of 0.075 mol L^{-1} acetate buffer of pH ± 0.1 containing 7.5×10^{-5} mol L^{-1} $Pb(NO_3)_2$ and 5.0×10^{-6} mol L^{-1} TST were recorded at scan rates from 5 to 250 mV s^{-1}. Figure 5A demonstrates the CVs obtained for three scan rate values (35, 50, and 75 mV s^{-1}). There is a cathodic peak and no anodic peak in the CVs of TST, indicating an irreversible electrode process. The TST reduction mechanism (Figure 5C) is well described in the literature [3]. It shows that the electrode process

for TST is two-proton coupled two-electron transfer. As can be seen in Figure 5B, the TST signal (I_p) increases non-linearly with the square root of the scan rate (υ). The non-linear I_p/υ plot with the regression equation of I_p (μA) = 0.74 × $\upsilon^{1/2}$ ((mV s^{-1})$^{1/2}$) − 2.17 indicates that the faradic reaction is controlled by an adsorption process.

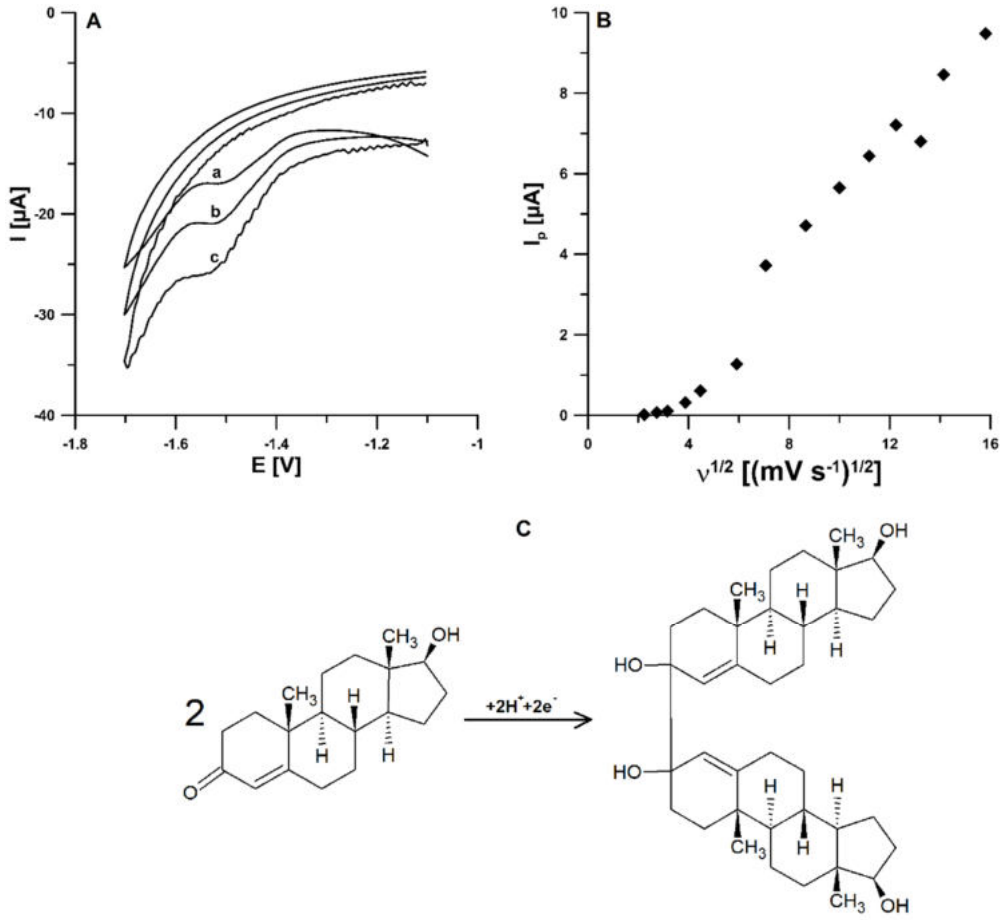

Figure 5. (**A**) CVs obtained at the pSPCE/PbNPs in the 0.075 mol L^{-1} acetate buffer of pH 4.6 ± 0.1 containing 7.5 × 10^{-5} mol L^{-1} $Pb(NO_3)_2$ and 5.0 × 10^{-6} mol L^{-1} TST (υ of 35, 50, 75 mV s^{-1}). (**B**) The dependence between TST signal (I_p) and the square root of the scan rate (υ) (υ in the range of 5–250 mV s^{-1}). (**C**) The possible TST reduction mechanism.

Additionally, the effect of pH value (acetic acid and acetate buffer) on the reduction peak current of 1.0 × 10^{-8} mol L^{-1} TST was studied. The progress of I_p with pH shows that (Figure 6A) this parameter increased up to pH 4.6 ± 0.1, and therefore, an acetate buffer of pH 4.6 ± 0.1 was selected for further studies. Furthermore, the TST reduction process was analyzed at various concentrations (from 0.025 to 0.125 mol L^{-1}) of acetate buffer (pH 4.6 ± 0.1) at the pSPCE/PbNPs. The fixed concentration of TST (1.0 × 10^{-8} mol L^{-1}) was added to the supporting electrolyte. According to the results, the highest peak current was obtained at an acetate buffer concentration of 0.075 mol L^{-1}. Then, the effect of $Pb(NO_3)_2$ concentration was evaluated in the range of 2.5 × 10^{-5} to 1.25 × 10^{-4} mol L^{-1} towards the reduction peak current of 1.0 × 10^{-8} mol L^{-1} TST. As exposed in Figure 6B, when increasing the $Pb(NO_3)_2$ concentration, the TST response also increases up to 7.5 × 10^{-5} mol $L^{-1,}$ and therefore, this concentration value was chosen. Moreover, the impact of DPAdSV procedure parameters, such as simultaneous modification of the surface with PbNPs and accumulation of TST potential ($E_{Pb\ dep.\ and\ TST\ acc.}$) and time ($t_{Pb\ dep.\ and\ TST\ acc.}$), amplitude ($\Delta E_A$), scan rate (ν), and modulation time (t_m), on the peak currents of 1.0 × 10^{-8} mol L^{-1} TST was investigated. The $E_{Pb\ dep.\ and\ TST\ acc.}$ were tested in the range from −0.8 to −1.3 V. The results (Figure 6C) show that the highest TST signal was

obtained for −1.1 V ($t_{Pb\ dep.\ and\ TST\ acc.}$ was equal to 120 s), and hence this value was chosen as optimal. Next, for the selected value of the potential, the effect of $t_{Pb\ dep.\ and\ TST\ acc.}$ in the range of 15–300 s was examined. The $t_{Pb\ dep.\ and\ TST\ acc.}$ of 120 s was selected for further study (Figure 6D), but the stage of simultaneous modification of the surface with PbNPs and accumulation of TST can be extended to obtain lower detection limits.

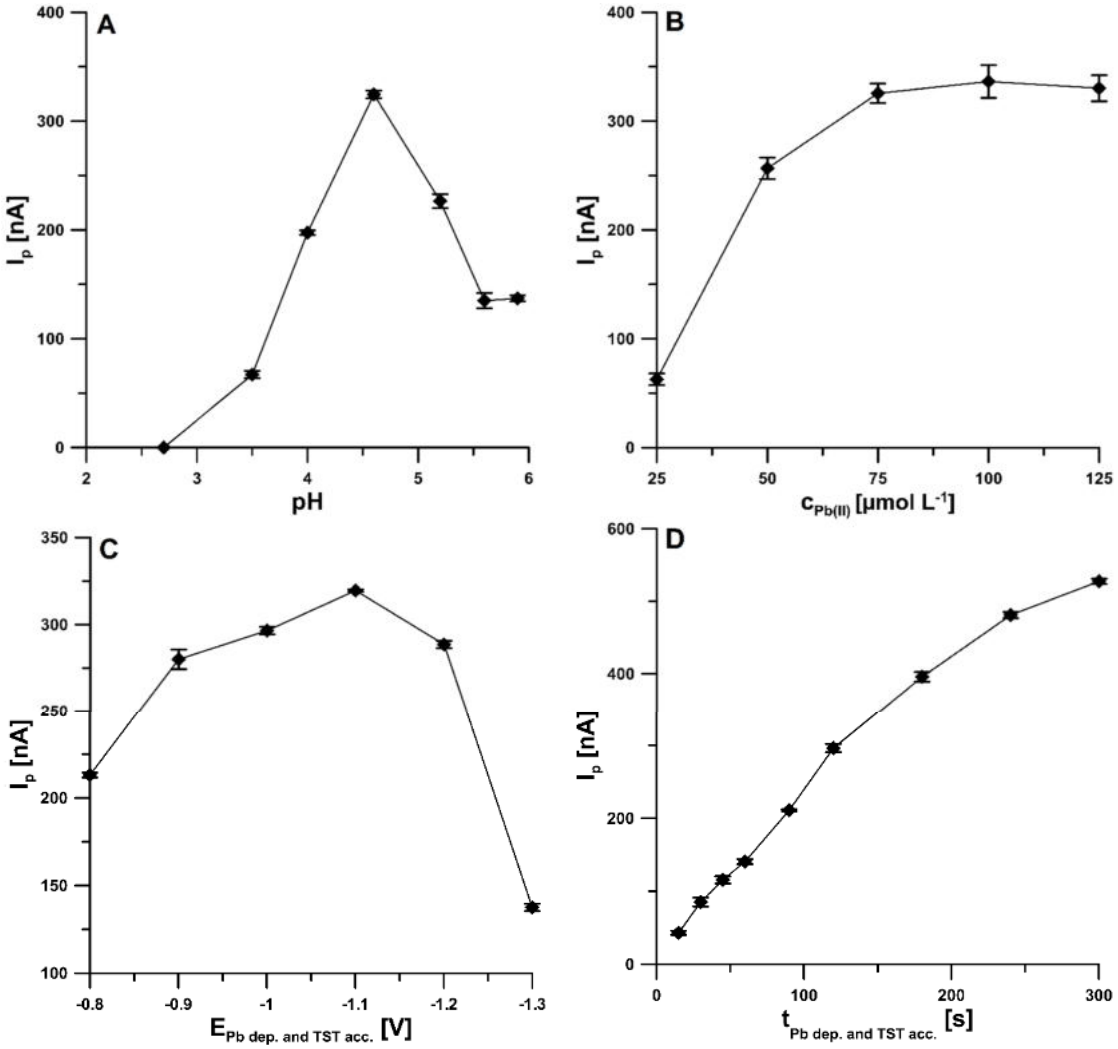

Figure 6. The dependence of pH (**A**), $Pb(NO_3)_2$ concentration (**B**), $E_{Pb\ dep.\ and\ TST\ acc.}$ (**C**), and $t_{Pb\ dep.\ and\ TST\ acc.}$ (**D**) on 1×10^{-8} mol L^{-1} TST signal. The DPAdSV parameters: t_m of 10 ms, ΔE_A of 50 mV and ν of 40 mV s^{-1}. The mean values of I_p are given with the standard deviation for $n = 3$.

In order to investigate the effect of ΔE_A (from 25 to 200 mV), the reduction peak current of TST was measured (Figure 7A). The best responses were obtained with ΔE_A of 150 and 175 mV. For further studies, the value of 150 mV was chosen. Figure 7B depicts the effect of ν in the range of 25–200 mV s^{-1} on the TST signal. The TST reduction signal increased by increasing υ up to 200 mV s^{-1}. Due to the better repeatability of the TST signal, υ of 175 mV s^{-1} was selected as optimal. The t_m was checked in the range from 2 to 40 ms. The highest TST signal was recorded for the t_m of 5 ms (Figure 7C).

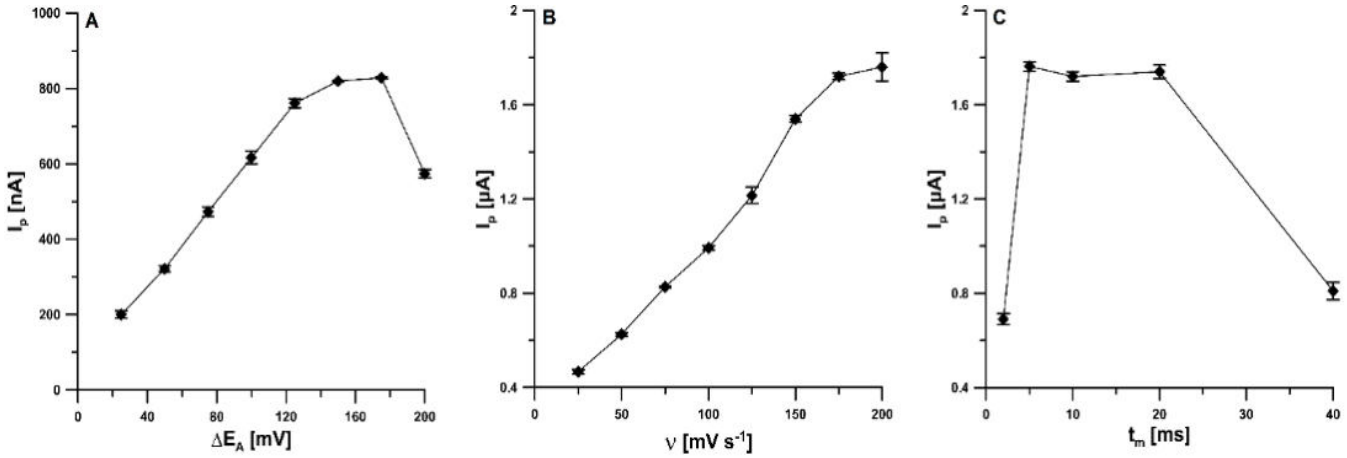

Figure 7. The dependence of ΔE_A (**A**), ν (**B**), and t_m (**C**) on 1×10^{-8} mol L^{-1} TST signal. The DPAdSV parameters: $E_{Pb\ dep.\ and\ TST\ acc.}$ of −1.1 V and $E_{Pb\ dep.\ and\ TST\ acc.}$ of 120 s. The mean values of I_p are given with the standard deviation for $n = 3$.

3.3. Voltammetric Determination of TST

The determination of TST at different concentrations was performed at the pSPCE/PbNPs by the DPAdSV technique under the developed conditions. Figure 8 shows the obtained results. A_s the concentration of TST increased, the related reduction peak current also increased. The plot of the peak current against TST concentration exhibited three linear ranges. The first one was from 1.0×10^{-11} to 1.0×10^{-10} mol L^{-1}, the second one was from 1.0×10^{-10} to 2.0×10^{-9} mol L^{-1}, and the third one was from 2.0×10^{-9} to 2.0×10^{-8} mol L^{-1}. The detection (LOD) and quantification (LOQ) limits were estimated to be 2.2×10^{-12} and 7.3×10^{-12} mol L^{-1}, respectively, using LOD = $3SD_a/b$ and LOQ = $10\ SD_a/b$ equations (SD_a—standard deviation of intercept ($n = 3$); b—slope of calibration curve) [45].

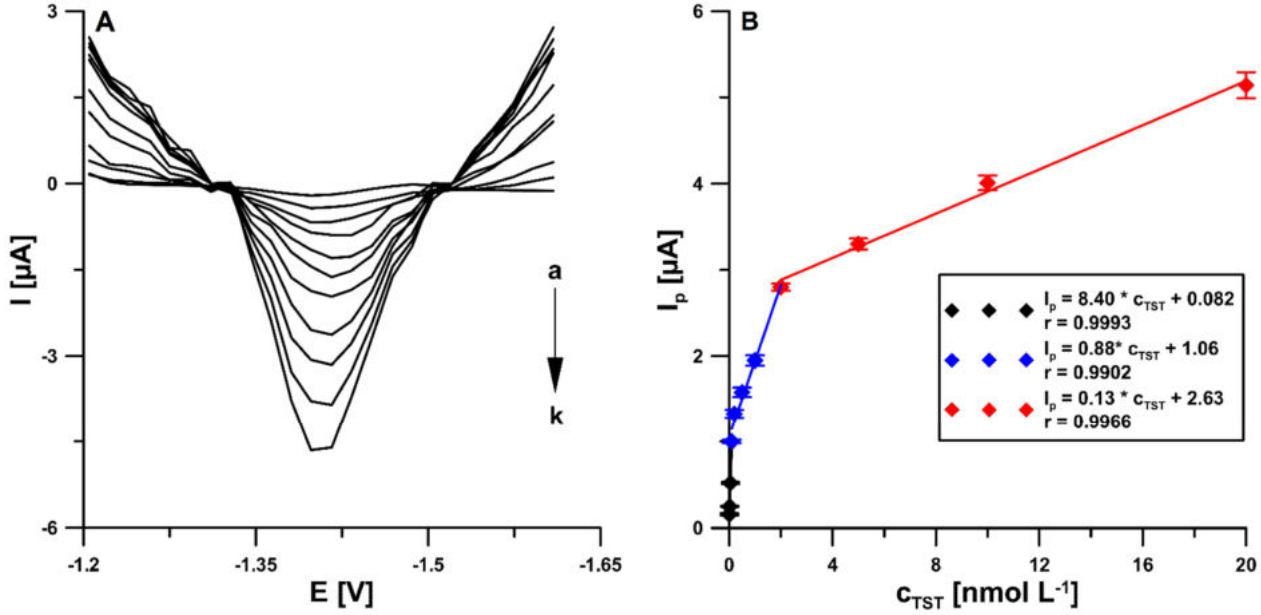

Figure 8. The DPAdSVs of the pSPCE/PbNPs in the presence of various TST concentrations (a → k, 1.0×10^{-11}–2.0×10^{-8} mol L^{-1}) in 0.075 mol L^{-1} acetate buffer of pH 4.6 ± 0.1 and 7.5×10^{-5} mol L^{-1} $Pb(NO_3)_2$ (**A**).Calibraion graph of TST (**B**). The obtained average values of the peak current are shown with standard deviation for $n = 3$. The DPAdSV parameters: t_m of 5 ms, ΔE_A of 150 mV, ν of 175 mV s^{-1}, $E_{Pb\ dep.\ and\ TST\ acc.}$ of −1.1 V and $E_{Pb\ dep.\ and\ TST\ acc.}$ of 120 s.

The linear range and the LOD of the pSPCE/PbNPs were compared with other previously reported voltammetric sensors, and the data are presented in Table 1. It can be seen that only two studies describe the determination of TST with a lower LOD [21,41]. However, the preparation of these electrodes (SPEs modified with a molecularly imprinted polymer and AuE modified with a double-layered molecularly imprinted polymer) requires a more expensive apparatus; the procedures are more labor-intensive, and more chemicals are used.

Table 1. Comparison of techniques for analysis of TST.

Electrode	Method	Linear Range [mol L^{-1}]	LOD [mol L^{-1}]	Application	Ref.
SWNT-EPPGE	SWV	5.0×10^{-9}–1.0×10^{-6}	2.8×10^{-9}	Urine	[2]
GCE/BiF + CTAB	SWAdSV	1.0×10^{-9}–4.5×10^{-8}	3.0×10^{-10}	Pharmaceutical formulations, urine	[3]
HMDE	AdSV	1.0×10^{-8}–7.3×10^{-6}	5.0×10^{-9}	Pharmaceutical formulations	[20]
MD/graphite	DPV	1.0×10^{-8}–1.0×10^{-6}	4.1×10^{-8}	Saliva	[1]
MD/Graphene	DPV	1.0×10^{-7}–1.0×10^{-6}	6.7×10^{-9}	Saliva	[1]
MD/CNTs	DPV	1.0×10^{-10}–1.0×10^{-6}	1.4×10^{-11}	Saliva	[1]
MD/fullerene C_{60}	DPV	1.0×10^{-8}–1.0×10^{-6}	1.5×10^{-8}	Saliva	[1]
SPE/MIP	CV	3.5×10^{-18}–3.5×10^{-15}	3.5×10^{-17}	Urine	[41]
PbFE (GCE/PbF)	SWAdSV	2.0×10^{-8}–3.0×10^{-7}	9.0×10^{-9}	Urine	[19]
AuE/DMIP	SWV	1.0×10^{-14}–1.0×10^{-13}	1.0×10^{-14}	Urine	[21]
GCE/CTAB	SWAdSV	1.0×10^{-8}–7.0×10^{-8}	1.2×10^{-9}	Pharmaceutical formulations, urine	[4]
pSPCE/PbNPs	DPAdSV	1.0×10^{-11}–1.0×10^{-10} 2.0×10^{-10}–2.0×10^{-9} 2.0×10^{-9}–2.0×10^{-8}	2.2×10^{-12}	Urine, wastewater	This work

SWNT-EPPGE—edge plane pyrolytic graphite electrode modified with single-walled carbon nanotubes; GCE/BiF + CTAB—glassy carbon electrode modified with bismuth film and cetyltrimethylammonium bromide; HMDE—hanging mercury drop electrode; MD/graphite—maltodextrin-modified paste electrode based on graphite; MD/graphene—maltodextrin-modified paste electrode based on grapheme; MD/CNTs—maltodextrin-modified paste electrode based on carbon nanotubes; MD/fullerene C_{60}—maltodextrin-modified paste electrode based on fullereneC_{60}; SPE/MIP—screen-printed electrode modified with molecularly imprinted polymer; PbFE—lead film electrode; AuE/DMIP—gold electrode modified with a double-layered molecularly imprinted polymer; GCE/CTAB—glassy carbon electrode modified with cetyltrimethylammonium bromide; pSPCE/PbNPs—electrochemically pretreated screen-printed carbon electrode modified with lead nanoparticles; SWV—square-wave voltammetry; SWAdSV—square-wave adsorptive stripping voltammetry; AdSV—adsorptive stripping voltammetry; DPV—differential-pulse voltammetry; CV—cyclic voltammetry; DPAdSV—differential-pulse adsorptive stripping voltammetry.

In order to investigate the selectivity of the DPAdSV procedure with the use of the pSPCE/PbNPs for TST determination, increasing concentrations of potential interferents were added to the supporting electrolyte. The tolerance limit was defined as the concentration that gave an error of $\leq$10% in the determination of 1.0×10^{-9} mol L^{-1} TST. It was noted that studied substances have negligible effects on the peak current of TST (Figure 9).

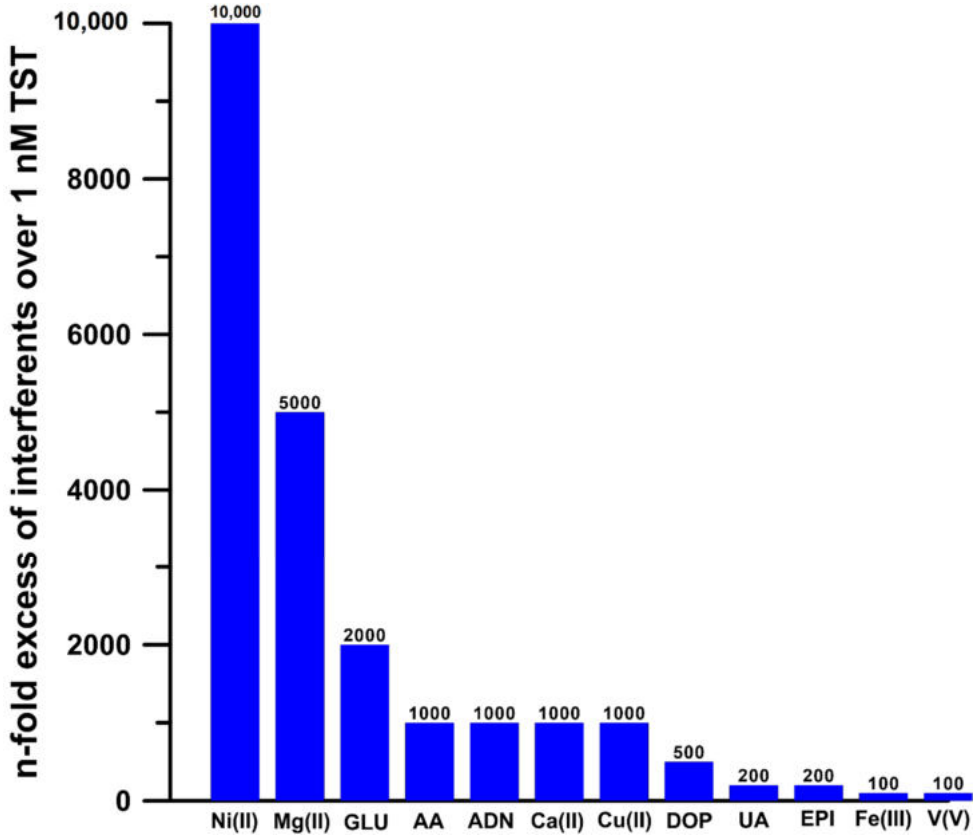

Figure 9. Histogram of the selectivity of pSPCE/PbNPs for TST determination. GLU—glucose, AA—ascorbic acid, ADN—adenine, DOP—dopamine, UA—uric acid, EPI—epinephrine.

3.4. TST Determination in Real Samples

The high performance of the DPAdSV procedure at the pSPCE/PbNPs for TST determination makes it a great potential for the analysis of environmental and biological samples. Therefore, the practical ability of DPAdSV at the pSPCE/PbNPs was checked by the determination of TST in reference material of human urine and wastewater samples purified in a sewage treatment plant without any separation steps. The samples were spiked with a known concentration of TST standard solution and analyzed by the standard addition method. Table 2 presents the obtained results. The very low value of LOD (2.2×10^{-12} mol L^{-1}) allows for the use of small sample volumes and multiple dilutions of the sample in the electrolyte solution (10 × dilution of wastewater and 1000 × dilution of urine, which contributes to minimizing the interference from the sample matrix). The coefficient of variation values obtained between 0.8 and 4.7% indicate very good repeatability of the signal. The recovery values were between 98.7 and 104.5%, which confirms a satisfactory degree of accuracy of the DPAdSV procedure at the pSPCE/PbNPs. The DPAdSVs registered during the determination of TST in real samples are shown in Figure 10. The HPLC/PDA was applied to compare the results of TST analysis in samples without preliminary preparation. However, the concentrations of TST were below the LOD and LOQ of HPLC/PDA. The calculated LOD and LOQ for the standard solution were 7.5×10^{-8} and 2.5×10^{-7} mol L^{-1}, respectively.

Table 2. The outcomes of TST determination in reference material of human urine and wastewater purified in a sewage treatment plant.

TST Concentration [μmol L^{-1}] ± SD (n = 3)					
Sample	**Added**	**Found DPAdSV**	**Found in Electrochemical Cell**	**Coefficient of Variation * [%]**	**Recovery ** [%]**
Purified wastewater	0.0003	0.000297 ± 0.000012	0.0000297 ± 0.0000012	4.05	99.0
	0.002	0.00201 ± 0.000026	0.000209 ± 0.0000017	0.80	100.5
RM of human urine	0.03	0.0296 ± 0.0012	0.0000296 ± 0.0000012	4.07	98.7
	0.02	0.209 ± 0.0017	0.000209 ± 0.0000017	1.29	104.5

* Coefficient of variation [%] = (SD × 100)/Found DPAdSV, ** Recovery [%] = (Found DPAdSV × 100)/Added.

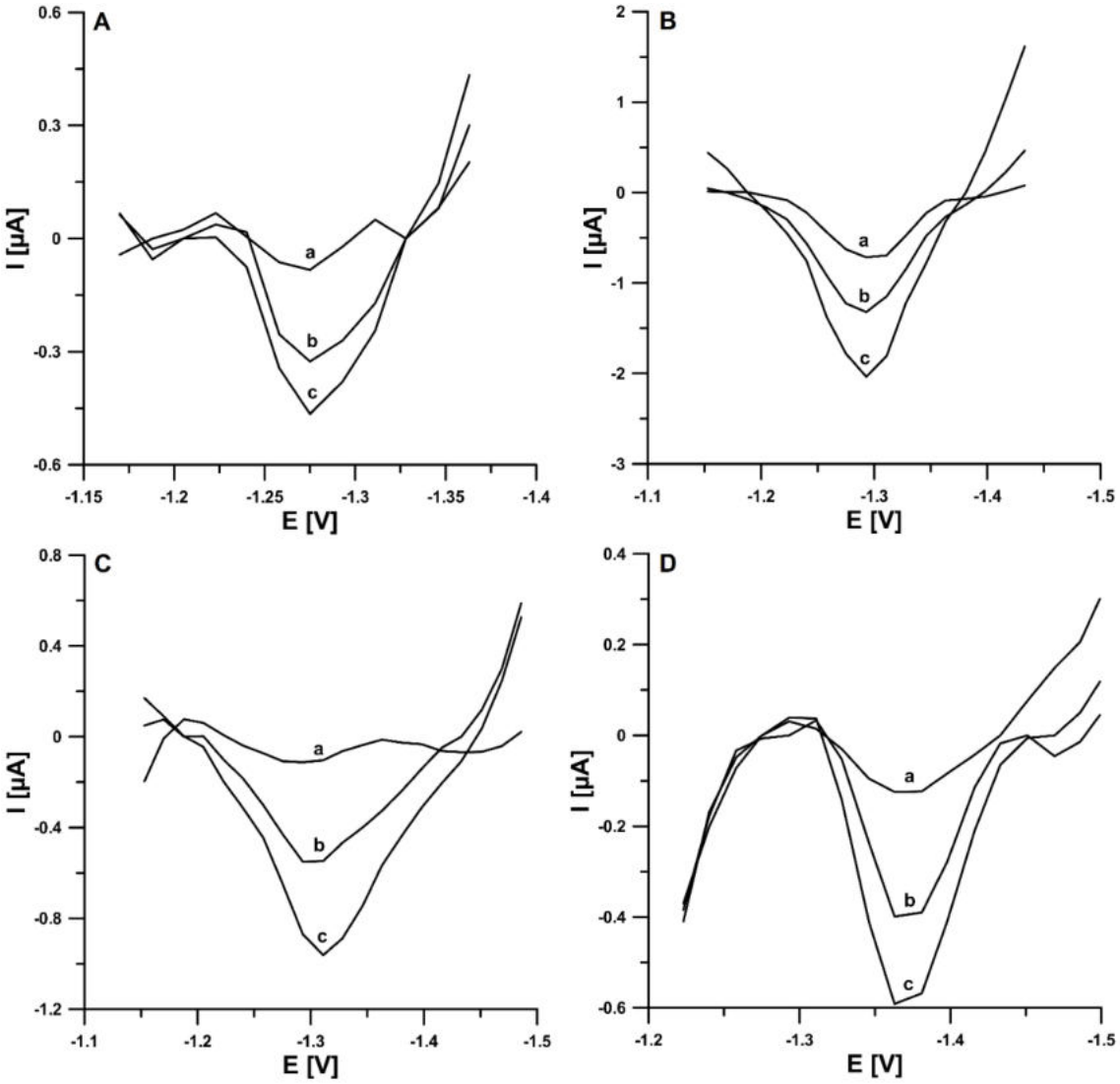

Figure 10. The DPAdSVs recorded for the determination of TST in reference material of human urine (**A**,**B**) and wastewater samples purified in a sewage treatment plant (**C**,**D**): (**A**): (**a**) 10 μL of sample + 0.03, (**b**) as (**a**) + 0.03, (**c**) as (**a**) + 0.06 nM TST, (**B**): (**a**) 10 μL of sample + 0.2, (**b**) as (**a**) + 0.2, (**c**) as (**a**) + 0.4 nM TST, (**C**): (**a**) 1 mL of sample + 0.03, (**b**) as (**a**) + 0.03, (**c**) as (**a**) + 0.06 nM TST, and (**D**): (**a**) 1 mL of sample + 0.2, (**b**) as (**a**) + 0.2, (**c**) as (**a**) + 0.4 nmol $L^{-1.}$ TST. The DPAdSV parameters: ΔE_A of 150 mV, t_m of 5 ms, ν of 175 mV s^{-1}, $E_{Pb\ dep.\ and\ TST\ acc.}$ of −1.1 V and $E_{Pb\ dep.\ and\ TST\ acc.}$ of 120 s.

4. Conclusions

In summary, in this study, for the first time, an electrochemically pretreated screen-printed carbon electrode modified with lead nanoparticles (pSPCE/PbNPs) was introduced for trace analysis of testosterone (TST). The pSPCE/PbNPs were characterized by cyclic voltammetry (CV), electrochemical impedance spectroscopy (EIS), scanning and transmission electron microscopy (SEM and TEM), and energy-dispersive X-ray spectroscopy (EDS). The electrochemical pretreatment of the SPCE surface and electrochemical modification with PbNPs reduce the charge transfer resistance, inhibit the electron transfer kinetics, and significantly increase the active surface area of the sensor, which is translated into a significant increase in the TST reduction peak current. The DPAdSV procedure using the pSPCE/PbNPs is a highly sensitive and selective method for the determination of TST. The use of the pSPCE/PbNPs allows obtaining a very low limit of TST detection (2.2×10^{-12} mol L^{-1}) and wide linear ranges of the calibration graph (1.0×10^{-11}–1.0×10^{-10}, 1.0×10^{-10}–2.0×10^{-9}, and 2.0×10^{-9}–2.0×10^{-8} mol L^{-1}). The practical ability of DPAdSV at the pSPCE/PbNPs was successfully confirmed by the determination of TST in spiked reference material of human urine and wastewater samples purified in a sewage treatment plant without any separation steps. These findings suggest that it is a promising analytical electrochemical sensing procedure for TST analysis in environmental and biological samples. Furthermore, the advantage of the sensor is its portability, which is very promising for quick field analysis.

Author Contributions: Conceptualization, J.K. and K.T.-R.; methodology, J.K. and K.T.-R.; investigation, J.K., K.T.-R., M.W., I.S. and M.R.; writing—original draft preparation, J.K. and K.T.-R.; writing—review and editing, J.K., K.T.-R., M.W., I.S. and M.R.; supervision, K.T.-R. All authors have read and agreed to the published version of the manuscript.

Funding: This research received no external funding.

Institutional Review Board Statement: Not applicable.

Informed Consent Statement: Not applicable.

Data Availability Statement: The data presented in this study are available on request from the corresponding author.

Acknowledgments: The authors would like to thank the employees of Municipal Water Supply and Waste Water Treatment Company Ltd. (Lublin, Poland) for the wastewater samples.

Conflicts of Interest: The authors declare no conflict of interest.

References

1. Gugoasa, L.A.; Stefan-van Staden, R.-I.; Calenic, B.; Legler, J. Multimode sensors as new tools for molecular recognition of testosterone, dihydrotestosterone and estradiol in children's saliva. *J. Mol. Recognit.* **2015**, *28*, 10–19. [CrossRef] [PubMed]
2. Goyal, R.N.; Gupta, V.K.; Chatterjee, S. Electrochemical investigations of corticosteroid isomers—testosterone and epitestosterone and their simultaneous determination in human urine. *Anal. Chim. Acta* **2010**, *657*, 147–153. [CrossRef] [PubMed]
3. Levent, A.; Altun, A.; Taş, S.; Yardım, Y.; Şentürk, Z. Voltammetric behavior of testosterone on bismuth film electrode: Highly sensitive determination in pharmaceuticals and human urine by square-wave adsorptive stripping voltammetry. *Electroanalysis* **2015**, *27*, 1219–1228. [CrossRef]
4. Levent, A.; Altun, A.; Yardım, Y.; Şentürk, Z. Sensitive voltammetric determination of testosterone in pharmaceuticals and human urine using a glassy carbon electrode inthe presence of cationic surfactant. *Electrochim. Acta* **2014**, *128*, 54–60. [CrossRef]
5. Moon, J.Y.; Kwon, W.; Suh, S.; Cheong, J.C.; In, M.K.; Chung, B.C.; Kim, J.Y.; Choi, M.H. Reference ranges for urinary levels of testosterone and epitestosterone, which may reveal gonadal function, in a Korean male population. *J. Steroid Biochem. Mol. Biol.* **2014**, *140*, 100–105. [CrossRef]
6. Bulut, U.; Sanli, S.; Cevher, S.C.; Cirpan, A.; Donmez, S.; Timur, S. A biosensor platform based on amine functionalized conjugated benzenediamine-benzodithiophene polymer for testosterone analysis. *J. Appl. Polym. Sci.* **2020**, *137*, 49332. [CrossRef]
7. Lyubimenko, R.; Cardenas, O.I.G.; Turshatov, A.; Richards, B.S.; Schäfer, A.I. Photodegradation of steroid-hormone micropollutants in a flow-through membrane reactor coated with Pd(II)-porphyrin. *Appl. Catal. B* **2021**, *291*, 120097. [CrossRef]
8. Bexfield, L.M.; Toccalino, P.T.; Belitz, K.; Foreman, W.T.; Furlong, E.T. Hormones and pharmaceuticals in groundwater used as a source of drinking water across the united states. *Environ. Sci. Technol.* **2019**, *53*, 2950–2960. [CrossRef]

9. Kolodziej, E.P.; Gray, J.L.; Sedlak, D.L. Quantification of steroid hormones with pheromonal properties in municipal wastewater effluent. *Environ. Toxicol. Chem.* **2003**, *22*, 2622–2629. [CrossRef]
10. Vicente, F.B.; Smith, F.A.; Sierra, R.; Wang, S. Measurement of serum testosterone using high-performance liquid chromatography/tandem mass spectrometry. *Clin. Chem. Lab. Med.* **2006**, *44*, 70–75. [CrossRef]
11. Sun, G.; Xue, J.; Li, L.; Li, X.; Cui, Y.; Qiao, B.; Wei, D.; Li, H. Quantitative determination of human serum testosterone via isotope dilution ultra-performance liquid chromatography tandem mass spectrometry. *Mol. Med. Rep.* **2020**, *22*, 1576–1582. [CrossRef] [PubMed]
12. Wang, Y.; Gay, G.D.; Botelho, J.C.; Caudill, S.P.; Vesper, H.W. Total testosterone quantitative measurement in serum by LC-MS/MS. *Clin. Chim. Acta* **2014**, *436*, 263–267. [CrossRef] [PubMed]
13. French, D. Development and validation of a serum total testosterone liquid chromatography–tandem mass spectrometry (LC-MS/MS) assay calibrated to NIST SRM 971. *Clin. Chim. Acta* **2013**, *415*, 109–117. [CrossRef]
14. Kannenberg, F.; Fobker, M.; Schulte, E.; Pierściński, G.; Kelsch, R.; Zitzmann, M.; Nofer, J.R.; Schüring, A.N. The Simultaneous measurement of serum testosterone and 5α-dihydrotestosterone by gas chromatography–mass spectrometry (GC-MS). *Clin. Chim. Acta* **2018**, *476*, 15–24. [CrossRef]
15. Matysik, S.; Schmitz, G. Determination of steroid hormones in human plasma by GC-triple quadrupole MS. *Steroids* **2015**, *99*, 151–154. [CrossRef]
16. Du, B.; Zhang, J.; Dong, Y.; Wang, J.; Lei, L.; Shi, R. Determination of testosterone/epitestosterone concentration ratio in human urine by capillary electrophoresis. *Steroids* **2020**, *161*, 108691. [CrossRef]
17. Chen, H.-X.; Deng, Q.-P.; Zhang, L.-W.; Zhang, X.-X. Quantification of testosterone and epitestosterone in biological samples by capillary electrophoresis with immunoaffinity extraction. *Talanta* **2009**, *78*, 464–470. [CrossRef] [PubMed]
18. Tan, Y.; Jing, L.; Ding, Y.; Wei, T. A novel double-layer molecularly imprinted polymer film based surface plasmon resonance for determination of testosterone inaqueous media. *Appl. Surf. Sci.* **2015**, *342*, 84–91. [CrossRef]
19. Tyszczuk, K. Application of an in situ plated lead film electrode to the analysis of testosterone by adsorptive stripping voltammetry. *Anal. Bioanal. Chem.* **2018**, *390*, 1951–1956. [CrossRef]
20. Hu, S.; Chen, Z.; Zhang, T. Adsorptive stripping voltammetry of testosterone propionate in pharmaceutical preparations. *Fresenius J. Anal. Chem.* **1993**, *346*, 1008–1010. [CrossRef]
21. Fourou, H.; Braiek, M.; Bonhomme, A.; Lagarde, F.; Zazoua, A.; Jaffrezic-Renault, N. Voltammetric sensor based on a double layered molecularly imprinted polymer for testosterone. *Anal. Lett.* **2018**, *51*, 312–322. [CrossRef]
22. Ma, L.-L.; He, Y.; Qin, D.; Chang, A.; Huang, A.; Xie, X.-J.; Zhang, Y. Fabrication, Characterization and performance evaluation of screen-printed carbon electrodes: Determination of acetaminophen in Tylenol. *Chin. J. Anal. Chem.* **2021**, *49*, 21187–21196. [CrossRef]
23. Raymundo-Pereira, P.A.; Gomes, N.O.; Machado, S.A.S.; Oliveira Jr, O.N. Simultaneous, ultrasensitive detection of hydroquinone, paracetamol and estradiol for quality control of tap water with a simple electrochemical method. *J. Electroanal. Chem.* **2019**, *848*, 113319. [CrossRef]
24. Bagherinasab, Z.; Beitollahi, H.; Yousefi, M.; Bagherzadeh, M.; Hekmati, M. Rapid sol gel synthesis of $BaFe_{12}O_{19}$ nanoparticles: An excellent catalytic application in the electrochemical detection of tramadol in the presence of acetaminophen. *Microchem. J.* **2020**, *156*, 104803. [CrossRef]
25. Kondori, T.; Tajik, S.; Akbarzadeh-T, N.; Beitollahi, H.; Graiff, C.; Jang, H.W.; Shokouhimehr, M. Synthesis and characterization of bipyridine cobalt(II) complex modified graphite screen printed electrode: An electrochemical sensor for simultaneous detection of acetaminophen and naproxen. *RSC Adv.* **2021**, *11*, 3049–3057. [CrossRef]
26. Tyszczuk-Rotko, K.; Kozak, J.; Czech, B. Screen-printed voltammetric sensors—tools for environmental water monitoring of painkillers. *Sensors* **2022**, *22*, 2437. [CrossRef]
27. Gonzalez-Sanchez, M.I.; Gomez-Monedero, B.; Agrisuelas, J.; Iniesta, J.; Valero, E. Highly activated screen-printed carbon electrodes by electrochemical treatment with hydrogen peroxide. *Electrochem. Commun.* **2018**, *91*, 36–40. [CrossRef]
28. Yuan, X.; Ma, L.; Zhang, J.; Zheng, Y. Simple pre-treatment by low-level oxygen plasma activates screen-printed carbon electrode: Potential for mass production. *Appl. Surf. Sci.* **2021**, *544*, 148760. [CrossRef]
29. Wei, H.; Sun, J.-J.; Xie, Y.; Lin, C.-G.; Wang, Y.-M.; Yin, W.-H.; Chen, G.-N. Enhanced electrochemical performance at screen-printed carbon electrodes by a new pretreating procedure. *Anal. Chim. Acta* **2007**, *588*, 297–303. [CrossRef]
30. Lee, J.; Arrigan, D.W.M.; Silvester, D.S. Mechanical polishing as an improved surface treatment for platinum screen-printed electrodes. *Sens. Bio-Sens. Res.* **2016**, *9*, 38–44. [CrossRef]
31. Cumba, L.R.; Foster, C.W.; Brownson, D.A.C.; Smith, J.P.; Iniesta, J.; Thakur, B.; do Camo, D.R.; Banks, C.E. Can the mechanical activation (polishing) of screen-printed electrodes enhance their electroanalytical response? *Analyst* **2016**, *141*, 2791–2799. [CrossRef] [PubMed]
32. Montiel, N.F.; Parilla, M.; Beltran, V.; Nuyts, G.; Van Durme, F.; De Wael, K. The opportunity of 6-monoacetylmorphine to selectively detect heroin at preanodized screen printed electrodes. *Talanta* **2021**, *226*, 122005. [CrossRef] [PubMed]
33. de Oliveira Silva, R.; da Silva, E.A.; Fiorucci, A.R.; Ferreira, V.S. Electrochemically activated multi-walled carbon nanotubes modified screen-printed electrode for voltammetric determination of sulfentrazone. *J. Electroanal. Chem.* **2019**, *835*, 220–226. [CrossRef]

34. Kozak, J.; Tyszczuk-Rotko, K.; Wójciak, M.; Sowa, I.; Rotko, M. First screen-printed sensor (electrochemically activated screen-printed boron-doped diamond electrode) for quantitative determination of rifampicin by adsorptive stripping voltammetry. *Materials* **2021**, *14*, 4231. [CrossRef]
35. Yaghoubian, H.; Tajik, S.; Beitollahi, H.; Sardahi, H.; Sheikhshoaie, I. Fe_2MoO_4 magnetic nanocomposite modified screen printed graphite electrode as a voltammetric sensor for simultaneous determination of nalbuphine and diclofenac. *J. Mater. Sci.* **2021**, *32*, 17311–17323. [CrossRef]
36. Cumba, L.R.; Camisasca, A.; Giordani, S.; Foster, R.J. Electrochemical properties of screen-printed carbon nano-onion electrodes. *Molecules* **2020**, *25*, 3884. [CrossRef]
37. Kozak, J.; Tyszczuk-Rotko, K.; Sadok, I.; Sztanke, K.; Sztanke, M. Application of a screen-printed sensor modified with carbon nanofibers for the voltammetric analysis of an anticancer disubstituted fused triazinone. *Int. J. Mol. Sci.* **2022**, *23*, 2429. [CrossRef]
38. Ibanez-Redin, G.; Furuta, R.H.M.; Wilson, D.; Shimizu, F.M.; Materon, E.M.; Arantes, L.M.R.B.; Melendez, M.E.; Carvalho, A.L.; Reis, R.M.; Chaur, M.N.; et al. Screen-printed interdigitated electrodes modified with nanostructured carbon nano-onion films for detecting the cancer biomarker CA19-9. *Mater. Sci. Eng. C* **2019**, *99*, 1502–1508. [CrossRef]
39. Sawan, S.; Maalouf, R.; Errachid, A.; Jaffrezic-Renault, N. Metal and metal oxide nanoparticles in the voltammetric detection of heavy metals: A review. *Trends Anal. Chem.* **2020**, *131*, 116014. [CrossRef]
40. Hezard, T.; Fajerwerg, K.; Evrard, D.; Colliere, V.; Behra, P.; Gros, P. Gold nanoparticles electrodeposited on glassy carbon using cyclic voltammetry: Application to Hg(II) trace analysis. *J. Electroanal. Chem.* **2012**, *664*, 46–52. [CrossRef]
41. Lee, M.-H.; Thomas, J.L.; Liu, W.-C.; Zhang, Z.-X.; Liu, B.D.; Yang, C.-H.; Lin, H.-Y. A multichannel system integrating molecularly imprinted conductive polymers for ultrasensitive voltammetric determination of four steroid hormones in urine. *Microchim. Acta* **2019**, *186*, 695–705. [CrossRef] [PubMed]
42. Gonzalo-Lumbreras, R.; García-Miguens, M.A.; Izquierdo-Hornillos, R. HPLC method development for testosterone propionate and cipionate in oil-based injectables. *J. Pharm. Biomed. Anal.* **2005**, *38*, 757–762. [CrossRef] [PubMed]
43. Rana, A.; Baig, N.; Saleh, T.A. Electrochemically pretreated carbon electrodes and their electroanalytical applications–A review. *J. Electroanal. Chem.* **2019**, *833*, 313–332. [CrossRef]
44. Gosser, D.K. *Cyclic Voltammetry: Simulation and Analysis of Reaction Mechanism*; VCH: New York, NY, USA, 1993.
45. Mocak, J.; Bond, A.M.; Mitchell, S.; Scollary, G. A statistical overview of standard (IUPAC and ACS) and new procedures for determining the limits of detection and quantification: Application to voltammetric and stripping techniques. *Pure Appl. Chem.* **1997**, *69*, 297–328. [CrossRef]

RD6

J. Kozak, K. Tyszczuk-Rotko, I. Sadok, K. Sztanke, M. Sztanke, *Application of a screen-printed sensor modified with carbon nanofibers for the voltammetric analysis of an anticancer disubstituted fused triazinone,*
International Journal of Molecular Sciences, 23 (5) (2022) 2429-2442.

International Journal of
Molecular Sciences

MDPI

Article

Application of a Screen-Printed Sensor Modified with Carbon Nanofibers for the Voltammetric Analysis of an Anticancer Disubstituted Fused Triazinone

Jędrzej Kozak [1], Katarzyna Tyszczuk-Rotko [1], Ilona Sadok [2], Krzysztof Sztanke [3,*] and Małgorzata Sztanke [4]

1 Faculty of Chemistry, Institute of Chemical Sciences, Maria Curie-Skłodowska University in Lublin, 20-031 Lublin, Poland; jedrekkozak@onet.pl (J.K.); katarzyna.tyszczuk-rotko@mail.umcs.pl (K.T.-R.)
2 Laboratory of Separation and Spectroscopic Method Applications, Centre for Interdisciplinary Research, Faculty of Science and Health, The John Paul II Catholic University of Lublin, 20-708 Lublin, Poland; ilona.sadok@kul.pl
3 Laboratory of Bioorganic Synthesis and Analysis, Chair and Department of Medical Chemistry, Medical University of Lublin, 4A Chodźki Street, 20-093 Lublin, Poland
4 Chair and Department of Medical Chemistry, Medical University of Lublin, 4A Chodźki Street, 20-093 Lublin, Poland; malgorzata.sztanke@umlub.pl
* Correspondence: krzysztof.sztanke@umlub.pl

Abstract: In this paper, we propose the first analytical procedure—using a screen-printed carbon electrode modified with carbon nanofibers (SPCE/CNFs)—for the detection and quantitative determination of an electroactive disubstituted fused triazinone, namely 4-Cl-PIMT, which is a promising anticancer drug candidate. The electrochemical performances of the sensor were investigated by cyclic voltammetry (CV), electrochemical impedance spectroscopy (EIS), and square-wave adsorptive stripping voltammetry (SWAdSV). The presence of carbon nanofibers on the sensor surface caused a decrease in charge-transfer resistance and an increase in the active surface compared to the bare SPCE. Under the optimised experimental conditions, the proposed voltammetric procedure possesses a good linear response for the determination of 4-Cl-PIMT in the two linear ranges of 0.5–10 nM and 10–100 nM. The low limits of detection and quantification were calculated at 0.099 and 0.33 nM, respectively. In addition, the sensor displays high reproducibility and repeatability, as well as good selectivity. The selectivity was improved through the use of a flow system and a short accumulation time. The SWAdSV procedure with SPCE/CNFs was applied to determine 4-Cl-PIMT in human serum samples. The SWAdSV results were compared to those obtained by the ultra-high-performance liquid chromatography coupled with electrospray ionization/single-quadrupole mass spectrometry (UHPLC-ESI-MS) method.

Keywords: disubstituted fused triazinone; anticancer agent candidate; square-wave adsorptive stripping voltammetry; screen-printed sensor; carbon nanofibers; flow system

Citation: Kozak, J.; Tyszczuk-Rotko, K.; Sadok, I.; Sztanke, K.; Sztanke, M. Application of a Screen-Printed Sensor Modified with Carbon Nanofibers for the Voltammetric Analysis of an Anticancer Disubstituted Fused Triazinone. *Int. J. Mol. Sci.* **2022**, *23*, 2429. https://doi.org/10.3390/ijms23052429

Academic Editor: Vijay Kumar Thakur

Received: 9 February 2022
Accepted: 18 February 2022
Published: 23 February 2022

1. Introduction

Among pharmaceutically important disubstituted fused triazinones, 4-Cl-PIMT (i.e., 8-(4-chlorophenyl)-3-phenyl-7,8-dihydroimidazo[2,1-*c*][1,2,4]triazin-4(6*H*)-one; Figure 1), with a fully defined molecular structure, is the most promising anticancer drug candidate. This innovative nucleobase-like molecule revealed significant, concentration-dependent antiproliferative effects in human peripheral blood myeloma cells, indicating a possible usefulness in the treatment of such haematological malignancies. Furthermore, this compound proved to have the strongest antimigratory property in human tumour cells of the cervix among all disubstituted fused triazinones, suggesting the highest antimetastatic potential and, consequently, an applicability in the prevention of metastasis [1]. It is worth noting that 4-Cl-PIMT, as a promising candidate for an anticancer

agent, was found to be completely nontoxic to normal human skin fibroblast [1] and African green monkey kidney (data not published) cells and low in toxicity for mice (LD_{50} > 2000 mg kg^{-1}, i.p.) [2]. This compound was predicted (using OSIRIS Property Explorer: http://www.organic-chemistry.org/prog/peo/) (accessed on 7 February 2022) to have no adverse side effects, such as mutagenicity, tumorigenicity, irritating and reproductive effects, due to the lack of "genotoxicophore" fragments in its structure. Based on the highly significant QSARs between the experimentally determined lipophilicity parameters (on columns imitating biosystems) and pharmacokinetic parameters, as well as the reliable and predictive QSAR models developed for assessing the penetration of the blood–brain barrier, this small molecule could be expected to have good bioavailability and high permeability through biological barriers [2–4]. The ability to penetrate the blood–brain barrier was also confirmed by its effect on the central nervous system in mice [2]. The above features indicate that this anticancer fused triazinone can be qualified as a promising candidate for further pharmacological in vivo studies.

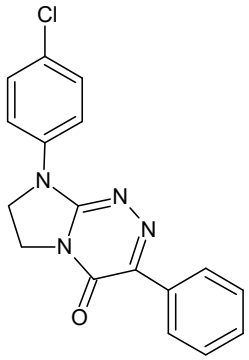

Figure 1. 8-(4-Chlorophenyl)-3-phenyl-7,8-dihydroimidazo[2,1-*c*][1,2,4]triazin-4(6*H*)-one (4-Cl-PIMT)—an electroactive molecule used in this study.

Chromatography and spectroscopy are among the popular methods used in the analysis of organic compounds, especially pharmaceuticals. However, these techniques are time-consuming, labour-intensive, and generate a high consumption of reagents. In addition, they require expensive equipment, and due to their complexity, highly qualified analysts are required [5,6]. In contrast to the above-mentioned methods, electrochemical methods, which include voltammetry, are characterised by a relatively low cost and simplicity of operations, as well as high stability and sensitivity [5,7]. Electrochemical analysis is practically free of organic solvents, is fast, and can be used on a large scale, thanks to portable, miniaturised tools [6,8,9]. Electrochemical methods, including voltammetry, use electrodes as a conversion element, the surface of which interacts with the analyte and converts the information obtained into a signal that can be measured and identified by means of electrochemical analysis control devices [10]. The most frequently used method in quantitative analysis is voltammetry coupled with pulse waveform and the accumulation of analyte on the electrode surface, e.g., square-wave adsorptive stripping voltammetry (SWAdSV). Techniques of this kind are considered a tool to obtain the very low limits of detection (LODs) and quantification (LOQs) [11].

A whole range of working electrodes is used in voltammetry, e.g., mercury electrodes, glassy carbon electrodes, carbon paste electrodes, or boron-doped diamond electrodes [12]. Since the initial development of screen-printed carbon electrodes (SPCEs) in the 1980s, these sensors have found applications in biomedical, environmental, and industrial analyses. Unlike individual electrodes in traditional electrochemical analysis, all SPCEs are printed and integrated on an inert plastic or ceramic substrate, where a carbon ink and silver pseudo-electrodes usually serve as working, counter, and reference electrodes [13,14]. Screen-printing techniques offer simple means of possible mass production of disposable, stable, and low-cost screen-printed electrodes to be used in on-site analyses [15,16].

Screen-printed electrodes are often employed in analytical applications due to their specific characteristics, including small dimensions and determination limits, quick response duration, reproducibility, ability to operate at room temperature, and low background current [5,17,18]. Additional advantages of screen-printed electrodes are diversification of the selection of electrode materials, portability, reliability for detecting different substances, and an ease of surface modification for various uses [19].

Often, both conventional and screen-printed electrodes require surface modification for improved selectivity and sensitivity in determining the analyte. The modifier applied to the electrode increases its active surface and improves electron transfer. Among the currently popular modifiers, various types of nanoparticles and nanomaterials are used, including carbon nanomaterials [12,20]. Nanomaterials are chemicals or materials that are produced and used on a very small scale. Nanomaterials are being developed to exhibit new properties compared to the same material without nanoscale features [21]. Carbon-based nanomaterials have attracted much attention due to their large surface area, interconnecting network, low electrical resistance, and excellent electrical conductivity, as well as good chemical and physical stability toward electrochemical purposes [22]. Among carbon nanomaterials, we can distinguish carbon nanofibers (CNFs); carbon nanohorns (CNHs); and carbon nanotubes, including single-walled (SWCNTs), double-walled (DWCNTs) and even multiwalled (MWCNTs) nanotubes [23–25]. Carbon nanofibers (CNFs) are graphitic materials with a high surface area-to-volume ratio and excellent mechanical strength, flexibility, chemical stability, and biocompatibility [26].

Despite the above-mentioned facts, no analytical procedure has been described in the literature to date for the quantitative determination of an anticancer fused triazinone (4-Cl-PIMT). On the other hand, this promising small molecule is the subject of our current electrochemical studies due to the attendance (in its structure) of an electroactive azomethine moiety of the ketimine-type, which may be the most susceptible to electrochemical reduction under experimental conditions. The purpose of the present study is to develop and optimise the first analytical procedure—using the most suitable screen-printed sensor coupled with a flow system—which would enable the detection and subsequent quantitative determination of this potential anticancer drug in both solution and enriched serum samples.

2. Results and Discussion

2.1. Initial Studies

In the initial stage of the experiments, we compared the voltammetric response of the title compound at the commercially available unmodified screen-printed carbon electrode (SPCE), screen-printed carbon electrode modified with carbon nanofibers (SPCE/CNFs), and screen-printed carbon electrode modified with multiwalled carbon nanotubes (SPCE/MWCNTs). SWV curves of 0.05 and 0.1 μM 4-Cl-PIMT were recorded at all electrodes after 45 s of solution stirring (Figure 2). The analytical signals obtained at the SPCE/CNFs were significantly improved compared to those obtained at the SPCE and the SPCE/MWCNTs. Therefore, the commercially available screen-printed carbon electrode modified with carbon nanofibers was selected for further study.

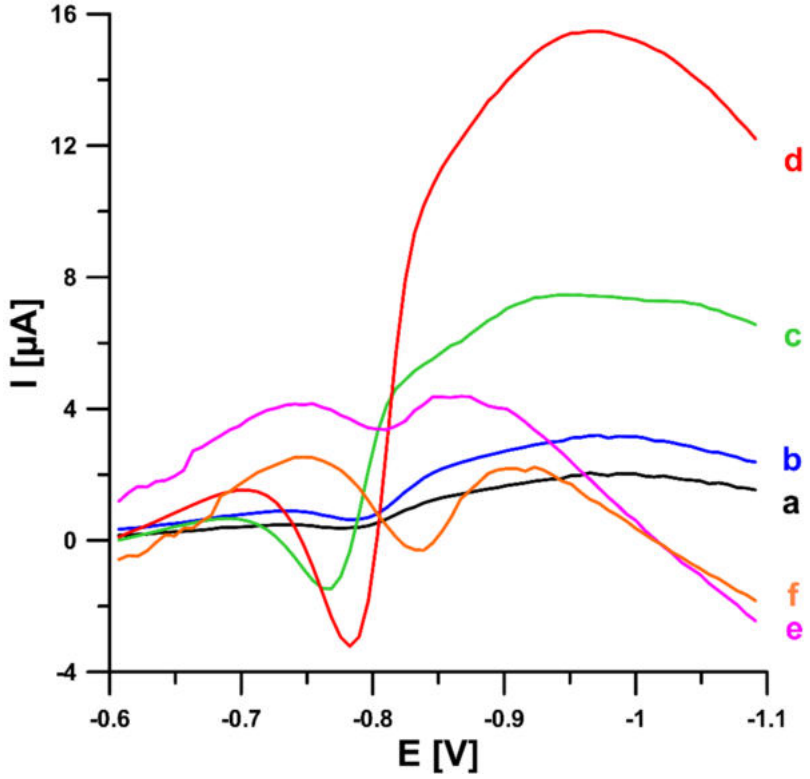

Figure 2. SW voltammograms of 0.05 (a, c, and e) and 0.1 µM (b, d, and f) 4-Cl-PIMT in 0.1 M H_2SO_4 solution at the screen-printed carbon electrode (SPCE) (a and b), screen-printed carbon electrode modified with carbon nanofibers (SPCE/CNFs) (c and d), and screen-printed carbon electrode modified with multiwalled carbon nanotubes (SPCE/MWCNTs) (e and f). SWV parameters: open-circuit potential, t of 45 s, initial E of −0.2 V, final E of −1.1 V, f of 50 Hz, E_{SW} of 50 mV, and ΔE of 7 mV.

To explain the advisability of modification of the electrode surface by carbon nanofibers, the commercially available, unmodified screen-printed carbon electrode (SPCE) and screen-printed carbon electrode modified with carbon nanofibers (SPCE/CNFs) were examined using the electrochemical impedance spectroscopy (EIS) method. Impedance spectra (Nyquist plots) were recorded in the frequency range from 20.0 kHz to 1.0 Hz at a potential of 0.2 V from a solution of 0.1 M KCl containing 5.0 mM $K_3[Fe(CN)_6]$. The obtained curves (Figure 3) clearly show that the presence of carbon nanofibers on the surface of the SPCE (black curve) causes a decrease in the charge-transfer resistance (R_{ct}) compared to the bare SPCE (blue curve) (63.5 vs. 197.3 Ω cm^2). Moreover, a better electrochemical performance of the SPCE/CNFs compared to the SPCE is observed as a result of the increase in its active surface due to modification (0.0809 ± 0.0014 vs. 0.061 ± 0.00058 cm^2 (n = 3), respectively) [27–29].

2.2. Effect of Type and pH of Supporting Electrolytes

The effect of the type of supporting electrolytes on the voltammetric response of 0.05 and 0.1 µM 4-Cl-PIMT was checked using 0.1 M solutions of H_2SO_4, HNO_3, CH_3COOH, and acetate buffers with pH values of 3.5 ± 0.1, 4.0 ± 0.1, and 5.0 ± 0.1, respectively; the corresponding data are depicted in Figure 4A. It is clearly visible that the highest peak current of the reduction was obtained in acidic media. Figure 4B shows a comparison of the SWV curves recorded for 0.1 µM 4-Cl-PIMT in 0.1 M solutions of acetic (red), sulfuric (blue), and nitric (black) acids. Considering the obtained results, the nitric acid solution was found to be the most suitable for the determination of 4-Cl-PIMT. Moreover, the concentration of nitric acid from 0.01 to 0.125 M was evaluated (Figure 4C). The highest and best-shaped analytical signal of 4-Cl-PIMT was attained for the 0.025 M concentration of HNO_3, so it was selected for subsequent experiments.

In addition, the linearity of peak potential (E_p) of 4-Cl-PIMT vs. pH plot (Figure 4D) was obtained within the pH range of 1.0–5.0 (r = 0.9910). The equation slope is identical to the theoretical value of 0.059 V pH^{-1}, indicating that the electrode process involves an equal number of protons and electrons. This is demonstrated in the reduction mechanism of our anticancer agent candidate (Figure 4E). It was found that the reduction process of 4-Cl-PIMT occurs at the surface of screen-printed carbon electrode modified with carbon nanofibers (SPCE/CNFs)—as a sensor—through an electron-gain mechanism, with the transfer of two electrons and two protons. The analyte possesses two azomethine moieties of the ketimine-type (C=N). The reduction of each of these azomethine groups (C3=N2, C8a=N1) implies the same number of protons and electrons. On the basis of previous findings [29–32], it was proposed that the C=N moiety located at positions 3 and 2 would be exclusively susceptible to the electrochemical reduction under these experimental conditions, leading to a protonated CH–NH group. This proposal may be supported by the proven susceptibility of this azomethine moiety to electrochemical reduction in structures of monocyclic, as well as fused, triazinones with single N–N bonds [29–31]. In addition, this may be supported by the experimentally observed reduction peak potential, the value of which is close to that of the same azomethine moiety of the ketimine-type undergoing regioselective electrochemical reduction in a structurally similar triazinone [32].

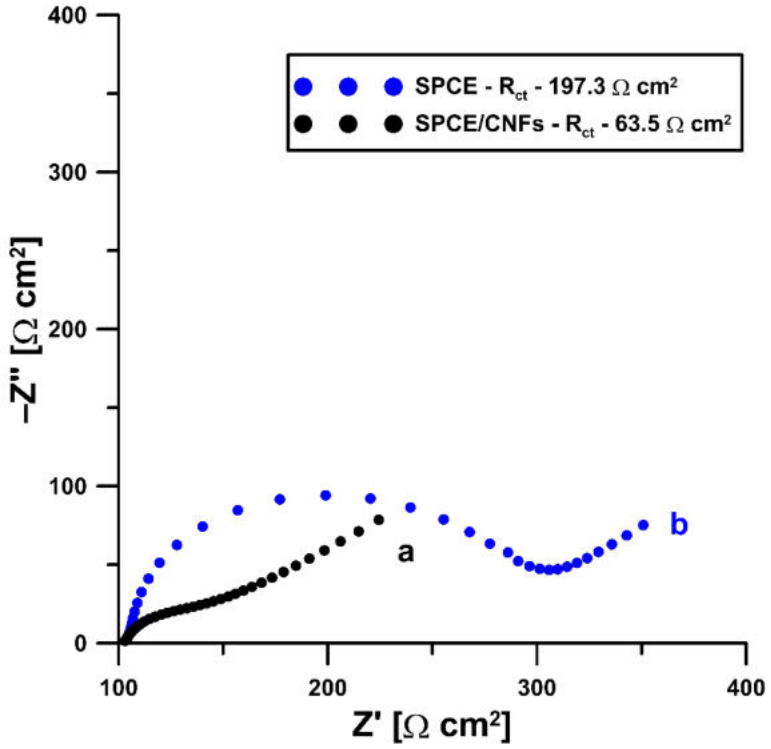

Figure 3. Nyquist plots of SPCE/CNFs (a) and SPCE (b).

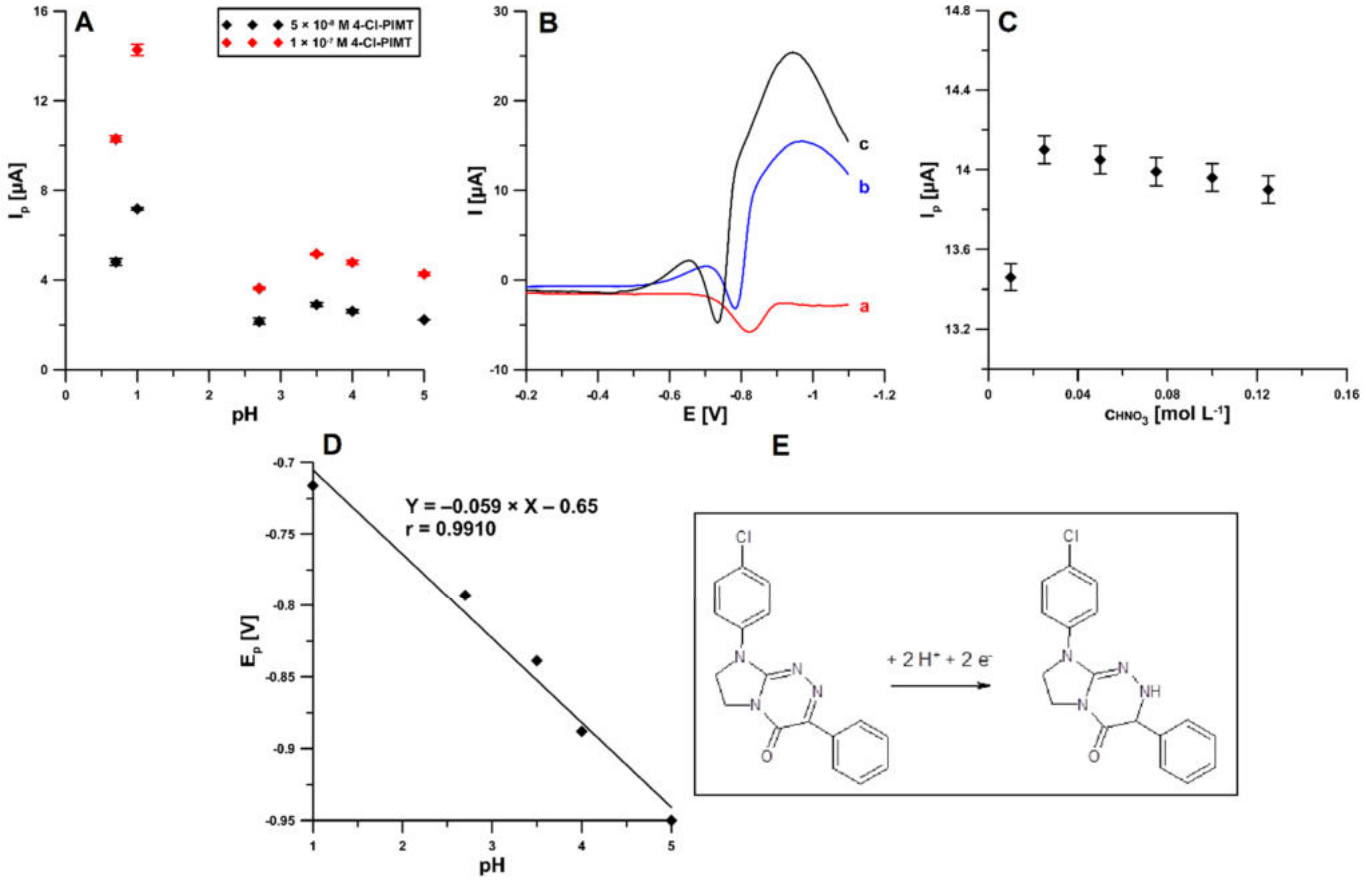

Figure 4. (**A**) Influence of the type of supporting electrolytes (0.1 M H_2SO_4, HNO_3, CH_3COOH and acetate buffers with pH values of 3.5 ± 0.1, 4.0 ± 0.1, and 5.0 ± 0.1) on the 4-Cl-PIMT peak current. The mean values of I_p are given with the standard deviation for n = 3. (**B**) SWV curves recorded in 0.1 M solutions of acetic acid (a), sulfuric acid (b), and nitric acid (c) containing 0.1 µM 4-Cl-PIMT. (**C**) Influence of the concentration of nitric acid on the peak current of 0.1 µM 4-Cl-PIMT. (**D**) Effect of pH on the E_p of 0.1 µM 4-Cl-PIMT. (**E**) The proposed reduction mechanism of 4-Cl-PIMT at the surface of SPCE/CNFs.

2.3. CV Studies

The electrochemical responses of 4-Cl-PIMT (10.0 µM) at the SPCE/CNFs in 0.025 M HNO_3 were examined using cyclic voltammetry (CV). The CV curves were recorded for different values of scan rate (ν) from 20 to 450 mV s^{-1}. Figure 5A shows the CV curves for the selected ν of 50, 100, and 200 mV s^{-1}. In the potential range used, one irreversible cathode peak was visible at -0.88 V (ν = 100 mV s^{-1}). The reduction peak potential shifted toward more negative values with the increase in scan rate, which confirmed that the analyte (4-Cl-PIMT) was irreversibly reduced. More information about the electrochemical behaviour of 4-Cl-PIMT at the SPCE/CNFs was obtained based on the measured values of the reduction peak current at various scan rates (20–450 mV s^{-1}). The dependence between the intensity of the peak current (I_p) and the square root of the scan rate ($\nu^{1/2}$) was plotted (Figure 5B), the non-linear course of which indicates that the 4-Cl-PIMT reduction process on the SPCE/CNF surface was adsorption-controlled. Furthermore, the relationship between the log of the peak current ($\log I_p$) and the log of the scan rate ($\log\nu$) was plotted (Figure 5C). The slope of 1.011 in the plot of $\log I_p$ vs. $\log\nu$ indicates that this process was purely adsorption-controlled [33].

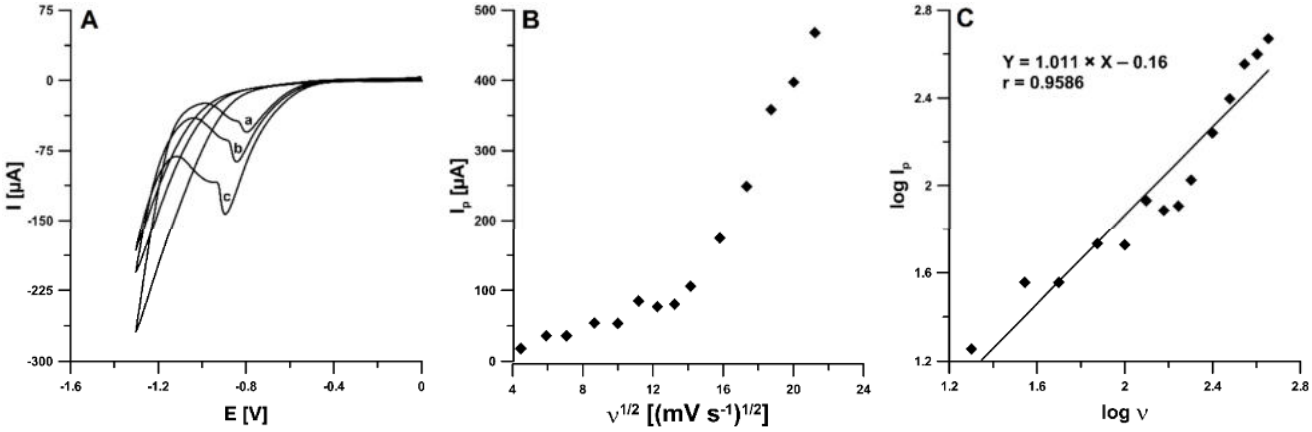

Figure 5. (**A**) Cyclic voltammograms of 10.0 µM 4-Cl-PIMT at ν of 50 (a), 100 (b), and 200 (c) mV s^{-1}. (**B**) The dependence between I_p and $\nu^{1/2}$. (**C**) The dependence between logI_p and logν for ν from 20 to 450 mV s^{-1}.

2.4. Effect of SWAdSV Parameters

Due to the confirmation of the adsorption of the 4-Cl-PIMT onto the surface of SPCE/CNFs by CV, we decided to evaluate the influence of parameters such as the accumulation potential (E_{acc}) and time (t_{acc}) on the peak current of this compound. The accumulation potential was varied over the range from −0.2 to 0.3 V, and t_{acc} was equal to 45 s. Figure 6A shows that the peak current increased when the accumulation potential was changed from −0.2 V towards more positive values and reached its maximum intensity at 0.1 V. Further increasing the potential value did not increase the analytical signal. For the selected value of E_{acc}, the effect of accumulation time was investigated in the range of 15–600 s. As can be seen, in Figure 6B, the highest peak current was obtained for an accumulation time of 600 s; however, to make the analysis less time consuming, 120 s was chosen for further study. To further improve the detection limit, an accumulation time greater than 120 s is recommended.

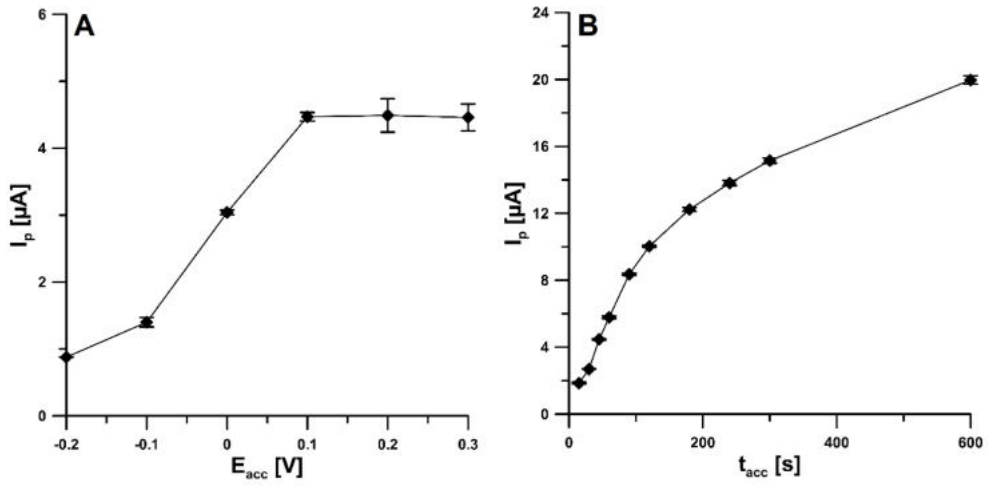

Figure 6. Influence of E_{acc} (**A**) and t_{acc} (**B**) on the peak current intensity of 20.0 nM 4-Cl-PIMT. The mean values of I_p are given with the standard deviation for n = 3.

The influence of the square-wave frequency (f) on the analytical signal of the 20.0 nM 4-Cl-PIMT was studied in the range of 10–200 Hz (Figure 7A). For further research, we decided to choose an f value of 75 Hz. The next step was to select the appropriate step-potential (ΔE) value. For this purpose, the influence of this parameter was investigated from 2 to 9 mV (Figure 7B). An increase in the peak current was observed as the step potential increased to 7 mV and then decreased. Therefore, 7 mV was considered the

optimal value. In addition, an influence of the square-wave amplitude (E_{SW}) was checked over the range from 25 to 200 mV (Figure 7C, f of 75 Hz and ΔE of 7 mV). The highest 4-Cl-PIMT peak current was obtained for the E_{SW} value of 150 mV.

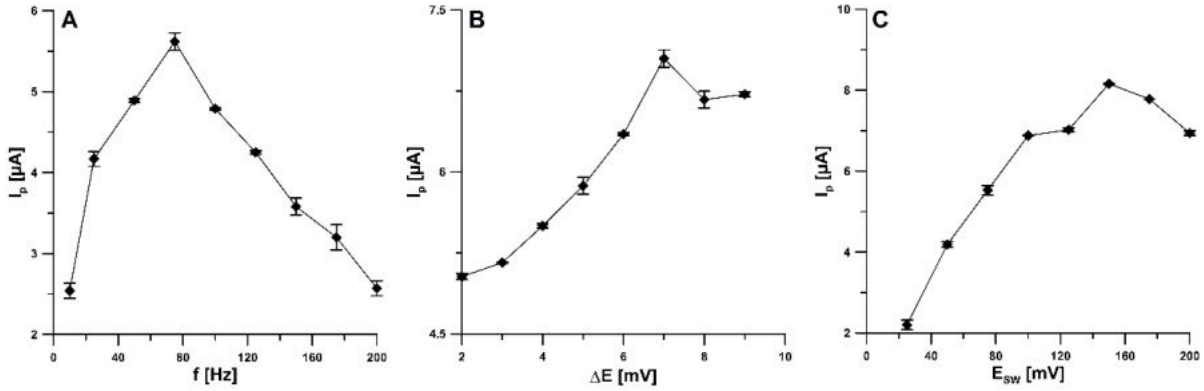

Figure 7. Effect of f (**A**), ΔE (**B**), and E_{SW} (**C**) on the analytical signal of 20 nM 4-Cl-PIMT. E_{acc} of 0.1 V and t_{acc} of 120 s. The mean values of I_p are given with the standard deviation for n = 3.

2.5. Analytical Performance

Under the optimised experimental conditions presented above, the 4-Cl-PIMT was analysed on the SPCE/CNFs by SWAdSV. The reduction current responses were found to be proportional in the two linear ranges of 0.5–10 nM and 10–100 nM (Figure 8A,B). This is probably connected with the fact that at concentrations higher than 10 nM, saturation took place or the analyte transport mechanism was altered. The limits of detection (LOD) and quantification (LOQ) were calculated at 0.099 and 0.33 nM, respectively, using the following formulas: LOD = 3SDa/b and LOQ = 10SDa/b (SDa, standard deviation of intercept (n = 3); b, slope of calibration curve) [34].

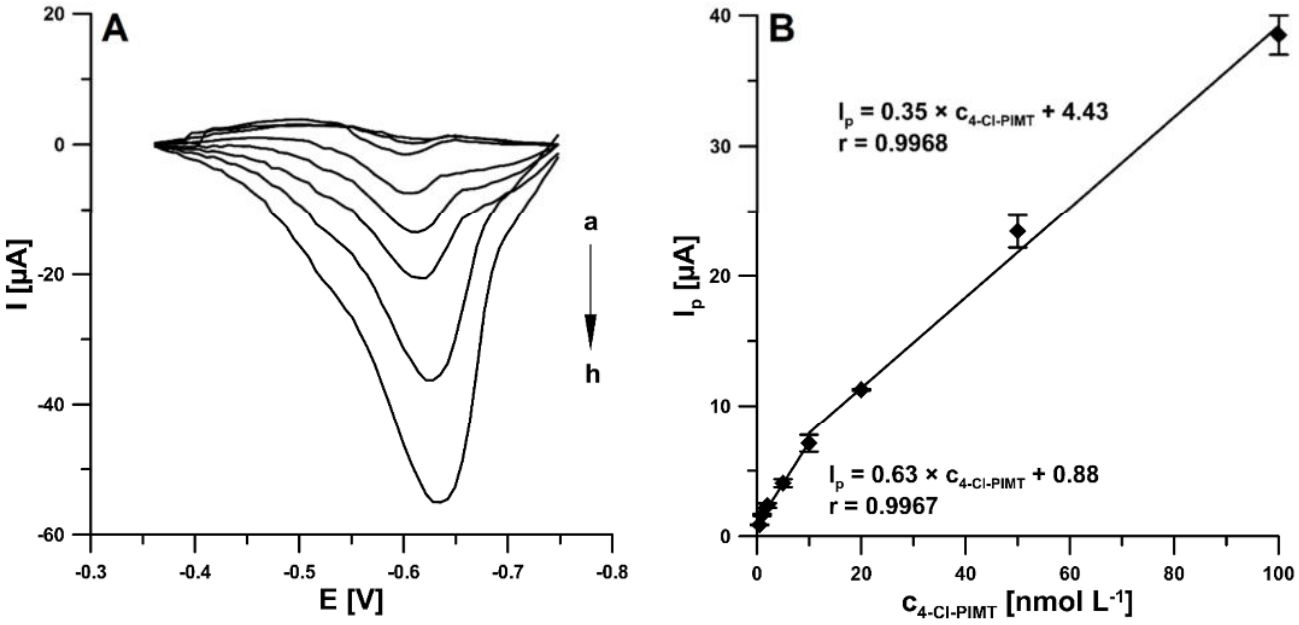

Figure 8. (**A**) Voltammograms obtained at the SPCE/CNFs in the 0.025 M solution of HNO_3 containing increasing concentrations of 4-Cl-PIMT: (a) 0.5, (b) 1.0, (c) 2.0, (d) 5.0, (e) 10.0, (f) 20.0, (g) 50.0, and (h) 100.0 nM. (**B**) Calibration plot of 4-Cl-PIMT. SWAdSV parameters: E_{acc} of 0.1 V, t_{acc} of 120 s, f of 75 Hz, ΔE of 7 mV, and E_{SW} of 150 mV. The mean values of I_p are given with the standard deviation for n = 3.

The 4-Cl-PIMT analytical peak at the SPCE/CNFs displays very good repeatability, with an RSD of 2.2% (20.0 nM 4-Cl-PIMT, n = 10). To examine the reproducibility of SPCE/CNFs, three different sensors were applied for the analysis of 20.0 nM 4-Cl-PIMT. The RSD value of 5.1% (n = 9) confirmed the acceptable reproducibility of the SPCE/CNFs.

2.6. Selectivity

We examined the effect of interferences that can potentially occur in biological fluids on the electrochemical response of 4-Cl-PIMT. The tolerance limit was defined as the concentration that gave an error of ≤10% in the assay of 5 nM 4-Cl-PIMT. It was observed that glucose (up to 2000-fold excess), epinephrine (up to 1000-fold excess), ascorbic acid (up to 1000-fold excess), uric acid (up to 1000-fold excess), Cl(-I) (up to 1000-fold excess), adenine (up to 200-fold excess), Ca(II) (up to 200-fold excess), dopamine (up to 100-fold excess), Mg(II) (up to 100-fold excess), and Fe(III) (up to 40-fold excess) had negligible effects on the assay of 4-Cl-PIMT (Figure 9). Considering that the developed procedure is intended to be used for the determination of 4-Cl-PIMT in biological samples, the influence of human serum on the analytical signal of 5 nM 4-Cl-PIMT was also investigated. Due to the significant influence of the serum matrix on the analyte peak current, we decided to use a flow system in the analysis of real samples in order to reduce the influence of interferents present therein. A comparison of the effect of serum on the voltammetric response of 5 nM 4-Cl-PIMT in the classical and flow systems is presented in Figure 10.

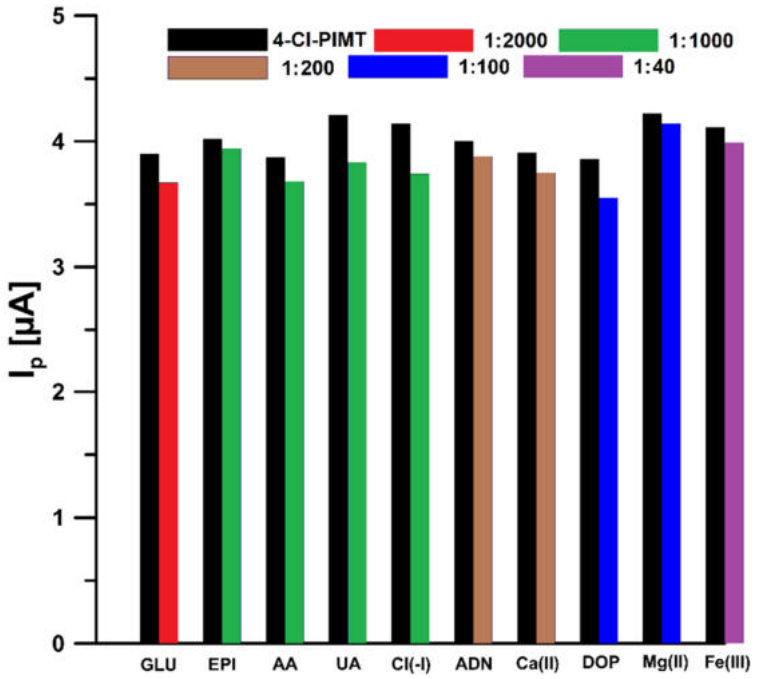

Figure 9. Histogram bars of the 5 nM 4-Cl-PIMT peak current in the presence of interferents. GLU—glucose, EPI—epinephrine, AA—ascorbic acid, UA—uric acid, ADN—adenine, DOP—dopamine.

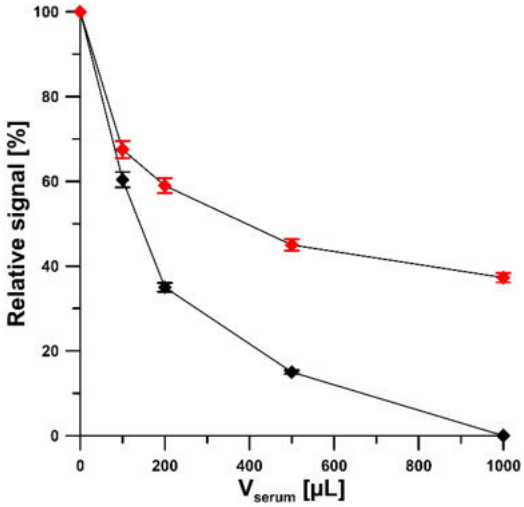

Figure 10. Effect of human serum on the 5 nM 4-Cl-PIMT peak current in the classic (black) and flow (red) systems.

2.7. Serum Sample Analysis

In order to confirm the usefulness of the developed voltammetric procedure using SPCE/CNFs, 4-Cl-PIMT was determined in spiked human serum samples. As mentioned in Section 2.6, in order to minimise interference from the sample matrix, a flow system was used, in which, after the accumulation step, a supporting electrolyte solution was introduced to the flow cell, followed by recording of the voltammograms. This procedure was aimed at removing the sample solution from the near-electrode space in order to reduce the probability of reducing interferents at the stage of recording the analytical signal. Additionally, for the same purpose, we decided to reduce the accumulation time from 120 to 30 s. Table 1 summarises the results obtained in the flow electrochemical cell. The recovery values obtained by SWAdSV were 100.7 and 105.0%. The SWAdSV results were compared to those obtained by ultra-high-performance liquid chromatography coupled with electrospray ionization/single-quadrupole mass spectrometry (UHPLC-ESI-MS). As can be seen, the relative error values between the results obtained by SWAdSV and UHPLC-ESI-MS are satisfying, amounting to 2.18 and 9.48%, respectively.

Table 1. Results of 4-Cl-PIMT determination in human serum samples.

4-Cl-PIMT Concentration [nM] ± SD (n = 3)					
Added	**Found SWAdSV**	**Found UHPLC-ESI-MS**	**Recovery * SWAdSV [%]**	**Recovery ** UHPLC-ESI-MS [%]**	**Relative Error *** [%]**
2.0	2.10 ± 0.072	2.32 ± 0.34	105.0	116.0	9.48
20.0	20.13 ± 0.55	19.7 ± 0.30	100.7	98.5	2.18

* Recovery [%] = (Found SWAdSV × 100)/Added; ** Recovery [%] = (Found UHPLC-ESI-MS × 100)/Added; *** Relative error [%] = ((|Found UHPLC-ESI-MS—Found SWAdSV|)/Found UHPLC-ESI-MS) × 100.

3. Materials and Methods

3.1. The Investigated Electroactive Molecule

4-Cl-PIMT was chosen for the current electrochemical research and was freshly re-synthesised from 1-(4-chlorophenyl)-2-hydrazinylideneimidazolidine hydroiodide (as the starting nucleophilic building block) and α-oxophenylacetic acid (as the electrophilic annulation reagent), according to one of the original synthetic approaches described in [1]. The analyte had a fully defined molecular structure, as all its spectroscopic data (see Supplementary Material Table S1) were consistent with those previously reported [1]. This highly pure white organic compound had a sharp melting point (275–276 °C) after recrystallization from a binary solvent mixture of dichloromethane/methanol. Furthermore, when dis-

solved in buffer/acetonitrile and injected into the immobilised-artificial-membrane (IAM) column, the 4-Cl-PIMT revealed a symmetric peak of a Gaussian shape in its chromatogram (Figure S1 in the Supplementary Materials).

3.2. Apparatus

Voltammetric measurements were performed using a μAutolab analyser (Eco Chemie, Utrecht, The Netherlands) controlled by GPES 4.9 software in an electrochemical quartz cell with a commercially available screen-printed sensor (Metrohm-DropSens, Oviedo, Spain). The same analyser controlled by FRA 4.9 software was also used to record Nyquist plots in the electrochemical impedance spectroscopy (EIS) method. The three-electrode commercially available sensors consisted of a carbon working electrode unmodified or modified with carbon nanofibers or multiwalled carbon nanotubes, as well as a carbon auxiliary electrode and a silver pseudo-reference electrode (SPCE, ref. 110; SPCE/CNFs, ref. 110CNF and SPCE/MWCNTs, ref. 110CNT). The experiments on the flow system were carried out using a peristaltic pump-type MS-CA (Ismatec, Wertheim, Germany) and a commercially available methacrylate wall-jet flow cell (FLWCL, DropSens, Llanera, Spain). Chromatographic measurements were conducted using an Agilent Technologies 1200 Infinity ultra-high-performance liquid chromatography system consisting of an autosampler, degasser, binary pump, and column thermostat connected to an Agilent Technologies 6120 quadrupole mass spectrometer equipped with an electrospray ionization source (API-ESI) (Wilmington, DE, USA). Chromatographic separation was achieved on a Zorbax Eclipse Plus C18 rapid-resolution HT (2.1 × 50 mm, 1.8 μm) analytical column protected by a Zorbax Eclipse Plus-C18 narrow-bore guard column (2.1 × 12.5 mm, 5 μm), both purchased from Agilent Technologies.

3.3. Reagents and Solutions

The solutions of sulfuric acid, acetic acid, nitric acid, and acetate buffers of different pH were prepared from Sigma-Aldrich reagents. Merck (Darmstadt, Germany) standard solutions of Ca(II), Mg(II), Fe(II), and Cl(-I), as well as Sigma-Aldrich (Saint Louis, MO, USA) reagents (adenine, dopamine, epinephrine, glucose, uric acid, and ascorbic acid) were used in interference studies. For voltammetric measurements, a 1.0 mM solution of 4-Cl-PIMT was prepared in N,N-dimethylformamide (Sigma-Aldrich, Saint Louis, MO, USA). For UHPLC-ESI-MS analysis, acetonitrile (Merck, Darmstadt, Germany), formic acid (LC-MS, Sigma, Saint Louis, MO, USA), and trichloroacetic acid (TCA, Sigma-Aldrich, Saint Louis, MO, USA) were used. A stock solution of the analyte (1 g L^{-1}) was prepared in dimethyl sulfoxide (DMSO, Merck, Darmstadt, Germany). Working solutions of the analyte were prepared in 0.1% (v/v) formic acid in acetonitrile. All solutions were prepared using ultra-purified water (>18 MΩ cm, Milli-Q system, Millipore, UK).

3.4. 4-Cl-PIMT SWAdSV Analysis

Voltammetric measurements of 4-Cl-PIMT were carried out in a classic electrochemical cell under optimised conditions in 0.025 M solution of HNO_3. An accumulation potential (E_{acc}) of 0.1 V was applied during stirring for 120 s (accumulation time, t_{acc}). Voltammograms were recorded within the potential range from −0.2 to −1.0 V with a frequency (f) of 75 Hz, a step potential (ΔE) of 7 mV, and a square-wave amplitude (E_{SW}) of 150 mV. The background curve was subtracted from each voltammogram. In the flow system during serum sample analysis, in the first step 0.025 M solution of HNO_3 containing the spiked sample for 40 s was directed through the cell in order to accumulate the analyte on the surface of SPCE/CNFs. During this step, an accumulation potential of 0.1 V was used. Then, 0.025 M HNO_3 was directed to the cell for 10 s in order to remove the sample solution, and voltammograms were recorded. The average values of I_p are shown with the standard deviation of n = 3.

3.5. 4-Cl-PIMT UHPLC-ESI-MS Analysis

Volumes of 0.1% (v/v) formic acid in water (A) and acetonitrile (B) were used as solvents for elution (flow rate of 0.3 mL min^{-1}). The gradient used for the analysis was as follows: 15% B at 0 min, 70% B at 7–8 min, 15% B at 10 min (post run: 2 min). The injection volume and column temperature were 5 µL and 40 °C, respectively. Spectra were recorded in positive-ion mode, with a capillary voltage of 4000 V, nebuliser pressure of 45 psi, drying gas flow of 11 L min^{-1} at 350 °C, and fragmentor voltage of 140 V. Selected ion monitoring (SIM) was used to record the abundance of the $[M + H]^+$ ion peak at m/z 325.1 (retention time: ~6.78 min)

3.6. Serum Sample Analysis

Normal human serum purchased from Merck (Darmstadt, Germany) was tested. Frozen human serum was thawed at room temperature. Then, 100 µL of the human serum sample was 100 times diluted in deionised water spiked with appropriate concentrations of the analyte, transferred to a centrifugal tube, mixed with 50 µL of 7.5% (w/v) TCA solution (Sigma-Aldrich, Saint Louis, MO, USA) in order to precipitate proteins, centrifuged at 4000× g for 10 min, and filtered through a 0.22 µm Millipore filter. The supernatant was analysed in triplicate by the optimised voltammetric procedure and UHPLC-ESI-MS method.

4. Conclusions

In the present studies, a screen-printed carbon electrode modified with carbon nanofibers (SPCE/CNFs) was proposed as the sensor in the first analytical procedure allowing for the selective and sensitive determination of the most promising anticancer drug candidate from a class of disubstituted fused triazinones, i.e., 4-Cl-PIMT. The increase in the analytical signal of the 4-Cl-PIMT at the SPCE/CNFs compared to an unmodified SPCE results from an increase in the active surface of the working electrode and a reduction in the charge-transfer resistance. The developed SWAdSV procedure is characterised by good sensitivity and selectivity. The calculated LOD and LOQ values were found to be 0.099 and 0.33 nM, respectively. The developed procedure using SPCE/CNFs was successfully used to determine the title analyte in human serum samples. The flow system minimised the effect of human serum matrix on the analyte signal. The SWAdSV results were compared to those obtained by the UHPLC-ESI-MS method, and the relative error values between the results obtained by both methods proved to be satisfying (2.18% and 9.48%). The 4-Cl-PIMT analytical peak at the SPCE/CNFs as a sensor displayed high reproducibility and repeatability.

Supplementary Materials: The following supporting information can be downloaded at: https://www.mdpi.com/article/10.3390/ijms23052429/s1.

Author Contributions: Conceptualization, J.K., K.T.-R. and K.S.; investigation, J.K, K.T.-R., I.S., K.S. and M.S.; writing—original draft preparation, J.K, K.T.-R., I.S., K.S. and M.S.; writing—review and editing, J.K, K.T.-R., I.S., K.S. and M.S.; supervision, K.T.-R. and K.S. All authors have read and agreed to the published version of the manuscript.

Funding: This research received no external funding.

Institutional Review Board Statement: Not applicable.

Informed Consent Statement: Not applicable.

Data Availability Statement: The data presented in this study are available on request from the corresponding author. A sample of the investigated compound (4-Cl-PIMT) is available from the corresponding author.

Acknowledgments: The authors gratefully acknowledge the use of the services and facilities of the Center for Interdisciplinary Research of The John Paul II Catholic University of Lublin, Lublin, Poland, supported by the European Union through the European Regional Development Fund under

the Operational Programme Development of Eastern Poland 2007–2013 (agreement POPW.01.03.00-06-003/09-00).

Conflicts of Interest: The authors declare no conflict of interest.

References

1. Sztanke, K.; Pasternak, K.; Sztanke, M.; Kandefer-Szerszeń, M.; Kozioł, A.E.; Dybała, I. Crystal structure, antitumour and antimetastatic activities of disubstituted fused 1,2,4-triazinones. *Bioorg. Med. Chem. Lett.* **2009**, *19*, 5095–5100. [CrossRef]
2. Janicka, M.; Sztanke, M.; Sztanke, K. Reversed-phase liquid chromatography with octadecylsilyl, immobilized artificial membrane and cholesterol columns in correlation studies with in silico biological descriptors of newly synthesized antiproliferative and analgesic active compounds. *J. Chromatogr. A* **2013**, *1318*, 92–101. [CrossRef] [PubMed]
3. Janicka, M.; Sztanke, M.; Sztanke, K. Predicting the blood-brain barrier permeability of new drug-like compounds via HPLC with various stationary phases. *Molecules* **2020**, *25*, 487. [CrossRef]
4. Sztanke, M.; Tuzimski, T.; Janicka, M.; Sztanke, K. Structure-retention behaviour of biologically active fused 1,2,4-triazinones—Correlation with in silico molecular properties. *Eur. J. Pharm. Sci.* **2015**, *68*, 114–126. [CrossRef] [PubMed]
5. Cao, F.; Dong, Q.; Li, C.; Chen, J.; Ma, X.; Huang, Y.; Song, D.; Ji, C.; Lei, Y. Electrochemical sensor for detecting pain reliever/fever reducer drug acetaminophen based on electrospun CeBiOx nanofibers modified screen-printed electrode. *Sens. Actuators B* **2018**, *256*, 143–150. [CrossRef]
6. Seguro, I.; Pacheco, J.G.; Delerue-Matos, C. Low cost, easy to prepare and disposable electrochemical molecularly imprinted sensor for diclofenac detection. *Sensors* **2021**, *21*, 1975. [CrossRef]
7. Jahani, P.M.; Mohammadi, S.Z.; Khodabakhshzadeh, A.; Asl, M.S.; Jang, H.W.; Shokouhimehr, M.; Zhang, K.; Van Le, Q.; Peng, W. Simultaneous voltammetric detection of acetaminophen and tramadol using molybdenum tungsten disulfide-modified graphite screen-printed electrode. *Int. J. Electrochem. Sci.* **2020**, *15*, 9024–9036. [CrossRef]
8. Zhang, Y.; Jiang, X.; Zhang, J.; Zhang, H.; Li, Y. Simultaneous voltammetric determination of acetaminophen and isoniazid using MXene modified screen-printed electrode. *Biosens. Bioelectron.* **2019**, *130*, 315–321. [CrossRef]
9. Baezzat, M.R.; Tavakkoli, N.; Zamani, H. Construction of a new electrochemical sensor based on MoS_2 nanosheets modified graphite screen printed electrode for simultaneous determination of diclofenac and morphine. *Anal. Bioanal. Chem. Res.* **2022**, *9*, 153–162.
10. Zhang, C.; Cao, Z.; Zhang, G.; Yan, Y.; Yang, X.; Chang, J.; Song, Y.; Jia, Y.; Pan, P.; Mi, W.; et al. An electrochemical sensor based on plasma-treated zinc oxide nanoflowers for the simultaneous detection of dopamine and diclofenac sodium. *Microchem. J.* **2020**, *158*, 105237J. [CrossRef]
11. Amin, S.; Soomro, M.T.; Memon, N.; Solangi, A.R.; Uddin, S.; Qureshi, T.; Behzad, A.R. Disposable screen printed graphite electrode for the direct determination of ibuprofen in surface water. *Environ. Nanotechnol. Monit. Manag.* **2014**, *1–2*, 8–13. [CrossRef]
12. Serrano, N.; Castilla, O.; Ariño, C.; Diaz-Cruz, M.S.; Diaz-Cruz, J.M. Commercial screen-printed electrodes based on carbon nanomaterials for a fast and cost-effective voltammetric determination of paracetamol, ibuprofen and caffeine in water samples. *Sensors* **2019**, *19*, 4039. [CrossRef] [PubMed]
13. Ma, L.-L.; He, Y.; Qin, D.; Chang, A.; Huang, A.; Xie, X.-J.; Zhang, Y. Fabrication, characterization and performance evaluation of screen-printed carbon electrodes: Determination of acetaminophen in Tylenol. *Chin. J. Anal. Chem.* **2021**, *49*, 21187–21196. [CrossRef]
14. Sima, V.; Cristea, C.; Bodoki, E.; Duţu, G.; Săndulescu, R. Screen-printed electrodes modified with HRP-zirconium alkoxide film for the development of a biosensor for acetaminophen detection. *Cent. Eur. J. Chem.* **2010**, *8*, 1034–1040.
15. Raymundo-Pereira, P.A.; Gomes, N.O.; Machado, S.A.S.; Oliveira, O.N., Jr. Simultaneous, ultrasensitive detection of hydroquinone, paracetamol and estradiol for quality control of tap water with a simple electrochemical method. *J. Electroanal. Chem.* **2019**, *848*, 113319. [CrossRef]
16. Kruanetr, S.; Prabhu, R.; Pollard, P.; Fernandez, C. Pharmaceutical electrochemistry: The electrochemical detection of aspirin utilising screen printed Graphene electrodes as sensors platforms. *Surf. Eng. Appl. Electrochem.* **2015**, *51*, 283–289. [CrossRef]
17. Stefano, J.S.; Montes, R.H.O.; Richter, E.M.; Munoz, R.A.A. Flow-injection analysis with multiple-pulse amperometry for simultaneous determination of paracetamol and naproxen using a homemade flow cell for screen-printed electrodes. *J. Braz. Chem. Soc.* **2014**, *25*, 484–491. [CrossRef]
18. Kondori, T.; Tajik, S.; Akbarzadeh, T.N.; Beitollahi, H.; Graiff, C.; Jang, H.W.; Shokouhimehr, M. Synthesis and characterization of bipyridine cobalt(II) complex modified graphite screen printed electrode: An electrochemical sensor for simultaneous detection of acetaminophen and naproxen. *RSC Adv.* **2021**, *11*, 3049–3057. [CrossRef]
19. Bagherinasab, Z.; Beitollahi, H.; Yousefi, M.; Bagherzadeh, M.; Hekmati, M. Rapid sol gel synthesis of BaFe12O19 nanoparticles: An excellent catalytic application in the electrochemical detection of tramadol in the presence of acetaminophen. *Microchem. J.* **2020**, *156*, 104803. [CrossRef]
20. Jahani, P.M.; Mohammadi, S.Z.; Khodabakhshzadeh, A.; Cha, J.W.; Asl, M.S.; Jang, H.W.; Shokouhimehr, M.; Zhang, K.; Van Le, Q.; Peng, W. Simultaneous voltammetric detection of morphine and diclofenac using graphene nanoribbon modified screen-printed electrode. *Int. J. Electrochem. Sci.* **2020**, *15*, 9037–9048. [CrossRef]

21. Yaghoubian, H.; Tajik, S.; Baitollahi, H.; Sarhadi, H.; Sheikhshoaie. Fe_2MoO_4 magnetic nanocomposite modified screen printed graphite electrode as a voltammetric sensor for simultaneous determination of nalbuphine and diclofenac. *J. Mater. Sci. Mater. Electron.* **2021**, *32*, 17311–17323. [CrossRef]
22. Jahromi, Z.; Mirzael, E.; Savardashtaki, A.; Afzali, M.; Afzali, Z. A rapid and selective electrochemical sensor based on electrospun carbon nanofibers for tramadol detection. *Microchem. J.* **2020**, *157*, 104942. [CrossRef]
23. Apetrei, I.M.; Bejinaru, A.A.; Boev, M.; Apetrei, C.; Buzia, O.D. Determination of ibuprofen based on screen-printed electrodes modified with carbon nanofibers. *Farmacia* **2017**, *65*, 790–795.
24. Bounegru, A.V.; Apetrei, C. Voltamperometric sensors and biosensors based on carbon nanomaterials used for detecting of caffeic acid-a review. *Int. J. Mol. Sci.* **2020**, *21*, 9275. [CrossRef] [PubMed]
25. Sipa, K.; Brycht, M.; Leniart, A.; Skrzypek, S. The application of carbon nanomaterials as electrode surface modifiers for the voltammetric sensing of nitroxinil—A comparative studies. *J. Electroanal. Chem.* **2019**, *848*, 113294. [CrossRef]
26. Kaewket, K.; Karuwan, C.; Sonsupap, S.; Maensiri, S.; Ngamchuea, K. Anti-fouling effects of carbon nanofiber in electrochemical sensing of phenolic compounds. *J. Electrochem. Soc.* **2021**, *168*, 067501. [CrossRef]
27. Sasal, A.; Tyszczuk-Rotko, K.; Wójciak, M.; Sowa, I. First electrochemical sensor (screen-printed carbon electrode modified with carboxyl functionalized multiwalled carbon nanotubes) for ultratrace determination of diclofenac. *Materials* **2020**, *13*, 781. [CrossRef] [PubMed]
28. Sasal, A.; Tyszczuk-Rotko, K.; Wójciak, M.; Sowa, I.; Kuryło, M. Simultaneous analysis of paracetamol and diclofenac using MWCNTs-COOH modified screen-printed carbon electrode and pulsed potential accumulation. *Materials* **2020**, *13*, 3091. [CrossRef] [PubMed]
29. Tyszczuk-Rotko, K.; Kozak, J.; Sztanke, M.; Sztanke, K.; Sadok, I. A screen-printed sensor coupled with flow system for quantitative determination of a novel promising anticancer agent candidate. *Sensors* **2020**, *20*, 5217. [CrossRef]
30. Ludvik, J.; Zuman, P. Electrochemical proof of the single bond character of the N–N bonds in some 1,2,4-triazines. *Indian J. Chem.* **2003**, *42A*, 847–848.
31. Stępniowska, A.; Sztanke, M.; Tuzimski, T.; Korolczuk, M.; Sztanke, K. A simple stripping voltammetric method for the determination of a new anticancer prodrug in serum. *Biosens. Bioelectron.* **2017**, *94*, 584–588. [CrossRef] [PubMed]
32. Ludvik, J.; Riedl, F.; Liska, F.; Zuman, P. Electrochemical reduction of metamitron. *J. Electroanal. Chem.* **1998**, *457*, 177–190. [CrossRef]
33. Gosser, D.K. *Cyclic Voltammetry, Simulation and Analysis of Reaction Mechanisms*; Wiley VCH: New York, NY, USA, 1993.
34. Mocak, J.; Bond, A.M.; Mitchell, S.; Scollary, G. A statistical overview of standard (IUPAC and ACS) and new procedures for determining the limits of detection and quantification: Application to voltammetric and stripping techniques. *Pure Appl. Chem.* **1997**, *69*, 297–328. [CrossRef]

RD7

J. Kozak, K. Tyszczuk-Rotko, R. Metelka, *Voltammetric quantification of anti-cancer antibiotic bleomycin using an electrochemically pretreated and decorated with lead nanoparticles screen-printed sensor,* International Journal of Molecular Sciences, 24 (1) (2022) 472-484.

International Journal of
Molecular Sciences

MDPI

Article

Voltammetric Quantification of Anti-Cancer Antibiotic Bleomycin Using an Electrochemically Pretreated and Decorated with Lead Nanoparticles Screen-Printed Sensor

Jędrzej Kozak [1], Katarzyna Tyszczuk-Rotko [1,*] and Radovan Metelka [2]

[1] Faculty of Chemistry, Institute of Chemical Sciences, Maria Curie-Skłodowska University, 20-031 Lublin, Poland
[2] Department of Analytical Chemistry, Faculty of Chemical Technology, University of Pardubice, 532 10 Pardubice, Czech Republic
* Correspondence: katarzyna.tyszczuk-rotko@mail.umcs.pl

Abstract: In this paper, we report a highly sensitive voltammetric sensor for the determination of the anti-cancer antibiotic bleomycin (BLM) based on a screen-printed carbon sensor that is electrochemically pretreated and decorated with lead nanoparticles in the sample solution (pSPCE/PbNPs). These sensor surface manipulations contribute to significant amplification of the analytical signal and improvement of its shape and repeatability. The effect of the electrochemical behavior of BLM on the pSPCE/PbNPs was examined by electrochemical strategies. CV, EIS, and XPS were used to compare the sensor surface modifications. The effects of the type and pH of the supporting electrolyte and the procedure parameters were optimized. The features of the proposed procedure include: (a) very low limits of detection and quantification (2.8×10^{-11} and 9.3×10^{-11} M, respectively), (b) linear ranges (1.0×10^{-10}–2.0×10^{-9} M and 2.0×10^{-9}–2.0×10^{-8} M, and (c) a high sensitivity of 0.32 μA/nM. The electrochemical sensor was successfully applied for the determination of BLM in wastewater and reference material of human urine samples.

Keywords: electrochemically prepared screen-printed carbon electrode; lead nanoparticles; anti-cancer antibiotic; bleomycin; voltammetry; human urine and wastewater sample

Citation: Kozak, J.; Tyszczuk-Rotko, K.; Metelka, R. Voltammetric Quantification of Anti-Cancer Antibiotic Bleomycin Using an Electrochemically Pretreated and Decorated with Lead Nanoparticles Screen-Printed Sensor. *Int. J. Mol. Sci.* **2023**, *24*, 472. https://doi.org/10.3390/ijms24010472

Academic Editors: Gohar Khachatryan and Magdalena Krystyjan

Received: 24 November 2022
Revised: 16 December 2022
Accepted: 20 December 2022
Published: 28 December 2022

1. Introduction

Cancer is one of the most dangerous diseases and one of the greatest challenges of modern medicine. The use of anti-cancer drugs is still the basic method of treatment [1]. One of the anti-cancer drugs is bleomycin (BLM), which is a mixture of natural structurally related glycopeptide antibiotics produced by the bacterium *Streptomyces verticillus*. Clinically used bleomycin contains mainly bleomycin A2 and B2 and small amounts of other subfractions [2–4]. In combination with other chemotherapeutic agents, BLM is used in the treatment of many types of cancer. It is the first-line drug in the treatment of Hodgkin's lymphoma [5], but it is also used in the treatment of non-Hodgkin lymphomas and head, neck, and skin cancers. In combination therapy with cisplatin and etoposide, it is highly effective against testicular cancer [6]. BLM is also used in the treatment of malignant pleural effusion [7] and in sclerotherapy in patients with vascular malformations [8]. The wide use of BLM results from the fact that it causes myelosuppression and immunosuppression at a relatively low level [7,9].

The anti-tumor activity of BLM is related to the fact that it induces selective DNA cleavage. BLM produces this effect on both single-stranded and double-stranded DNA. In the presence of oxygen, BLM forms binary Fe(II)•BLM complexes with Fe(II) ions. When Fe(II) is oxidized to Fe(III), oxygen is reduced to free radicals, which then induce DNA cleavage, ultimately leading to cell death [7,10,11]. Despite the aforementioned relatively

low toxicity of BLM, the use of this substance is, however, associated with serious dose-limiting side effects, such as kidney and lung toxicity. Treatment with BLM may result in pneumonia progressing to irreversible pulmonary fibrosis with high mortality. An important risk factor is the cumulative BLM dose exceeding 300 mg [5,8,11]. Therefore, in order to achieve the best possible results of BLM therapy while minimizing its side effects, it is necessary to develop sensitive and selective methods of BLM determination in clinical samples.

Several methods allowing the determination of BLM can be found in the literature. High-performance liquid chromatography (HPLC) [2,12,13], high-performance liquid chromatography quadrupole-time of flight mass spectrometry (HPLC-QTOF-MS) [4], electrogenerated chemiluminescence (ECL) [7] or radioimmunoassay (RIA) can be mentioned here [9]. However, these methods require expensive equipment, are often time-consuming and labor-intensive, and generate a high consumption of reagents.

As an alternative, electrochemical methods can be proposed; they require relatively inexpensive devices, are simple, very sensitive, and selective, and also allow analyses to be performed in a short time. Only a few papers describing the voltammetric procedures for BLM determination are available. One of them [14] shows the use of a hanging mercury drop electrode (HMDE). The remaining articles [1,11,15] present voltammetric assays based on BLM-induced DNA strand scission. The lowest limit of detection (LOD), 7.4×10^{-13} mol L^{-1}, was obtained using the procedure described in [1]. Nonetheless, this procedure, similar to those described in [11,15], requires the complicated and time-consuming preparation of a working electrode modifier, which is DNA in this case, and the subsequent immobilization of DNA on the surface of the electrode. The DNA cleavage reaction itself, which is the basis for obtaining the BLM analytical signal, also takes a relatively long time (10 min, while in the case of other works, even several hours).

To the best of our knowledge, there have been no attempts to use screen-printed electrodes (SPEs) in BLM analysis so far. SPEs have been an increasingly popular type of electrode in recent years. They are characterized by low production costs and high commercial availability. The diversity of electrode materials used to produce SPEs and the ease of modification of the electrode surface make them a very versatile tool for the determination of a whole range of substances [16–18]. One of the ways to modify the electrode surface is the electrochemical deposition of metal particles, e.g., lead. The lead film electrode exhibited interesting characteristics, such as lower toxicity and volatility compared with the mercury electrodes, a wide potential window, the ability to operate in a wide range of pH media, good reproducibility, simple preparation, and a simple way of electrochemical surface renewal [19]. This paper presents for the first time the use of modified screen-printed electrodes for BLM detection. The use of the electrochemically prepared screen-printed carbon electrode decorated with lead nanoparticles (pSPCE/PbNPs) allowed highly sensitive and selective determination of BLM in urine and also, in environmental samples, in this case, municipal wastewater.

2. Results and Discussion

2.1. Sensor Characterization

Initially, the BLM voltammetric response at the electrochemically prepared screen-printed carbon electrode decorated with lead nanoparticles (pSPCE/PbNPs) was examined using square-wave adsorptive stripping voltammetry (SWAdSV). Measurements were made in 0.075 M acetate buffer (pH 4.5) with the addition of 75 µM Pb(II) and 2 nM BLM. Then, under the same conditions, SWAdSV curves were recorded on an unmodified screen-printed carbon electrode (SPCE), and the screen-printed carbon electrode was decorated with lead nanoparticles (SPCE/PbNPs) that had not been pretreated. In Figure 1, it can be seen that the modification of the electrode with PbNPs is necessary to obtain the BLM peak. In the case of the bare SPCE, no BLM reduction signal was observed (2 nM BLM—curve a), which was confirmed by measuring a higher concentration of the analyte (5 nM BLM—curve b). As can be seen, electrochemical pretreatment does not significantly affect the BLM

peak current intensity but causes a slight shift of the peak potential towards less negative potential values (−1.50 vs. −1.46 V) and improves the shape of the BLM peak. Moreover, pretreatment of the sensor before its use in a series of BLM measurements significantly improves the repeatability of the signal (5 nM BLM, RSD of 17.74% for the SPCE/PbNPs, and 3.25% for the pSPCE/PbNPs, n = 10), which is in line with our previous research [20]. We tried to explain this phenomenon using various analytical techniques.

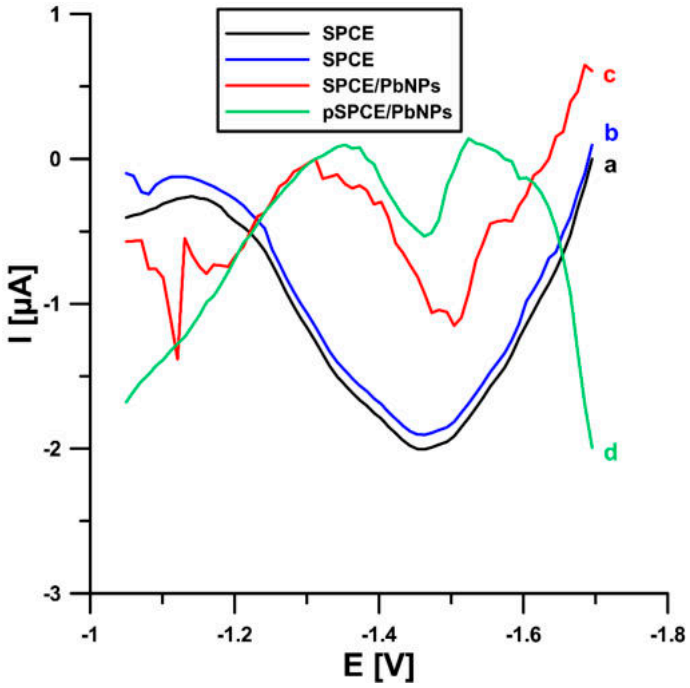

Figure 1. Comparison of the SWAdSV response for: (a and b) unmodified SPCE, (c) SPCE/PbNPs, and (d) pSPCE/PbNPs. BLM concentration of 2 (a, c, and d) and 5 (b) nM. $E_{acc.}$ = −1.0 V, $t_{acc.}$ = 120 s, f = 50 Hz, E_{SW} = 50 mV, and ΔE = 10 mV.

The pSPCE/PbNPs and the bare SPCE had been characterized using cyclic voltammetry (CV), electrochemical impedance spectroscopy (EIS), scanning and transmission electron microscopy (SEM and TEM), and energy-dispersive X-ray spectroscopy (EDS) in our previous research [20]. In paper [20], we stated that the electrochemically deposited lead nanoparticles were not visible in SEM images, but the PbNPs presence on the electrode surface was confirmed using a TEM–EDS. In this work, the research was supplemented by the analysis of the sensors using X-ray photoelectron spectroscopy (XPS) and the CV and EIS characteristics. The parameters for all tested sensors are summarized in Table 1. The active area of the SPCE/PbNPs electrode was calculated in the same way as for the other electrodes: CV measurements were made in a 0.1 M KCl solution containing 5 mM $K_3[Fe(CN)_6]$, and the Randles-Sevcik equation was used here [21]. It can be seen that the active surface area (A_s) significantly increases with modification with PbNPs (0.072 cm^2 for the SPCE, 0.23 cm^2 for the SPCE/PbNPs, 0.22 cm^2 for the pSPCE/PbNPs). However, electrochemical pretreatment does not contribute to an increase in As. Similarly, in the case of the value of the charge transfer resistance (R_{ct}), only the modification with PbNPs causes a slight decrease in the resistance in relation to the unmodified electrode (146.7 Ω cm^2 for the SPCE, 121.5 Ω cm^2 for the SPCE/PbNPs, 121.3 Ω cm^2 for the pSPCE/PbNPs). The XPS analysis shows that the percentage atomic concentration of Pb is as follows: 0.3% for the SPCE/PbNPs and 0.9% for the pSPCE/PbNPs. The higher content of lead is associated with its additional deposition during the electrochemical pretreatment of the sensor. However, this increase does not translate into an increase in As. A very interesting conclusion can be drawn after a careful analysis of the deconvoluted Pb4f signal. The metallic form of lead (55.6%) prevails over lead oxides (i.e., PbO) at the electrochemically pretreated

SPCE/PbNPs. In the case of the non-pretreated electrode, an opposite situation is observed since the metallic form of lead accounts for 40.3% of the total deposited lead film. Most probably, the increased proportion of metallic lead affects the repeatability of the deposited lead film before each measurement, thus contributing to the improvement in the shape of the BLM signal and its repeatability. Figure 2 shows the XPS spectrum of the SPCE/PbNPs and pSPCE/PbNPs, and the deconvoluted Pb4f region.

Table 1. Characteristics of the sensors.

Electrode	A_S [cm^2]	R_{ct} [Ω cm^2]	RSD [%] (n = 10)	Ref.
SPCE	0.072	146.7	-	[20]
SPCE/PbNPs	0.23	121.5	17.74	This work
pSPCE/PbNPs	0.22	121.3	3.25	[20]

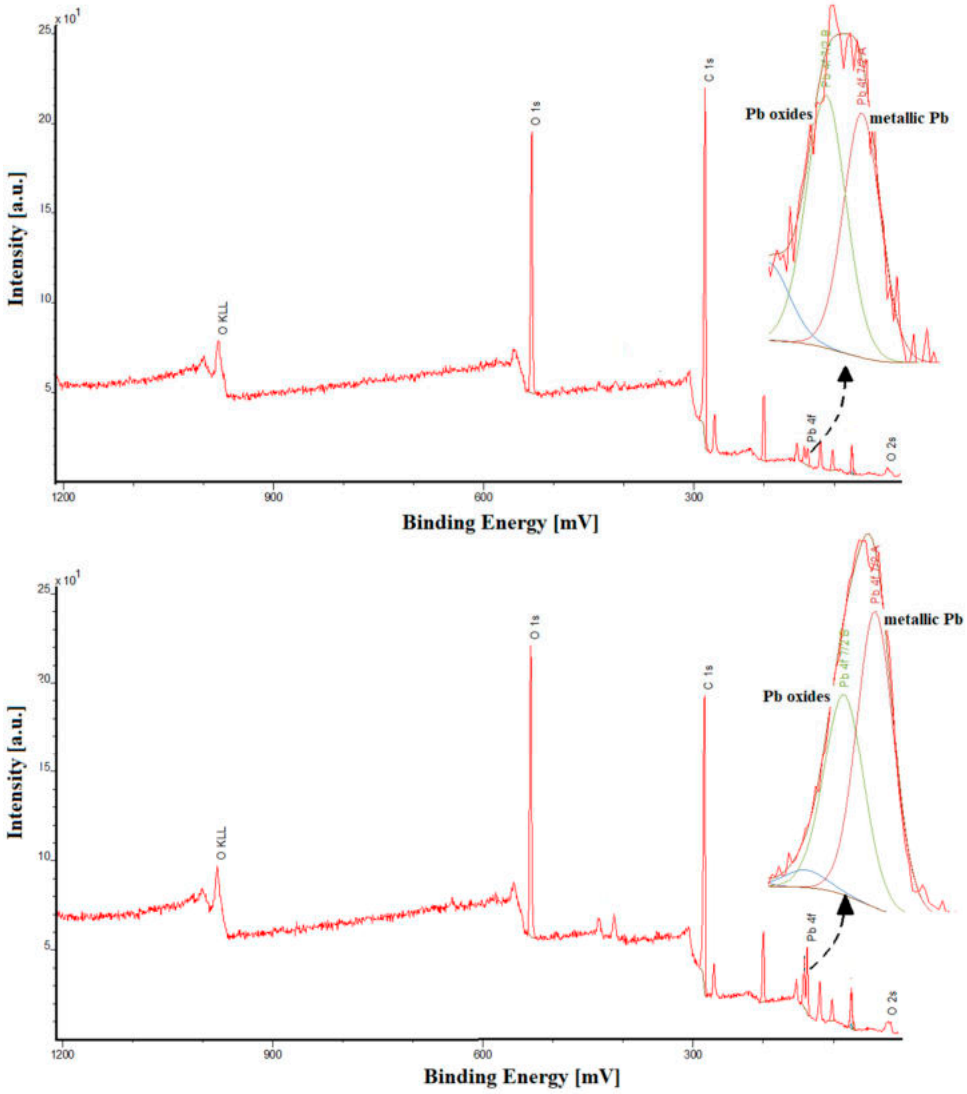

Figure 2. The XPS spectrum of the SPCE/PbNPs and pSPCE/PbNPs, and the deconvoluted Pb4f region.

2.2. Supporting Electrolyte Composition

The first step in optimizing the procedure was to select the appropriate type and pH of the supporting electrolyte. For this purpose, the influence of the pH value on the reduction signal of 2 nM BLM in the environment of acetic acid and NaAc—HAc solutions

with different pH were evaluated. An increase in the BLM peak current was observed with an increase in pH to 4.5, and then a decrease in the BLM signal above this value until it disappeared completely at a pH value of 5.9 (Figure 3A). In view of the obtained results, NaAc—HAc solution (pH 4.5) was selected for further research. Subsequently, the effect of the selected NaAc—HAc buffer concentration on the 2 nM BLM signal was also examined in the range from 0.01 to 0.1 M. The highest peak current was obtained with a buffer concentration of 0.05 M (Figure 3B), and therefore this concentration was considered optimal. The last component of the base electrolyte whose influence on the BLM peak current was checked was Pb(II). The effect of Pb(II) concentration on the 2 nM BLM reduction signal was investigated over a concentration range of 0.01 to 0.1 mM. The highest peak current was obtained at the Pb(II) ion concentration of 0.05 mM (Figure 3C), and this value was chosen for further studies.

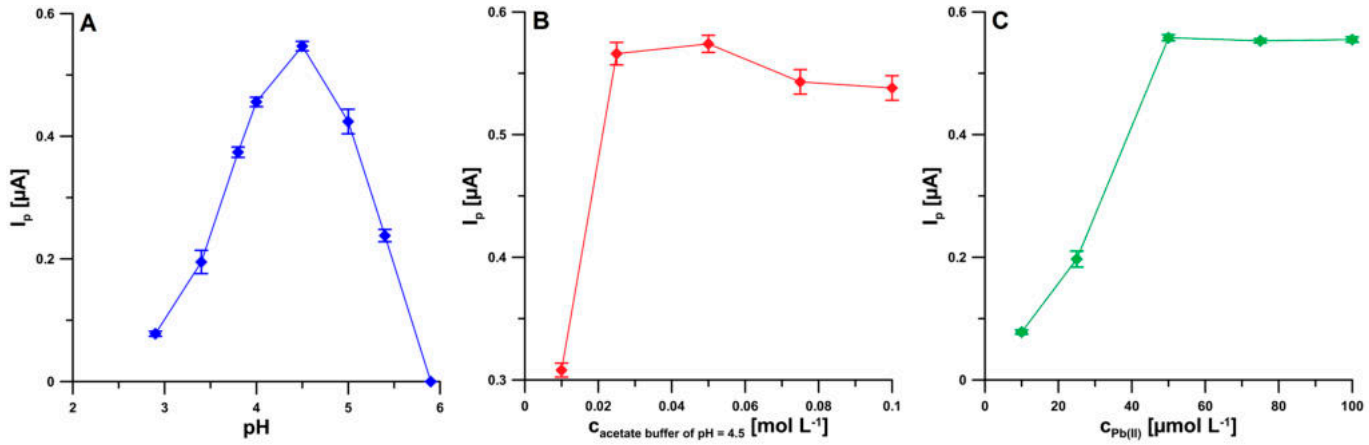

Figure 3. The dependence of pH (**A**), acetate buffer (**B**), and Pb(II) concentration (**C**) on the 2 nM BLM peak current. $E_{acc.}$ = −1.0 V, $t_{acc.}$ = 120 s, f = 50 Hz, E_{SW} = 50 mV, and ΔE = 10 mV. The received average values of the peak current are shown with a standard deviation for n = 3.

2.3. Voltammetric Behavior of BLM on the pSPCE/PbNPs

The voltammetric behavior of BLM at the pSPCE/PbNPs in the supporting electrolyte solution (0.05 M NaAc—HAc buffer of pH 4.5 and 0.05 mM Pb(II)) containing 0.1 µM BLM was examined using cyclic voltammetry. Figure 4A shows the CVs recorded for the supporting electrolyte (dashed line) and for 0.1 µM BLM (solid line) at a scan rate (υ) of 50, 100, and 200 mV/s. With the potential range used in the measurements, three cathode peaks were visible at potentials of −1.15, −1.45, and −1.65 V (ν = 200 mV/s). However, no oxidation signals were observed, which suggests that the BLM electroreduction process on the electrode is irreversible. Due to the best shape and repeatability of the signal at the potential of −1.45 V on the SWV voltammograms, this peak was selected for further study. In an attempt to determine the nature of the electrode process, the BLM reduction peak current was measured for increasing scan rates ranging from 5 to 200 mV/s. The linear course of the dependence of the peak current (I_p) on the square root of the scan rate ($\upsilon^{1/2}$) (Figure 4B) suggests that the process is diffusion-controlled, but the slope (0.81) in the plot of the relationship between the log of the peak current and the log of the scan rate (Figure 4C) shows that the process has a mixed nature because it is not fully controlled by diffusion, but also partially by adsorption.

The information on the electrochemical response of BLM was also obtained from the analysis of differential capacity curves of the double-layer interface pSPCE/PbNPs/NaAc—HAc buffer (pH 4.5) (frequency of 200 Hz). As shown in Figure 5, in the presence of 2 and 5 µM BLM, three desorption peaks (−1.17, −1.4, and −1.59 V) are visible. This proves the adsorption of BLM onto the electrode surface.

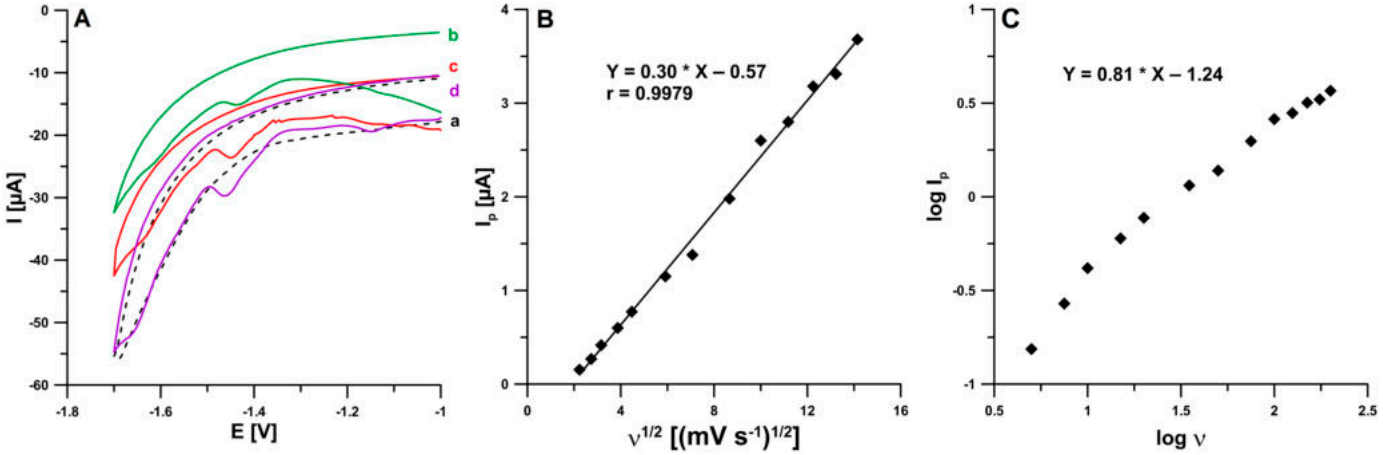

Figure 4. (**A**) CV curves obtained at the pSPCE/PbNPs in the 0.05 M NaAc—HAc buffer (pH 4.5) containing 0.05 mmol L^{-1} Pb(II) and 0 M BLM (dashed line, a) or 0.1 µM BLM (solid line, b, c, and d) (υ = 50, 100 and 200 mV/s). (**B**) The dependence between the BLM peak current (I_p) and the square root of the scan rate ($\upsilon^{1/2}$) (υ in the range of 5–200 mV/s). (**C**) The dependence between the log of the BLM peak current (log I_p) and the log of the scan rate (log υ) (υ in the range of 5–200 mV/s).

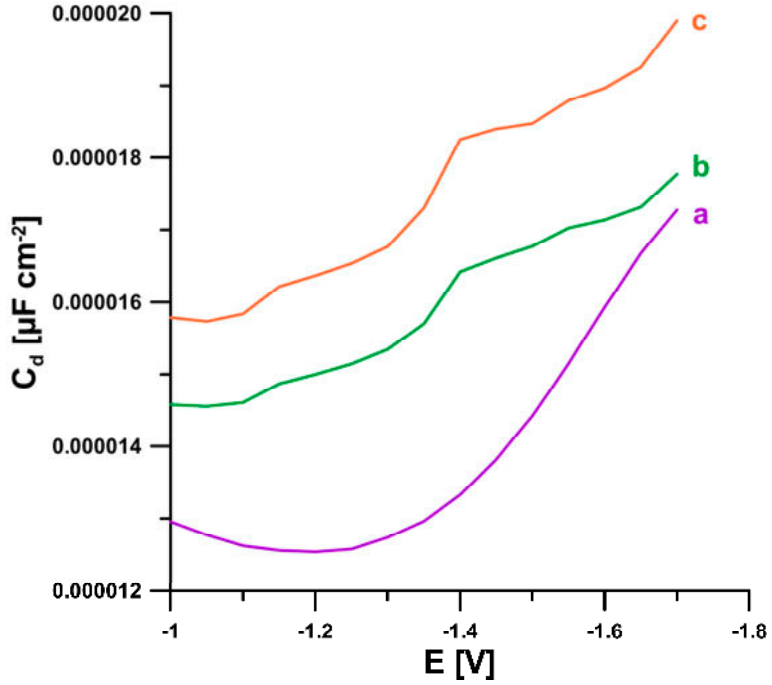

Figure 5. The differential capacity-potential curves of the double layer interface pSPCE/PbNPs/NaAc—HAc buffer (pH 4.5) in the presence of 0 (a), 2 (b), and 5 (c) µM BLM.

2.4. Optimization Step

In order to achieve the best analytical signal, and thus the best sensitivity and accuracy of the determinations, the SWAdSV procedure parameters were optimized, such as the potential for simultaneous deposition of PbNPs and BLM accumulation on the electrode surface ($E_{acc.}$) as well as time ($t_{acc.}$), frequency (f), square-wave amplitude (E_{SW}), and step potential (ΔE). BLM at a fixed concentration (2 nM) was added to the supporting electrolyte solution, and then the effect of the potential ($E_{acc.}$) on the reduction peak ranging from −0.8 to −1.3 V was examined. The highest peak current intensity was obtained at −1.0 V, and therefore this value was considered optimal (Figure 6A). In the next stage, the influence of the time of applying this potential was tested for the selected potential value. A deposition

time ($t_{acc.}$) of 120 s was chosen; however, since the signal continues to increase with accumulation up to 600 s (Figure 6B), it is possible to attain an even lower detection limit when a longer accumulation time is chosen.

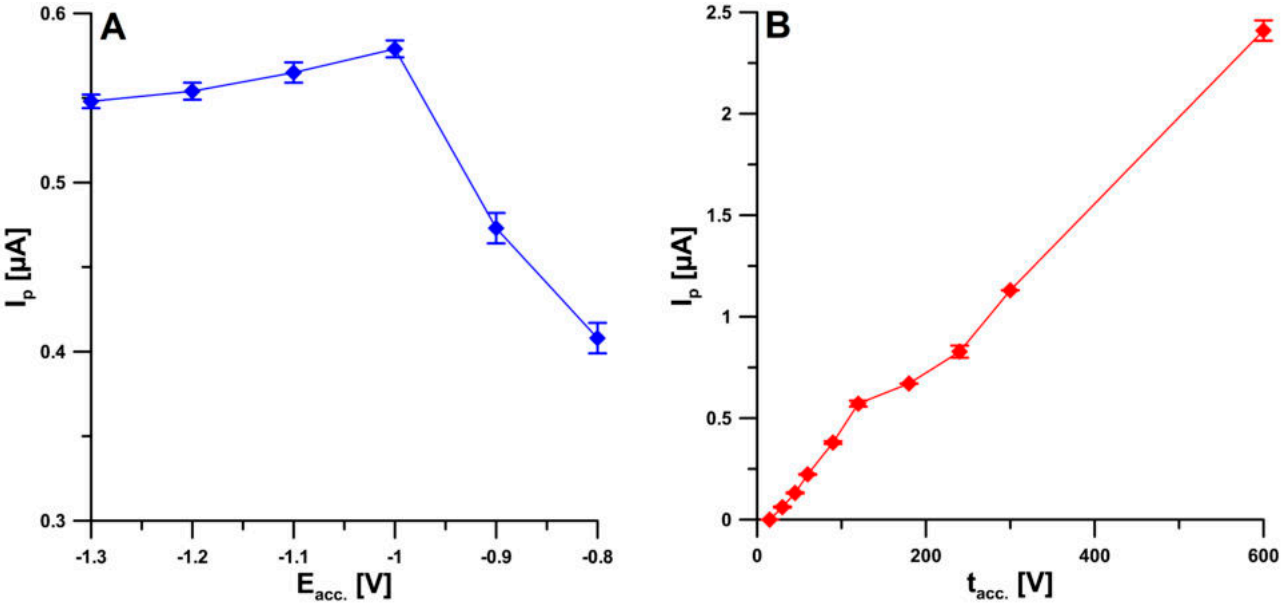

Figure 6. The dependence on $E_{acc.}$ (**A**) and $t_{acc.}$ (**B**) on the 2 nM BLM peak current. f = 50 Hz, E_{SW} = 50 mV, and ΔE = 10 mV. The received average values of the peak current are shown with a standard deviation for n = 3.

For the E_{SW} of 50 mV and the ΔE of 10 mV, the frequency was varied in the range from 10 to 200 Hz. The peak current increased with increasing frequency up to 50 Hz; higher frequencies caused a decrease in the signal, and therefore the value of 50 Hz was selected for subsequent studies (Figure 7A). Then, the influence of ΔE was checked by changing the value of this parameter from 3 to 11 mV. The best result was obtained for the value of 10 mV (Figure 7B). Finally, the effect of E_{SW} values in the range of 25–175 mV was optimized. The highest BLM analytical signal was observed for the E_{SW} of 50 mV (Figure 7C).

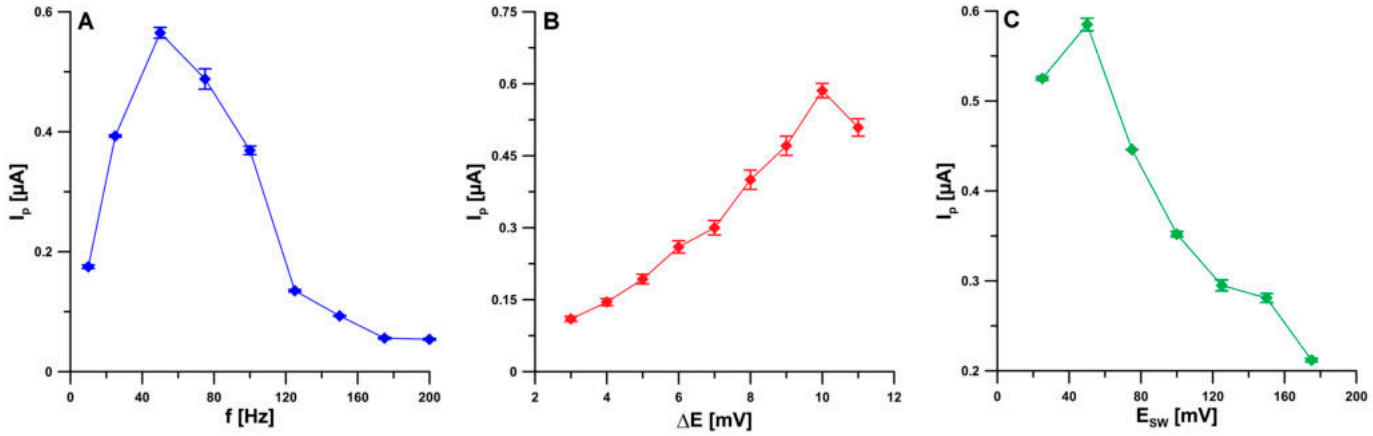

Figure 7. The dependence of f (**A**), ΔE (**B**), and E_{SW} (**C**) on the 2 nM BLM peak current. The received average values of the peak current are shown with a standard deviation for n = 3.

2.5. Selectivity Studies and Sensor Reproducibility

In order to test the selectivity of the pSPCE/PbNPs sensor, the voltammetric response of 2 nM BLM was checked in the presence of increasing concentrations of potential interferents. It was found that a 2500-fold excess of epinephrine and a 1000-fold excess of Mg(II),

Ca(II), glucose, dopamine, ascorbic acid, and uric acid do not significantly alter the peak current of BLM (they do not cause changes greater than 10%). Moreover, a 500-fold excess of V(V), a 200-fold excess of Ni(II), and a 100-fold excess of Fe(III), Cd(II), Cu(II), adenine, and testosterone had negligible effects on the BLM analytical signal. Since natural waters contain surfactants with a surface-active effect corresponding to 0.2–2.0 ppm of Triton X-100 [22], the influence of the presence of 2.0 ppm of this surfactant on the 2 nM BLM signal was also investigated, and no peak current changes exceeding 10% were observed.

Furthermore, three sensors were prepared independently and employed in the SWAdSV analysis of 2 nM BLM. The RSD value equal to 7.5% (n = 9) confirms the acceptable reproducibility of the pSPCE/PbNPs sensor.

2.6. Voltammetric Determination of BLM

The determination of the effect of increasing BLM concentrations on the electrode was performed under optimized conditions using square-wave adsorptive stripping voltammetry (SWAdSV) (Figure 8A). It was observed that the BLM analytical signal increased linearly with increasing concentration over two ranges, the first one from 1×10^{-10} to 2×10^{-9} M and the second one from 2×10^{-9} to 2×10^{-8} M (Figure 8B). The limits of detection and quantification were calculated to be 2.8×10^{-11} and 9.3×10^{-11} M, respectively, using the LOD = $3SD_a/b$ and LOQ = $10\ SD_a/b$ equations (SD_a—standard deviation of intercept (n = 3); b—slope of calibration curve) [23]. The analytical performance of the proposed sensor was compared with other voltammetric BLM determination procedures described in the literature. The collected data are presented in Table 2. Only one of the procedures [1] allows a lower limit of detection to be achieved, but it requires many hours and multi-stage preparation of the working electrode, and the analysis time is relatively long.

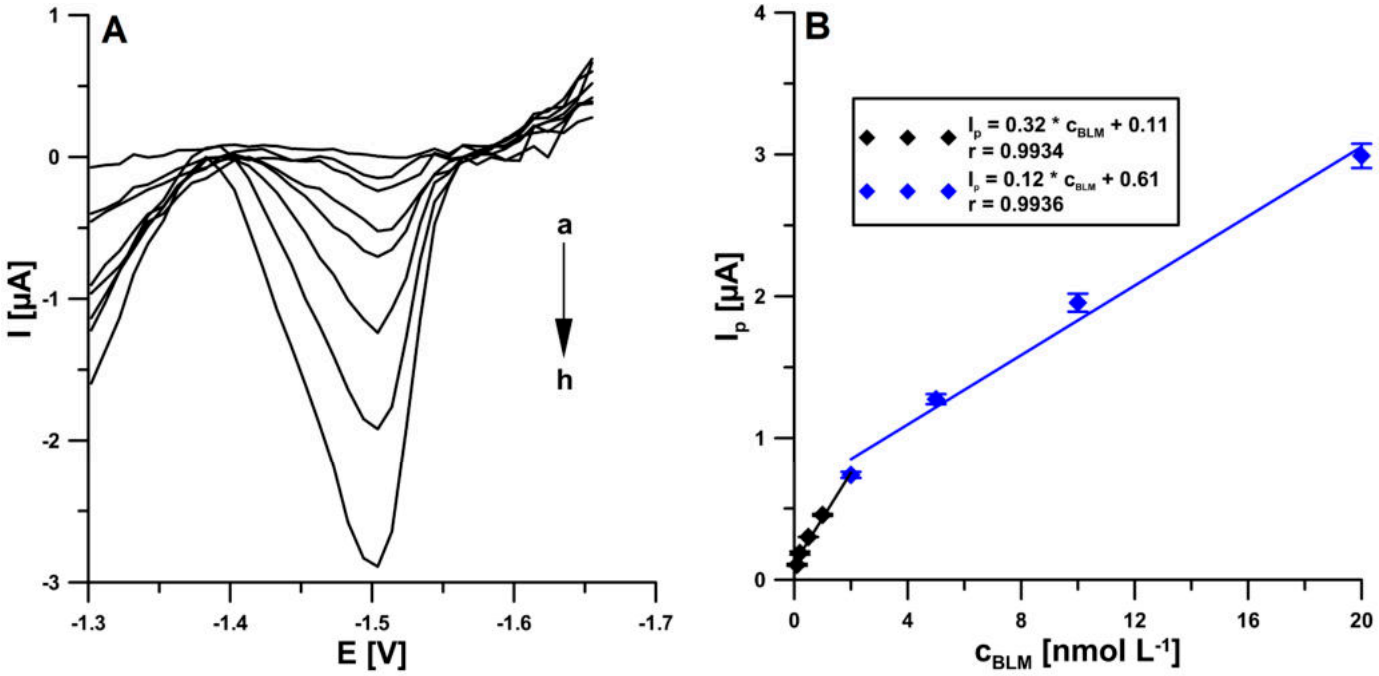

Figure 8. (**A**) The SWAdSV curves obtained on the pSPCE/PbNPs in the presence of increasing BLM concentration (a → h, 0.1–20 nM) in 0.05 M NaAc—HAc buffer (pH 4.5) and 0.05 mM Pb(II). (**B**) Linear ranges of BLM. The received average values of the peak current are shown with a standard deviation for n = 3. $E_{acc.}$ = −1.0 V, $t_{acc.}$ = 120 s, f = 50 Hz, E_{SW} = 50 mV, and ΔE = 10 mV.

Table 2. Comparison of voltammetric analyses of BLM.

Electrode	Method	Linear Range (M)	LOD (M)	Application	Ref.
AuE/DNA	DPV	1.0×10^{-12}–1.0×10^{-7}	7.4×10^{-13}	Serum	[1]
AuE/DNA (E-DNA sensor)	SWV	1.0×10^{-10}–1.0×10^{-6}	1.0×10^{-10}	Serum	[11]
HMDE	AdSV	1.0×10^{-9}–1.0×10^{-7}	5.0×10^{-10}	Serum	[14]
ITO/MB-DNA	DPV	1.0×10^{-10}–1.0×10^{-7}	3.3×10^{-11}	Serum	[15]
pSPCE/PbNPs	SWAdSV	1.0×10^{-10}–2.0×10^{-9} 2.0×10^{-9}–2.0×10^{-8}	2.8×10^{-11}	Urine, wastewater	This work

AuE/DNA—DNA probe modified gold electrode; HMDE—hanging mercury drop electrode; ITO/MB-DNA—methylene blue-DNA modified indium oxide electrode; pSPCE/PbNPs—electrochemically pretreated screen-printed carbon electrode decorated with lead nanoparticles; DPV—differential-pulse voltammetry; SWV—square-wave voltammetry; AdSV—adsorptive stripping voltammetry; SWAdSV—square-wave adsorptive stripping voltammetry.

2.7. Real Samples Analysis

The last stage of the research was to confirm the usefulness of the proposed SWAdSV procedure for BLM determination in real samples. Samples of human urine and purified municipal sewage were analyzed. In a single session during BLM therapy, the maximum dose of the drug is 15 IU, which corresponds to 15 g L^{-1}, and 50–70% of BLM is excreted within 24 h after administration in the urine in the unchanged form [24,25]. Accordingly, the BLM concentrations in the urine of the patients are in the order of 10^{-5} M, and therefore, when analyzing human urine samples, multiple sample dilutions (10,000×) could be used. The wastewater samples, on the other hand, were diluted 10× and analyzed with an additional 1×10^{-5} mol L^{-1} DTPA in order to minimize the possible influence of metal ions present in the sample. Spiked samples were analyzed using the standard addition method. The small values of the coefficient of variation (1.16–2.5%) and the values of recoveries (96.0–103.5%) prove the good repeatability of the analytical signal and the good accuracy of the applied method, respectively (Table 3). Figure 9 shows the voltammograms obtained during the determination of BLM in the human urine and municipal sewage samples.

Table 3. The results of BLM determination in reference material of human urine and wastewater purified in a sewage treatment plant.

Sample	BLM Concentration [μM] ± SD (n = 3)			Coefficient of Variation * [%]	Recovery ** [%]
	Added	Found SWAdSV	Found in Electrochemical Cell		
Purified wastewater	0.005	0.0048 ± 0.00012	0.00048 ± 0.000012	2.13	103.5
	0.02	0.0193 ± 0.00035	0.00193 ± 0.000035	1.16	99.0
RM of human urine	20.0	20.7 ± 0.44	0.00207 ± 0.000044	2.50	96.0
	40.0	39.6 ± 0.46	0.00396 ± 0.000046	1.81	96.5

* Coefficient of variation [%] = (SD × 100)/Found SWAdSV, ** Recovery [%] = (Found SWAdSV × 100)/Added.

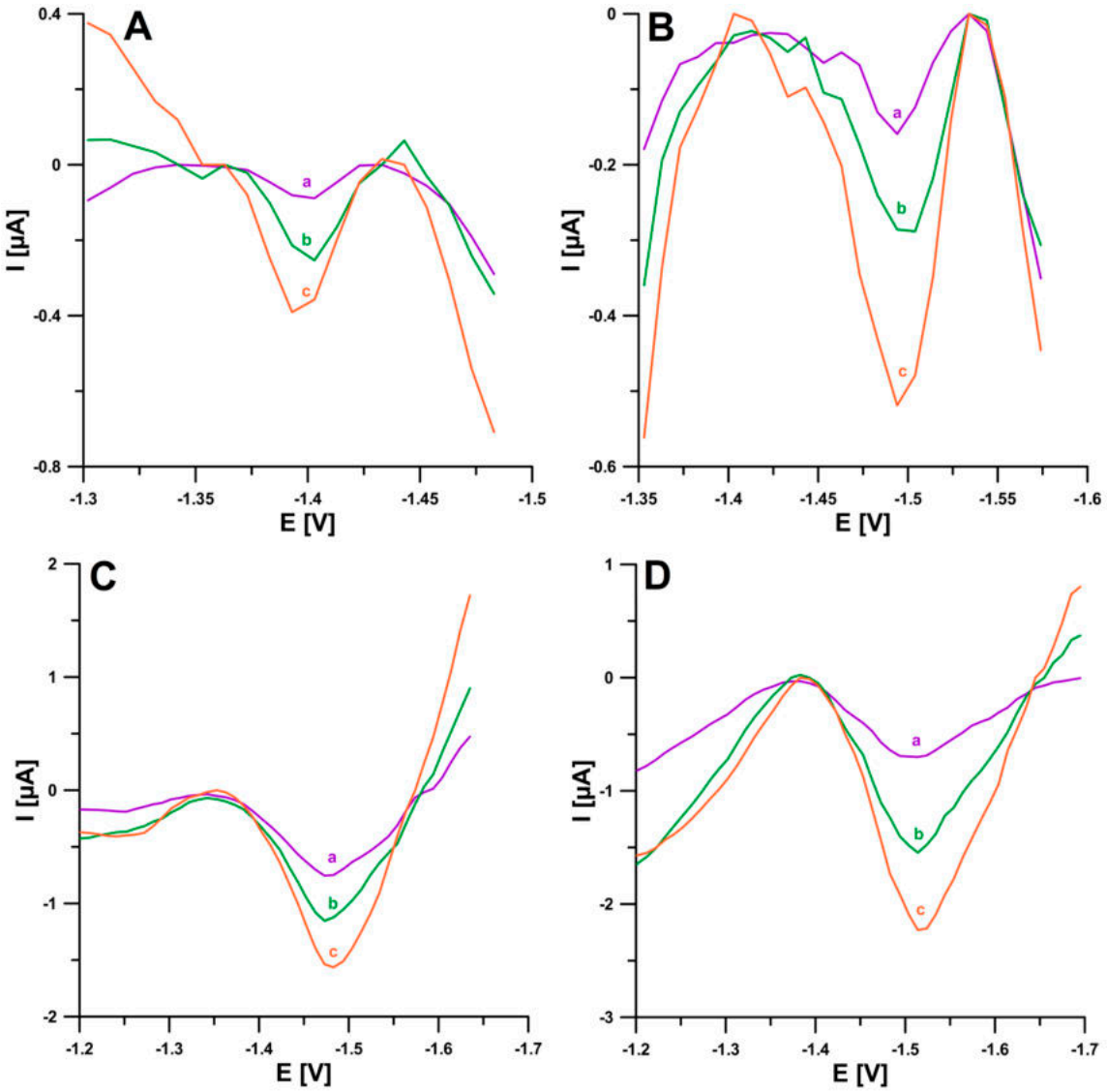

Figure 9. Voltammograms recorded for the determination of BLM in reference material of human urine (**A**,**B**) and wastewater samples purified in a sewage treatment plant (**C**,**D**). (**A**): (a) 1 µL of sample + 2, (b) as (a) + 2, (c) as (a) + 4 nM BLM, (**B**): (a) 1 µL of sample + 4, (b) as (a) + 4 (c) as (a) + 8 nM BLM, (**C**): (a) 1 mL of sample + 0.5, (b) as (a) + 0.5, (c) as (a) + 1 nM BLM, and (**D**): (a) 1 mL of sample + 2, (b) as (a) + 2, (c) as (a) + 4 nM BLM. $E_{acc.} = -1.0$ V, $t_{acc.} = 120$ s, f = 50 Hz, $E_{SW} = 50$ mV, and $\Delta E = 10$ mV.

3. Materials and Methods

3.1. Apparatus

The electrochemical studies were performed using a µAutolab electrochemical analyzer (Eco Chemie, Utrecht, Netherlands) controlled by GPES 4.9 software (voltammetric measurements) and FRA 4.9 software (electrochemical impedance spectroscopy (EIS) studies). The standard quartz electrochemical cell with a volume of 10 mL and a commercially available screen-printed carbon sensor (SPCE, DropSens, Llanera, Spain, Ref. C150) were applied for the experiments. The SPCE sensor consisted of a screen-printed carbon working electrode with a diameter of 4 mm, a silver screen-printed pseudo-reference electrode, and a platinum screen-printed auxiliary electrode.

X-ray photoelectron spectroscopy (XPS) spectra were obtained using a Multi-Chamber Analytical System (Prevac, Rogów, Poland) with monochromated Kα-Al radiation (1486.6 eV) (Gammadata Scienta, Uppsala, Sweden) and an X-ray power of 450 W.

3.2. Reagents and Solutions

A 1 mM standard BLM solution was prepared by dissolving an appropriate amount of bleomycin sulfate (Merck, Darmstadt, Germany) in a 0.9% NaCl (saline) solution. This BLM solution was further diluted with saline to obtain BLM solution with a concentration of 10 μM. Sodium acetate and acetic acid used to make an acetate buffer (NaAc—HAc) of pH 4.5, which acted as the supporting electrolyte, were purchased from Merck. There were 1 mM stock solutions of Ni(II), Cd(II), Ca(II), V(V), Fe(III), Mg(II), Cu(II), glucose, ascorbic acid, dopamine, adenine, epinephrine, uric acid and testosterone that were prepared from Merck reagents in deionized water or ethanol (testosterone) and stored at 4 °C in the dark until the influence of interferents was examined. Diethylenetriaminepentaacetic acid (DTPA) was purchased from Merck. Ultra-purified water from a Milli-Q system (Millipore, Livingston, Scotland, UK) was used to prepare the solutions.

3.3. Preparation of the pSPCE/PbNPs and Bleomycin (BLM) Analysis

For electrochemical pretreatment and simultaneous decoration of the electrode with nanoparticles of lead (PbNPs), a fresh electrode was placed in a 0.05 M NaAc—HAc solution (pH 4.5) containing 50 μM Pb(II), and subsequently, ten consecutive scans were performed using square-wave voltammetry (SWV). Apart from recording the voltammetric curve, each measurement consisted of electrochemical cleaning at a potential of 0.5 V ($E_{clean.}$) for 10 s ($t_{clean.}$) and then deposition of PbNPs on the electrode surface at a potential of −1.0 V during 120 s. SWV curves were recorded in the range from −1.0 to −1.7 V using a frequency (f) of 50 Hz, a square-wave amplitude (E_{SW}) of 50 mV, and a step potential (ΔE) of 10 mV. After the presented sequence of measurements was performed, the electrode was rinsed with water and allowed to dry in the air. The pretreatment of the electrode was conducted only once before it was used in a series of measurements.

The BLM determination on the pSPCE/PbNPs was performed in the same solution that had been used for the pretreatment of the electrode. Only appropriate amounts of the sample or BLM standard were added to the solution. The square-wave adsorptive stripping voltammetric (SWAdSV) procedure also consisted of the same steps as outlined above, i.e., simultaneous electrodeposition of PbNPs and BLM accumulation at a potential ($E_{acc.}$) of −1.0 V for a time ($t_{acc.}$) of 120 s, followed by electrochemical cleaning of the electrode surface at a potential of 0.5 V ($E_{clean.}$) for 10 s ($t_{clean.}$). SWV curves were recorded from −1.0 to −1.7 V with f of 50 Hz, E_{SW} of 50 mV, and ΔE of 10 mV.

3.4. Real Sample Analysis

The samples of purified municipal wastewater obtained from a municipal sewage treatment plant (Lublin, Poland), as well as samples of reference material (human urine) (Medidrug Basis-line U), were used for BLM determination at the pSPCE/PbNPs. The samples were spiked with a specific concentration of BLM and analyzed without any preparation.

4. Conclusions

In summary, we proposed the application of electrochemical pretreatment (p) of the screen-printed carbon electrode (SPCE) surface and its modification with nanoparticles of lead (PbNPs) in the sample solution as an easy-to-employ method to prepare sensors and further use them for voltammetric determination of the anti-cancer antibiotic bleomycin (BLM). The modification of the electrode with PbNPs is necessary to obtain the BLM signal (no BLM reduction signal was observed at the bare SPCE). Moreover, electrochemical pretreatment does not significantly affect the BLM peak current intensity but causes a slight shift of the peak potential towards less negative potential values and improves the shape of the BLM peak. Furthermore, pretreatment of the sensor before its use in a series of BLM measurements significantly improves the repeatability of the signal.

The results obtained using cyclic voltammetry (CV), electrochemical impedance spectroscopy (EIS), and X-ray photoelectron spectroscopy (XPS) were used to characterize the sensors (bare SPCE, SPCE/PbNPs, and pSPCE/PbNPs). The active surface area (A_s) increases,

and the charge transfer resistance (R_{ct}) decreases with PbNPs modification. However, electrochemical pretreatment does not contribute to a change in A_s and R_{ct} compared to the SPCE/PbNPs. Most probably, the increased proportion of metallic lead (confirmed by the XPS analysis) affects the repeatability of the deposited lead film before each measurement, thus contributing to the improvement of the shape of the BLM signal and its repeatability.

It was confirmed based on the CV results that the process of BLM reduction on the pSPCE/PbNPs is not purely diffusion- or adsorption-controlled. The developed sensor was validated for selectivity, repeatability, and reproducibility toward BLM. The specific features of the proposed sensor include wide linear ranges (1.0×10^{-10}–2.0×10^{-9} M and 2.0×10^{-9}–2.0×10^{-8} M), very low limits of detection and quantification (2.8×10^{-11} and 9.3×10^{-11} M, respectively), and a high sensitivity of 0.32 µA/nM. The pSPCE/PbNPs sensor and the SWAdSV procedure were effectively applied for direct analysis of human urine and wastewater samples towards the determination of BLM. The results show the potential of the pSPCE/PbNPs in using it as an electrochemical sensor for direct BLM analysis in real samples with a good recovery rate.

Author Contributions: Conceptualization, J.K. and K.T.-R.; methodology, J.K. and K.T.-R.; investigation, J.K., K.T.-R. and R.M.; writing—original draft preparation, J.K. and K.T.-R.; writing—review and editing, J.K., K.T.-R. and R.M.; supervision, K.T.-R. All authors have read and agreed to the published version of the manuscript.

Funding: This research received no external funding.

Institutional Review Board Statement: Not applicable.

Informed Consent Statement: Not applicable.

Data Availability Statement: The data presented in this study are available on request from the corresponding author.

Conflicts of Interest: The authors declare no conflict of interest.

References

1. Lu, S.; Yang, M.; Li, X.; Liu, X.; Yin, Y.; Cao, Y. Amplified detection of bleomycin based on an electrochemically driven recycling strategy. *Anal. Methods* **2014**, *6*, 5573–5577. [CrossRef]
2. Shiu, G.K.; Goehl, T.J.; Pitlick, W.H. Rapid high-performance liquid chromatographic determination of bleomycin A2 in plasma. *J. Pharm. Sci.* **1979**, *68*, 232–234. [CrossRef] [PubMed]
3. Miura, T. The peroxidase activity of bleomycin-Fe3+ is associated with damage to biological components. *J. Biochem.* **2015**, *157*, 217–224. [CrossRef] [PubMed]
4. Galba, J.; Veizerová, L.; Piešťanský, J.; Mego, M.; Novotný, L.; Dokupilová, S.; Maráková, K.; Havránek, E.; Mikuš, P. HPLC-QTOF-MS method for identification and determination of bleomycin A2 and B2 Fractions. *J. Liq. Chromatogr. Relat. Technol.* **2015**, *38*, 294–302. [CrossRef]
5. Falay, O.; Öztürk, E.; Bölükbaşı, Y.; Gümüş, T.; Örnek, S.; Özbalak, M.; Çetiner, M.; Demirkol, O.; Ferhanoğlu, B. Use of fluorodeoxyglucose positron emission tomography for diagnosis of bleomycin-induced pneumonitis in hodgkin lymphoma. *Leuk. Lymphoma* **2017**, *58*, 1114–1122. [CrossRef] [PubMed]
6. Murray, V.; Chen, J.; Chung, L. The interaction of the metallo-glycopeptide anti-tumour drug bleomycin with DNA. *Int. J. Mol. Sci.* **2018**, *19*, 1372. [CrossRef] [PubMed]
7. Li, Y.; Huang, C.; Zheng, J.; Qi, H. Ultrasensitive electrogenerated chemiluminescent DNA-based biosensing switch for the determination of bleomycin. *Talanta* **2013**, *103*, 8–13. [CrossRef]
8. Mack, J.M.; Peterson, E.C.; Crary, S.E.; Moran, J.H.; Neville, K.; Pierce, C.D.; Richter, G.T. Pharmacokinetics of bleomycin sclerotherapy in patients with vascular malformations. *Pediatr. Blood Cancer* **2022**, *69*, e29733. [CrossRef]
9. Elson, M.K.; Oken, M.M.; Shafer, R.B.; Broughton, A.; Strong, J.; Braun, C.T.; Crooke, S.T. Comparison of two radioimmunoassays and a microbiologic assay for bleomycin. *Med. Pediatr. Oncol.* **1978**, *5*, 213–218. [CrossRef]
10. Rajani, C.; Kincaid, J.R.; Petering, D.H. Resonance Raman studies of HOO−Co(III)bleomycin and Co(III)bleomycin: Identification of two important vibrational modes, ν(Co−OOH) and ν(O−OH). *J. Am. Chem. Soc.* **2004**, *126*, 3829–3836. [CrossRef]
11. Yin, B.-C.; Wu, D.; Ye, B.-C. Sensitive DNA-based electrochemical strategy for trace bleomycin detection. *Anal. Chem.* **2010**, *82*, 8272–8277. [CrossRef] [PubMed]
12. Zubair Malik, M.; Ahmad, M.; Muahammad, S. Rapid and simultaneous determination of adriamycin, bleomycin, vinblastine and dacarbazine in plasma of hodgkin's lymphoma patients by a reversed phase HPLC method. *J. Chil. Chem. Soc.* **2013**, *58*, 1674–1677. [CrossRef]

13. Aszalos, A.; Crawford, J.; Vollmer, P.; Kantor, N.; Alexander, T. High-performance liquid chromatographic determination of components of bleomycin preparations. *J. Pharm. Sci.* **1981**, *70*, 878–880. [CrossRef] [PubMed]
14. Tan, X.; Hu, J.; Li, Q. Adsorptive stripping voltammetry of bleomycin. *Analyst* **1997**, *122*, 991–994. [CrossRef] [PubMed]
15. Chang, J.; Gai, P.; Li, H.; Li, F. Target-induced diffusivity enhancement for rapid and highly sensitive homogeneous electrochemical detection of BLM in human serum. *Talanta* **2018**, *190*, 492–497. [CrossRef]
16. Zhang, Y.; Jiang, X.; Zhang, J.; Zhang, H.; Li, Y. Simultaneous voltammetric determination of acetaminophen and isoniazid using MXene modified screen-printed electrode. *Biosens. Bioelectron.* **2019**, *130*, 315–321. [CrossRef]
17. Bagherinasab, Z.; Beitollahi, H.; Yousefi, M.; Bagherzadeh, M.; Hekmati, M. Rapid sol gel synthesis of BaFe12O19 nanoparticles: An excellent catalytic application in the electrochemical detection of tramadol in the presence of acetaminophen. *Microchem. J.* **2020**, *156*, 104803. [CrossRef]
18. Serrano, N.; Castilla, Ò.; Ariño, C.; Diaz-Cruz, M.; Díaz-Cruz, J. Commercial screen-printed electrodes based on carbon nanomaterials for a fast and cost-effective voltammetric determination of paracetamol, ibuprofen and caffeine in water samples. *Sensors* **2019**, *19*, 4039. [CrossRef]
19. Tyszczuk-Rotko, K. Metal film electrodes prepared with a reversibly deposited mediator in voltammetric analysis of metal ions. *Curr. Opin. Electrochem.* **2019**, *17*, 128–133. [CrossRef]
20. Kozak, J.; Tyszczuk-Rotko, K.; Wójciak, M.; Sowa, I.; Rotko, M. Electrochemically pretreated sensor based on screen-printed carbon modified with Pb nanoparticles for determination of testosterone. *Materials* **2022**, *15*, 4948. [CrossRef]
21. Gosser, D.K. *Cyclic Voltammetry, Simulation and Analysis of Reaction Mechanisms*; Wiley VCH: New York, NY, USA, 1993.
22. Grabarczyk, M.; Koper, A. How to determine uranium faster and cheaper by adsorptive stripping voltammetry in water samples containing surface active compounds. *Electroanalysis* **2011**, *23*, 1442–1446. [CrossRef]
23. Mocak, J.; Bond, A.M.; Mitchell, S.; Scollary, G. A statistical overview of standard (IUPAC and ACS) and new procedures for determining the limits of detection and quantification: Application to voltammetric and stripping techniques (technical report). *Pure Appl. Chem.* **1997**, *69*, 297–328. [CrossRef]
24. Arafat, S.; Abdelmabood, A.A.; Mohamed, W.; El-Tagy, G.; El-Swify, A. Bleomycin intralesional injections of maxillofacial venous malformations in pediatric patients. *Oral Maxillofac. Surg. Cases* **2022**, *8*, 100256. [CrossRef]
25. Reinert, T.; da Rocha Baldotto, C.S.; Nunes, F.A.P.; de Souza Scheliga, A.A. Bleomycin-induced lung injury. *J. Cancer Res.* **2013**, *2013*, 480608. [CrossRef]

RD8

J. Kozak, K. Tyszczuk-Rotko, K. Sztanke, M. Sztanke, *Sensitive and selective voltammetric sensor based on anionic surfactant-modified screen-printed carbon for the quantitative analysis of an anticancer active fused azaisocytosine-containing congener,* International Journal of Molecular Sciences, 24 (1) (2023) 564-574.

International Journal of
Molecular Sciences

MDPI

Article

Sensitive and Selective Voltammetric Sensor Based on Anionic Surfactant-Modified Screen-Printed Carbon for the Quantitative Analysis of an Anticancer Active Fused Azaisocytosine-Containing Congener

Jędrzej Kozak [1], Katarzyna Tyszczuk-Rotko [1], Krzysztof Sztanke [2] and Małgorzata Sztanke [3,*]

[1] Faculty of Chemistry, Institute of Chemical Sciences, Maria Curie-Skłodowska University in Lublin, 20-031 Lublin, Poland
[2] Laboratory of Bioorganic Compounds Synthesis and Analysis, Medical University of Lublin, 4A Chodźki Street, 20-093 Lublin, Poland
[3] Department of Medical Chemistry, Medical University of Lublin, 4A Chodźki Street, 20-093 Lublin, Poland
* Correspondence: malgorzataszt5@gmail.com

Abstract: 3-(4-Nitrophenyl)-8-(2,3-dimethylphenyl)-7,8-dihydroimidazo[2,1-*c*][1,2,4]triazin-4(6*H*)-one (NDIT) is one of the most promising candidates for anticancer agents. Hence, a sensitive and selective sodium dodecyl sulfate-modified screen-printed carbon sensor (SPCE/SDS) was used for its quantitative analysis. The SPCE/SDS, in contrast to the SPCE, showed excellent behavior in the electrochemical reduction of NDIT by differential-pulse adsorptive stripping voltammetry (DPAdSV). Cyclic voltammetric (CV) studies reveal an irreversible, two-stage and not purely diffusion-controlled reduction process in 0.01 M HNO_3. The sensor was characterized by CV and electrochemical impedance spectroscopy (EIS). Under the optimized conditions (t 45 s, ΔE 175 mV, ν 150 mV/s, and t_m 5 ms), the DPAdSV procedure with the SPCE/SDS presented a very wide linear range from 1 to 2000 nM and a low detection limit of 0.29 nM. A 1000-fold excess concentration of potential interferents commonly present in biological samples did not significantly alter the peak current of NDIT. The practical application of the proposed DPAdSV procedure with the SPCE/SDS was successfully checked by analyzing spiked human serum samples.

Keywords: fused azaisocytosine-containing congener with the *para*-nitrophenyl group; anticancer agent candidate; voltammetry; screen-printed sensor; anionic surfactant

Citation: Kozak, J.; Tyszczuk-Rotko, K.; Sztanke, K.; Sztanke, M. Sensitive and Selective Voltammetric Sensor Based on Anionic Surfactant-Modified Screen-Printed Carbon for the Quantitative Analysis of an Anticancer Active Fused Azaisocytosine-Containing Congener. *Int. J. Mol. Sci.* **2023**, *24*, 564. https://doi.org/10.3390/ijms24010564

Academic Editor: Claudiu T. Supuran

Received: 25 November 2022
Revised: 23 December 2022
Accepted: 27 December 2022
Published: 29 December 2022

1. Introduction

Among antiproliferative active disubstituted fused azaisocytosine-containing congeners with fully defined and patented molecular structures [1,2], 3-(4-nitrophenyl)-8-(2,3-dimethylphenyl)-7,8-dihydroimidazo[2,1-*c*][1,2,4]triazin-4(6*H*)-one, abbreviated in this paper as NDIT (Figure 1), has previously been disclosed as one of the most promising candidates for anticancer agents [1]. This innovative nucleobase-like small molecule evoked a concentration-dependent growth-inhibitory effect in human epithelial tumor cells of the breast, cervix, lung, and ovary, which was the strongest in breast and cervical cancer cells [1,2]. In light of the current knowledge, the mechanism of its anticancer action may be related to the selective activation (via reduction with the participation of a number of flavoproteins) of this nitroaromatic-containing prodrug in tumor tissue into an anticancer active agent (i.e., the cytotoxic nitroanion radical and the cytotoxic hydroxylamine molecule) [1,3]. Furthermore, it has been found that NDIT—as a drug candidate for pharmaceutical use [2]—is distinctly less toxic towards normal epithelial Vero cells, reveals the optimal lipophilicity for high bioavailability after per os administration [1], as well as high thermal stability and high chemical purity [4]. These advantageous features indicate that this heterocyclic

compound can be classified as a promising candidate for further in vivo pharmacological studies in the drug development process.

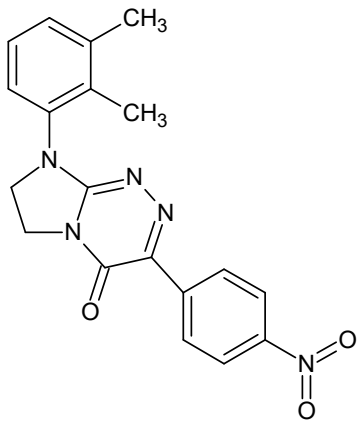

Figure 1. 3-(4-Nitrophenyl)-8-(2,3-dimethylphenyl)-7,8-dihydroimidazo[2,1-*c*][1,2,4]triazin-4(6*H*)-one (NDIT)—an electroactive small molecule used in the present study.

Taking into account the potential usefulness of NDIT in cancer chemotherapy [2], it is of great importance to develop a sensitive, selective, and reliable analytical procedure as the first method for its quantitative determination in solution, as well as biological samples. Such a method with optimized experimental and instrumental parameters could be used in the future to detect and determine the concentration of this substance in the blood serum of treated patients. It is supposed that such a method, after evaluating its linearity, selectivity, sensitivity, limit of detection, and limit of quantification, would have a chance for the prospective use in clinical analytics. Notwithstanding, as yet, no analytical procedure allowing the quantitative analysis of this small molecule has been developed to date or described. NDIT, as a drug candidate for pharmaceutical use, is the subject of our current electrochemical investigation due to the presence of an electroactive (prone to reduction both in in vitro and in vivo systems) *para*-nitrophenyl moiety at the *C*3 of the heterocyclic scaffold in its molecule. To date, no information about the electrochemical behavior of NDIT has been disclosed. Moreover, so far, no voltammetric sensor has been designed and applied for the quantification of NDIT.

In general, electrochemical methods are characterized by simplicity, the use of relatively inexpensive equipment, high sensitivity, speed, and high accuracy [5,6]. The main challenge of voltammetry as an electrochemical method is the fabrication of a suitable electrode. An ideal electrode should be mechanically stable and chemically non-reactive and should have a wide range of operating potentials [7]. Among the whole range of working electrodes used in voltammetry, in recent years, screen-printed electrodes (SPEs) are gaining more and more popularity. The screen-printing technique is considered to be an effective method of producing electrodes individually or in the form of entire electrode systems consisting of a working electrode, a reference electrode, and an auxiliary electrode. SPEs can be fabricated on different kinds of substrates, such as ceramic, glass, and flexible polymer polyimide, based on the characteristics of printing [8]. SPEs have been developed as single-use, disposable sensors for a variety of applications in environmental, clinical, and industrial analysis [9]. Disposable electrodes can be easily mass-produced, making them readily available and relatively inexpensive. Due to their small size, SPEs can be used with portable devices in field analysis. SPEs also allow working with small sample volumes. Moreover, these electrodes do not require laborious pretreatment and the cleaning of the surface. SPEs are easy to modify, which can be conducted by immobilizing the modifier on the electrode surface or by adding it to the ink that will be used to make the electrode [10–15].

Among the numerous modifiers of working electrodes used in voltammetry, we can distinguish surfactants. Due to their unique molecular structure, surfactants are widely used in the field of electrochemistry and electroanalytical chemistry for various purposes. They are often used as the selective masking agents to improve the selectivity and sensitivity of the electrochemical analysis [16]. The surfactant adsorbs on the electrode surface in the form of a layer that aggregates the electron allocation and enhances the peak current [17]. Furthermore, surfactants stabilize the electrochemical signal, enhancing the electron transfer rate and improving the detection limits [18]. Additionally, a medium containing a surfactant can prevent the fouling of the electrode [19,20]. There are many examples of voltammetric determinations with the use of surfactants in the literature. These are anionic surfactants such as sodium dodecyl sulfate (SDS) [15,20–24], cationic surfactants such as cetyltrimethylammonium bromide (CTAB) [18,25], and amphoteric [26] or non-ionic ones such as Triton X-100 [27].

Because NDIT may be useful in the future as a new anticancer agent, the present study was conducted with the goal of developing and optimizing the first analytical procedure allowing its quantitative determination based on a screen-printed carbon electrode (SPCE) modified with anionic surfactant, sodium dodecyl sulfate (SDS). The assimilation of SDS on the SPC surface of the electrode forms an adsorptive layer, which charges the surface negatively, prevents the accumulation of interferents, and enhances the NDIT peak current in acidic media. Therefore, an SDS-modified SPC sensor has outstanding electrochemical performance in highly sensitive and selective NDIT analysis. The results presented in this paper are important because the development of such a method, employing a reusable sensor, may be useful in the future for monitoring the concentrations of this potential anticancer agent in body fluids.

2. Results and Discussion

2.1. Characterization of SPCE and SPCE/SDS

The interfacial electron transport ability of the SPCE and the SDS-modified SPCE was analyzed using cyclic voltammetry (CV) and electrochemical impedance spectroscopy (EIS) in the $K_3[Fe(CN)_6]$ solution, as well as in the HNO_3 supporting electrolyte. Figure 2A shows CV curves at the SPCE and SPCE/SDS in 5.0 mM $K_3[Fe(CN)_6]$ and 0.1 M KCl at a scan rate of 150 mV/s. According to the experimental results, the SPCE depicts a slightly lower Fe(II) and Fe(III) peak current intensity than the SPCE/SDS. This relationship translates into a similar active surface area (A_s) of a modified electrode (0.0521 $\pm$ 0.0023 vs. 0.0551 $\pm$ 0.0028 cm^2). It is worth adding that for A_s calculation, the relationship between the oxidation peak current of Fe and the square root of the scan rate (υ from 5 to 300 mV/s, Figure 2B), as well as the Randles–Sevcik equation, were used [28]. Moreover, the relative peak separations (χ^0) were calculated for ν of 150 mV/s. It was found that the χ^0 value of 2.86 for the SPCE/SDS is closer to the theoretical value (χ^0 = 1) than the χ^0 value of 4.12 obtained for the SPCE. In summary, the experimental results indicate that the SDS adsorption layer improves the electron transfer kinetics.

The influence of the surfactant on the peak current of NDIT was analyzed by adding an increasing concentration of SDS to the supporting electrolyte. As shown in Figure 3A, the introduction of SDS (10 mg/L) allows for a significant increase in the 50 nM NDIT reduction signals (0.57 vs. 2.2 µA for peak 1 (peak potential of −0.37 V) and 0.54 vs. 1.4 µA for peak 2 (peak potential around −0.65 V)). In an acidic pH range, NDIT must exist in cationic form because the SDS molecules aggregate the species with alike charges and repel the species with like charges. SDS enhances the polarity on the exterior surface of the SPCE, as an outcome of which the enhancement of NDIT current signals can be observed. The adsorption of SDS on the SPCE surface was evidenced by the difference in the curves of the double-layer interface SPCE/HNO_3 in the absence and presence of SDS (10 and 20 mg/L) (Figure 3B). The additional peak that appears at the potential of −0.7 V shows the desorption of previously adsorbed SDS during the recording of the differential capacity–potential curves. Moreover, Figure 3C shows the changes in the intensity of the

50 nM NDIT analytical signal with the changing concentration of SDS (0 to 15 mg/L). In the presence of 15 mg/L SDS, a large standard deviation of the peak current intensity was observed. Therefore, taking into account the NDIT peak current and the repeatability of the signal, an SDS concentration of 10 mg/L was selected for further measurements.

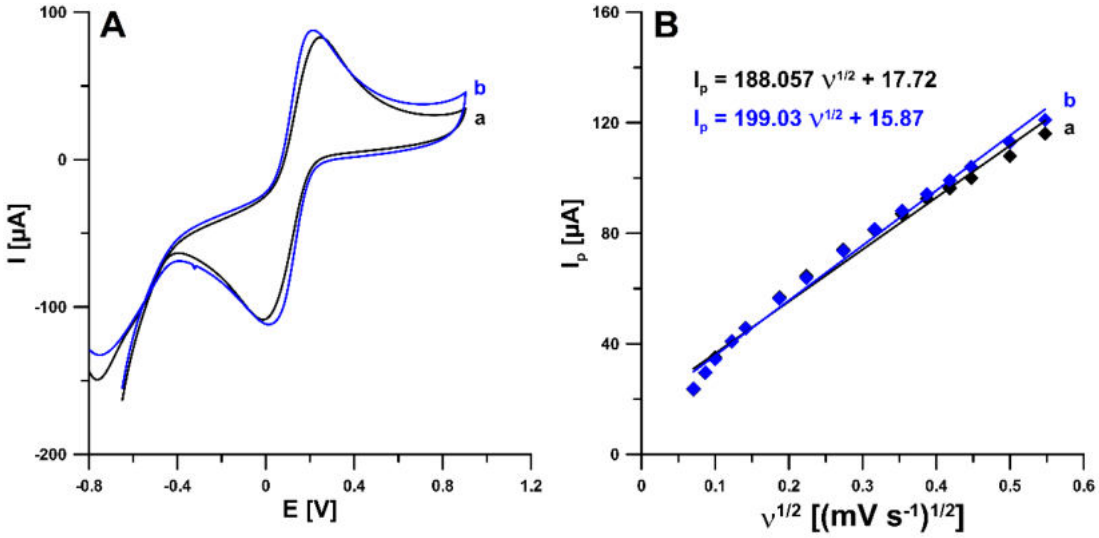

Figure 2. (**A**) Cyclic voltammograms of 5.0 mM $K_3[Fe(CN)_6]$ and 0.1 M KCl at the SPCE (a) and SPCE/SDS (b) (ν of 150 mV/s). (**B**) The relationship between I_p and $\nu^{1/2}$ for ν from 5 to 300 mV/s.

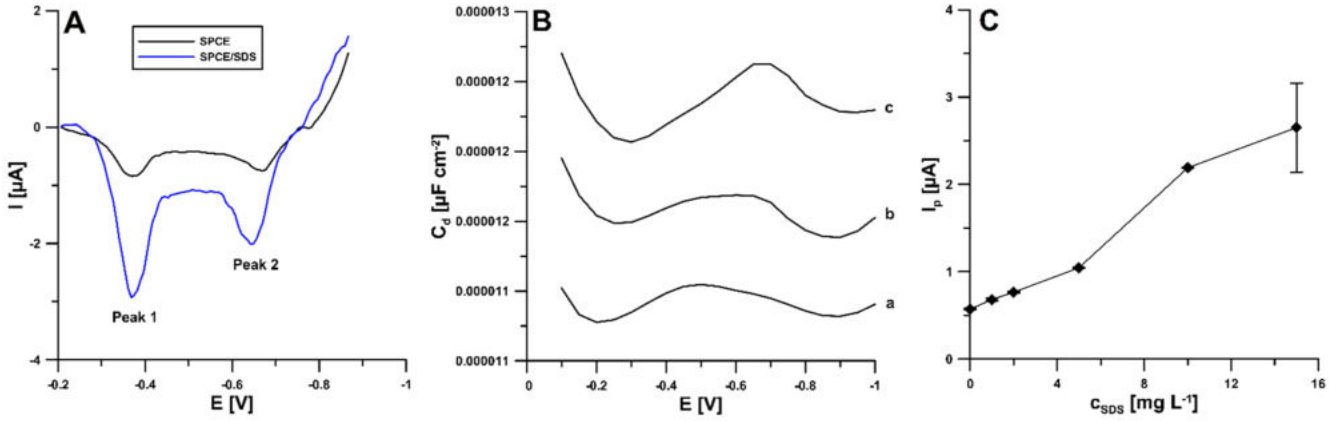

Figure 3. (**A**) Voltammograms of 50 nM NDIT obtained at the SPCE and SPCE/SDS (in the presence of 10 mg/L SDS). (**B**) The differential capacity–potential curves of the double-layer interface SPCE/supporting electrolyte in the presence of 0 (a), 10 (b), and 20 (c) mg L^{-1} SDS. (**C**) The relationship between the 50 nM NDIT peak current and SDS concentration from 0 to 15 mg/L.

2.2. Electrochemical Reduction of NDIT over SPCE/SDS

The effects of the scan rate were evaluated in the range of 5–300 mV/s towards NDIT. Figure 4A shows the CVs at the SPCE/SDS with 10 mM NDIT for different scan rates (υ of 50, 100, and 150 mV/s). The electroreduction of NDIT occurs irreversibly and in two stages (potential peak 1 of −0.66 and peak 2 of −0.97 V for υ of 150 mV/s) in 0.01 M HNO_3. The reduction signal responses have good linearity with the square root of the scan rates for the two NDIT peaks (Figure 4B). These results explained that the reduction of NDIT at the SPCE/SDS is followed by a diffusion-controlled process. However, the relationships between the log of the peak current and the log of the scan rate (Figure 4C) indicate that the process of NDIT reduction at the SPCE/SDS was not purely diffusion-controlled. Therefore, the influence of the selected potentials (0.1, 0, −0.1, and −0.25 V for 60 s) on the NDIT signal was examined. However, no improvement in the peak current was observed. Only

examining the influence of mixing time (without applying the potential), before recording the signal, confirmed that the mixing solution would facilitate diffusion to the electrode surface and the adsorption of NDIT on the electrode surface (Figure 5A). Furthermore, the process of 50 nM NDIT reduction was studied in various supporting electrolytes (0.1 and 0.01 M solutions of HNO_3, 0.1 M CH_3COOH, and 0.1 M acetate buffers with a pH of 3.5, 4.0, and 4.5) (Figure 5B). The highest and best-shaped peak current with a low standard deviation was obtained for peak 1 in 0.01 M HNO_3. Therefore, this solution was used in further studies.

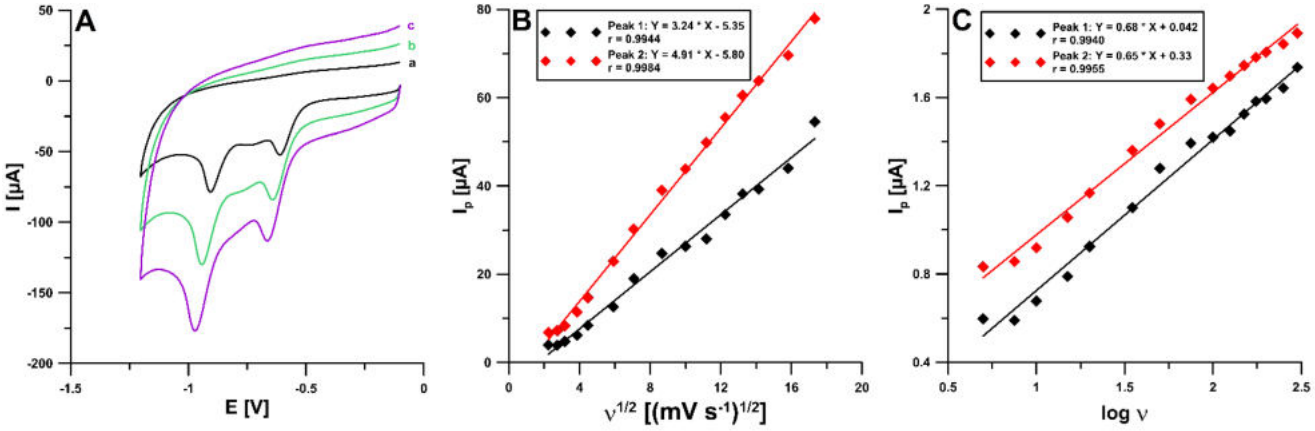

Figure 4. (**A**) Cyclic voltammograms of 0.01 M HNO_3 at the SPCE/SDS for ν of 50 (a), 100 (b), and 150 (c) mV/s. (**B**) The relationship between I_p and $\nu^{1/2}$ for ν from 5 to 300 mV/s. (**C**) The relationship between I_p and log ν for ν from 5 to 300 mV/s.

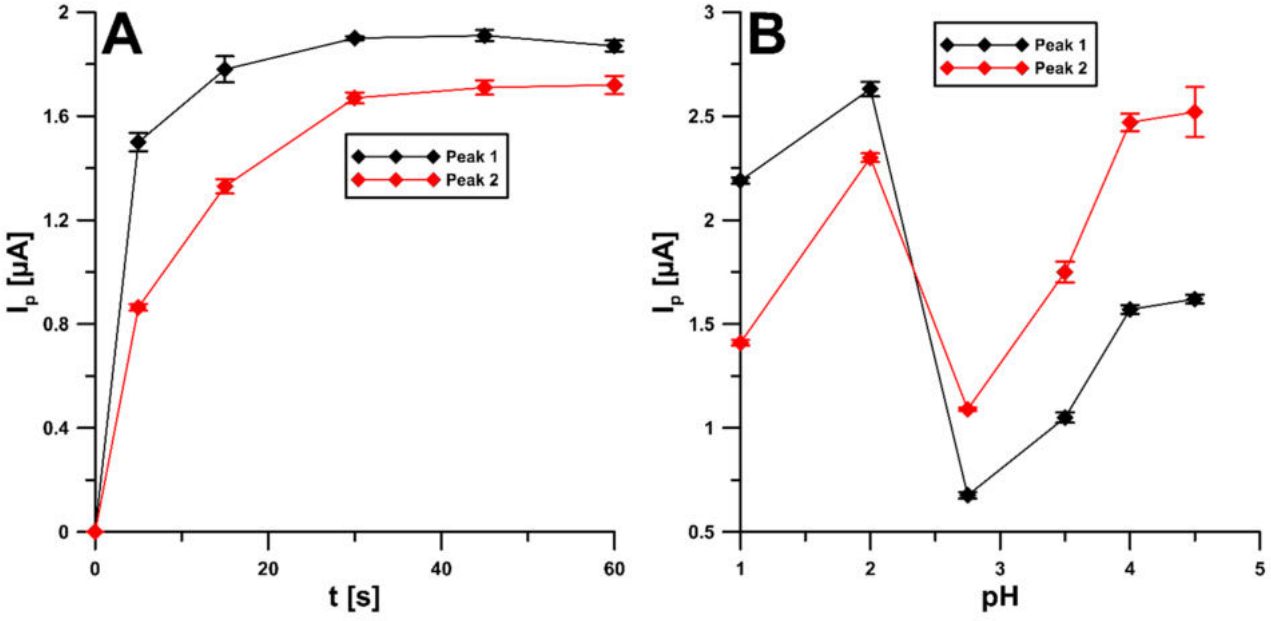

Figure 5. Influence of: (**A**) solution mixing time and (**B**) the type of supporting electrolytes (0.1 and 0.01 M solutions of HNO_3, 0.1 M CH_3COOH, and 0.1 M acetate buffers with a pH of 3.5, 4.0, and 4.5) on the 50 nM peak current of NDIT. The mean values of I_p are given with the standard deviation for n = 3.

As mentioned above, in the case of NDIT, an irreversible two-step reduction process took place at the surface of the SPCE/SDS as a sensor. The proposed electrochemical NDIT reduction course proceeding through an electron-gain mechanism is outlined in Figure 6. At

the pretreatment step, due to the presence of strong nitric acid as the supporting electrolyte, the prior protonation [29,30] of NDIT to a cationic form at the sensor surface is most likely.

$$R–NO_2 + H^+ \rightarrow R–NO_2H^+$$

$$R–NO_2H^+ + 4e^- + 3H^+ \rightarrow R–NHOH + H_2O$$

$$R–NHOH + H^+ \rightarrow R–NHOH_2^+$$

$$R–NHOH_2^+ + 2e^- + H^+ \rightarrow R–NH_2 + H_2O$$

R =

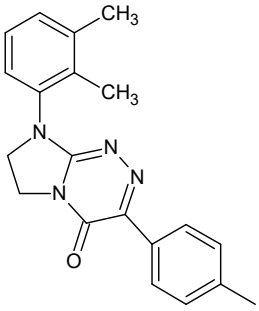

Figure 6. The hypothetical NDIT reduction mechanism.

It has been proved in previous studies that the course of the electrochemical reduction of nitro-containing pharmaceutics strictly depends on the reaction conditions (e.g., the electrolyte solution pH and the electrode potential) [3,31,32]. Thus, the most probable course is that under acidic conditions the electrochemical reduction of NDIT in the first step leads to the NDIT hydroxylamine derivative, while in the second step (preceded by further protonation of the previously formed hydroxylamine derivative), it leads to the NDIT amino derivative, as shown in Figure 6.

2.3. Effect of DPV Parameters

Further studies focused on the reduction peak 1 (the peak at less negative potential) due to the higher intensity of the peak current and the better repeatability of the signal. Much better reproducibility of the first signal (RSD of 3.5% for n = 10) was observed compared to the second signal (RSD of 10.7% for n = 10). Furthermore, the influence of the differential-pulse voltammetric (DPV) parameters (amplitude—ΔE_A; scan rate—ν; and modulation time—t_m) on the analytical signal of 50 nM NDIT was studied. In order to examine the influence of ΔE_A (from 25 to 200 mV), the NDIT reduction signal was measured (Figure 7A). The highest responses were obtained with an ΔE_A of 175 and 200 mV, so for further studies, the value of 175 mV was selected. Figure 7B represents the relationship between the ν in the range of 25–200 mV/s and the NDIT peak current. The highest responses were obtained with a ν of 150 and 175 mV/s, and therefore, a ν of 150 mV/s was selected as optimal. A t_m was studied in the range from 2 to 40 ms. As can be seen in Figure 7C, the highest NDIT signal was obtained for a t_m of 5 ms.

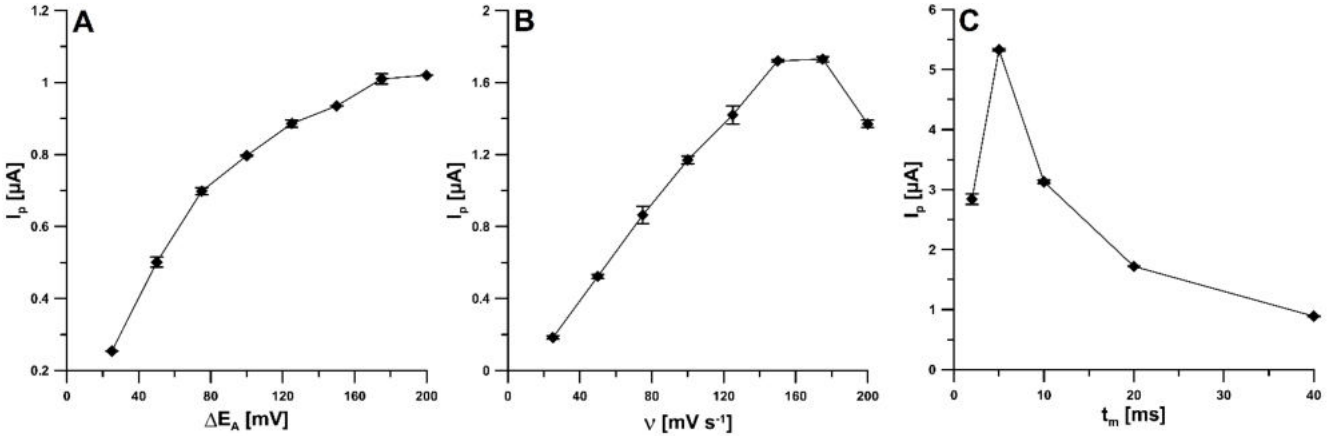

Figure 7. Influence of (**A**) ΔE_A, (**B**) ν, and (**C**) t_m on the analytical signal of 50 nM NDIT. The mean values of I_p are given with the standard deviation for n = 3.

2.4. Sensitive and Selective Voltammetric Determination of NDIT

It is evident from Figure 8 that the NDIT reduction peaks at the SPCE/SDS increase with an increasing concentration of NDIT. The SDS film allowed better electron transfer on the SPCE surface and showed an extremely good linear response towards NDIT. As mentioned above, due to the higher intensity of the peak current (Figure 8A,B) and the better repeatability, the signal 1 is recommended for the quantitative analysis of NDIT. The reduction signal was found to be proportional in a very wide linear range of NDIT concentrations (1–2000 nM, Figure 8C,D). The detection limit (LOD) and quantification limit (LOQ) were calculated at 0.29 and 0.96 nM, respectively, using the following formulas: LOD = $3SD_a/b$ and LOQ = $10SD_a/b$ (SD_a—standard deviation of intercept (n = 3); b—slope of calibration curve).

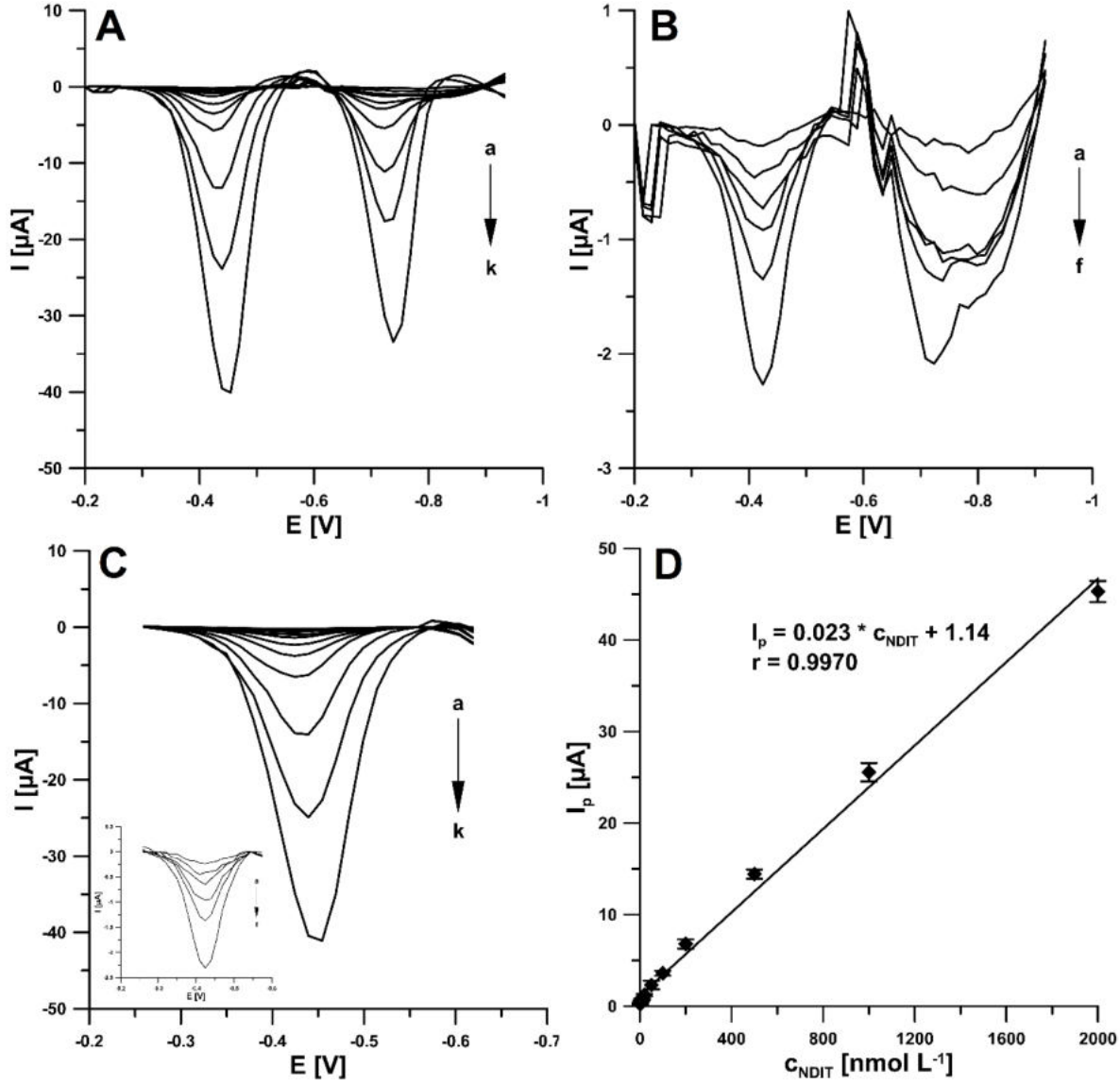

Figure 8. DPAdSV curves registered at the SPCE/SDS in 0.01 M solution of HNO_3 containing 10 mg/L SDS and increasing concentrations of NDIT: (**A**) (a) 1, (b) 2, (c) 5, (d) 10, (e) 20, (f) 50, (g) 100, (h) 200, (i) 500, (j) 1000, and (k) 2000 nM; (**B**) (a) 1, (b) 2, (c) 5, (d) 10, (e) 20 and (f) 50 nM; (**C**) (a) 1, (b) 2, (c) 5, (d) 10, (e) 20, (f) 50, (g) 100, (h) 200, (i) 500, (j) 1000, and (k) 2000 nM; and insert in **C**) (a) 1, (b) 2, (c) 5, (d) 10, (e) 20, and (f) 50 nM. (**D**) Calibration plot of NDIT (peak 1). DPAdSV parameters: t of 45 s, ΔE of 175 mV, ν of 150 mV/s, and t_m of 5 ms. The mean values of I_p are given with the standard deviation for n = 3.

The interference studies were performed under the optimized conditions (0.01 M HNO_3, 10 mg/L SDS and 50 nM NDIT) in the presence of various ions and organic substances commonly present in body fluids. On the basis of the conducted research, it was found that a 1000-fold excess of Fe(III), Ca(II), Mg(II), Cl(-I), glucose, epinephrine, ascorbic acid, and uric acid does not significantly alter the peak current of NDIT (does not cause changes greater than 10%). In the case of dopamine, a 100 times higher concentration than that of NDIT caused no significant influence on the NDIT response. In summary, the SPCE/SDS with a high interference withstanding ability permits the selective determination of NDIT.

2.5. Serum Sample Analysis

The DPAdSV procedure with the SPCE/SDS was used for NDIT determination in spiked human serum samples to prove its viability in real sample analysis. The samples were prepared as follows: 10 mL of human serum thawed at room temperature was spiked with 2.5 mL of 15% (*w/v*) TCA solution and the appropriate NDIT concentration. Then, the resultant solution was transferred to a centrifugal tube, centrifuged at 4000× *g* for 10 min, and filtered through a 0.22 µm Millipore filter. Next, 1 mL of sample was added to the supporting electrolyte, and the DPAdSV curves (Figure 9) were recorded under the optimized conditions. The recovery values were found to be very close to 100% (Table 1), which proves that the fabricated sensor is a reliable tool for the sensitive and selective determination of NDIT in real samples.

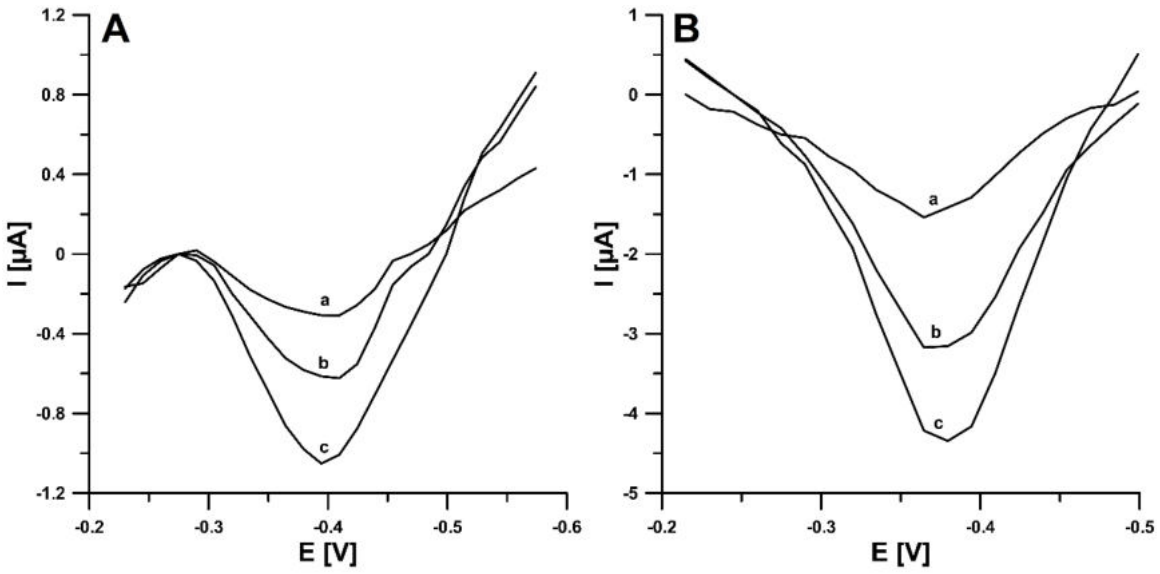

Figure 9. DPAdSV curves registered at the SPCE/SDS in 0.01 M solution of HNO_3 containing 10 mg/L SDS during human serum analysis: (**A**) (a) sample + 20 nM NDIT, (b) as (a) + 20 nM NDIT, and (c) as (a) + 40 nM NDIT; (**B**) (a) sample + 50 nM NDIT, (b) as (a) + 100 nM NDIT, and (c) as (a) + 150 nM NDIT. DPAdSV parameters: t of 45 s, ΔE of 175 mV, ν of 150 mV/s, and t_m of 5 ms.

Table 1. Results of NDIT determination in human serum samples.

NDIT Concentration (nM) ± SD (n = 3)		
Added	**Found DPAdSV**	**Recovery * (%)**
20	20.1 ± 0.88	100.5
50	50.4 ± 1.44	100.8

* Recovery (%) = (Found DPAdSV × 100)/Added.

3. Materials and Methods

3.1. The Investigated Electroactive Molecule

For current electrochemical research needs, an electroactive NDIT molecule with a fully defined structure (i.e., 3-(4-nitrophenyl)-8-(2,3-dimethylphenyl)-7,8-dihydroimidazo[2,1-*c*][1,2,4]triazin-4(6*H*)-one [1,2], which is prone to reduction in biological systems, was chosen. The analyte was obtained from 1-(2,3-dimethylphenyl)-2-hydrazinylideneimidazolidine hydroiodide and ethyl 2-(4-nitrophenyl)-2-oxoacetate, according to the synthetic procedure, which was described in an earlier paper [1].

3.2. Instrumentation, Reagents, and Solutions

The electrochemical experiments were performed using a μAutolab analyzer (Eco Chemie, Utrecht, The Netherlands) controlled by GPES 4.9 software (CV, AdSV) or FRA 4.9 software (EIS) in a 10 mL quartz cell with a commercially available screen-printed sensor (Metrohm-DropSens, Oviedo, Spain). The sensors consisted of a carbon working electrode (diameter of 4 mm), a carbon auxiliary electrode, and a silver pseudo-reference electrode (SPCE, ref. 110).

The 1 M solution of HNO_3, CH_3COOH, and acetate buffers with a pH of 3.5, 4.0, and 4.5 were prepared from Merck (Darmstadt, Germany) reagents. Additionally, Merck standard solutions of Ca(II), Mg(II), Fe(III), and Cl(-I), as well as Sigma-Aldrich (Saint Louis, MO, USA) reagents (epinephrine, dopamine, uric acid, glucose, and ascorbic acid) were used in interference studies. The 1.0 and 0.1 mM solutions of NDIT were prepared in *N*,*N*-dimethylformamide (Sigma-Aldrich, Saint Louis, MO, USA). Normal human serum was purchased from Merck (Darmstadt, Germany). In order to precipitate proteins from serum samples, 15% (*w*/*v*) TCA solution (Sigma-Aldrich, Saint Louis, MO, USA) was used.

3.3. Fabrication of SPCE/SDS and Assay Procedure

The SPCE/SDS sensor was fabricated during the NDIT analysis. Under the optimized conditions, the supporting electrolyte consisted of 0.01 M HNO_3 and 10 mg/L SDS. The 45 s solution mixing time before recording the signal facilitates the diffusion of the NDIT molecules from the solution to the electrode surface and the adsorption of the NDIT particles on the electrode surface. Sometimes, adsorption of SDS takes place on the surface of the SPCE. The DPAdSV curves were registered within the potential range from −0.2 to −1.1 V with amplitude–ΔE_A–of 175 mV, scan rate–ν–of 150 mV/s and modulation time–t_m–of 5 ms. The background curve was subtracted from each voltammogram and the baseline was corrected.

4. Conclusions

In summary, for the fabrication of the screen-printed carbon modified sodium dodecyl sulfate sensor (SPCE/SDS), we report the adsorption of anionic surfactant molecules on the electrode surface during the analysis. The unmodified SPCE and the SPCE/SDS sensors were characterized by cyclic voltammetry (CV) and electrochemical impedance spectroscopy (EIS). Furthermore, the SPCE/SDS sensor showed an electrochemical response towards 3-(4-nitrophenyl)-8-(2,3-dimethylphenyl)-7,8-dihydroimidazo[2,1-*c*][1,2,4]triazin-4(6*H*)-one (NDIT), one of the most promising candidates for anticancer agents. The substantial increase in the NDIT peak current with a sharper and well-defined peak at the SPCE/SDS reflects the faster electron transfer kinetics due to the presence of the SDS film. The SPCE/SDS sensor with its outstanding electrochemical performance is highly sensitive and selective for NDIT analysis. The DPAdSV procedure with the SPCE/SDS presented a very wide linear range from 1 to 2000 nM and a low detection limit of 0.29 nM. It should be highlighted that this is the first analytical procedure developed for the NDIT analysis. The results suggest a promising analytical tool for NDIT analysis in human serum samples.

Author Contributions: Conceptualization, J.K., K.T.-R. and K.S.; investigation, J.K., K.T.-R., K.S. and M.S.; writing—original draft preparation, J.K., K.T.-R., K.S. and M.S.; writing—review and editing, J.K., K.T.-R., K.S. and M.S.; supervision, K.T.-R. and K.S. All authors have read and agreed to the published version of the manuscript.

Funding: This research received no external funding.

Institutional Review Board Statement: Not applicable.

Informed Consent Statement: Not applicable.

Data Availability Statement: The data presented in this study are available on request from the corresponding author.

Conflicts of Interest: The authors declare no conflict of interest.

References

1. Sztanke, M.; Rzymowska, J.; Janicka, M.; Sztanke, K. Synthesis, structure elucidation, determination of antiproliferative activities, lipophilicity indices and pharmacokinetic properties of novel fused azaisocytosine-containing congeners. *Arab. J. Chem.* **2019**, *12*, 4044–4064. [CrossRef]
2. Sztanke, M.; Sztanke, K. Derivatives of 3-(4-nitrophenyl)-7,8-dihydroimidazo[2,1-*c*][1,2,4]triazin-4(6*H*)-one Substituted by phenyl, alkylphenyl, dialkylphenyl and alkoxyphenyl, Method for Obtaining Them and Medical Application. Polish Patent PL 225419, 28 April 2017.
3. Chiavassa, L.D.; Camilo, F.F.; La Scalea, M.A. Voltammetric generation and kinetic stability of nitro anion radical from nitrofurazone in ionic liquids. *J. Braz. Chem. Soc.* **2021**, *32*, 889–899. [CrossRef]
4. Worzakowska, M.; Sztanke, M.; Sztanke, K. Decomposition mechanism of annelated triazinones bearing the *para*-nitrophenyl group. *J. Anal. Appl. Pyrolysis* **2020**, *149*, 104856. [CrossRef]
5. Jahani, P.M.; Beitollahi, H. Screen-printed graphite electrode modified with Co_3O_4 nanoparticles and 2D graphitic carbon nitride as an effective electrochemical sensor for 4-aminophenol detection. *Nanotechnology* **2022**, *33*, 395702. [CrossRef] [PubMed]
6. Darroudi, A.; Nazari, S.; Marashi, S.A.; Abad, M.K.N. Determination of simvastatin by voltammetry method at screen-printed electrode modified by graphene oxide nanosheets and sodium dodecyl sulfate. *J. Electrochem. Soc.* **2022**, *169*, 026501. [CrossRef]
7. Zhao, G.; Tran, T.-T.; Modha, S.; Sedki, M.; Myung, N.V.; Jassby, D.; Mulchandani, A. Multiplexed anodic stripping voltammetry detection of heavy metals in water using nanocomposites modified screen-printed electrodes integrated with a 3D-printed flow cell. *Front. Chem.* **2022**, *10*, 815805. [CrossRef] [PubMed]
8. Tyszczuk-Rotko, K.; Metelka, R.; Vytras, K. Screen-printed carbon electrodes modified with lead film deposited using different plating methods as sensors in anodic stripping voltammetry. *Electrochim. Acta* **2013**, *92*, 335–340. [CrossRef]
9. Ustabasi, G.S.; Perez-Rafols, C.; Serrano, N.; Diaz-Cruz, J.M. Simultaneous determination of iron and copper using screen-printed carbon electrodes by adsorptive stripping voltammetry with *o*-phenanthroline. *Microchem. J.* **2022**, *179*, 107597. [CrossRef]
10. Frutos-Puerto, S.; Hurtado-Sanchez, M.C.; Cerrato-Alvarez, M.; Miro-Rodriguez, C.; Pinilla-Gil, E. A pocket-size device for monitoring gaseous elemental mercury by passive sampling on a Nano-Au screen-printed electrode and detection by single drop smartphone-controlled voltammetry. *Microchem. J.* **2022**, *179*, 107642. [CrossRef]
11. Buffon, E.; Stradiotto, N.R. Using a disposable platform based on reduced graphene oxide, iron nanoparticles and molecularly imprinted polymer for voltammetric determination of vanillic acid in fruit peels. *Food Chem.* **2022**, *397*, 133786. [CrossRef]
12. Ott, C.E.; Cunha-Silva, H.; Kuberski, S.L.; Cox, J.A.; Arcos-Martinez, M.J. Electrochemical detection of fentanyl with screen-printed carbon electrodes using square-wave adsorptive stripping voltammetry for forensic applications. *J. Electroanal. Chem.* **2020**, *873*, 114425. [CrossRef]
13. Prezilius, A.C.M.; dos Santos, G.F.S.; Silva, L.R.G.; Barbieri, E.M.S.; Brandao, G.P.; Ferreira, R.Q. Development of an electroanalytical methodology associated with screen-printed electrodes for the determination of glyphosate in river waters. *Ionics* **2022**, *28*, 4035–4043. [CrossRef]
14. Zabolestani, H.; Sardahi, H.; Beitollahi, H. Electrochemical sensor based on modified screen printed electrode for vitamin B_6 detection. *Surf. Engin. Appl. Electrochem.* **2021**, *57*, 277–285. [CrossRef]
15. Yardim, Y. Sensitive detection of capsaicin by adsorptive stripping voltammetry at a boron-doped diamond electrode in the presence of sodium dodecylsulfate. *Electroanalysis* **2011**, *23*, 2491–2497. [CrossRef]
16. Monnappa, A.B.; Manjunatha, J.G.; Bhatt, A.S. Design of a sensitive and selective voltammetric sensor based on a cationic surfactant-modified carbon paste electrode for the determination of alloxan. *ACS Omega* **2020**, *5*, 23481–23490. [CrossRef]
17. Angelis, P.N.; de Cassia Mendonca, J.; de Rocha, L.R.; Capelari, T.B.; Prete, M.C.; Segatelli, M.G.; Borsato, D.; Tarley, C.R.T. Feasibility of a nano-carbon black paste electrode for simultaneous voltammetric determination of antioxidants in food samples and biodiesel in the presence of surfactant. *Electroanalysis* **2020**, *32*, 1198–1207. [CrossRef]
18. Pınar, P.T. Electrooxidation and low-tech determination of pantoprazole on a disposable pencil graphite electrode by the use of cationic surfactant. *Acta Chim. Slov.* **2020**, *67*, 212–220. [CrossRef]

19. Abdullah, A.A.; Yardim, Y.; Senturk, Z. The performance of cathodically pretreated boron-doped diamond electrode in cationic surfactant media for enhancing the adsorptive stripping voltammetric determination of catechol-containing flavonoid quercetin in apple juice. *Talanta* **2018**, *32*, 156–164. [CrossRef]
20. Tigari, G.; Manjunatha, J.G. A surfactant enhanced novel pencil graphite and carbon nanotube composite paste material as an effective electrochemical sensor for determination of riboflavin. *J. Sci. Adv. Mater. Dev.* **2020**, *5*, 56–64. [CrossRef]
21. Atta, N.F.; Darwish, S.A.; Khalil, S.E.; Galal, A. Effect of surfactants on the voltammetric response and determination of an antihypertensive drug. *Talanta* **2007**, *72*, 1438–1445. [CrossRef]
22. da Silva, E.M.; de Oliveira, G.C.; de Sequeira, A.B.; Terezo, A.J.; Castilho, M. Development of a composite electrode based on graphite and polycaprolactone for the determination of antihypertensive drugs. *Microchem. J.* **2020**, *158*, 105228. [CrossRef]
23. Kumar, N.; Goyal, R.N. A simple and highly selective determination of telmisartan at sodium dodecyl sulfate modified pyrolytic graphite surface. *Electroanalysis* **2018**, *30*, 892–900. [CrossRef]
24. Raril, C.; Manjunatha, J.G.; Tigari, G. Low-cost voltammetric sensor based on an anionic surfactant modified carbon nanocomposite material for the rapid determination of curcumin in natural food supplement. *Instrum. Sci. Tech.* **2020**, *48*, 561–582. [CrossRef]
25. Nurdin, I.; Fitri, H.R.; Widiatmoko, P.; Devianto, H.; Prakoso, T. The effect of cationic CTAB on the performance of graphene electrode for supercapacitor. *IOP Conf. Ser. Mater. Sci. Eng.* **2020**, *823*, 012038. [CrossRef]
26. Decarli, N.O.; Zapp, E.; de Souza, B.S.; Santana, E.R.; Winiarski, J.P.; Vieira, I.C. Biosensor based on laccase-halloysite nanotube and imidazolium zwitterionic surfactant for dopamine determination. *Biochem. Eng. J.* **2022**, *186*, 108565. [CrossRef]
27. Ziyatdinova, G.; Ziganshina, E.; Budnikov, H. Voltammetric sensing and quantification of eugenol using nonionic surfactant self-organized media. *Anal. Methods* **2013**, *5*, 4750–4756. [CrossRef]
28. Gosser, D.K. *Cyclic Voltammetry: Simulation and Analysis of Reaction Mechanism*; VCH: New York, NY, USA, 1993.
29. Cadle, S.H.; Tice, P.R.; Chambers, J.Q. Electrochemical reduction of aromatic nitro compounds in the presence of proton donors. *J. Phys. Chem.* **1967**, *71*, 3517–3522. [CrossRef]
30. Exner, O.; Böhm, S. Protonated nitro group: Structure, energy and conjugation. *Org. Biomol. Chem.* **2005**, *3*, 1838–1843. [CrossRef]
31. Squella, A.J.; Bollo, S.; Nunez-Vergara, J.L. Recent developments in the electrochemistry of some nitro compounds of biological significance. *Curr. Org. Chem.* **2005**, *9*, 565–581. [CrossRef]
32. De Lima Brito, C.; Goulart-Trossini, G.H.; Ferreira, E.I.; La-Scalea, M.A. Nitrofurazone and its nitroheterocyclic analogues: A study of the electrochemical behavior in aqueous medium. *J. Braz. Chem. Soc.* **2013**, *24*, 1964–1973. [CrossRef]

RD9

J. Kozak, K. Tyszczuk-Rotko, *Screen-printed gold electrode for ultrasensitive voltammetric determination of the antipsychotic drug thioridazine,* Measurement, 217 (2023) 113107.

Measurement 217 (2023) 113107

Contents lists available at ScienceDirect

Measurement

journal homepage: www.elsevier.com/locate/measurement

Screen-printed gold electrode for ultrasensitive voltammetric determination of the antipsychotic drug thioridazine

Jędrzej Kozak, Katarzyna Tyszczuk-Rotko *

Faculty of Chemistry, Institute of Chemical Sciences, Maria Curie-Skłodowska University in Lublin, 20-031 Lublin, Poland

ARTICLE INFO

Keywords:
Thioridazine
Schizophrenia
Screen-printed gold sensor
Stripping voltammetry
Adsorption
Human serum
Municipal sewage

ABSTRACT

A highly sensitive, fast and simple analytical procedure for analysis of the antypsychotic drug thioridazine (TDZ) using an original screen-printed gold electrode (SPAuE) was developed. The cyclic voltammetry, scanning electron microscopy, electrochemical impedance and energy-dispersive X-ray spectroscopy were used for the SPAuE characterization. The results showed the advantage of the commercially available SPAuE in terms of working electrode active surface and the efficiency of kinetics of electron transfer compare to unmodified and *ex situ* modified gold film screen-printed carbon electrode. Moreover, the results displayed that an irreversible, adsorption-controlled oxidation process of TDZ in phosphate buffered saline of pH 2.6 is connected with the strong affinity of sulfur atoms for gold. The SPAuE allows for a much lower detection limit (2.9×10^{-12} M) than in the case of other electrochemical sensors used for TDZ analysis. The measurements results were validated by official and standard addition methods.

1. Introduction

Antipsychotics are the mainstay of treatment for psychotic disorders, including schizophrenia. Drugs in this group are commonly used to treat psychotic symptoms such as paranoia, hallucinations, agitation, and delirium. They are also used to treat psychotic depression, bipolar disorder, and anxiety. One of the drugs used in the treatment of schizophrenia is thioridazine; it is administered to patients who do not respond adequately to treatment with other antipsychotics [1]. Thioridazine is a phenothiazine neuroleptic drug and in pharmaceuticals it is present in the form of thioridazine hydrochloride (TDZ) [2]. This drug works by regulating the level of substances such as serotonin, dopamine and glutamate in the human brain, inadequate amounts of which cause symptoms in schizophrenia [3]. In addition to schizophrenia, TDZ is used to control mania and agitation, and can be used to treat anxiety and behavioral problems in children. The use of TDZ in combating infections with methicillin-resistant Staphylococcus aureus (MRSA) and multidrug-resistant Mycobacterium tuberculosis is also known [4–6].

Despite numerous therapeutic applications, high doses of TDZ can cause serious side effects, such as the potentially fatal neuroleptic malignant syndrome exerting its effect through central dopamine-blocking, adrenergic-blocking and minor anticholinergic activity [5,7]. Other side effects include arrhythmia, dry mouth and cardiac death [2]. Therapeutic doses for an adult are usually in the range of 50–800 mg TDZ per day. During therapy, the maximum concentration of TDZ in the blood of patients ranges from 3.2×10^{-7} to 1.3×10^{-6} M [8,9].

Nowadays, the problem is the release of various groups of pharmaceuticals into the environment, which is related to their increasing consumption. Psychotropic drugs, also after being excreted with urine and feces, are transported to the sewage treatment plant. However, treatment plants are not designed to eliminate drugs and their metabolites, and therefore a certain amount of administered drugs is released into the environment [10]. The presence of TDZ at low concentration levels in wastewater in various regions of the world has been reported. For example, $1.5 \times 10^{-11} - 5.4 \times 10^{-10}$ M TDZ was detected at the site of discharge of sewage into the Medway River in the UK [11]. In the same country, while examining the degree of removal of various pharmaceuticals, TDZ was determined in the sewage flowing in and out of the Motney Hill treatment plant and the concentrations of TDZ were 1.1×10^{-10} and 8.1×10^{-11} M, respectively [12]. In turn, in the Tehran South Municipal Wastewater Treatment Plant, up to 1.2×10^{-9} M TDZ was detected in the wastewater flowing in, and about 7×10^{-11} M in the wastewater flowing out of the treatment plant [13].

Taking into account the dangerous side effects of TDZ overdose as well as the presence of this drug in environmental samples, it is essential to create highly sensitive assay methods. The literature describes the

* Corresponding author.
E-mail address: katarzyna.tyszczuk-rotko@mail.umcs.pl (K. Tyszczuk-Rotko).

https://doi.org/10.1016/j.measurement.2023.113107
Received 28 March 2023; Received in revised form 10 May 2023; Accepted 25 May 2023
Available online 30 May 2023

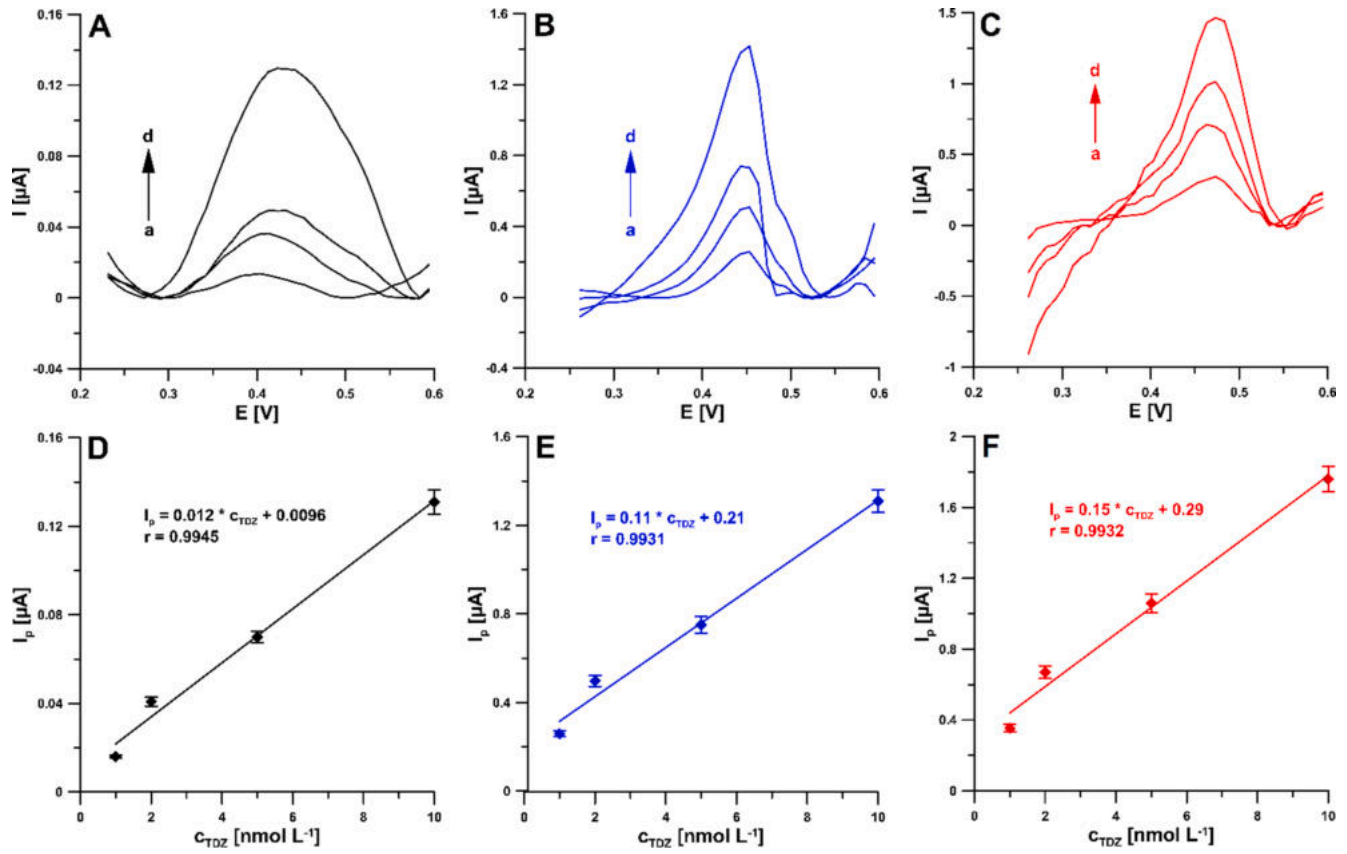

Fig. 1. The DPAdSVs of the SPCE (A), SPCE/AuF (B) and SPAuE (C) in the presence of following TDZ concentration: (a) 1.0×10^{-9}, (b) 2.0×10^{-9}, (c) 5.0×10^{-9}, (d) 1.0×10^{-8} M in 0.1 M PBS of pH 7.2. Linear dependences between I_p and TDZ concentration ($1.0 \times 10^{-9} - 1.0 \times 10^{-8}$ M) obtained on SPCE (A), SPCE/AuF (B) and SPAuE (C). The DPAdSV parameters: ν of 100 mV s^{-1}, t_m of 10 ms, ΔE_A of 100 mV, $E_{acc.}$ of −0.2 V and $t_{acc.}$ of 60 s.

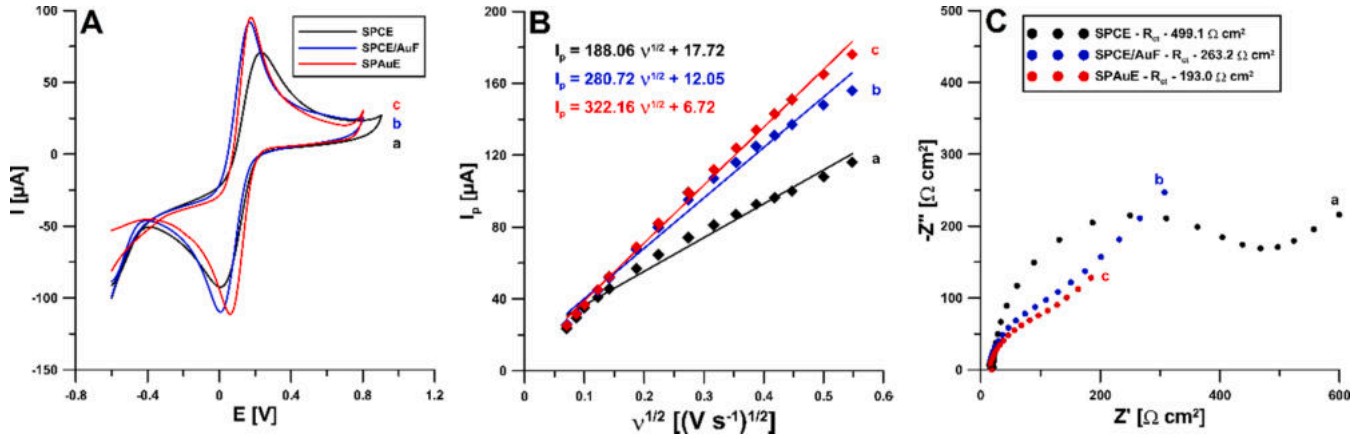

Fig. 2. (A) CV curves recorded at the SPCE (a), SPCE/AuF (b) and SPAuE (c) using the scan rate of 100 mV s^{-1}; (B) the relationship between the anodic I_p and the square root of the scan rate ($\nu^{1/2}$) obtained at the SPCE (a) SPCE/AuF (b) and SPAuE (c) using the scan rate ranging from 5 to 300 mV s^{-1}; (C) Nyquist plots of the SPCE (a) SPCE/AuF (b) and SPAuE (c) recorded at a potential of 0.2 V, in the frequency range from 50 kHz to 1 Hz. All measurements were performed in 0.1 M KCl and 0.005 M $[Fe(CN)_6]^{3-}$.

methods of TDZ determination using, e.g., colorimetry [14], spectrophotometry [15], spectrofluorimetry [16], gas–liquid chromatography [17], supercritical fluid chromatography [18], and high-performance liquid chromatography [19,20]. However, these methods are mostly time-consuming, requiring laborious sample pretreatment and expensive equipment. An alternative are electrochemical methods, including voltammetry, the undoubted advantages of which are the simplicity of the procedures used, high accuracy and precision, repeatability and selectivity as well as short analysis time [21,22].

Among the multitude of voltammetric sensors, screen-printed electrodes are used nowadays, apart from classic electrodes. This type of electrodes is part of the trend of miniaturization of measuring devices due to the possibility of integrating the working, auxiliary and reference electrodes on the same substrate (plastic or ceramic) [23–26]. The advantages of SPEs are their design flexibility, low cost, portability, the possibility of using them for the determination of various substances, and the diversity of electrode materials. In addition, these electrodes have a low background current and ease of operation, and can be

Table 1
Electrochemical characteristics of SPCE, SPCE/AuF and SPAuE using EIS and CV in 0.1 M KCl and 0.005 M $[Fe(CN)_6]^{3-}$.

Electrode	A_S [cm^2]	R_{ct} [Ω cm^2]	χ^0 (for ν of 100 mV s^{-1})	Sensitivity [μM nA^{-1}]
SPCE	0.052	499.1	3.45	0.012
SPCE/AuF	0.078	263.2	2.68	0.11
SPAuE	0.089	193.0	1.90	0.15

modified for various applications [27,28].

One of frequently used modifiers of working electrodes in voltammetry are metals in the form of particles of different sizes. Metal particles deposited on the surface of the working electrode increase the active surface. Their use also provides a fast transfer of electrons between the surface of electrode and the electroactive species and as well as the speed of mass transport, which translates into high sensitivity of analyses performed [29,30]. A number of analytical procedures can be found in the literature using electrodes modified with films or metal nanoparticles, including Pb, Bi, and Sb [31], but also with noble metals such as Ag [32] or Au [33,34]. Gold is also a popular electrode material, widely used in electrochemical studies of many substances. The advantages of the gold electrode are inertness in the presence of most reagents, a wide range of work potentials, stability, and very favorable kinetics of electron transfer [35–37].

In this paper, we describe a highly sensitive, fast and simple procedure for voltammetric analysis of thioridazine (TDZ) in human serum and sewage samples, based on a screen-printed gold electrode (SPAuE) that does not require any preliminary preparation. In the study, the SPAuE was characterized using a scanning electron microscope (SEM), electrochemical impedance spectroscopy (EIS), and cyclic voltammetry (CV), and the obtained parameters were compared with those obtained for other compared electrodes, i.e. a screen-printed carbon electrode (SPCE) and a SPCE modified with gold film (SPCE/AuF).

2. Materials and equipment

2.1. Apparatus

The μAutolab potentiostat/galvanostat (Netherlands, Eco Chemie) connected with FRA 4.9 (EIS studies) and GPES 4.9 software (voltammetric studies) was applied for the electrochemical experiments. The standard 10 mL electrochemical cell made of quartz with a screen-printed gold sensor (SPAuE, Ref. 250BT, commercially available, DropSens, Spain) was adopted for experiments. This sensor consisted of a gold working electrode, a silver pseudo-reference electrode, and a platinum counter electrode. For characterization and comparison of the SPAuE, a screen-printed carbon electrode (SPCE, DropSens; Ref. 110) and the SPCE electrochemically plated during experiment with gold film (SPCE/AuF) were used.

A scanning electron microscope (SEM, high-resolution, Quanta 3D FEG, FEI, USA, was applied for the microscopic images of the studied sensors. The equivalent diameters of Au particles and agglomerates were determined using NIS-Elements Advanced Research software.

2.2. Chemicals

Thioridazine (hydrochloride form, Merck, Germany) was dissolved in deionized water to obtain a 10^{-3} M TDZ. The 10^{-5} or 10^{-6} M solutions of TDZ were obtained by dilution of 10^{-3} M standard by 0.1 M PBS (pH = 7.2). The dilutions were prepared each day. 0.1 M PBS (phosphate buffered saline) solutions with the following pH values: 2.6, 3.9, 6.0, 7.2, 9.1 and 11.0, were used to evaluate the pH effect on the analytical signal of TDZ. The 10^{-3} M solutions of Cd(II), Mg(II), Fe(III), Ca(II), Pb (II), Cu(II), Ni(II), dopamine (DOP), glucose (GLU), adenine (ADN), ascorbic acid (AA), epinephrine (EPI) and uric acid (UA) were made from chemicals bought from Merck in ultrapurified water before measurements, stored in the refrigerator and protected from light. The following samples were analyzed: normal human serum (Merck, Germany) and purified wastewater (Municipal Water Supply and Waste Water Treatment Company Ltd, Lublin, Poland).

2.3. DPAdSV analysis of TDZ

DPAdSV analysis of TDZ under optimized conditions was carried out in a 0.075 M PBS of pH = 2.6. TDZ accumulation was performed at a potential of −0.2 V for 60 s. The procedure consisted of electrochemical cleaning of the electrode surface before each measurement by applying a potential of 0.5 V ($E_{clean.}$) for 10 s ($t_{clean.}$), followed by TDZ accumulation at −0.2 V ($E_{acc.}$) for 60 s ($t_{acc.}$). DPAdSV scans were recorded from 0 to 1.2 V with t_m (the modulation time) of 10 ms, ν (the scan rate) of 75 mV s^{-1} and ΔE_A (the amplitude) of 100 mV. The baseline was corrected and blank was subtracted from every voltammogram.

2.4. Sample analysis

The determination of TDZ in samples of spiked human serum and treated wastewater the DPAdSV was applied to demonstrate its usefulness in analysis of real samples. The serum samples were prepared by mixing 10 mL of human serum thawed at room temperature with 2.5 mL of trichloroacetic acid (15% solution) and TDZ standard solution. Then, the samples were centrifuged at 4000 (rotations per minute) for 10 min and filtered through syringe filter (Millipore) with 0.22 μm pore size. Then, 10 μL of sample was introduced into the electrochemical cell, and the voltammograms were registered.

The samples of treated wastewater were spiked with the desired concentration of TDZ and 100 μL of sample was introduced into the electrochemical cell and analyzed directly.

3. Experimental section

3.1. Initial experiments

In the early stage of the tests, the voltammetric response of TDZ was compared on a SPAuE, a bare SPCE, and a SPCE modified with *ex situ* deposited gold film (SPCE/AuF). The electrode was modified by immersing the SPCE in 0.2 M sulfuric acid and 2.0×10^{-4} M chloroauric acid, applying a potential of −0.2 V for 90 s. The electrode prepared in this way was rinsed and transferred to the supporting electrolyte solution. Voltammograms were registered on each electrode for four increasing concentrations (1.0×10^{-9}, 2.0×10^{-9}, 5.0×10^{-9} and 1.0×10^{-8} M) of TDZ after 10 s of electrode electrochemical cleaning at 0.5 V and after analyte accumulation at −0.2 V for 60 s. The obtained analytical signals show more clearly that the modification of the SPCE with a gold film results in a significant enhancement (Fig. 1B) relative to the bare SPCE (Fig. 1A). The use of the SPAuE, in turn, allows higher signals to be obtained (Fig. 1C) than on the SPCE/AuF. Measurements conducted for four concentrations of TDZ made it possible to plot a linear dependence of the peak current (I_p) on the concentration of TDZ, and thus calculate the sensitivity of each of the three electrodes. The highest sensitivity was shown by the SPAuE (Fig. 1F), while the SPCE/AuF is slightly less sensitive (Fig. 1E). The SPCE has the lowest sensitivity (Fig. 1D) among the tested electrodes, about 10 times lower than the SPCE/AuF and SPAuE. Such a huge increase in sensitivity of gold-based electrodes is most likely due to the strong affinity of sulfur for gold. Sulfur atoms, especially in thiol groups, adsorb on the gold surface forming strong covalent bonds [38–40]. Therefore, TDZ with two sulfur atoms in the molecule, including one in the thiomethyl group, should most likely be adsorbed on the surface of gold electrodes.

All the three electrodes studied were characterized electrochemically using EIS and CV in a solution of 0.1 M KCl and 0.005 M $[Fe(CN)_6]^{3-}$.

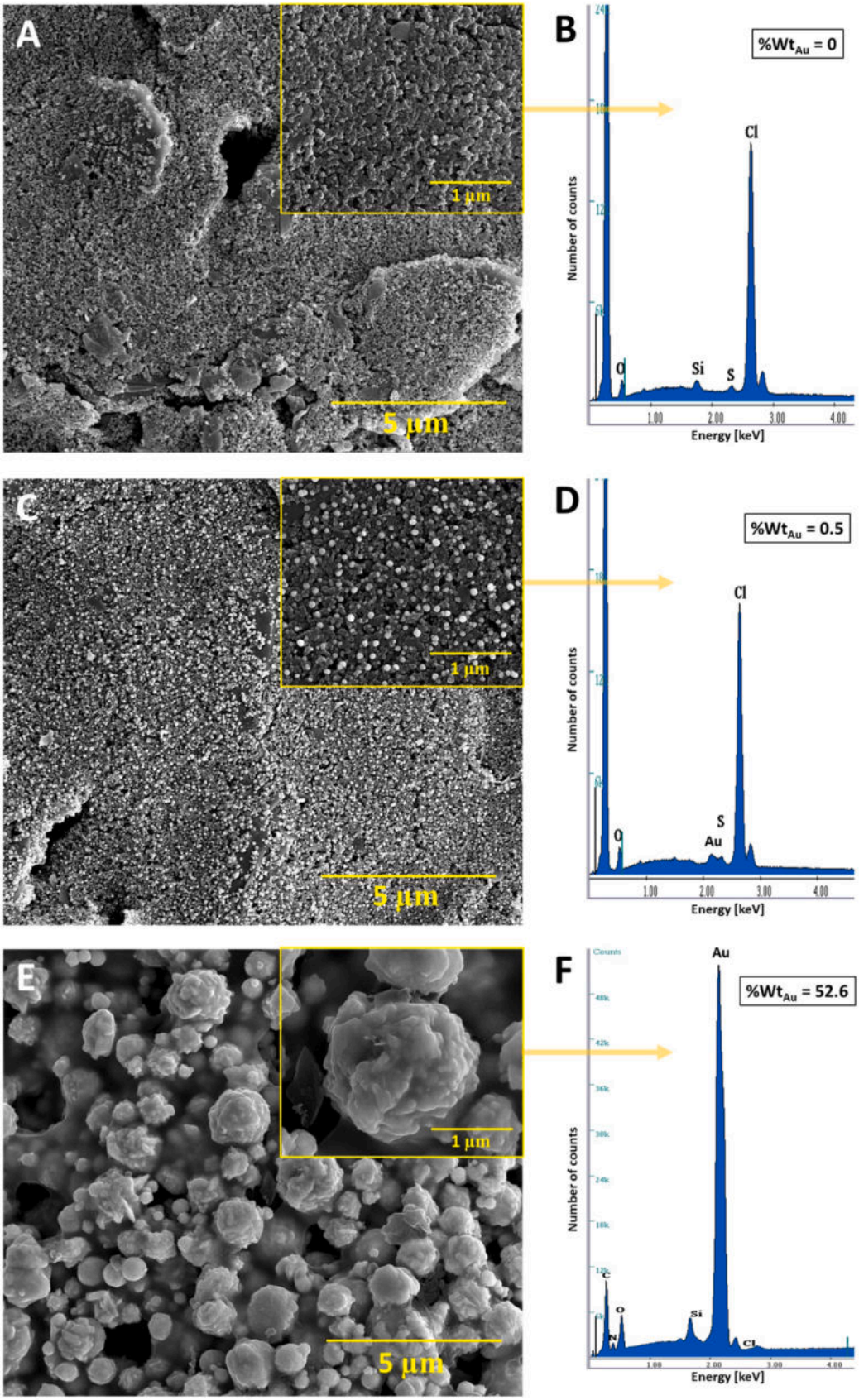

Fig. 3. SEM images of SPCE (A), SPCE/AuF (C) and SPAuE (E). EDS spectra of SPCE (B), SPCE/AuF (D) and SPAuE (F).

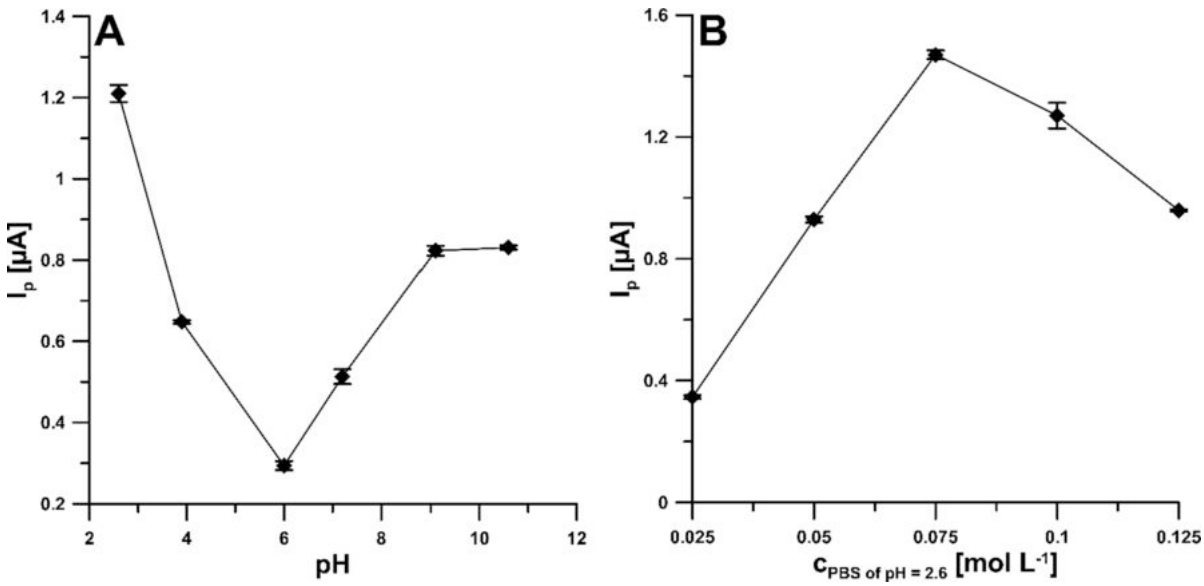

Fig. 4. Effect of pH value (A) and concentration of the PBS of pH 2.6 (B) on TDZ I_p. The DPAdSV parameters: ν of 100 mV s^{-1}, t_m of 10 ms, ΔE_A of 100 mV, $E_{acc.}$ of −0.2 V and $t_{acc.}$ of 60 s.

Fig. 2A illustrates the CVs recorded on the SPCE, SPCE/AuF and SPAuE at a scan rate of 100 mV s^{-1}. Both the SPCE/AuF and SPAuE show an amplification of the Fe(II) to Fe(III) oxidation signal (107.0 µA for the SPCE/AuF and 112.0 µA for the SPAuE) relative to the SPCE (81.1 µA). For each of the electrodes, the relative peak separation (χ^0) was calculated and a value closest to the theoretical value ($\chi^0 = 1$) was obtained for the SPAuE, which proves its best kinetics of electron transfer among the tested electrodes. In addition, based on the entire scan rate range in which the CV measurements were made (5–300 mV s^{-1}), the equation of Randles-Sevcik [41] and the dependence of I_p and the scan rate square root ($\nu^{1/2}$) (Fig. 2B), the electrochemically active area (A_s) of the electrodes, were calculated. EIS studies showed that the modification of the SPCE with a gold film results in a significant lowering of the charge-transfer resistance (R_{ct}), and also that the lowest R_{ct} value, compared to the rest of the electrodes, was obtained for the SPAuE (Fig. 2C). In Table 1 all the mentioned parameters are summarized, the analysis of which allows us to clearly state that due to its very efficient electron transfer, high sensitivity and large active surface, the SPAuE has the best properties among the tested sensors. Therefore, this type of sensor was used for further experiments.

The morphology of all three sensor surfaces was characterized using a SEM-EDS (Fig. 3). It was shown that in the case of the SPCE/AuF the gold film is composed of nanoparticles with an equivalent diameter ranging from 44.59 to 88.86 nm. The SPAuE, on the other hand, consists of particles and agglomerates of gold with a size of 143.93 to 2100.23 nm.

3.2. Effect of pH and concentration of the measurement solution

The effect of pH value on the oxidation peak of 2.0×10^{-9} M TDZ was examined in PBS (0.1 M, pH values from 2.6 to 11) (Fig. 4A). The highest I_p was obtained for pH of 2.6 and this value was considered optimal. The next step was to evaluate the effect of PBS concentration in the range of 0.025–0.125 M (Fig. 4B). The highest values of the TDZ signal were attained in 0.075 M PBS with a pH value of 2.6 and therefore it was adopted for the next stages of the studies.

3.3. CV studies

The voltammetric responses of 2.0×10^{-5} M TDZ at the SPAuE in 0.075 M PBS of pH = 2.6 was tested using CV. The CVs were registered for ν ranging from 0.005 to 0.4 V s^{-1}. Fig. 5A illustrates the CV curves for the following values of the scan rate: 0.05, 0.1 and 0.2 V s^{-1}. One irreversible TDZ oxidation signal was observed. The anode peak at about 1.0 V is due to gold oxidation, and the visible reduction peaks are most likely the result of a quasi-reversible reduction process of previously oxidized gold. An additional confirmation of the irreversibility of TDZ oxidation is the shift of the peak potential (E_p) in the positive direction with increasing scan rate. More information was obtained by analyzing the relationship between the measured values of the TDZ I_p over the entire potential range (5–400 mV s^{-1}) and the square root of the scan rate ($\nu^{1/2}$) (Fig. 5B). The non-linear course of this relationship indicates that the oxidation process of TDZ on the SPAuE is controlled by adsorption. The above conclusion was confirmed by the dependence of the TDZ I_p logarithm (log I_p) and the scan rate logarithm (log ν) (Fig. 5C), the slope of which is 1.01, which allows us to state unequivocally that the process is purely adsorption-controlled. In addition, based on Laviron's equation [42] of the linear relationship between the peak potential (E_p) and the square root of the scan rate ($\nu^{1/2}$) (Fig. 5D), the number of electrons involved in the TDZ oxidation reaction was calculated. The calculated value is 2.36, which corresponds to two electrons and is confirmed in literature data [5,6,21]. The probable mechanism of TDZ oxidation involving two electrons is illustrated in Fig. 5E.

3.4. Effect of DPAdSV parameters

Due to the adsorption of TDZ on the SPAuE surface, demonstrated by the CV studies, we considered it necessary to investigate the effect of $E_{acc.}$ and $t_{acc.}$ on the current intensity of the TDZ peak. For $t_{acc.}$ of 60 s, the $E_{acc.}$ was changed from 0.1 to −0.4 V. In Fig. 6A, it can be seen that the TDZ I_p increases when the potential is shifted in the negative direction, reaches a maximum at −0.2 V and then decreases for lower potentials. Therefore, the $E_{acc.}$ of −0.2 V was selected for further research. Next, the influence of the $t_{acc.}$ in the range of 15–240 s was studied. Fig. 6B shows that the highest signal was obtained for 240 s, but to shorten the analysis time, 60 s was selected for further testing. In order to possibly lower the detection limit, it is recommended to use $t_{acc.}$ of 240 s.

The effect of ΔE_A on the 2.0×10^{-9} M TDZ I_p intensity was evaluated over the range from 0.025 to 0.15 V (Fig. 7A). The I_p reached maximum value for ΔE_A of 0.1 V, so this value was adopted for further research.

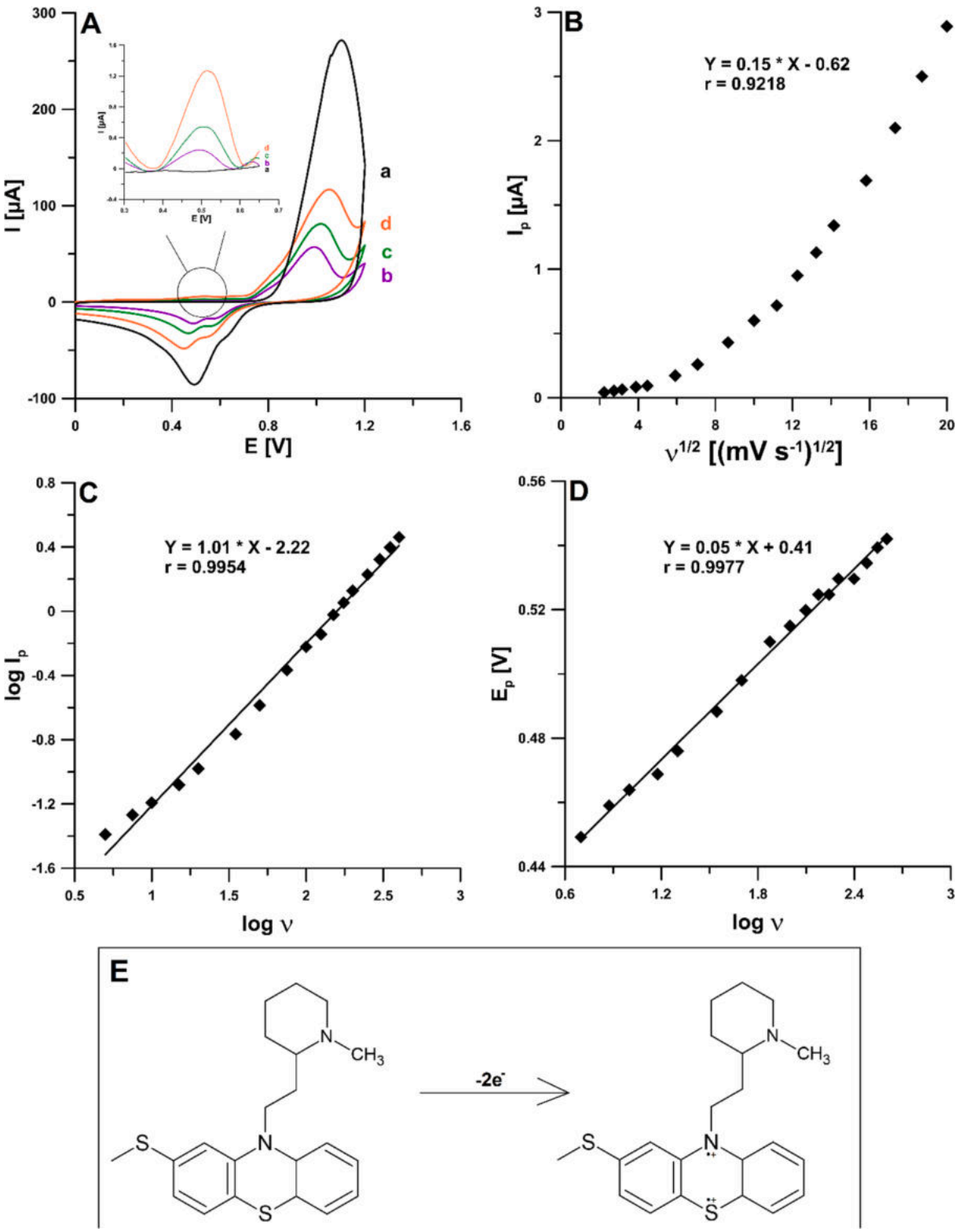

Fig. 5. (A) CVs obtained at the SPAuE in 0.075 M PBS of pH 2.6 and 0 M TDZ (a) and 2.0×10^{-5} M TDZ (b, c and d) (ν of 50, 100 and 200 mV s^{-1}). The relationship between I_p and $\nu^{1/2}$ (ν from 5 to 400 mV s^{-1}) (B), log I_p and log ν (C) and E_p and log ν (D). (E) TDZ oxidation mechanism.

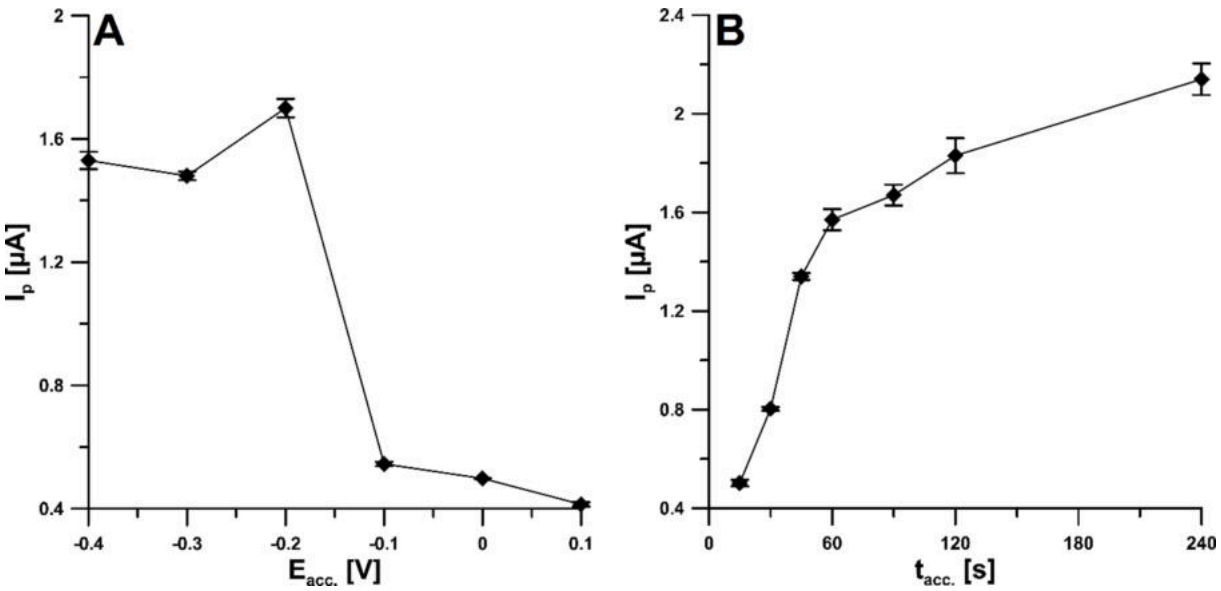

Fig. 6. The dependence of $E_{acc.}$ (A) and $t_{acc.}$ (B) on 2.0×10^{-9} M TDZ signal. ν of 100 mV s^{-1}, t_m of 10 ms, ΔE_A of 100 mV.

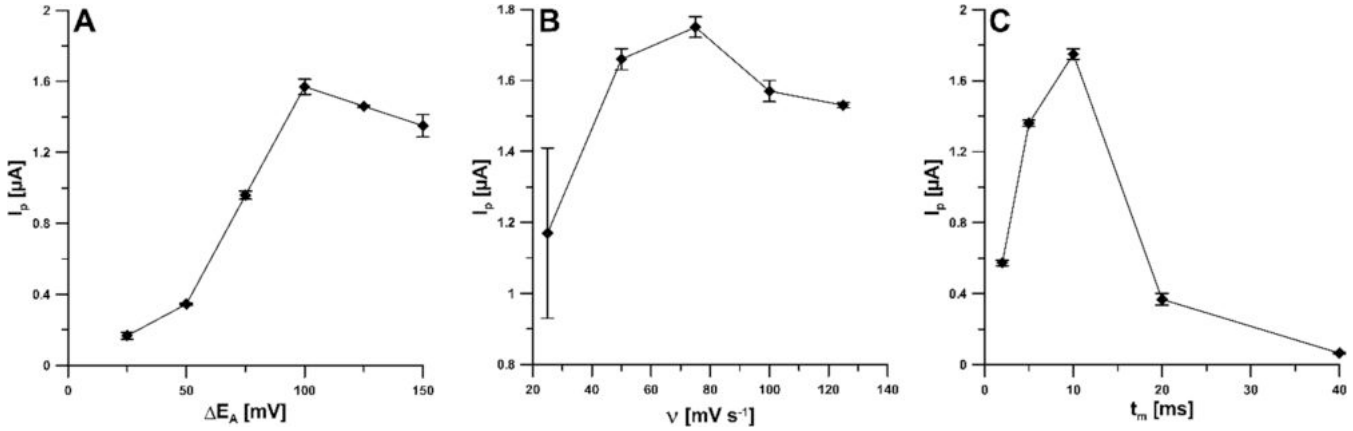

Fig. 7. The influence of ΔE_A (A), ν (B), and t_m (C) on 2.0×10^{-9} M TDZ I_p. $E_{acc.}$ of −0.2 V and $t_{acc.}$ of 60 s.

The next step was to check the influence of the ν, which was done by altering its value from 0.025 to 0.125 V s^{-1}. With the increase of ν, the I_p increased, reaching the highest intensity at the scan rate of 75 mV s^{-1}. Further increasing ν resulted in a lower analytical signal (Fig. 7B), so a value of 75 mV s^{-1} was considered optimal. The last optimized parameter was the t_m, the influence of which was evaluated over the range of 2–40 ms. The maximum TDZ signal height was recorded at 10 ms (Fig. 7C).

3.5. Voltammetric determination of TDZ

Table 2 presents a comparison of the developed procedure using the SPAuE with other voltammetric procedures for the TDZ analysis [2–6,8,21,22,43–45]. In optimized conditions, the determination of increasing concentrations of TDZ (1.0×10^{-11} to 2.0×10^{-8} M) on the SPAuE was performed (Fig. 8A). The analytical signal of TDZ linearly increases with the concentration in three ranges (1.0×10^{-11}–2.0×10^{-10}, 2.0×10^{-10}–2.0×10^{-9} and 2.0×10^{-9}–2.0×10^{-8} M) (Fig. 8B) with the limits of detection (LOD) and quantification (LOQ) of 2.9×10^{-12} and 9.8×10^{-12} M, respectively, (LOD was calculated as (3 × SD of intercept, n = 3) divided by slope of calibration plot, LOQ was calculated as 3.3(3) × LOD) [46]. It can be undoubtedly stated that the SPAuE is characterized by extraordinary sensitivity and allows for a much lower detection limit than in the case of other electrochemical sensors used for TDZ detection. It should also be emphasized that the sensor used is commercially available, which avoids the time-consuming process of preparing the sensor as well as the reagents needed for it.

The SPAuE selectivity was examined studying voltammetric response of TDZ in the presence of various organic compounds and metal ions. The tolerance limit was considered to be 1.0×10^{-9} M TDZ peak current changes not exceeding 10% (Fig. 9). The presence of 0.2–2.0 ppm Triton X-100 in voltammetric cell has a similar effect on the signal as surfactants in natural waters [47]. Therefore, the effect of 2 ppm of Triton X-100 on the TDZ peak was examined and found to be negligible.

In addition, repeatability of the determination of 1.0×10^{-8} M TDZ on the SPAuE was examined. The RSD (relative standard deviation) of 3.5% (n = 10) was reached, which confirms good repeatability of the TDZ signal. Reproducibility was determined based on the results of measurements made for 0.1 nM TDZ on three SPAuEs in the separate solutions. The RSD was 6.25%, which proves that reproducibility is

Table 2
Comparison of procedures for analysis of TDZ.

Electrode	Method	Linear range (mol L^{-1})	LOD (mol L^{-1})	Application	Ref.
SPCE/FeV NPs	DPV	2.0×10^{-8} – 1.2×10^{-4}	8.0×10^{-9}	Serum	[8]
CPE/NiAlPO-5	DPAdSV	1.0×10^{-7} – 1.0×10^{-5}	9.0×10^{-8}	Pharmaceutical formulations, serum	[21]
CoNP/MWCNT/GCE	CV	5.0×10^{-7} – 1.0×10^{-4}	5.0×10^{-8}	Pharmaceutical formulations, serum	[6]
NGO-500/SPCE	DPV	4.0×10^{-8} – 1.5×10^{-4}	4.0×10^{-9}	Urine, serum	[22]
P-MCO/GCE	DPV	5.0×10^{-7} – 1.4×10^{-3}	4.7×10^{-8}	Serum	[5]
BDDE	DPV	2.0×10^{-7} – 4.0×10^{-5}	1.2×10^{-7}	Urine	[4]
ZIF-67/Bio-MCM-41/CQDs/GCE	DPV	6.0×10^{-8} – 7.0×10^{-5}	3.1×10^{-8}	Pharmaceutical formulations, serum	[2]
AgNPs-NDG/PGE	CV	8.0×10^{-8} – 1.0×10^{-4}	1.0×10^{-8}	Pharmaceutical formulations, serum	[7]
Bi/PSi/CNTPE	DPV	1.0×10^{-7} – 2.6×10^{-4}	3.0×10^{-8}	Plasma	[3]
β-CD/CPE	DPV	1.0×10^{-8} – 1.0×10^{-7}	7.0×10^{-9}	Pharmaceutical formulations	[43]
Ru-Bi_2S_3/GCE	DPV	5.0×10^{-9} – 1.4×10^{-3}	1.0×10^{-9}	Serum	[44]
N-CNTs/gold-modified GCE	DPV	1.2×10^{-5} – 8.5×10^{-4}	1.3×10^{-6}	–	[45]
SPAuE	DPAdSV	1.0×10^{-11} – 2.0×10^{-10} 2.0×10^{-10} – 2.0×10^{-9} 2.0×10^{-9} – 2.0×10^{-8}	2.9×10^{-12}	Serum, wastewater	This work

SPCE/FeV NPs – screen-printed carbon electrode modified with iron vanadate nanoparticles; CPE/NiAlPO-5 – carbon paste electrode modified with nickel (II) incorporated aluminophosphate; CoNP/MWCNT/GCE – glassy carbon electrode modified with multi-walled carbon nanotubes with immobilized cobalt nanoparticles;
NGO-500/SPCE – screen-printed carbon electrode modified with spherical-like microstructures of NiO and Gd_2O_3; P-MCO/GCE – glassy carbon electrode modified with magnesium cobalt oxide; BDDE – boron-doped diamond electrode; ZIF-67/Bio-MCM-41/CQDs/GCE glassy carbon electrode modified with nanocomposite based on zeolitic imidazolate framework-67 (ZIF-67), bio-mobile crystalline material-41 (Bio-MCM-41) and carbon quantum dots (CQDs); AgNPs-NDG/PGE – nanodiamond graphite (NDG) decorated with Ag nanoparticles pyrolytic graphite electrode; Bi/PSi/CNTPE – bismuth@porous silicon carbon nanotubes paste electrode; β-CD/CPE – carbon paste electrode modified with β-cyclodextrin; Ru-Bi_2S_3/GCE – glassy carbon electrode modified with ruthenium doped bismuth sulfide; N-CNTs/gold-modified GCE – glassy carbon electrode modified with nitrogen doped carbon nanotubes/gold nanoparticles composites; SPAuE – screen-printed gold electrode; DPV – differential-pulse voltammetry; CV – cyclic voltammetry; DPAdSV – differential-pulse adsorptive stripping voltammetry.

acceptable.

3.6. Application

To examine the practicality of the proposed TDZ determination procedure with the SPAuE, human serum and purified wastewater samples analysis was performed. The results are presented in Table 3. Considering the very low LOD of the developed procedure (2.9×10^{-12} M) and the fact that TDZ reaches a concentration of 10^{-7}–10^{-6} M in human serum [8,9], it was possible to use a high dilution of serum samples to minimize interference (1000×). Wastewater samples were diluted 100-fold. The high accuracy of the DPAdSV procedure at the SPAuE is evidenced by the obtained recovery in the range of 98.5–102.5%. The coefficient variation between 0.76 and 4.88 indicates a good repeatability [48]. Fig. 10 shows obtained voltammograms.

4. Conclusions

Summarizing, this paper presents a fast, extremely sensitive and simple voltammetric procedure using a screen-printed gold electrode (SPAuE) for quantification of thioridazine (TDZ). The sensor was characterized by cyclic voltammetry (CV), electrochemical impedance spectroscopy (EIS), scanning electron microscopy (SEM) and energy-dispersive X-ray spectroscopy (EDS). Using these methods, the SPAuE was compared with the SPCE and SPCE/AuF. The obtained results show the advantage of the SPAuE in terms of working electrode active surface and the efficiency of kinetics of electron transfer, which, combined with the high chemical affinity of gold atoms to sulfur atoms present in the structure of the analyte molecule, makes this sensor an extremely effective tool in the detection of TDZ. The CV studies of the TDZ electrooxidation process at the SPAuE showed that this process is controlled purely by adsorption. In addition, the developed procedure shows good selectivity, and the calculated LOD and LOQ were 2.9×10^{-12} and 9.8×10^{-12} M, respectively. The practicality of the procedure was verified by successfully determining TDZ in spiked purified wastewater and human serum samples. The results suggest that the SPAuE has the potential to be used as a sensor for electrochemical determination of TDZ in real samples. The statistical evaluation of DPAdSV procedure showed satisfactory accuracy and precision.

CRediT authorship contribution statement

Jędrzej Kozak: Conceptualization, Methodology, Investigation, Writing – original draft, Writing – review & editing. **Katarzyna Tyszczuk-Rotko:** Conceptualization, Methodology, Investigation, Writing – original draft, Writing – review & editing, Supervision.

Declaration of Competing Interest

The authors declare that they have no known competing financial interests or personal relationships that could have appeared to influence the work reported in this paper.

Data availability

Data will be made available on request.

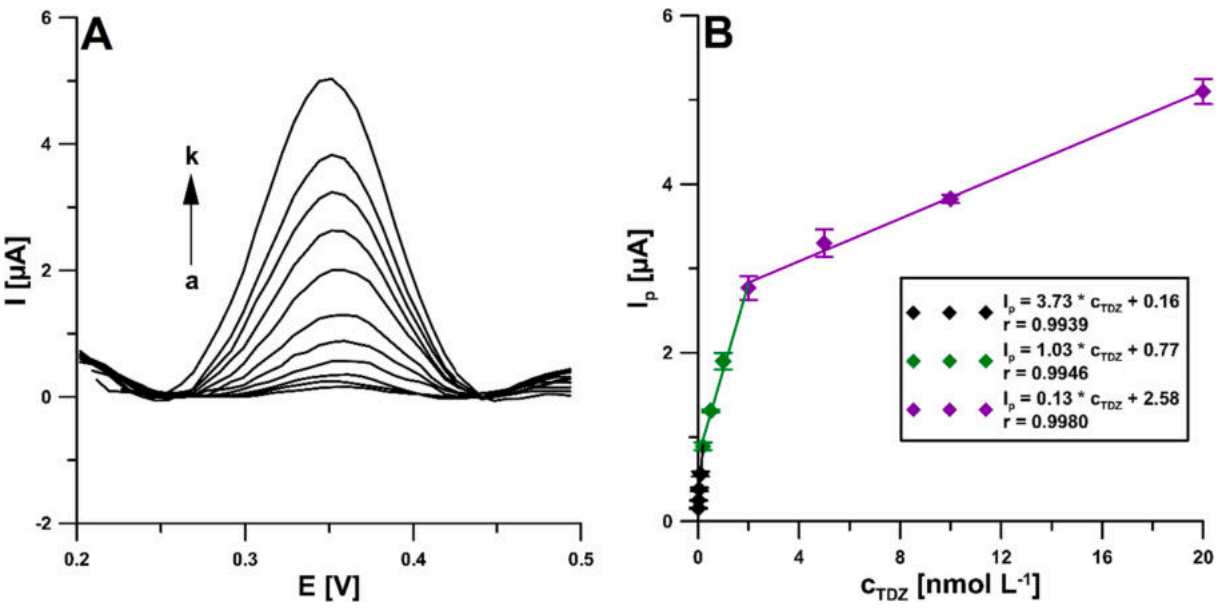

Fig. 8. (A) The DPAdSVs obtained on the SPAuE in the presence of various TDZ concentration (a → k, 1.0×10^{-11} – 2.0×10^{-8} M) in 0.075 mol L^{-1} PBS of pH 2.6. (B) Calibration plot of TDZ. The obtained average values of the I_p are shown with standard deviation for n = 3. The DPAdSV parameters: ν of 75 mV s^{-1}, t_m of 10 ms, ΔE_A of 100 mV, $E_{acc.}$ of −0.2 V and $t_{acc.}$ of 60 s.

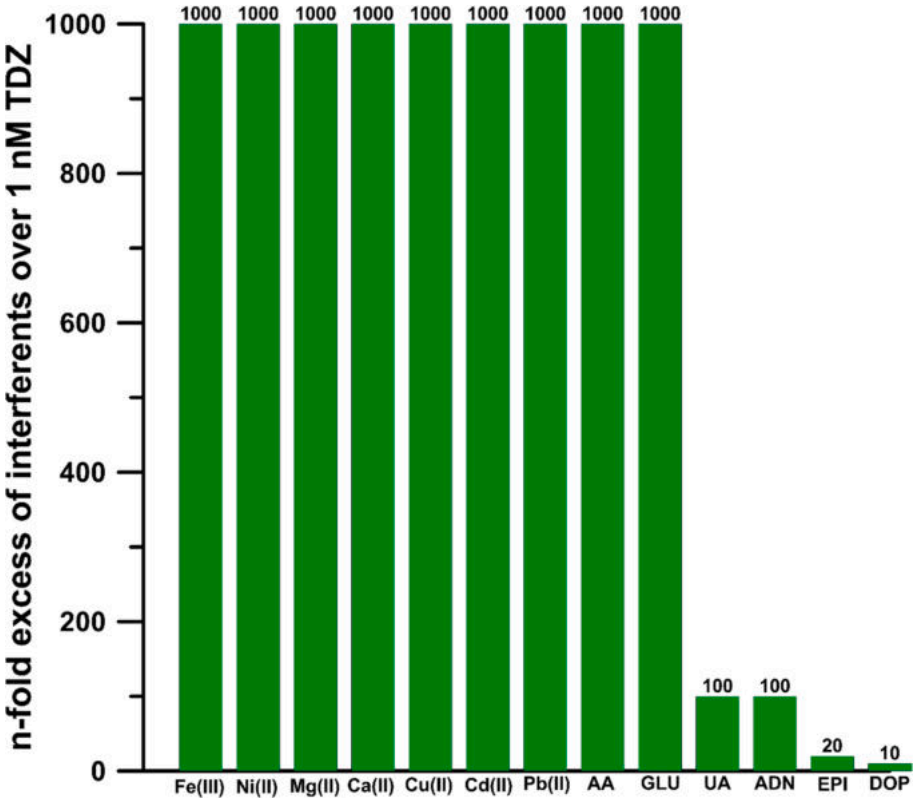

Fig. 9. Histogram bars of the selectivity of SPAuE for determination of TDZ. AA–ascorbic acid, GLU–glucose, UA–uric acid, ADN–adenine, EPI–epinephrine, DOP–dopamine.

Table 3
The results of TDZ determination in real samples.

Sample	TDZ concentration [μmol L^{-1}] ± SD (n = 3)			Coefficient variation* [%]	
	Added	Found DPAdSV	Found in electrochemical cell		Recovery** [%]
Human serum	0.05	0.0503 ± 0.0024	0.0000503 ± 0.0000024	4.77	100.6
	0.2	0.205 ± 0.01	0.000205 ± 0.00001	4.88	102.5
Purified wastewater	0.005	0.005 ± 0.00021	0.00005 ± 0.0000021	4.20	100.0
	0.02	0.0197 ± 0.00015	0.000197 ± 0.0000015	0.76	98.5

* Coefficient variation [%] = (SD × 100)/ Found DPAdSV, ** Recovery [%] = (Found DPAdSV × 100)/Added.

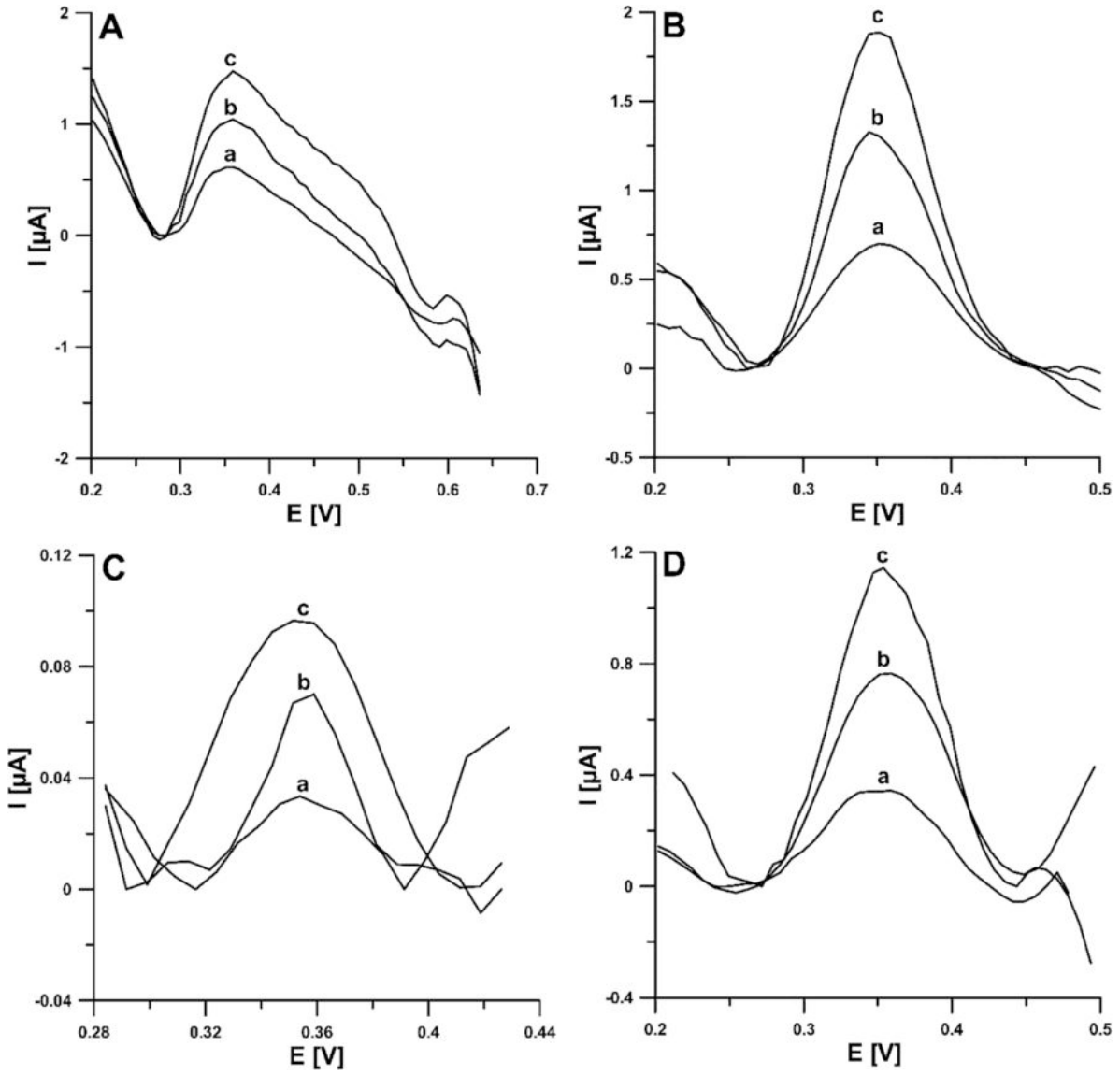

Fig. 10. The DPAdSVs recorded during determination of TDZ in human serum (A and B) and purified wastewater samples (C and D): (A): (a) 10 μL of sample + 5.0 × 10^{-11}, (b) as (a) + 5.0 × 10^{-11}, (c) as (a) + 1.0 × 10^{-10} M TDZ, (B): (a) 10 μL of sample + 2.0 × 10^{-10}, (b) as (a) + 2.0 × 10^{-10}, (c) as (a) + 4.0 × 10^{-10} M TDZ, (C): (a) 100 μL of sample + 5.0 × 10^{-11}, (b) as (a) + 5.0 × 10^{-11}, (c) as (a) + 1.0 × 10^{-10} M TDZ, and (D): (a) 100 μL of sample + 2.0 × 10^{-10}, (b) as (a) + 2.0 × 10^{-10}, (c) as (a) + 4.0 × 10^{-10} M TDZ. The DPAdSV parameters: ν of 75 mV s^{-1}, t_m of 10 ms, ΔE_A of 100 mV, $E_{acc.}$ of −0.2 V and $t_{acc.}$ of 60 s.

Acknowledgment

We would like to thank employees of Municipal Water Supply and Waste Water Treatment Company Ltd (Lublin, Poland) for the wastewater samples.

References

[1] L. Karadurmus, D. Kır, S. Kurbanoglu, S.A. Ozkan, Electrochemical analysis of antipsychotics, Curr. Pharm. Anal. 15 (2019) 413–428.
[2] B. Habibi, S. Pashazadeh, L.A. Saghatforoush, A. Pashazadeh, A thioridazine hydrochloride electrochemical sensor based on zeolitic imidazolate framework-67-functionalized bio-mobile crystalline material-41 carbon quantum dots, New J. Chem. 45 (2021) 14739–14750.

[3] A. Ensafi, P. Hedayati, M.M. Abarghoui, B. Rezaei, Bismuth nanoparticles@porous silicon nanostructure, application as a selective and sensitive electrochemical sensor for the determination of thioridazine, Electroanalysis 29 (2017) 2461–2469.
[4] B.B. Petković, D. Kuzmanović, T. Dimitrijević, M.P. Krstić, D.M. Stanković, Novel strategy for electroanalytical detection of antipsychotic drugs chlorpromazine and thioridazine; possibilities for simultaneous determination, Int. J. Electrochem. Sci. 3709–3720 (2017).
[5] C. Koventhan, V. Vinothkumar, S.-M. Chen, P. Veerakumar, K.-C. Lin, Polyol-assisted synthesis of spinel-type magnesium cobalt oxide nanochains for voltammetric determination of the antipsychotic drug thioridazine, J. Electroanal. Chem. 898 (2021), 115600.
[6] S. Shahrokhian, M. Ghalkhani, M. Adeli, M.K. Amini, Multi-walled carbon nanotubes with immobilised cobalt nanoparticle for modification of glassy carbon electrode: application to sensitive voltammetric determination of thioridazine, Biosens. Bioelectron. 24 (2009) 3235–3241.
[7] S. Shahrokhian, N. Hosseini Nassab, Nanodiamond decorated with silver nanoparticles as a sensitive film modifier in a jeweled electrochemical sensor: application to voltammetric determination of thioridazine, Electroanalysis 25 (2013) 417–425.
[8] G. Kesavan, M. Pichumani, S.-M. Chen, C.-J. Wu, Hydrothermal synthesis of iron vanadate nanoparticles for voltammetric detection of antipsychotic drug thioridazine, J. Alloys Compd. 885 (2021), 160880.
[9] E. Mortensson, B.-E. Roos, Serum levels of thioridazine in psychiatric patients and healthy volunteers, Eur. J. Clin. Pharmacol. 6 (1973) 181–186.
[10] J. Escudero, J.L. Muñoz, T. Morera-Herreras, R. Hernandez, J. Medrano, S. Domingo-Echaburu, D. Barceló, G. Orive, U. Lertxundi, Antipsychotics as environmental pollutants: an underrated threat? Sci. Total Environ. 769 (2021), 144634.
[11] A.J. Ebele, M. Abou-Elwafa Abdallah, S. Harrad, Pharmaceuticals and personal care products (PPCPs) in the freshwater aquatic environment, Emerg. Contam. 3 (2017) 1–16.
[12] M.L. Wilde, J. Menz, C. Trautwein, C. Leder, K. Kümmerer, Environmental fate and effect assessment of thioridazine and its transformation products formed by photodegradation, Environ. Pollut. 213 (2016) 658–670.
[13] S. Golbaz, M. Zamanzadeh, K. Yaghmaeian, R. Nabizadeh, N. Rastkari, H. Esfahani, Occurrence and removal of psychiatric pharmaceuticals in the Tehran South Municipal Wastewater Treatment Plant, Environ. Sci. Pollut. Res. (2022).
[14] M. Amjadi, T. Hallaj, M.A. Mayan, Green synthesis of nitrogen-doped carbon dots from lentil and its application for colorimetric determination of thioridazine hydrochloride, RSC Adv. 6 (2016) 104467–104473.
[15] A. El-Didamony, S. Hafeez, Spectrophotometric determination of thioridazine hydrochloride in tablets and biological fluids by ion-pair and oxidation reactions, J. Spectrosc. 27 (2012) 129–141.
[16] M.A. Omar, O.H. Abdelmageed, S.M. Derayea, T. Uno, T.Z. Atia, Spectrofluorimetric determination of certain antidepressant drugs in human plasma, J. Anal. Sci. Technol. 4 (2013) 5.
[17] F.A.J. Vanderheeren, D.J.C.J. Theunis, Gas-liquid chromatographyc determination of perazine, thioridazine and thioridazine metabolites in human plasma, J. Chromatogr. 120 (1976) 123–128.
[18] F. Geiser, M. Schultz, L. Betz, M. Shaimi, J. Lee, W. Champion, Direct, preparative enantioselective chromatography of propranolol hydrochloride and thioridazine hydrochloride using carbon dioxide-based mobile phases, J. Chromatogr. A 865 (1999) 227–233.
[19] A. Asghari, E. Fahimi, M. Bazregar, M. Rajabi, L. Boutorabi, Rapid determination of some psychotropic drugs in complex matrices by tandem dispersive liquid–liquid microextraction followed by high performance liquid chromatography, J. Chromatogr. B 1052 (2017) 51–59.
[20] L. Qi, L.-M. Duan, X.-H. Sun, J. Zhang, Z.-Q. Zhang, Simultaneous determination of three banned psychiatric drugs in pig feed and tissue using solid-phase reactor on-line oxidizing and HPLC-fluorescence detection: HPLC-fluorescence determination of three banned psychiatric drugs, Biomed. Chromatogr. 29 (2015) 1535–1540.
[21] M. Amiri, S. Sohrabnezhad, A. Rahimi, Nickel (II) incorporated AlPO-5 modified carbon paste electrode for determination of thioridazine in human serum, Mater. Sci. Eng. C 37 (2014) 342–347.
[22] V. Vinothkumar, G. Kesavan, S.-M. Chen, Highly selective voltammetric detection of antipsychotic drug thioridazine hydrochloride based on NiO@Gd_2O_3 modified screen printed carbon electrode, J. Electroanal. Chem. 895 (2021), 115535.
[23] L.-L. Ma, Y. He, D. Qin, A. Chang, A. Huang, X.-J. Xie, Y. Zheng, Fabrication, characterization and performance evaluation of screen-printed carbon electrodes: determination of acetaminophen in tylenol, Chinese J. Anal. Chem. 49 (2021) e21187–e21196.
[24] P.A. Raymundo-Pereira, N.O. Gomes, S.A.S. Machado, O.N. Oliveira, Simultaneous, ultrasensitive detection of hydroquinone, paracetamol and estradiol for quality control of tap water with a simple electrochemical method, J. Electroanal. Chem. 848 (2019), 113319.
[25] S.N. Ashakirin, M.H.M. Zaid, M.A.S.M. Haniff, A. Masood, M.F.M.R. Wee, Sensitive electrochemical detection of creatinine based on electrodeposited molecular imprinting polymer modified screen printed carbon electrode, Measurement 210 (2023), 112502.
[26] O.K. Topsoy, F. Muhammad, S. Kolak, A. Ulu, Ö. Güngör, M. Şimşek, S. Köytepe, B. Ateş, Fabrication of electrospun polycaprolactone/chitosan nanofiber-modified screen-printed electrode for highly sensitive detection of diazinon in food analysis, Measurement 187 (2023), 110250.
[27] Z. Bagherinasab, H. Beitollahi, M. Yousefi, M. Bagherzadeh, M. Hekmati, Rapid sol gel synthesis of $BaFe_{12}O_{19}$ nanoparticles: An excellent catalytic application in the electrochemical detection of tramadol in the presence of acetaminophen, Microchem. J. 156 (2020) 104803.
[28] T. Kondori, S. Tajik, N. Akbarzadeh-T, H. Beitollahi, C. Graiff, H.W. Jang, M. Shokouhimehr, Synthesis and characterization of bipyridine cobalt(II) complex modified graphite screen printed electrode: an electrochemical sensor for simultaneous detection of acetaminophen and naproxen, RSC Adv. 11 (2021) 3049–3057.
[29] S. Sawan, R. Maalouf, A. Errachid, N. Jaffrezic-Renault, Metal and metal oxide nanoparticles in the voltammetric detection of heavy metals: A review, Trends Analyt. Chem.131 (2020) 116014.
[30] T. Hezard, K. Fajerwerg, D. Evrard, V. Collière, P. Behra, P. Gros, Gold nanoparticles electrodeposited on glassy carbon using cyclic voltammetry: Application to Hg(II) trace analysis, J. Electroanal. Chem. 664 (2012) 46–52.
[31] K. Tyszczuk-Rotko, Metal film electrodes prepared with a reversibly deposited mediator in voltammetric analysis of metal ions, Curr. Opin. Electrochem. 17 (2019) 128–133.
[32] G. Wang, G. Shi, X. Chen, R. Yao, F. Chen, A glassy carbon electrode modified with graphene quantum dots and silver nanoparticles for simultaneous determination of guanine and adenine, Microchim. Acta 182 (2015) 315–322.
[33] J. Tang, R. Huang, S. Zheng, S. Jiang, H. Yu, Z. Li, J. Wang, A sensitive and selective electrochemical sensor based on graphene quantum dots/gold nanoparticles nanocomposite modified electrode for the determination of luteolin in peanut hulls, Microchem. J. 145 (2019) 899–907.
[34] A.M. Mahmoud, M.M. El-Wekil, M.H. Mahnashi, M.F.B. Ali, S.A. Alkahtani, Modification of N, S co-doped graphene quantum dots with p-aminothiophenol-functionalized gold nanoparticles for molecular imprint-based voltammetric determination of the antiviral drug sofosbuvir, Microchim. Acta 186 (2019) 617.
[35] L. Angnes, E.M. Richter, M.A. Augelli, G.H. Kume, Gold electrodes from recordable CDs, Anal. Chem. 72 (2000) 5503–5506.
[36] H. Yun Xia, X. Ya Hu, Determination of isoniazid using a gold electrode by differential pulse voltammetry, Anal. Lett. 38 (2005) 1405–1414.
[37] P. Masawat, The Underpotential determination of lead using the laboratory-made gold electrode flow cell, Chiang Mai J. Sci. 35 (2008) 355–369.
[38] E. Pensa, E. Cortés, G. Corthey, P. Carro, C. Vericat, M.H. Fonticelli, G. Benítez, A. A. Rubert, R.C. Salvarezza, The chemistry of the sulfur–gold interface: in search of a unified model, Acc. Chem. Res. 45 (2012) 1183–1192.
[39] L.J. Opuchlik, J. Pawłowska, S. Sęk, R. Bilewicz, Ferrocenylated gold nanoparticles self-assemble at carbon surfaces to form stable films, J. Electroanal. Chem. 825 (2018) 22–29.
[40] N.P. Shetti, S.J. Malode, S.T. Nandibewoor, Electro-oxidation of captopril at a gold electrode and its determination in pharmaceuticals and human fluids, Anal. Methods 7 (2015) 8673–8682.
[41] D.K. Gosser. Cyclic voltammetry: Simulation and analysis of reaction mechanism, VCH, New York, NY, USA, 1993.
[42] E. Laviron, General expression of the linear potential sweep voltammogram in the case of diffusionless electrochemical systems, J. Electroanal. Chem. 101 (1979) 19–28.
[43] A. Ferancova, E. Korgova, Determination of tricyclic antidepressants using a carbon paste electrode modified with b-cyclodextrin, J. Electroanal. Chem. 492 (2000) 74–77.
[44] R. Sakthivel, S. Kubendhiran, S.-M. Chen, One-pot sonochemical synthesis of marigold flower-like structured ruthenium doped bismuth sulfide for the highly sensitive detection of antipsychotic drug thioridazine in the human serum sample, J. Taiwan Inst. Chem. Eng. 111 (2020) 270–282.
[45] X. Feng, C. Wang, R. Cui, X. Yang, W. Hou, The synthesis of nitrogen-doped carbon nanotubes/gold composites and their application to the detection of thioridazine, J. Solid State Electrochem. 16 (2012) 2691–2698.
[46] J. Mocak, A.M. Bond, S. Mitchell, G. Scollary, A statistical overview of standard (IUPAC and ACS) and new procedures for determining the limits of detection and quantification: application to voltammetric and stripping techniques, Pure Appl. Chem. 69 (1997) 297–328.
[47] M. Grabarczyk, A. Koper, How to determine uranium faster and cheaper by adsorptive stripping voltammetry in water samples containing surface active compounds, Electroanalysis 23 (2011) 1442–1446.
[48] P. Konieczka, Jacek Namiesnik. Quality Assurance and Quality Control in the Analytical Chemical Laboratory, WNT, Warsaw, Poland, 2013.

RD10

J. Kozak, K. Tyszczuk-Rotko, D. Gorylewski, *A nanoporous screen-printed carbon sensor for environmental and clinical monitoring of the antibiotic ciprofloxacin***,** Measurement (zaakceptowana do druku 26.09.2023 r.).

Date: Sep 26, 2023
To: "Katarzyna Tyszczuk-Rotko" katarzyna.tyszczuk-rotko@mail.umcs.pl
From: "Measurement" support@elsevier.com
Subject: Your Submission has been Accepted MEAS-D-23-06084

Ms. Ref. No.: MEAS-D-23-06084
Title: A nanoporous screen-printed carbon sensor for environmental and clinical monitoring of the antibiotic ciprofloxacin
Measurement

Dear Professor Katarzyna Tyszczuk-Rotko,

I am pleased to confirm that your paper "A nanoporous screen-printed carbon sensor for environmental and clinical monitoring of the antibiotic ciprofloxacin" has been accepted for publication in Measurement.

Comments from the Editor and Reviewers can be found below (if available).

Thank you for submitting your work to this journal.

What happens next?

1. Our production department will create a proof of your article, which will be shared with you for approval.
2. We will send you a link to your post-acceptance online author forms. These forms include the publishing agreement for you to complete as well as confirming whether your article is to be published open access or subscription. We kindly request you complete the forms as soon as possible upon receipt of the link.

If we need any further information from you during the typesetting process, we will let you know.

For further information about the proofing process, please click this link:
https://service.elsevier.com/app/answers/detail/a_id/6007/p/10592/supporthub/publishing/related/

We appreciate and value your contribution to Measurement. We regularly invite authors of recently published articles to participate in the peer review process. You are now part of the Measurement reviewer pool. We look forward to your continued participation in our journal, and we hope you will consider us again for future submissions.

We encourage authors of original research papers to share the research objects – including raw data, methods, protocols, software, hardware and other outputs – associated with their paper. More information on how our open access Research Elements journals can help you do this is available at https://www.elsevier.com/authors/tools-and-resources/research-elements-journals?dgcid=ec_em_research_elements_email.

With kind regards,

Noritaka Yusa
Editor
Measurement

Comments from the Editors and Reviewers(if available):

Reviewer #1: The manuscript meets the conditions for publication, based on the improvements and clarifications provided by the author.

Register as a reviewer:

As an accepted author in Measurement, we would now like to ask you if you would be willing to contribute towards the review process for this journal, giving some of your time to help other authors. If you are keen to become a reviewer, please see the information provided on our website at:
https://www.journals.elsevier.com/measurement/news/volunteer-for-peer-review-with-measurement

Here, you can register to become a regular reviewer and thus contribute towards the continued growth and quality development of this journal.

Thank you for your engagement with Measurement!

****
For further assistance, please visit our customer support site at http://help.elsevier.com/app/answers/list/p/7923 Here

you can search for solutions on a range of topics, find answers to frequently asked questions and learn more about EM via interactive tutorials. You will also find our 24/7 support contact details should you need any further assistance from one of our customer support representatives.

This journal uses the Elsevier Article Transfer Service. This means that if an editor feels your manuscript is more suitable for an alternative journal, then you might be asked to consider transferring the manuscript to such a journal. The recommendation might be provided by a Journal Editor, a dedicated Scientific Managing Editor, a tool assisted recommendation, or a combination. For more details see the journal guide for authors.

At Elsevier, we want to help all our authors to stay safe when publishing. Please be aware of fraudulent messages requesting money in return for the publication of your paper. If you are publishing open access with Elsevier, bear in mind that we will never request payment before the paper has been accepted. We have prepared some guidelines (https://www.elsevier.com/connect/authors-update/seven-top-tips-on-stopping-apc-scams) that you may find helpful, including a short video on Identifying fake acceptance letters (https://www.youtube.com/watch?v=o5l8thD9XtE). Please remember that you can contact Elsevier s Researcher Support team (https://service.elsevier.com/app/home/supporthub/publishing/) at any time if you have questions about your manuscript, and you can log into Editorial Manager to check the status of your manuscript (https://service.elsevier.com/app/answers/detail/a_id/29155/c/10530/supporthub/publishing/kw/status/).
#AU_MEAS#

To ensure this email reaches the intended recipient, please do not delete the above code

---

4

Measurement

A nanoporous screen-printed carbon sensor for environmental and clinical monitoring of the antibiotic ciprofloxacin

--Manuscript Draft--

Manuscript Number:	MEAS-D-23-06084
Article Type:	Research Paper
Keywords:	antibiotics; screen-printed sensor; nanoporous carbon; stripping voltammetry; human urine; hospital and municipal wastewater
Corresponding Author:	Katarzyna Tyszczuk-Rotko Maria Curie-Sklodowska University Lublin, POLAND
First Author:	Jędrzej Kozak
Order of Authors:	Jędrzej Kozak
	Katarzyna Tyszczuk-Rotko
	Damian Gorylewski
Abstract:	A very sensitive, fast and simple electrochemical procedure using a nanoporous screen-printed carbon electrode (NPSPCE) was developed for the determination of the fluoroquinolone antibiotic ciprofloxacin (CFX). Changes in the surface morphology and electrochemical properties of the SPCE before and after pre-anodization were examined using scanning electron microscopy (SEM), electrochemical impedance spectroscopy (EIS) and cyclic voltammetry (CV). CV studies also demonstrated unequivocally adsorption controlled and irreversible oxidation of CFX. Using optimized conditions, the developed procedure is characterized by excellent selectivity and high sensitivity, allowing to achieve a very low limit of detection (6.3 × 10-11 mol L-1). The measurements taken allow us to consider the NPSPCE as a very effective tool for direct determination of CFX in samples with a complex matrix such as sewage and body fluids. The developed environment friendly sensor and procedure meet the requirements of green chemistry (reduction of toxic chemicals/reagents, and generation of minimal waste).

Cover Letter

MARIA CURIE-SKLODOWSKA UNIVERSITY in LUBLIN
Institute of Chemical Sciences
Faculty of Chemistry
Department of Analytical Chemistry

Prof. dr hab. Katarzyna Tyszczuk-Rotko

Measurement ***August 28, 2023***

Dear Editor,

According to the decision of Noritak Yusa (Editor of Measurment), I am re-submiting the manuscript (MEAS-D-23-03392R1). **The work received three positive reviews (reviews and responses for reviewers are below).The manuscript has been thoroughly revised to the suggestions/comments pointed out by Reviewers.** The decision of Editor of Measurment was related to the lack of changes marked on the revised manuscript. These changes are now marked in red. The error (unmarked changes) resulted from the information in the system ("Revised manuscript with no changes marked"). We are very sorry if it was our mistake. In response to the reviewers, we added the corrected fragments. In addition, we found a few typos in the revised manuscript, which have also been highlighted. **Morover, figures and tables have been removed from the revised manuscript and added as separate files.**
We would be grateful if you could consider the possibility of publishing our manuscript in Measurement.

Thank you very much for your kind consideration.

Sincerely,

Katarzyna Tyszczuk-Rotko

Response to Reviewers

Response to Reviewer 1:

I would recommend the paper for publication in Measurement after addressing the following concerns:
1- Why the frequency range starts at 50000 Hz usually it should be in order of 1 Hz
We would like to thank the Reviewer for invaluable time and comments that have significantly improved the previous version of our manuscript.
Impedance spectra were recorded in KCl solution (0.1 mol L^{-1}) with the addition of $K_3[Fe(CN)_6]$ (5.0 × 10^{-3} mol L^{-1}) for frequencies in the range of 50000 - 1 Hz and at a potential of 0.2 V. In this range, the kinetic and diffusion area for both electrodes is well outlined. You can easily read and compare the charge transfer resistance (R_{ct}) for both electrodes.

2- This explanation totally disagrees with previous parts where the actives surface area calculated CVs and the SEM where the preanodization caused a pore structure.
Thank you for your attention. The text was corrected. The SPCE was pre-anodized in a strongly alkaline medium (0.1 mol L^{-1} NaOH) in accordance with the procedure already used in our previous studies [32]. In our previously mentioned studies [32], an electrochemically activated boron-doped screen-printed diamond electrode (aSPBDDE) also provided a much higher analyte (rifampicin) peak current. A number of parameters were also improved compared to the non-activated electrode. As in the case of the NPSPCE, R_{ct} was lowered as a result of activation. The visible changes in the surface of the working electrode and a slight increase in the active surface were observed at that time. However, a highly porous structure of SPBDDE as a result of pre-anodization as in the case of SPCE was not observed. It can therefore be concluded that the same type of electrochemical pretreatment

pl. Marii Curie-Skłodowskiej 3/541, 20-031 Lublin, www.umcs.lublin.pl
tel: +48 81 537 55 85
e-mail: katarzyna.tyszczuk-rotko@mail.umcs.pl

may affect the different properties of the electrodes depending on the material from which they are made.

3- In this equation the 3SDa/b and LOQ = 10SDa/b, thw SDa and b are not defined.
Thank you for your attention. The information was added to the text "*(SD_a: standard deviation of intercept, b: slope of calibration plot, n = 3)".*

4- It must be explained in experimental how the repeatability and reproducibility were determined
Thank you for your attention. The repeatability of the signal of 5.0×10^{-9} mol L^{-1} CFX on the NPSPCE was checked. The relative standard deviation (RSD) of 1.58% (n = 10) was received, which confirms satisfying repeatability of the CFX signal. Reproducibility was determined based on the results of measurements made for the same CFX concentration on the three sensors. The obtained RSD of 4.77% indicates good reproducibility of the NPSPCE.

5- The style of numbers in Table 2 must be corrected, please use µM or nM not to use so many digits , or you can use mol L-1 but report in power of ten.
The concentrations are shown in the µM. Due to the multiple dilution of the sample in the electrochemical cell, there will always be a difference between the determined values in the samples and electrochemical cell. Thanks to the low LOD allowed by the NPSPCE, high dilutions of the analyzed samples were possible, thus minimizing interference. In the case of urine, it was 10,000-fold because CFX reaches a concentration of 10^{-4} – 10^{-6} mol L^{-1} in the urine [8,12,13]. Municipal wastewater was diluted 10-fold, while hospital wastewater was diluted 20-fold. Additionally, there are differences in analyte concentrations in different samples. We have reduced the number of significant digits to 3. We can't reduce it anymore so as not to affect the accuracy of the result of the calculated error.

6- All the graphs should have the same number of significant digits .
Due to the changes in parameters used during the optimization of the procedure, different measured values were obtained. Using the same number of significant digits in each graph will result in the need to use for example additionally at least two zeros after the dot. That's why I tried to unify the number of significant digits but after a dot on each of the graphs.

<u>Response to Reviewer 2:</u>

The manuscript is clearly written and the data are presented in a logical flow and well proved. From the presented results and discussions supports the conclusions reached.
My question is about the sensors repeatability '(RSD) of 1.58% (n = 10)' and the reproducibility 'RSD 4.77% (n=3) results presented in the manuscript. In figure 2 A and B the acquired signal is in fig. 2A~0.9 uA at pH 7 while in figure 2B it is about 1.1 uA when the same amount of CFX (2x10-8 M) in 0.1 mol/L PBS was added in both cases. Here is not fully consistent with the conclusion for RSD of repeatability/reproducibility.
We would like to thank the Reviewer for invaluable time and comments that have significantly improved the previous version of our manuscript. Yes, I agree that there was a difference in the current in Figures 2 A and 2 B. But it was due to the stage of work on the analytical procedure. The repeatability of the signal and the reproducibility of the electrode to the electrode were determined after full optimization, i.e. not only the pH and electrolyte concentration were checked, but also the analyte accumulation parameters and analytical signal registration parameters were examined.

Response to Reviewer 3:

Comments and requests to the manuscript are as follows:Minor Revisions:

1- The motivation behind the modifier selection must be clearly mentioned in the introduction.

We would like to thank the Reviewer for invaluable time and comments that have significantly improved the previous version of our manuscript.

Thank you for your attention. We have added the following text *"The SPCE was pre-anodized in a strongly alkaline medium in accordance with the procedure already used for an electrochemically activated screen-printed boron-doped diamond electrode (aSPBDDE) preparation [32]. We wanted to take advantage of the fact that the electrochemical activation of the electrode surface results in changes in its morphology and a decrease in the charge transfer resistance, which translates into a significant increase in the analytical signal [32]. The morphological and electrochemical characterization of the developed sensor and its application for the determination of CFX in municipal and hospital wastewater and also human urine were performed."*

2- The abstract should be revised to make it more attractive, and the novelty involved in this research should be highlighted.

Thank you for your attention. The abstract was corrected. The abstract in the revised manuscript is as below

"A very sensitive, fast and simple electrochemical procedure using a nanoporous screen-printed carbon electrode (NPSPCE) was developed for the determination of the fluoroquinolone antibiotic ciprofloxacin (CFX). Changes in the surface morphology and electrochemical properties of the SPCE before and after pre-anodization were examined using scanning electron microscopy (SEM), electrochemical impedance spectroscopy (EIS) and cyclic voltammetry (CV). CV studies also demonstrated unequivocally adsorption controlled and irreversible oxidation of CFX. Using optimized conditions, the developed procedure is characterized by excellent selectivity and high sensitivity, allowing to achieve a very low limit of detection (6.3×10^{-11} mol L^{-1}). The measurements taken allow us to consider the NPSPCE as a very effective tool for direct determination of CFX in samples with a complex matrix such as sewage and body fluids. The developed environment friendly sensor and procedure meet the requirements of green chemistry (reduction of toxic chemicals/reagents, and generation of minimal waste)."

3- Introduction also needs to be revised and improved to emphasize the novelty of the proposed work. Include novelty statements.

The following text has been added *"The novelty of this work is the improvement of analytical procedures for the determination of CFX with respect to the limitations described so far in the literature, i.e. too low sensitivity, complicated procedures of sensor preparation and measurement."*

4- The conclusion is too much; please simplify that.

The conclusion was corrected.

The conclusion in the revised manuscript is as below

"In summary, in this study a very fast and simple DPAdSV procedure using a nanoporous, pre-anodized screen-printed carbon electrode (NPSPCE) for trace analysis of ciprofloxacin (CFX) was proposed. Methods such as EIS and CV were used to characterize the sensor. The obtained results showed numerous advantages of subjecting the SPCE to the pre-anodization process, including a significant increase in the active surface of the working electrode, a decrease in the resistance of charge transfer and improvement of the kinetics of electron transfer. The improvement of these parameters resulted in an extreme increase in the height of the CFX oxidation peak. In addition, SEM imaging showed that the electrode obtained a highly porous structure as a result of pre-anodization. The developed procedure is characterized by excellent selectivity and high sensitivity, allowing to

achieve a very low limit of detection (6.3 × 10^{-11} mol L^{-1}) with a wide range of linearity from 5.0 × 10^{-10} to 3.0 × 10^{-8} mol L^{-1}. The usefulness of the proposed procedure was confirmed by successfully determining CFX in spiked samples of treated municipal wastewater and human urine, as well as determining the real content of CFX in samples of hospital wastewater. The results of the study allow us to consider the NPSPCE as a very effective tool for direct determination of CFX in samples with a complex matrix such as sewage and body fluids. Moreover, the developed environment friendly sensor and procedure meet the requirements of green chemistry (reduction of toxic chemicals/reagents, and generation of minimal waste).”

5- The authors can use the following reference to develop different sections of the article and should be cited:
a-Zaki, M., et al., "Mn/Cu nanoparticles modified carbon paste electrode as a novel electrochemical sensor for nicotine detection." Electroanalysis 35.2 (2023): e202200143.
b-Zaki, M., et al., "Sensitive detection for nicotine using nickel/copper nanoparticle-modified carbon paste electrode." Ionics 28.10 (2022): 4881-4891.
c-Moustafa, Ayah, et al. "Electrochemical determination of vitamin B6 (pyridoxine) by a reformed carbon paste electrode with iron oxide nanoparticles," Ionics 28.9 (2022): 4471-4484.
d-Fekry, Amany M., et al. "A sensitive electrochemical sensor for moxifloxacin hydrochloride based on nafion/graphene oxide/zeolite modified carbon paste electrode." Electroanalysis 33.4 (2021): 964-974.
The references were added.

Highlights

- Ciprofloxacin (CFX) is a second-generation fluoroquinolone antibiotic that is effective against both Gram-negative and Gram-positive bacteria
- A nanoporous, pre-anodized screen-printed carbon electrode (NPSPCE) was used as CFX sensor
- New method for tracing changes of CFX concentration in the environmental and clinical samples
- Excellent detection limit (LOD of 6.3×10^{-11} mol L^{-1}) and sensitivity
- Low reagent and sample consumption

Response to Reviewer 1:

I would recommend the paper for publication in Measurement after addressing the following concerns:

1- Why the frequency range starts at 50000 Hz usually it should be in order of 1 Hz

We would like to thank the Reviewer for invaluable time and comments that have significantly improved the previous version of our manuscript.

Impedance spectra were recorded in KCl solution (0.1 mol L^{-1}) with the addition of $K_3[Fe(CN)_6]$ (5.0×10^{-3} mol L^{-1}) for frequencies in the range of 50000 - 1 Hz and at a potential of 0.2 V. In this range, the kinetic and diffusion area for both electrodes is well outlined. You can easily read and compare the charge transfer resistance (R_{ct}) for both electrodes.

2- This explanation totally disagrees with previous parts where the actives surface area calculated CVs and the SEM where the preanodization caused a pore structure.

Thank you for your attention. The text was corrected. The SPCE was pre-anodized in a strongly alkaline medium (0.1 mol L^{-1} NaOH) in accordance with the procedure already used in our previous studies [32]. In our previously mentioned studies [32], an electrochemically activated boron-doped screen-printed diamond electrode (aSPBDDE) also provided a much higher analyte (rifampicin) peak current. A number of parameters were also improved compared to the non-activated electrode. As in the case of the NPSPCE, R_{ct} was lowered as a result of activation. The visible changes in the surface of the working electrode and a slight increase in the active surface were observed at that time. However, a highly porous structure of SPBDDE as a result of pre-anodization as in the case of SPCE was not observed. It can therefore be concluded that the same type of electrochemical pretreatment may affect the different properties of the electrodes depending on the material from which they are made.

3- In this equation the 3SDa/b and LOQ = 10SDa/b, thw SDa and b are not defined.

Thank you for your attention. The information was added to the text "*(SD_a: standard deviation of intercept, b: slope of calibration plot, n = 3)*".

4- It must be explained in experimental how the repeatability and reproducibility were determined

Thank you for your attention. The repeatability of the signal of 5.0×10^{-9} mol L^{-1} CFX on the NPSPCE was checked. The relative standard deviation (RSD) of 1.58% (n = 10) was received, which confirms satisfying repeatability of the CFX signal. Reproducibility was determined based on the results of measurements made for the same CFX concentration on the three sensors. The obtained RSD of 4.77% indicates good reproducibility of the NPSPCE.

5- The style of numbers in Table 2 must be corrected , please use µM or nM not to use so many digits , or you can use mol L-1 but report in power of ten.

The concentrations are shown in the µM. Due to the multiple dilution of the sample in the electrochemical cell, there will always be a difference between the determined values in the samples and electrochemical cell. Thanks to the low LOD allowed by the NPSPCE, high dilutions of the analyzed samples were possible, thus minimizing interference. In the case of urine, it was 10,000-fold because CFX reaches a concentration of 10^{-4} – 10^{-6} mol L^{-1} in the urine [8,12,13]. Municipal wastewater was diluted 10-fold, while hospital wastewater was diluted 20-fold. Additionally, there are

differences in analyte concentrations in different samples. We have reduced the number of significant digits to 3. We can't reduce it anymore so as not to affect the accuracy of the result of the calculated error.

6- All the graphs should have the same number of significant digits .
Due to the changes in parameters used during the optimization of the procedure, different measured values were obtained. Using the same number of significant digits in each graph will result in the need to use for example additionally at least two zeros after the dot. That's why I tried to unify the number of significant digits but after a dot on each of the graphs.

Response to Reviewer 2:

The manuscript is clearly written and the data are presented in a logical flow and well proved. From the presented results and discussions supports the conclusions reached. My question is about the sensors repeatability '(RSD) of 1.58% (n = 10)' and the reproducibility 'RSD 4.77% (n=3) results presented in the manuscript. In figure 2 A and B the acquired signal is in fig. 2A~0.9 uA at pH 7 while in figure 2B it is about 1.1 uA when the same amount of CFX (2x10-8 M) in 0.1 mol/L PBS was added in both cases. Here is not fully consistent with the conclusion for RSD of repeatability/reproducibility.
We would like to thank the Reviewer for invaluable time and comments that have significantly improved the previous version of our manuscript.
Yes, I agree that there was a difference in the current in Figures 2 A and 2 B. But it was due to the stage of work on the analytical procedure. The repeatability of the signal and the reproducibility of the electrode to the electrode were determined after full optimization, i.e. not only the pH and electrolyte concentration were checked, but also the analyte accumulation parameters and analytical signal registration parameters were examined.

Response to Reviewer 3:

Comments and requests to the manuscript are as follows:
Minor Revisions:
1- The motivation behind the modifier selection must be clearly mentioned in the introduction.

We would like to thank the Reviewer for invaluable time and comments that have significantly improved the previous version of our manuscript.

Thank you for your attention. We have added the following text *"The SPCE was pre-anodized in a strongly alkaline medium in accordance with the procedure already used for an electrochemically activated screen-printed boron-doped diamond electrode (aSPBDDE) preparation [32]. We wanted to take advantage of the fact that the electrochemical activation of the electrode surface results in changes in its morphology and a decrease in the charge transfer resistance, which translates into a significant increase in the analytical signal [32]. The morphological and electrochemical characterization of the developed sensor and its application for the determination of CFX in municipal and hospital wastewater and also human urine were performed."*

2- The abstract should be revised to make it more attractive, and the novelty involved in this research should be highlighted.

Thank you for your attention. The abstract was corrected. The abstract in the revised manuscript is as below

"A very sensitive, fast and simple electrochemical procedure using a nanoporous screen-printed carbon electrode (NPSPCE) was developed for the determination of the fluoroquinolone antibiotic ciprofloxacin (CFX). Changes in the surface morphology and electrochemical properties of the SPCE before and after pre-anodization were examined using scanning electron microscopy (SEM), electrochemical impedance spectroscopy (EIS) and cyclic voltammetry (CV). CV studies also demonstrated unequivocally adsorption controlled and irreversible oxidation of CFX. Using optimized conditions, the developed procedure is characterized by excellent selectivity and high sensitivity, allowing to achieve a very low limit of detection (6.3×10^{-11} mol L^{-1}). The measurements taken allow us to consider the NPSPCE as a very effective tool for direct determination of CFX in samples with a complex matrix such as sewage and body fluids. The developed environment friendly sensor and procedure meet the requirements of green chemistry (reduction of toxic chemicals/reagents, and generation of minimal waste)."

3- Introduction also needs to be revised and improved to emphasize the novelty of the proposed work. Include novelty statements.

The following text has been added ***"The novelty of this work is the improvement of analytical procedures for the determination of CFX with respect to the limitations described so far in the literature, i.e. too low sensitivity, complicated procedures of sensor preparation and measurement."***

4- The conclusion is too much; please simplify that.

The conclusion was corrected.

The conclusion in the revised manuscript is as below

"In summary, in this study a very fast and simple DPAdSV procedure using a nanoporous, pre-anodized screen-printed carbon electrode (NPSPCE) for trace analysis of ciprofloxacin (CFX) was proposed. Methods such as EIS and CV were used to characterize the sensor. The obtained results showed numerous advantages of subjecting the SPCE to the pre-anodization process, including a significant increase in the active surface of the working electrode, a decrease in the resistance of charge transfer and improvement of the kinetics of electron transfer. The improvement of these parameters resulted in an extreme increase in the height of the CFX oxidation peak. In addition, SEM imaging showed that the electrode obtained a highly porous structure as a result of pre-anodization. The developed procedure is characterized by excellent selectivity and high sensitivity, allowing to achieve a very low limit of detection (6.3×10^{-11} mol L^{-1}) with a wide range of linearity from 5.0×10^{-10} to 3.0×10^{-8} mol L^{-1}. The usefulness of the proposed procedure was confirmed by successfully determining CFX in spiked samples of treated municipal wastewater and human urine, as well as determining the real content of CFX in samples of hospital wastewater. The results of the study allow us to consider the NPSPCE as a very effective tool for direct

determination of CFX in samples with a complex matrix such as sewage and body fluids. Moreover, the developed environment friendly sensor and procedure meet the requirements of green chemistry (reduction of toxic chemicals/reagents, and generation of minimal waste).”

5- The authors can use the following reference to develop different sections of the article and should be cited:
a-Zaki, M., et al., "Mn/Cu nanoparticles modified carbon paste electrode as a novel electrochemical sensor for nicotine detection." Electroanalysis 35.2 (2023): e202200143.
b-Zaki, M., et al., "Sensitive detection for nicotine using nickel/copper nanoparticle-modified carbon paste electrode." Ionics 28.10 (2022): 4881-4891.
c-Moustafa, Ayah, et al. "Electrochemical determination of vitamin B6 (pyridoxine) by a reformed carbon paste electrode with iron oxide nanoparticles," Ionics 28.9 (2022): 4471-4484.
d-Fekry, Amany M., et al. "A sensitive electrochemical sensor for moxifloxacin hydrochloride based on nafion/graphene oxide/zeolite modified carbon paste electrode." Electroanalysis 33.4 (2021): 964-974.

The references were added.

Figure 1

Click here to access/download;Figure(s);Fig. 1.tif

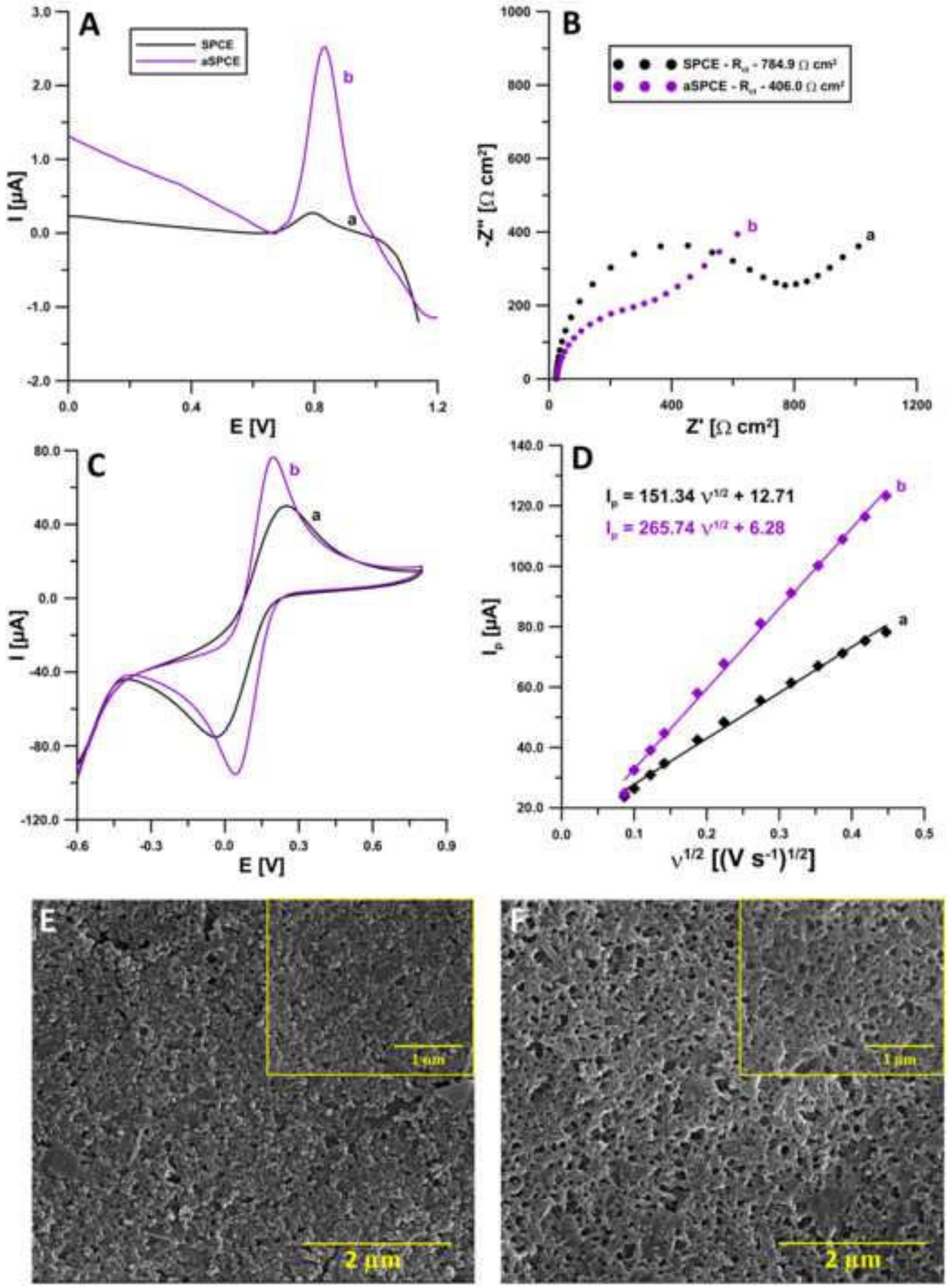

Figure 2

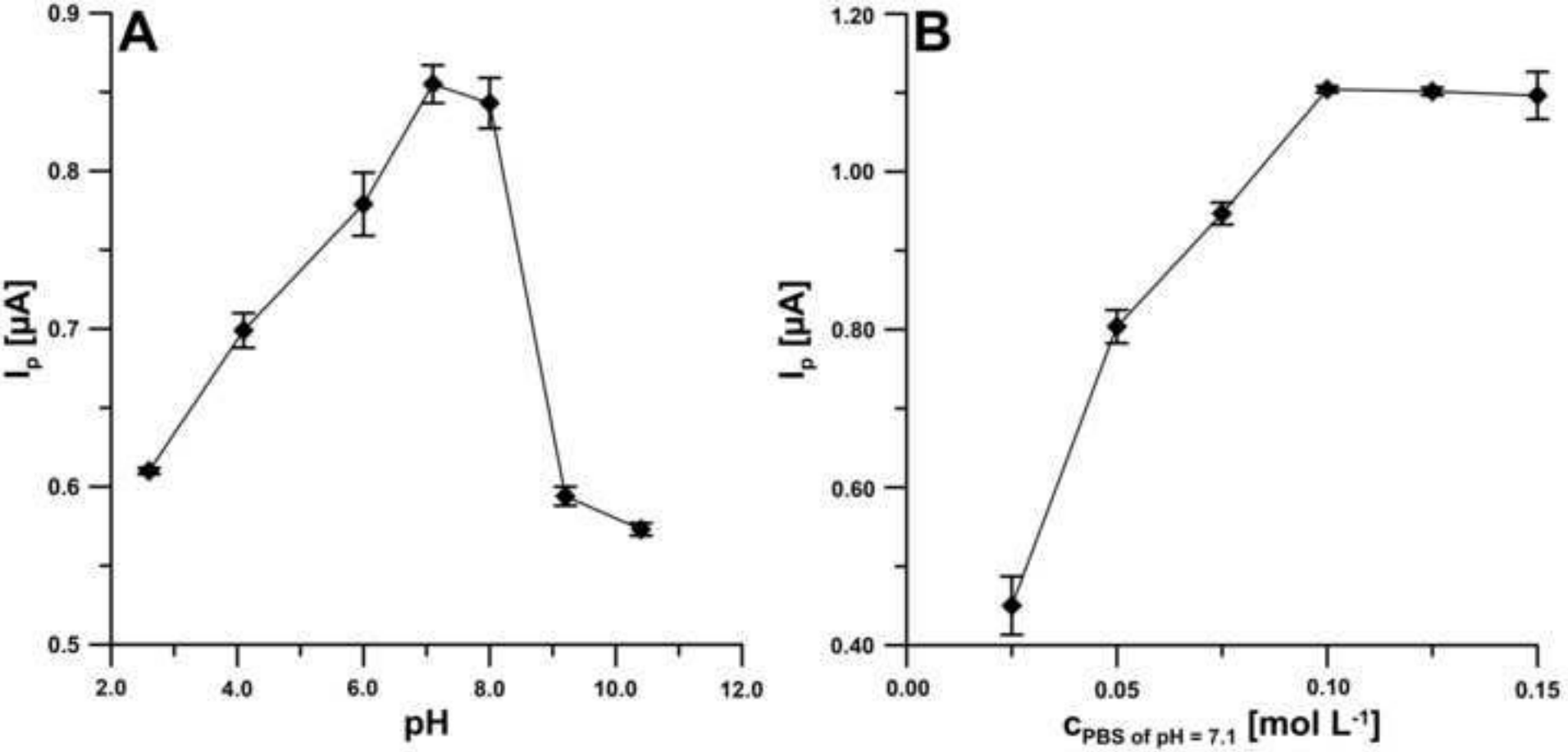

Figure 3

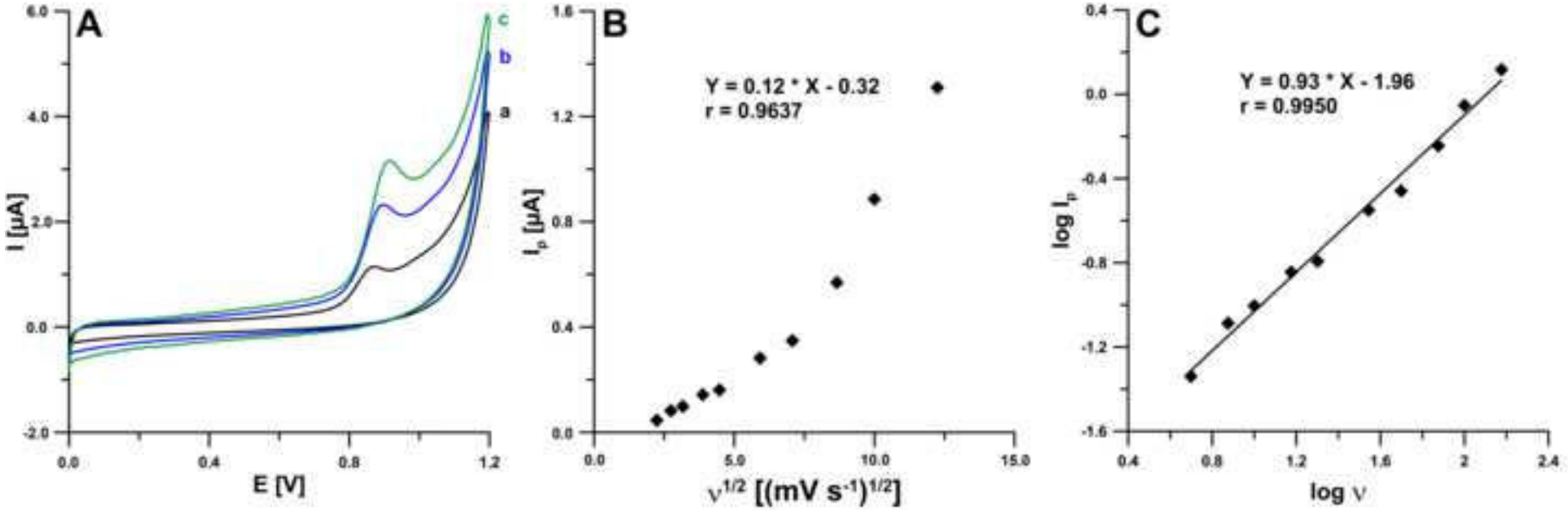

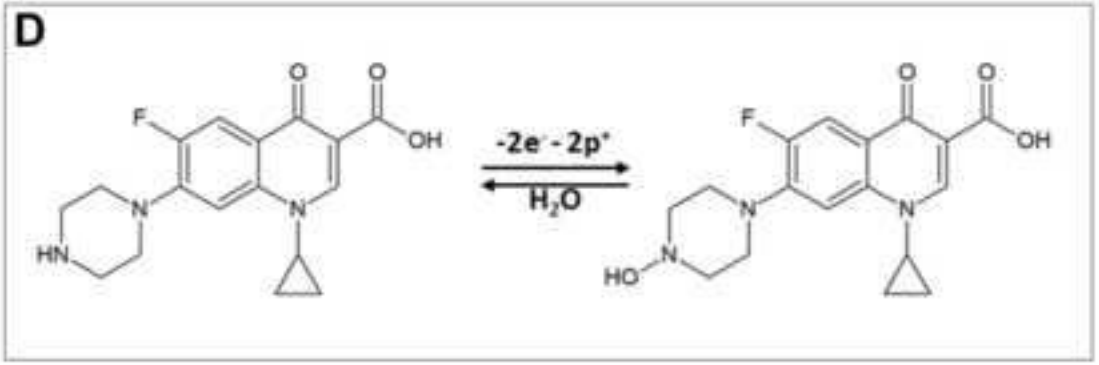

Figure 4

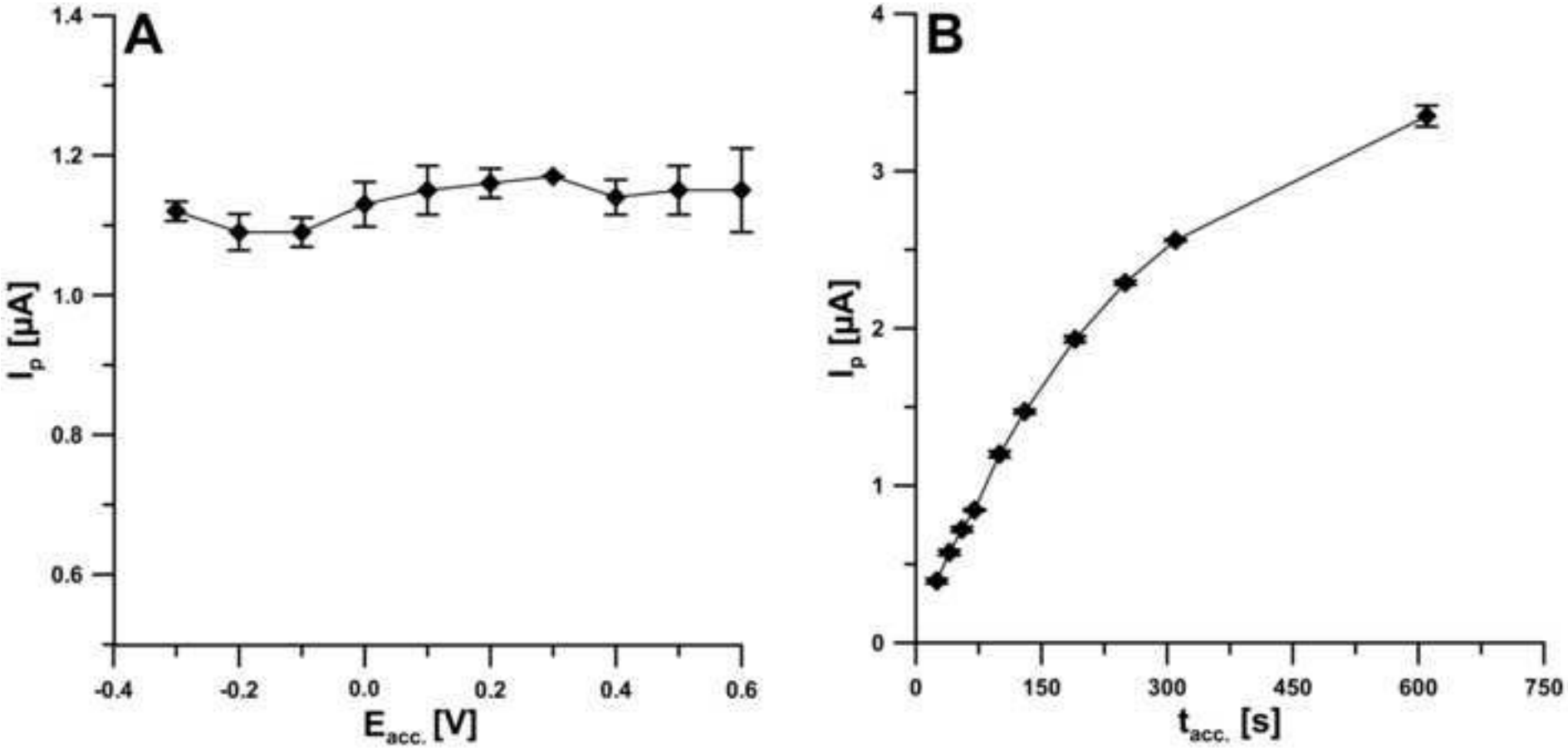

Figure 5

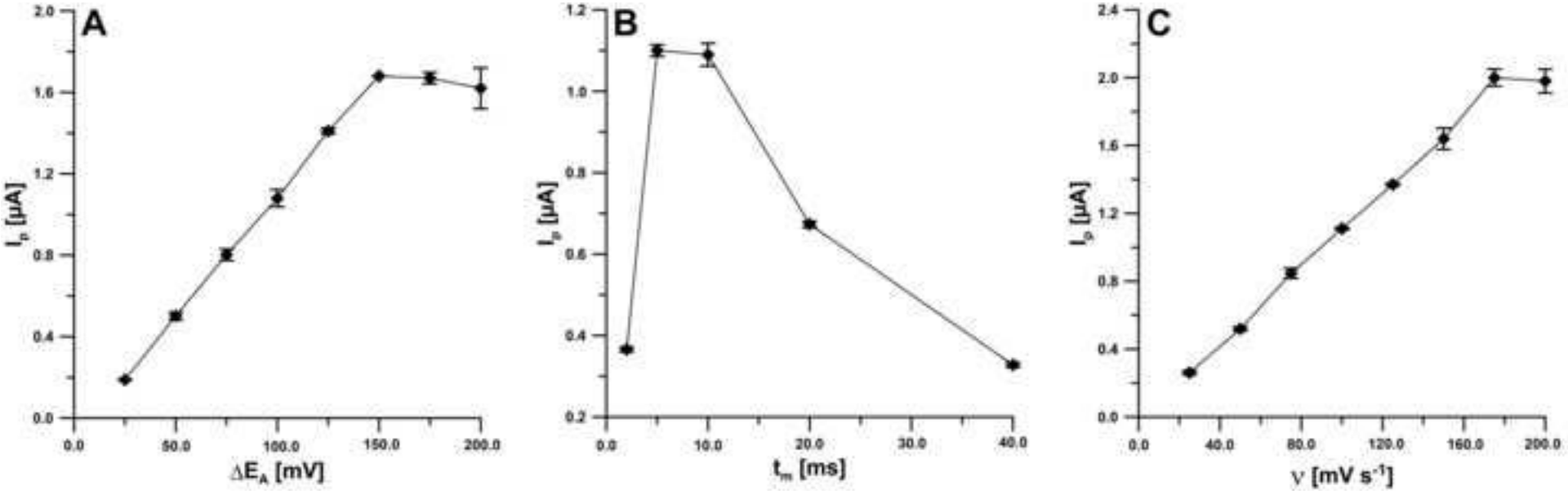

Figure 6

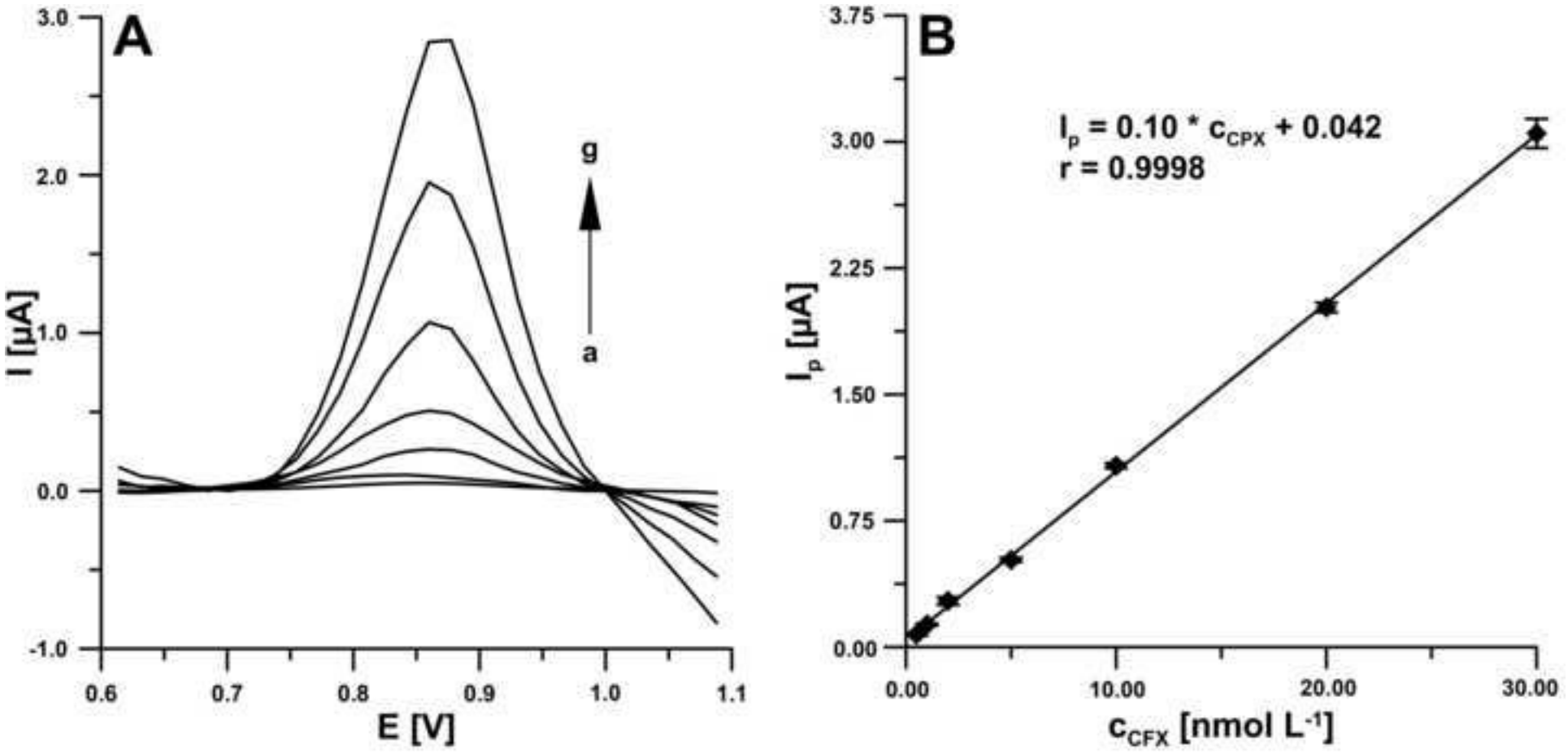

Figure 7

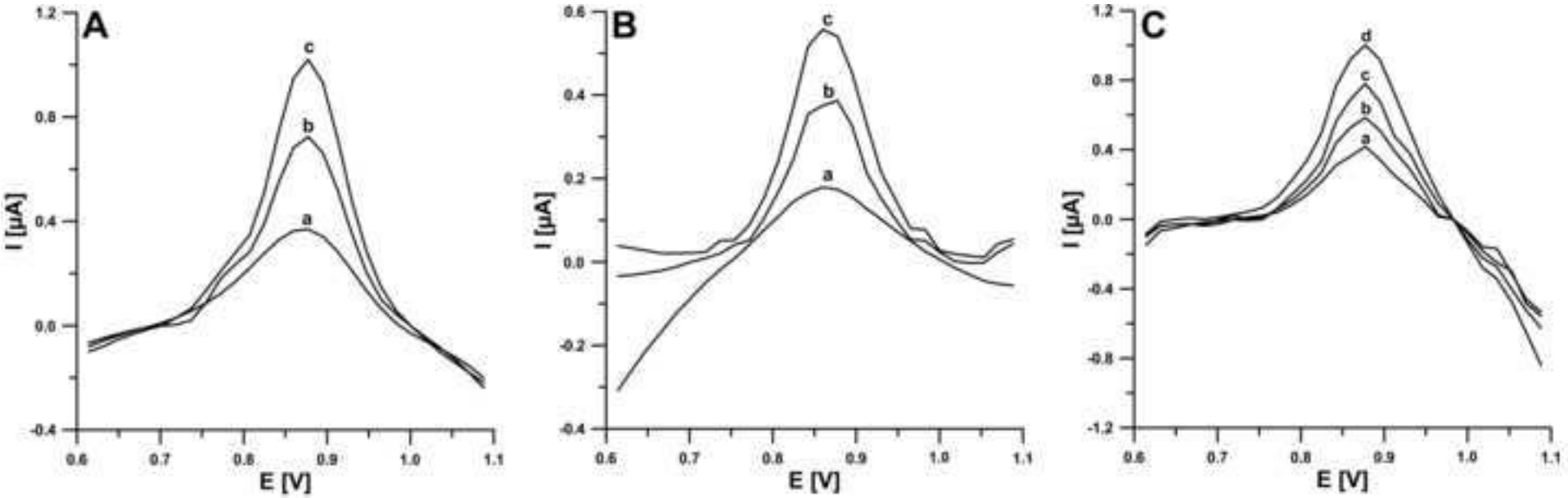

Table 1. Comparison of voltammetric assays for analysis of CFX.

Electrode	Method	Linear range (mol L^{-1})	LOD (mol L^{-1})	Application	Ref.
PAR/EGR/GCE	DPV	$4.0 \times 10^{-8} - 1.2 \times 10^{-4}$	1.0×10^{-8}	Pharmaceutical formulations, serum	[34]
NiONPs-GO-CTS:EPH/GCE	SWV	$4.0 \times 10^{-8} - 9.7 \times 10^{-7}$	6.0×10^{-9}	Urine, serum	[35]
TiO_2/PB/AuNPs/CMK-3/Nafion/GE	CV	$1.0 \times 10^{-6} - 5.2 \times 10^{-5}$	1.1×10^{-7}	River water, CRM of wastewater	[11]
AuNPs/CHI/SPE	SWV	$1.0 \times 10^{-7} - 1.5 \times 10^{-4}$	1.0×10^{-9}	Urine, serum, plasma	[30]
Graphene-modified GCE	DPV	$1.0 \times 10^{-7} - 1.0 \times 10^{-5}$	5.9×10^{-8}	Pharmaceutical formulations, urine	[38]
rGO/PPR/GCE	DPV	$2.0 \times 10^{-9} - 4.0 \times 10^{-4}$	2.0×10^{-9}	Serum	[36]
ChCl/CPE	SWV	$5.0 \times 10^{-9} - 2.0 \times 10^{-4}$	3.6×10^{-10}	Eye drops, river water, eggs	[31]
CRGO/GCE	SWV	$6.0 \times 10^{-6} - 4.0 \times 10^{-5}$	2.1×10^{-7}	Pharmaceutical formulations, milk	[39]
HMDE	AdCSV	$1.5 \times 10^{-7} - 4.5 \times 10^{-7}$	3.0×10^{-8}	Urine	[40]
UiO-66/RGO	ASV	$2.0 \times 10^{-8} - 1.0 \times 10^{-6}$	6.7×10^{-9}	Water	[41]
Graphene SPCE	SWV	$1.0 \times 10^{-7} - 1.0 \times 10^{-4}$	1.0×10^{-7}	Urine, serum	[42]
MMWCNTs@MIP/CPE	DPV	$5.0 \times 10^{-9} - 8.5 \times 10^{-7}$	1.7×10^{-9}	Pharmaceutical formulations, urine, serum	[43]
CZF-CME	DPAdSV	$9.1 \times 10^{-7} - 4.7 \times 10^{-3}$	2.6×10^{-9}	Pharmaceutical formulations, urine, serum	[44]
CMNP-CPE	DPV	$5.0 \times 10^{-8} - 7.5 \times 10^{-5}$	1.0×10^{-8}	Serum, urine	[45]
BDDE	SWV	$1.5 \times 10^{-7} - 2.1 \times 10^{-6}$	5.0×10^{-8}	Urine	[46]
PGE	SWV	$1.2 \times 10^{-5} - 5.5 \times 10^{-5}$	5.6×10^{-6}	Pharmaceutical formulations	[47]
Cu MOF/GC	DPV	$5.0 \times 10^{-8} - 7.5 \times 10^{-5}$	1.0×10^{-8}	Tap water	[48]
mag@MIP-CB-NF/SPE	DPV	$5.0 \times 10^{-7} - 7.0 \times 10^{-6}$	8.4×10^{-9}	Urine, river water	[49]
Ag-β-CD/GCE	DPV	$1.0 \times 10^{-10} - 5.0 \times 10^{-8}$	2.8×10^{-11}	Serum, runoff water	[50]
CB/$ZnWO_4$/GCE	DPV	$2.0 \times 10^{-8} - 1.2 \times 10^{-4}$	2.0×10^{-8}	River water, tap water	[51]

$BaCuSi_4O_{10}$/GCE	DPV	$5.0 \times 10^{-8} - 1.5 \times 10^{-4}$	9.0×10^{-9}	Natural waters, wastewater	[52]
f-MWCNT/GCE	SWV	$5.0 \times 10^{-6} - 1.0 \times 10^{-4}$	1.6×10^{-7}	Natural water, hospital and domestic wastewater	[53]
GO/SPCE	SWV	$1.0 \times 10^{-6} - 8.0 \times 10^{-6}$	3.0×10^{-7}	Milk	[54]
N-prGO/CPE	DPV	$1.0 \times 10^{-7} - 1.0 \times 10^{-5}$	3.9×10^{-8}	Serum, Pharmaceutical formulations	[55]
Co/TiO_2/CPE	DPV	$1.0 \times 10^{-7} - 7.0 \times 10^{-5}$	3.0×10^{-8}	Serum, urine	[56]
MIP/PGE	SWV	$1.0 \times 10^{-9} - 1.0 \times 10^{-3}$	7.6×10^{-11}	Pharmaceutical formulations	[57]
NPSPCE	DPAdSV	$5.0 \times 10^{-10} - 3.0 \times 10^{-8}$	6.3×10^{-11}	Urine, municipal wastewater, hospital wastewater	This work

PAR/EGR/GCE – glassy carbon electrode modified with poly(alizarin red)/electrodeposited graphene; **NiONPs-GO-CTS:EPH/GCE** – glassy carbon electrode modified with NiO nanoparticles, graphene oxide, polysaccharide and epicatechin; **TiO_2/PB/AuNPs/CMK-3/Nafion/GE** – graphite electrode modified with Nafion, mesoporous carbo, gold nanoparticles and titanium dioxide; **AuNPs/CHI/SPE** – screen-printed electrode modified with gold nanoparticles and chitosan; **rGO/PPR/GCE** – reduced graphene oxide/poly(phenol red) modified glassy carbon electrode; **CRGO/GCE** – chemically reduced graphene oxide GCE; **HMDE –** hanging mercury drop electrode; **MIP/PGE** – molecular imprinted polymer modified pencil graphite electrode; UiO-66/RGO – Zr(IV)-based metal−organic frameworks and reduced graphene oxide sensor; **MMWCNTs@MIP/CPE** – carbon paste electrode modified with molecular imprinted polymer and magnetic multiwalled carbon nanotubes; **CZF-CME** – copper zinc ferrite nanoparticle modified carbon paste electrode; **CMNP-CPE** – chitosan-coated magnetic nanoparticle modified carbon paste electrode; **BDDE** – boron doped diamond electrode; **Cu MOF/GC** – copper based organic framework modified glassy carbon electrode; **mag@MIP-CB-NF/SPE** – screen-printed electrode modified with magnetic molecular imprinted polymer, carbon black and Nafion; **Ag-β-CD/GCE –** GCE modified with silver modified β-cyclodextrin nanoparticles; **CB/ZnWO4/GCE –** GCE modified $ZnWO_4$ and carbon black nanocomposite; **$BaCuSi_4O_{10}$/GCE** – GCE modified with Effenbergerite; with voltammetry; ***f*-MWCNT/GCE** – COOH-functionalized multiwalled carbon nanotube-coated GCE; **GO/SPCE –** graphene oxide modified screen-printed electrode; **N-prGO/CPE** – CPE modified with nitrogen doped porous reduced graphene oxide; **CV** – cyclic voltammetry; **DPV** – differential-pulse voltammetry; **SWV –** square-wave voltammetry; **AdCSV** – adsorptive cathodic stripping voltammetry; **DPAdSV** – differential-pulse adsorptive stripping voltammetry

Table 2. The results of CFX determination in human urine, municipal and hospital wastewater.

Sample	CFX concentration [µmol L^{-1}] ± SD (n = 3)			Coefficient of variation* [%]	Recovery** [%]
	Added	Found DPAdSV	Found in electrochemical cell		
RM of human serum	20.0	20.7 ± 0.82	0.00207 ± 0.000082	3.96	103.5
	50.0	49.2 ± 1.10	0.00492 ± 0.00011	2.24	98.4
Purified municipal wastewater	0.02	0.0196 ± 0.00069	0.00196 ± 0.000069	3.52	98.0
	0.05	0.0514 ± 0.0011	0.00514 ± 0.00011	2.14	102.2
Hospital wastewater	0	0.208 ± 0.009	0.0104 ± 0.00045	4.33	-
	0.1	0.299 ± 0.0007	0.0150 ± 0.000035	0.23	97.1

*Coefficient of variation [%] = (SD × 100)/ Found DPAdSV, ** Recovery [%] = (Found DPAdSV × 100)/Added

Declaration of interests

☒The authors declare that they have no known competing financial interests or personal relationships that could have appeared to influence the work reported in this paper.

☐The authors declare the following financial interests/personal relationships which may be considered as potential competing interests:

CRediT authorship contribution statement

Jędrzej Kozak: Conceptualization, Methodology, Investigation, Writing – original draft, Writing – review and editing. **Katarzyna Tyszczuk-Rotko:** Conceptualization, Methodology, Investigation, Writing – original draft, Writing – review and editing, Supervision. **Damian Gorylewski:** Investigation, Writing – review and editing.

A nanoporous screen-printed carbon sensor for environmental and clinical monitoring of the antibiotic ciprofloxacin

Jędrzej Kozak , Katarzyna Tyszczuk-Rotko *, Damian Gorylewski

Faculty of Chemistry, Institute of Chemical Sciences, Maria Curie-Skłodowska University in Lublin, 20-031 Lublin, Poland

* Corresponding author: katarzyna.tyszczuk-rotko@mail.umcs.pl

Abstract: A very sensitive, fast and simple electrochemical procedure using a nanoporous screen-printed carbon electrode (NPSPCE) was developed for the determination of the fluoroquinolone antibiotic ciprofloxacin (CFX). Changes in the surface morphology and electrochemical properties of the SPCE before and after pre-anodization were examined using scanning electron microscopy (SEM), electrochemical impedance spectroscopy (EIS) and cyclic voltammetry (CV). CV studies also demonstrated unequivocally adsorption controlled and irreversible oxidation of CFX. ~~In 0.1 mol L^{-1} phosphate buffer saline (PBS) of pH 7.1,~~ U~~u~~sing optimized conditions, the developed procedure is characterized by excellent selectivity and high sensitivity, allowing to achieve a very low limit ~~the NPSPCE shows a~~ detection ~~limit~~ (~~LOD) of~~ 6.3×10^{-11} mol L^{-1}).~~.~~ The measurements taken allow us to consider the NPSPCE as a very effective tool for direct determination of CFX in samples with a complex matrix such as sewage and body fluids. The developed environment friendly sensor and procedure meet the requirements of green chemistry (reduction of toxic chemicals/reagents, and generation of minimal waste).

Keywords: antibiotics; screen-printed sensor; nanoporous carbon; stripping voltammetry; human urine; hospital and municipal wastewater

1. Introduction

Consuming a huge amount of antibiotics nowadays in the fight against diseases, but also to promote the growth of animals, among others in aquacultures, dairy or poultry farms, contributes to the presence of these biologically active compounds in the environment [1]. A significant amount of antibiotics is excreted unchanged or as active metabolites. For this reason, hospital, veterinary and even municipal wastewater often contains high concentrations of antibiotics. In addition, the processes of their removal from wastewater are not very effective [2,3]. Antibiotics are also found in drinking water and surface waters [4]. The constantly growing antibiotic pollution of the environment and aquatic ecosystems is a factor stimulating the evolution of antibiotic resistance in many pathogenic bacteria, which is a serious threat to public health on a global scale [5,6].

Fluoroquinolones are one of the most important and widely used antibacterial drugs. They are characterized by an affordable price, low toxicity and number of side effects, and a wide spectrum of activity [2,7]. The mechanism of action of this group of antibiotics consists in the inhibition of bacterial DNA replication by inhibiting DNA topoisomerase IV and DNA gyrase, which in turn leads to cell death [8,9]. Ciprofloxacin (CFX) is a second-generation

fluoroquinolone antibiotic that is effective against both Gram-negative and Gram-positive bacteria [10,11]. CFX is used to treat a wide range of infections affecting the urinary, respiratory and digestive systems. In addition, it is the drug of choice in the treatment of bone and joint infections, skin infections and sexually transmitted diseases [8,10]. CFX is a substance that, after oral administration, is excreted in about 50% through the urinary tract, which achieves relatively high concentrations in the urine, of the order of $10^{-4} – 10^{-6}$ mol L^{-1} [8,12,13]. Due to the widespread use of CFX in hospitals, this drug is detected in hospital wastewater, where its content often reaches 10^{-7} mol L^{-1} [3,5,7,14]. The presence of CFX in municipal wastewater was also noted at a concentration level of $10^{-10} – 10^{-9}$ mol L^{-1} [1].

Detection and quantification of drugs is an extremely important aspect of environmental and clinical research. CFX present in many types of samples, i.e. natural waters, sewage, pharmaceuticals or body fluids, is analyzed using a whole range of analytical methods. CFX assays use spectrophotometry [15,16], spectrofluorimetry [17], Rayleigh light scattering [18], electrogenerated chemiluminescence [19], high performance liquid chromatography coupled with tandem mass spectrometry [20], liquid chromatography coupled with tandem mass spectrometry [21,22], microemulsion electrokinetic chromatography [23], micellar electrokinetic chromatography [24] or capillary electrophoresis [25]. Most of the above-mentioned methods require very expensive equipment, large amounts of reagents, highly skilled operators, as well as time-consuming and multi-stage sample preparation. Electroanalytical methods enable the detection and quantification of a multitude of organic compounds [26-29]. These methods have a number of advantages, such as relatively inexpensive devices, low consumption of reagents, small sample volumes, simplicity, high selectivity and sensitivity, speed of response, as well as the possibility of miniaturization and use of sensors in portable analyzers [30~~26~~,31~~27~~].

The novelty of this work is the improvement of analytical procedures for the determination of CFX with respect to the limitations described so far in the literature, i.e. too low sensitivity, complicated procedures of sensor preparation and measurement. For this purpose,

~~In this work,~~ we propose a screen-printed sensor based on nanoporous carbon (NPSPCE) and present a fast and very simple electrochemical method to obtain an NPSPCE from a bare screen-printed carbon sensor (SPCE). The SPCE was pre-anodized in a strongly alkaline medium in accordance with the procedure already used for an electrochemically activated screen-printed boron-doped diamond electrode (aSPBDDE) preparation [32]. We wanted to take advantage of the fact that the electrochemical activation of the electrode surface

results in changes in its morphology and a decrease in the charge transfer resistance, which translates into a significant increase in the analytical signal [32]. The morphological and electrochemical characterization of the developed sensor and its application for the determination of CFX in municipal and hospital wastewater and also human urine were performed.

2. Experimental section

2.1. Apparatus

Voltammetric measurements were done using a μAutolab electrochemical analyzer (Netherlands, Eco Chemie) controlled by GPES 4.9 software and in the case of electrochemical impedance spectroscopy (EIS) studies by FRA 4.9 software. The standard 10 mL electrochemical cell made of quartz with a screen-printed carbon sensor with a carbon working electrode, a platinum counter electrode and a silver pseudo-reference electrode (SPCE, Ref. 150 commercially available from DropSens, Spain) was used for our studies.

Microscopic images of the sensors were obtained with a high-resolution scanning electron microscope Quanta 3D FEG (USA, FEI) (voltage of acceleration of 5000 V, working distance of 9.3 mm). The equivalent diameters of pores present in the working electrode material were measured using NIS-Elements Advanced Research software.

2.2.Reagents and solutions

An appropriate weighed amount of ciprofloxacin (Germany, Merck) was dissolved in 0.1 mol L^{-1} acetic acid obtaining a 10^{-3} mol L^{-1} solution of CFX. This solution was diluted using 0.1 mol L^{-1} phosphate buffer saline (PBS) with a pH value of 7.1 to obtain 10^{-4} and 10^{-5} mol L^{-1} solutions of CFX. The dilutions were prepared every day. 0.1 mol L^{-1} solutions of PBS with the following pH values: 2.6, 4.1, 6.0, 7.1, 8.0, 9.2 and 10.4, were used to check the influence of pH on the CFX analytical signal. The 10^{-3} mol L^{-1} solutions of the following metal ions: Fe^{3+}, Cu^{2+}, Ca^{2+}, Pb^{2+}, Cd^{2+}, Mg^{2+} and Ni^{2+}, as well as organic compounds such as ascorbic acid, dopamine, glucose, uric acid and adrenaline were made with chemicals purchased from Merck reagents in ultrapure water, stored in the refrigerator, and protected from light. Reference material of human urine was bought from Merck, hospital wastewater and purified municipal wastewater samples were obtained from Municipal Water Supply & Waste Water Treatment Company Ltd (Lublin, Poland).

2.3. Differential-pulse adsorptive stripping voltammetric (DPAdSV) analysis of CFX

Voltammetric analysis of CFX in optimized conditions was performed in 0.1 mol L^{-1} PBS (pH = 7.1). The analyte was accumulated on the working electrode surface at a potential of 0.5 V ($E_{acc.}$) for 130 s ($t_{acc.}$). Voltammograms were recorded in a potential range from 0 to 1.2 V with ν of 175 mV s^{-1}, t_m of 5 ms and ΔE_A of 150 mV. From each voltammogram the background curve was subtracted and the baseline was adjusted.

2.3. Sample analysis

The proposed DPAdSV procedure was applied for CFX determination in spiked municipal wastewater and human urine. It was also used to analyze the real content of CFX in hospital wastewater samples in order to prove its usefulness in analysis of real samples. The samples of purified municipal wastewater as well as the reference material of human urine were spiked with the appropriate concentration of CFX and directly analyzed without any pretreatment. In the case of hospital wastewater, the sample was also analyzed directly.

3. Results and discussion

3.1. Preparation and characterization of the NPSPCE

The SPCE was pre-anodized in a strongly alkaline medium (0.1 mol L^{-1} NaOH) in accordance with the procedure already used in our previous studies [~~28~~32]. This procedure involves the use of CV; 5 measurements were made in the potential range of 0 – 2 V at ν = 100 mV s^{-1}. First, the voltammetric response of CFX to the SPCE and NPSPCE was compared. DPAdSV measurements were performed in 0.1 mol L^{-1} PBS (pH = 7.1) and the analyte was accumulated at -0.2 V for 60 s. An approximately 10-fold increase in the peak height on the pre-anodized electrode was observed compared to the signal obtained on the SPCE (Fig. 1A). The next step was to investigate the effect of electrode pretreatment on its electrochemical properties. CV and electrochemical impedance spectroscopy (EIS) were used for this purpose. The i~~I~~mpedance spectra were recorded in KCl solution (0.1 mol L^{-1}) with the addition of $K_3[Fe(CN)_6]$ (5.0×10^{-3} mol L^{-1}) for frequencies in the range of 50000 - 1 Hz and at a potential of 0.2 V. The results are shown in Figure 1B, where it is clear that the NPSPCE has a much lower charge transfer resistance (R_{ct}) than the SPCE. Using a solution of the same composition, CV measurements were made for scanning rates from 7.5 to 200 mV s^{-1}. Figure 1C shows the CV curves recorded on both sensors for a scan rate (ν) of 100 mV s^{-1}. On the NPSPCE, not only an enhancement of the Fe(II) oxidation signal was observed, but also an improvement in the relative separation of the oxidation and reduction peaks (χ^0). The χ^0 values were 4.47 and 2.39 for the SPCE and NPSPCE, respectively, which indicates better electron transfer kinetics for

the NPSPCE, where χ^0 is closer to the theoretical value ($\chi^0 = 1$). On the basis of CV studies, the relationship between the intensity of the anode peak (I_p) and the square root of the scan rate was also plotted (Fig. 1D), based on which the active area (A_s) of both electrodes was calculated using equation of Randles-Sevcik [~~29~~33]. The obtained results showed a significant increase in the area of the NPSPCE compared to the SPCE (0.074 vs. 0.042 cm^2). The SEM images showing the surface morphology of the SPCE (Fig. 1E) and NPSPCE (Fig. 1F) were also compared and it proved that as a result of preanodization of SPCE, the surface of the working electrode obtains a highly porous structure. The size of the pores present in the NPSPCE material is in the range of 17.68 - 167.46 nm with an average value of 58.70 ± 31.29 (n = 100).

In our previously mentioned studies [32], an electrochemically activated boron-doped screen-printed diamond electrode (aSPBDDE) also provided a much higher analyte (rifampicin) peak current. A number of parameters were also improved compared to the non-activated electrode. As in the case of the NPSPCE, R_{ct} was lowered as a result of activation. The visible changes in the surface of the working electrode and a slight increase in the active surface were observed at that time. However, a highly porous structure of SPBDDE as a result of pre-anodization as in the case of SPCE was not observed. It can therefore be concluded that the same type of electrochemical pretreatment may affect the different properties of the electrodes depending on the material from which they are made. ~~In our previously mentioned studies [28], an electrochemically activated boron-doped screen-printed diamond electrode (aSPBDDE) also provided a much higher analyte (rifampicin) peak current. A number of parameters were also improved compared to the non-activated electrode. As in the case of the NPSPCE, R_{ct} was lowered as a result of activation. However, no significant changes in the surface morphology were observed at that time, and thus practically no change in the active area of the working electrode. It can therefore be concluded that the same type of electrochemical pretreatment may affect the different properties of the electrodes depending on the material from which they are made.~~

Formatted: Font: Not Italic

Formatted: Font: (Default) Times New Roman, 12 pt

Formatted: Font: (Default) Times New Roman, 12 pt

Formatted: Font: (Default) Times New Roman, 12 pt

Field Code Changed

Formatted: Font: (Default) Times New Roman, 12 pt

3.2. Effect of pH and concentration of the supporting electrolyte

In order to find the optimal pH value of the solution in which the experiments were carried out, the voltammetric response of 2 × ~~x~~ 10^{-8} mol L^{-1} CFX in 0.1 mol L^{-1} PBS for pH in the range from 2.6 to 10.4 was tested. The highest peak was obtained in buffer with pH of 7.1 and therefore this value was chosen (Fig. 2A). Then, it was examined how the current intensity of the CFX peak changes depending on the concentration of PBS with pH = 7.1, which was changed from 0.025 to 0.15 mol L^{-1} (Fig. 2B). The CFX analytical signal increased with

increasing electrolyte concentration, reached a maximum for 0.1 mol L^{-1} PBS solution and remained constant for higher concentrations, so the concentration of 0.1 mol L^{-1} was implemented for further stages of research.

3.3. CV behavior of CFX on the NPSPCE

Using CV, the electrochemical behavior of CFX on the NPSPCE in supporting electrolyte was studied. For this purpose, 1 ×~~x~~ 10^{-6} mol L^{-1} of CFX was added to the supporting electrolyte and CVs were registered varying ν from 5 to 200 mV s^{-1}. Figure 3A shows the CV curves obtained at ν values of 50, 100 and 150 mV s^{-1}. One irreversible oxidation peak of CFX can be clearly seen at 0.89 V (for ν of 100 mV s^{-1}). In addition, the potential of the peak shifts in the positive direction with increasing scan rate, which is an additional confirmation that the CFX oxidation process is irreversible. The nature of the electrode process is clearly indicated by the relationship between the CFX peak current (I_p) and the square root of the scan rate ($\nu^{1/2}$) (Fig. 3B), as well as the dependence between the peak current logarithm (log I_p) and the scan rate logarithm (log ν) (Fig. 3C). The first dependence is far from linear, while the slope of the linear regression equation in the second plot is close to 1.0, which ensures that the oxidation of CFX on NPSPCE is adsorption controlled. The mechanism of CFX oxidation is known and well described in the literature [~~26~~30,3~~40~~–3~~62~~]. This process involves two electrons and two protons as well as the oxidation of a secondary amino group to form hydroxylamine (Fig. 3D).

3.4. Optimization of DPAdSV parameters

The effect of the accumulation potential ($E_{acc.}$) on the efficiency of the CFX adsorption process on the NPSPCE surface was examined in the range from -0.3 to 0.6 V. It was noticed that the applied potentials practically do not affect the height of the 2.0×10^{-8} mol L^{-1} CFX peak (Fig. 4A), which remains at the same level as in the case of open-circuit accumulation. However, it was decided to conduct the accumulation step applying 0.5 V to oxidize compounds that could deposit on the surface of the working electrode and interfere with the analyte signal. Then, the effect of the accumulation time ($t_{acc.}$) was investigated by extending it from 25 to 610 s. The CFX analytical signal increased continuously up to 610 s (Fig. 4B), but to make the analysis less time-consuming, an accumulation time of 130 s was chosen for further research.

It was also checked how the height of the CFX peak is affected by the parameters of the signal recording technique, such as amplitude (ΔE_A), modulation time (t_m) and scan rate (ν). The amplitude was changed from 25 to 200 mV and it was noticed that the peak current reached the highest value at the ΔE_A of 150 mV; therefore, it was considered optimal (Fig. 5A). Then,

the modulation time effect was tested in the range of 2 – 40 ms (Fig. 5B) and t_m of 5 ms was selected for further testing. Lastly, the scan rate was optimized by evaluating its effect on the CFX signal in the range of 25 to 200 mV s^{-1} (Fig. 5C) and it was decided that the ν of 175 mV s^{-1} would be the most suitable.

3.5. Analytical characteristics

Under the conditions of properly selected parameters of the DPAdSV procedure, signals were recorded for successive CFX concentrations increasing linearly in the range from 5 × 10^{-10} to 3 × 10^{-8} mol L^{-1} (Fig. 6). The limits of detection (LOD) and quantification (LOQ) calculated as LOD = 3SD_a/b and LOQ = 10SD_a/b (SD_a: standard deviation of intercept, b: slope of calibration plot, n = 3) [37] [33] were 6.3 × 10^{-11} and 2.1 × 10^{-10} mol L^{-1}, respectively. The comparison of the results obtained with the proposed procedure using the NPSPCE with other voltammetric CFX determination procedures described in the literature [11,26,27,30,34–36,38 53,57] is presented in Table 1. To the best of our knowledge, there is only one procedure [46,50] that allows a lower limit to be obtained than with the use of the NPSPCE, but the electrode used requires a multi-stage preparation (synthesis, rinsing and drying) of the modifier (nanocomposite of silver and beta-cyclodextrin), which takes a total of four days. In contrast, the preparation of the NPSPCE takes only about two minutes as this sensor does not require complex and time-consuming modification.

The effect of potential interferents was tested for both inorganic ions and organic compounds, while the limit of tolerance was considered to be peak current changes not exceeding 10%. Based on the obtained results, it was concluded that a 1000-fold excess of Fe^{3+}, Cu^{2+}, Ca^{2+}, Pb^{2+}, Cd^{2+}, Mg^{2+} and Ni^{2+}, as well as glucose, dopamine, adrenaline, uric acid and ascorbic acid have a negligible effect on the 5.0 × 10^{-9} mol L^{-1} CFX analytical signal. Similarly, changes in the current intensity of the CFX peak greater than 10% were not observed in the presence of 2 ppm of Triton X-100.

Moreover, repeatability of the signal of 5.0 × 10^{-9} mol L^{-1} CFX on the NPSPCE was checked. The relative standard deviation (RSD) of 1.58% (n = 10) was received, which confirms satisfying repeatability of the CFX signal. Reproducibility was determined based on the results of measurements made for the same CFX concentration on the three sensors. The obtained RSD of 4.77% indicates good reproducibility of the NPSPCE.

3.6. Analytical application

The application of the proposed voltammetric procedure was tested for the determination of CFX in municipal wastewater, hospital wastewater and reference material of human urine. The voltammograms obtained during the analysis are depicted in Figure 7. Thanks to the low LOD allowed by the NPSPCE, high dilutions of the analyzed samples were possible, thus minimizing interference. In the case of urine, it was 10,000-fold because CFX reaches a concentration of 10^{-4} – 10^{-6} mol L^{-1} in the urine [8,12,13]. Municipal wastewater was diluted 10-fold, while hospital wastewater was diluted 20-fold. All samples were analyzed using the method of standard addition.

The obtained recoveries ranging from 9~~70~~.~~1~~8~~~~ to 103.5% prove the high accuracy of the proposed procedure (Table 2). Moreover, the coefficient of variation from 0.~~77~~ 23 to 3.96 indicates good CFX peak current repeatability. In addition, in samples of hospital wastewater, it was possible to determine the real content of CFX.

Formatted: Indent: First line: 0.49"

4. Conclusions

In summary, in this study a very fast and simple DPAdSV procedure using a nanoporous, pre-anodized screen-printed carbon electrode (NPSPCE) for trace analysis of ciprofloxacin (CFX) was proposed. ~~CFX is a second-generation fluoroquinolone antibiotic that is effective against both Gram-negative and Gram-positive bacteria. CFX is used to treat a wide range of infections affecting the urinary, respiratory and digestive systems.~~ Methods such as EIS and CV were used to characterize the sensor. The obtained results showed numerous advantages of subjecting the SPCE to the pre-anodization process, including a significant increase in the active surface of the working electrode, a decrease in the resistance of charge transfer and improvement of the kinetics of electron transfer. The improvement of these parameters resulted in an extreme increase in the height of the CFX oxidation peak. In addition, SEM imaging showed that the electrode obtained a highly porous structure as a result of pre-anodization. The developed procedure is characterized by excellent selectivity and high sensitivity, allowing to achieve a very low limit of detection (6.3×10^{-11} mol L^{-1}) with a wide range of linearity from 5.0×10^{-10} to 3.0×10^{-8} mol L^{-1}. The usefulness of the proposed procedure was confirmed by successfully determining CFX in spiked samples of treated municipal wastewater and human urine, as well as determining the real content of CFX in samples of hospital wastewater. The results of the study allow us to consider the NPSPCE as a very effective tool for direct determination of CFX in samples with a complex matrix such as sewage and body fluids. Moreover, the developed environment friendly sensor and procedure

meet the requirements of green chemistry (reduction of toxic chemicals/reagents, and generation of minimal waste). ~~green analytical chemistry encourages using energy efficient equipment, reducing the use of toxic chemicals/reagents, and generating minimal waste. The developed sensor and analytical procedure perfectly fit into this trend. The developed environment friendly sensor and analytical procedure perfectly fit into this trend. We are dealing here with a small consumption of chemical reagents, no chemical modifier of the sensor surface, direct analysis of samples and small volume of the analyzed solutions.~~

Data availability

Data will be made available on request.

Declaration of competing interest

The authors declare no competing financial interests or personal relationships that could have appeared to influence the work reported in this paper.

Acknowledgment: We would like to thank employees of Municipal Water Supply & Waste Water Treatment Company Ltd (Lublin, Poland) for the wastewater samples.

References

[1] B. Nas, T. Dolu, S. Koyuncu, Behavior and Removal of Ciprofloxacin and Sulfamethoxazole Antibiotics in Three Different Types of Full-Scale Wastewater Treatment Plants: A Comparative Study, Water Air Soil Pollut. 232 (2021) 127. https://doi.org/10.1007/s11270-021-05067-6.

[2] X. Ma, Z. Wang, Removal of Ciprofloxacin from Wastewater by Ultrasound/Electric Field/Sodium Persulfate (US/E/PS), Processes. 10 (2022) 124. https://doi.org/10.3390/pr10010124.

[3] A.F. Martins, T.G. Vasconcelos, D.M. Henriques, C. da S. Frank, A. König, K. Kümmerer, Concentration of Ciprofloxacin in Brazilian Hospital Effluent and Preliminary Risk Assessment: A Case Study, Clean Soil Air Water. 36 (2008) 264–269. https://doi.org/10.1002/clen.200700171.

[4] Y. Li, L. Chen, X. Tian, L. Lin, R. Ding, W. Yan, F. Zhao, Functional role of mixed-culture microbe in photocatalysis coupled with biodegradation: Total organic carbon

removal of ciprofloxacin, Science of The Total Environment. 784 (2021) 147049. https://doi.org/10.1016/j.scitotenv.2021.147049.

[5] L. Lien, N. Hoa, N. Chuc, N. Thoa, H. Phuc, V. Diwan, N. Dat, A. Tamhankar, C. Lundborg, Antibiotics in Wastewater of a Rural and an Urban Hospital before and after Wastewater Treatment, and the Relationship with Antibiotic Use—A One Year Study from Vietnam, IJERPH. 13 (2016) 588. https://doi.org/10.3390/ijerph13060588.

[6] R. Pei, S.-C. Kim, K.H. Carlson, A. Pruden, Effect of River Landscape on the sediment concentrations of antibiotics and corresponding antibiotic resistance genes (ARG), Water Research. 40 (2006) 2427–2435. https://doi.org/10.1016/j.watres.2006.04.017.

[7] C. Rodrigues-Silva, R. Porto, S. dos Santos, J. Schneider, S. Rath, Fluoroquinolones in Hospital Wastewater: Analytical Method, Occurrence, Treatment with Ozone and Residual Antimicrobial Activity Evaluation, J. Braz. Chem. Soc. (2019). https://doi.org/10.21577/0103-5053.20190040.

[8] P.D. Brown, Ciprofloxacin for the Management of Urinary Tract Infection, Womens Health (Lond Engl). 2 (2006) 509–516. https://doi.org/10.2217/17455057.2.4.509.

[9] S.S. Timofeeva, O.V. Tyukalova, S.S. Timofeev, Environmental risk and possibilities of ciprofloxacin phytoremediation, IOP Conf. Ser.: Earth Environ. Sci. 1061 (2022) 012025. https://doi.org/10.1088/1755-1315/1061/1/012025.

[10] L. Fotouhi, Z. Atoofi, M.M. Heravi, Interaction of ciprofloxacin with DNA studied by spectroscopy and voltammetry at MWCNT/DNA modified glassy carbon electrode, Talanta. 103 (2013) 194–200. https://doi.org/10.1016/j.talanta.2012.10.032.

[11] A. Pollap, K. Baran, N. Kuszewska, J. Kochana, Electrochemical sensing of ciprofloxacin and paracetamol in environmental water using titanium sol based sensor, Journal of Electroanalytical Chemistry. 878 (2020) 114574. https://doi.org/10.1016/j.jelechem.2020.114574.

[12] K.G. Naber, U. Theuretzbacher, G. Moneva-Koucheva, H. Staß, Urinary Excretion and Bactericidal Activity of Intravenous Ciprofloxacin Compared with Oral Ciprofloxacin, European Journal of Clinical Microbiology & Infectious Diseases. 18 (1999) 783–789. https://doi.org/10.1007/s100960050401.

[13] F.M.E. Wagenlehner, M. Kinzig-Schippers, F. Sörgel, W. Weidner, K.G. Naber, Concentrations in plasma, urinary excretion and bactericidal activity of levofloxacin (500mg) versus ciprofloxacin (500mg) in healthy volunteers receiving a single oral dose, International Journal of Antimicrobial Agents. 28 (2006) 551–559. https://doi.org/10.1016/j.ijantimicag.2006.07.026.

[14] L.J.M. Githinji, M.K. Musey, R.O. Ankumah, Evaluation of the Fate of Ciprofloxacin and Amoxicillin in Domestic Wastewater, Water Air Soil Pollut. 219 (2011) 191–201. https://doi.org/10.1007/s11270-010-0697-1.

[15] L. Fratini, Ciprofloxacin determination by visible light spectrophotometry using iron(III)nitrate, International Journal of Pharmaceutics. 127 (1996) 279–282. https://doi.org/10.1016/0378-5173(95)04290-3.

[16] R.S. Nijhu, Y.M. Jhanker, K.B. Sutradhar, Development of an Assay Method for Simultaneous Determination of Ciprofloxacin and Naproxen by UV Spectrophotometric Method, S.J. Pharm. Sci. 4 (1970) 84–90. https://doi.org/10.3329/sjps.v4i1.8876.

[17] A. Navalón, Determination of ciprofloxacin in human urine and serum samples by solid-phase spectrofluorimetry, Talanta. 52 (2000) 845–852. https://doi.org/10.1016/S0039-9140(00)00437-9.

[18] X. Li, Q. Cao, F. Wang, Determination of ciprofloxacin hydrochloride in pharmaceutical preparation and biological fluid by Rayleigh light scattering technique, Wuhan Univ. J. Nat. Sci. 14 (2009) 70–74. https://doi.org/10.1007/s11859-009-0115-y.

[19] D. Pavão e Pavão, C. Nascimento Botelho, R. Nunes Fernandes, C. Costa dos Santos, F. Santos Damos, R. Cássia Silva Luz, A Simple, Cost- effective, and Environmentally Friendly Method for Determination of Ciprofloxacin in Drugs and Urine Samples Based on Electrogenerated Chemiluminescence, Electroanalysis. 32 (2020) 1498–1506. https://doi.org/10.1002/elan.201900355.

[20] O. Szerkus, J. Jacyna, A. Gibas, M. Sieczkowski, D. Siluk, M. Matuszewski, R. Kaliszan, M.J. Markuszewski, Robust HPLC–MS/MS method for levofloxacin and ciprofloxacin determination in human prostate tissue, Journal of Pharmaceutical and Biomedical Analysis. 132 (2017) 173–183. https://doi.org/10.1016/j.jpba.2016.10.008.

[21] C.-L. Chan, H.K.-F. Wai, P. Wu, S.-W. Lai, O.S.-K. Chan, H.M. Tun, A Universal LC-MS/MS Method for Simultaneous Detection of Antibiotic Residues in Animal and Environmental Samples, Antibiotics. 11 (2022) 845. https://doi.org/10.3390/antibiotics11070845.

[22] M.K. Matta, A. Chockalingam, A. Gandhi, S. Stewart, L. Xu, K. Shea, V. Patel, R. Rouse, LC-MS/MS based quantitation of ciprofloxacin and its application to antimicrobial resistance study in Balb/c mouse plasma, urine, bladder and kidneys, Anal. Methods. 10 (2018) 1237–1246. https://doi.org/10.1039/C7AY02923C.

[23] S. Wei, J. Lin, H. Li, J.-M. Lin, Separation of seven fluoroquinolones by microemulsion electrokinetic chromatography and application to ciprofloxacin, lomefloxacin

determination in urine, Journal of Chromatography A. 1163 (2007) 333–336. https://doi.org/10.1016/j.chroma.2007.06.052.

[24] J.-Y. Ko, C.-Y. Chang, Y.-H. Yang, S.-H. Chen, Rapid Determination of Ciprofloxacin in Cerebrospinal Fluid by Micellar Electrokinetic Chromatography with Direct Sample Injection and its Application in Tuberculosis Meningitis, Journal of Liquid Chromatography & Related Technologies. 32 (2008) 418–431. https://doi.org/10.1080/10826070802634513.

[25] D. Barron, E. Jimenez-Lozano, J. Cano, J. Barbosa, Determination of residues of enrofloxacin and its metabolite ciprofloxacin in biological materials by capillary electrophoresisq, J. Chromatogr. B. 759 (2001) 73–9. doi: 10.1016/s0378-4347(01)00214-6.

[26] M. Zaki, E. El Shafie, S.A. Gawad, A.M. Fekry, R.S. El-Kamel, M. Shehata, Mn/Cu nanoparticles modified carbon paste electrode as a novel electrochemical sensor for nicotine detection, Electroanalysis 35 (2023) e202200143. https://doi.org/10.1002/elan.202200143.

[27] M. Zaki, E. El Shafie, S.A. Abdel-Gawad, A.M. Fekry, M. Shehata, Sensitive detection for nicotine using nickel/coppernanoparticle–modified carbon paste electrode, Ionics 28 (2022) 4881–4891. https://doi.org/10.1007/s11581-022-04649-6.

[28] A. Moustafa, R.S. El-Kamel, S. Abdelgawad, A.M. Fekry, M. Shehata, Electrochemical determination of vitamin B6 (pyridoxine) by reformedcarbon paste electrode with iron oxide nanoparticles, Ionics 28 (2022) 4471–4484. https://doi.org/10.1007/s11581-022-04673-6.

[29] A.M. Fekrya, S.A. Abdel-Gawad, S.M. Azab, Alain Walcarius, A Sensitive Electrochemical Sensor for Moxifloxacin Hydrochloride Based on Nafion/Graphene Oxide/Zeolite Modified Carbon Paste Electrode, Electroanalysis 33 (2021) 964-974. https://doi.org/10.1002/elan.202060355.

~~(2001).~~

[30~~26~~] K.R. Reddy, P.K. Brahman, L. Suresh, Fabrication of high performance disposable screen printed electrochemical sensor for ciprofloxacin sensing in biological samples, Measurement. 127 (2018) 175–186. https://doi.org/10.1016/j.measurement.2018.05.078.

[31~~27~~] W.D. Adane, B.S. Chandravanshi, M. Tessema, A simple, ultrasensitive and cost-effective electrochemical sensor for the determination of ciprofloxacin in various types of samples, Sensing and Bio-Sensing Research. 39 (2023) 100547. https://doi.org/10.1016/j.sbsr.2022.100547.

Formatted: Bibliography

Formatted: No underline

Field Code Changed

Formatted: No underline

Field Code Changed

Field Code Changed

Formatted: No underline

Field Code Changed

Formatted: No underline

[~~28~~32] J. Kozak, K. Tyszczuk-Rotko, M. Wójciak, I. Sowa, M. Rotko, First Screen-Printed Sensor (Electrochemically Activated Screen-Printed Boron-Doped Diamond Electrode) for Quantitative Determination of Rifampicin by Adsorptive Stripping Voltammetry, Materials. 14 (2021) 4231. https://doi.org/10.3390/ma14154231.

[~~29~~33] F. Beck, Cyclic voltammetry—simulation and analysis of reaction mechanisms. By David K. Gosser, Jr., VCH, New York 1993, xi, 154 pp., hardcover, DM 124.00, ISBN 3-527-28226-2, disks included (5 1/4″ and 3 1/2″), Electroanalysis. 7 (1995) 298–298. https://doi.org/10.1002/elan.1140070324.

[~~30~~34] X. Zhang, Y. Wei, Y. Ding, Electrocatalytic oxidation and voltammetric determination of ciprofloxacin employing poly(alizarin red)/graphene composite film in the presence of ascorbic acid, uric acid and dopamine, Analytica Chimica Acta. 835 (2014) 29–36. https://doi.org/10.1016/j.aca.2014.05.020.

[~~31~~35] A. Martin Santos, A. Wong, A. Araújo Almeida, O. Fatibello-Filho, Simultaneous determination of paracetamol and ciprofloxacin in biological fluid samples using a glassy carbon electrode modified with graphene oxide and nickel oxide nanoparticles, Talanta. 174 (2017) 610–618. https://doi.org/10.1016/j.talanta.2017.06.040.

[~~32~~36] R. Chauhan, A.A.S. Gill, Z. Nate, R. Karpoormath, Highly selective electrochemical detection of ciprofloxacin using reduced graphene oxide/poly(phenol red) modified glassy carbon electrode, Journal of Electroanalytical Chemistry. 871 (2020) 114254. https://doi.org/10.1016/j.jelechem.2020.114254.

[~~33~~37] J. Mocak, A.M. Bond, S. Mitchell, G. Scollary, A statistical overview of standard (IUPAC and ACS) and new procedures for determining the limits of detection and quantification: Application to voltammetric and stripping techniques (Technical Report), Pure and Applied Chemistry. 69 (1997) 297–328. https://doi.org/10.1351/pac199769020297.

[~~34~~38] J. Shan, Y. Liu, R. Li, C. Wu, L. Zhu, J. Zhang, Indirect electrochemical determination of ciprofloxacin by anodic stripping voltammetry of Cd(II) on graphene-modified electrode, Journal of Electroanalytical Chemistry. 738 (2015) 123–129. https://doi.org/10.1016/j.jelechem.2014.11.031.

[~~35~~39] L. Faria, J. Pereira, G. Azevedo, M. Matos, R. Munoz, R. Matos, Square-Wave Voltammetry Determination of Ciprofloxacin in Pharmaceutical Formulations and Milk Using a Reduced Graphene Oxide Sensor, J. Braz. Chem. Soc. (2019). https://doi.org/10.21577/0103-5053.20190108.

[~~36~~40] V. Hoang, N. Yen, Adsorptive Cathodic Stripping Voltammetric Determination of Ciprofloxacin in Bulk Powder, Pharmaceutical Dosage Forms and Urine, Trop. J. Pharm Res. 12 (2013) 783–790. https://doi.org/10.4314/tjpr.v12i5.19.

[~~37~~41] X. Fang, X. Chen, Y. Liu, Q. Li, Z. Zeng, T. Maiyalagan, S. Mao, Nanocomposites of Zr(IV)-Based Metal–Organic Frameworks and Reduced Graphene Oxide for Electrochemically Sensing Ciprofloxacin in Water, ACS Appl. Nano Mater. 2 (2019) 2367–2376. https://doi.org/10.1021/acsanm.9b00243.

[~~38~~42] S.A. Lim, M.U. Ahmed, A Simple DNA-based Electrochemical Biosensor for Highly Sensitive Detection of Ciprofloxacin Using Disposable Graphene, ANAL. SCI. 32 (2016) 687–693. https://doi.org/10.2116/analsci.32.687.

[~~39~~43] H. Bagheri, H. Khoshsafar, S. Amidi, Y. Hosseinzadeh Ardakani, Fabrication of an electrochemical sensor based on magnetic multi-walled carbon nanotubes for the determination of ciprofloxacin, Anal. Methods. 8 (2016) 3383–3390. https://doi.org/10.1039/C5AY03410H.

[~~40~~44] M.P. Kingsley, P.K. Kalambate, A.K. Srivastava, Simultaneous determination of ciprofloxacin and paracetamol by adsorptive stripping voltammetry using copper zinc ferrite nanoparticles modified carbon paste electrode, RSC Adv. 6 (2016) 15101–15111. https://doi.org/10.1039/C5RA19861E.

[~~41~~45] S. Dehdashtian, M.B. Gholivand, M. Shamsipur, A. Azadbakht, Z. Karimi, Fabrication of a highly sensitive and selective electrochemical sensor based on chitosan-coated Fe_3O_4 magnetic nanoparticle for determination of antibiotic ciprofloxacin and its application in biological samples, Can. J. Chem. 94 (2016) 803–811. https://doi.org/10.1139/cjc-2016-0129.

[~~42~~46] M. Radičová, M. Behúl, M. Marton, M. Vojs, R. Bodor, R. Redhammer, A. Vojs Staňová, Heavily Boron Doped Diamond Electrodes for Ultra Sensitive Determination of Ciprofloxacin in Human Urine, Electroanalysis. 29 (2017) 1612–1617. https://doi.org/10.1002/elan.201600769.

[~~43~~47] G.F. Alves, T.P. Lisboa, L.V. Faria, D.M. Farias, M.A.C. Matos, R.C. Matos, Disposable Pencil Graphite Electrode for Ciprofloxacin Determination in Pharmaceutical Formulations by Square Wave Voltammetry, Electroanalysis. 33 (2021) 543–549. https://doi.org/10.1002/elan.202060432.

[~~44~~48] R. Rani, A. Deep, B. Mizaikoff, S. Singh, Copper Based Organic Framework Modified Electrosensor for Selective and Sensitive Detection of Ciprofloxacin, Electroanalysis. 32 (2020) 2442–2451. https://doi.org/10.1002/elan.202060274.

[4549] A. Wong, A. M. Santos, T. A. Silva, F.C. Moraes, O. Fatibello- Filho, M.D.P.T. Sotomayor, Sensitive and Selective Voltammetric Determination of Ciprofloxacin Using Screen- printed Electrodes Modified with Carbon Black and Magnetic- molecularly Imprinted Polymer, Electroanalysis. 35 (2023). https://doi.org/10.1002/elan.202200165.

[4650] A.A.S. Gill, S. Singh, Z. Nate, C. Pawar, R. Chauhan, N.B. Thapliyal, R. Karpoormath, R. Patel, One-pot synthesis of β-cyclodextrin modified silver nanoparticles for highly sensitive detection of ciprofloxacin, Journal of Pharmaceutical and Biomedical Analysis. 203 (2021) 114219. https://doi.org/10.1016/j.jpba.2021.114219.

[4751] K. Mariappan, S. Alagarsamy, S.-M. Chen, S. Sakthinathan, Fabrication of ZnWO4/Carbon Black Nanocomposites Modified Glassy Carbon Electrode for Enhanced Electrochemical Determination of Ciprofloxacin in Environmental Water Samples, Materials. 16 (2023) 741. https://doi.org/10.3390/ma16020741.

[4852] G. Muungani, V. Moodley, W.E. van Zyl, Solid-state synthesis of the phyllosilicate Effenbergerite (BaCuSi4O10) for electrochemical sensing of ciprofloxacin antibiotic in pharmaceutical drug formulation, J Appl Electrochem. 52 (2022) 285–297. https://doi.org/10.1007/s10800-021-01633-2.

[4953] A. Chaabani, T. Ben Jabrallah, N. Belhadj Tahar, Electrochemical Oxidation of Ciprofloxacin on COOH-Functionalized Multi-Walled Carbon Nanotube–Coated Vitreous Carbon Electrode, Electrocatalysis. 13 (2022) 402–413. https://doi.org/10.1007/s12678-022-00725-7.

[540] M. Pan, P. Guo, H. Liu, J. Lu, Q. Xie, Graphene oxide modified screen-printed electrode for highly sensitive and selective electrochemical detection of ciprofloxacin residues in milk, J Anal Sci Technol. 12 (2021) 55. https://doi.org/10.1186/s40543-021-00309-y.

[551] R. Rahimpour, B. Sabeti, F. Chekin, Electrochemical Sensor Based on Nitrogen Doped Porous Reduced Graphene Oxide to Detection of Ciprofloxacin in Pharmaceutical Samples, Russ J Electrochem. 57 (2021) 654–662. https://doi.org/10.1134/S1023193520120186.

[5256] M. Shamsipur, M.B. Gholivand, S. Dehdashtian, M. Feyzi, F. Jafari, Synthesis of Co/TiO_2 Nanocomposite and its Use in Construction of a Sensitive and Selective Sensor for Determination of Ciprofloxacin, AMR. 829 (2013) 563–567. https://doi.org/10.4028/www.scientific.net/AMR.829.563.

[5357] C. Yan, J. Li, T. Meng, X. Liu, R. Zhang, Y. Chen, G. Wang, Selective Recognition of Ciprofloxacin Hydrochloride Based on Molecular Imprinted Sensor via Electrochemical

Copolymerization of Pyrrole and o-phenylenediamine, Int. J. Electrochem. Sci. (2016) 6466–6476. https://doi.org/10.20964/2016.08.56.

Legend for figures

Fig. 1. (A) Voltammograms of 5.0 x 10^{-8} mol L^{-1} CFX obtained on SPCE (a) and NPSPCE (b). (B) Impedance spectra of SPCE (a) and NPSPCE (b). (C) CVs recorded in KCl solution (0.1 mol L^{-1}) containing 5.0 × 10^{-3} mol L^{-1} $K_3[Fe(CN)_6]$ at a scan rate of 100 mV s^{-1} on the SPCE (a) and NPSPCE (b). (D) Dependence between the anodic peak currents and the square root of the scan rates for the SPCE (a) and NPSPCE (b) (ν from 7.5 to 200 mV s^{-1}). SEM images of SPCE (E) and NPSPCE (F).

Fig. 2. Influence of the pH value (A) and concentration of the supporting electrolyte (B) on CFX peak current. The DPAdSV parameters: ν of 100 mV s^{-1}, t_m of 10 ms, ΔE_A of 100 mV, $E_{acc.}$ of -0.2 V and $t_{acc.}$ of 60 s.

Fig. 3. (A) Cyclic voltammograms obtained at the NPSPCE in 0.1 M PBS (pH = 7.1) containing 1.0×10^{-6} M CFX at ν of 50 (a), 100 (b) and 150 (c) mV s^{-1}. The dependence between I_p and $\nu^{1/2}$ (ν from 5 to 200 mV s^{-1}) (B), log I_p and log ν (C) and CFX oxidation mechanism (D).

Fig. 4. The dependence of $E_{acc.}$ (A) and $t_{acc.}$ (B) on 2.0×10^{-8} M CFX peak current. ν of 100 mV s^{-1}, t_m of 10 ms, ΔE_A of 100 mV.

Fig. 5. The influence of ΔE_A (A), t_m (B), and ν (C) on 2.0×10^{-8} mol L^{-1} CFX peak current. $E_{acc.}$ of 0.5 V, $t_{acc.}$ of 130 s.

Fig. 6. The DPAdSV curves obtained during determination of the following CFX concentrations (a → g, $5.0 \times 10^{-10} - 3.0 \times 10^{-8}$ mol L^{-1}) in 0.1 mol L^{-1} PBS of pH 7.1. (B) Calibration graph of CFX. The obtained average values of the peak current are shown with standard deviation for n = 3. The DPAdSV parameters: ν of 175 mV s^{-1}, t_m of 5 ms, ΔE_A of 150 mV, $E_{acc.}$ of 0.5 V and $t_{acc.}$ of 130 s.

Fig. 7. The DPAdSV curves obtained during determination of CFX in RM of human urine (A), municipal wastewater (B) and hospital wastewater (C): (A): (a) 1 µL of sample + 2.0×10^{-9}, (b) as (a) + 2.0×10^{-9}, (c) as (a) + 4.0×10^{-9} mol L^{-1} CFX, (B): (a) 1 mL of sample + 2.0×10^{-9}, (b) as (a) + 2.0×10^{-9}, (c) as (a) + 4.0×10^{-9} mol L^{-1} CFX and (C): (a) 0.5 mL of sample, (b) as (a) + 5.0×10^{-9}, (c) as (a) + 1.0×10^{-8}, (d) as (a) + 1.5×10^{-8} mol L^{-1} CFX. The DPAdSV parameters: ν of 175 mV s^{-1}, t_m of 5 ms, ΔE_A of 150 mV, $E_{acc.}$ of 0.5 V and $t_{acc.}$ of 130 s.

Lublin, 26.09.2023r.

mgr Jędrzej Kozak
Katedra Chemii Analitycznej
Instytut Nauk Chemicznych
Wydział Chemii UMCS
pl. Marii Curie-Skłodowskiej 3
20-031 Lublin

Oświadczenie o współautorstwie

Oświadczam, że w pracach:

(RD1) K. Tyszczuk-Rotko, J. Kozak, M. Sztanke, K. Sztanke, I. Sadok, A screen-printed sensor coupled with flow system for quantitative determination of a novel promising anticancer agent candidate, Sensors, 20 (18) (2020) 5217-5227.

(RD2) J. Kozak, K. Tyszczuk-Rotko, M. Wójciak, I. Sowa, Electrochemically activated screen-printed carbon sensor modified with anionic surfactant (aSPCE/SDS) for simultaneous determination of paracetamol, diclofenac and tramadol, Materials, 14 (13) (2021) 3581-3596.

(RD3) J. Kozak, K. Tyszczuk-Rotko, M. Wójciak, I. Sowa, M. Rotko, First screen-printed sensor (electrochemically activated screen-printed boron-doped diamond electrode) for quantitative determination of rifampicin by adsorptive stripping voltammetry, Materials, 14 (15) (2021) 4231-4242.

(RD4) K. Tyszczuk-Rotko, J. Kozak, B. Czech, Screen-printed voltammetric sensors—tools for environmental water monitoring of painkillers, Sensors, 22 (7) (2022) 2437-2454.

(RD5) J. Kozak, K. Tyszczuk-Rotko, M. Wójciak, I. Sowa, M. Rotko, Electrochemically pretreated sensor based on screen-printed carbon modified with Pb nanoparticles for determination of testosterone, Materials, 15 (14) (2022) 4948-4964.

(RD6) J. Kozak, K. Tyszczuk-Rotko, I. Sadok, K. Sztanke, M. Sztanke, Application of a screen-printed sensor modified with carbon nanofibers for the voltammetric analysis of an anticancer disubstituted fused triazinone, International Journal of Molecular Sciences, 23 (5) (2022) 2429-2442.

(RD7) J. Kozak, K. Tyszczuk-Rotko, R. Metelka, Quantification of anti-cancer antibiotic bleomycin using an electrochemically pretreated and decorated with lead nanoparticles screen-printed sensor, International Journal of Molecular Sciences, 24 (1) (2022) 472-484.

(RD8) J. Kozak, K. Tyszczuk-Rotko, K. Sztanke, M. Sztanke, Sensitive and selective voltammetric sensor based on anionic surfactant-modified screen-printed carbon for the

quantitative analysis of an anticancer active fused azaisocytosine-containing congener, International Journal of Molecular Sciences, 24 (1) (2023) 564-574.

(RD9) J. Kozak, K. Tyszczuk-Rotko, Screen-printed gold sensor for ultrasensitive voltammetric analysis of the antipsychotic drug thioridazine, Measurement, 217 (2023) 113107.

(RD10) J. Kozak, K. Tyszczuk-Rotko, Damian Gorylewski, A nanoporous screen-printed carbon sensor for environmental and clinical monitoring of the antibiotic ciprofloxacin, Measurement (zaakceptowana 26.09.2023 r.).

mój wkład polegał na współudziale w tworzeniu koncepcji prac, optymalizacji woltamperometrycznych procedur oznaczania badanych związków, charakterystyce stosowanych czujników, badaniu selektywności i zastosowaniu opracowanych procedur do ilościowej analizy badanych związków w próbkach o rożnej matrycy, a także opracowaniu otrzymanych wyników, przygotowaniu i edycji manuskryptów.

Jędrzej Kozak

mgr Jędrzej Kozak

Lublin, 26.09.2023

prof. dr hab. Katarzyna Tyszczuk-Rotko
Katedra Chemii Analitycznej
Instytut Nauk Chemicznych
Wydział Chemii UMCS
pl. Marii Curie-Skłodowskiej 3
20-031 Lublin

Oświadczenie o współautorstwie

Oświadczam, że w pracach:

(RD1) K. Tyszczuk-Rotko, J. Kozak, M. Sztanke, K. Sztanke, I. Sadok, A screen-printed sensor coupled with flow system for quantitative determination of a novel promising anticancer agent candidate, Sensors, 20 (18) (2020) 5217-5227.

(RD2) J. Kozak, K. Tyszczuk-Rotko, M. Wójciak, I. Sowa, Electrochemically activated screen-printed carbon sensor modified with anionic surfactant (aSPCE/SDS) for simultaneous determination of paracetamol, diclofenac and tramadol, Materials, 14 (13) (2021) 3581-3596.

(RD3) J. Kozak, K. Tyszczuk-Rotko, M. Wójciak, I. Sowa, M. Rotko, First screen-printed sensor (electrochemically activated screen-printed boron-doped diamond electrode) for quantitative determination of rifampicin by adsorptive stripping voltammetry, Materials, 14 (15) (2021) 4231-4242.

(RD4) K. Tyszczuk-Rotko, J. Kozak, B. Czech, Screen-printed voltammetric sensors—tools for environmental water monitoring of painkillers, Sensors, 22 (7) (2022) 2437-2454.

(RD5) J. Kozak, K. Tyszczuk-Rotko, M. Wójciak, I. Sowa, M. Rotko, Electrochemically pretreated sensor based on screen-printed carbon modified with Pb nanoparticles for determination of testosterone, Materials, 15 (14) (2022) 4948-4964.

(RD6) J. Kozak, K. Tyszczuk-Rotko, I. Sadok, K. Sztanke, M. Sztanke, Application of a screen-printed sensor modified with carbon nanofibers for the voltammetric analysis of an anticancer disubstituted fused triazinone, International Journal of Molecular Sciences, 23 (5) (2022) 2429-2442.

(RD7) J. Kozak, K. Tyszczuk-Rotko, R. Metelka, Quantification of anti-cancer antibiotic bleomycin using an electrochemically pretreated and decorated with lead nanoparticles screen-printed sensor, International Journal of Molecular Sciences, 24 (1) (2022) 472-484.

(RD8) J. Kozak, K. Tyszczuk-Rotko, K. Sztanke, M. Sztanke, Sensitive and selective voltammetric sensor based on anionic surfactant-modified screen-printed carbon for the

quantitative analysis of an anticancer active fused azaisocytosine-containing congener, International Journal of Molecular Sciences, 24 (1) (2023) 564-574.

(RD9) J. Kozak, K. Tyszczuk-Rotko, Screen-printed gold sensor for ultrasensitive voltammetric analysis of the antipsychotic drug thioridazine, Measurement, 217 (2023) 113107.

(RD10) J. Kozak, K. Tyszczuk-Rotko, Damian Gorylewski, A nanoporous screen-printed carbon sensor for environmental and clinical monitoring of the antibiotic ciprofloxacin, Measurement (zaakceptowana 26.09.2023 r.).

mój wkład polegał na współudziale w tworzeniu koncepcji prac, merytorycznym nadzorze nad badaniami realizowanymi w ramach niniejszych prac oraz współudziale w opracowaniu otrzymanych wyników, przygotowaniu i edycji manuskryptów.

Prof. dr hab. Katarzyna Tyszczuk-Rotko
Uniwersytet Marii Curie-Skłodowskiej
Wydział Chemii
Instytut Nauk Chemicznych
Katedra Chemii Analitycznej
Pl. M. Curie-Skłodowskiej 3/519
20-031 Lublin
E-mail: katarzyna.tyszczuk-rotko@mail.umcs.pl

prof. dr hab. Katarzyna Tyszczuk-Rotko

Lublin, dn. 6.07.2023 r.

dr hab. Małgorzata Sztanke, prof. UM
Zakład Chemii Medycznej
Katedry Nauk Podstawowych
Uniwersytet Medyczny w Lublinie
ul. Chodźki 4a
20-093 Lublin

Oświadczenie o współautorstwie

Oświadczam, że w pracach:

(RD1) K. Tyszczuk-Rotko, J. Kozak, M. Sztanke, K. Sztanke, I. Sadok, A screen-printed sensor coupled with flow system for quantitative determination of a novel promising anticancer agent candidate, Sensors, 20 (18) (2020) 5217-5227.

(RD6) J. Kozak, K. Tyszczuk-Rotko, I. Sadok, K. Sztanke, M. Sztanke, Application of a screen-printed sensor modified with carbon nanofibers for the voltammetric analysis of an anticancer disubstituted fused triazinone, International Journal of Molecular Sciences, 23 (5) (2022) 2429-2442.

(RD8) J. Kozak, K. Tyszczuk-Rotko, K. Sztanke, M. Sztanke, Sensitive and selective voltammetric sensor based on anionic surfactant-modified screen-printed carbon for the quantitative analysis of an anticancer active fused azaisocytosine-containing congener, International Journal of Molecular Sciences, 24 (1) (2023) 564-574.

mój wkład polegał na syntezie i charakterystyce analizowanych związków, zaproponowaniu mechanizmów ich redukcji, a także na współudziale w przygotowaniu manuskryptu.

dr hab. Małgorzata Sztanke, prof. UM

Lublin, dn. 6.07.2023 r.

prof. dr hab. Krzysztof Sztanke
Pracownia Syntezy i Analizy Związków Bioorganicznych
Katedry Nauk Podstawowych
Uniwersytet Medyczny w Lublinie
ul. Chodźki 4a
20-093 Lublin

Oświadczenie o współautorstwie

Oświadczam, że w pracach:

(RD1) K. Tyszczuk-Rotko, J. Kozak, M. Sztanke, K. Sztanke, I. Sadok, A screen-printed sensor coupled with flow system for quantitative determination of a novel promising anticancer agent candidate, Sensors, 20 (18) (2020) 5217-5227.

(RD6) J. Kozak, K. Tyszczuk-Rotko, I. Sadok, K. Sztanke, M. Sztanke, Application of a screen-printed sensor modified with carbon nanofibers for the voltammetric analysis of an anticancer disubstituted fused triazinone, International Journal of Molecular Sciences, 23 (5) (2022) 2429-2442.

(RD8) J. Kozak, K. Tyszczuk-Rotko, K. Sztanke, M. Sztanke, Sensitive and selective voltammetric sensor based on anionic surfactant-modified screen-printed carbon for the quantitative analysis of an anticancer active fused azaisocytosine-containing congener, International Journal of Molecular Sciences, 24 (1) (2023) 564-574.

mój wkład polegał na syntezie i charakterystyce analizowanych związków, zaproponowaniu mechanizmów ich redukcji, a także na współudziale w przygotowaniu manuskryptu.

Kierownik
Pracowni Syntezy i Analizy
Związków Bioorganicznych
Katedry Nauk Podstawowych
Uniwersytetu Medycznego w Lublinie
Prof. dr hab. n. med. Krzysztof Sztanke

KATOLICKI UNIWERSYTET LUBELSKI JANA PAWŁA II
Wydział Medyczny
INSTYTUT NAUK BIOLOGICZNYCH
KATEDRA CHEMII
PRACOWNIA ZASTOSOWAŃ METOD SEPARACJI I SPEKTROSKOPII

Lublin, dn. 6 lipca 2023 r.

Oświadczenie o współautorstwie

Oświadczam, że w pracach:

(RD1) K. Tyszczuk-Rotko, J. Kozak, M. Sztanke, K. Sztanke, I. Sadok, A screen-printed sensor coupled with flow system for quantitative determination of a novel promising anticancer agent candidate, Sensors 20 (18) (2020) 5217-5227;

(RD6) J. Kozak, K. Tyszczuk-Rotko, I. Sadok, K. Sztanke, M. Sztanke, Application of a screen-printed sensor modified with carbon nanofibers for the voltammetric analysis of ananti cancer disubstituted fusedtriazinone, International Journal of Molecular Sciences 23 (5) (2022) 2429-2442

mój wkład polegał na wykonaniu chromatograficznych oznaczeń badanych związków w próbkach realnych oraz współudziale w opracowaniu i opisie otrzymanych wyników.

Sadok Ilona

dr Ilona Sadok

Al. Racławickie 14 | 20-950 Lublin | tel. 530 567 488| Ilona.sadok@kul.pl | www.kul.pl

Lublin, 5.07.2023

prof. dr hab. Magdalena Wójciak
Zakład Chemii Analitycznej
Katedra Chemii
Wydział Farmaceutyczny
Uniwersytet Medyczny w Lublinie
ul. Chodźki 4a
20-093 Lublin

Oświadczenie o współautorstwie

Oświadczam, że w pracach:

(RD2) J. Kozak, K. Tyszczuk-Rotko, M. Wójciak, I. Sowa, Electrochemically activated screen-printed carbon sensor modified with anionic surfactant (aSPCE/SDS) for simultaneous determination of paracetamol, diclofenac and tramadol, Materials, 14 (13) (2021) 3581-3596.

(RD3) J. Kozak, K. Tyszczuk-Rotko, M. Wójciak, I. Sowa, M. Rotko, First screen-printed sensor (electrochemically activated screen-printed boron-doped diamond electrode) for quantitative determination of rifampicin by adsorptive stripping voltammetry, Materials, 14 (15) (2021) 4231-4242.

(RD5) J. Kozak, K. Tyszczuk-Rotko, M. Wójciak, I. Sowa, M. Rotko, Electrochemically pretreated sensor based on screen-printed carbon modified with Pb nanoparticles for determination of testosterone, Materials, 15 (14) (2022) 4948-4964.

mój wkład polegał na wykonaniu chromatograficznych oznaczeń badanych związków w próbkach realnych oraz współudziale w opracowaniu i opisie otrzymanych wyników.

Wójciak Magda

prof. dr hab. Magdalena Wójciak

Lublin,05.07.2023

prof. dr hab. Ireneusz Sowa
Zakład Chemii Analitycznej
Katedra Chemii
Wydział Farmaceutyczny
Uniwersytet Medyczny w Lublinie
ul. Chodźki 4a
20-093 Lublin

Oświadczenie o współautorstwie

Oświadczam, że w pracach:

(RD2) J. Kozak, K. Tyszczuk-Rotko, M. Wójciak, I. Sowa, Electrochemically activated screen-printed carbon sensor modified with anionic surfactant (aSPCE/SDS) for simultaneous determination of paracetamol, diclofenac and tramadol, Materials, 14 (13) (2021) 3581-3596.

(RD3) J. Kozak, K. Tyszczuk-Rotko, M. Wójciak, I. Sowa, M. Rotko, First screen-printed sensor (electrochemically activated screen-printed boron-doped diamond electrode) for quantitative determination of rifampicin by adsorptive stripping voltammetry, Materials, 14 (15) (2021) 4231-4242.

(RD5) J. Kozak, K. Tyszczuk-Rotko, M. Wójciak, I. Sowa, M. Rotko, Electrochemically pretreated sensor based on screen-printed carbon modified with Pb nanoparticles for determination of testosterone, Materials, 15 (14) (2022) 4948-4964.

mój wkład polegał na wykonaniu chromatograficznych oznaczeń badanych związków w próbkach realnych oraz współudziale w opracowaniu i opisie otrzymanych wyników.

Uniwersytet Medyczny w Lublinie
Katedra Chemii, Zakład Chemii Analitycznej
prof. dr hab. n. farm. Ireneusz Sowa

prof. dr hab. Ireneusz Sowa

Lublin, 6.07.2023

dr Marek Rotko
Katedra Technologii Chemicznej
Instytut Nauk Chemicznych
Wydział Chemii UMCS
pl. Marii Curie-Skłodowskiej 3
20-031 Lublin

Oświadczenie o współautorstwie

Oświadczam, że w pracach:

(RD3) J. Kozak, K. Tyszczuk-Rotko, M. Wójciak, I. Sowa, M. Rotko, First screen-printed sensor (electrochemically activated screen-printed boron-doped diamond electrode) for quantitative determination of rifampicin by adsorptive stripping voltammetry, Materials, 14 (15) (2021) 4231-4242.

(RD5) J. Kozak, K. Tyszczuk-Rotko, M. Wójciak, I. Sowa, M. Rotko, Electrochemically pretreated sensor based on screen-printed carbon modified with Pb nanoparticles for determination of testosterone, Materials, 15 (14) (2022) 4948-4964.

mój wkład polegał na współudziale w analizie otrzymanych wyników i edycji manuskryptu.

dr Marek Rotko

Lublin, 6.07.2023

dr hab. Bożena Czech, prof. UMCS
Katedra Radiochemii i Chemii Środowiskowej
Instytut Nauk Chemicznych
Wydział Chemii UMCS
pl. Marii Curie-Skłodowskiej 3
20-031 Lublin

Oświadczenie o współautorstwie

Oświadczam, że w pracy:

(RD4) K. Tyszczuk-Rotko, J. Kozak, B. Czech, Screen-printed voltammetric sensors—tools for environmental water monitoring of painkillers, Sensors, 22 (7) (2022) 2437-2454.

mój wkład polegał na współudziale w przygotowaniu i edycji manuskryptu.

Bożena Czech

dr hab. Bożena Czech, prof. UMCS

Pardubice, 10. 7. 2023

Radovan Metelka, Ph. D.
Department of Analytical Chemistry
Faculty of Chemical Technology
University of Pardubice
Studentská 573
532 10 Pardubice

Declaration of co-autorship

I hereby declare that in the work:

(RD7) J. Kozak, K. Tyszczuk-Rotko, R. Metelka, Quantification of anti-cancer antibiotic bleomycin using an electrochemically pretreated and decorated with lead nanoparticles screen-printed sensor, International Journal of Molecular Sciences, 24 (1) (2022) 472-484.

my participation consisted in analyzing the obtained results and editing the manuscript.

Radovan Metelka, Ph. D.

Lublin, 26.09.2023r.

mgr Damian Gorylewski
Katedra Chemii Analitycznej
Instytut Nauk Chemicznych
Wydział Chemii UMCS
pl. Marii Curie-Skłodowskiej 3
20-031 Lublin

Oświadczenie o współautorstwie

Oświadczam, że w pracy:

(RD10) J. Kozak, K. Tyszczuk-Rotko, Damian Gorylewski, A nanoporous screen-printed carbon sensor for environmental and clinical monitoring of the antibiotic ciprofloxacin, Measurement (zaakceptowana 26.09.2023 r.).

mój wkład polegał na współudziale w analizie otrzymanych wyników i edycji manuskryptu.

Damian Gorylewski
mgr Damian Gorylewski